

Electronic and Photonic Applications of Polymers

Publication Date: October 1, 1988 | doi: 10.1021/ba-1988-0218.fw001

ADVANCES IN CHEMISTRY SERIES **218**

Electronic and Photonic Applications of Polymers

Murrae J. Bowden, EDITOR
Bell Communications Research

S. Richard Turner, EDITOR
Eastman Kodak Company

Developed from a symposium sponsored
by the Division of Polymeric Materials:
Science and Engineering
at the 192nd Meeting
of the American Chemical Society,
Anaheim, California
September 7–12, 1986



American Chemical Society, Washington, DC 1988



Library of Congress Cataloging-in-Publication Data

Electronic and photonic applications of polymers
Murrae J. Bowden, editor, S. Richard Turner, editor.
p. cm.—(Advances in chemistry series; 218)

“Developed from a symposium sponsored by the Division of Polymeric Materials: Science and Engineering at the 192nd Meeting of the American Chemical Society, Anaheim, California, September 7–12, 1986.”

Bibliography: p.

Includes index.

ISBN 0–8412–1400–X

1. Polymers and polymerization—Congresses. 2. Photoresists—Congresses. 3. Microlithography—Materials—Congresses.

I. Bowden, M. J., 1943– . II. Turner, S. Richard, 1942– . III. American Chemical Society. Division of Polymeric Materials: Science and Engineering. IV. American Chemical Society. Meeting (192nd: 1986: Anaheim, Calif.) V. Series.

QD1.A355 no. 218

[TK7871.15.P6]

540 s—dc19

[621.381]

88–21099

CIP

Copyright © 1988

American Chemical Society

All Rights Reserved. The appearance of the code at the bottom of the first page of each chapter in this volume indicates the copyright owner's consent that reprographic copies of the chapter may be made for personal or internal use or for the personal or internal use of specific clients. This consent is given on the condition, however, that the copier pay the stated per copy fee through the Copyright Clearance Center, Inc., 27 Congress Stret, Salem, MA 01970, for copying beyond that permitted by Sections 107 or 108 of the U.S. Copyright Law. This consent does not extend to copying or transmission by any means—graphic or electronic—for any other purpose, such as for general distribution, for advertising or promotional purposes, for creating a new collective work, for resale, or for information storage and retrieval systems. The copying fee for each chapter is indicated in the code at the bottom of the first page of the chapter.

The citation of trade names and/or names of manufacturers in this publication is not to be construed as an endorsement or as approval by ACS of the commercial products or services referenced herein; nor should the mere reference herein to any drawing, specification, chemical process, or other data be regarded as a license or as a conveyance of any right or permission, to the holder, reader, or any other person or corporation, to manufacture, reproduce, use, or sell any patented invention or copyrighted work that may in any way be related thereto. Registered names, trademarks, etc., used in this publication, even without specific indication thereof, are not to be considered unprotected by law.

PRINTED IN THE UNITED STATES OF AMERICA

Advances in Chemistry Series

M. Joan Comstock, *Series Editor*

1988 ACS Books Advisory Board

Paul S. Anderson
Merck Sharp & Dohme Research
Laboratories

Harvey W. Blanch
University of California—Berkeley

Malcolm H. Chisholm
Indiana University

Alan Elzerman
Clemson University

John W. Finley
Nabisco Brands, Inc.

Natalie Foster
Lehigh University

Marye Anne Fox
The University of Texas—Austin

Roland F. Hirsch
U.S. Department of Energy

G. Wayne Ivie
USDA, Agricultural Research Service

Michael R. Ladisch
Purdue University

Vincent D. McGinniss
Battelle Columbus Laboratories

Daniel M. Quinn
University of Iowa

James C. Randall
Exxon Chemical Company

E. Reichmanis
AT&T Bell Laboratories

C. M. Roland
U.S. Naval Research Laboratory

W. D. Shults
Oak Ridge National Laboratory

Geoffrey K. Smith
Rohm & Haas Co.

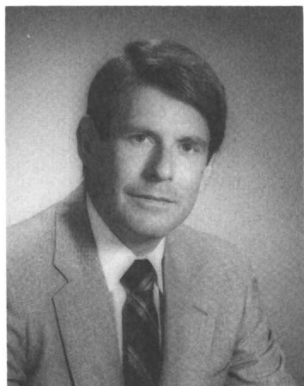
Douglas B. Walters
National Institute of
Environmental Health

Wendy A. Warr
Imperial Chemical Industries

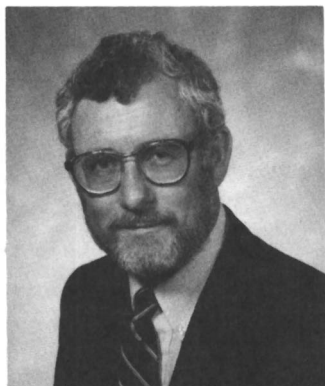
FOREWORD

The **ADVANCES IN CHEMISTRY SERIES** was founded in 1949 by the American Chemical Society as an outlet for symposia and collections of data in special areas of topical interest that could not be accommodated in the Society's journals. It provides a medium for symposia that would otherwise be fragmented because their papers would be distributed among several journals or not published at all. Papers are reviewed critically according to ACS editorial standards and receive the careful attention and processing characteristic of ACS publications. Volumes in the **ADVANCES IN CHEMISTRY SERIES** maintain the integrity of the symposia on which they are based; however, verbatim reproductions of previously published papers are not accepted. Papers may include reports of research as well as reviews, because symposia may embrace both types of presentation.

ABOUT THE EDITORS



MURRAE J. BOWDEN obtained his Ph.D. from the University of Queensland, Australia, in 1969, and after a 2-year postdoctoral appointment at the University of Manchester, England, he joined Bell Telephone Laboratories in the United States as a Member of Technical Staff in October 1971. In 1979, he was promoted to Supervisor of the Radiation Sensitive Materials and Applications group within the Organic Materials Chemical Engineering Department. With the divestiture of AT&T at the beginning of 1984, he joined Bell Communications Research where he is currently Division Manager of the Chemistry and Materials Science Research Division. His research interests have been primarily in the effects of high-energy radiation on polymeric materials, particularly in the application to high-resolution lithography for microcircuit manufacture. He is author or coauthor of over 80 technical publications and holds 8 patents. He is a member of the American Chemical Society and was a past president of the ACS Division of Polymeric Materials: Science and Engineering.



S. RICHARD TURNER received his Ph.D. in organic-polymer chemistry from the University of Florida in 1971 and did a year of postdoctoral work at the Institute of Macromolecular Chemistry in Darmstadt, Federal Republic of Germany. Before joining the Kodak Research Laboratories in 1980, he worked in the Xerox Research Laboratories in Webster, New York, and the Exxon Corporate Research Laboratories in Linden, New Jersey. He is currently a Research Associate in the Polymer Science Laboratories at Kodak. His research interests include synthesis and properties of photoactive polymers, ion-containing polymers, and water-soluble polymers. He has over 80 publications and patents in these areas. He is a member of the executive committee of the Division of Polymeric Materials: Science and Engineering of the American Chemical Society, where he currently serves as Program Chairman.

PREFACE

THE SCIENCE AND TECHNOLOGY of polymers have had a profound influence on the quality of life in the 20th century. Indeed, the utility of polymeric materials was widely appreciated long before scientists understood the molecular basis of this class of materials. Early telephone handsets, for example, were made from a condensation polymer of formaldehyde and phenol, but it was many years later before the macromolecular concept of a polymer molecule was proposed, much less accepted.

Many of the polymers in use at the beginning of the 1930s, such as rubber, proteins, nucleic acids, and polysaccharides (e.g., starch and cellulose), were of natural origin. These materials were used as construction materials, adhesives, and molded products. But the pioneering work of Staudinger, Mark, Carrothers, and others in the 1920s and 1930s had already laid the foundations for the tremendous revolution that would launch the world into the "plastic age". By establishing the molecular principles governing the formation and properties of polymers (or macromolecules, as they are often called), these early workers paved the way for the innovative onslaught and rich variety of synthetic polymers that have characterized the last 50 years.

The ease of manufacture and fabrication, wide range of physical and chemical properties, and low raw-material cost have made polymers ubiquitous in everyday life, allowing us to replace, in many instances, costly natural materials with cheap, attractive, and often vastly superior "plastic" alternatives with enormous impact on the quality and reliability of the product involved. A good example is the revolution in the telecommunications industry brought about by the introduction of polymeric materials. Applications have ranged from replacement of lead as a sheath in electric cable to meeting the stringent requirements for dielectrics in transoceanic communication. Where wires were once insulated with paper pulp and cotton serving, synthetic polymers such as poly(ethylene) and poly(vinyl chloride), which are markedly cheaper and vastly superior in performance, are now used.

The major use of polymers has been as replacements for naturally occurring materials. Synthetic fibers such as nylon and polyester have substantially replaced natural textiles; synthetic rubber is vastly superior to natural rubber, and the wide variety of engineering polymers (both thermosets and thermoplastics) have replaced traditional, naturally occurring materials such as metals and cellulosic compounds in many applications.

Polymers have also found widespread use in the electronics industry, where they have been traditionally used as insulating materials. In recent years, however, polymers have been used increasingly in many other areas of electronics. They have been used as electromechanical transducers, as lithographic resists and intermetal dielectrics in the fabrication of integrated circuits, and as passivation and insulating materials in electronics packaging. These examples are representative of what might be called passive applications, in the sense that the polymer does not play an active role in the performance of the device. But active applications, in which the device performance depends on active participation of the polymer, are increasing. Active applications include electrically conductive and photoconductive polymers and polymers for nonlinear optics and molecular electronics. These areas constitute the research frontier of polymer science. While it is unlikely that some new polymer will be introduced with the cost advantage and impact of poly(ethylene) or nylon, advances will be made in specialty applications of polymers, where the unique properties of polymers are central to the overall success of the new technology.

Recognition of the worldwide activity on the exciting research frontier of polymer science spawned the symposium upon which this book is based, and provided the catalyst to publish the plenary lectures from that meeting. The contributed papers from the plenary sessions were published as ACS Symposium Series No. 346, *Polymers for High Technology: Electronics and Photonics*.

We appreciate the many hours expended by the authors in writing their respective chapters. Their efforts are reflected in the high quality of this book, which represents a unique compilation of the various applications of polymers in electronics and photonics. We acknowledge the Division of Polymeric Materials: Science and Engineering for sponsoring the symposium upon which this book is based. We thank Lois Damick of Bell Communications Research for handling many of the administrative details associated with the book. Special thanks are due to Robin Giroux, Keith Belton, and the staff of the Books Department of the American Chemical Society for their patience, effort, and editorial assistance in assembling the book.

MURRAE J. BOWDEN
Bell Communications Research
Corporate Research Laboratories
Red Bank, NJ 07701-7020

S. RICHARD TURNER
Navesink Research and Engineering Center
Eastman Kodak Company
Rochester, NY 14650

Polymers for Electronic and Photonic Applications

Murrae J. Bowden

Bell Communications Research, 331 Newman Springs Road, Red Bank, NJ 00701

The application of polymers to selected areas of electronics and photonics is reviewed. These areas include microlithography, packaging, conducting polymers, molecular electronics, optical fiber coatings, integrated optics, nonlinear optics, and optical recording. This chapter provides an overview of the various technologies and highlights the advantages offered by the unique properties of polymers in meeting the material requirements of each technology.

POLYMERS ARE INCREASINGLY BEING USED in a wide variety of applications in electronics and photonics, most of which use polymers in their traditional role as engineering materials (e.g., circuit boards, molded products, wire and cable insulation, encapsulants, and adhesives). In addition, many other unique applications require material properties that only polymers can provide. Examples include resist materials for the lithographic fabrication of integrated circuits (IC) and polymers for optical recording. These types of applications may be considered “passive” in the sense that the polymer does not play an active role in the operation of the device or circuit. Rather, it serves some other function such as mechanical support, electrical insulation, or in the case of resists, some intermediate function in the fabrication of the device.

Technology is reaching a point, however, where the unique properties of polymers make them suitable not only for these so-called passive applications, but also for “active” applications, wherein the polymer plays an active role in the functioning of the device. Examples of such applications include nonlinear optics, molecular electronics, and conductors: electronic

0065-2393/88/0218-0001\$16.95/0
© 1988 American Chemical Society

(conducting polymers) and photonic (waveguides). In this chapter, various applications of polymers in electronics and photonics will be briefly reviewed with emphasis on the subject areas just mentioned. Brief descriptions of the various technologies are included so that the advantages of polymers might be better appreciated in terms of matching their unique properties to the requirements of the technology. This chapter is intended to provide sufficient background to put the rest of the book in perspective. A more detailed treatment of the various topics can be found in subsequent chapters.

1.1 Polymers for Electronic Applications

The modern electronics era began at Bell Telephone Laboratories in 1948 with the invention of the solid-state transistor, which replaced the large thermionic vacuum tube, the mainstay of the electronics industry for the previous 40 years. Transistors were smaller and much more robust than their vacuum tube counterparts and required much less power to operate. Electronic circuits of the 1950s and early 1960s were assembled from discrete transistors, diodes, and resistors, for example, but rapid advances in circuit complexity and density, driven by developments in computer technology, soon led to an impasse, namely, how to approach the problem of interconnecting hundreds, perhaps thousands, (some visionaries would have said millions) of discrete devices into a complex circuit.

This Herculean problem was solved in 1960 with the invention of the IC, which ushered in the microelectronics revolution whose impact we continue to experience. This technology allowed individual solid-state components to be fabricated on a single wafer of crystalline silicon—the chip—by a mass production technique and interconnected via a network of conductors on the surface of the chip. The first ICs contained only a few transistors on a chip, whereas the number of components integrated into a single circuit today number in the hundreds of thousands, even millions. Along with this revolution have come many opportunities for innovative materials technology. Polymers possess unique properties that have enabled them to meet many of the materials requirements of microelectronics engineering. Some of these applications in microelectronics will be discussed in the following section. Later sections will briefly review conducting polymers and also molecular electronics, which is believed by many to represent the next revolution in electronics.

1.1.1 From Silicon to Circuit Board

The modern-day circuit board is testimony to the pervasive intrusion of polymers into the electronics industry. As seen in Figure 1.1, a typical mounted circuit board contains a large number of packaged devices, prin-

Publication Date: October 1, 1988 | doi: 10.1021/ba-1988-0218.ch001

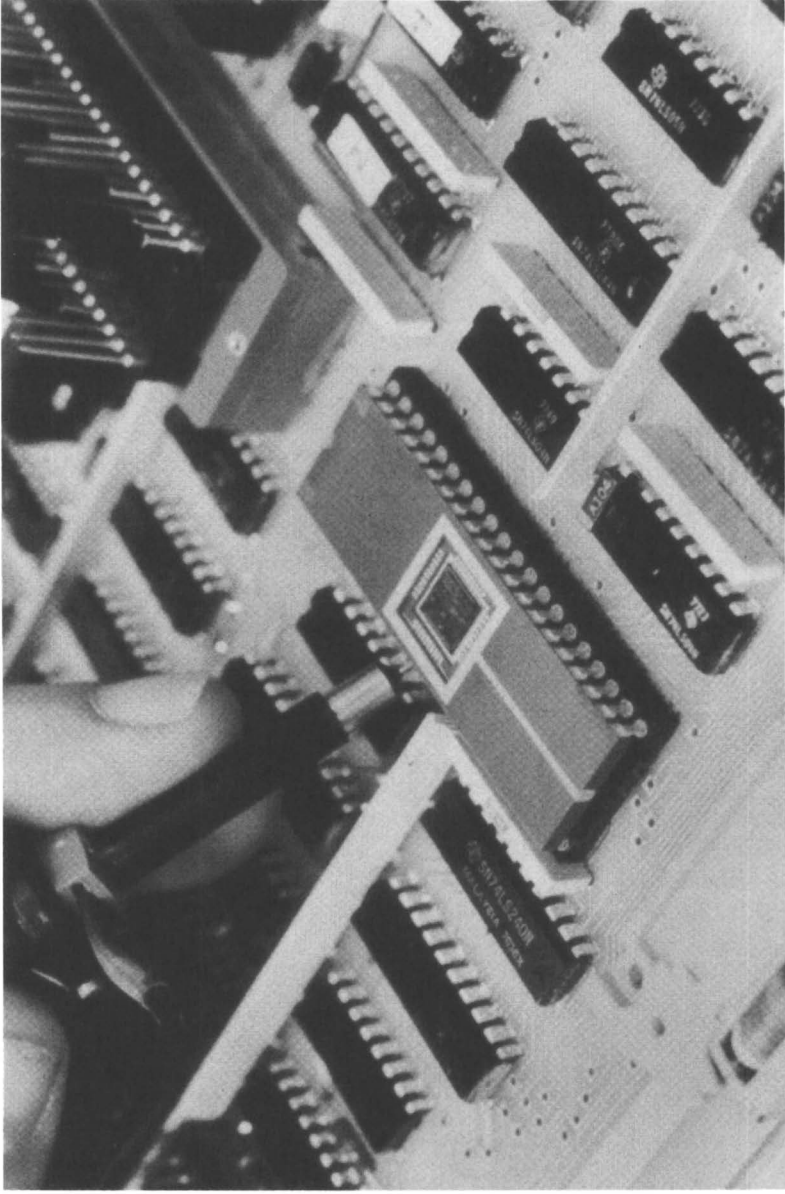


Figure 1.1. A typical circuit board.

cipally ICs, which are soldered into a plastic laminated circuit board and interconnected, typically on both sides of the board, with printed wiring. The board itself may contain up to six layers of interconnection with line widths of 6 mils. To appreciate the role played by polymers in constructing and assembling such a circuit board, it will be instructive to start at the beginning (i.e., with the fabrication of the individual IC itself) and follow the various applications of polymers in the evolution from silicon to circuit board.

1.1.1.1 RESIST MATERIALS

All silicon integrated circuits (SICs) begin life as a silicon wafer, which has been cut from a silicon ingot and polished on one side to provide a smooth surface upon which thousands, even millions, of circuit elements such as transistors, diodes, and resistors will be fabricated and interconnected to yield a set of complete circuits. Circuit fabrication requires the selective diffusion of tiny amounts of impurities into specific regions of the silicon substrate to produce the desired electrical characteristics of the circuit. These regions are defined by lithographic processes that consist of two steps:

1. delineation of the desired circuit pattern in a resist layer (usually a polymeric film that is spin-coated onto the substrate), and
2. transfer of that pattern via processes such as etching into the underlying substrate. The "substrate" in this case is an oxidized silicon wafer with an oxide thickness typically 0.1–0.5 μm .

The primary definition of the circuit pattern in the resist is a two-stage process consisting of the formation of a latent image by exposure to some form of patterned radiation followed by development of that image to produce a three-dimensional relief structure. In the case of photolithography or X-ray lithography, the latent image is formed by exposure of the resist through a mask that contains clear and opaque features outlining the circuit pattern. The basic steps of the process are outlined in Figure 1.2. In electron beam lithography, pattern information is stored digitally in a computer that controls the beam blanking and deflection function. The wafer surface is divided into a geometric array of pixels, and each pixel is either exposed (beam on) or not exposed (beam off or blanked) as the beam is scanned across the resist surface (Figure 1.3). In this way, the pattern is "written" in serial fashion as opposed to a mask process, which "writes" in parallel. Of course, the end result is the same, namely, formation of an exposed latent image in the resist.

The next step in the process is the development of the latent image to

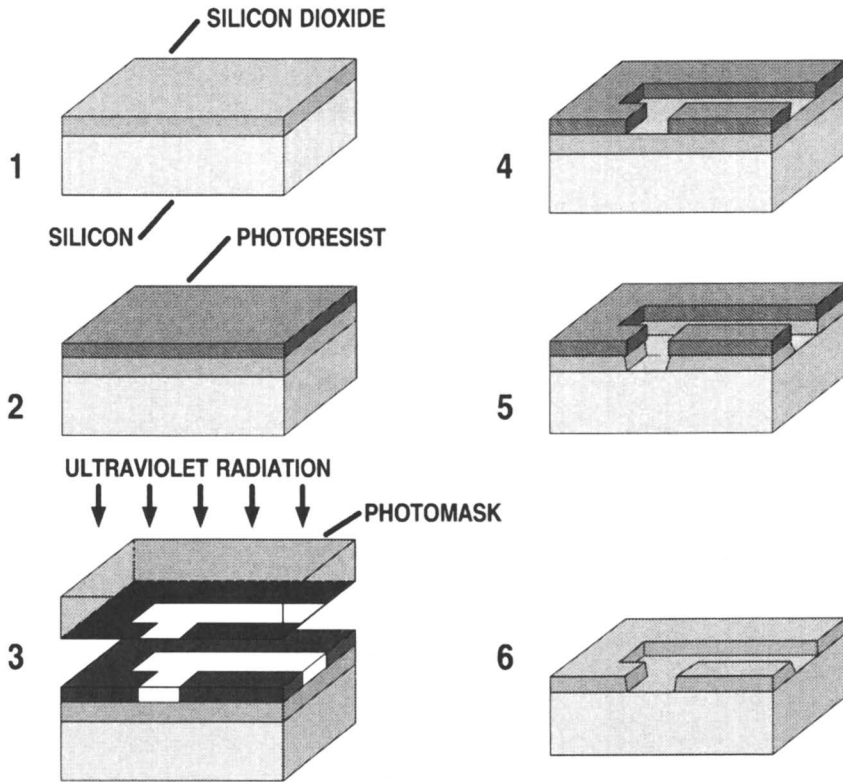


Figure 1.2. Basic steps of the photolithographic process: (1) oxidizing, (2) spin coating, (3) exposing, (4) developing, (5) etching, and (6) stripping.

give a three-dimensional relief image of the mask pattern in the resist. Exposure to actinic radiation causes chemical changes in the resist that enable the exposed and unexposed areas to be differentiated through differences in solubility or plasma etch resistance. Depending on the chemical nature of the resist, the exposed areas may be rendered more soluble in the developer than the unexposed areas, thereby producing a positive-tone image of the mask. Conversely, the exposed areas may be rendered less soluble, producing a negative-tone image. Either way, the result is a wafer with sections of the substrate exposed and the remainder still covered with resist. The remaining resist must now withstand the wide variety of chemicals used to etch the exposed substrate. The resist must possess excellent adhesion to prevent undercutting during etching (and developing) that would result in loss of resolution and line width control. The end objective is a perfect three-dimensional replication of the two-dimensional mask pattern in the wafer surface.

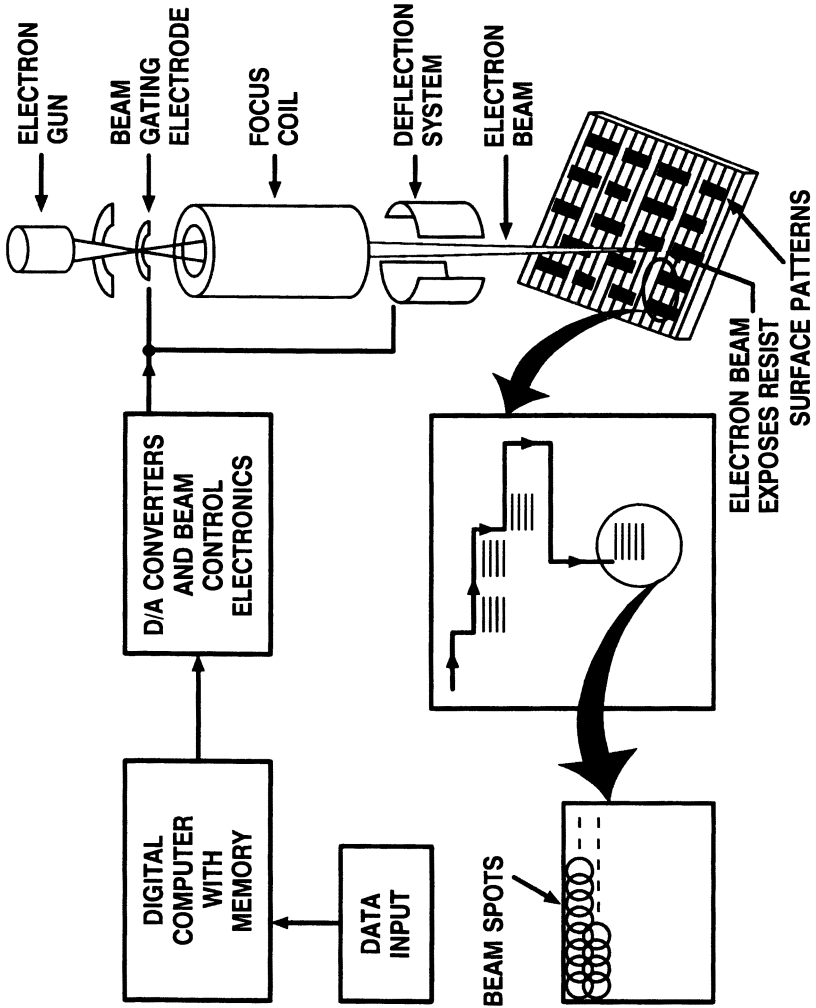


Figure 1.3. Electron beam system and exposure process.

This brief overview of the lithographic process is sufficient to appreciate the unique properties required of the resist:

- It must be capable of being uniformly deposited as a thin (typically 0.5–2.0 μm) film across a wafer, which may be as much as 8 in. (20.3 cm) in diameter.
- It must be sensitive to specific actinic radiation (UV light in the case of photolithography) and must undergo a chemical transformation that will enable exposed and unexposed areas to be differentiated by an appropriate developing scheme such as solvent or plasma development.
- It must adhere to a variety of substrates and withstand the various etching environments encountered in IC processing. These environments include high temperatures, exceedingly corrosive etching chemicals such as strong acids, and reactive plasmas.

Another very important requirement of the resist is resolution. Lithographic tools are capable of imaging submicrometer features in the resist. The resist must be able to “resolve” such features. In some cases, the resist may even be expected to do more, such as compensate for the loss of mask resolution that has been degraded in the aerial image because of fundamental limitations associated with the physics of image generation. In projection photolithography, for example, the aerial image of an object such as a mask containing an equal line and space pattern corresponds to a sinusoidal pattern of light intensity when operating at the diffraction limit of the projection tool. Such a pattern is in marked contrast to the square-wave pattern of light intensity that would correspond to perfect image transfer (*I*). (In electron beam lithography, the “aerial” image quality is degraded by scattering processes within the resist.) The net result of processes such as these is the deposition of energy in regions of the resist not specified in the original circuit (mask) layout. Ideally, one would like to use chemistry to transform this sinusoidal *aerial* image into a square-wave *latent* image in the resist (Figure 1.4).

Polymers can be designed with a unique blend of properties to meet most if not all of these requirements. Their macromolecular architecture permits them to be deposited as uniform thin films by spin coating and also provides for solubility differentiation by means of radiation-induced changes in the molecular weight. Radiation-induced scission and cross-linking are particularly important for those lithographic technologies such as electron beam or X-ray lithography, where the exposing radiation has sufficient energy to break carbon–carbon bonds. By incorporating groups that render the main chain susceptible to cleavage upon exposure to radiation, the molecular weight can be reduced, thereby making the exposed area soluble in solvents

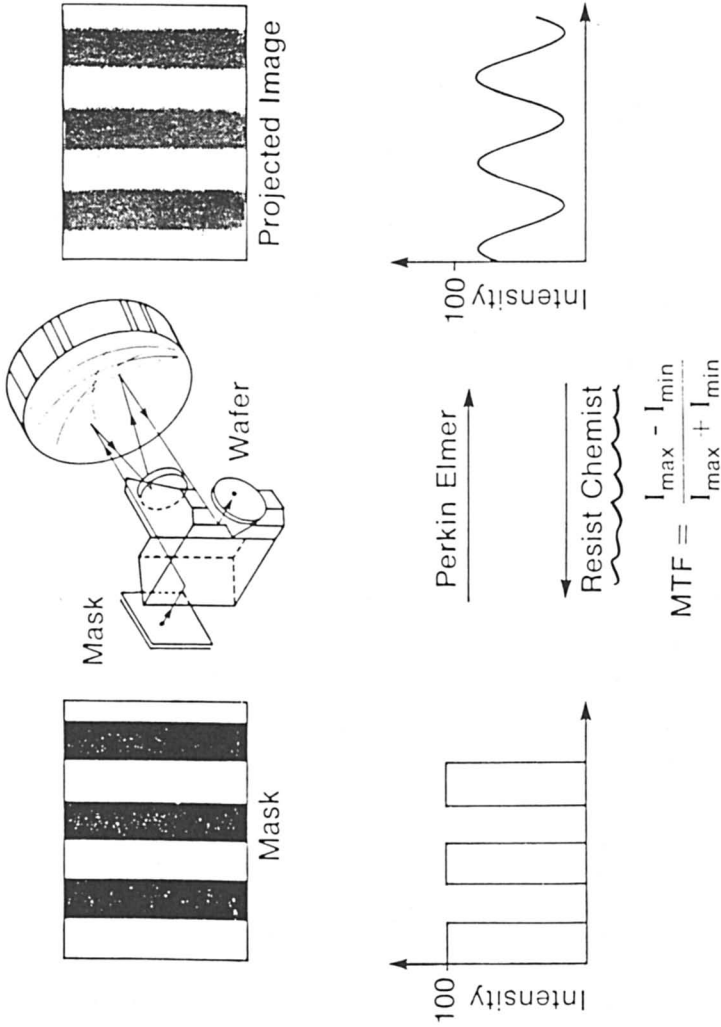


Figure 1.4. Degradation of the projected image at the diffraction limit of the lens. Diffraction effects transform an initially square-wave image into a sinusoidal pattern of intensity at the image plane.

that do not dissolve the unexposed, larger molecules. For example, the alternating copolymers of olefins and sulfur dioxide contain a relatively weak carbon–sulfur bond in the main chain. When exposed to high-energy radiation, this bond is preferentially broken, leading to a reduction in the molecular weight and consequent positive resist action (2). Alternatively, incorporation of cross-linking groups such as epoxy, vinyl, or halomethyl groups into the polymer chain will have the opposite effect, causing the polymer to become totally insoluble in all solvents. Many such chain-scissioning and cross-linking polymers have been devised and their lithographic properties reviewed in the literature. Reference 3 is an in-depth review of resist materials for fine-line lithography before the year 1985. The more recent literature is covered in Chapters 2 and 3 of this book.

In cases where the exposing radiation does not have sufficient energy to rupture bonds directly (e.g., at the wavelengths encountered in traditional photolithography), other differential solubility schemes have been devised on the basis of polarity changes in the matrix resulting from polarity changes of the sensitizer (e.g., novolac-based photoresists) or of the matrix itself. An example of matrix polarity changes is the extensive work by Willson and co-workers (4, 5) on acid-induced cleavage of protective groups substituted on a suitable polymeric binder. In this case, the acid is generated from different onium salts acting as sensitizers. Cleavage of tertiary butoxycarbonyloxy groups, for example, substituted on the aromatic ring of polystyrene converts the polymer from the hydrophobic poly(*tert*-butoxycarbonyloxystyrene) (*t*-BOC) to the hydrophilic poly(hydroxystyrene). Either positive or negative tone can be generated depending on the polarity of the developer. In cases where the polymeric component functions purely as a binder, its chemical composition depends on factors such as dissolution requirements and etch resistance.

One limitation of solvent development is swelling of the remaining resist. Swelling is particularly a problem with rubbery negative resists where it limits resolution of the residual pattern to about 1.5 μm . The resolution of negative resists may be improved by using glassy polymers, but in general, resolution is not as high as that which can be obtained with positive resists.

Today, all submicrometer imaging in photolithography is done with positive photoresists. These materials are two-component systems based on diazonaphthoquinone-sensitized novolac resins. In this case, the dissolution mechanism depends on a change of polarity of the irradiated matrix (*see* Chapter 2) resulting from chemical changes in the sensitizer that render the novolac binder soluble in aqueous base. Because the polarity of the unexposed resist is unchanged, resolution is not limited by swelling of the unexposed resist during development in aqueous base. Schemes have been devised to reverse the tone of these resists, enabling negative-tone patterns to be generated with resolution comparable to positive-tone patterns. This approach also has an added advantage over the corresponding positive pro-

cess in that it permits better control of line widths over topographic features on the wafer surface (*see* Chapter 2).

Many chemical modifications have been devised to improve resistance to specific etchants. Multilevel resist processing schemes, for example, require materials that are highly resistant to dry processing environments such as oxygen reactive ion etching (3). The resist chemist has responded to this demand by incorporating an oxide-forming element such as silicon or tin in the polymer structure. Silicon has been extensively used in this way because of the availability of a wide variety of organosilicon monomers. In an oxygen plasma, the silicon moiety in the polymer is converted to silicon dioxide at the surface of the resist (Figure 1.5). Although only typically a few hundred angstroms thick, the silicon dioxide essentially passivates the surface and thus protects the underlying resist against further erosion. Much of the research on resists over the past few years has been directed toward organosilicon resists, spurred by the growing importance of multilevel processing schemes for fabricating devices with feature sizes less than 1.0 μm . Table 1.1 lists several of these resists that have been principally designed for deep-UV (DUV) and electron beam lithography.

In the processes described so far, the resist is removed after etching, baring the patterned oxide that serves as a mask during subsequent high-temperature diffusion of dopants into the exposed silicon substrate. There are examples, however, where the resist material is left behind to become

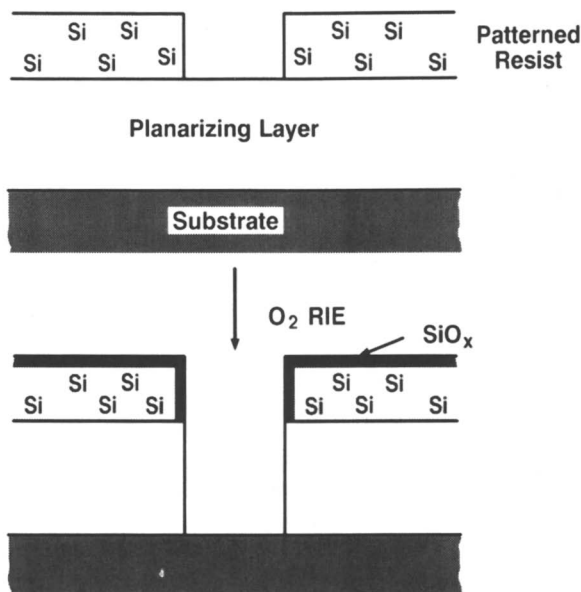
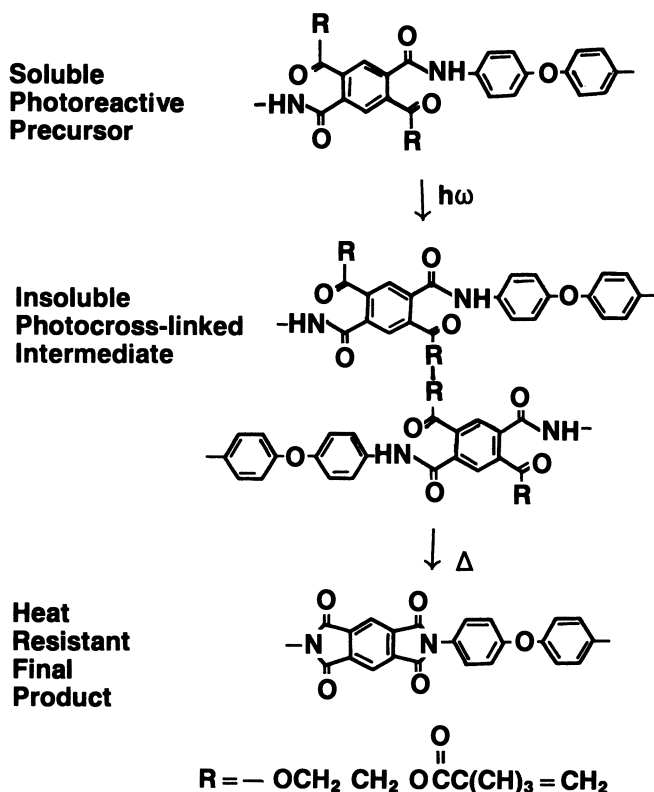


Figure 1.5. Surface passivation of silicon-containing resists in an oxygen plasma.

an integral part of the IC (e.g., an inner layer dielectric in multilayered ICs). Polyimides have been proposed for such applications (17). Polyimides exhibit excellent dielectric and thermal properties (the transition glass temperature (T_g) ~ 400 °C), are available with high purity, and may be patterned photolithographically, either directly or indirectly (e.g., to fabricate contact holes). In indirect patterning, the polyimide is spin-coated on the substrate, partially cured, and then overcoated with a conventional photoresist. The photoresist is imaged in the usual way by exposing selected areas of polyimide that are removed by development in a solvent such as hydrazine. The photoresist is then stripped, and the remaining polyimide pattern fully cured (imidized). This process has been simplified through the introduction of photosensitive polyimides, which facilitate direct patterning of the film (Scheme 1.1).





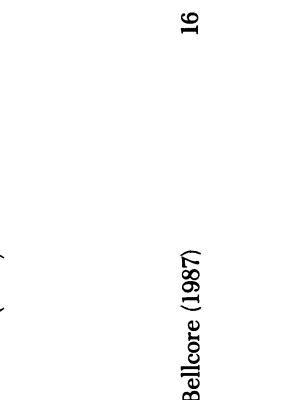
The microelectronics revolution is due, in part, to the advances in design and operation of the lithographic hardware. But the high-resolution devices that characterize this revolution would not have been possible were it not



Scheme 1.1. Chemistry of photosensitive polyimides: exposure and cure.

Table 1.1. Organosilicon Resists for Bilayer Multilevel Resist Systems

Structure	Type	Company	Reference
$\begin{array}{c} \text{CH}_3 \\ \\ \text{---Si-O---Si-O---} \\ \quad \\ \text{CH}_3 \quad \text{CH}=\text{CH}_2 \end{array}$	Negative-tone, electron beam	IBM (1981)	6
$\begin{array}{c} \text{---(CH}_2\text{---CH)}\text{---} \\ \\ \text{---Si(CH}_3\text{)}_3 \\ \\ \text{---(CH}_2\text{---CH)}\text{---} \\ \\ \text{---C}_6\text{H}_4\text{---} \\ \\ \text{---CH}_2\text{Cl} \end{array}$	Negative-tone, electron-beam, DUV	NEC (1982)	7
$\begin{array}{c} \text{---(CH}_2\text{---CH)}\text{---} \\ \\ \text{---C}_6\text{H}_4\text{---} \\ \\ \text{---Si(CH}_3\text{)}_3 \\ \\ \text{---(CH}_2\text{---CH)}\text{---} \\ \\ \text{---C}_6\text{H}_4\text{---} \\ \\ \text{---Cl} \end{array}$	Negative-tone, electron-beam, DUV	IBM (1983)	8
$\begin{array}{c} \text{Ph} \\ \\ \text{---Si-O---Si-O---} \\ \quad \\ \text{Ph} \quad \text{---C}_6\text{H}_4\text{---} \\ \\ \text{---CH}_2\text{Cl} \end{array}$	Negative-tone, electron-beam, X-ray, DUV	NTT (1983)	9
$\begin{array}{c} \text{R} \quad \text{R} \\ \quad \\ \text{---Si---Si---} \\ \quad \\ \text{R} \quad \text{R} \end{array}$	Positive-tone, DUV, mid-UV	IBM (1983) Sandia (1983)	10 11

	Positive-tone, DUV	Hitachi (1984)	12
	Positive-tone, electron-beam, DUV	AT&T (1984)	13
	Positive-tone, near-UV	AT&T (1984)	14
	Positive-tone, electron-beam	Bellcore (1986)	15
	Positive-tone, DUV	Bellcore (1987)	16

for the ingenuity of the synthetic polymer chemist and the versatility afforded by macromolecular architecture.

1.1.1.2 ELECTRONICS PACKAGING

The IC is fabricated by a series of lithographic processes similar to that described in the previous section. Each individual step constitutes a "level" in the device, the final level being a metalization pattern to interconnect the circuit elements that have been fabricated in the surface of the silicon wafer. The completed wafer is then diced, a step that involves cutting the wafer, typically with a diamond saw, to separate the individual IC chips. The next step is to package the chips in some way, attach the devices along with other components to the printed wiring board (PWB), and interconnect them to produce the completed circuit board.

Polymers are playing an increasingly important role in the protection and interconnection of the chips. SICs are exceedingly fragile, and any number of environmental factors can cause the device to fail unless the chip is protected in some way. Thus, the IC should be shielded from mechanical damage, humidity, corrosion, and other detrimental environmental effects. One approach is to hermetically seal the chip in some kind of inert package. Indeed, hermetically sealed ceramic-based packages, for example, are very reliable. They are, however, extremely costly, and given the billions of ICs produced worldwide, there is clear incentive to develop a low-cost package, which is where polymers again come to the forefront.

Figure 1.6 shows a hypothetical IC packaging structure that makes wide use of polymers in a number of components. First, the chip is bonded to the base of the chip carrier or lead frame by means of an adhesive that may also be required to provide electrical conductivity and heat dissipation. Polymeric adhesives offer very large materials cost savings over gold eutectic bonding. The adhesive may be applied to the bonding pad by dispensing directly, transfer printing, or screen printing. Screen printing is particularly suited to hybrid circuit assembly, where many chips may need to be attached to a ceramic substrate. The chips are then put in place and the assembly is cured at elevated temperature, typically 150 °C.

Many factors must be taken into consideration in designing an adhesive. The requirements include low level of ionic impurities, no voids under the chip caused by evaporation of solvent or other volatiles, no resin bleed during cure, and thermal expansion properties that match those of the substrate and chip. A significant mismatch in the thermal expansion coefficient can lead to development of thermal stresses that can result in cracking or distortion of the chip. This problem is becoming more and more important as die sizes continue to increase.

Epoxy resins are almost exclusively used for such chip-attach purposes; polyimides are used to a lesser extent. Polyimides provide excellent protection in accelerated humidity tests, but it is difficult to obtain void-free

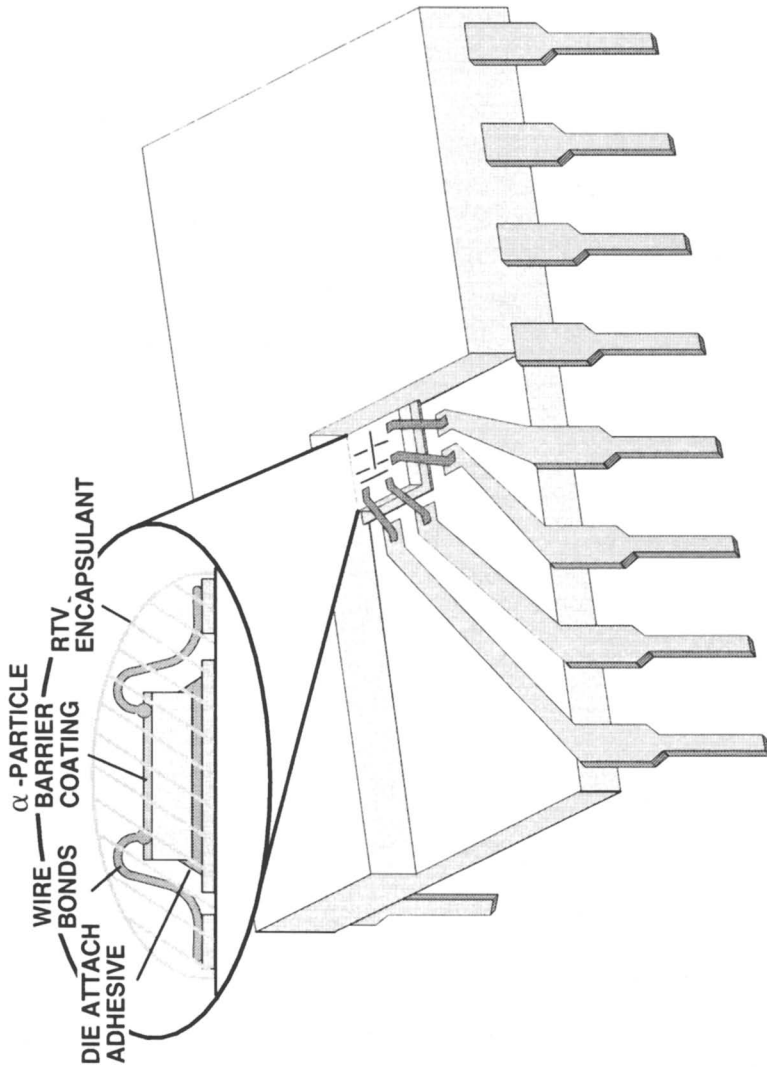


Figure 1.6. Cutaway view of a DIP.

bonds between the substrate and chip. Polyimides also tend to be more rigid and brittle than epoxy resins, and this characteristic causes lifting and cracking of the chip as the size of the chip increases. Epoxy resins, on the other hand, provide better bond strengths, are tougher, and possess greater elongation under stress. They are easier and faster to process than the polyimides; they provide one-step cures with no evolution of volatile products. The overall cost of materials and processing is also lower. In the case of conductive adhesives, metallic fillers such as silver or gold are mixed with the adhesive; for those applications where conductivity is not required, SiO_2 is the filler of choice.

Once the chip has been attached to the bonding pad of the lead-frame or ceramic substrate, it must be connected electrically to the individual leads or conductor paths on the substrate, respectively. Such connections are often made by using thin gold wires in a process known as *wire bonding*. As shown in the hypothetical package in Figure 1.6, the chip is bonded face-up, and the gold wires connect the bonding pads at the edges of the IC to the individual leads on the frame. In other processes, notably flip-chip bonding or beam-lead bonding, the chip is attached face-down to the substrate through solder bumps on the periphery of the chip, or via beam leads, which extend from the edges of the chip. Both processes leave a gap between the active chip surface and the substrate.

The chip must now be protected in some way from the wide variety of environmental factors encountered during both subsequent assembly and real-life operation that could cause the chip to fail. These environmental conditions may include:

- thermal shock (e.g., during soldering, which subjects the device to temperature differentials of several hundred degrees),
- moisture (board cleaning and humid environments),
- chemicals and salts (fluxes, board-cleaning solutions, industrial fumes, and sea air),
- mechanical shock (test and assembly, handling, and careless use), and
- extended thermal cycling (e.g., if the chip heats up during operation).

Although the surface of most IC chips has been passivated with a layer of inorganic dielectric material such as silicon dioxide or silicon nitride (polyimides have also been used as final passivating layers), the protection provided by such layers is not sufficient to ensure reliable operation throughout the lifetime of the device. The three basic methods of protection are

1. incorporation into a preformed metal, glass, plastic, or ceramic package;

2. embedment of the device in a hard plastic (epoxy, silicone-epoxy, or other thermosetting resin) by transfer or injection molding; and
3. the application of flowable materials (barrier coatings) to the assembly.

Which technique to use generally depends on the desired reliability during end-use operation. Certain military applications, for example, will demand expensive hermetically sealed packages, whereas an inexpensive calculator may make do with a simple “glob” of encapsulant on top of the chip.

Barrier coatings are often applied prior to total encapsulation in transfer-molded packages. The coating provides additional protection against moisture and gases and also provides relief from stresses that can develop during the subsequent transfer-molding operation. Figure 1.7 shows a device encapsulated by a silicone elastomer. Silicones are widely used for this purpose because they offer excellent protection against moisture and their hydrophobic nature limits water absorption. Room-temperature-vulcanizing (RTV) silicone rubber is a one-component cure system frequently used in such barrier-coating applications as shown in the hypothetical package in Figure

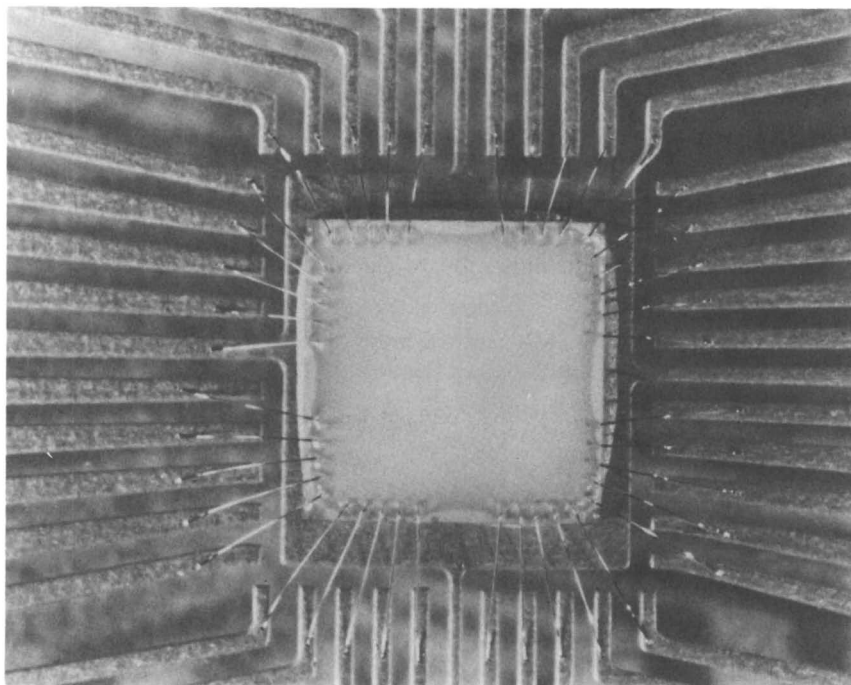


Figure 1.7. An encapsulated chip prior to transfer molding.

1.6. The RTV silicones contain methoxy groups substituted along the polysiloxane chain, which react with moisture to form silanol groups, which undergo self-condensation to form cross-links. Methanol is produced as a byproduct.

A barrier coating may also be required for protection against alpha particles. High-density devices can suffer soft errors when alpha particles emitted from trace quantities of thorium or uranium in packaging materials strike the active surface. Thus, the surface must be protected against this possibility. Polyimides are again recommended for such applications.

In many cases, the protection provided by a simple barrier coating such as RTV silicone will be sufficient to ensure long-term reliability of the device. Small, ceramic-based, hybrid ICs designed to be inserted into a PWB are often protected in this manner. However, for other applications, additional protection is required to provide impact and shock resistance (RTV silicones are very soft and offer little mechanical protection), better environmental protection, and a well-defined structure for subsequent assembly and handling. Such protection is provided by embedment in a hard plastic by transfer or injection molding as shown in Figure 1.6. The molding process leaves two parallel rows of pins exposed for subsequent connection to the PWB.

Choice of the transfer-molding compound is again dictated by the various environmental factors listed previously. The material should be of sufficiently low viscosity during mold filling to minimize stresses on the delicate wire bonds. The material should also completely fill the mold before gelling or setting to maximize the yield of encapsulated devices. Moreover, the cure cycle should be repeatable. The molding compound's expansion coefficient should match that of the lead frame to minimize stresses during thermal cycling, and it should exhibit low shrinkage on curing to further minimize stresses. The material should contain a very low level of ionic impurities that might diffuse to the device and cause circuit failure. In addition, many requirements are imposed by the need to ensure long-term protection. These requirements include high T_g , heat stability, fire retardancy, hydrolytic stability, low moisture/vapor diffusion, good dielectric properties, and high mechanical strength.

Epoxy polymers (including epoxy novolacs) have been designed to meet most of these requirements and are almost universally used in such encapsulant applications. Epoxy polymers exhibit superior adhesion that in many cases eliminates the need for a barrier or junction coating. They have a low coefficient of thermal expansion; low shrinkage; and low injection velocity, which means that low transfer or injection pressures can be used. These polymers also possess excellent mechanical properties coupled with low moisture and gas permeability. Above all, they are cheap and readily available. Other transfer-molding materials used to a limited extent include silicones, phenolic materials, and even polyesters. Most molding formulations are highly filled (70–75%) with materials such as quartz, fused silica, short

glass fibers, and other minerals. Such fillers minimize the thermal expansion mismatch between the transfer-molding compound and the chip substrate material, thereby reducing stresses on the chip and its delicate wire bonds. The existence of thermal stresses make it extremely difficult to transfer mold large ceramic packages such as hybrid integrated circuits (HICs). As mentioned previously, these devices are most often protected with a simple barrier coating such as RTV. Alternatively, they may be coated in a fluidized-bed process in which epoxy materials are again typically used.

The hypothetical package in Figure 1.6 is representative of the plastic dual in-line package (DIP) that has been the mainstay of the semiconductor industry for many years. Although not as reliable as the hermetically sealed ceramic package, it nevertheless offers a level of reliability sufficient for a wide variety of applications. The plastic DIP does, however, have a number of limitations. The increasing complexity of ICs, which is characterized in part by the large number of input-output leads required for many of today's state-of-the-art devices, has caused research efforts in IC packaging technology to be intensified. Here again, polymers play an integral role in the development of low-cost packaging methods. One of the most promising new technologies, for example, is tape automated bonding (TAB) (18). Supported by fully automated processing and assembly techniques, this approach involves patterning of cantilevered metallic leads on a continuous polyimide film in reel format (Figure 1.8). All of the leads are bonded simultaneously to the chip at contact bumps located around the periphery of the active chip surface. After testing, an epoxy encapsulant is deposited on the chip to create a miniature, surface-mountable chip packaged on tape. The method is reported to offer reliability equal to that of DIP packaging. The choice of polyimides as the base film reflects the chemical stability and heat stability of these polymers as required during subsequent circuit board mounting.

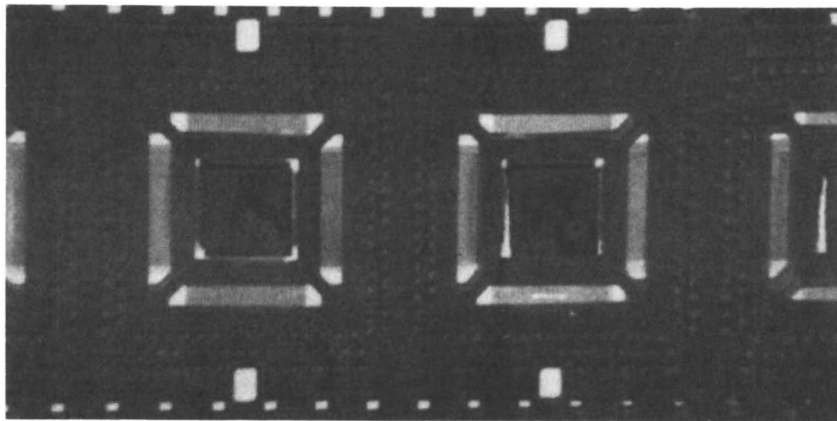


Figure 1.8. TAB packaged chips.

1.1.1.3 PRINTED WIRING BOARDS

The PWB (also called printed circuit board) is the mounting platform for all of the electronic components such as packaged ICs, HICs, and resistors. It provides a rigid mechanical support for the various components as well as a convenient means for interconnecting the components via thin conducting lines that have been "printed" on the board. The modern PWB dates back to the mid-1950s, when it was introduced by RCA. These original boards were based on copper-clad, epoxy, glass-reinforced laminates on which the conductor pattern was defined in a screen-printing process and the copper etched away with ferric chloride.

Over the years, several refinements to this process have been introduced, but the essentials have changed very little. PWBs are ubiquitous, being found in applications ranging from consumer electronics to military hardware. Again, their widespread use provides motivation for developing a cheap, reliable substrate for which polymers are eminently suitable. Polymers possess good dielectric characteristics and can be designed with acceptable mechanical and thermal properties as well. Thermosetting epoxy resins, typically containing a reinforcing material such as chopped or woven glass, are by far the most commonly encountered substrate material. The widely used FR-4 laminated PWB, for example, consists of a brominated epoxy resin reinforced with glass cloth. Other substrate materials include phenolic materials, epoxy novolacs, polyesters, polyimides, and bismaleimides. Polyimides and bismaleimides are mainly used in military applications, where continuous high-temperature performance is required. Polyimides are also used as substrates in flexible circuitry applications. Such circuits are used to provide interconnection between rigid boards, as well as in space-saving specialty applications such as cameras and telephones (Figure 1.9). Other substrate materials considered for flexible circuitry include polyesters, fluorocarbons, and epoxy-glass composites.

The manufacture of a PWB begins with coating the woven reinforcement with the resin. This coating is done in a continuous operation (Figure 1.10), in which glass cloth, for example, is fed through the resin bath and then passed through a curing oven where the epoxy material is partially cured in a process referred to as B staging to produce what is called a *prepreg*. The prepreg is then cut to the desired size, several layers are stacked together, and copper foil (typically 36 μm thick) is placed on both sides to produce a laminated lay-up. This laminate assembly is then cured in a press at elevated temperature ($\sim 350^\circ\text{F}$) and pressure to produce a fully cured laminate. The clad laminates come in almost any thickness but are most commonly 1.5 mm thick.

The next step in the process is to create the intricate interconnection patterns on one or both sides of the board. To create patterns on both sides of the board, holes must first be drilled through the board through which the electronic components (e.g., the leads of the plastic DIP), will eventually

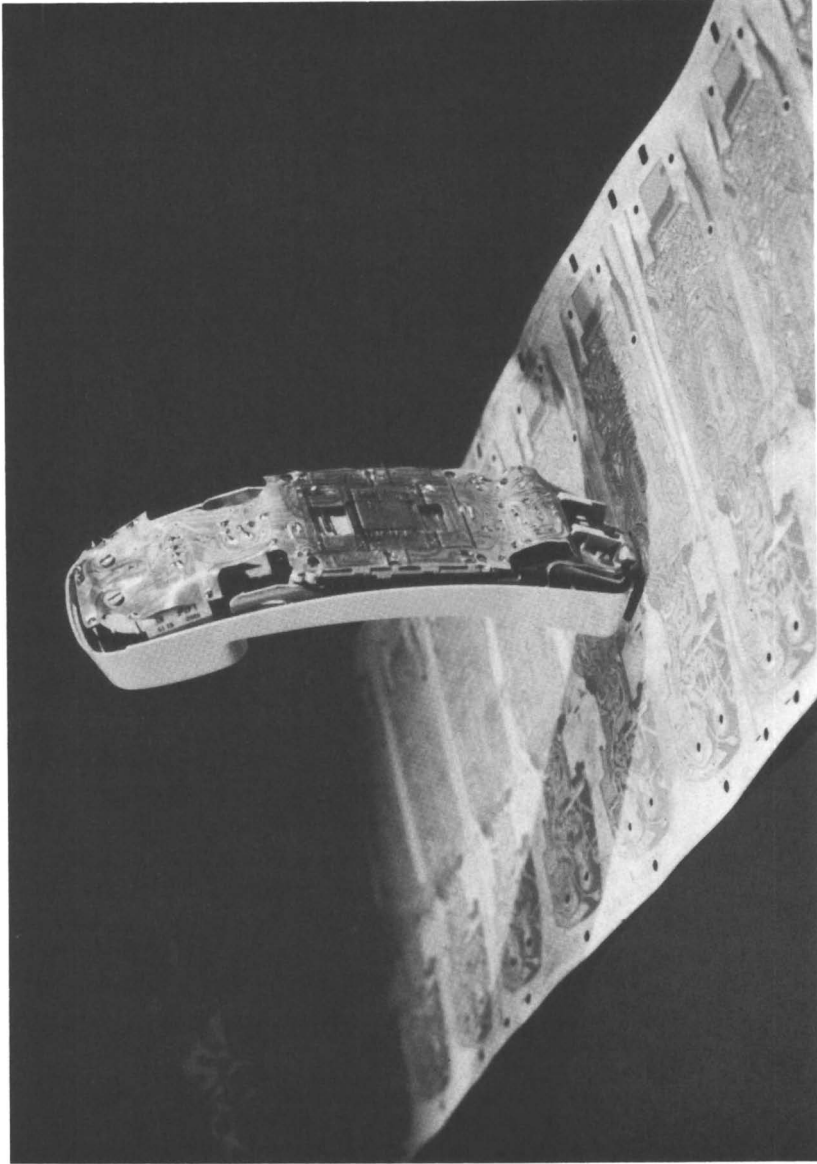


Figure 1.9. Application of flexible circuitry in a telephone handset.

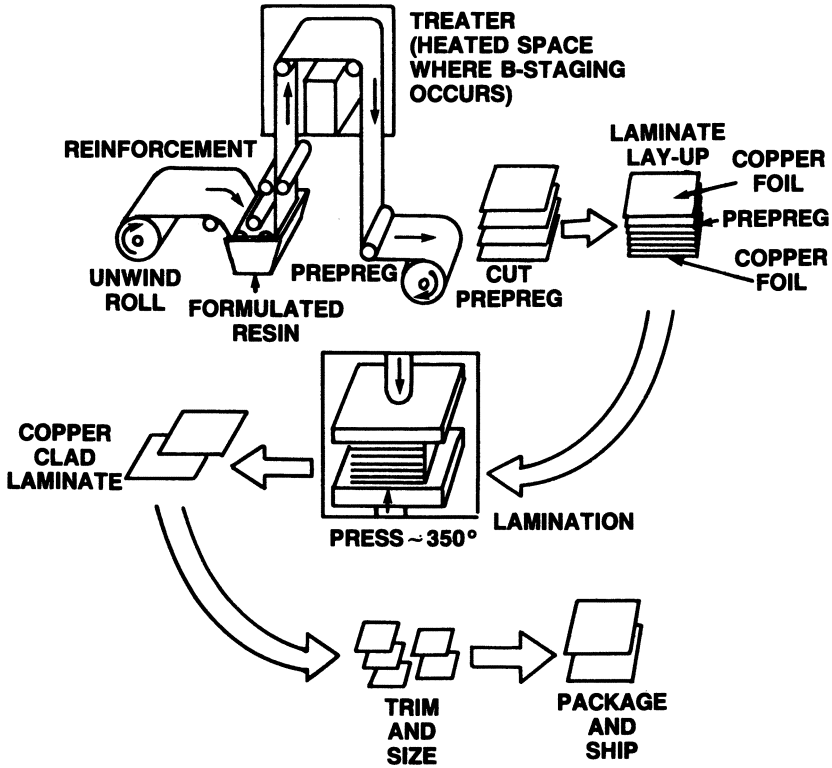


Figure 1.10. Prepreg process in the manufacture of PWBs.

be inserted. The conductor paths are then defined lithographically. The original screen printing process described previously can resolve 10-mil features, but such feature sizes are insufficient for many of today's circuit boards. A new technology based on a dry-film photoresist (19) was introduced in the late 1960s and is now used to fabricate most of the high-density circuit boards for computer, telecommunication, and aerospace applications.

A dry-film photoresist has a three-layer structure consisting of a clear strong polyester support film, a photopolymerizable resist layer, and a polyolefin separator sheet (Figure 1.11). The polyester film is similar to that used as the base for many photographic films and is only about 25 μm thick. The middle layer is the photopolymer resist that has been coated on the polyester film by the dry-film manufacturer. This layer, which ranges in thickness from 17 to 100 μm depending on the intended application, consists principally of a polymeric binder, a monomer, and photoinitiator. The binder consists of a tough film-forming material such as a methacrylate polymer. The resist is applied to the copper-clad laminated substrate in a lamination process and then exposed through a photographic mask outlining the circuit pattern. Processing is similar to that discussed earlier in Section 1.1.1.1.

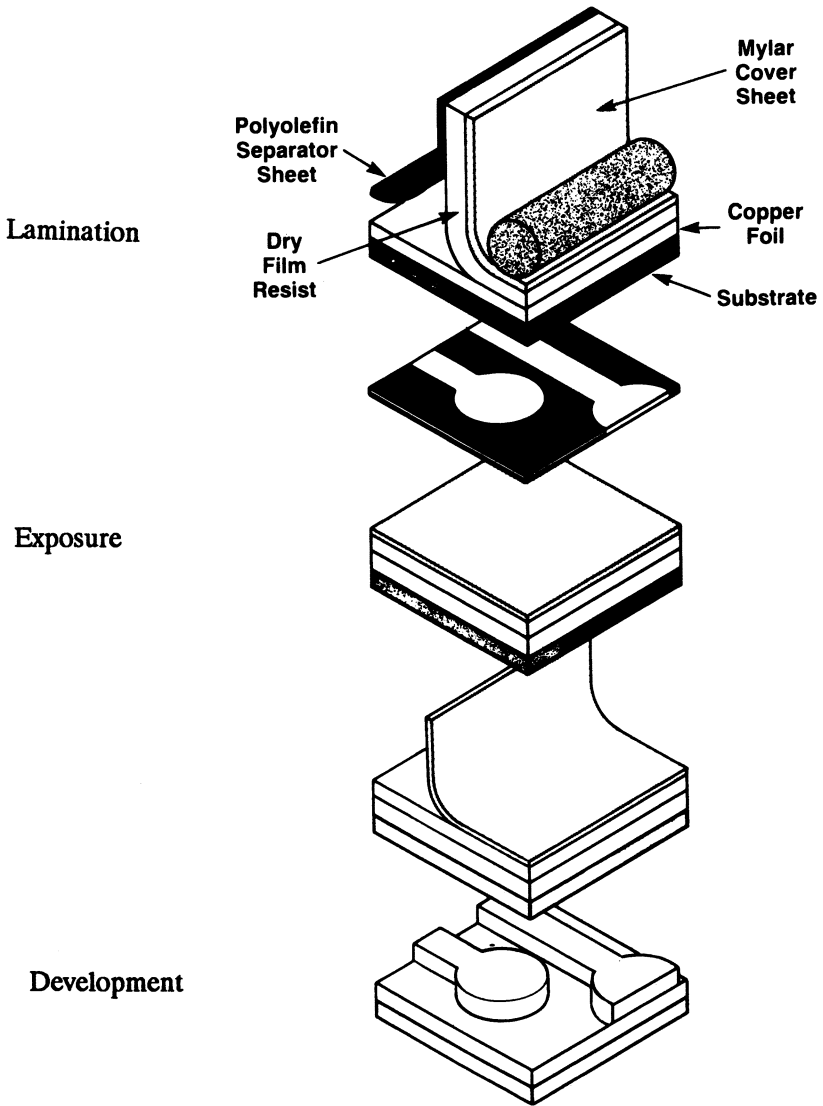


Figure 1.11. Dry-film photoresist process.

Exposure to UV light polymerizes the monomer to a cross-linked matrix and enables a negative image of the mask to be formed by solvent development.

Several techniques can be used to produce the actual conductor paths on the PWB substrate. These techniques are depicted in Figure 1.12. Subtractive processing starts with a PWB coated on one or both sides with copper foil ranging in thickness between 5 and 70 μm . In the case of double-sided PWBs containing plated-through holes, the holes are first drilled and

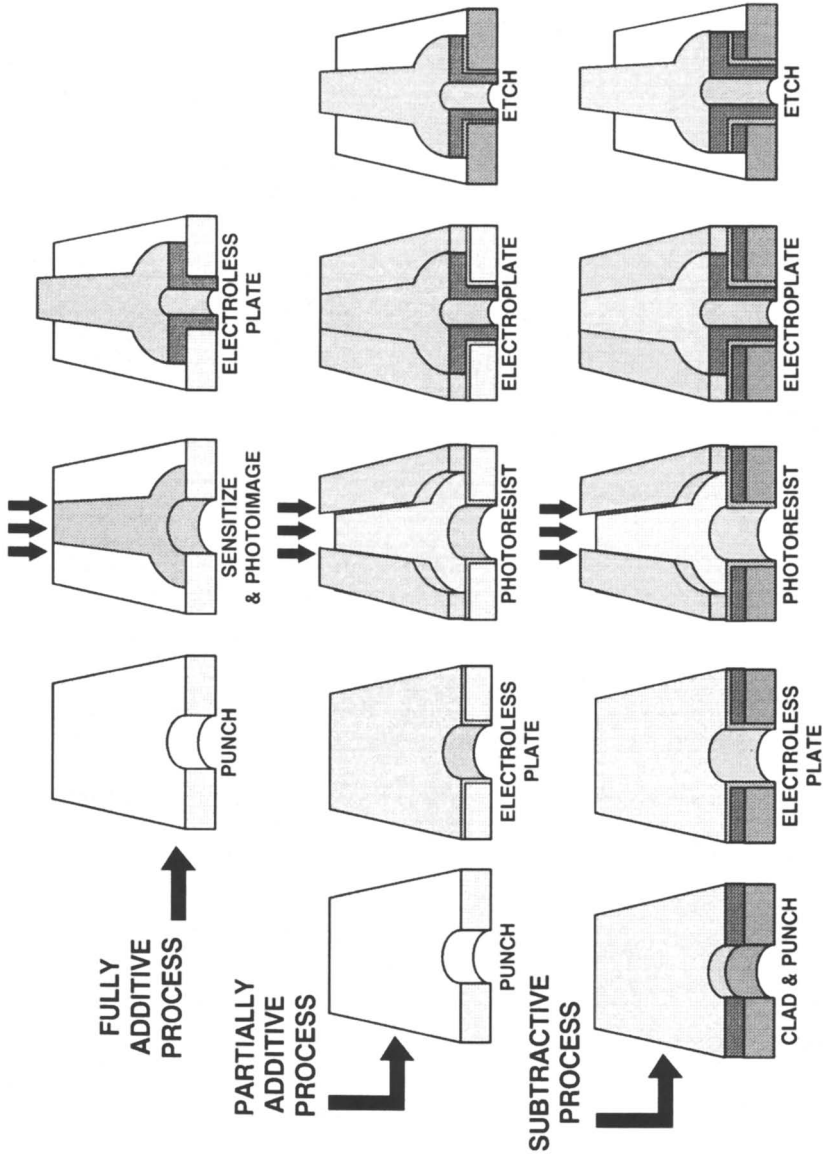


Figure 1.12. Techniques for defining conductor paths on PWBs.

copper is deposited in the drilled hole by electroless plating, which is a process that deposits copper on all surfaces including the inner surface of the nonconducting hole. Next, the copper thickness is built up by electroplating to the requisite thickness within the hole. At this point, the dry-film resist is applied, imaged, developed, and the exposed copper is etched away. The plated-through holes are protected by the resist during the etching process.

Other variations of this theme include partially additive and fully additive processing. In partially additive processing, an unclad circuit board is punched (to form the holes), and a thin layer of electroless copper is deposited on all surfaces. The substrate is then imaged lithographically, and the exposed copper surface is plated to the desired thickness. The final step involves removal of the thin flash coat of copper from the protected areas; this process also removes a similar thickness from the plated-up areas. The fully additive process also starts with an unclad board to which an adhesion promoter and activator (usually a Pd salt) is applied on the surface. The resist is applied, imaged, and patterned, thereby exposing the activated surface upon which copper is plated in an electroless process. The advantages of this process include depositing copper only where it is required as opposed to subtractive etching, where 80% of the copper is discarded.

Printed circuitry today is at the crossroads. The density of components on the PWB continues to increase and is accompanied by shrinkage of the dimensions of the conductor paths on the surface of the board. Furthermore, the PWBs frequently contain several layers of metalization. There is a marked trend toward surface-mounted devices, which are increasing in complexity and generating more heat. These trends are creating a demand for boards that exhibit better thermal properties, higher density (resolution), and lower thermal expansion coefficients (facilitating direct mounting of ICs on the board). Polymers will play an important part in this continuing evolution. Already, considerable interest has been generated in directly molded circuit boards (20), which use the newer high-temperature resins such as polyether imides, polysulfones, polyether ether ketones (PEEK), and polyphenylene sulfide reinforced with chopped glass fibers. Direct molding offers the advantage that features such as spaces, stand-offs, and brackets can be directly fabricated. Holes can be molded rather than punched, and boards can be molded to suit specific styling requirements. The liquid crystalline polyesters, such as poly(hydroxybenzoic acid) and various derivatives and modifications thereof, hold promise for future applications, particularly for specialized uses. These materials are characterized by very high modulus and temperature stability, low thermal expansion coefficients, and high resistance to chemicals. Such specialty materials are very expensive at the moment, and the humble epoxy laminate may well remain the mainstay of the industry for many years to come.

One final area that is having a significant impact on PWB technology

is that of high-speed electronics (21). Silicon and GaAs technologies are driving device speeds into the gigahertz frequency range with rise times in the order of fractions of a nanosecond. At such signal frequencies, electrical energy no longer resides as voltage and current within the conductors. Energy flows as electromagnetic waves outside of and between conductors, whose propagation velocity is determined by the dielectric constant of the surrounding material. Generally speaking, the higher the dielectric constant, the greater the penalty in terms of propagation delay. For most PWBs, the polymeric substrate has a dielectric constant from 3 to 5, which translates into a speed penalty of 50% for most PWBs and flexible circuits. Another factor that must be taken into consideration is control of the physical dimensions of the conductors and spacing between conductors, which determines impedance and cross-talk characteristics. These requirements will place increasingly stringent demands on the lithography and on the materials components of the PWB itself. Poly(tetrafluoroethylene) and its derivatives, for example, are being used as PWB substrate materials because of the lower dielectric constant (ϵ) of these polymers compared with epoxy materials and polyimides (21). With ϵ values of 2.2–2.8, propagation delays are reduced by as much as 30% compared with the woven-glass, fabric-reinforced epoxy and polyimide materials, and by as much as 10% over the newer polyimide laminates reinforced with quartz or poly(*p*-phenylene terephthalamide) (Kevlar) fabric.

1.1.2 Conducting Polymers

Electrical conductivity refers to the transport of charge carriers through a medium under the influence of an electric field or temperature gradient and is thus dependent on the number of charge carriers and their mobility. The charge carriers may be generated intrinsically or from impurities, in which case they may be electrons, holes, or ions. Alternatively, electrons or holes may be injected from electrodes. Conduction may therefore be of two types—ionic and electronic—both of which have been the focus of intense research, particularly ionic conduction, which has been studied for many years and has been the subject of several books. Advantage is taken of ionic conduction in certain polymers, for example, in the design of polymeric electrolytes for solid-state batteries. Poly(ethylene oxide) has been extensively studied in this regard. Electronic conduction in polymers, on the other hand, is a relatively new phenomenon, having been discovered only about 10 years ago and is the subject of this section.

In general, polymers are insulating materials having conductivities ranging from $10^{-10} (\Omega \text{ cm})^{-1}$ for poly(vinyl chloride) to $10^{-18} (\Omega \text{ cm})^{-1}$ for poly(tetrafluoroethylene), which are many orders of magnitude below the conductivities associated with metals (Figure 1.13). Indeed, low conductivity (and consequent low dielectric constant) is one of the major reasons polymers have found widespread acceptance in a myriad of insulating and structural

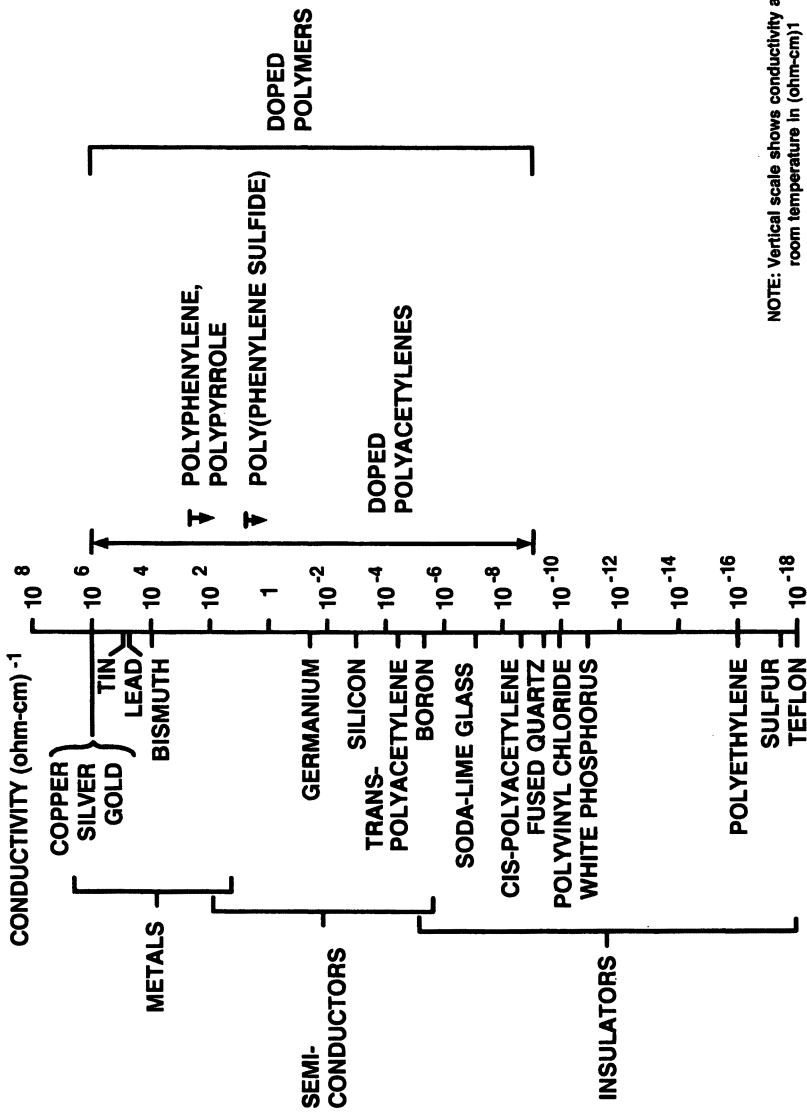


Figure 1.13. Conductivity of various metallic, semiconductor, and insulating materials.

applications throughout the electronics industry. Nevertheless, the discovery in 1973 (22) that poly(sulfur nitride) (SN)_x was intrinsically conducting provided proof that polymers could be conducting and greatly stimulated the search for other conducting polymers.

1.1.2.1 BAND THEORY OF SOLIDS

To provide a framework for discussing conduction in polymers and why polymers are normally classified as insulators, some of the basic ideas of band theory in solids should be reviewed. Cowan and Wlygul (23), in their review of the organic solid state, discussed this topic from the organic viewpoint and provided a useful framework within which chemists can appreciate the salient features of the theory.

When a large number of atoms (e.g., as in metals or semiconductors) or molecules (e.g., organic metals) are brought together in the crystalline state, the electronic states mix so as to form bands, each band consisting of electronic states whose energies form a continuous range. This situation is analogous to the splitting of atomic energy levels as two atoms are brought together to form a molecule. For example, the ethylene molecule consists of two *sp*²-hybridized carbon atoms, each containing an unpaired electron in a *p* orbital; the two orbitals overlap to form a π bond. According to Hückel theory, the interaction of these two *p* orbitals forms two molecular orbitals corresponding to the π bonding and π antibonding orbitals (Figure 1.14), separated by an energy Δ . If these orbitals are allowed to interact with the π and π^* orbitals of a second ethylene molecule stacked directly above the first, two sets of two molecular orbitals are formed that are separated by energy 2δ , where δ is the resonance or transfer integral. Likewise, if *n* ethylene molecules are allowed to interact, *n* states from each of the π and π^* orbitals are formed. For large values of *n*, the energy states are close enough together to correspond to a continuous band. The $2n$ electrons are then allowed to fill the bands in a manner analogous to the Aufbau principle for atoms (i.e., electrons are placed in these states in pairs starting with the lowest energy state and filling the higher energy states successively). The highest occupied state is called the Fermi level.

As seen in Figure 1.14, the band formed from the highest occupied molecular orbital (HOMO) in the stack of ethylene molecules is entirely full, but the band formed from the lowest unoccupied molecular orbital (LUMO) is entirely empty. According to band theory, if the highest filled band (referred to as the valence band) is only partially full, the empty states which exist close to the Fermi level will facilitate conduction. In the case of the hypothetical stack of ethylene molecules, the HOMO band is completely full. For the stack to be conductive, energy must be supplied (either thermally or photolytically) to move an electron into the next lowest state, which in this case happens to be the lowest energy level in the LUMO band (also called the conduction band). This energy gap separating the two bands is

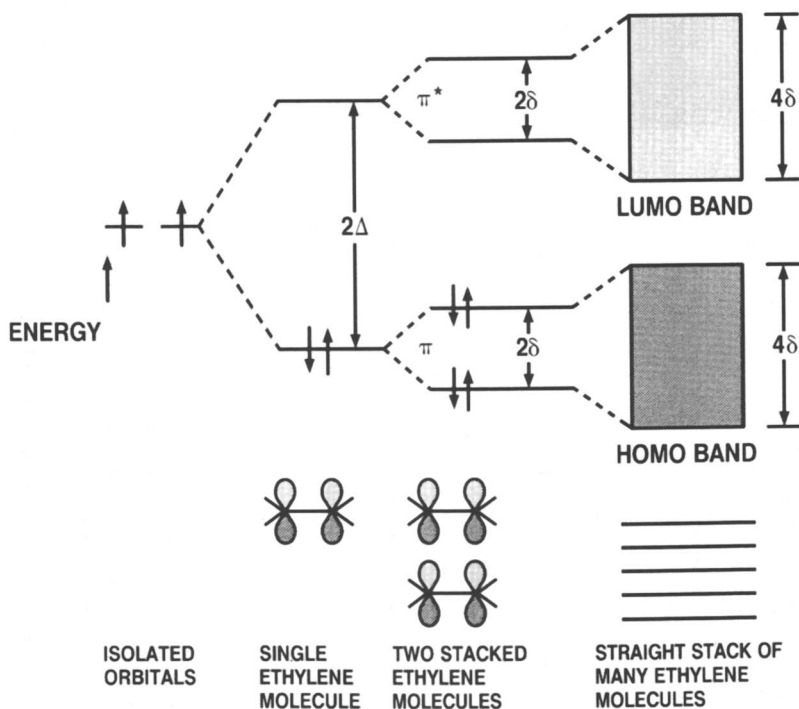


Figure 1.14. Band formation obtained by mixing of electronic states. (Reproduced from reference 23. Copyright 1986 American Chemical Society.)

called the band-gap energy, and its magnitude determines whether such a material is a semiconductor or an insulator (Figure 1.15).

The intrinsic conducting properties of $(SN)_x$ derive from the presence of one unpaired electron for each S–N unit. As a result, the highest occupied electronic levels (i.e., the valence band) are only half-occupied. Because no forbidden gap exists between the highest occupied and lowest unoccupied levels (both exist within the HOMO band), the unpaired electrons can readily move under the application of an electric field and give rise to metalliclike conductivity.

Unlike $(SN)_x$, most polymers correspond to closed-shell systems where all the electrons are paired. Such a configuration leads to insulating or semiconducting properties as noted previously. Polyacetylenes and related conjugated polymers, for example, have conductivities that classify them as semiconductors. The carbon atom in polyacetylene is sp^2 hybridized, which leaves one p electron out of the bond-forming hybrid orbitals. In principle, such a structure might be expected to give rise to extended electronic states formed by overlap of the p (π) electrons and thus provide a basis for metallic behavior in polymers.

In practice, the quasi-one-dimensional structure just described is not

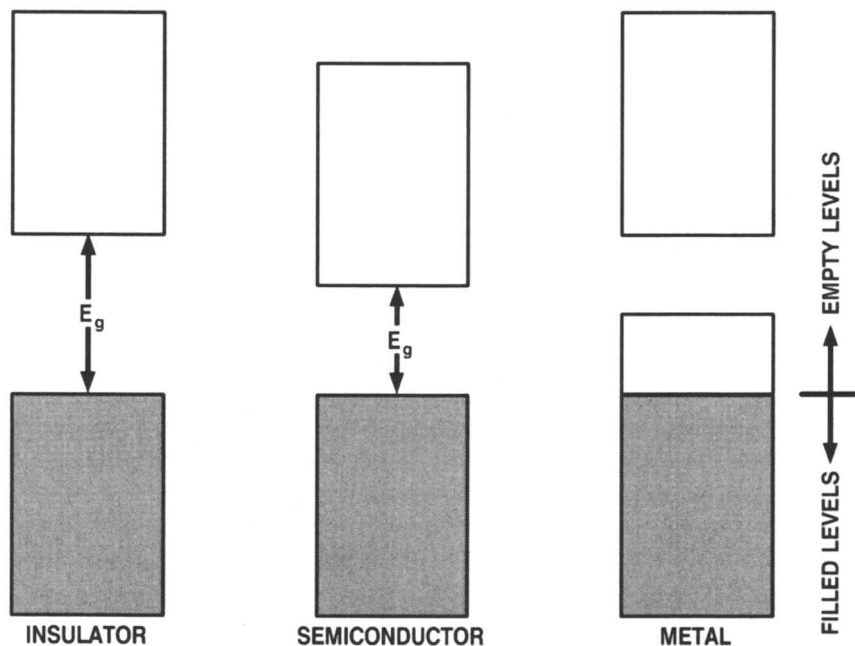


Figure 1.15. The allowed energy states for an insulator, semiconductor, and metal. Blackened regions represent regions filled with electrons. E_g is the energy gap between filled and empty states. (Reproduced from reference 23. Copyright 1986 American Chemical Society.)

stable. Instead, the π electrons overlap in an alternating fashion, resulting in the familiar conjugated π -bond structure of polyacetylene. In energetic terms, bond alternation causes a gap (E_g) to be opened at the Fermi level that converts the system from a conductor to a semiconductor (Figure 1.16). Physicists refer to this as a *Pierls transition*.

A major breakthrough in the search for conducting polymers occurred in 1977 (24) with the discovery that polyacetylene could be readily oxidized (by electron acceptors such as iodine or arsenic pentafluoride) or reduced (by donors such as lithium). The resulting material had a conductivity that was orders of magnitude greater than the original, untreated sample. This process is often referred to as *doping* by analogy with the doping of inorganic semiconductors, but it contrasts with the inorganic semiconductor doping in that doping in polymers is a redox process involving charge transfer with subsequent creation of charged species. The redox reaction may be carried out in the vapor phase, in solution, or electrochemically.

1.1.2.2 CONDUCTION MECHANISMS

Since the first report of metallic conductivity in doped polyacetylene, a number of other conjugated polymers have been shown to possess high

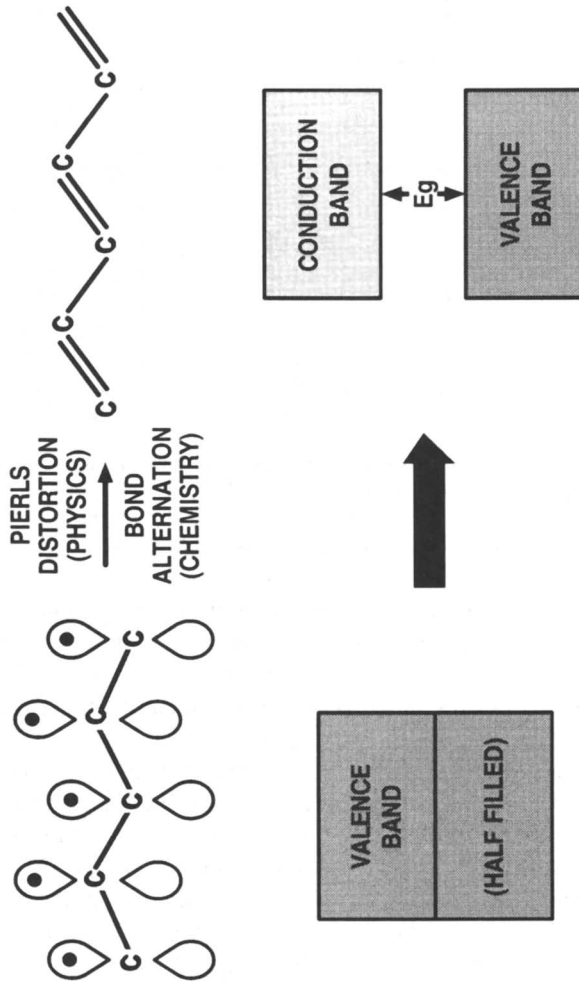


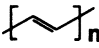
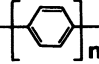
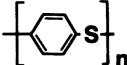
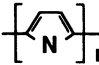
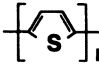
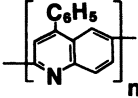
Figure 1.16. Splitting of the valence band caused by overlap of p electrons to form the alternating double bond sequence of polyacetylene.

conductivity. The structures of the principal conducting polymer systems are shown in Table 1.2. The maximum dopant concentrations are on the order of several mole percent, which is considerably higher than required for the inorganic semiconductors.

The origin of the conduction mechanism has been a source of controversy ever since conducting polymers were first discovered. At first, doping was assumed to simply remove electrons from the top of the valence band (oxidation) or add electrons to the bottom of the conduction band (reduction). This model associates charge carriers with free spins (unpaired electrons). However, the measured conductivity in doped polyacetylene (and other conducting polymers such as polyphenylene and polypyrrole) is far greater than what can be accounted for on the basis of free spin alone.

To account for this phenomenon of spinless conductivity, physicists have introduced the concept of transport via structural defects in the polymer chain. In a conventional semiconductor, an electron can be removed from the valence band and placed in the conduction band, and the structure can be assumed to remain rigid. In contrast, an electronic excitation in polymeric materials is accompanied by a distortion or relaxation of the lattice around the excitation, which minimizes the local lattice strain energy. The combined

Table 1.2. Structures and Conductivity of Doped Conjugated Polymers

<i>Polymer</i>	<i>Structure</i>	<i>Typical Methods of Doping</i>	<i>Typical Conductivity ($\Omega \text{ cm}$)⁻¹</i>
Polyacetylene		Electrochemical, chemical (AsF ₅ , I ₂ , Li, K)	500–1.5 × 10 ⁵
Polyphenylene		Chemical (AsF ₅ , Li, K)	500
Poly(phenylene sulfide)		Chemical (AsF ₅)	1
Polypyrrole		Electrochemical	600
Polythiophene		Electrochemical	100
Poly(phenyl-quinoline)		Electrochemical, chemical (sodium naphthalide)	50

structural and electronic excitation will now look like a defect on the chain. From a chemical viewpoint, this defect is interpreted as a radical cation (or radical anion in the case of reduction). Physicists refer to it as a *polaron*. Because these defects represent localized distortions of the lattice, the associated energy level must be split off from the continuum of band states (Figure 1.17a). The two polaron states corresponding to a radical cation and radical anion are symmetrically disposed around the Fermi level (i.e., the midpoint of the gap). Removal of an electron leaves an unpaired spin near the valence band edge (*p* doping), and addition of an electron fills the corresponding state near the conduction band edge (*n* doping). These energy levels are depicted in Figure 1.17b.

Further oxidation (or reduction) results in the formation of what physicists call a *bipolaron*. In the oxidation case, it is energetically much more favorable to take the second electron from the polaron than to form a second polaron (25); thus, the oxidation process may be viewed as leading to the formation of a localized doubly charged species (i.e., a dication, or dianion in the case of reduction). The bipolaron is thus identified as a dication or dianion associated with a strong local lattice distortion. Because the lattice relaxation around the charges is stronger than in the case of a single charge, the electronic states appearing in the band edge are further away from the band edges (closer to the Fermi level) than they are for polarons (Figure 1.17c). Coulombic repulsion might be expected to result in charge separation, but as will be seen, separation is only feasible if the polymer possesses a degenerate ground state. In polypyrrole, for example, the charges associated with the bipolaron are separated, but only over about four pyrrole units.

As seen in Figure 1.17c, bipolarons contain no free spins. All energy levels in the gap are either empty or full. These species are believed to be involved in the conduction process, thereby accounting for the observed "spinless" conductivity. Evidence for their existence comes from spectroscopic studies, although the precise mechanism of charge conduction is not really known. For one thing, the charges should be fixed in position along the chain by the counterion derived from the dopant species. Furthermore, polymers themselves contain many defects such as cross-links, chain ends, and bends, and it is difficult to see how even a mobile bipolaron or polaron could move past such obstacles.

Conduction mechanisms have been proposed, at least in the case of polyacetylene itself, that involve a different type of defect structure called a *soliton*. *trans*-Polyacetylene is unique among conducting polymers in that it possesses a degenerate ground state corresponding to the two geometric forms shown in Figure 1.18. As a consequence, the two charges associated with the bipolaron can easily separate and become independent, charged species. No associated energy penalty occurs because the geometric structure appearing between the two charges has the same energy as the configuration

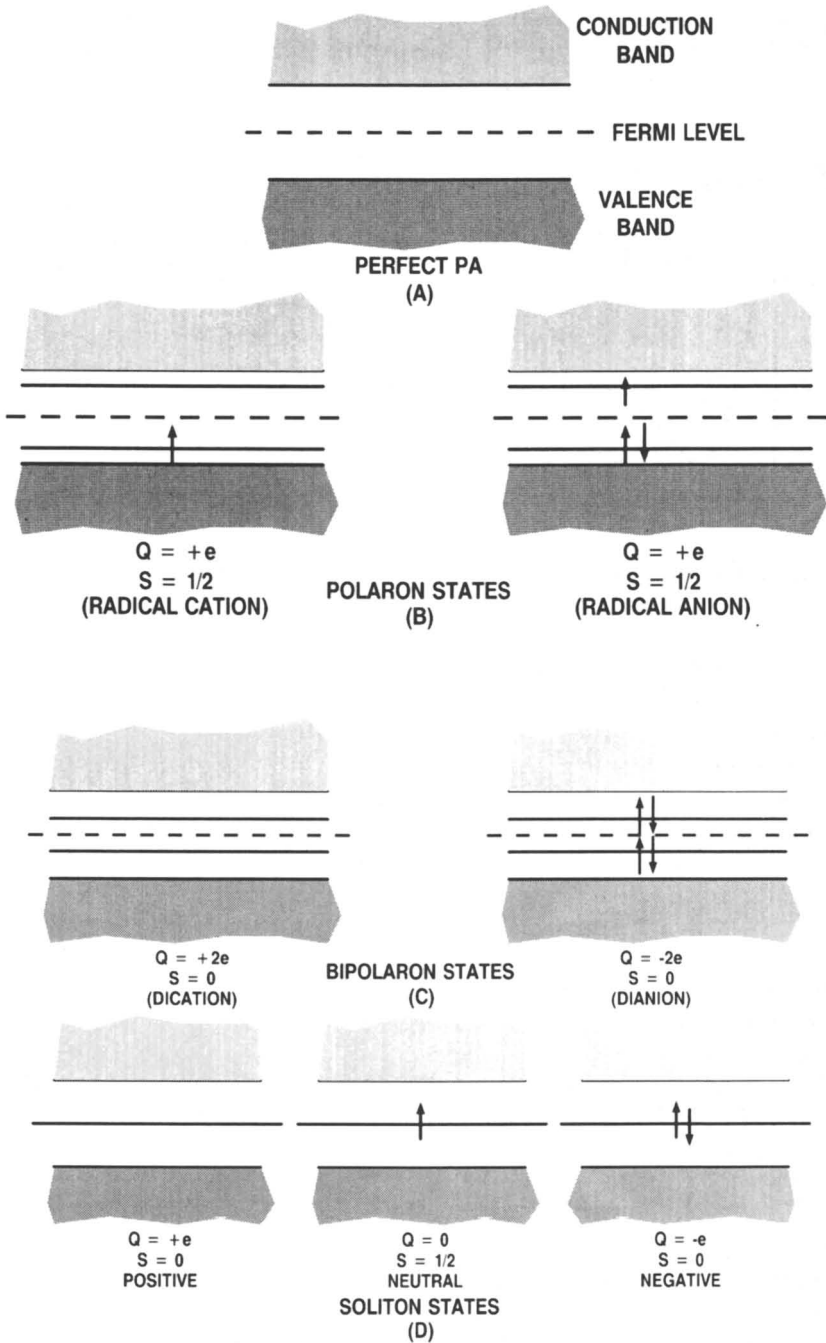


Figure 1.17. Electronic energy levels associated with various types of defect structures found in doped polyacetylene.

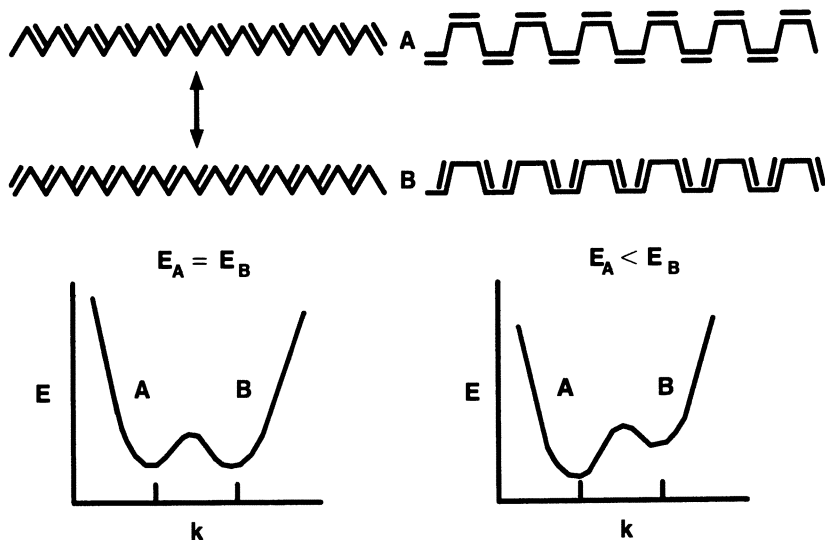


Figure 1.18. Energy diagram for ground-state geometric isomers of polyacetylene.

on the other side of the charge. On the contrary, the two geometric isomers of *cis*-polyacetylene or polypyrrole are not energetically equivalent. In polypyrrole, the quinoidlike geometric isomer has a higher total energy than the aromatic (ground state) structure; hence, charge separation of the bipolaron is not favored. The fact that limited charge separation does occur to the extent of about four pyrrole units is attributed to the larger electron affinity of the quinoid structure relative to that of the aromatic structure. Maximum stabilization of the dication occurs at a separation of about four units.

Similar defect structures may be envisioned as arising during isomerization of *cis*-polyacetylene to *trans*-polyacetylene. If two *trans* sequences with opposite bond alternation approach each other along a chain containing an odd number of conjugated carbon atoms, an unpaired electron (radical) will be left at the point where the two sequences meet. This defect, which chemists call a free radical, is similar to the solitary charged defect produced by separation of a bipolaron, except that it is neutral.

Physicists call this type of defect a soliton, which is defined as a phase-boundary defect linking two energetically equivalent configurations. The electronic energy level associated with the soliton in *trans*-polyacetylene is located in the middle of the gap because the phase boundary effectively represents a single nonbonding p orbital that has the energy (E) of the local atomic orbital, defined to be at $E = 0$. The soliton can exist in any of three spin-charge configurations (Figure 1.17d): neutral ($S = \frac{1}{2}$), negatively charged ($S = 0$), or positively charged ($S = 0$). Neutral solitons are believed

to be the origin of the free spins (~ 1 per 4000 carbon atoms) formed during thermal isomerization of *cis*-polyacetylene to the *trans* isomer.

The diagrammatic representation of the soliton depicts the defect as being centered on a single carbon atom. Spin density measurements indicate, however, that the spin is not localized on a single carbon atom but is spread over several (~ 15) carbon atoms. Likewise, the charge density associated with charged solitons is spread over a similar number of carbon atoms.

The picture that emerges is that at low doping levels, charged solitons are formed, either directly from neutral solitons or by recombination of polarons to form bipolarons, which then move apart to become individually charged solitons. But the question of the mechanism of actual charge transport still remains. Central to many of the proposed theories is the assumption that the soliton can move freely along the chain. One proposed mechanism, due to Kivelson (26), is depicted in Figure 1.19. A neutral soliton moving

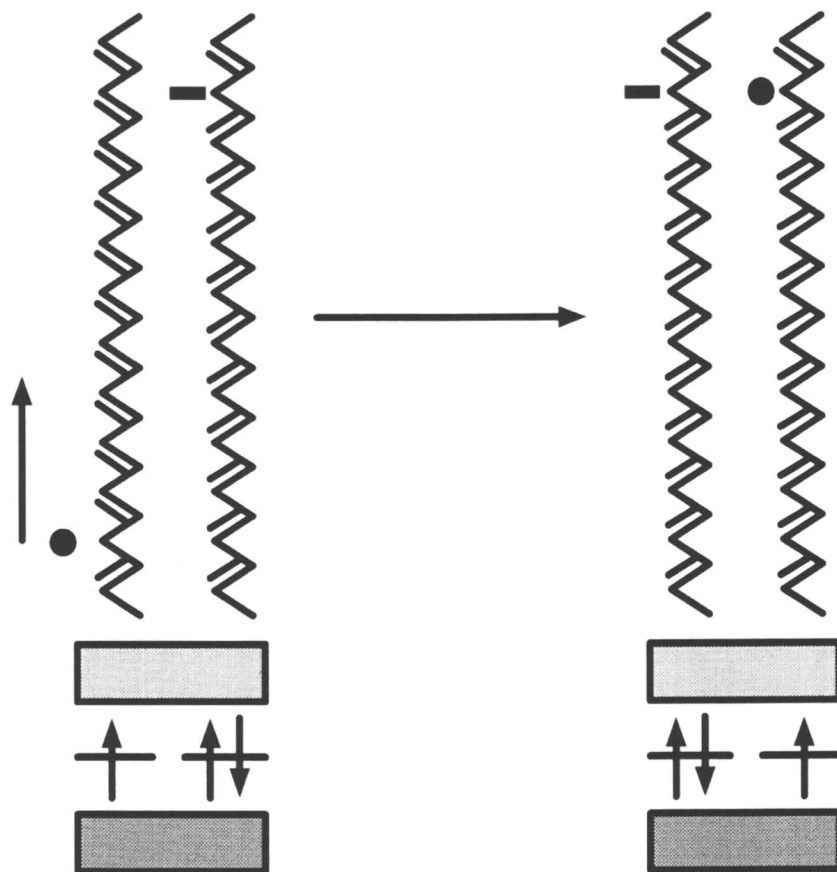


Figure 1.19. Kivelson mechanism for charge transport involving mobile neutral solitons.

along the polymer chain encounters a charged soliton, which is spatially pinned by its counterion. Transfer of an electron results in the appearance of the soliton on the neighboring chain. The mechanism thus purports to account for both interchain and intrachain conduction and predicts that the conductivity should vary with the number of free spins. However, recent experiments (27) on specially prepared polyacetylenes, in which the spin concentration was deliberately varied, have cast doubt on such theories. These studies indicate that conductivity does not vary with spin concentration in the manner predicted by the Kivelson theory. Additional studies based on techniques such as electron nuclear double resonance (ENDOR) (28) and electron spin-echo multiple quantum nuclear magnetic resonance (ESEMQR) (29), which probe the local environment of the soliton, indicate that the soliton does not move (i.e., it is static). Much work remains to be done to unravel the transport mechanism responsible for conduction in these systems.

1.1.2.3 COMMERCIAL APPLICATIONS

Conducting polymers appear to be on the brink of commercial exploitation. Progress in commercialization has been hampered by poor stability (polyacetylene, for example, is rapidly oxidized in air and thus loses conductivity) and by poor processability. Many of the materials are intractable and therefore are not amenable to easy fabrication. Nevertheless, work has continued on developing a new generation of stable, processable conducting polymers. Naarmann and coworkers (30) at BASF modified the standard method for polymerizing acetylene, and the result was a material with a higher degree of crystallinity and consequent greater thermal stability than polyacetylene prepared by the older technique. Perhaps more importantly though, the new material reportedly exhibits conductivity that, on a weight basis, is twice that of copper. Although the BASF material is highly conducting and much more stable than earlier films, it is still a highly intractable polymer and thus not processable. The Feast technique (31) for preparing polyacetylene involves formation of a soluble precursor via ring-opening metathesis. The precursor can be processed (e.g., stretched to orient the chains) and then thermally converted to polyacetylene. Doped polypyrrole can be produced in a continuous process to give films that appear to be relatively stable. The conductivity of these materials is higher than that of plastics extended with conductive fillers. This characteristic suggests possible application as an electromagnetic interference shield.

A major goal of the research on conducting polymers has been the development of a rechargeable plastic battery. Cells based on polypyrrole and lithium electrodes have been developed in which the energy per unit mass and discharge characteristics are comparable to nickel-cadmium cells. Current interest appears to center around stable, processable polymers, such as polythiophene and its derivatives, and polyaniline.

1.1.3 Polymers for Molecular Electronics

One of the buzz words in the world of science today is the term “molecular electronics”. One has only to open the pages of the popular scientific literature to find such headlines as “And Now—the Biochip”, or “The Organic Computer”. The premise behind these articles is the idea that a single molecule might function as a self-contained electronic device; thus, the possibility arises to develop a computer based on molecular-sized electronic elements. This possibility was first discussed by Carter in 1979 and was the subject of two international workshops in 1981 and 1983 (32). The genesis of these ideas may be seen in the relentless progress of the semiconducting industry in diminishing the size of circuit features of microelectronic devices. Circuit densities have doubled virtually every year since the invention of the IC in 1960, primarily through shrinking the size of the individual circuit elements. Minimum feature sizes in today’s devices are on the order of $1\ \mu\text{m}$, and $0.5\text{-}\mu\text{m}$ -sized devices are likely by the early 1990s. A simple linear extrapolation of the feature size vs. time plot (Figure 1.20) leads to the conclusion that within 30 years or so, the size of electronic components will be on the order of nanometers (i.e., the size of individual molecules).

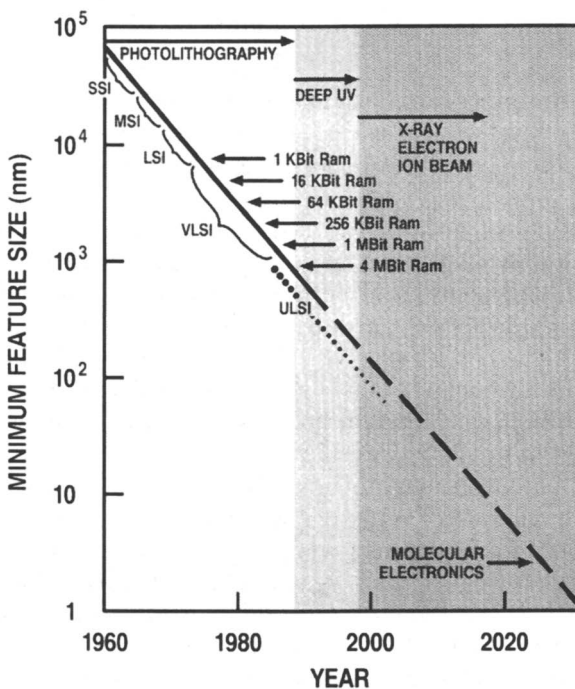


Figure 1.20. Microlithographic trends in minimum device feature size and imaging technology. The figure illustrates the time evolution of random access memory (RAM) devices.

1.1.3.1 DEVICE FABRICATION CONSIDERATIONS

Current IC fabrication technology, which involves sculpturing microstructures from single crystalline blocks of silicon, is not likely to fabricate devices at molecular dimensions. Molecular electronics, on the other hand, offers the possibility of building up complex structures by using atomic and molecular forces. Devices will be constructed by assembly of individual molecular electronic components into arrays, thereby engineering from small to large rather than from large to small as do current lithographic techniques.

At our current level of technology, many of these concepts are still in the realm of science fiction. Ideas have been suggested for devices such as molecular switches, but these devices still await experimental realization and verification. A molecular switch, for example, must possess a variety of properties for it to be classified as operational (33):

- It must possess bistability (i.e., capable of existing in two or more stable states).
- The switching process must be controllable (i.e., it must be possible to unambiguously set the state of the switch).
- The state of the switch must be readable (i.e., it must be possible to unambiguously sense whether the switch is on or off).
- The two preceding functions must be executable at the molecular level with full addressability. That is, it must be possible to selectively switch or address an individual molecule.

Thus, whereas many systems have been suggested that exhibit optical bistability, they have yet to be fabricated into an operational switch.

The same argument could be made for design of molecular interconnects. Proposals have been made for molecular "wires" constructed from conducting polymers. But how would one isolate an individual molecular strand, much less attach it to a molecular switch? Would such a one-dimensional wire exhibit conduction properties akin to bulk conduction? These questions have yet to be answered.

In addition, the subject of assembly looms as an apparently insurmountable obstacle. It is not at all clear how researchers would go about assembling individual molecular components into a functioning device, although bioengineering offers a potential solution to this problem. Examples of self-assembled structures exist everywhere in nature from the helical secondary structure of DNA to the human brain. Current knowledge of such systems is simply inadequate to allow scientists to employ similar forces to create synthetic molecular electronic devices. Clearly, an enormous amount of groundwork needs to be laid if the concept of the molecular electronic device or biochip computer is ever to become a reality.

The field of molecular electronics may be considered to encompass much more than molecular electronic devices. In its broadest context, molecular electronics may be regarded as simply the application of molecules, primarily organic molecules, to electronics. This definition would include such areas as liquid crystalline materials, piezoelectric materials such as poly(vinylidene fluoride), chemically sensitive field-effect transistors (CHEMFET), and the whole range of electroactive polymers. These applications are beyond the scope of this book and are covered in other reviews (34, 35). However, given the basic tenet of molecular electronics, namely, the ability to engineer and assemble molecular structures into a useful device, the broader definition raises the question of whether organic molecules can be specifically assembled or engineered for unique applications in electronics.

1.1.3.2 LANGMUIR–BLODGETT FILMS

The Langmuir–Blodgett (LB) technique is one of the few methods available for manipulating the architecture of an assembly of organic molecules (36). It may be regarded as the organic analog of molecular beam epitaxy, which is extremely important to solid-state electronics as a means of fabricating precise microstructures with novel charge-transport properties. The LB technique offers the means to construct similar organic analogs by building up organic layers one monolayer at a time and enables precise geometries (e.g., molecular orientation and thickness) to be constructed. The technique involves spreading some suitable organic molecule onto a water surface, compressing the film to form a compact monolayer, and then transferring this layer to a suitable substrate. The processing sequence is depicted in Figure 1.21.

Very few materials are suitable for LB film formation. Typical monolayer-forming molecules possess both hydrophobic and hydrophilic end groups such as long alkyl and carboxylic groups, respectively. Certain polymers will also form monolayers as will certain aromatic macrocycles such as porphyrins and phthalocyanines. Phthalocyanines tend not to have highly oleophilic or hydrophilic parts, but consist of a roughly circular aromatic disk, often with a metal atom at the center and with a minimum of side groups. The material is usually dissolved in an organic solvent and carefully spread onto the surface of water contained in a Langmuir trough. The concentration is such that the molecules spread to a depth of one monolayer. If the surface pressure F is small, the monolayer behaves as a two-dimensional gas obeying the equation

$$FA = kT \quad (1.1)$$

where A is the area per molecule, k is Boltzmann's constant, and T is absolute temperature. The surface pressure is increased by compressing the film by means of a sliding barrier. Eventually, a point is reached where all the

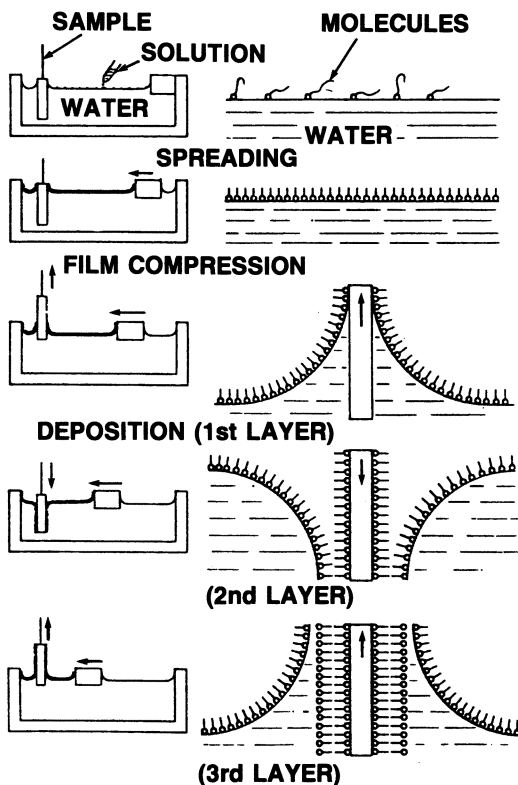


Figure 1.21. The LB sequence: spreading, compression, and deposition. (Reproduced with permission from reference 45. Copyright 1987 Academic Press.)

molecules touch, forming a “perfect” pinhole-free monolayer. The change in surface pressure as the area per molecule is decreased is shown in Figure 1.22. The correct degree of compression is determined by monitoring the surface tension of the water, which starts to drop when the molecules are nearly dense-packed. At higher pressures, the monolayer will buckle and collapse. Below the collapse pressure, the monolayer can be transferred to a suitable substrate by lowering the substrate carefully through the film into the water and slowly withdrawing it (Figure 1.21). Alternatively, transfer may be effected horizontally by contacting the surface with the substrate oriented horizontally to the film surface. These procedures may be repeated successively until the required number of monolayers is obtained. The thickness will thus be an integral multiple of the length of the amphiphilic species.

In this way, ultrathin, compact, pinhole-free (at least in theory) films of constant, well-controlled thickness can be prepared. The films are solids with a lamellar structure, and by properly choosing the chemical composition, they can serve a variety of useful electronic functions. Molecules can

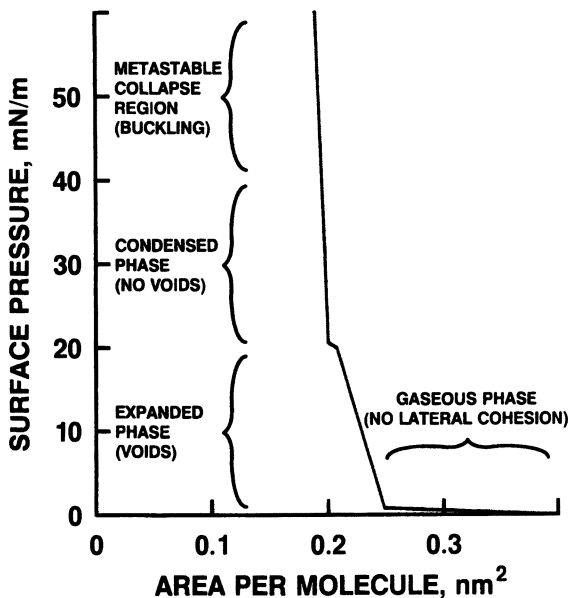


Figure 1.22. A typical monolayer isotherm.

be designed, for example, with unsaturated groups either near the hydrophobic end (e.g., vinyl stearate), near the hydrophilic end (e.g., tricosenoic acid), or around the center of the molecular chain as with diacetylenes. These molecules can be polymerized without disruption of the lamellar structure and thus improve the mechanical and thermal stability of the LB film. One proposed application of these films is as resists for microlithography (37), although the complexities of film deposition and concerns of pinhole density in these ultrathin films make the LB approach a doubtful practical technique for semiconductor device fabrication. LB films have been proposed as passive optical waveguides (*see* Section 1.2.2), where they allow closer control of the waveguide parameters (both dimensional and optical) than is possible with evaporated layers. One problem with LB films in optical applications is that they are not truly single-crystalline materials. Instead, they consist of crystallites separated by domain boundaries that act as scattering centers and limit applications in nonlinear and guided-wave optics.

The attractiveness of silicon as a semiconductor material for ICs derives in part from the fact that this important material forms a naturally insulating surface oxide. Use is made of this fact, for example, in metal-oxide-semiconductor (MOS) field-effect transistors (FET), where the oxide serves as the gate insulator. No such naturally insulating oxide occurs with any of the compound semiconductors that offer improved performance over silicon in many device applications. Roberts et al. (38) demonstrated the feasibility of such metal-insulator-semiconductor (MIS) structures as FETs and chemical sensors shown schematically in Figure 1.23. These researchers

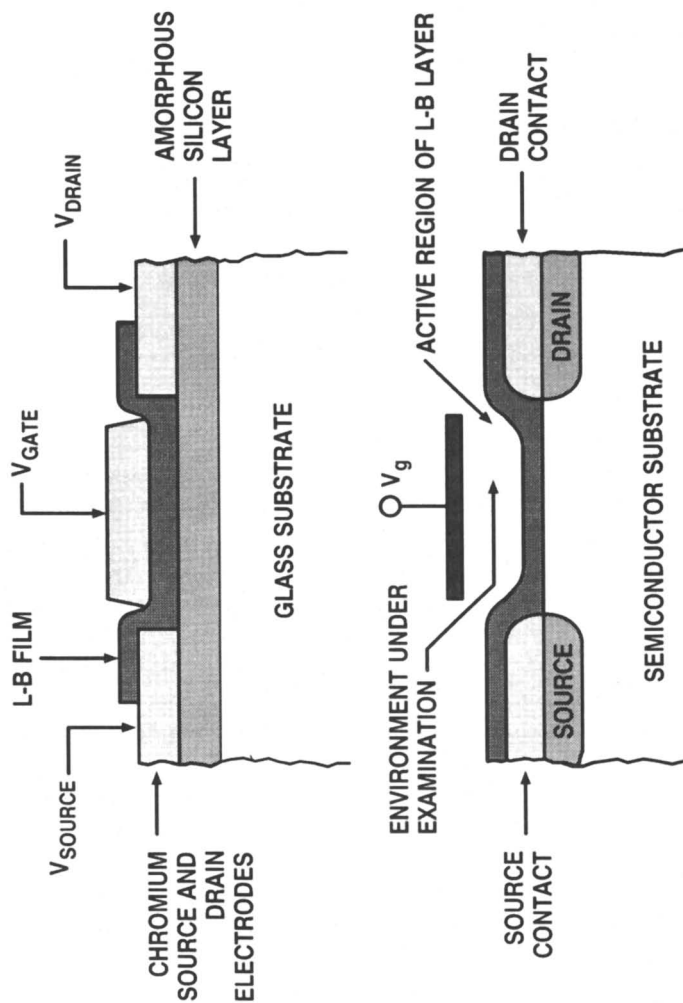


Figure 1.23. Cross-sections of FET structures employing LB films as gate insulators. The top diagram illustrates a thin-film FET using an amorphous silicon source and drain structures. The bottom diagram illustrates a chemically sensitive FET (CHEMFET) in which the electrical characteristics of the LB gate insulator are sensitive to specific chemical species in the environment.

showed that by applying LB films to the surfaces of amorphous Si, GaAs, GaP, InSb, CdTe, and (HgCd)Te, charge-density profiles can also be modified. By using films of tunneling dimensions, charge injection leading to enhanced electroluminescence efficiency was achieved. The efficiency of devices that incorporate layers of quantum-mechanical tunneling dimensions is critically dependent on the control of the insulator thickness. This dependency is why the LB approach is eminently suitable for fabricating such devices.

These examples of LB film application give only a cursory view of the many structures and processes currently being investigated. This field has undergone a marked resurgence over the last decade as scientists have begun to realize that functional devices can be constructed by a molecular engineering approach, although as yet, such devices generally remain an experimental curiosity. The ultimate objective, namely, that of utilizing individual molecules as functional elements and the assembly of such elements into a device, is as elusive as ever. Nevertheless, should a breakthrough be achieved, it promises to be every bit as revolutionary as was the transistor.

1.2 Polymers for Photonic Applications

The microelectronics revolution, which began with the invention of the transistor in 1948 and rapidly accelerated following the invention of the IC in 1960, has had a profound influence on modern society, particularly in the processing and transport of information. The heart of today's telecommunications network, for example, is the highly sophisticated electronic switching machine, which offers a wide variety of service options that cannot be provided by electromechanical switches. Voice and data are switched over a network that ranges from twisted copper pairs to microwave communication towers. However, two inventions during the 1960s have begun to radically change the way in which information is transmitted and may, in the future, lead to a totally new switching technology. Those two inventions are the laser and the optical fiber, which together have spawned the photonics revolution upon whose dawn we are now entering.

Simply speaking, photons are to photonics what electrons are to electronics. In electronic transmission, information, encoded in the form of digital or analog electronic signals, is routed along a conductor path such as a copper wire. In an optical transmission system, information is transmitted in digital format as pulses of light along glass fibers specifically designed to confine the light to the interior of the fiber. Lasers and light-emitting diodes are ideal light sources for optical transmission. These solid-state devices can be turned on and off billions of times per second, providing an ideal mechanism for conveying digital information where the presence of light corresponds to a "1" and its absence signifies a "0". The driving force behind

optical transmission is the enormous capacity, or bandwidth, available. A laser pulsed at 540 megabits per second is equivalent to 24,000 telephone conversations that can be transmitted simultaneously over a single hair-thin optical fiber. Not only does optical transmission offer the potential of essentially unlimited bandwidth, but it is also free from interference effects that plague electronic transmission and offers enormous cost savings in space and materials. As will be shown in the following discussion, polymers play an enormously important role in this rapidly expanding technology.

1.2.1 Optical Fiber Coatings

The glass fibers used in light-wave telecommunications systems must be protected from mechanical abrasion to preserve their strength. Flaws in the glass surface as small as $1.0\ \mu\text{m}$ will reduce the tensile strength of the fiber from over 10^6 kpsi to less than 10^5 kpsi, and lead to breaking of the fiber during cabling. Accordingly, optical fibers must be treated with a protective coating immediately after being drawn in a furnace. A schematic diagram of the process is shown in Figure 1.24. The fiber is drawn from a glass preform that is fed at a controlled rate into the top of a tubular high-temperature ($2200\ ^\circ\text{C}$) furnace. A fiber diameter monitor provides an electronic signal that can be used to adjust the speed of a capstan drive, which pulls the fiber at the base of the machine. Equipment for coating the fiber and solidifying it is located between the diameter monitor and the capstan. This in-line coating procedure enables the coating to be applied and hardened before

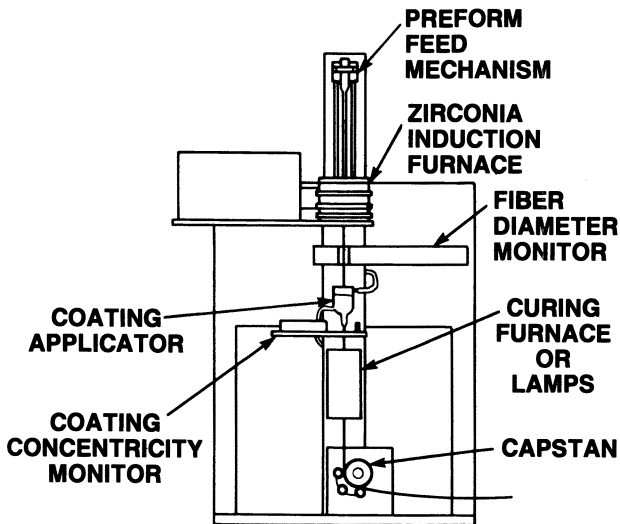


Figure 1.24. A fiber-drawing apparatus. (Reproduced with permission from reference 39.)

the fiber contacts any surface. For this reason, the most successful coating techniques involve the application of a low viscosity (10–50 poise) oligomeric liquid to the fiber followed by rapid solidification. Three coating processes have been developed to meet this requirement of rapid solidification. These processes use

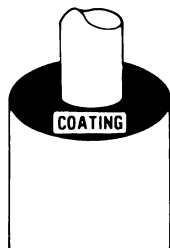
1. UV-radiation-curable polymer formulations,
2. thermally cross-linkable prepolymers capable of being force-cured at high rates (e.g., silicones), or
3. hot-melt thermoplastics that can be solidified by rapid cooling (39).

In addition to providing mechanical and environmental protection to the optical fiber, the polymer coating should reduce microbending losses. As a result of their very small diameters, typically 100–150 μm , optical fibers bend readily. This feature is advantageous in that the transmission medium is flexible and easily routed. However, when the spatial period of the bending becomes very small, some of the light rays normally guided by the fiber are lost through radiation. Such small-period distortions may occur when a fiber is wound on a spool under tension, or when it is placed in a cable structure. The phenomenon is called *microbending loss*, which in extreme cases can result in transmission losses amounting to several decibels per kilometer, thereby seriously degrading the performance of an optical fiber transmission link. This problem can be minimized through use of low-modulus coatings.

The preferred coating design involves a dual-coated fiber consisting of a soft, low-modulus primary coating (to minimize microbending losses) and a hard, high-modulus secondary coating (for mechanical protection) (Figure 1.25). The second coating can be applied either in-line or off-line. Thermally

Chief Advantage

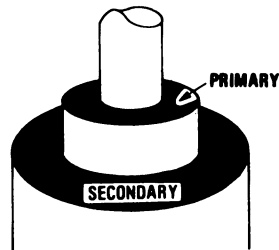
HIGH STRENGTH



SINGLE COATING

Chief Advantage

HIGH MICROBENDING RESISTANCE



DUAL COATING

Figure 1.25. Protecting glass optical fibers by employing single and dual coatings.

curable silicones and UV-curable epoxy acrylates are used commercially for the soft primary coating. High-modulus UV-curable epoxy acrylates have been used for the hard secondary coating as have extrudable thermoplastics such as nylon.

Polymers have broad application in cabling, sheathing, and connecting operations. Cabling of optical fibers is quite different from cabling of copper conductors. The coated fibers are usually assembled or packaged prior to sheathing. A typical fiber-packaging structure used in cable designs is shown in Figure 1.26. In this structure, known as a ribbon, 12 fibers are packaged in a linear array by sandwiching them between two adhesive-coated polyester tapes. The ribbons are then grouped along with metallic strength members and enclosed in a polymeric sheath in a final extrusion process.

Deployment of optical fibers in the field requires the fibers to be spliced (joined) at various junction points. Fusion splicing is the most reliable method for permanently joining optical fibers and has been successfully applied in the field. However, the fusion splice needs a protective package because the spliced section has no protective coating and its strength is weakened by the splicing operation. One type of packaging system, shown in Figure 1.27, consists of a heat-shrinkable tube of cross-linked polyethylene, a hot-melt adhesive inner tube, and a strength member rod of stainless steel.

Connectors that operate by physical alignment have also been designed. A typical example is shown in Figure 1.28. The extremely narrow tolerances required demand high-dimensional stability and precision. As a consequence, most connectors are made of metals and ceramics by precision machining techniques. Plastic connectors are also available but are better suited to connection of multimode fibers, where the larger core imposes less severe alignment tolerances than required for single-mode fibers.

One application that has not been mentioned is the use of polymers for the optical core in place of silica. Attenuation losses essentially preclude such applications in long-haul transmission systems. For example, poly(methyl methacrylate) has been studied as a potential plastic optical fiber, but intrinsic absorption losses due to overtones of the C–H vibration limit attenuation to 55 dB/km at 570 nm (40). The losses caused by overtone absorptions can be eliminated by deuterating the polymer. The overtone absorptions associated with C–D vibrations (where D is deuterium) occur at longer wavelengths and are of lower intensity than C–H overtones (Figure 1.29). Attenuation losses of 20 dB/km at 650–680 nm have been reported for perdeuterated poly(methyl methacrylate), but this value is still over 2 orders of magnitude higher than that of silica fibers, for which attenuations of 0.2 dB/km at 1300 nm have been reported. The theoretical minimum attenuation for plastic fibers is believed to be 9 dB/km at 680 nm. This minimum makes such materials clearly unacceptable for transmission over long distances. Plastic optical fibers may, however, find application in back-plane interconnections, for example, where transmission distances may be on the order of inches.

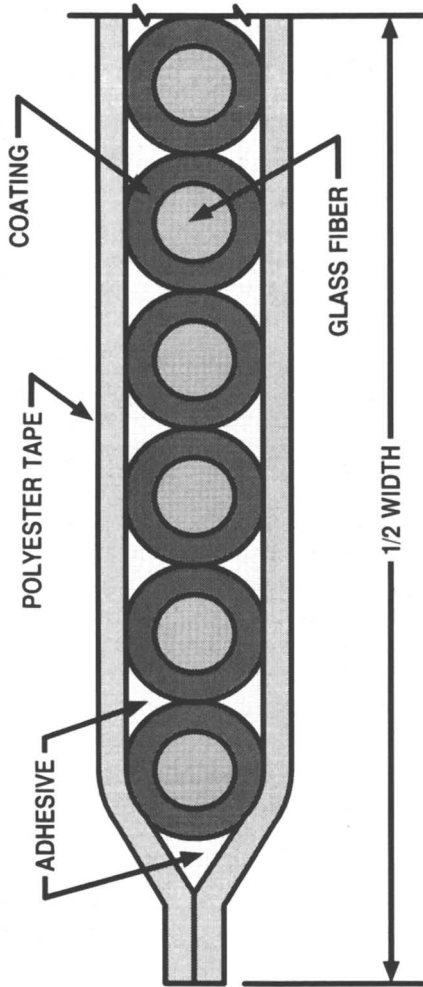


Figure 1.26. Section of a 12-fiber ribbon. (Reproduced with permission from reference 39.)

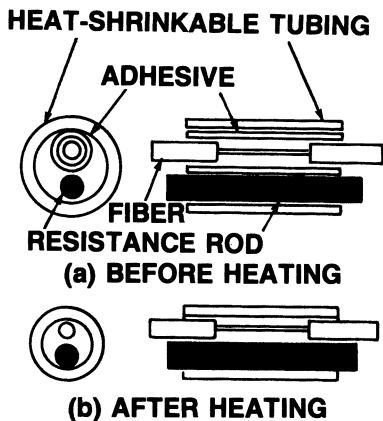


Figure 1.27. A heat-shrinkable tubing package for protecting spliced fibers. Shrinking is accomplished by means of an internally heated resistance rod. (Reproduced with permission from reference 40.)

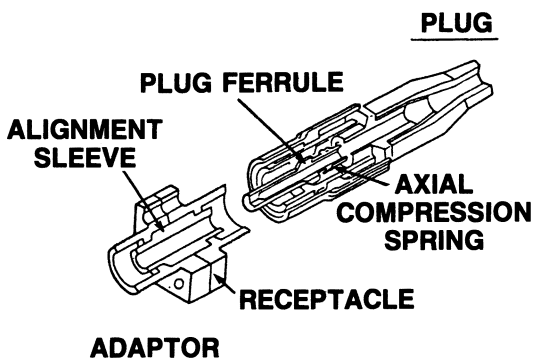


Figure 1.28. A precision-molded plastic connector. (Reproduced with permission from reference 40.)

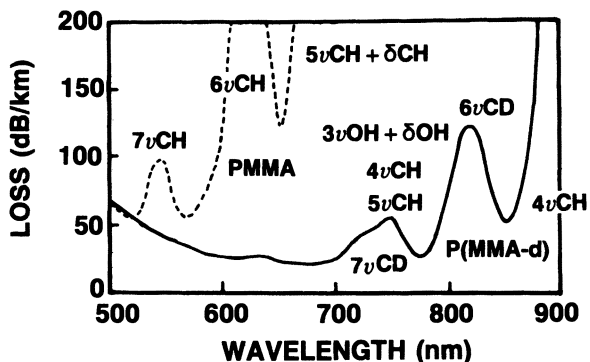


Figure 1.29. Transmission spectra of PMMA and perdeuterated PMMA core plastic optical fibers. (Reproduced with permission from reference 40.)

1.2.2 Polymers for Integrated Optics

In long-haul transmission, the light intensity decreases with distance and must be regenerated (amplified) at intervals determined by the intrinsic loss in the fiber. This regenerative process is accomplished electronically. The light pulses received at the end of an optical fiber are converted to electronic signals by a photodetector (photodiode). These signals are then amplified and used to modulate the output of a laser that forms part of the repeater circuit. A new set of pulses are therefore generated and launched into the fiber. It would be advantageous to perform such functions photonically rather than going to the trouble of converting from photonics to electronics and back to photonics. Likewise, photonic switching has the potential to be much faster than electronic switching (with resulting higher bandwidths) and carries with it the possibility of parallel processing.

Although the implementation of an all-optical network lies well in the future, much of the technological framework is being developed. The attendant passive components associated with multimode fibers (e.g., couplers, power dividers, wavelength filters, and connectors) may be constructed by using miniature versions of familiar bulk optical components such as lenses, prisms, and diffraction gratings. Further scaling down of equivalent multimode components for monomode applications is not usually practical owing to stringent alignment tolerances between fiber and component. One approach to solve this dilemma is to integrate such devices on a single chip. The basic motivation of this field of integrated optics is to do for optical circuits what integrated electronics has done for electrical circuits, namely, replace a set of large, individually fabricated elements with integrated, miniaturized circuit elements that are interconnected on a single chip.

A major concept of integrated optics is that in all of the elements and interconnections, the optical signals are confined in compact optical waveguides, and thus the field is often referred to as *guided-wave optics*, and the devices are referred to as photonic circuits. The fabrication of such circuits again involves lithographic processes in which polymeric resists are used for the imaging steps. Relatively complex assemblies of devices have been demonstrated (e.g., an 8×8 matrix switch integrating $64 \times 2 \times 2$ interconnected switch elements on a single chip) (41).

The construction of an optical waveguide in the surface of a substrate requires alteration of the refractive index of the substrate along the length of the guide. By increasing the refractive index of the region, light can be guided or channeled in the same way as takes place in the core of an optical fiber. These guides are then used both to form the various circuit elements (both active and passive) and to make interconnections between elements. The basic concepts are illustrated in Figure 1.30, which is a schematic drawing of an integrated, optical, four-channel, wavelength-division multiplexer. The waveguides have been constructed such that light of a particular

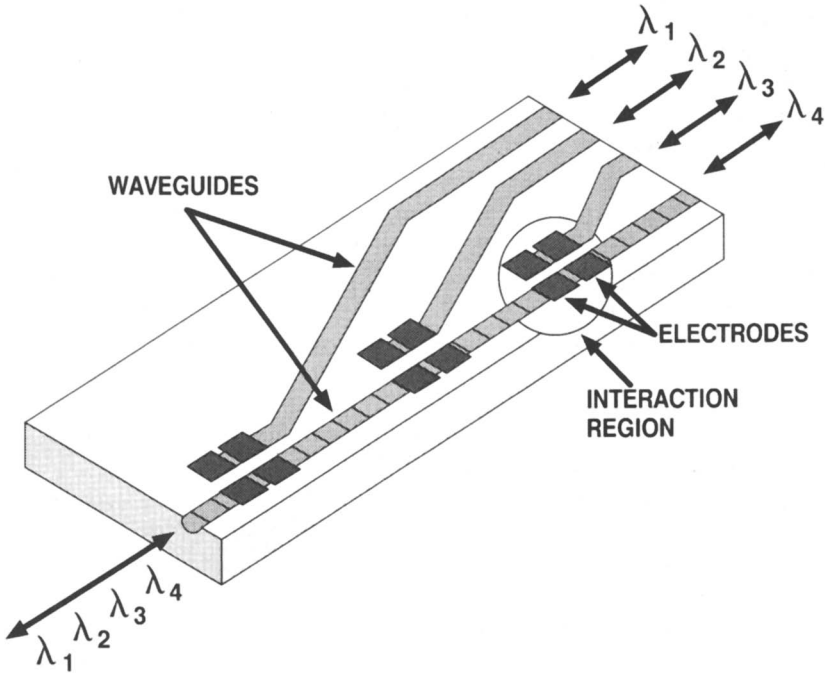


Figure 1.30. An integrated, optical, four-channel, wavelength-division multiplexer.

wavelength entering the interaction region of the first two guides will transfer to the second guide, but light at other wavelengths will remain in the first guide. For waveguides built into substrates exhibiting a large electrooptic effect (e.g., lithium niobate), one can use an electric field to control the interaction wherein the wavelength selected by the coupler can be controlled by the voltage applied to the electrodes.

As with electronic ICs, the fabrication of optical waveguides is preceded by the design and construction of a mask outlining the path light will take in the guiding layer of the structure. Lithium niobate is the favored dielectric material for use in integrated optics. This material can be routinely formed to give large crystals of optical quality and exhibits a reasonably large electrooptic figure-of-merit (i.e., change of refractive index with change of applied field strength). Once the path has been defined by lithographic techniques, the waveguides are fabricated by depositing a thin layer of titanium on the exposed surface, removing the remaining photoresist, and finally diffusing the metal into the crystal at temperatures on the order of 1000 °C for 6 h. Guides can also be made by an ion-exchange process in which Li^+ ions in the substrate are replaced by H^+ ions. In this process, the surface of the crystal is covered by a gold film, except where one wants to form guides. The crystal is then placed in an acid bath for a period of

time (e.g., benzoic acid at 250 °C for a few hours), during which ion exchange takes place through the openings in the gold mask.

Polymers are also well suited for waveguide applications. Total bulk optical losses in the red and near-IR spectral regions are typically <1 dB/cm. For many polymers, losses are <0.1 dB/cm. Most organic materials have refractive indices in the range 1.4–1.7, and a number of simple fabrication techniques such as embossing and casting and photolocking have been shown to be effective in producing regions of different refractive index separated by extremely smooth surfaces (42). In the case of three-dimensional waveguides, the refractive index differential required between the guide and its surroundings depends on the sharpest bend that must be traversed by the guide. A 1% increment is sufficient for most purposes. Refractive index differentials of this magnitude can be generated via photochemically enhanced processes. Although changes in optical polarizability resulting from photochemically induced processes involving bond breaking result in much smaller changes in refractive index than the 1% needed for waveguide fabrication, advantage can be taken of such reactions to alter the chemical composition or density by subsequent chemistry to achieve large refractive index differences.

The photolocking technique, shown schematically in Figure 1.31, has been widely used to fabricate waveguides. A film consisting of a matrix resin [e.g., polycarbonate ($n = 1.59$)], volatile monomeric dopant, and photosen-

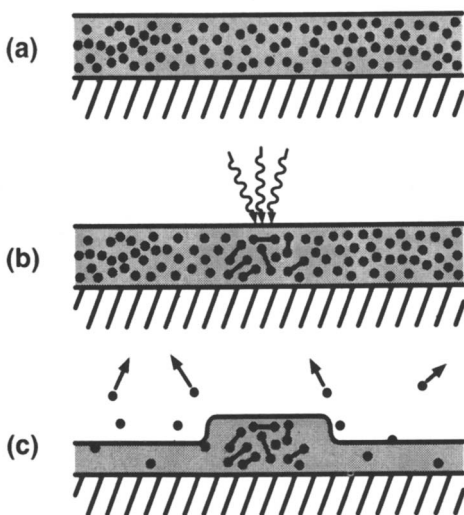


Figure 1.31. The photolocking process: (a) Initial film, dots represent the dopant. (b) Exposure induces reaction of the dopant illustrated here as dimerization. (c) Heating the film evaporates the unreacted dopant. (Reproduced with permission from reference 42. Copyright 1974 American Institute of Physics.)

sitizer is irradiated through a mask with UV light, which polymerizes the monomer in the irradiated region, thereby effectively immobilizing it. The monomeric dopant is then removed from the unirradiated portions of the film by evaporation in a vacuum. By selecting dopants with higher refractive index than the matrix material, the photolocked region will have a higher refractive index than the surrounding matrix. Alternatively, using dopants of lower refractive index such as methyl acrylate ($n = 1.48$) results in regions of lower refractive index. Additional monomer may then be introduced at the outer edges to produce an enclosed waveguide structure (Figure 1.32).

1.2.3 Polymers for Nonlinear Optics

All of the applications involving waveguides discussed in the previous section may be considered “passive”. The polymer serves some structural, protective, or guiding function but is not integral to the functioning of a device. A number of photonic device applications are available, however, where polymers may be useful as active elements. These applications require some type of nonlinear optical response when the material is irradiated with light of very high intensity, usually from a laser.

Nonlinear optics is concerned with the interactions of electromagnetic fields with materials to produce new fields altered in phase, frequency, amplitude, or other propagation characteristics from the incident fields. An example of such an effect is second harmonic generation (SHG). When certain crystalline materials are irradiated with light of frequency ω , there is generated a second beam of frequency 2ω that emerges from the crystal at an angle different from that of the emerging primary beam. The efficiency of conversion is determined by the optical properties of the material. Other examples include third harmonic generation, optical bistability, degenerate four-wave mixing, and phase conjugation.

The origin of these effects lies in the polarization P induced in a molecule by a local electric field E (due to the electromagnetic radiation). P is expressed as a power series of the local field:

$$P = \alpha E + \beta E^2 + \gamma E^3 + \dots \quad (1.2)$$

The coefficients α , β , and γ are the second, third, and fourth rank tensors and are referred to as the polarizability, first hyperpolarizability, and second hyperpolarizability, respectively. The hyperpolarizability terms are responsible for the nonlinear response of the molecule to impinging radiation. These coefficients are not very large, and the associated nonlinear optical effects are usually studied by taking advantage of the high optical field obtainable with laser beams.

An understanding of these effects can be simplified by assuming that polarization is a scalar quantity (as opposed to a vector). Following the approach of Williams (43), when electromagnetic radiation interacts with a

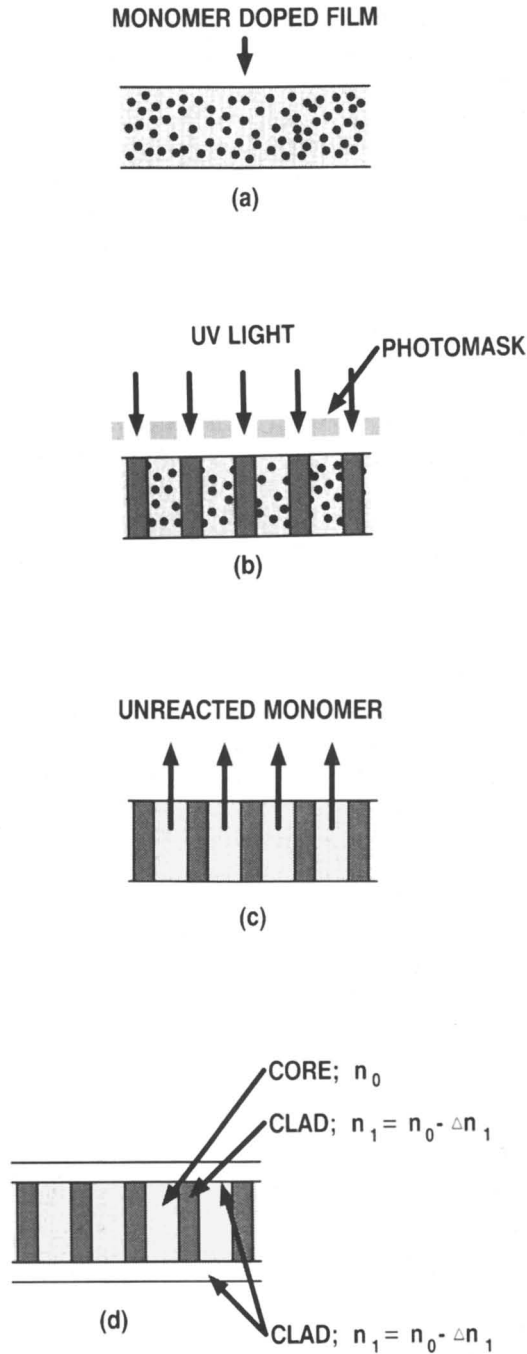


Figure 1.32. Formation of an optical waveguide obtained by using the photolocking technique. (Reproduced with permission from reference 40.)

molecule or medium consisting of many molecules, the field polarizes the molecules which in turn act as oscillating dipoles radiating electromagnetic waves in all directions. In a nonlinear medium, P is a nonlinear function of the applied field. This concept is illustrated in Figure 1.33, where P exhibits an asymmetric response to the applied field E . A medium exhibiting such a response might be envisaged as a crystal composed of molecules with asymmetric charge distribution arranged in such a way that a polar orientation is maintained throughout the crystal. Such a crystal is said to be *noncentrosymmetric*. Molecules exemplifying noncentrosymmetric crystalline orientations include *m*- and *p*-nitroaniline and various substituted derivatives. Such molecules are more easily polarized in the direction from the electron-rich substituent (donor) to the electron-deficient substituent A (acceptor) (i.e., polarization is more effective in one direction than the other). This consequence is reflected in the asymmetric response of P in Figure 1.33. Such a nonsinusoidal response can be broken down into its Fourier components consisting of the fundamental frequency ω and an appropriate summation of the even harmonics (i.e., 2ω , 4ω). In other words, the oscillating dipoles induced in the molecules by the incident field contain not only the fundamental frequency characteristic of the incident radiation, but also components of the second and higher even harmonics. The magnitude of 4ω and the higher even-multiple frequencies is extremely small and is usually ignored.

In the case of a *centrosymmetric crystal*, the polarization induced by the first nonlinear term in equation 1.2 is βE^2 . If a field $-E$ is applied, the

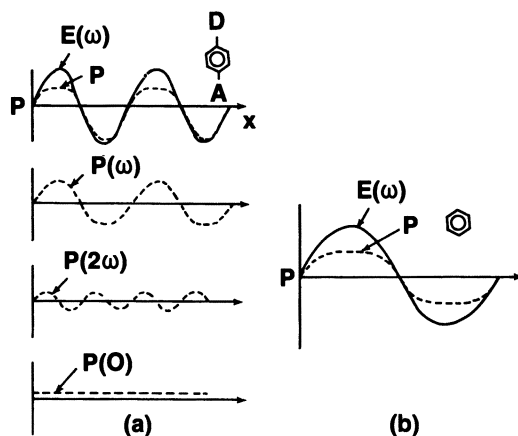


Figure 1.33. Plot of polarization response P to an incident electromagnetic wave of field strength $E(\omega)$ at frequency ω in (a) a noncentrosymmetric medium and (b) a centrosymmetric medium. The Fourier components for the noncentrosymmetric response are also shown. (Reproduced with permission from reference 43. Copyright 1984 VCH.)

polarization will still equal $+\beta^2$, whereas in a centrosymmetric medium it should be $-\beta^2$. This contradiction can only be resolved if $\beta = 0$ in a centrosymmetric medium. No such contradiction occurs with the next higher order term because $+E$ produces a polarization $+\gamma E^3$, and $-E$ produces a polarization $-\gamma E^3$ as required by symmetry. The polarization will therefore vary symmetrically with the applied field, and only the fundamental and higher odd harmonics (3ω , 5ω , etc.) will be present in the Fourier decomposition of the response curve. Thus, the efficiency of third-order harmonic generation will be determined by the magnitude of the third-order coefficient. The electrooptic effect depicted in the wavelength division multiplexing device in Figure 1.30 is a second-order nonlinear effect. In this case, the polarization has components arising both from the field of the light-wave propagating through the optical fiber, $E(\omega)$, and from the field applied to the electrode $E(0)$. The change in polarization resulting from the interaction of these two interacting field components effectively alters the refractive index of the medium. This phenomenon is also known as the *Pockels effect*.

The basic molecular properties that give rise to high values of the hyperpolarizabilities β and γ are reasonably well understood (44). Efficient quadratic molecular effects (high β) require conjugation and intramolecular charge transfer. The absolute magnitude of the charge-transfer component of β is directly proportional to the change in dipole moment between the excited-state dipole moment and the ground-state dipole moment. Likewise, the magnitude of the component attributable to conjugation is proportional to the cube of the conjugation length. Organic compounds that have extended conjugated π systems substituted with both electron-donating (*D*) and electron-withdrawing (*A*) groups meet these criteria. Such groups combine to perturb the electron density in a mesomeric fashion. The value of β is determined as the sum of two contributions due to an additivity term and a charge-transfer term:

$$\beta_{\text{tot}} = \beta_{\text{CT}} + \beta_{\text{add}} \quad (1.3)$$

The β_{add} term involves a substituent-induced charge asymmetry, and β_{CT} is the contribution resulting from charge transfer or mesomerism. The relative contributions of β_{add} and β_{CT} are determined by the individual characteristics of the specific *D* and *A* groups.

It is necessary but not sufficient for an organic molecule to exhibit a large β to be an efficient SHG material. Such molecules must also pack in a crystal lattice in such a way as to result in an overall dipole moment. Polar molecules frequently crystallize in centrosymmetric crystalline structures in which the internal fields cancel. Thus, the search for the efficient organic nonlinear crystal is, in reality, a search for the "polar" crystal in which the macroscopic properties reflect the internal asymmetric molecular relation-

ships. The polarization (P) induced in a medium by an external electric field is expressed by the equation

$$P = \chi^{(1)}E + \chi^{(2)}E^2 + \chi^{(3)}E^3 \quad (1.4)$$

where the $\chi^{(n)}$ values are the macroscopic coefficients that measure the projection of the microscopic molecular tensors on the unit cell. Because the $\chi^{(n)}$ values are tensor quantities, the unit-cell characteristics and the orientations of the molecules within the crystal lattice are highly important if the molecular properties are to be fully manifested. One such molecule that has been extensively studied for its nonlinear optical properties is 2-methyl-4-nitroaniline (MNA). Compared with the inorganic crystals commonly used for frequency doubling, MNA generates radiation at twice the frequency of the incoming beam much more efficiently. Organic crystals are also generally more useful than their inorganic counterparts because of increased transparency and associated resistance to laser damage. Lithium niobate, for example, exhibits a damage threshold between 1 and 100 MW/cm² compared with $2\text{--}3 \times 10^3$ MW/cm² for organic crystals, although potassium dihydrogen phosphate has about the highest damage threshold of any material at 2.3×10^4 MW/cm².

Organic crystals have not yet found widespread use in guided-wave optics or as bulk components for parametric processes. The difficulty of growing large high-quality single crystals with the required processability, lack of mechanical integrity, and ambient stability has impeded their implementation. Efforts to artificially create a noncentrosymmetric environment in a crystal lattice include (1) LB techniques (which control molecular architecture via the dipping sequence) (45), and (2) molecular doping of an appropriate nonlinear chromophore into a polymeric host (46). In the second approach, the chromophore is aligned in the host medium by poling in an electric field, followed by permanent fixation of the induced alignment. Poly(methyl methacrylate) has been used as a typical isotropic host medium. Other workers have sought to improve the alignment by inclusion of guest molecules in liquid crystalline host matrices.

Cubic-nonlinearity-related effects are enhanced in one-dimensional conjugated structures such as linear conjugated polymer chains of the polyene, polyacetylene, or polydiacetylene type. No charge-transfer-induced asymmetric environment is required. Polydiacetylenes (Figure 1.34) in particular have been extensively studied (47) because certain diacetylenic monomers can be topochemically polymerized in the solid state to give polymeric single crystals in which the chains are aligned parallel to a crystallographic direction. This orientation enhances the value of $\chi^{(3)}$ along this direction, although there are no constraints as to the centrosymmetric nature of the lattice. Values of $\chi^{(3)}$ are on the same order of magnitude as that of Ge and GaAs,

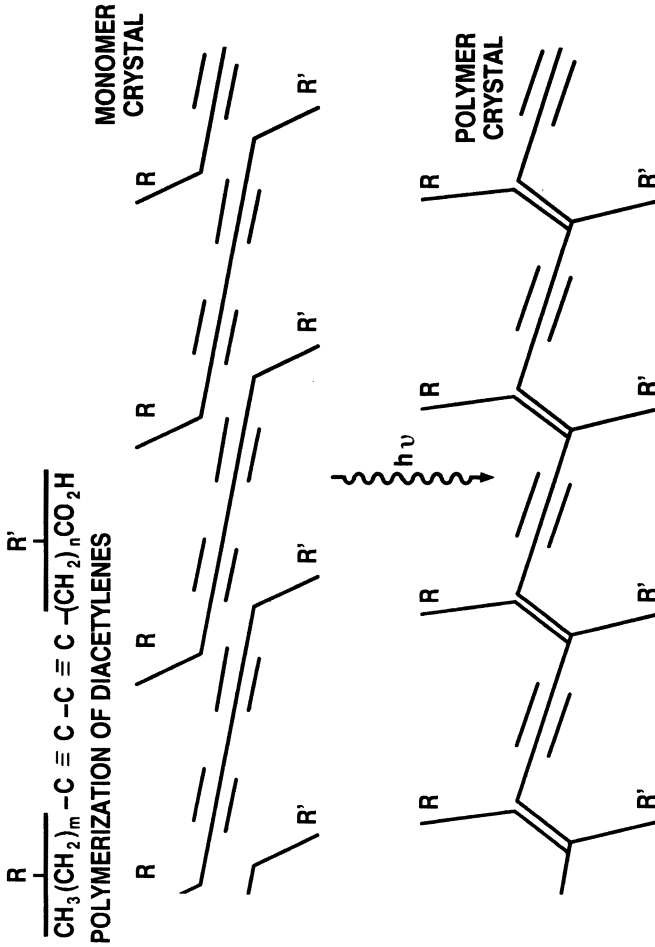


Figure 1.34. Polymerization of polydiacetylenes.

with recent reports on polyacetylene indicating an order-of-magnitude improvement.

The nonlinear response time in the nonabsorptive (off-resonance) region has been estimated to be in the subpicosecond domain, which may have major importance in the emerging ultrafast signal processing technologies. Such processing schemes rely on a material's intensity-dependent index of refraction as the basic nonlinear mechanism, and this parameter can be related to the third-order susceptibility. A high $\chi^{(3)}$ would enable the refractive index to be altered at relatively low incident intensities, thereby controlling the passage of a second light beam. This principle can be extended to four-wave mixing experiments in which two intersecting beams of light create a refractive index grating in the material. A third beam directed at the same spot will be deflected by the grating and emerge as a fourth beam (Figure 1.35). Degenerate four-wave mixing is a special case in which all the input beams and the scattered beam have the same frequency. The degenerate four-wave mixing experiment is directly relevant to such technologically important phenomena as self-focusing, phase conjugation, saturable absorption, and self-induced transparency. Such effects form the basis of a completely photonic switching technology, which constitutes a major driving force behind research on nonlinear optical materials (48).

Various techniques have been used to prepare single crystals of polydiacetylene. Bulk crystals obtained by conventional crystallization procedures (e.g., slow cooling or evaporation from solution) tend to be riddled with defects such as grain boundaries or stacking faults, and are not suitable for optical applications. The LB technique, on the other hand, has been

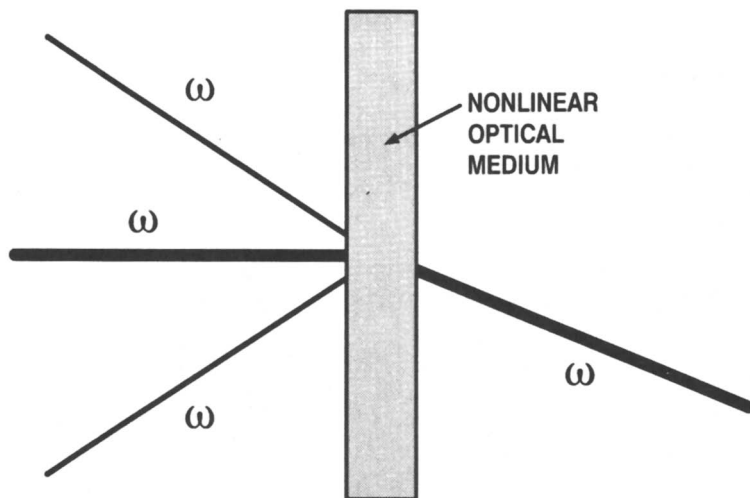


Figure 1.35. Principle of degenerate four-wave mixing.

widely used to fabricate thin films of polydiacetylenes for waveguiding applications. Suitable monomers have been synthesized that contain hydrophobic and hydrophilic groups, which facilitate alignment of the molecules on the film balance. The monomeric monolayer is then polymerized by UV irradiation, and the polymerized film is deposited on the substrate by subsequent dipping. By repeating this process, multilayers as thick as 500 nm have been built up on quartz and silicon substrates, enabling fabrication of planar optical waveguides (49).

Single crystals prepared by the LB technique still contain grain boundaries that reduce optical transmission. These imperfections are not found in monomer single crystals grown by a melt-shear technique (50), in which crystals are grown either from the melt or from solution by confining the liquid between two optically flat opposing surfaces. Pressure is applied to the substrate–monomer–substrate assembly while the mobile phase is subjected to a shearing force via a slow linear translation of one of the substrates with respect to the other. The uniaxial shear introduces a preferred orientation of the diacetylenic molecules perpendicular to the substrate interface. This method has been reported to yield single crystals that are 4 orders of magnitude larger than what had previously been reported and are of superior optical quality.

Most of the work so far on new nonlinear materials has involved dealing with bulk materials coupled to high-powered lasers. However, to bridge the gap between mere observation of nonlinear effects and their actual use in relatively low-power semiconductor-laser-driven systems, fully optimized nonlinear structures will be needed. This is an extremely active field of current research involving crystal design and growth, crystal thin-film technology, and polymer thin-film technology.

1.2.4 Polymers in Optical Recording Media

The development of low-cost lasers has also made optical information storage a practical reality, as evidenced by the rapid proliferation of such consumer items as digital audio disks and video disks. In a video disk, the picture and sound information is stored on the disk as a succession of small pits of varying length and repetition frequency (Figure 1.36). The information is read optically with monochromatic light from a laser by focusing the beam (typical diameter $\sim 1.0 \mu\text{m}$) onto the surface of the rotating disk, and monitoring the intensity of reflected light by a light-sensitive diode. The reflectivity of the pit differs from that of the surface or land area; hence, the intensity of the reflected light (and consequently the electrical output of the photodiode) will be modulated according to the pattern of pits. The intensity-modulated output is converted by the photodiode to a current (I), whose magnitude will depend on the position (x) along the information track. The waveform of the electrical output represents a frequency-modulated analog signal (Fig-

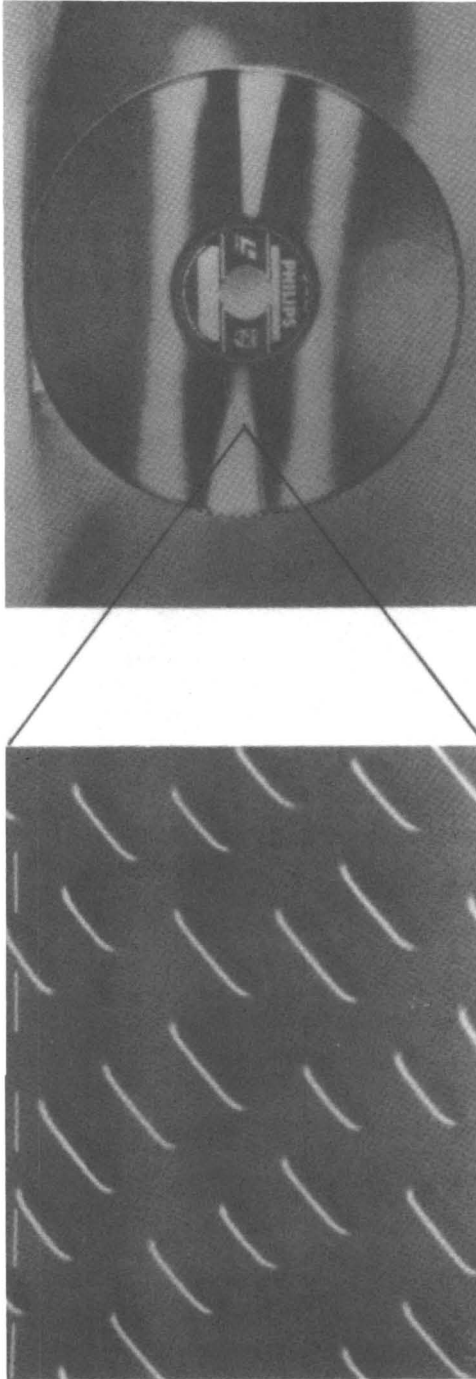


Figure 1.36. Scanning electron microscope picture showing topography of a typical video disk. The information track consists of small pits of constant width and depth with variable length and spacing.

ure 1.37) that can be electronically translated into picture and sound signals appropriate to a television receiver.

The analog format of a video disk is in contrast to an optical audio disk on which information is encoded digitally. Because of the higher bandwidth required for video use, the sampling rate required to digitally encode a video signal is many times greater than that needed to encode an audio signal (100 megabits per second vs. 1.4 megabits per second, respectively). Digital encoding of a video signal would require a storage density many times greater than that obtainable with current technology, which is, however, sufficient to permit digital encoding of an audio signal. Thus, although the waveform of the electrical output obtained from an audio disk is similar to that from a video disk, the waveform of the audio disk output can be analyzed by digital processing techniques. These techniques convert the distance, both between and within pits, to a series of bits by convoluting the time between two successive changes in reflectivity (signifying the beginning and end of a pit) with a particular clock rate (determined in part by the angular or linear velocity of rotation of the disk). If reflection from a land area is associated with a "1", and that from a pit is associated with a "0", then the length of

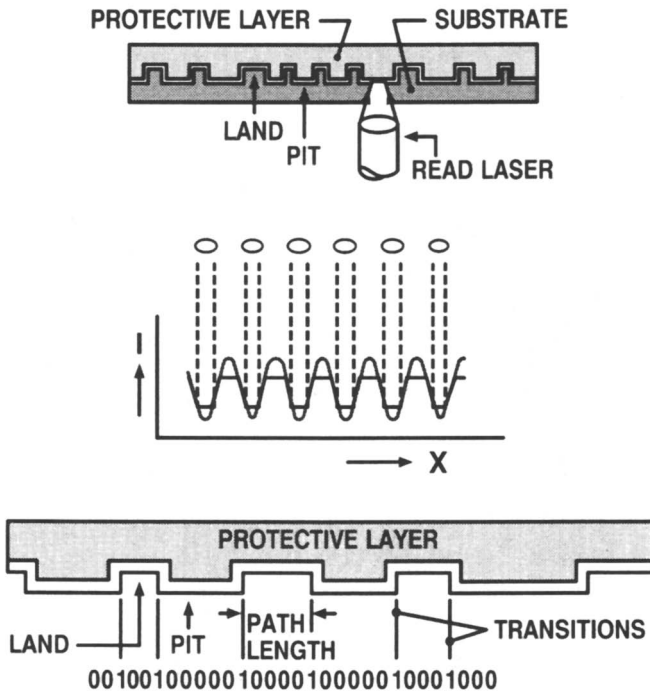


Figure 1.37. The relationship between the pattern of pits and the signal on read-out. The output represents a frequency-modulated signal.

the land area or pit thus determines the number of bits (0s or 1s) between each change in reflectivity.

1.2.4.1 SUBSTRATES

The largest volume use of polymers in optical recording media is in the disk substrate. A schematic of a typical double-sided disk substrate is shown in Figure 1.38, which illustrates the properties required of the substrate material:

1. It must be dimensionally stable, and although expansion with temperature or humidity can be tolerated to some degree, this expansion must occur isotropically.
2. The material chosen must be capable of being formed into a disk either by molding or machining.

Polymers are again ideally suited for such applications in that they exhibit a wide range of mechanical properties and can be molded, for example, by injection molding to the desired physical form.

In addition to these two criteria, there may be additional stringent optical requirements that the polymeric substrate must meet, especially when the substrate is an integral part of the optical pathway. Here it is imperative that the substrate be nonabsorbing at the read and write wavelengths. It must also be transparent (i.e., free of particulates and occlusions that would act as scattering centers). The refractive index of the substrate must be uniform across the diameter of the disk, which should also be free of birefringence. Polymers such as poly(methyl methacrylate), poly(4-methyl-1-pentene), and bisdiallylpolycarbonates are amorphous, optically isotropic, engineering resins that can be easily molded or cut from cast sheet to form disk-shaped substrates (51). These polymers offer the optical quality of glass in terms of high transmission and low birefringence.

1.2.4.2 IMAGING LAYERS

The next step in the manufacture of a video disk is the creation of the imaged layer (i.e., the series of pits) on the surface of the substrate. This process could be accomplished by lithographic processes by exposing a resist-coated substrate to modulated laser light. This technique is used to fabricate the "master" video disk from which molds are fabricated for subsequent mass production. However, lithographic processes require development and are not practical for digital optical recording involving direct read after write (DRAW), (i.e., data read within 500 ns of the recording event). Such requirements have led to the introduction of extremely sophisticated imaging systems, particularly where read, write, and erase capability is required.

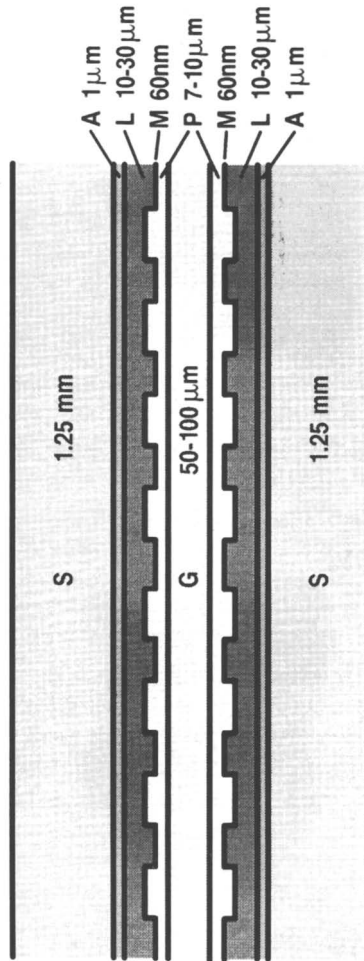


Figure 1.38. A double-sided video disk. Abbreviations are as follows: S is the transparent substrate, A is the adhesion layer, L is the polymeric information layer with picture and sound information in the form of pits, M is the mirror coating, PR is the protective layer, and G is the adhesive layer holding both sides together. (Reproduced with permission from reference 55. Copyright 1982 Philips Research Laboratories.)

First, surface imperfections must be eliminated from the substrate because the specular quality of the imaging layer in most optical recording media is determined by the quality of the surface on which the imaging layer is deposited. The surface of plastic disk substrates commonly contains many surface imperfections that can cause output errors. Thus, a polymeric surfacing-subbing layer is commonly deposited on the substrate from solution to cover the defects and produce a defect-free surface. In this sense, the function of the subbing layer is much like that of the planarizing layer in lithographic multilayer resist processing.

The most common method for optical digital recording is laser-induced ablation or decomposition of thin films. This method is suitable for write-once applications such as archival storage. Typical classes of materials include metals (particularly tellurium), metal alloys, chalcogenides, and chalcogenide alloys deposited as thin films on a suitable substrate (52). The device options include simple single layers, bilayers in which the recording material is deposited on a reflective layer of metal such as aluminum, and trilayer structures in which the recording material is deposited on top of a transparent dielectric spacer separating it from a reflective layer of aluminum. In these constructions, polymers are frequently used as the spacer and dielectric layers and are deposited by either spin coating or plasma deposition.

Ablative imaging systems that consist of a thin film of an organic dye have been designed, although difficulties with film preparation of such systems have led to modifications in which the organic dye is dissolved or dispersed in a polymeric binder. Excitation energy absorbed by the dye is converted to thermal energy that initiates decomposition of the dye-polymer matrix. This decomposition leads to formation of a pit surrounded by a rim of solidified material. The precise kinematics of the process are very complex and appear to depend on the molecular parameters of the ablative material. This principle has also been extended to include polymeric matrices that readily depolymerize. Such polymers include poly(methyl methacrylate), poly(α -methylstyrene), poly(oxymethylene), and poly(2-methylpentenesulfone). A constraint of such systems is that one is committed to use wavelengths that fall within the absorption spectrum of the dye. The thin metal films, on the other hand, are broadly absorptive across the visible and IR spectrum.

The ability to erase what has just been written offers several advantages over the write-once disks just described. Erasable optical recording materials enable errors to be detected and corrected (i.e., re-recorded), as is possible with magnetic recording materials. Several schemes have been proposed, but the technology of erasable optical recording materials is not as advanced as the technology of write-once materials. Many potential systems are not suitable because of speed or stability considerations. For example, the change in the absorption spectrum that occurs when photochromic materials are irradiated with light of an appropriate wavelength can, in certain in-

stances, occur virtually instantaneously. Erasure capability is provided through reversal of the color change by absorption of light in a different spectral region. However, lack of thermal stability of the written image, together with the propensity of photochromic materials to undergo irreversible, photochemical side reactions, has hindered acceptance of this class of materials.

An interesting extension of this technology is photochemical hole burning (53). The absorption spectrum of a dye dispersed in a polymeric matrix consists of a relatively broad band that reflects the different energies associated with the variety of molecular environments surrounding each dye molecule. A laser with a much narrower line width or profile will excite molecules only in those selected orientations whose energies correspond to the energy of the exciting radiation. The photochromic spectral shift thus results in a "hole" in the absorption spectrum at this specific region of the total absorption. By tuning the laser frequency across the inhomogeneously broadened line, different sets of molecules *within the same region of illumination* can be addressed, and thus storage capacity is greatly enhanced. The maximum storage density will be determined by the number of distinct laser profiles that can be accommodated in the total absorption line width. Such systems are stable only at very low temperatures, where the molecular orientation remains temporally fixed.

One erasable technique that has shown some promise is magneto-optical recording. Information is recorded by local heating of a thin film of a thermomagnetic material such as an amorphous alloy of the rare-earth transition metals [e.g., GdTbFe (54)]. In the recording process, a beam of light from an AlGaAs diode laser is focused onto the surface of the film, causing a local increase in temperature. This increase causes a localized decrease in coercivity that, with the aid of a small external magnetic field, facilitates reversal of the magnetization direction and forms a cylindrical domain with dimensions approximately equal to that of the focused laser beam. Erasure may be accomplished by application of a magnetic field large enough to overcome room-temperature sensitivity and oriented in the original magnetization direction. Read-out is accomplished via the magnetic Kerr or Faraday effect, whereby the plane of polarization of plane-polarized light reflected by the layer is rotated. The rotation is positive or negative depending on the direction of the local magnetization. Polymers are again used in the construction of these disks, which are designed in monolayer, bilayer, trilayer, and even quadrilayer configurations.

Some erasable materials contain the polymer as an integral part of the record and erase process. Figure 1.39 depicts such a system consisting of two polymer layers called the expansion and retention layer. The expansion layer is an elastomer containing a dye sensitive to light at 840 nm. The retention layer contains a dye sensitive to light at 780 nm. In the write operation, the system is exposed to an 840-nm diode laser that heats the expansion layer, thus causing it to expand and deform the retention layer.

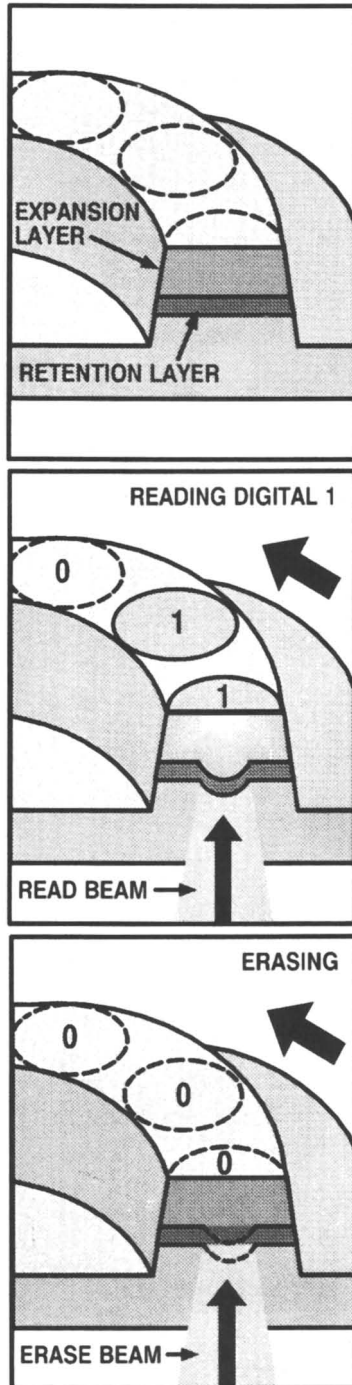


Figure 1.39. Erasable dye-polymer recording scheme.

The deformation appears as a surface bump that can be detected during the read operation because the intensity of light reflected back to the detector will be different from that reflected from a flat area. Erasure is effected by exposure to a second laser beam at 780 nm. Here, light is absorbed by the dye in the retention layer but not the expansion layer; the retention layer is softened, and the elastic energy stored in the expansion layer restores planarity to the laminated structure.

1.2.4.3 PROTECTIVE COATINGS

The final step in the production of the optical disk is protection of the imaged layer from dust and physical damage. Several procedures are possible. Either the layer can be protected in an air-sandwich configuration or by overcoating with a protective polymeric layer. The air-sandwich structure is particularly well suited to ablative recording, whereas conformal coatings can interfere with the marking process. In the case of polymeric encapsulated structures, the encapsulant is an integral part of the read-write optical path. Consequently, it must be transparent and defect-free, and it must exhibit negligible birefringence. Cross-linked siloxane elastomers have been employed most extensively for this purpose. The thickness of this layer must be sufficient to remove dust particles from the focus plane of the read-write laser to eliminate signal defects.

Video and audio disks serve a read-only function and must be reproduced by using mass production techniques to make them available at reasonable cost. Injection molding provides a convenient reproduction technique. The mold is typically made from a "master" disk that has been manufactured from a master video tape by lithographic processes described earlier. Following molding, the surface of the disk is metalized and overcoated with a protective polymeric film. Care must be taken to minimize birefringence during the molding process. Birefringence refers to the anisotropy of refractive index in the same plane and can occur during injection molding through orientation of the polymer chains induced by the shear stresses associated with the molding process. Factors such as holding pressure, injection speed, and melt index are important parameters in ensuring disks of high quality. Workers at Philips (55) have devised a photopolymerization replication process, shown schematically in Figure 1.40, in which a photopolymerizable liquid is sandwiched between a master mold and substrate backing plate. The reactive monomer is polymerized by exposing the sandwich to UV light through the substrate. The mold is then separated, and the "imaged" layer on the substrate is metalized. The final step is the application of a protective overcoating. By joining two such structures back-to-back, one can create the double-sided video disk shown in Figure 1.38. Multifunctional acrylates are generally used for the photopolymerizable

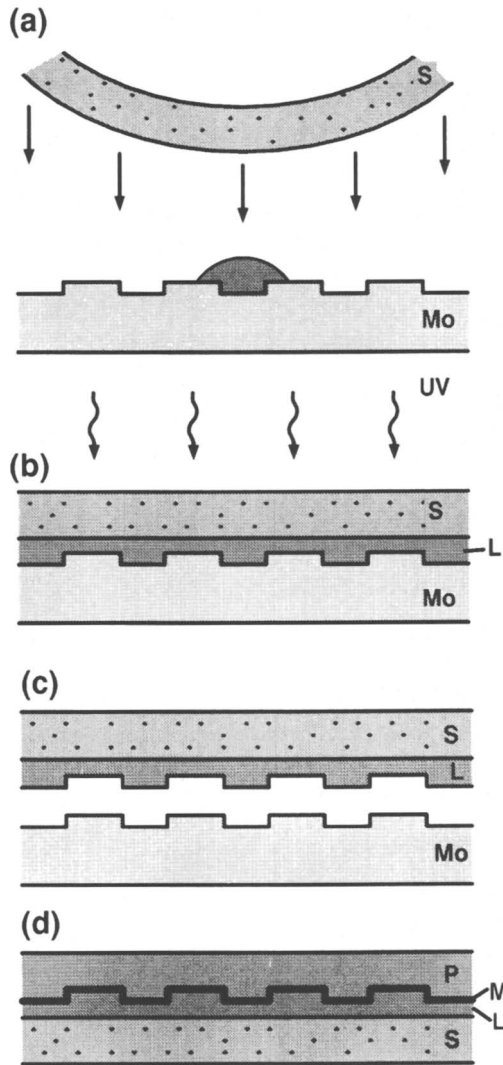


Figure 1.40. The Philips photopolymerization process for replicating video disks. (a) The liquid layer L is spread over the mold Mo by deforming the substrate S to make it slightly convex. (b) Exposure to UV light polymerizes the liquid coating. (c) The substrate with coating is separated from the mold. (d) The information layer is coated with a mirror M and protective layer P. (Reproduced with permission from reference 55. Copyright 1982 Philips Research Laboratories.)

resin. Acrylates exhibit very high cure rates (important for throughput), good dimensional stability (required during subsequent metalization), and proper adhesive properties (required for mold release).

1.3 Conclusions

It would be difficult to imagine a world without the benefits of polymer science. This chapter has given some insight into the enormously important and enabling role played by polymers just in the fields of electronics and photonics. Indeed, it does not seem presumptuous to state that were it not for the unique properties of polymers, there would be no microelectronics or photonics revolution. This review has concentrated on several major applications of polymers to these two technologies. Needless to say, there are many other applications. Perhaps the one thing that can be said with confidence is that polymers will continue to make significant contributions to electronics and photonics through improved materials and new applications.

Abbreviations and Symbols

α	polarizability (second rank tensor)
β	first hyperpolarizability (third rank tensor)
β_{add}	contribution to β_{tot} resulting from a substituent-induced charge asymmetry
β_{CT}	contribution to β_{tot} resulting from charge transfer or mesomerism
β_{tot}	sum of β_{CT} and β_{add}
γ	second hyperpolarizability (fourth rank tensor)
δ	resonance or transfer integral
ϵ	dielectric constant
ω	frequency
χ	macroscopic coefficient that measures the projection of the molecular tensors on the unit cell
A	area per molecule
CHEMFET	chemically sensitive field-effect transistor
DIP	dual in-line package
DRAW	direct read after write
E	(1) electrical field; (2) gap opened at the Fermi level caused by band alteration
ENDOR	electron nuclear double resonance
ESEMQRNMR	electron spin-echo multiple quantum nuclear magnetic resonance
F	surface pressure
FET	field-effect transistors
HIC	hybrid integrated circuits

HOMO	highest occupied molecular orbital
<i>I</i>	current
IC	integrated circuit
<i>k</i>	Boltzmann's constant
LB	Langmuir–Blodgett
LUMO	lowest unoccupied molecular orbital
MIS	metal–insulator–semiconductor
MNA	methyl-4-nitroaniline
MOS	metal–oxide–semiconductor
P	poise
<i>P</i>	polarization
PEEK	polyether ether ketone
PMMA	poly(methyl methacrylate)
PWB	printed wiring board
RAM	random access memory
RTV	room-temperature-vulcanizing
<i>S</i>	spin quantum number
SHG	second harmonic generation
SIC	silicon integrated circuit
<i>t</i> -BOC	poly(<i>tert</i> -butoxycarbonyloxystyrene)
<i>T</i>	absolute temperature
TAB	tape automated bonding
<i>T_g</i>	transition glass temperature

References

1. Thompson, L. F.; Bowden, M. J. In *Introduction to Microlithography*; Thompson, L. F.; Willson, C. G.; Bowden, M. J., Eds.; ACS Symposium Series 219; American Chemical Society: Washington, DC, 1983; p 15.
2. Bowden, M. J.; O'Donnell, J. H. In *Developments in Polymer Degradation-6*; Grassie, N., Ed.; Elsevier: New York, 1985; p 21.
3. Bowden, M. J. In *Materials for Microlithography*; Thompson, L. F.; Willson, C. G.; Frechet, J. M. T., Eds.; ACS Symposium Series 266; American Chemical Society: Washington, DC, 1984; p 39.
4. MacDonald, S. A.; Ito, H.; Willson, C. G. *Microelectron. Eng.* **1983**, *1*, 269.
5. Ito, H.; Willson, C. G. In *Polymers in Electronics*; Davidson, T., Ed.; ACS Symposium Series 242; American Chemical Society: Washington, DC, 1983; p 11.
6. Hatzakis, M.; Paraszczak, J.; Shaw, J. *Proceedings, International Conference on Microcircuit Engineering*; Lausanne, 1981; p 386.
7. Suzuki, M.; Saigo, K.; Gokan, H.; Ohnishi, Y. *J. Electrochem. Soc.* **1983**, *130*, 1962.
8. MacDonald, S. A.; Ito, H.; Willson, C. G. *Microelectron. Eng.* **1983**, *1*, 269.
9. Morita, K.; Tanaka, A.; Imamura, S.; Tamamura, T.; Kogure, O. *Jpn. J. Appl. Phys.* **1983**, *22*, L659.
10. Hofer, D. C.; Miller, R. D.; Willson, C. G. *Proc. SPIE* **1984**, *469*, 16.
11. Ziegler, J. M.; Harrah, L. A.; Johnson, A. W. *Proc. SPIE* **1984**, *469*, 166.

12. Nate, K.; Sugiyama, H.; Inove, T. *Electrochem. Soc. Extended Abstracts* 1984, 94(2), 778.
13. Reichmanis, E.; Smolinsky, G. *Proc. SPIE* 1984, 469, 38.
14. Wilkins, C. W.; Reichmanis, E.; Wolf, T. M.; Smith, B. C. *J. Vac. Sci. Technol.* 1985, 3(1), 306.
15. Gozdz, A. S.; Carnazza, C.; Bowden, M. J. *Proc. SPIE* 1986, 631, 2.
16. Gozdz, A. S.; Baker, G. L.; Klausner, C.; Bowden, M. J. *Proc. SPIE* 1987, 771, 18.
17. Rohde, O.; Riediker, M.; Schaffner, A.; Bateman, J. *Solid State Technol.* 1986, 29(9) 109.
18. Marshall, J.; Hullmann, J. *Semicond. Int.* 1985, 8(8), 170.
19. Wopschall, R. H. *Solid State Technol.* 1986, 29(6), 153.
20. Thompson, M. K.; Noble, P. W. *Proceedings, 4th International Conference on Plastics in Telecommunications*; Plastics and Rubber Institute: London, 1986; p 5-1.
21. Allison, J. F.; Chang, W. H.; Holdeman, L. B.; Smith, T. *Solid State Technol.* 1986, 29 (6), 169.
22. Walatka, V. V.; Labes, M. M.; Perlstein, J. H. *Phys. Rev. Lett.* 1973, 31, 1139.
23. Cowan, D. O.; Wlygul, F. M. *Chem. Eng. News* 1986, 64(29), 28.
24. Chiang, C. K.; Fincher, C. R.; Park, Y. W.; Heeger, A. J.; Shirakawa, H.; Louis, E. J.; Gau, S. C.; McDiarmid, A. G. *Phys. Rev. Lett.* 1977, 39, 1098.
25. Bredas, J. L.; Street, G. B. *Acc. Chem. Res.* 1985, 18, 309.
26. Kivelson, S. *Phys. Rev.* 1982, B25, 3798.
27. Baker, G. L.; Shelburne, J. A., III; Bates, F. S. *J. Am. Chem. Soc.* 1987, 108, 7377.
28. Thomann, H.; Baker, G. L. *J. Am. Chem. Soc.* 1987, 109, 1569.
29. Thomann, H.; Jin, H.; Baker, G. L. *Phys. Rev. Lett.* 1987, 59, 509.
30. *Chem. Eng. News* 1987, 65(25), 20.
31. Edwards, J. H.; Feast, W. J.; Bott, D. C. *Polymer* 1984, 25, 395.
32. (a) *Molecular Electronic Devices*; Carter, F. L., Ed.; New York: Marcel Dekker, 1982. (b) *Molecular Electronic Devices II*; Carter, F. L. Ed.; New York: Marcel Dekker, 1984.
33. Haddon, R. C.; Lamola, A. A. *Proc. Nat. Acad. Sci. USA* 1985, 82, 1874.
34. Chidsey, C. E. D.; Murray, R. W. *Science* 1986, 31, 25.
35. Munn, R. W. *Chem. Bri.* 1984, 20, 518.
36. Roberts, G. G. *Contemp. Phys.* 1984, 25(2), 109.
37. Barraud, A.; Rosilio, C.; Ruaudel-Teixier, A. *Solid State Technol.* 1979, 22(8), 120.
38. Roberts, G. G.; Petty, M. C.; Dharmadasa, I. M. *Proc. IEEE, Pt. 1, Solid State and Electron Devices* 1981, 128, 197.
39. Aloisio, C. J.; Blyler, L. L.; Chapin, J. T. *Proceedings, 4th International Conference on Plastics in Telecommunications*; Plastics and Rubber Institute: London, 1986, p 12-1.
40. Katayama, Y. *Ibid*, p 7-1.
41. Granestand, P.; Stoltz, B.; Thylen, L.; Bergvall, K.; Doldissen, W.; Heidrich, H.; Hoffman, D. *Electron. Lett.* 1986, 22, 816.
42. Chandross, E. A.; Pryde, C. A.; Tomlinson, W. J.; Weber, H. P. *Appl. Phys. Lett.* 1974, 24, 72.
43. Williams, D. G. *Angew Chem. Int. Ed. Eng. I* 1984, 23, 690.
44. Nicoud, J. F.; Twieg, R. J. In *Nonlinear Optical Properties of Organic Molecules and Crystals, Vol 1.*; Chmela, D. S.; Zyss, J., Eds.; Academic: 1987; p 227.
45. Barraud, A.; Vandevyver, M. *Ibid*, p 357.
46. Williams, D. J. *Ibid*, p 450.

47. Zyss, J. J. *Mol. Electron.* **1985**, *1*, 25.
48. Smith, P. W. *Bell Syst. Tech. J.* **1982**, *61* (8), 1975.
49. Ulrich, H. *Res. Dev.* **1985**, *27*, 82.
50. Thakur, M.; Meyler, S. *Macromolecules* **1985**, *18* (11), 2341.
51. Smith, T. W. *J. Vac. Sci. Technol.* **1981**, *18*(1), 100.
52. Croucher, M. D.; Hopper, M. A. *CHEMTECH* **1987**, *17*(7), 426.
53. Kharlamov, B. M.; Personov, R. I.; Bykovskaya, L. A. *Opt. Commun.* **1974**, *12*, 191.
54. Kryder, M. H.; Meiklejohn, W. H.; Skoda, R. E. *Proc. SPIE* **1983**, *420*, 236.
55. Haverkorn van Rijsewijk, H. C.; Legierse, P. E. J.; Thomas, G. E. *Philips Tech. Rev.* **1982**, *40*, 287.

RECEIVED for review June 29, 1987. ACCEPTED November 12, 1987.

Organic Resist Materials

C. Grant Willson¹ and Murrae J. Bowden²

¹IBM Almaden Research Center, San Jose, CA 95120

²Bell Communications Research, Red Bank, NJ 07701

Recent developments in applications of polymers as resists in microlithography are reviewed. Emphasis is placed on the advances in materials and processes associated with current photolithographic resists designed to extend the utility of photolithography into the submicrometer regime and to ensure continued dominance of photolithographic technology in commercial manufacture of integrated circuits.

ORGANIC IMAGING MATERIALS have undergone a period of rapid change in the past decade. Advances in organic and polymer chemistry and in innovative processing techniques have led to remarkable improvements in the resist materials and processes available for microlithographic applications. This area of research is expanding at an ever-increasing pace and has become the focus of groups working in academic laboratories as well as those of the microelectronics and chemical industries throughout the world. Several excellent reviews of this topic have been published (1–3). The goal of this chapter is to highlight important developments that have occurred in the resist area in recent years and to provide some insight into the trends of current research activities.

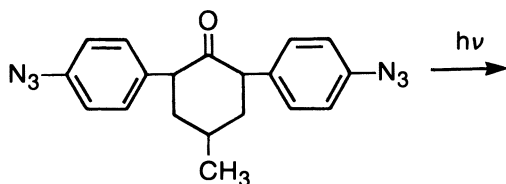
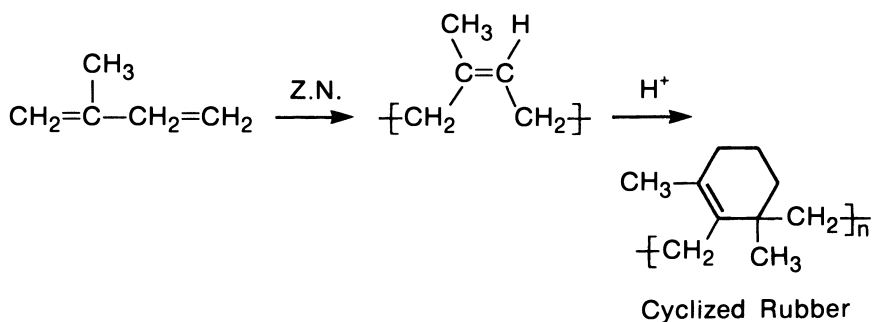
2.1 Diazoquinone–Novolac Resists

During the early years of the microelectronics industry, the imaging process used to define the layers of patterned conductor, insulator, and semiconductor materials that constitute active devices was accomplished by using contact printing in conjunction with resists based on photo-induced cross-linking to generate differential solubility. The resolution of the processes in

0065–2393/88/0218–0075\$09.50/0
© 1988 American Chemical Society

use at that time was limited by the ability to control mask-to-wafer separation and the pervasive use of isotropic, wet etching techniques. The resist materials that found widest acceptance were based on bisazide sensitization of partially cyclized synthetic rubber (1, 2) (Chart 2.1). As the industry migrated from contact (or proximity) printing to projection printing and started to introduce anisotropic etching technology based on reactive ion etching (RIE), the limit to resolution became more and more an issue of the resist material itself. The relatively low contrast of the bisazide-rubber resists; their propensity for swelling during development; and their relatively poor resistance to plasma-based, anisotropic etching processes led to the introduction of positive resist chemistry that is in pervasive use today.

The microelectronics manufacturing process is at present operating at a resolution of 1 μm that allows efficient production of, for example, 1-



Bis-arylazide

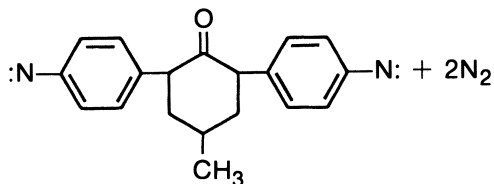


Chart 2.1. The negative-tone resists that were first used in semiconductor manufacturing were based on a matrix resin of synthetic rubber prepared by Ziegler-Natta polymerization of isoprene followed by acid-catalyzed cyclization to improve the mechanical properties. This cyclized rubber was rendered photosensitive by addition of a bisarylazide that undergoes photolysis to produce a bisnitrene. The nitrene reacts with the cyclized rubber to create intermolecular cross-links that render the exposed areas insoluble.

megabit dynamic access random memories (DRAMs), and is rapidly moving toward production of 4-megabit DRAMs with submicrometer design rules (4) (Figure 2.1). All of the semiconductor device fabrication lines have evolved toward the combination of projection printing in positive resists and plasma-based, anisotropic etching techniques. The resist materials that support this technology are all versions of the diazonaphthoquinone-sensitized novolac resin system (DQN) first introduced by the Kalle Co. many years ago (Chart 2.2). These materials (1–3) are positive in tone and provide both higher resolution and greater etch resistance to plasma-based etching processes than the bisazide–rubber resists. The improved etch resistance is a manifestation of the aromatic character of the novolac matrix resin (5–8) as compared to the aliphatic nature of the cyclized rubber materials. The improved resolution exhibited by the positive DQN materials relative to the negative bisazide–rubber resists results from their superior contrast and the fact that the development process does not cause swelling of the unexposed areas of the resist film.

The DQN resist system is able to resolve images much smaller than 0.5 μm . Thus, the resists available today are not the limiting factor in defining device dimensions. In fact, the resolution limit that can be reached in a manufacturing environment is limited not by the intrinsic properties of the resist materials available but by the physical limitations of the exposure equipment and by practical issues that include contamination control, level-to-level alignment capability, etc. Consequently, resist materials research has been, and will continue to be, focused on devising material approaches to extending the resolution limits imposed by the physics of the available exposure equipment.

The factors that contribute to limit resolution in projection optics are well known (2) and are manifested in the form of a degradation in the “free space” image as the exposure systems are operated near their diffraction limit. To some extent, this lens-generated degradation of image quality can be compensated by designing resist systems with a nonlinear dissolution response to dose.

Many positive resist materials, such as poly(methyl methacrylate) (PMMA) have linear dissolution kinetics. The rate of change in thickness of such materials as a function of time in the developing solvent is constant with respect to depth into the film. This rate is directly proportional to the exposure and increases with increasing dose. Properly formulated DQN resists can exhibit highly nonlinear dissolution kinetics such that the dissolution rate in the surface regions of the film is substantially lower than it is in the bulk of the film. The consequence of this nonlinear rate function is improved contrast (Figure 2.2). Nonlinear dissolution kinetics is achieved by proper choice of the monomer composition of the novolac (9), the polydispersity of the resin, and the processing conditions. Examination of Figure 2.2 shows that the nonlinear materials exhibit a greatly reduced

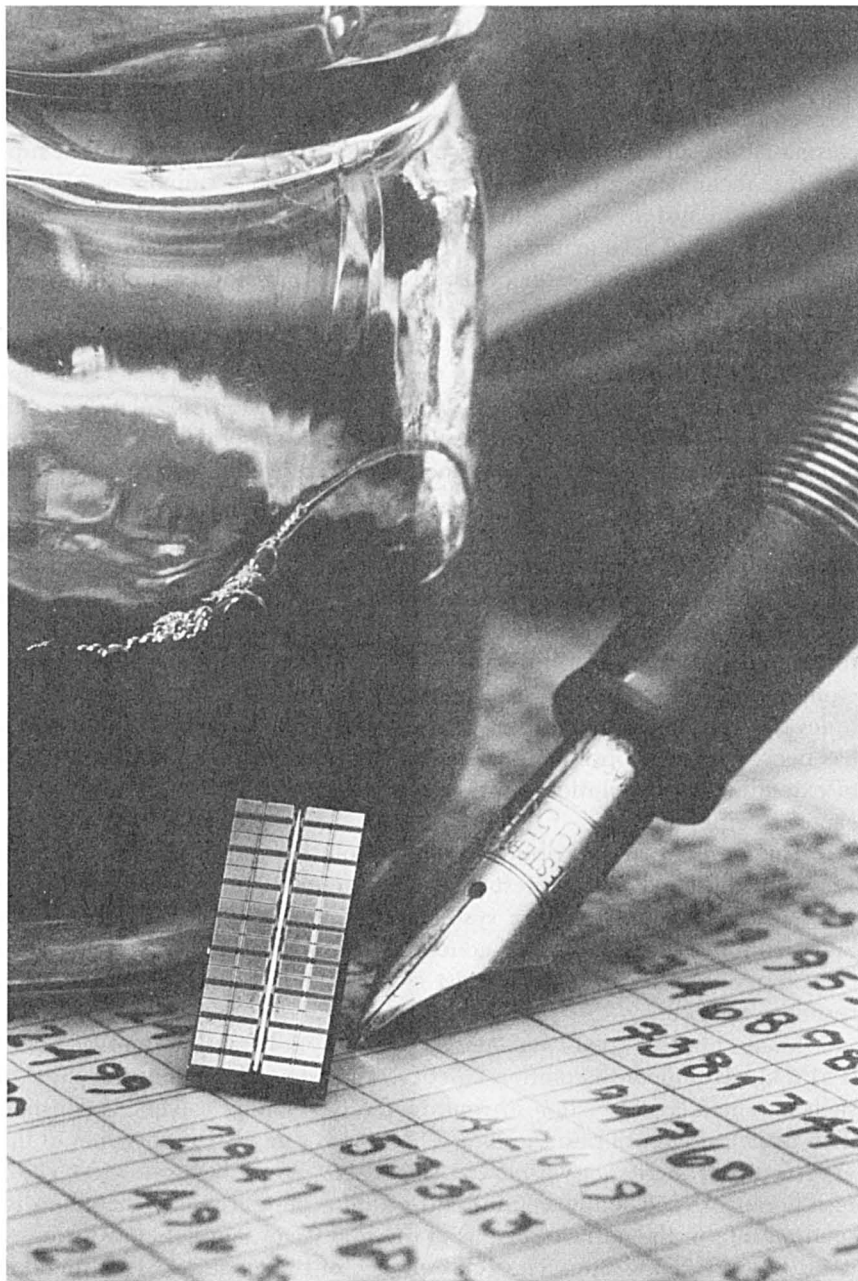


Figure 2.1. IBM's 4-megabit DRAM is a retrograde n-well CMOS device with 0.8- μm minimum features. The access time of this chip is 65 ns, and the chip size is 78 mm².

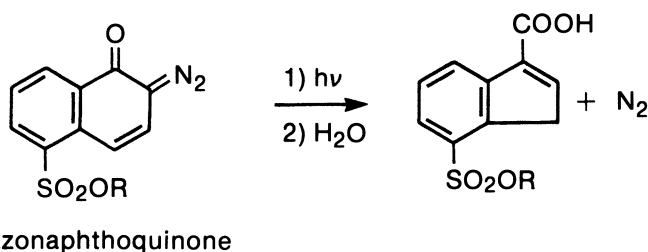
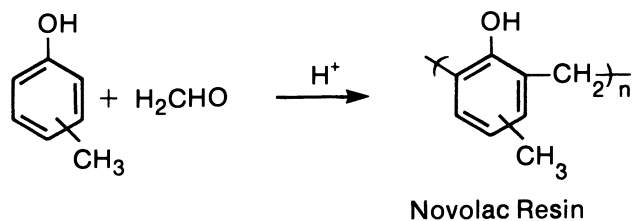


Chart 2.2. This DQN system employs a cresol-formaldehyde novolac resin as the matrix material. The resin is rendered photosensitive by addition of a diazonaphthoquinone that undergoes photolysis to produce a ketene intermediate that rapidly reacts with water present in the resin to yield an indenecarboxylic acid. The lipophilic diazoquinone serves to reduce the solubility of novolac films in aqueous base. Photolysis leads to production of an acidic photoproduct that renders exposed areas of the film soluble in aqueous base. Hence, this system functions as a positive resist.

dissolution rate of the unexposed film compared with that of linear materials with the same photospeed. The reduced attack on the unexposed resist represents an improvement in contrast.

Resist contrast in DQN systems is also determined to some extent by the structure of the diazonaphthoquinone sensitizer. According to published reports (10), the use of diazoquinone structures bearing multiple chromophores on a single molecule provides higher contrast resist formulations than formulations based on diazoquinones with fewer chromophores per molecule. Presumably, some threshold number of chromophores must be photoconverted to acid to render the multifunctional molecules soluble in base. Hence, the dissolution rate response to dose of resist formulated from multifunctional diazoquinones should be nonlinear. This argument assumes that the major contribution to the change in dissolution rate in DQN systems is the change in polarity or base solubility associated with conversion of the diazoquinone into the corresponding indenecarboxylic acid.

There are conflicting reports on this mechanism. One group compared the dissolution rate of DQN systems in which the diazoquinone was photolytically converted to the corresponding acid to that of resists formulated

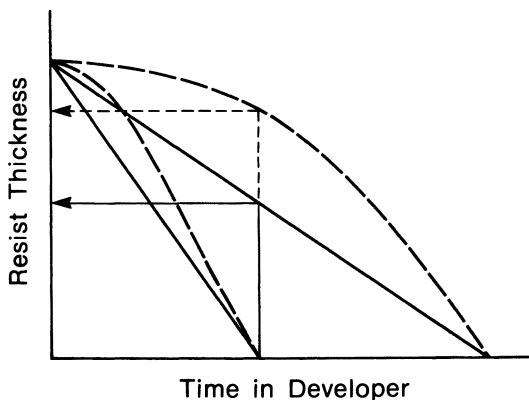


Figure 2.2. This plot depicts the time evolution of the development process for two resist films with identical starting thickness and identical overall development rates. The nonlinear system (dashed lines) has approximately 80% of the unexposed film remaining at the time when the exposed film is developed to the substrate. The linear system (solid lines) has only approximately 50% of the unexposed film remaining at the time when the exposed film is developed to the substrate. This difference in the extent of unexposed film loss represents a difference in contrast. The nonlinear system has higher contrast than the linear system.

from novolac and the pure acid photoproduct (11). The result was much higher rates for films in which the acid was photogenerated, leading to the conclusion that nitrogen evolution, which is a byproduct of the photolysis of the diazoquinone, is a major contributor to photogenerated changes in dissolution rate in these systems. Presumably, the nitrogen evolved upon photolysis causes an increase in free volume that is known to have a profound effect on the dissolution rate of polymer films (12). Another group studying a closely related system reported conflicting results, which led to the conclusion that the polarity change was the overriding contributor to the photo-induced changes in dissolution rate (13). Further experimentation is required to resolve this controversy, but the ability to formulate positive resist materials that have a thresholdlike nonlinear response to dose is a valuable skill that resist chemists use to improve the resolution and latitude of the imaging process.

2.2 Image Reversal

The chemistry of the DQN materials has been modified such that they function as a high-resolution, high-contrast, negative-tone resist system that is as devoid of distortion due to swelling as the standard, positive DQN system (14, 15). This tone reversal of the DQN system is accomplished by addition of an appropriate base to the formulation.

The first step in the image-reversal process (Figure 2.3) is patterned exposure. During this exposure, a latent image of photogenerated indene-

carboxylic acid is produced. When the exposed film is treated with base and baked to a temperature above $\sim 76^\circ\text{C}$, base-catalyzed decarboxylation of the indenecarboxylic acid occurs, and a latent image of an indene derivative is produced. The indene derivative also functions as a dissolution inhibitor but is not photosensitive. The next process step is a flood exposure that converts the diazoquinone in previously unexposed regions of the film into the corresponding indenecarboxylic acid, thereby rendering these regions more soluble in aqueous base than the patterned regions in which the diazoquinone has been converted into the indene derivative.

The base required for catalysis of the decarboxylation can be added to the formulation prior to spin coating of the resist or can be added after coating and patterned exposure. Addition after exposure is accomplished by immersing the exposed film in an atmosphere of a volatile base such as ammonia or an alkylamine. When most bases are added to the DQN resist formulation, a slow degradation in the resulting mixture occurs. The for-

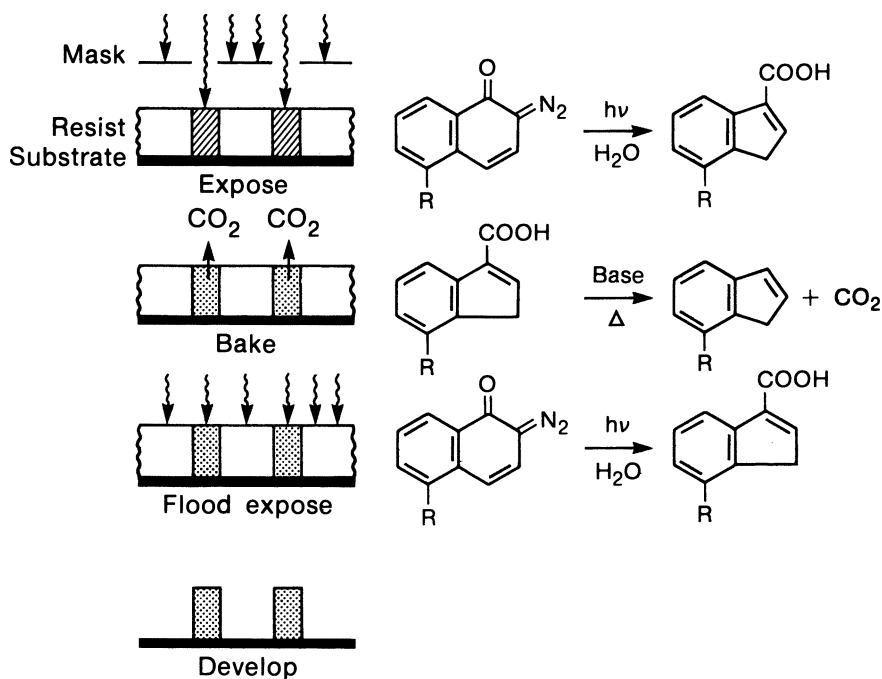


Figure 2.3. The base-catalyzed image-reversal process involves a patternwise exposure that converts the diazoquinone to the corresponding indenecarboxylic acid, followed by a bake step that causes base-catalyzed decarboxylation that produces the nonphotosensitive indene derivative. Subsequent flood exposure converts the diazoquinone in the previously unexposed areas of the film into the indenecarboxylic acid. Development then yields a negative image of the mask because the originally patterned areas containing the lipophilic indene derivative are less soluble in base than those containing the acidic photoproduct.

mulation undergoes spectral changes, and the viscosity increases with time. This shelf-life problem has led to a preference, in many cases, for the gaseous amine postexposure treatment process.

Because the latent image produced in the resist film during patterned exposure has a positive wall slope angle (Figure 2.4), the developed image following reversal can have walls with a positive, vertical, or negative slope depending on the processing and developing conditions. The positive wall slope stems from the fact that the top of the insolubilized area determines the line width in the negative mode, whereas the foot of the resist structure determines the width of the image in the positive mode. The ability to generate vertical wall profiles has important implications for imaging over topographical features, which will be discussed in Section 2.6. The undercut, or negatively sloped resist images, are particularly useful as stencils for additive (lift-off) metallization (15).

2.3 Contrast Enhancement

Attempts to compensate for the limitations of the projection lens systems currently available have led to some other very interesting innovations including contrast-enhancement materials. These materials are, in essence, dyes that absorb strongly at the exposure wavelength and undergo efficient photoconversion to products that are transparent at the exposure wavelength. The dyes are spin coated, in an appropriate vehicle, over the photoresist prior to exposure. Upon exposure, the dyed layer is bleached. This step enables the underlying photoresist to be exposed in a dynamic process. Because the dyes bleach most rapidly in areas of high intensity, the center areas of exposed lines bleach more rapidly than the edges; thus, the sloping, low-contrast character of the edges of the free space image are compensated for (Figures 2.5 and 2.6). The dyes that are used for contrast-enhancing materials range from the nitrones (16) to various diazonium salts (17, 18) and

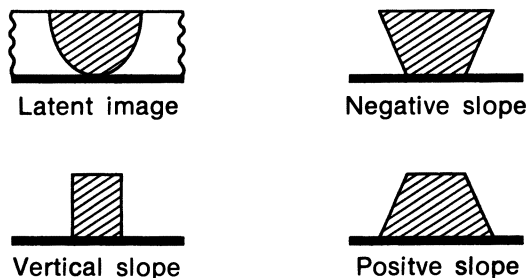


Figure 2.4. The latent image in the resist has essentially the shape indicated because of the sloping nature of the free space image and the absorption of the resist film. Depending on the processing conditions, either negatively sloped (undercut profiles) vertical profiles or positively sloped profiles can be obtained.

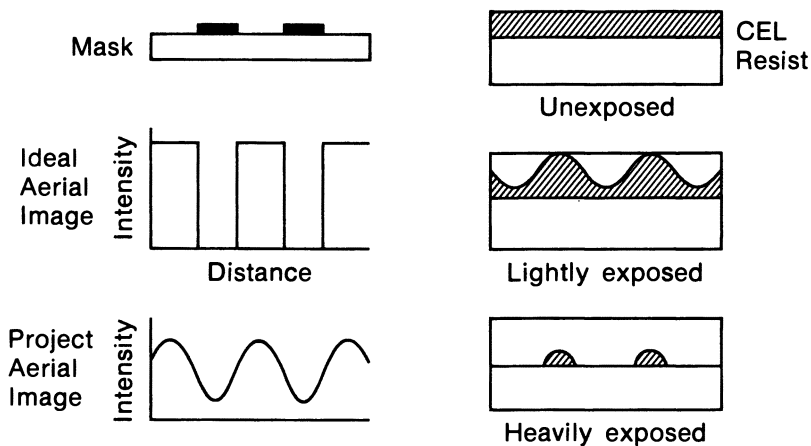


Figure 2.5. The intensity function or aerial image of a mask is ideally a square wave. However, projection optics operating near their diffraction limit degrade this square wave into a sinusoid with a small direct current (dc) term. When this intensity function is imposed on the contrast-enhancement lithographic material, bleaching occurs most rapidly in the high-intensity areas such that the transmitted intensity function that exposes the resist is modified and thus leads to improved contrast.

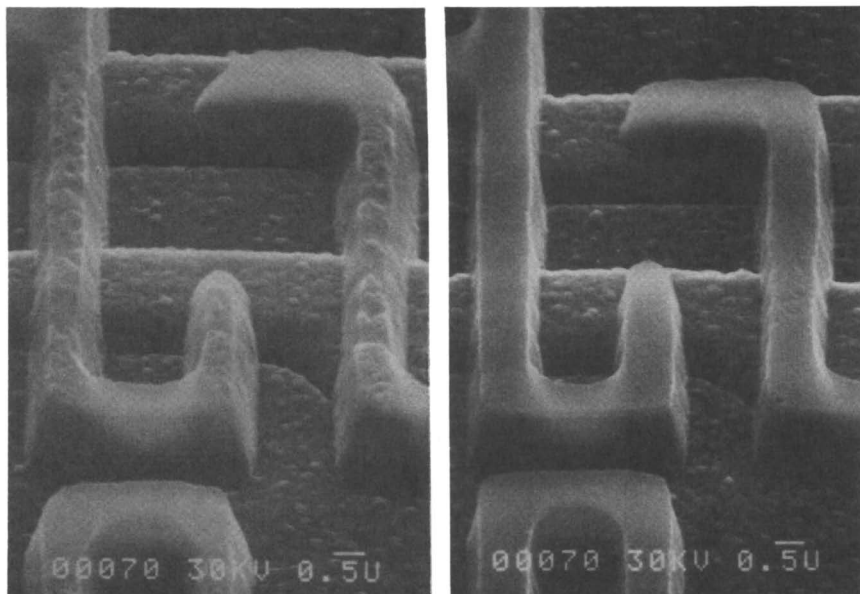


Figure 2.6. SEM images of 0.8- μm lines and spaces printed with (right) and without (left) contrast-enhancement lithography. (Courtesy of Cliff Takemoto of National Semiconductor.)

polysilanes (19) (Chart 2.3). Contrast-enhancement lithography unquestionably improves the resolution limit of a given lens system. The extent of resolution improvement is a complex function of the properties of the dye, the thickness of the dye layer, and the characteristics of the underlying photoresist. In general, the improvement in resolution is achieved at the expense of lower productivity (throughput). Hence, the process allows a trade to be made between resolution and throughput (20).

Another interesting use of a dye layer to improve the resolution limit of a lens system is found in the built-on mask (BOM) process (21). The BOM material is coated over the photoresist prior to exposure in a manner analogous to the contrast-enhancing material. The BOM material is, in essence, photochromic in that exposure at one wavelength generates a photoproduct that is transparent at the exposure wavelength but absorbs strongly in a different spectral region at which the photoresist is sensitive. The other important characteristic of the dye is that it can be "fixed", or rendered

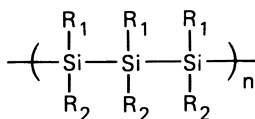
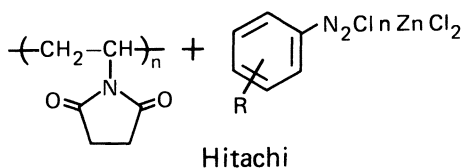
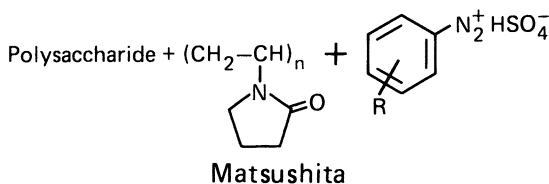
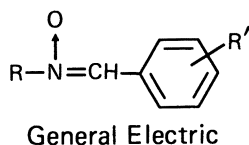


Chart 2.3. Various dyes used as contrast-enhancement materials. The polysilanes are useful in the mid-UV region (308–313 nm); the other materials are designed for use in the near-UV region (365–436 nm).

insensitive to exposure. Imines have been used as the chromophore for the BOM process, and perhalohydrocarbons such as CBr_4 have been used as a source of photogenerated acid. The imine absorbs strongly at 365 nm but not at 436 nm, and the protonated form, the iminium salt, behaves in the reverse (i.e., it absorbs strongly at 436 nm but not at 365 nm). Hence, exposure to essentially any wavelength at which the perhalohydrocarbon absorbs produces patterned areas of local acid concentration that lead to iminium salt formation, thereby rendering these areas opaque at 436 nm. The films are then baked to volatilize unexposed CBr_4 in the fixing process; thus, the films are rendered insensitive to subsequent exposure. This process photochemically generates a "built-on mask" in perfect contact with the resist for contact printing at 365 nm. Subsequent flood exposure at 365 nm followed by development leads to a positive-tone image of the mask (Figures 2.7 and 2.8). Adaptations of this interesting technique to X-ray exposure and to generation of negative-tone images have been discussed (21).

2.4 Deep-UV Resists

For a given lens system operating at a specified wavelength, the contrast-enhancement lithography or BOM techniques represent chemists' contributions to improvement in useful or functional resolution. The functional resolution of a given lens system can also be improved by reducing the exposure wavelength because resolution is directly proportional to the exposure wavelength and inversely proportional to the numerical aperture. Exposure tools based on all-reflecting optics such as the Perkin-Elmer Miralign 600HT are not subject to chromatic aberration distortion of the free space image. Hence, the resolution of such systems can be substantially improved by reduction of the exposure wavelength. The usual exposure wavelength for DQN resists is in the region of 405–436 nm. Materials have now been tailored to allow efficient exposure at 300–350 nm (22) and thus provide improved resolution for exposure tools such as the Miralign 600HT that can provide variable wavelength exposure.

Attempts to tailor DQN materials to still shorter, deep-UV (DUV) wavelengths (near 250 nm) have been largely unsuccessful because of the strong absorbance of the novolac resins and the extremely weak DUV output of standard, high-pressure, mercury arc lamps of the sort used in today's exposure tools. Some interesting approaches have been made toward tailoring the optical properties of both the resin and the sensitizer materials for DUV exposure. A system based on base-soluble acrylic resins that are transparent in the DUV, in combination with *o*-nitrobenzyl esters of lipophilic carboxylic acids that undergo photolysis to produce carboxylic acids, has been described (23) (Chart 2.4). These materials are reported to have sensitivity comparable to the DQN systems and remarkably high contrast. However, the aliphatic

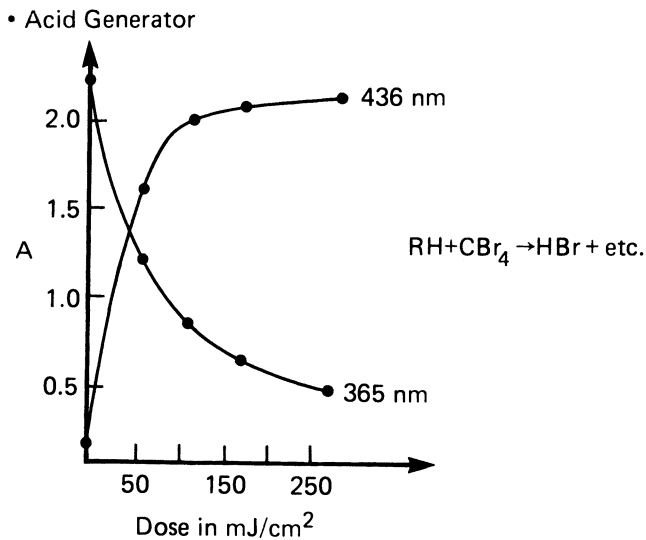
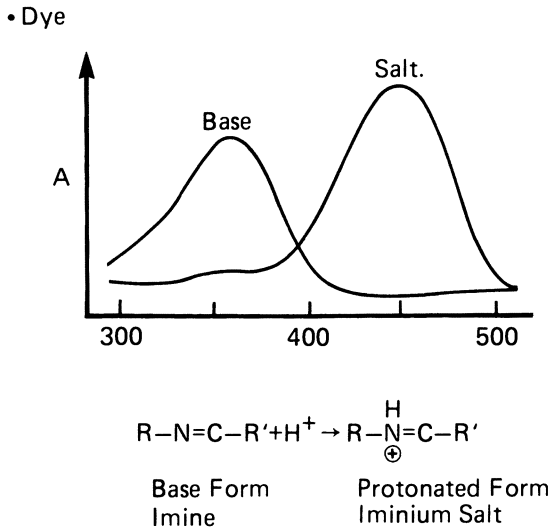


Figure 2.7. The materials used for the BOM process. Exposure at 365 nm produces acid derived from CBr_4 . This photogenerated acid protonates the imine dye, which causes a dramatic bathochromic shift in the absorbance. As exposure proceeds, the absorbance at 365 nm is bleached and the absorbance at 436 nm increases because of iminium salt formation.

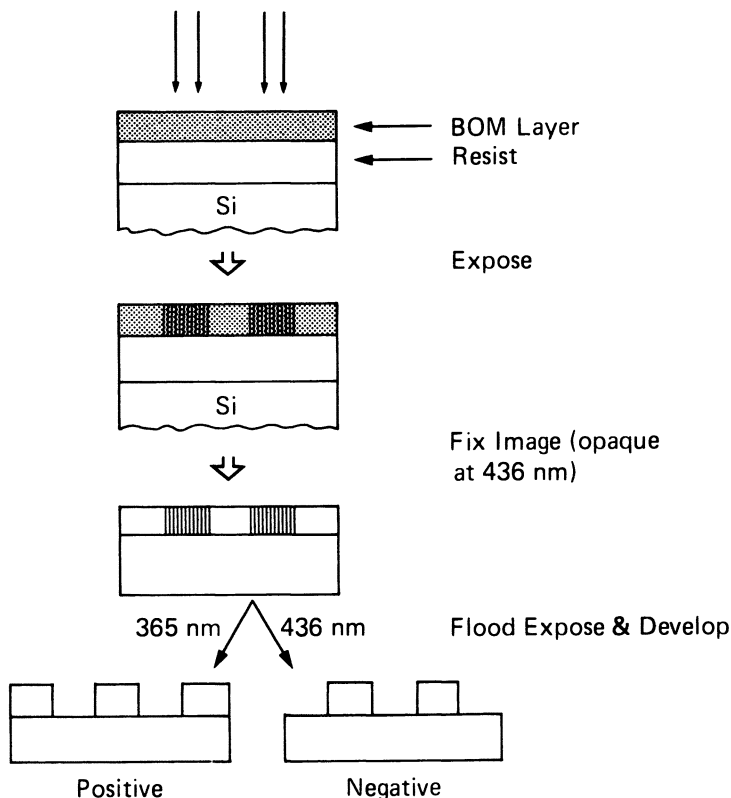


Figure 2.8. The BOM process.

nature of the acrylic matrix resin materials leads to resists that have less etch resistance in plasma environments than the DQN systems.

The synthesis and characterization of a novel class of diazoketones that function in a manner analogous to the diazoquinones but have bleachable absorbance maxima in the DUV region have been described (Figure 2.9). These systems are reported to function with photosensitivity comparable to that of the DQN systems, but their utility still appears to be limited by the fact that they are employed in conjunction with a novolac resin, which has a substantial, unbleachable absorbance in the DUV region. This undesirable resin absorbance leads to reduced contrast (24, 25).

2.5 Chemical Amplification

Although the tailored sensitizers and resins presumably improve DUV performance, systems based on the DQN design have a sensitivity limit imposed by the quantum efficiency of the sensitizer to photoproduct conversion that

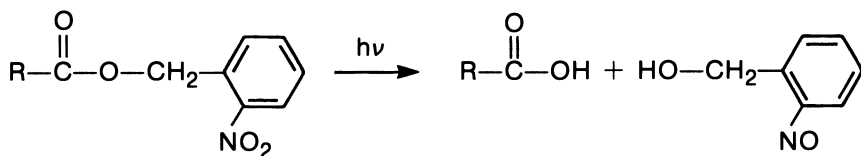
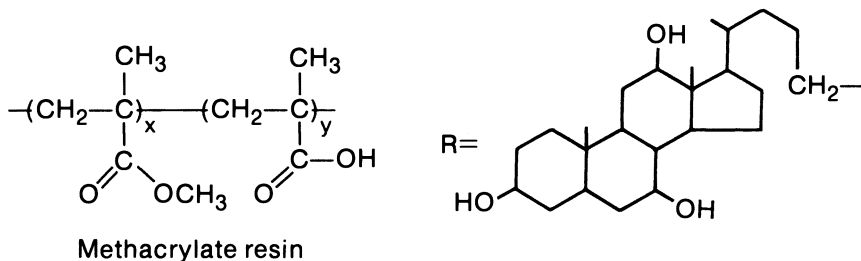


Chart 2.4. The o-nitrobenzylcholate DUV resist system uses a copolymer of methyl methacrylate and methacrylic acid as the base-soluble matrix resin. This resin is rendered photosensitive by addition of the o-nitrobenzyl ester of cholic acid. Upon exposure, the ester is photolyzed to yield cholic acid and an o-nitrosobenzyl alcohol. The system functions in a manner analogous to the DQN system and is positive in tone.

is simply too low for practical use in current DUV projection aligners. These tools are based on mercury lamp light sources, and the DUV power that these systems can deliver at the wafer plane is almost 2 orders of magnitude lower than that available in the near-UV range (Figure 2.10). Consequently, although resolution may be extended by DUV exposure of such resist systems, the productivity loss is intolerable.

New DUV resist materials with greatly enhanced sensitivity seem to offer the possibility of providing useful productivity in the DUV region. These systems are based on *chemical amplification* (26), wherein a single photoevent generates a catalytic species that acts on the matrix resin material to alter its solubility in some subsequent process step. Orders-of-magnitude improvement in sensitivity apparently can be realized with systems based on this sort of design without significant loss of resolution. Several examples of resist materials that function on the basis of chemical amplification are described in detail in Chapter 3. The material problems and the advances that have been made in resists for DUV lithography are also detailed in Chapter 3. However, regardless of the exposure wavelength, several important factors limit resolution in the practical application of microlithography to device fabrication. These factors warrant discussion and have been the focus of an interesting body of materials research.

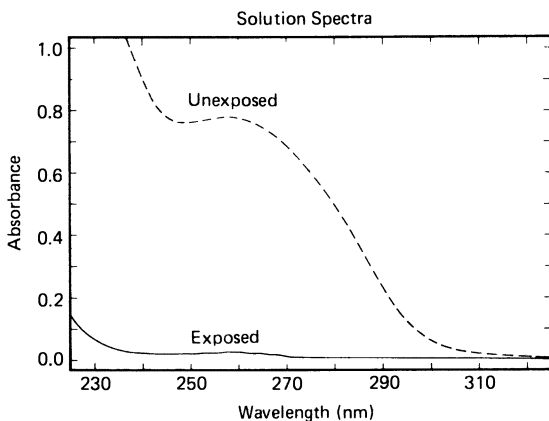
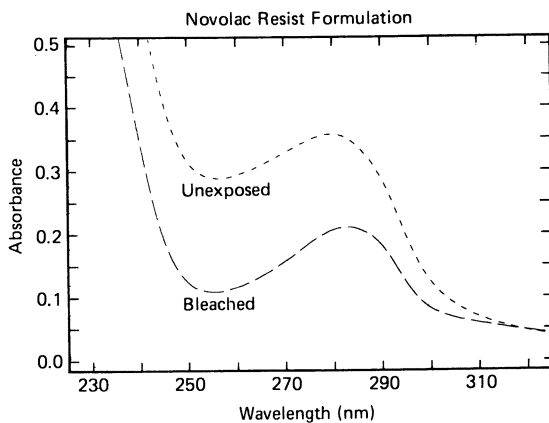
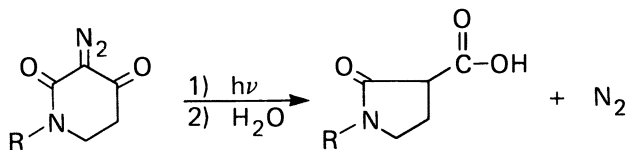


Figure 2.9. The N-alkyldiazopiperidinedione structure is typical of the 1,3-diacyl-2-diazo compounds studied at IBM. Photolysis produces a carboxylic acid analogous to the chemistry of diazonaphthoquinones. These materials absorb strongly in the DUV region, but bleach completely as indicated in the spectra of a methanolic solution (bottom). Resists formulated from these materials in novolac show residual unbleachable absorbance due to the resin as shown in the spectra of thin films (top).

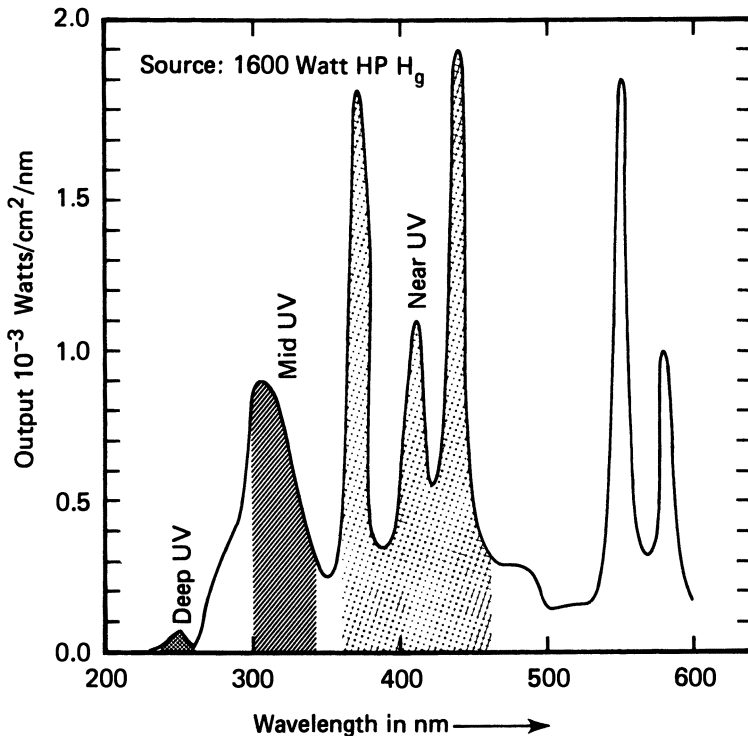


Figure 2.10. This plot shows the flux at the wafer plane as a function of wavelength for the Perkin-Elmer Micralign 500. The ratio of the flux available in the DUV (UV-2) region compared to that in the near-UV (UV-4) region is approximately the ratio of the indicated areas under this curve.

2.6 Multilevel Resist Processes

Chief among the contributions to resolution limitations other than lens-related physics is the contribution of the structure upon which the image must be printed. Resolution is generally considered in terms of only two dimensions. Yet, unlike the photographic processes, the goal of the micro-lithographic process is to generate three-dimensional relief images of the mask pattern. The impact of this third dimension limits the practical resolution limit. Typical device structures are not planar. They have local topographic features that approach the desired line widths in vertical extent (Figure 2.11). The influence of these topographic features on patterning of subsequent layers is very significant and can be divided into two areas:

1. resist thickness modulation, and
2. modulation of light.

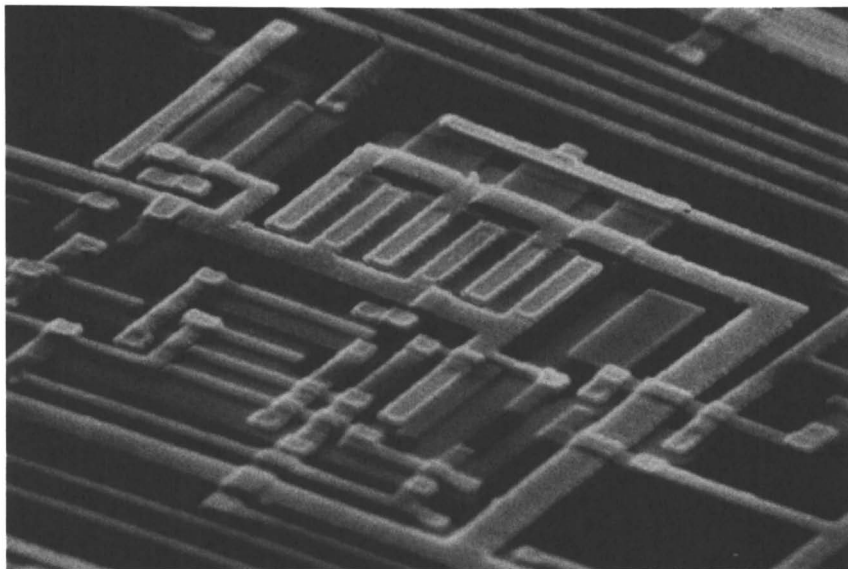


Figure 2.11. Scanning electron micrograph of an active device after defining the conductor pattern. The extent of the topography is evident. (Courtesy of H.E. Luhn of IBM).

Resist films that are spin-coated over topographic features have a tendency to planarize or smooth out the bumps. The extent to which this occurs is never perfect and depends on both substrate and resist material parameters (27). Two types of planarization influence resolution:

1. *local planarization*, or the extent to which closely spaced or regular features are planarized, and
2. *global planarization*, which represents the extent to which pattern density over a larger area affects the nominal resist thickness.

Local planarization is achieved far more easily than global planarization, but both contribute to resolution loss.

The loss in resolution that attends imaging of resists coated over topographic features results from the requirement to generate three-dimensional relief structures (trenches) in varying thicknesses of material. Only when development can be controlled such that it produces images with absolutely vertical side walls can the images in both the thick and the thin areas be developed to proper dimensions. If the profiles are not vertical, the time required to develop an image to the proper dimension at the substrate in a thin area is insufficient to develop an image to the substrate

in the thick area. Conversely, when the development time is extended until the desired dimension is achieved in the thick area, the thin area will be overdeveloped to give lines that are too wide. The geometry of this problem is easily quantified (Figure 2.12). Unfortunately, a combination of factors make it very difficult to achieve 90° wall profiles in projection-printed resist images. These factors include the sloping nature of the intensity function (free space image) and the necessity for some finite absorption in the resist layer.

The topographic features not only modulate the thickness of the resist coating but also contribute to local differences in light reflected from the resist-substrate interface. Light reflected from this interface has profound effects on resist exposure. These effects are particularly severe for step-and-repeat projection printing, where narrow bandwidth exposure is used to minimize chromatic aberrations in lens construction. Perhaps the most widely known effect is the production of *standing waves*, which cause regular indentations in the side wall of developed resist images (Figure 2.13). This phenomenon results from alternating constructive and destructive interference between the ray transmitted through the resist and that reflected from the substrate. Very subtle variations in thickness can render the resist film more or less reflective; thus, more or less power is coupled into the film as an alternating function of thickness. Topographic features also vary in material composition and therefore refractive index, further modifying the intensity of the reflected ray. In addition, light is scattered at odd angles from facets of the topography back through the photosensitive resist layer, producing an effect known as reflective notching. The combination of these phenomena produces large line width variations when attempts are made to pattern lines over steps of highly reflective materials such as metals and silicides (Figure 2.14).

One approach to minimize these problems is the image-reversal process described in Section 2.2 (28, 29). Another approach has been to increase the nonbleachable absorbance of the resist by adding a dye (30). This ap-

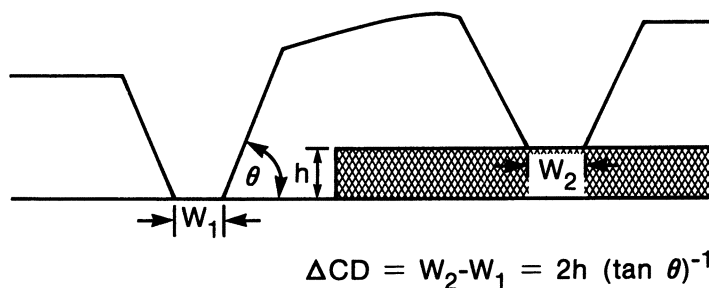


Figure 2.12. The difference in widths ($W_2 - W_1$) of a critical dimension (ΔCD) developed in a thick area of resist and in a thinner area is related to the resist wall angle (θ) and height (h) of the topographic feature.

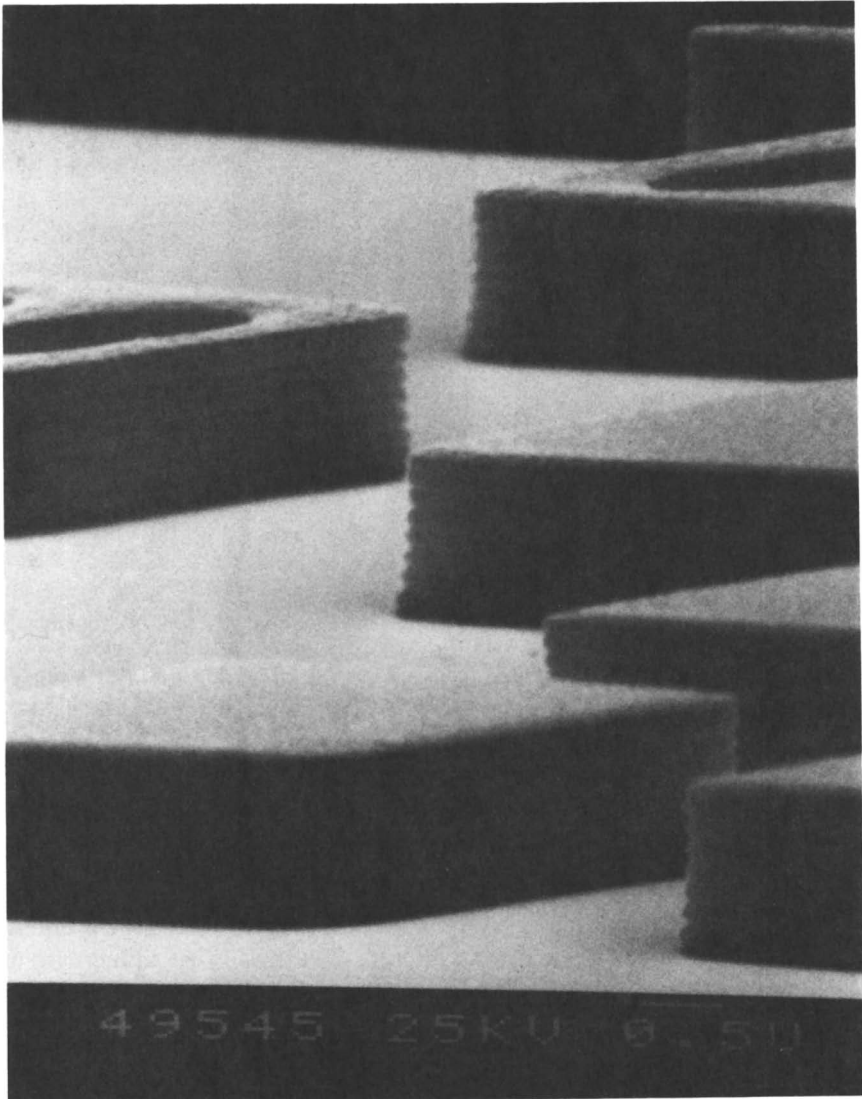


Figure 2.13. Scanning electron micrograph of images printed in a DQN resist by using narrow bandwidth (436 nm) light. The regular pattern of indentations on the side wall results from the standing wave interference of the light transmitted through the resist and that reflected from the resist-substrate interface.

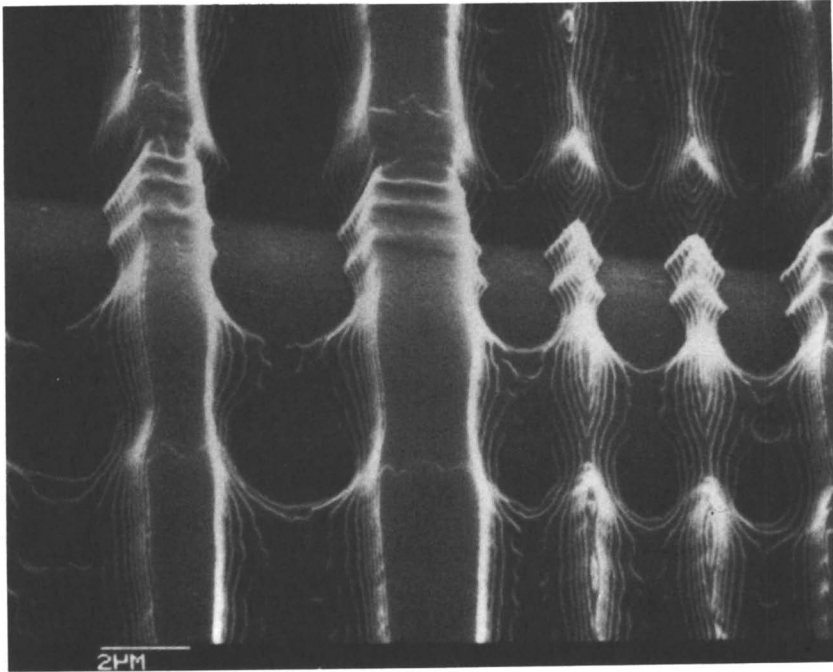


Figure 2.14. Scanning electron micrograph of resist lines passing over a step in the substrate. This figure shows the variations in line width caused by the topographic feature. (Reproduced from reference 3. Copyright 1984 American Chemical Society)

proach is reported to minimize distortions due to reflected light simply by reducing the transmitted intensity at the resist–substrate interface and by more rapidly attenuating what light is reflected back into the resist film. This approach should also reduce the standing wave effect. For example, Bolsen et al. (31) reported that use of a dyed resist provided a significant reduction in line width variation for 1- μm patterns printed over a grainy aluminum substrate. Simulation studies (24, 32) showed that an increase in the unbleachable absorbance of such a resist, such as that resulting from adding dye, results in a much higher exposure dose requirement for imaging, loss of side-wall control, and an increase in the variation in critical dimensions. Yet Bohland et al. (33) reported that addition of a dye actually improved resist profiles and resulted in improved line width control.

Such contradictory claims regarding the effectiveness of the dye in improving a line width control appear to reflect a complex interdependence of the various materials and processing parameters that is not adequately accounted for in the simulation programs. In general, dyed resists are believed to provide improved control of dimensions in lines printed over highly reflective substrates, and several vendors have made dyed resist formulations

commercially available. One aspect of the simulation studies, the prediction that a dyed resist will require much higher exposure doses for imaging, is certainly accurate. Adding dye to a resist is apparently not as effective in controlling line width variation as the multilayer resist processes that are becoming increasingly prevalent.

The simplest multilevel process involves the use of an antireflection coating (ARC) that is deposited over the substrate prior to coating the resist. Typical ARC materials are polyimide or polyamic acid formulations containing a dye (34–37). They function by absorbing the light that is transmitted through the resist film before it reaches the reflective substrate, thereby eliminating distortions caused by interference phenomena and diffuse reflections. Like contrast-enhancement lithography and BOM, the ARC technique is sometimes referred to as a quasimultilevel process because the resist structure consists of more than one layer, but only one image formation step is required. In contrast, true multilevel processes involve at least two coating steps and require an image-transfer step. Multilevel resist technology provides a generic solution to the topography problem (38). In the multilevel resist process, a relatively thick opaque layer is coated over the topographic features to attain maximum possible planarization, which in current technology is less than perfect (27). The resist is then coated on top of the planarizing layer and imaged. Unlike the single layer process, this top layer of resist is of nearly uniform thickness and can be quite thin, which facilitates high-resolution imaging. The resulting resist image is then transferred in some anisotropic process through the planarizing layer to yield high aspect ratio relief images with vertical walls. Because the walls of the images in the planarizing layer are vertical, the process is insensitive to variations in the coating thickness of the planarizing layer (Figure 2.15).

The practice of multilevel resist technology has evolved rapidly since its introduction in 1973 (39) largely through resist materials innovation. The first applications of this technology involved use of DQN-type resists over poly(methyl methacrylate) (PMMA) as the planarizing layer. The pattern was

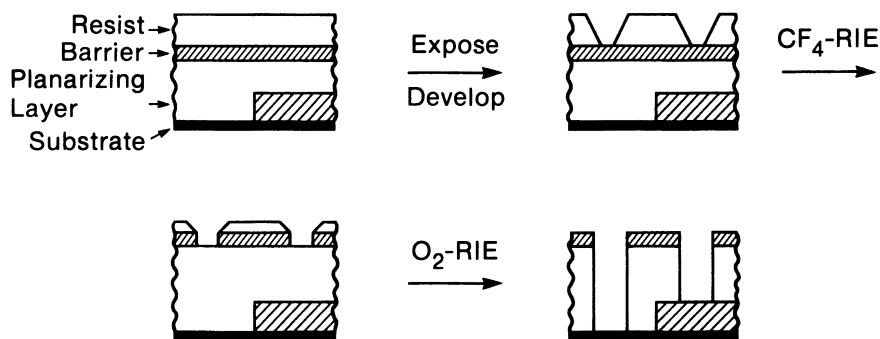


Figure 2.15. The trilayer process sequence.

first generated in the DQN resist that then served as a conformable contact mask for printing of the PMMA by DUV flood exposure (38–40). This approach has been improved by the availability of new photosensitive planarizing materials that have both higher thermal stability and improved processing characteristics (41). The optical influence of the topography on the primary patterning step has been eliminated by adding dyes to the planarizing material that are opaque at the wavelength used for exposure of the DQN resist (42, 43).

Perhaps the area of multilevel resist processing that has inspired the most innovative chemistry is that of oxygen RIE image transfer. In this process, the primary resist image is transferred through the underlying planarizing layer by anisotropic oxygen RIE. This process requires generation of an oxygen etch resistant pattern on the surface of the planarizing layer. Early versions of the process used an intervening layer of a barrier material sandwiched between the resist and the planarizing layer that was impervious to oxygen etching. Intermediate layer materials include “spin-on-glass”, which is typically a siloxane ladder polymer, SiO_2 , metal, Si_3N_4 , or any of a host of organometallic polymers. In this so-called trilayer process, the primary resist image is transferred through the barrier material by fluorocarbon RIE, for example. The pattern in the barrier material is then transferred through the planarizing layer by anisotropic oxygen RIE. The patterns that can be generated by such a process are truly impressive (Figure 2.16), but the process is complex and costly.

The trilayer process was significantly simplified by combining the properties of the barrier layer and the resist into a single material. This was accomplished by using radiation-sensitive organometallic polymers that incorporate an element such as silicon, which when exposed to oxygen plasma generates a nonvolatile, refractory oxide. Thus, when patterns of such a material are subjected to oxygen RIE, a thin coating of the oxide is rapidly generated on the surface of the resist that protects the underlying material from further attack from the plasma (Figure 2.17). The first example of a process based on such a material involved the use of polysiloxanes as the oxygen-RIE-resistant imaging layer (44, 45). The seminal work on the polysiloxanes led to a proliferation of materials with similar properties and a resurgence of interest in the radiation chemistry of organometallic polymers. Examples of such materials, sensitive to a range of wavelengths covering the far-UV, DUV, X-ray, and electron-beam radiation, now abound (44–48).

Further simplification of this process can be derived by metallization of the resist over a planarizing layer subsequent to the development of the primary image and prior to the oxygen RIE image-transfer step. This procedure has been accomplished by treatment of DQN resists with chlorosilanes (49) and by treatment of certain novel DUV resists with silylating agents (50, 51).

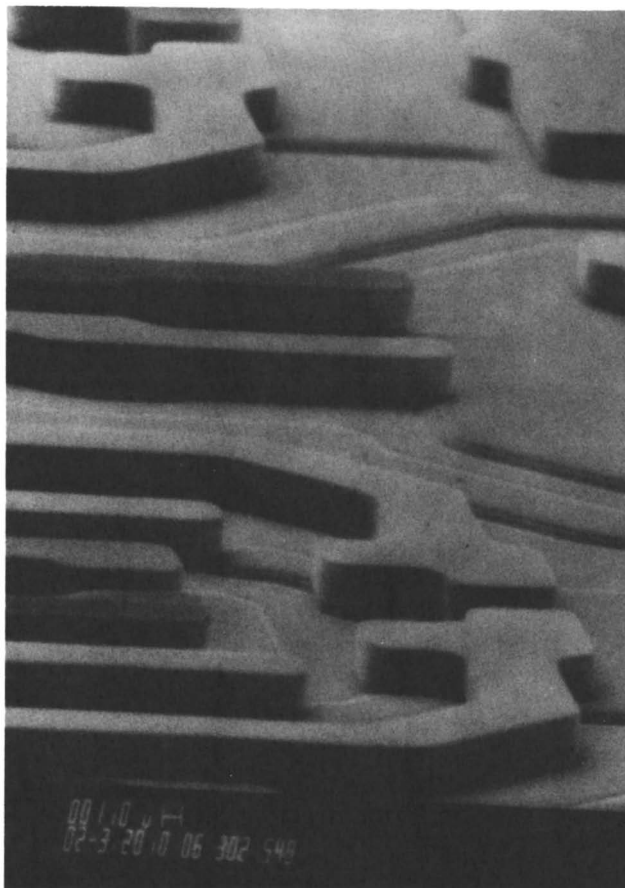


Figure 2.16. Scanning electron micrograph of resist images generated in a trilayer process. This figure shows the vertical walls and the absence of line width variations where the pattern crosses topographic features. (Reproduced from reference 3. Copyright 1984 American Chemical Society)

The most recent improvement or simplification of this process involves combining all of the layer functions into a single coating. This procedure is accomplished by coating a single layer of an appropriate resist material and then imaging the layer under exposure conditions at which it is opaque such that only a thin surface layer of the material undergoes photochemistry. In optical exposure, this step is accomplished by simply rendering the coating opaque at the exposure wavelength by addition of an appropriate dye. A similar shallow image can be generated under electron-beam exposure by using low-voltage electrons. The thin, surface-exposed region of the film is then rendered oxygen RIE resistant by a selective metallization process (50,

52, 53) (Figure 2.18). Subjecting the metallated pattern to oxygen RIE results in the desired, high aspect ratio, high-resolution pattern that is insensitive to underlying topography. These new materials and processes are quite interesting because they do not involve any wet development step; they can incorporate good RIE and thermal resistance through use of aromatic polymers; and they are insensitive to both the thickness and optical effects of topography, save some small contribution to focus error that remains due to imperfect global planarization. The availability of modern, high-speed, anisotropic, magnetron-enhanced oxygen RIE makes these materials and processes even more interesting.

The chemistry of the selective-surface metallization process has taken two paths. One approach (53) involves photo-induced local modifications in

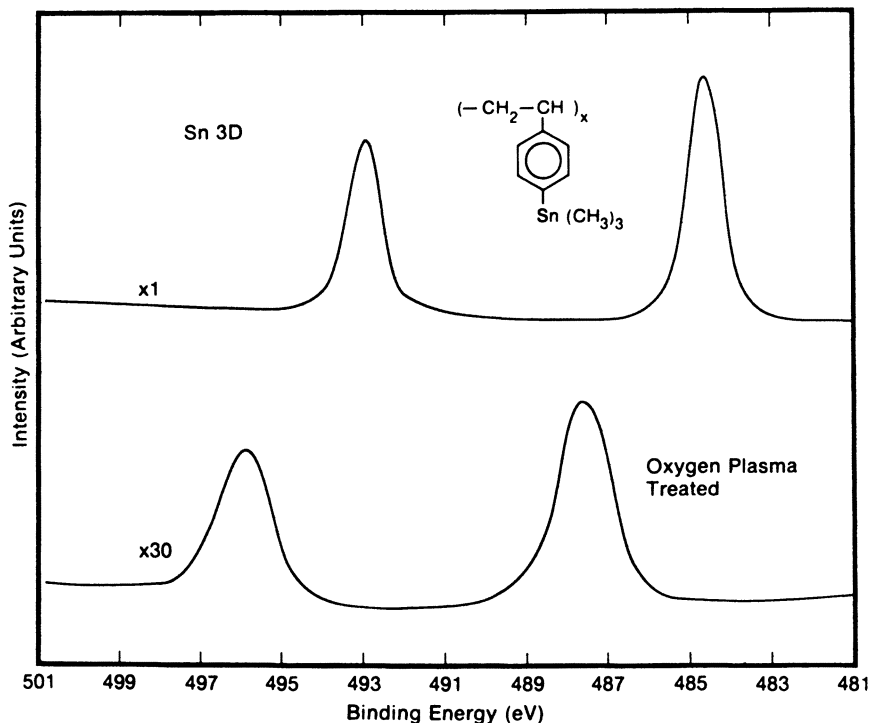


Figure 2.17. Electron spectroscopy for chemical analysis (ESCA) spectra of organometallic polymer films before and after exposure to oxygen plasma. The silicon 2p transition (page 99) is shifted from 99.7 to 102.4 eV. The magnitude of the shift is consistent with conversion to SiO_x , where x is between 1.5 and 2. The Sn 3d transitions of the organotin compound (above) undergo a similar shift (1.7 eV), consistent with generation of a SnO_x surface, where x is again between 1.5 and 2. Argon sputter etching followed by ESCA analysis indicates that these oxide films are less than 100 Å thick.

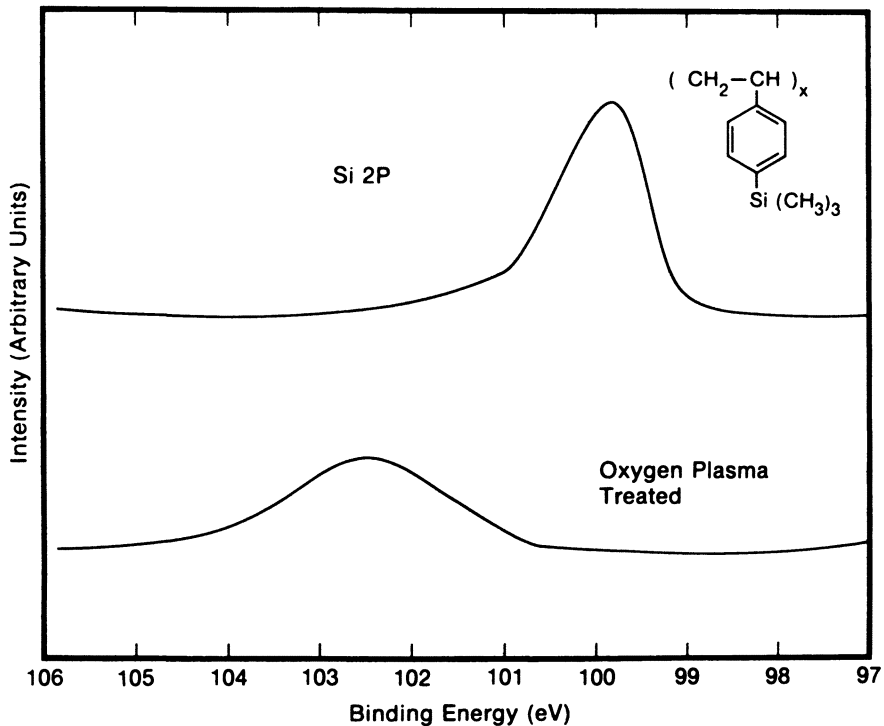


Figure 2.17.—Continued.

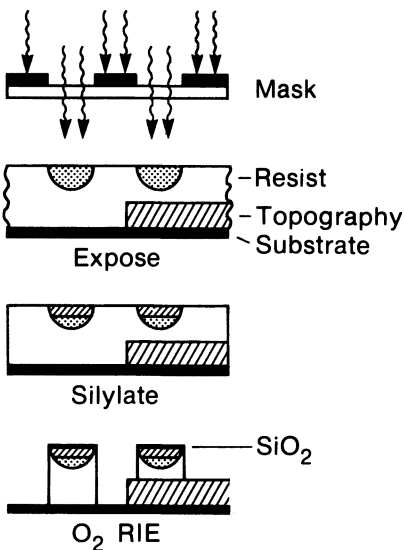


Figure 2.18. The surface-layer imaging process. Patternwise exposure results in radiochemical modification of only a thin surface layer of the resist (i.e., the resist film is opaque at the exposure wavelength). The surface area modified by exposure is then metalated with an appropriate organometallic reagent, and the resulting structure is dry developed by treatment with oxygen RIE.

the diffusion rate of an organometallic reagent. Exposure of these systems, reportedly based on DQN chemistry, renders the exposed areas more permeable to the organometallic reagent than the unexposed areas, and thereby allows area-selective metallization of the resist film. The photo-induced change in the diffusion rate presumably stems from the generation of free volume resulting from the nitrogen evolution that occurs upon exposure of the diazoquinone. The mechanism and kinetics of this reaction have been explored in some detail (54).

An alternative approach involves radiation-induced conversion of a non-reactive polymer into one that is highly reactive toward organometallic reagents (50, 52). This system includes the chemical amplification concept and can be processed either as a single-layer, dry-developed, surface-modified system or as a bilayer, dry-developed system. The chemistry reported is the same as that of the DUV resist system. It is based on radiochemical generation of a strong acid from an onium salt precursor. The radiochemically generated acid is then used as a catalyst in the thermolysis of a protected phenolic polymer (Figure 2.19). The deprotected phenolic moieties are readily converted to the phenyl ethers of organometallic compounds (e.g., by treatment with hexamethyldisilazane), whereas the protected precursors are inert toward reaction with these reagents (Figure 2.20). The kinetics and mechanism of this chemistry have been studied (51).

2.7 New Approaches

As the physics and engineering of high-resolution exposure equipment advances with the advent of excimer-laser-powered, DUV projection printers (55), synchrotron and laser-pulse-powered X-ray step-and-repeat aligners (56), advanced electron-beam exposure systems (57), and ion-beam patterning technology, resist chemists will continue to be challenged to provide new materials that do not limit either the resolution or productivity of these new exposure tools and are available in a timely fashion. Meeting this challenge will require continued innovation.

An interesting example of a capability, born recently from application of material research and pure innovation that awaits a practical implementation, is the generation of a third dimension in microlithographic patterning. Researchers (58) have demonstrated that doping a normal DQN resist with a melamine precursor allows controlled generation of a third dimension to patterning. Photodecomposition of the diazoquinone generates a local concentration of acid that, when heated prior to development, catalyzes carbonium-ion-mediated cross-linking of the novolac through the hydroxymethylmelamine. A combination of this chemistry with a mask having transparent, opaque, and gray pattern elements allows generation of remarkable three-level relief structures with cantilevered beams and bridges in a resist layer (Chart 2.5, Figures 2.21–2.23). The application of this new

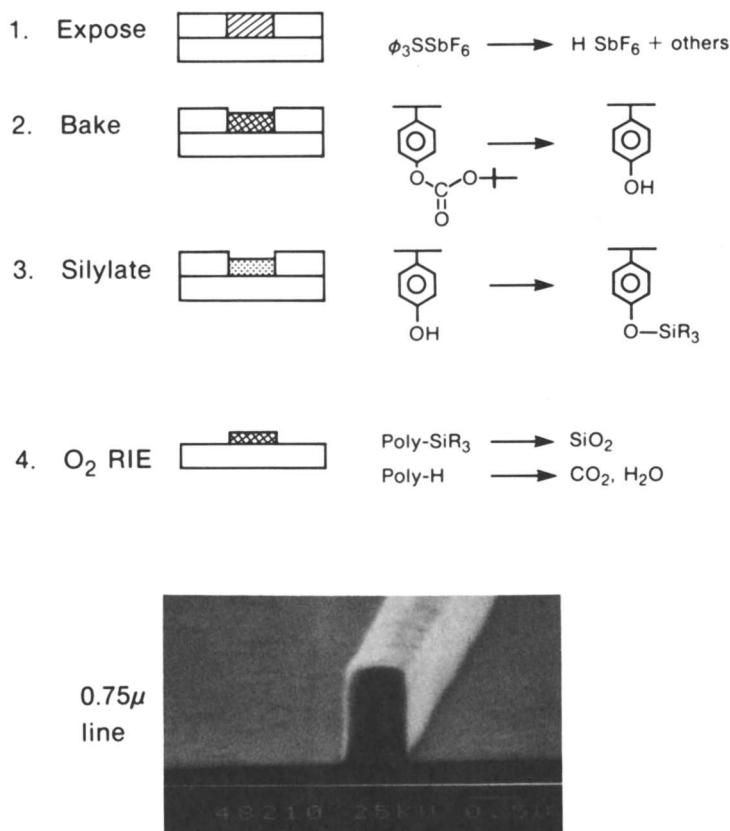


Figure 2.19. IBM's dry process. Exposure generates a latent image of strong acid that catalyzes thermolysis of the phenolic resin protected by poly(tert-butoxycarbonyloxystyrene) (t-BOC) in the exposed areas during a postexposure bake step. Subsequent treatment with a silylating reagent creates a pattern of high silicon content. Oxygen RIE efficiently removes the unexposed areas, but the thin film of SiO_x formed in the silylated areas masks etching to produce a negative-tone image of the mask.

capability in pattern generation to the design of novel device structures seems sure to follow.

2.8 Conclusions

Despite the considerable advances that have been made in exposure and etching systems and in the area of resist materials and processing for the various advanced lithographic technologies, photolithography continues to

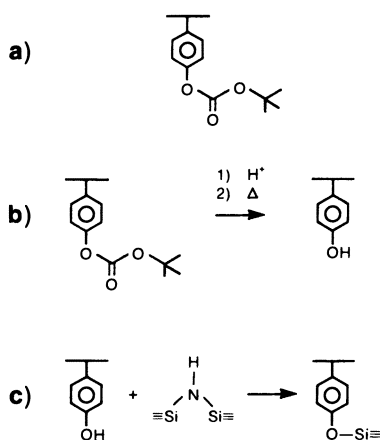
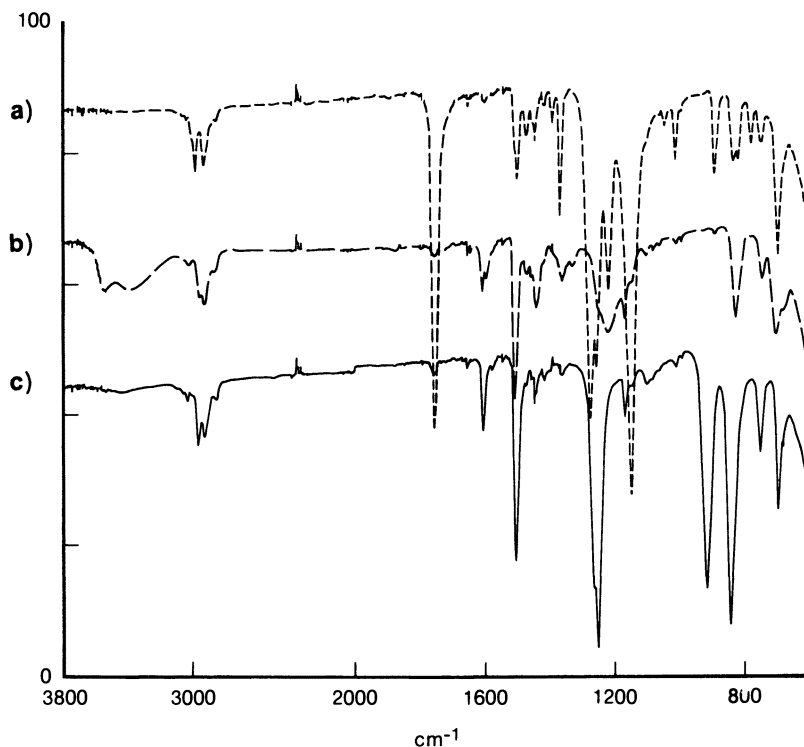
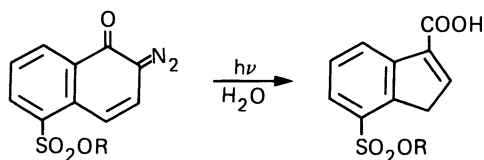


Figure 2.20. IR spectra of the t-BOC-protected phenolic resin (a) prior to exposure (the intense 1755-cm^{-1} band corresponds to a carbonate or carbonyl group), (b) after exposure and baking (the carbonyl band disappears and the broad phenolic OH band is generated at $3300\text{--}3500\text{ cm}^{-1}$) and (c) after treatment with hexamethyldisilazane (the formation of the silyl ether is characterized by the band at $\sim 1250\text{ cm}^{-1}$ and the two bands at 820 and 900 cm^{-1}).

1. Photoacid generation



2. Acid catalyzed crosslinking

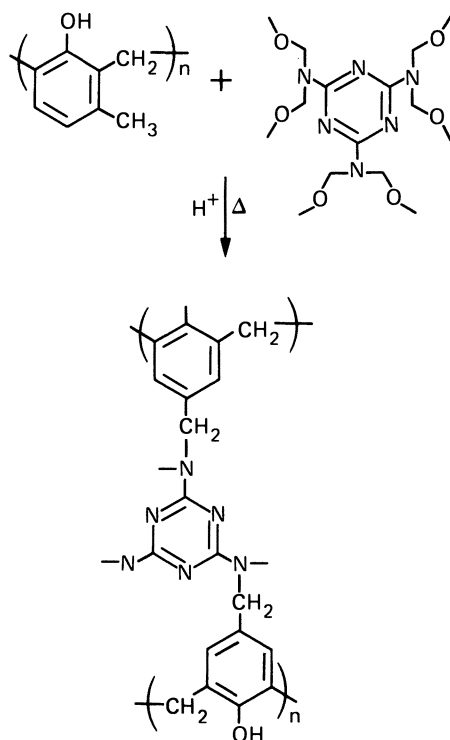


Chart 2.5. Chemistry of the Rohm & Haas resist. Photolysis of the diazoquinone generates a latent image of acid. Subsequent heating causes acid-catalyzed coupling in the exposed areas mediated by the hydroxymethylmelamine.

dominate production and seems poised on the brink of a full commitment to DUV technology. This realization has not been lost on resist chemists and process engineers who have devoted the major part of their efforts over the past several years to extending the utility of conventional DQN resists and developing new materials for DUV application.

The importance of DUV technology is reflected in Chapter 3, which is

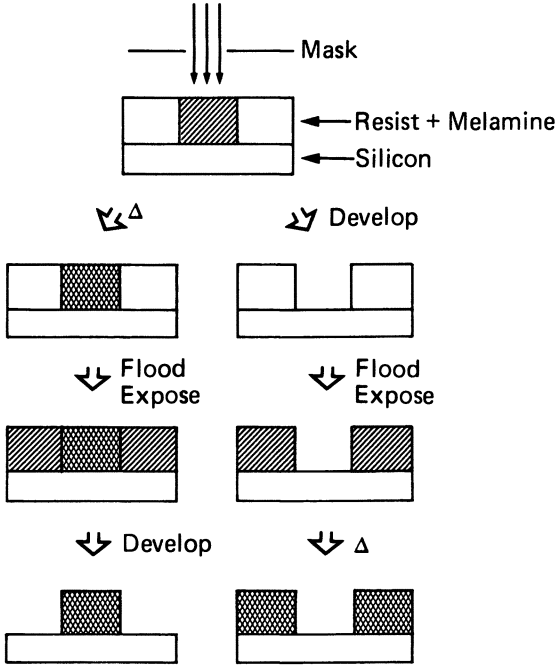


Figure 2.21. Resist hardening and image-reversal processes for the Rohm & Haas resist.

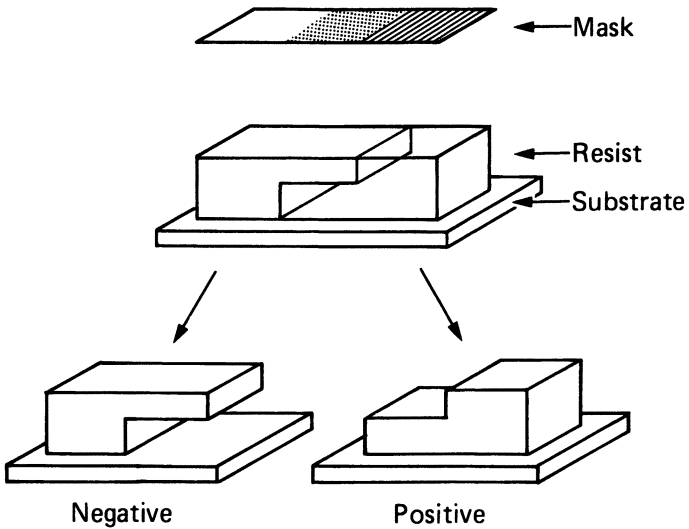


Figure 2.22. Three-tone mask exposure of the Rohm & Haas resist allows generation of a third dimension to the pattern. This third dimension allows formation of steps and overhangs.

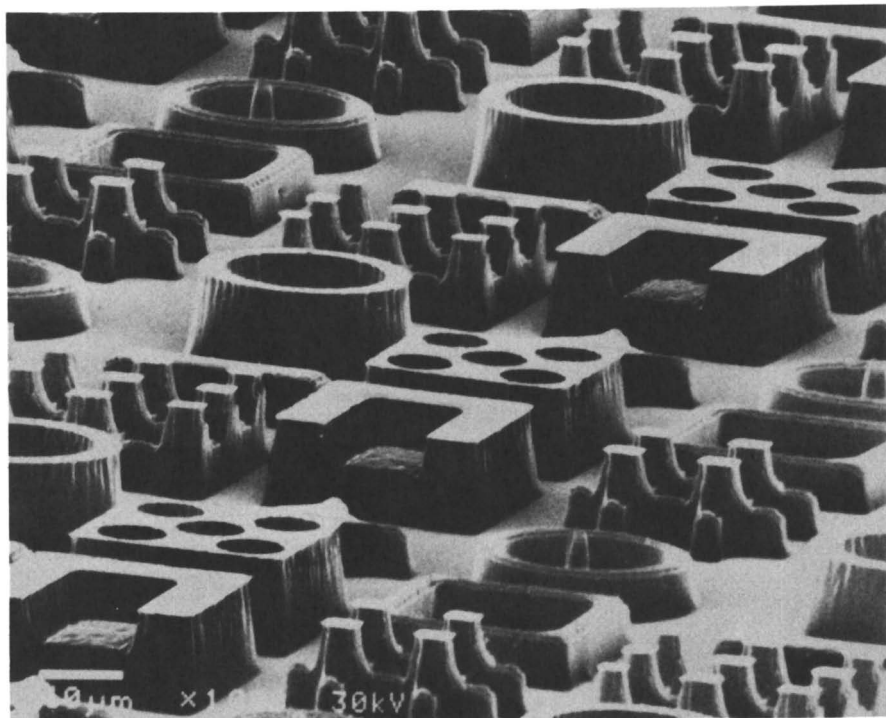


Figure 2.23. Scanning electron micrograph of a two-level resist structure printed in Rohm & Haas resist obtained by using a three-tone mask. (Courtesy of W. E. Feeley, Rohm & Haas.)

devoted entirely to DUV resist materials and processes. By comparison, research on electron-beam and X-ray resists has been less intense in recent years. Nevertheless, innovations in both materials and processes for electron beam and X-ray lithography continue to be made. Should either or both of these technologies emerge in the 1990s as dominant lithography strategies for production, the materials should be available to meet these requirements.

Abbreviations and Symbols

ARC	antireflection coating
BOM	built on mask
DQN	diazoquinone–novolac resist systems
DRAM	dynamic random access memory
DUV	deep-UV
ESCA	electron spectroscopy for chemical analysis
h	height
O ₂ -RIE	oxygen reactive ion etching

PMMA	poly(methyl methacrylate)
RIE	reactive ion etching
SEM	scanning electron micrograph
t-BOC	poly(<i>tert</i> -butoxycarbonyloxystyrene)

Acknowledgment

We acknowledge the assistance of Bette Murray and Julia Cox in the preparation of this chapter.

References

1. DeForest, W. *Photoresist Materials and Processes*; McGraw Hill: New York, NY, 1975.
2. Willson, C. G. In *Introduction to Microlithography*; Thompson, L. F.; Willson, C. G.; Bowden, M. J., Eds.; ACS Symposium Series 219; American Chemical Society: Washington, DC, 1983; p 87.
3. Bowden, M. J. In *Materials for Microlithography*; Thompson, L. F.; Willson, C. G.; Frechet, J. M. J., Eds.; ACS Symposium Series 266; American Chemical Society: Washington, DC, 1984; p 39.
4. Sinzer, P. H. *Semicond. Int.* **1987**, (10)6, 50.
5. Helbert, J. N.; Schmidt, M. A.; Malkiewicz, C.; Wallace, E., Jr.; Pittman, C. U. In *Polymers in Electronics*; Davidson, T., Ed.; ACS Symposium Series 242; American Chemical Society: Washington, DC, 1984; Chapter 8, p 91.
6. Pederson, L. A. *J. Electrochem. Soc.* **1982**, 129(1), 205.
7. Taylor, G. N.; Wolf, T. M. *Polym. Eng. Sci.* **1980**, 20(16), 1087.
8. Gokan, H.; Esho, S.; Ohnishi, Y. *J. Electrochem. Soc.* **1983**, 130, 143.
9. Hanabata, M.; Furuta, A.; Uemura, Y. *Proc. SPIE* **1987**, 771, 85.
10. Trefonas, P., III; Daniels, B. K.; Fischer, R. L., Jr. *Solid State Technol.* **1987**, 8, 131 and Trefonas, P., III; Daniels, B. K. *Proc. SPIE* **1987**, 771, 194.
11. Hinsberg, W. D.; Willson, C. G.; Kanazawa, K. K. *Proc. SPIE* **1985**, 539, 6.
12. Ouano, A. C. In *Polymers for Electronics*; Davidson, T., Ed.; ACS Symposium Series 242; American Chemical Society: Washington, DC, 1983; p 79.
13. Blum, L.; Perkins, M. E.; McCullough, A. W. *Proc. SPIE* **1987**, 771, 148.
14. (a) MacDonald, S. A.; Miller, R. D.; Willson, C. G.; Feinberg, G. M.; Gleason, R. T.; Halverson, R. M.; MacIntyre, M. W.; Motsiff, W. T. In *Proceedings of Kodak Microelectronics Seminar Interface '82*; Eastman Kodak: Rochester, NY, 1982; pp 114–117. (b) MacDonald, S. A.; Ito, H.; Willson, C. G. *Microelectron. Eng.* **1983**, 1, 269.
15. Moritz, H. *IEEE Trans. Electron Devices* **1985**, ED-32(3), 672.
16. West, P. R.; Davis, G. C.; Griffing, B. F. *J. Imaging Sci.* **1986**, 30, 65.
17. Sasago, M.; Endo, M.; Hirai, Y.; Ogawa, K.; Ishihara, T. *Proc. SPIE* **1986**, 631, 321.
18. Uchino, S.; Iwayanagi, T.; Ueno, T.; Hashimoto, M.; Nonogaki, S. *Proc. SPIE* **1987**, 771, 11.
19. Hofer, D. C.; Miller, R. D.; Willson, C. G.; Neureuther, A. R. *Proc. SPIE* **1984**, 469, 108.
20. Neureuther, A. R.; Hofer, D. C.; Willson, C. G. In *Microcircuit Engineering 84*; Heuberger, A.; Beneking, H., Eds.; Academic: London, 1985; p 53.

21. Vollenbroek, F. A.; Nijssen, W. P. M.; Kroon, H. J. J.; Yilmaz, B. In *Proceedings of the SPIE Regional Technical Conference*; Mid-Hudson Section, Society of Plastic Engineers: Ellenville, NY, 1985; p 309.
22. Willson, C. G.; Miller, R. D.; McKean, D. R.; Clecak, N. J.; Tompkins, T. C.; Michl, J.; Downing, J. *Polym. Eng. Sci.* **1983**, *23*, 1004.
23. Wilkins, C. W., Jr.; Reichmanis, E.; Chandross, E. A. *J. Electrochem. Soc.* **1982**, *129(11)*, 2552.
24. Grant, B. D.; Clecak, N. J.; Twieg, R. J.; Willson, C. G. *IEEE Trans. Electron Devices* **1981**, *ED-28(11)*, 1300.
25. Willson, C. G.; Miller, R. D.; McKean, D. R.; Clecak, N. J.; Pederson, L. A.; Regitz, M. *Proc. SPIE* **1987**, *771*, 2.
26. Willson, C. G.; Ito, H.; Frechet, J. M. J.; Tessier, T. G.; Houlihan, F. M. *J. Electrochem. Soc.* **1986**, *133(1)*, 181.
27. LaVergne, D.; Hofer, D. C. *Proc. SPIE* **1985**, *539*, 2.
28. Gijzen, R. M. R.; Kroon, H. J. J.; Vollenbroek, F. A.; Vervoordeldonk, R. *Proc. SPIE* **1986**, *631*, 108.
29. Marriott, V.; Garza, C. M.; Spak, M. *Proc. SPIE* **1987**, *771*, 221.
30. Bol, I. I. "High Resolution Optical Lithography Using Dyed Single-Layer Resist" In *Proceedings of Kodak Microelectronics Seminar-Interface '84*; Eastman Kodak: Rochester, NY, 1984.
31. Bolsen, M.; Buhr, G.; Merrem, H. T.; Van Werden, K. *Solid State Technol.* **1986**, *29*, 83.
32. Arden, N.; Mader, L. *Proc. SPIE* **1985**, *539*, 219.
33. Bohland, J. F.; Sandford, H. F.; Fine, S. A. *Proc. SPIE* **1985**, *539*, 267.
34. Jeffries, A. T.; Toukhy, M.; Sarubbi, T. R. *Ibid*, p 342.
35. Lin, Y. C.; Marriott, V.; Orvek, K.; Fuller, G. *Proc. SPIE* **1984**, *469*, 30.
36. Brewer, T.; Carlson, R.; Arnold, J. *J. Appl. Photogr. Eng.* **1981**, *7(6)*, 184.
37. Ting, C. H. *IBM Technical Disclosure Bulletin* **1981**, *24(5)*, 2400.
38. Lin, B. J. In *Introduction to Microlithography*; Willson, C. G.; Thompson, L. F.; ACS Symposium Series 210; American Chemical Society: Washington, DC, 1983; p 304.
39. Havas, J. R. *Electrochemical Society Extended Abstracts*; **1976**, *2*, 743 and Franco, J. R.; Havas, J. R.; Levine, H. A. U.S. Patent 3 873 361, 1973.
40. Watts, M. P. C. *Proc. SPIE* **1984**, *469*, 2.
41. McCullough, A. W.; Vidusek, D. A.; Legenza, M. W.; deGrandpre, M.; Imhoff, J. *Proc. SPIE* **1986**, *631*, 316.
42. O'Toole, M. M.; Liu, E. D.; Chang, M. S. *IEEE Trans. Electron Devices* **1981**, *ED-28(11)*, 1405.
43. Bartlett, K.; Hillis, G.; Chen, M.; Trutna, R.; Watts, M. P. C. *Proc. SPIE* **1983**, *394*, 49.
44. Hatzakis, M.; Paraszczak, J.; Shaw, J. *Proc. Microcircuit Eng. (Lausanne)* **1981**, *1981*, 396.
45. Shaw, J.; Babich, E.; Hatzakis, M.; Paraszczak, J. *Solid State Technol.* **1987**, *6*, 83.
46. Hatzakis, M. *Solid State Technol.* **1981**, *24(8)*, 74.
47. Ohnishi, Y.; Suzuki, M.; Saigo, K.; Saotome, Y.; Gokan, H. *Proc. SPIE* **1985**, *539*, 62.
48. Gozdz, A. S. *Solid State Technol.* **1987**, *30(6)*, 75.
49. Morgan, R. A. *Plasma Etching in Semiconductor Fabrication*; Elsevier: Oxford, England, 1985; p 302 and U.K. Patent Application 8403698; "Silylation of Photoresists".
50. MacDonald, S. A.; Ito, H.; Hiraoka, H.; Willson, C. G. In *Proceedings, SPIE*

- Regional Technical Conference*; Mid-Hudson Section, Society of Plastic Engineers: Ellenville, NY, 1985; p 177.
51. Brust, T. B.; Turner, S. R. *Proc. SPIE* 1987, 771, 102.
 52. MacDonald, S. A.; Pederson, L. A.; Patlach, A. M.; Willson, C. G. *Polym. Mater. Sci. Eng.* 1986, 55, 721.
 53. Coopmans, F.; Roland, B. *Solid State Technol.* 1987, 30(6), 93.
 54. Visser, R. J.; Schellekens, J. P. W.; Renhman-Huisken, M. E.; Van Ijzendoorn, J. *Proc. SPIE* 1987, 771, 111.
 55. Pol, V. *Solid State Technol.* 1987, 30(1), 71.
 56. Frankel, R. D.; Drumheller, J. P.; Kaplan, A. S.; Lubin, M. J. "X-Ray Lithography Process Optimization Using Laser-Based X-Ray Source"; In *Proceedings of Kodak Microelectronics Seminar-Interface '86*; Eastman Kodak: Rochester, NY, 1986.
 57. Bolen, H.; Behringer, U.; Nehmiz, P.; Zapka, W.; Kulcke, W.; Keyer, J. *Solid State Technol.* 1984, 27(9), 210.
 58. Feely, W. E. *Proc. SPIE* 1986, 631, 48.

RECEIVED for review August 17, 1987. ACCEPTED November 12, 1987.

Materials and Processes for Deep-UV Lithography

Takao Iwayanagi¹, Takumi Ueno¹, Saburo Nonogaki¹, Hiroshi Ito²,
and C. Grant Willson²

¹Central Research Laboratory, Hitachi, Ltd., Kokubunji, Tokyo 185, Japan

²IBM Almaden Research Center, San Jose, CA 95120-6099

This chapter provides a comprehensive review of the resist materials and processes that have been designed and developed to support high-resolution, deep-UV (DUV) lithography (i.e., lithography using radiation in the 200–300 - nm wavelength range). Special emphasis is placed on materials, their lithographic performance, and the chemistry responsible for their function. Topics include the fundamental relationships between resolution and exposure wavelength, sources of DUV radiation, and progress in the development of DUV exposure equipment. Unique applications including multilayer patterning schemes and excimer laser lithography are also discussed.

THE FABRICATION OF INTEGRATED CIRCUITS involves a series of steps that defines insulator, conductor, and semiconductor structures in and on single crystals of silicon or gallium arsenide (1). As practiced today, the circuit elements are as small as 1 micrometer (1 μm) in dimension. Reproducible device performance and yield issues require control of both the dimension and placement of these 1- μm structures to tolerances of fractions of 1 μm . The number of such circuit elements per chip has steadily increased during the past three decades, mainly through a decrease in the size of the elements. This reduction in the feature size and the increase in circuit complexity and integration that it allows is largely responsible for the dramatic improvement in the performance and cost-performance ratio that has occurred and is expected to continue to occur.

Circuit elements are patterned through a series of sophisticated imaging processes collectively called *lithography*. Photolithographic processing,

0065-2393/88/0218-0109\$22.60/0
© 1988 American Chemical Society

which is the form of lithography used to delineate the circuit elements in today's large-scale integrated devices, is, however, approaching its physical resolution limit. The resolution limit of an imaging system is a function of the wavelength of the exposing radiation (i.e., higher resolution can be attained with shorter wavelength radiation). Consequently, on the basis of this simple principle, lithographic systems including the exposure tools, resist systems, and the associated processes have been under intensive development since the 1960s for short-wavelength radiation including

- ion and electron beams,
- X-ray, and
- short-wavelength UV (2).

Electron beam lithography employs finely focused electron beams that are rastered or vectored and modulated under computer control to delineate patterns in resist films (3). Because the de Broglie wavelength of electrons is extremely small at common accelerating potentials (10–50 kV), these beams can be focused to diameters of several tens of angstroms. Because this technology is based essentially on serial delineation of the pattern pixel by pixel (4), these systems have low throughput. The complexity of the exposure system and its associated electronics and supporting computer hardware makes these systems quite expensive. Despite these limitations, the primary pattern-generation capability of electron beam systems has found wide use in the fabrication of masks for optical lithography and, in certain cases, for production of custom logic devices. Because of its resolution capability, electron beam lithography has been exploited in laboratories to produce extremely small structures including active devices with conductor dimensions of a few hundred angstroms in line width (5).

X-ray lithography is based on the use of radiation in the soft X-ray region of wavelength ranging from about 0.1 to 0.4 nm (6). This technology is capable of resolving very small features in resist films. X-ray lithography and, in particular, X-ray lithography based on synchrotron or "storage ring" X-ray sources is currently an extremely active area of research. This technology is advancing rapidly but has not yet reached the stage of practical implementation because of a variety of technical problems related to sources, mask fabrication, alignment, and resist materials.

The use of short-wavelength UV radiation to extend the resolution of photolithography was first reported by Moreau and Schmidt in 1970 (7), and Lin (8) further refined this technique. The wavelength of radiation used in what is now generally accepted as deep-UV (DUV) lithography and that which we will consider for the purposes of this review is between 200 and 300 nm. This range can be compared to the wavelength of the common "g-line" (436-nm) step-and-repeat printing tools that are the workhorses of today's factories and to the "i-line" (365-nm) printing tools that are just

becoming commercially available. DUV lithography, supported by the development of new exposure sources, advances in lens design, and new resist materials, is destined to become a powerful tool for the fabrication of semiconductor devices. We expect that during the next decade, the majority of production will migrate to some version of this patterning technology. Thus, this review of the resist materials and processes developed for DUV lithography is timely. The special emphasis in this chapter is on materials, their performance, and the chemistry responsible for their lithographic response.

3.1 *Deep-UV Lithography*

3.1.1 Historical Development

Moreau and Schmidt (7) demonstrated the sensitivity of poly(methyl methacrylate) (PMMA) to DUV radiation in 1970 and described most of the features of DUV lithography. The main objective of their work was to employ DUV radiation to allow larger mask-to-wafer separation at constant resolution in proximity printing. Their work demonstrated the utility of PMMA as a DUV resist, and they predicted that DUV radiation would be employed with an acrylate polymer of some type in future projection printing systems that should allow reliable printing of submicrometer features.

The term "DUV lithography" was coined by B. J. Lin in his pioneering paper that appeared in 1975 (8). Lin demonstrated the high-resolution potential of DUV lithography by contact printing 0.5- μm "T-bar" (T-shaped) bubble-propagation patterns separated by 0.25- μm gaps in 1.78- μm -thick PMMA films. Shortly after Lin's report, Feldman et al. (9) published the results of their experiments involving exposure of poly(butene-1 sulfone) to 185-nm radiation. Since these early reports, a variety of resist materials and processes have been developed and are the subject of this review. But the application of DUV lithography to practical device fabrication requires development of *both* the exposure system and the resist materials.

Significant changes in current exposure equipment are required to realize the potential for resolution improvement that shorter wavelength can provide. The materials used for fabrication of optical elements, including lenses, must be replaced by materials that have acceptable transmission in the DUV. This step represents a major challenge, particularly for lens designers, because they have few transparent materials from which to choose and yet require an inventory of transparent materials with varying refractive indices from which to construct lenses that are corrected for chromatic aberrations. The alternative is to use very narrow band-pass filtering of the source that, for the usual high-pressure mercury lamp, corresponds to an intolerable reduction in source brightness. Mirror-lens-based projection systems have less critical demands on materials because chromatic aberration correction does not require refractive elements, but filters and coatings

designed to isolate the desired DUV wavelength range must be developed. Even the standard high-pressure mercury lamp sources must be fabricated with special attention given to the transmission characteristics of the envelope material.

Most of these challenges, many of which are quite formidable, have been met at some level. Commercially available contact printers and mirror-based projection printers are now being used in device manufacturing. Refracting-lens-based projection printers (steppers) that use DUV light sources are currently under development by tooling manufacturers and have been demonstrated in laboratory environments (10). Apparently, manufacturing engineers will have a range of DUV exposure equipment from which to choose and around which to develop processes before the end of the decade.

In contact printing, DUV radiation provides improved resolution and the ability to pattern thicker resist films because of a reduction in the extent of diffraction-based distortion of the intensity function (aerial image) within the resist film (11). In proximity printing, where the mask is deliberately separated from the resist film surface by a small but controlled distance, a change to shorter wavelength can allow, as Moreau and Schmidt recognized, either a larger gap at constant resolution or improved resolution at constant gap. A detailed analysis of the effect of wavelength on the intensity function in the resist film for proximity printing was provided by Lin (11), and a more qualitative description is also available (1*b*). The resolution in both contact and proximity printing is proportional to the $\frac{1}{2}$ power of the wavelength. The effect of reducing the exposure wavelength is greatest in projection printing, where the resolution is directly proportional to the exposure wavelength and inversely proportional to the lens numerical aperture (NA). For a fixed NA, reducing the exposure wavelength can be exploited to provide an increase in the depth of focus at constant resolution. These relationships have been derived (1*b*, 11).

3.1.2 Deep-UV Light Sources

The source of radiation for photolithography has traditionally been a Hg or Hg-rare gas discharge lamp (12). The conventional discharge lamp consists of a quartz envelope that encloses two refractory metal (usually W) electrodes that are charged with a carefully metered amount of elemental Hg and a rare gas (usually Xe). These lamps are excited by external power supplies in the range of 0.5–2.0 kW. The equilibrium pressure of Hg and the rare gas determine the spectral distribution of the light output. This output is high in the near-UV region (350–450 nm), lower in the mid-UV region (300–350 nm), and very low in the DUV region (200–300 nm).

The low efficiency of these lamps in the DUV region can be explained in terms of the energy level diagram shown in Figure 3.1. The transitions involving the ground state of the atom (resonance lines) have the greatest

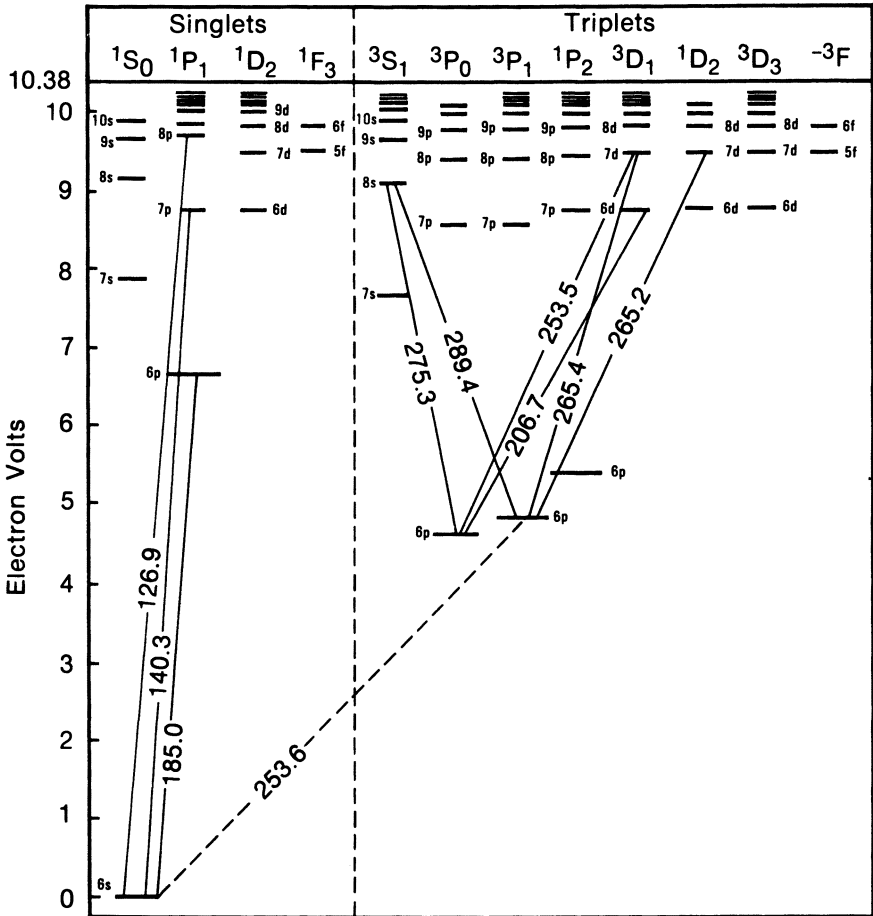


Figure 3.1. Energy level diagram for Hg. (Reproduced with permission from reference 12a. Copyright 1984 Academic Press.)

probability of occurrence. Hg has only one resonant line at 253.7 nm, corresponding to the emission associated with transition from the excited state $3P_1$ to the ground state $1S_0$. This resonant line is the strongest or characteristic output of a low-pressure discharge, but, with increasing pressure, it becomes almost completely reabsorbed.

Figure 3.1 shows that emission between 200 and 300 nm occurs from transitions between highly excited states to the group of 6 $3p$ triplet levels lying around 5 eV. Thus, to emit DUV photons, Hg atoms must be excited to a state with energy 8–10 eV above the ground state. The major mechanism for excitation in these lamps involves inelastic collision of Hg atoms with electrons from the plasma. The average energy of these electrons is only 0.5–1.0 eV; thus, individual electrons do not, on the average, have sufficient

energy to excite the required transitions. One obvious method for increasing the average energy of the plasma electrons would be to increase the discharge temperature. However, these lamps are already operated near the thermal stability limit of quartz in steady-state discharge applications. Despite their low output, discharge lamps have the attractive feature of small source size that makes condenser design simple and operation stable.

Deuterium lamps have been considered for DUV sources because these lamps have a broad-band emission in the desired spectral region. However, they are difficult to run at high power because of out-diffusion of deuterium, plasma instability, and short lifetime (13).

One method of improving the efficiency of the Hg discharge lamp is to dope it with Zn or Cd (11, 12). This approach probably deserves more attention. Another method is to simply apply higher power but in short pulses. This method allows achievement of the high electron velocities required for excitation to the required energy levels without overheating the quartz envelope. This method is used in pulsed Xe lamps. These lamps operate with high conversion efficiency and pulse widths of milliseconds. However, the pulsed nature of these lamps, their low repetition rate, and special cooling requirements have precluded their use, particularly in mirror-based scanning exposure systems.

Microwave-powered Hg discharge lamps have very high source brightness in the DUV region. Their efficiency stems from the fact that the microwave-induced plasma forms in a narrow shell very near the lamp wall. As a result, most of the light is emitted near the lamp wall and there is less reabsorption. The efficiency of these lamps is high because the average electron energy is higher than that in an arc lamp. The main drawback of these sources is their large source size that greatly complicates condenser optics design. These lamps are extremely useful in applications of blanket DUV exposure.

Another interesting source of DUV radiation for microlithography is excimer lasers (13). This relatively new class of very efficient and extremely powerful pulsed lasers became commercially available in 1978. They operate at several characteristic wavelengths ranging from less than 200 nm to greater than 400 nm. The output is typically 10–20-ns wide pulses with repetition rates from ten to several hundred Hertz. Jain (14) provided a recent review of laser application to microlithography.

An important characteristic of excimer lasers that sets them apart from traditional UV lasers is their lack of spatial coherence. The interference phenomena that result from the high spatial coherence of traditional single-mode continuous wave lasers produces a random intensity variation in projected patterns called *speckle*. This speckle phenomenon has historically made use of lasers in high-resolution lithography very difficult. The beam of excimer lasers is so highly multimode that speckles are, for all practical purposes, nonexistent in projected patterns. The application of excimer laser

sources to DUV lithography has been demonstrated for contact printing (15), mirror projection printing (16), and, most recently, for reduction projection printing in step-and-repeat fashion by using specially constructed refracting lenses (10). The use of excimer lasers in production has been hampered by the high cost and inconvenience of operating these devices in a production environment and difficulty in designing optical couplers that would be the analog of conventional condenser systems that efficiently fill the entrance pupil of the projection lens with uniform illumination of appropriate partial coherence. Furthermore, the lasers currently available suffer from pulse-to-pulse power irreproducibility and limited operational stability on a single gas fill. However, significant progress has been made in all of these areas. Improvements in electrode materials, gas handling systems, and pulse-control electronics have demonstrated major extensions in power stability. When the engineering difficulties have been overcome, excimer lasers will become an important part of the lithographic process. In fact, one commercial contact printer can be purchased with an excimer laser source (16).

3.1.3 Deep-UV Printer Systems

3.1.3.1 DEEP-UV CONTACT/PROXIMITY PRINTERS

In DUV contact printing, a photomask and a resist-coated wafer are brought into tight contact. The wafer is then exposed to DUV radiation of controlled collimation through the mask. In proximity printers, some mechanism is provided that allows exposure with a small, controlled gap between the mask and the wafer surface. Operation of such systems in the DUV requires certain modifications. These modifications are exemplified in the Canon PLA520FA printer (17). The optical system of this printer is shown in Figure 3.2. The transmission elements of the system are of high quality quartz to minimize absorption in the DUV. The system has a specifically designed dichroic, dielectric stack "cold mirror" that has high reflectivity in the DUV region but transmits visible and IR radiation from the source on to a heat sink. Figure 3.3 shows the spectral output of this system with two different cold mirrors. The Canon PLA520FA can be operated in either the contact or proximity mode. The time required to expose PMMA has been reported to be 40 s when cold mirror CM250 is used (17c).

3.1.3.2 DEEP-UV PROJECTION PRINTERS

The all-reflecting 1:1 projection system was first reported by Moller in 1973 (18). The optical and scanning configuration of such a system is illustrated in Figure 3.4. In these systems, a set of spherical mirrors is used to generate a narrow, ring-shaped aberration-free arc of light. Wafers are scanned past this arc to produce an image as the mask is moved synchronously in the object plane. An arc of the mask is thereby illuminated and imaged onto

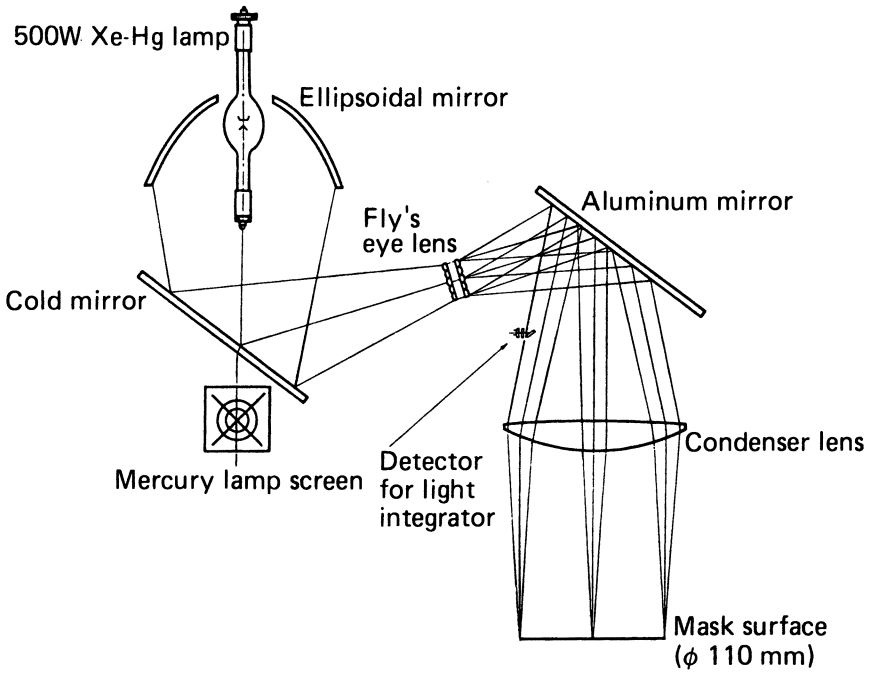


Figure 3.2. Optical layout of the illuminator in the Cannon PLA520FA contact/proximity printer. (Reproduced with permission from reference 17a.)

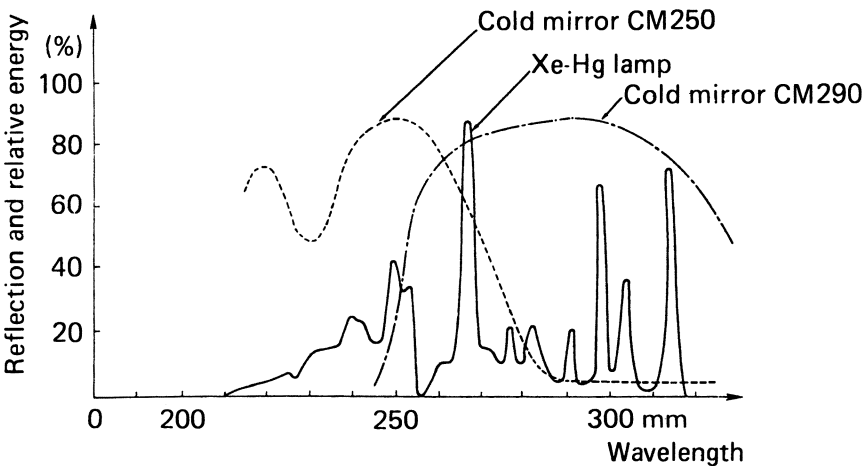


Figure 3.3. Spectral deflection of cold mirrors. (Courtesy of Cannon.)

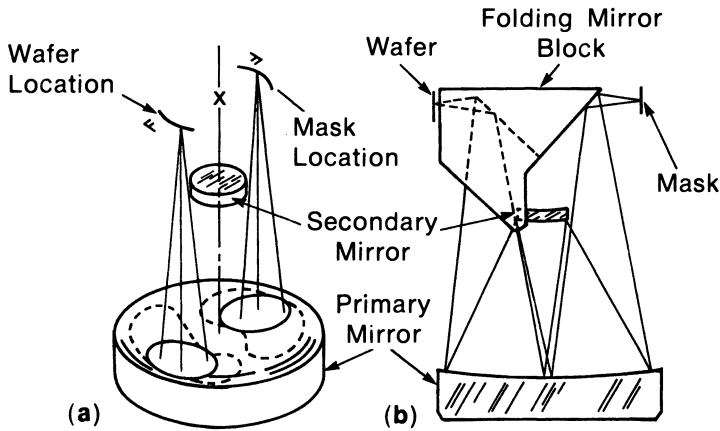


Figure 3.4. All-reflecting 1:1 projection optical system.

the wafer so that scanning once across the wafer and mask achieves exposure of the entire wafer surface.

One of the outstanding features of this system is the flexibility it offers. In particular, the mirror lens system in this configuration has essentially no chromatic aberration. Hence, one can vary the exposure wavelength simply by imposing the appropriate transmission filter between the condenser system and the mask. Many improvements have been made in the design of these tools since their first commercial introduction by Perkin-Elmer (19). The projection optics of the Perkin-Elmer Micralign 500 are shown in Figure 3.5. The NA of this system is 0.16. The refracting elements (shells) are all single elements and fabricated of high quality quartz. Another example of such a system is the Canon MPA520FA (Figure 3.6).

The illumination source in these printers is a high-pressure Hg-Xe lamp. The spectral irradiance of the Perkin-Elmer lamp is shown in Figure 3.7. Perkin-Elmer provides band-pass filters for operation in the "UV-2" (DUV), "UV-3" (mid-UV) and "UV-4" (near-UV) spectral regions as shown in Figure 3.8. The output in the UV-4 mode is similar to Perkin-Elmer's earlier projection printers, the PE100 and PE200 series, and passes the spectral lines at 365, 405, and 436 nm. The UV-3 mode transmits between 290 and 340 nm in the mid-UV region, and the UV-2 filter transmits in the DUV region between 220 and 290 nm. The relative output of the Micralign 500 at the wafer plane in the absence of any filtering is shown in Figure 3.8. In Figure 3.8, the area under the curve in the DUV is a very small proportion of that under the curve in the near-UV (UV-4) region of the spectrum because of the output inefficiency of the Hg discharge source. Although these systems have been designed and engineered such that a shift into the DUV will provide nearly a twofold improvement in resolution, either a much brighter light source or a far more sensitive resist is required

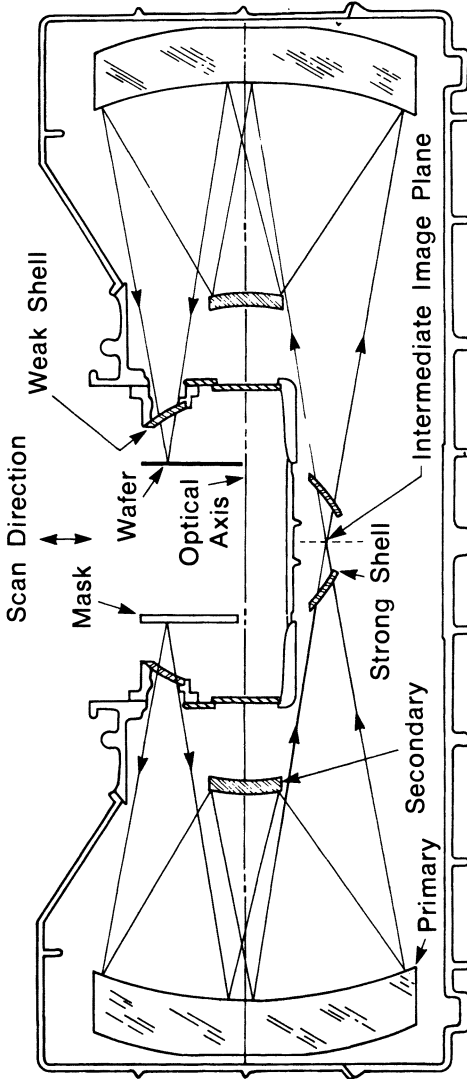


Figure 3.5. *Micralign 500 projection optics system. (Reproduced from Perkin-Elmer User's Manual.)*

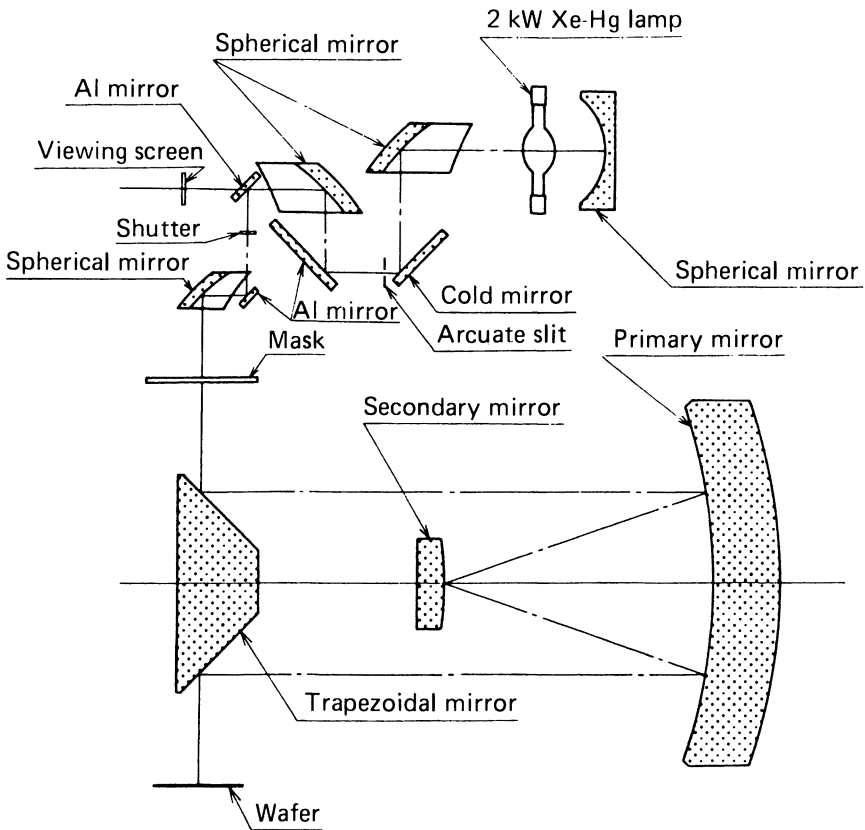


Figure 3.6. Illumination and projection systems of the Cannon MPA520FA. (Courtesy of Cannon.)

to maintain the wafer throughput (productivity) that can be achieved in the UV-4 mode.

3.2 Deep-UV Resist Materials

3.2.1 Positive Resists

3.2.1.1 DISSOLUTION-INHIBITOR SYSTEMS

Conventional positive photoresists consist of a matrix resin and a photoactive compound. The matrix resin is a cresol-formaldehyde novolac resin (structure 3.1) that is soluble in aqueous base solution, and the photoactive compound is a substituted diazonaphthoquinone (structure 3.2) that functions as a dissolution inhibitor for the matrix resin. As outlined in Scheme 3.1 (20), the photoactive compound undergoes a structural transformation upon UV radiation, known as Wolff rearrangement, followed by reaction with water

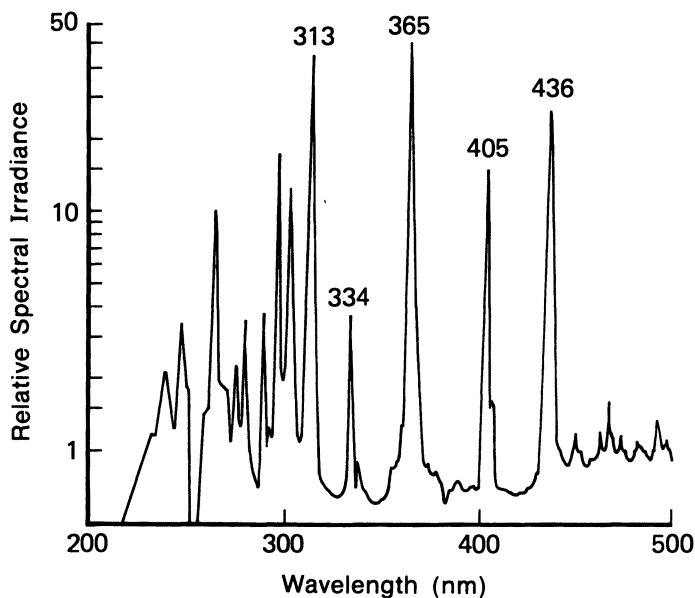


Figure 3.7. Spectral irradiance of the Perkin-Elmer Xe-Hg lamp. (Courtesy of Perkin-Elmer.)

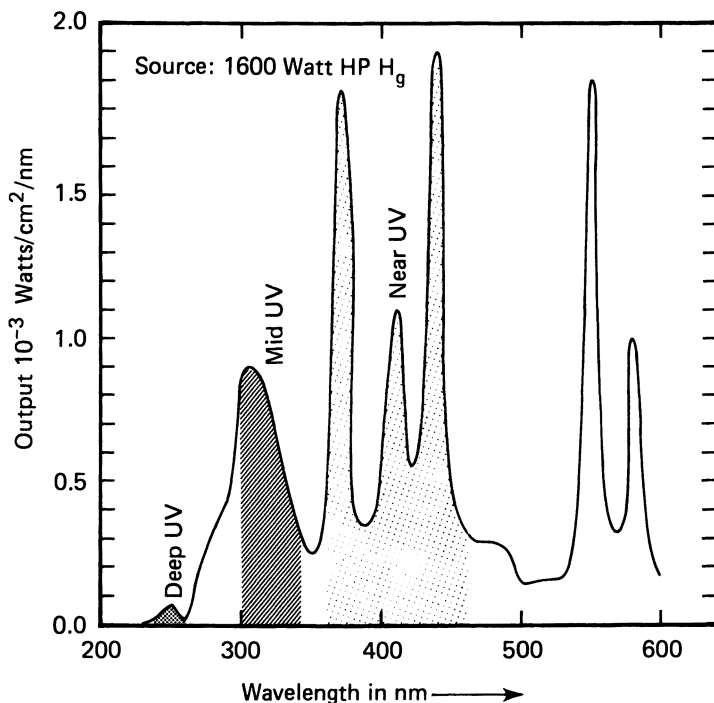
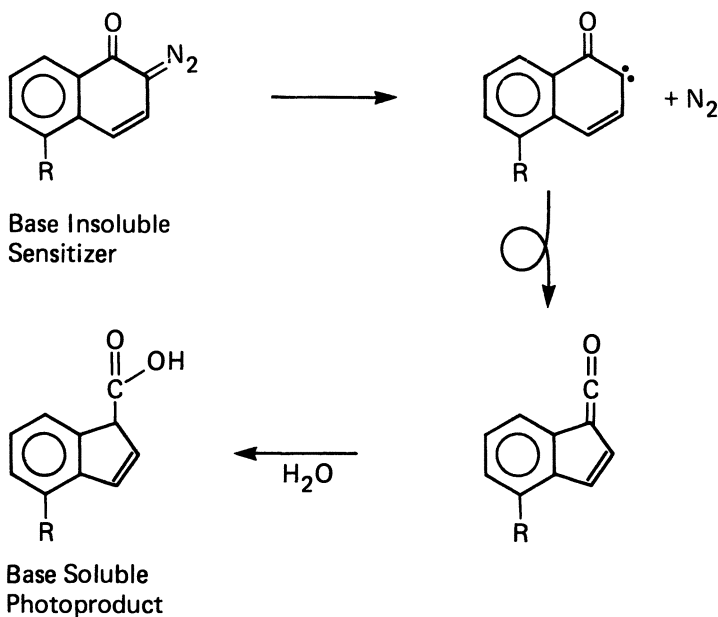
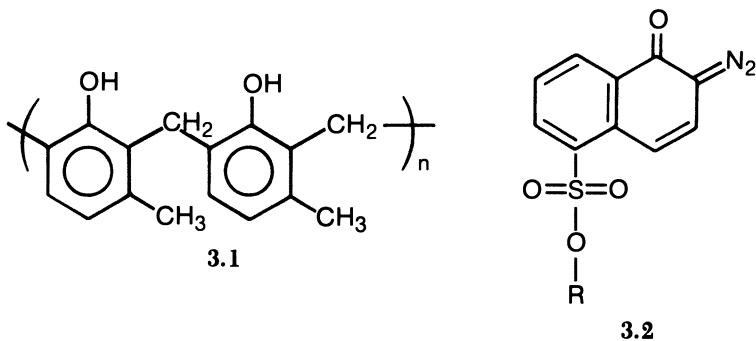


Figure 3.8. Optical output at wafer plane of Perkin-Elmer Micralign 500. (Courtesy of Perkin-Elmer.)



Scheme 3.1. Photochemical transformation of diazoquinone sensitizer.

to form a base-soluble indenecarboxylic acid that no longer inhibits dissolution of the novolac matrix resin in alkaline developer. Consequently, the exposed regions of the film are rendered more soluble than the unexposed regions, and the photochemically induced differential solubility rate is used to generate positive-tone images of the mask.

The positive photoresists based on a novolac matrix resin and a diazoquinone sensitizer evolved from materials originally designed by Kalle Corporation in Germany to produce photoplates used in the printing industry. These positives photoresists have become the “workhorses” of the microelectronics industry because of their high resolution and dry etch resistance.

3.2.1.1.a Mid-UV Resists Based on Diazoquinone–Novolac

Bruning and co-workers (21–23) demonstrated that the theoretical improvement in resolution can be achieved by reducing the exposing wavelength from the near-UV to the mid-UV. They exposed a positive photoresist, HPR204, coated on Ta-metalized wafers through a meander pattern mask on a modified Perkin–Elmer 111 projection printer operating in the near-UV and mid-UV ranges. After plasma etching of the substrate, the Ta pattern integrity was examined by electrical probing. The percentage of good patterns is plotted as a function of line size in Figure 3.9. This figure indicates that mid-UV exposure results in an improvement in both resolution and yield. This improvement is roughly proportional to the mean wavelength of the exposing radiation.

However, commercially available positive photoresists such as AZ1350J and HPR204 demonstrate greatly reduced sensitivity in the mid-UV region in comparison to their performance in the near-UV region. The reasons for this loss in sensitivity are as follows:

- The molar extinction coefficient of the 1-oxo-2-diazonaphthoquinone-5-arylsulfonate (structure 3.2) sensitizers that are used to formulate most commercial photoresists is very low at 313 nm compared to that at 405 nm.

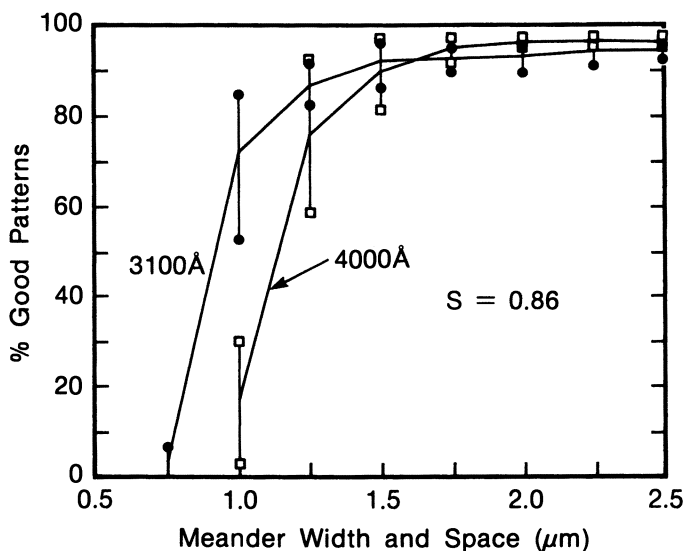


Figure 3.9. Electrical probe yield of meander patterns versus design feature size and wavelength. The vertical bars indicate the total yield range for the wafer tested. (Reproduced with permission from reference 23.)

- These materials undergo photochemistry, ultimately leading to a photoproduct that is transparent at 405 nm but absorbs at 313 nm.
- The phenolic resins used in most of the commercial resists have a significant unbleachable absorbance at 313 nm but are essentially transparent above 350 nm.

These accumulated undesirable optical characteristics are shown in Figure 3.10 for AZ1350J and Figure 3.11b for HPR204.

AZ2400 is different from most other commercial positive photoresists in both formulation and response to mid-UV radiation. This resist is formulated with a resin that is relatively transparent in the mid-UV and 1-oxo-2-diazonaphthoquinone-4-arylsulfonate (structure 3.3) rather than the 5-arylsulfonate (structure 3.2) that is commonly used in most commercial photoresists (24).

A transmittance spectrum for AZ2400 is provided in Figure 3.11a. This

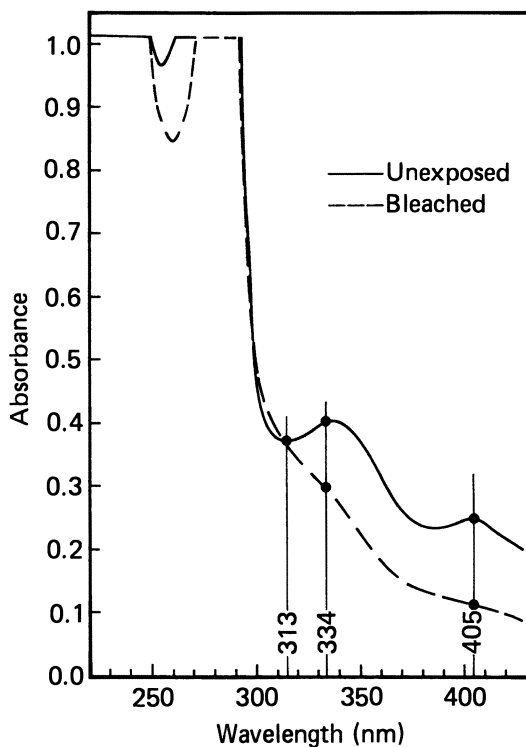


Figure 3.10. Unexposed and bleached spectra of AZ1350J resist spin-coated on quartz at a thickness of 1 μm . (Reproduced with permission from reference 30.)

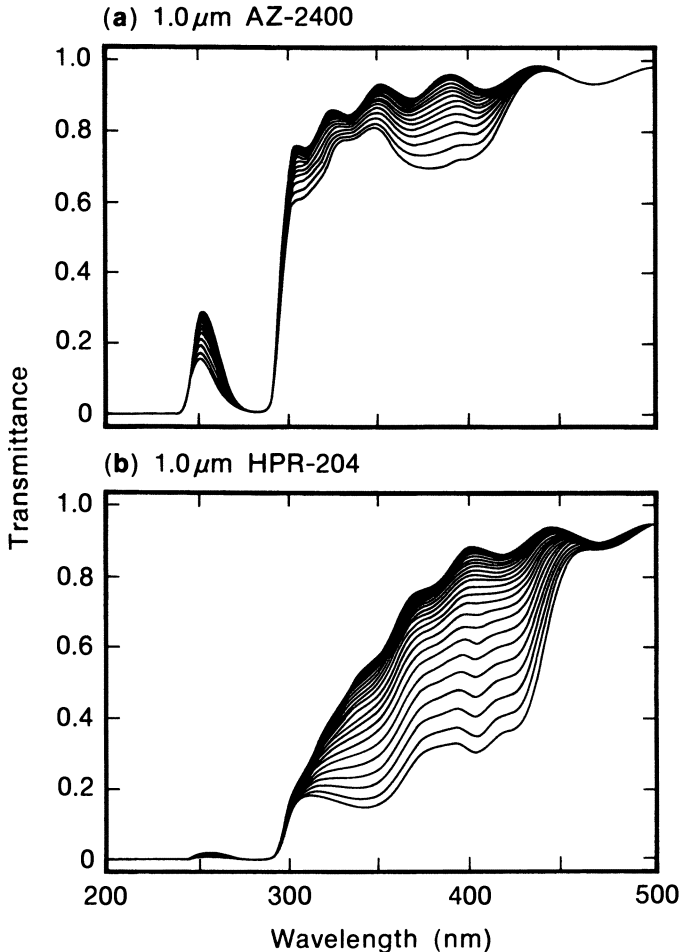
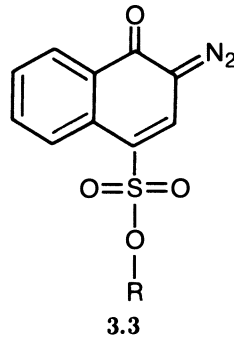


Figure 3.11. Dynamic bleaching absorption spectra of diazonaphthoquinone resists: (a) 1.0- μm AZ2400 and (b) 1.0- μm HPR204. (Reproduced with permission from reference 23.)

resist is clearly more suited for use in mid-UV lithography than the systems based on the 5-sulfonate esters because the initial absorbance at 313 nm is lower and exposure results in a significant bleaching even in the mid-UV region. In fact, AZ2400 has been shown to function satisfactorily under mid-UV-exposure conditions in terms of resolution, resist profile, and edge acuity (25–28). Bruning and co-workers (21, 23) obtained more than 90% yield for 1- μm meander patterns when using this resist. The applicability of AZ2400 to mid-UV lithography was extensively modeled by Hofer et al. (26).

Babie et al. (29) attempted to enhance the sensitivity of diazonaphthoquinone-5-arylsulfonate-based resist in the mid-UV region by adding py-



rene as a photosensitizer. The addition of the singlet sensitizer increased the conversion of diazonaphthoquinone by 20%–30% and consequently increased the dissolution-rate ratio of the exposed to the unexposed films by a factor of 5 at a given exposure dose.

Willson et al. (30) and Miller et al. (31) described a new mid-UV resist based on diazonaphthoquinone and a novolac resin specifically designed for use in the mid-UV region. The novolac resin was chosen to be transparent above 300 nm. The structure of the naphthoquinone was designed with the aid of semiempirical molecular orbital calculations to provide increased optical absorbance at the 313-nm emission line. They found that 5-alkylsulfonates of diazonaphthoquinone exhibit a greatly improved extinction at both 313 and 334 nm over their aryl counterparts. Furthermore, these compounds photolyze to give substituted indenecarboxylic acids that are transparent above 300 nm, whereas the photoproducts of all of the corresponding aryl derivatives studied retain residual absorbance at 313 nm. They chose a mixed 4,5-disulfonate of an aliphatic diol (structure 3.4) as a spectrally matched sensitizer for the mid-UV resist.

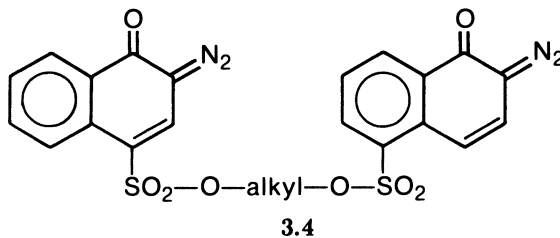


Figure 3.12 demonstrates the bleaching of the IBM mid-UV resist. This spectrum should be compared with that of AZ1350J (Figure 3.10). The new resist bleaches upon irradiation effectively across the range of wavelengths from 300 to 450 nm, whereas AZ1350J bleaches effectively in the near-UV region but does not bleach at all at 313 nm.

Scanning electron micrographs (SEMs) of 2.5- μm pitch gratings printed

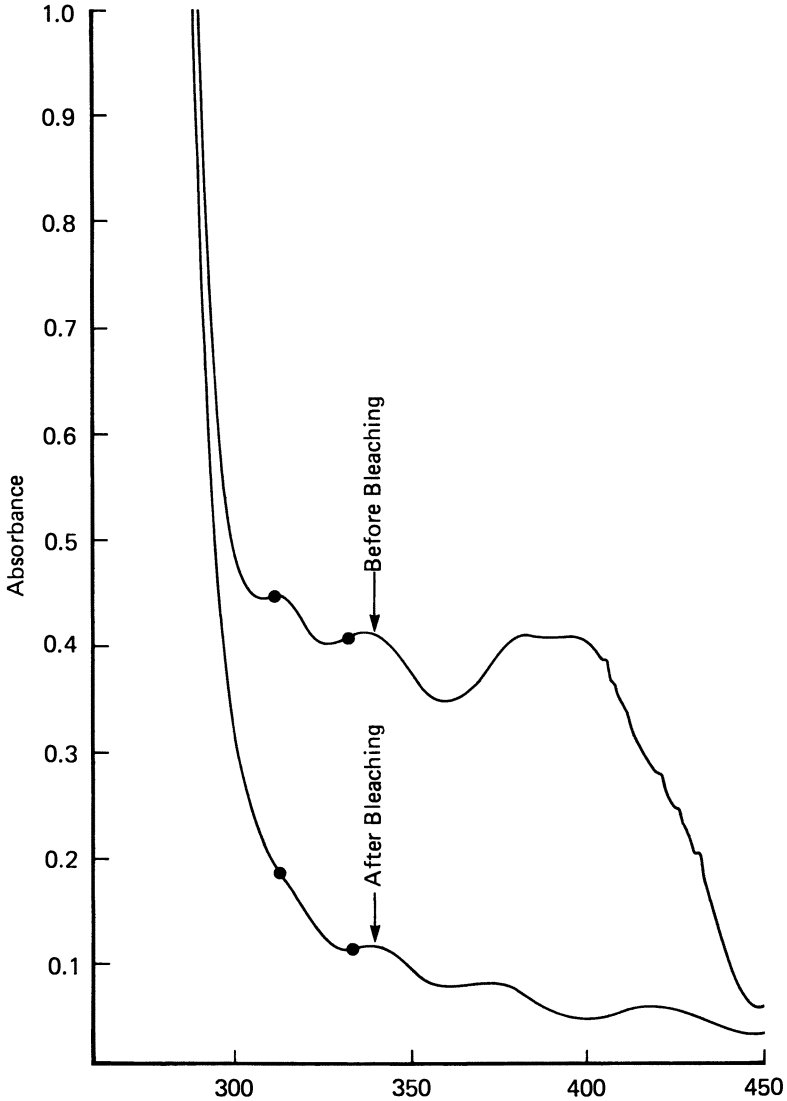


Figure 3.12. Unexposed and bleached spectra of an IBM mid-UV resist formulated from a 4,5-disulfonate of an aliphatic diol. (Reproduced with permission from reference 30.)

in the IBM mid-UV resist on a Perkin-Elmer M500 (Micralign 500) projection aligner are provided in Figure 3.13. These results should be compared with the calculated free space image at the wafer plane demonstrated in Figure 3.14. The square-wave image intensity function across the grating at the mask surface is degraded in the printer optical path such that a nearly

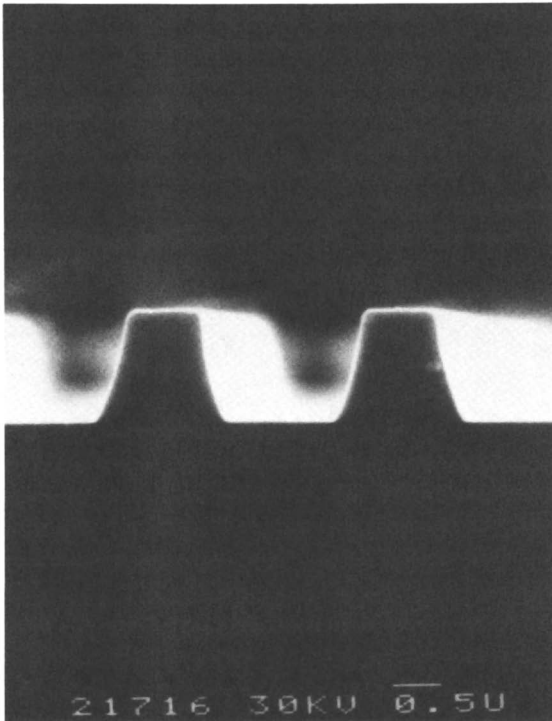


Figure 3.13. SEM of 2.5- μm pitch ($1.25 \times 1.25 \mu\text{m}$) gratings printed in an IBM mid-UV resist (Perkin-Elmer M500, scan speed 5000, DP-9 filter, aperture 1). (Reproduced with permission from reference 30.)

sinusoidal intensity function is presented at the wafer surface, as shown in Figure 3.14. The response of the resist, in terms of its dissolution rate as a function of dose, must be tailored so that it will convert this degraded intensity function back into a square-wave relief image representative of that which existed at the mask surface. This requirement is not trivial as the resist must recognize the mask edge in an intensity pattern of the sort depicted in Figure 3.14. A resist formulation that exhibits a dissolution rate that responds linearly to dose faithfully reproduces the image intensity function at the resist surface as shown in Figure 3.15. The new IBM resist formulation was adjusted to provide a nonlinear, thresholdlike response and therefore generates square-wave relief patterns. A plot of the dissolution rate of this formulation as a function of normalized photoactive compound concentration, which is inversely dependent on dose, is provided in Figure 3.16, which clearly shows the thresholdlike response. A mid-UV resist based on this design is being used in conjunction with a scanning projection printer to produce 1-megabit dynamic random access memory chips (32).

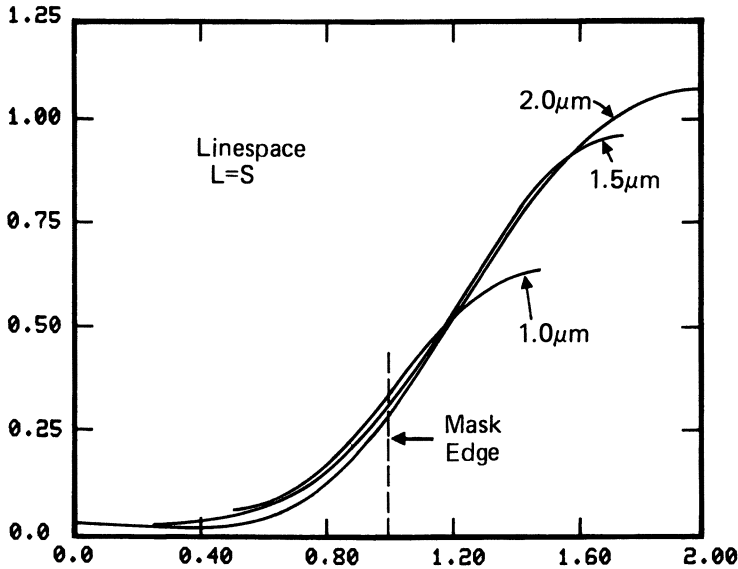


Figure 3.14. Free space image at the wafer plane for 1.0-, 1.5-, and 2- μm lines and spaces at $\text{NA} = 0.167$, partial coherence 0.71, and $\lambda = 313 \text{ nm}$. (Reproduced with permission from reference 30.)

3.2.1.1.b Deep-UV Dissolution-Inhibitor System

Lin evaluated the photosensitivity and lithographic performance of AZ2400 resist in the DUV mode in comparison with PMMA and AZ1350J (33). Gipstein et al. (34) synthesized cresol-formaldehyde novolac resins that are more transparent in the 254-nm region than novolac resins used in commercial photoresists. They also evaluated the resin's utility as a matrix for diazonaphthoquinone resist formulations for DUV lithography. However, the diazonaphthoquinone-novolac systems have not been successfully applied to DUV lithography. These systems suffer in DUV imaging from the same problems that limit their utility in the mid-UV region, namely, photoproduct absorbance and the strong absorption of novolac resins (Figures 3.10 and 3.11).

The magnitude of the deleterious effect that unbleachable absorbance has on developed profiles can be demonstrated by using SAMPLE (simulation and modeling of profiles in lithography and etching) (35), a computer program that simulates lithographic performance based on modulation transfer function, wavelength, dose, and the resist performance parameters of Dill et al. (36). The Dill parameter B represents the unbleachable absorbance of a resist, (i.e., the combined absorbance of the resin and the photoproducts). Figure 3.17 shows a SAMPLE simulated profile for a given set of exposure and development conditions for AZ1350J exposed at 436 nm (37).

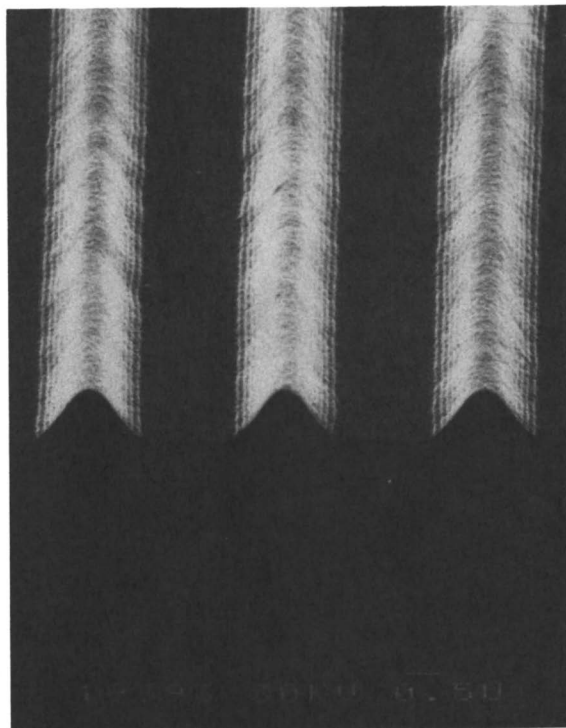
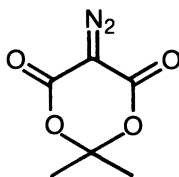


Figure 3.15. SEM of 3- μm pitch gratings printed in a linear experimental resist (Perkin-Elmer M500, scan speed 5000, aperture 0). (Reproduced with permission from reference 30.)

The curve is accompanied by one in which only B has been changed such that it represents the absorbance of the resist at 254 nm ($B = 1.96$) rather than at 436 nm ($B = 0.058$), with all other parameters kept constant. The effect is very large and sufficient to render the image useless for subsequent processes. Thus, conventional positive photoresists do not function adequately in DUV lithography.

Two interesting attempts to redesign the dissolution-inhibitor-matrix-resin systems have been reported. Grant et al. (37) proposed an alternative inhibitor for novolac resins. They found that 5-diazo-Meldrum's acid (structure 3.5) exhibits an intense, bleachable absorbance at 254 nm with a sharp



3.5

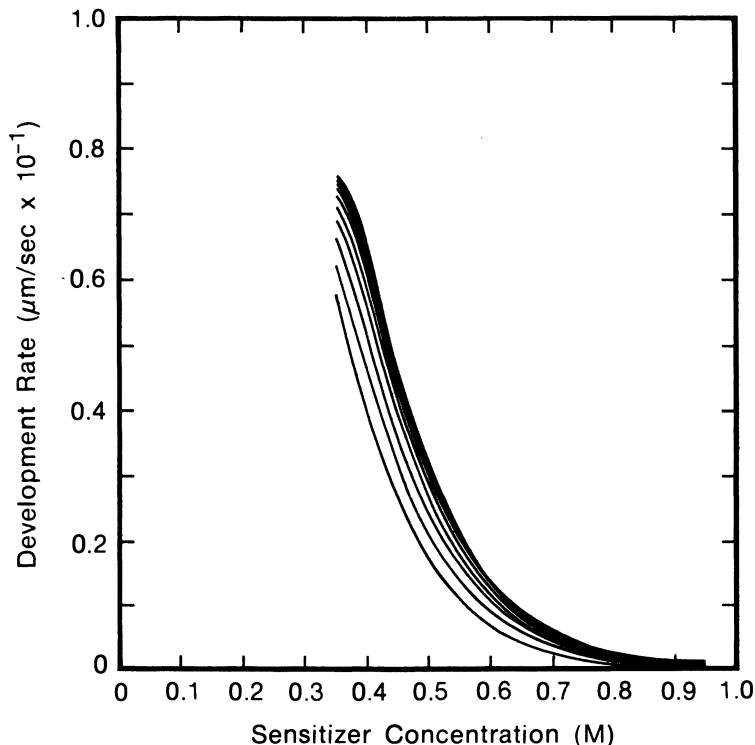


Figure 3.16. Development rate function of an IBM mid-UV resist at 1.0- μm increments from the surface. (Reproduced with permission from reference 30.)

cutoff above 300 nm (Figure 3.18) and is converted into volatile photoproducts upon irradiation. Photolysis of structure 3.5 results in a Wolff rearrangement to afford a ketene intermediate that decomposes further into carbon monoxide and acetone (Scheme 3.2) (37). The resists formulated with these sensitizers exhibited a reasonable sensitivity but suffered from sensitizer volatility and solubility problems. Profile degradation was experienced in films of over 0.5- μm thickness because of the strong absorption of the novolac matrix resin (Figure 3.18).

Reichmanis et al. (38, 40), Wilkins et al. (39), and Chandross et al. (41) redesigned both the dissolution inhibitor and the matrix resin. They evaluated a variety of *o*-nitrobenzylcholates (structure 3.6) that are initially insoluble in alkaline developer but are cleaved upon UV radiation to form base-soluble species. As shown in Scheme 3.3, irradiation of the *o*-nitrobenzyl ester results in rearrangement and degradation to generate a carboxylic acid and *o*-nitrosobenzaldehyde ($R = \text{H}$ in Scheme 3.3) (42). The matrix resin chosen is a copolymer of methyl acrylate and methacrylic acid that is far more transparent in the DUV than novolac resins and is soluble

in aqueous alkali. The new resist is reported to have useful sensitivity and extremely high contrast. The best result has been obtained in the case of 2,6-dinitrobenzylcholate (sensitivity is 90 mJ/cm^2 at $260 \pm 20 \text{ nm}$, contrast > 5) (40). A nearly thresholdlike exposure-dissolution response has been observed in this unusually high contrast resist. The resist formulation is essentially aliphatic and would be less stable in dry etching environments than resists based on aromatic resins (43, 44).

3.2.1.2 POSITIVE RESISTS BASED ON MAIN-CHAIN SCISSION

Moreau and Schmidt (7) showed that the electron beam positive resist, PMMA, responds to DUV radiation. Lin demonstrated its high-resolution capability by DUV contact printing $0.5\text{-}\mu\text{m}$ bars separated by $0.25\text{-}\mu\text{m}$ gaps in $1.78\text{-}\mu\text{m}$ -thick films of PMMA as shown in Figure 3.19 (8). Photolysis of PMMA leads to chain scission (Scheme 3.4): homolysis of the side chain is followed by decarbonylation to form a stable tertiary radical on the main chain, which, in turn, undergoes cleavage through β -scission of the chain to generate an acyl-stabilized tertiary radical. This process generates fragments of carbon monoxide, carbon dioxide, and methyl and methoxy radicals (45–50).

The chain scission initiated by the photolysis of PMMA results in the reduction of the molecular weight, which is primarily responsible for increased solubility rate of the exposed region. In addition to the molecular

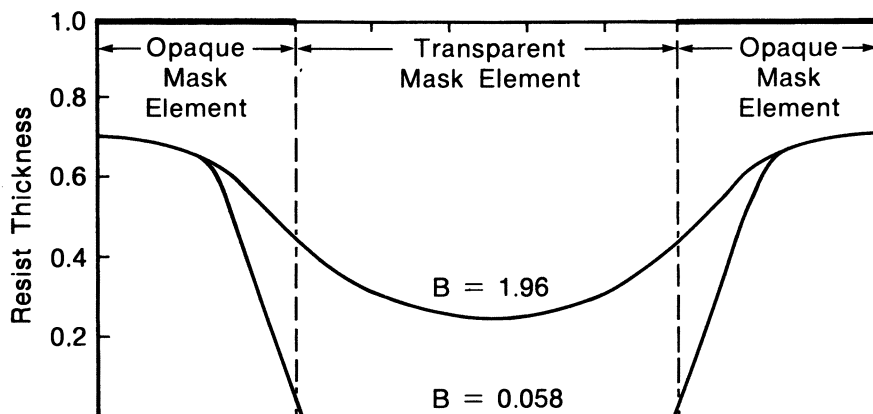


Figure 3.17. Computer-simulated resist profiles (SAMPLE). Operating input parameters include matched substrate, AZ1350J resist, 4358 \AA , 90 mJ/cm^2 , $NA = 0.35$, $\sigma = 9.99$, defocus 0.0 , development 80 s . The open image ($B = 0.058$) simulates AZ1350J performance. The shallow profile ($B = 1.96$) was generated from identical input parameters with the exception that the unbleachable absorbance (B) was adjusted to the value corresponding to the absorbance of $1 \mu\text{m}$ of novolac at 254 nm . (Reproduced with permission from reference 37. Copyright 1981 Institute of Electrical and Electronics Engineers.)

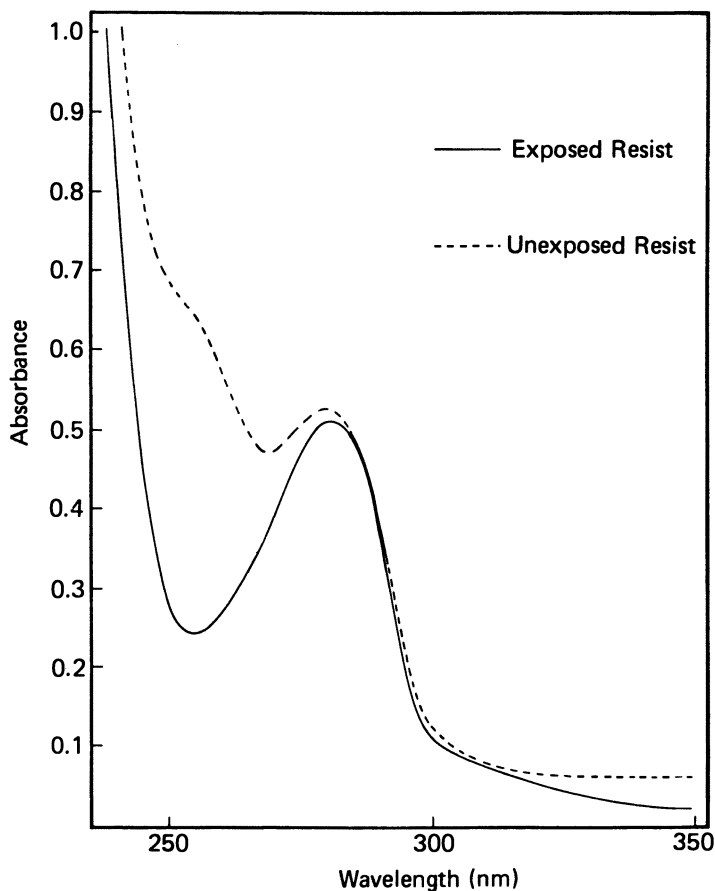
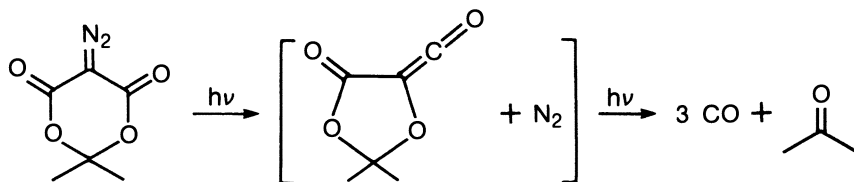
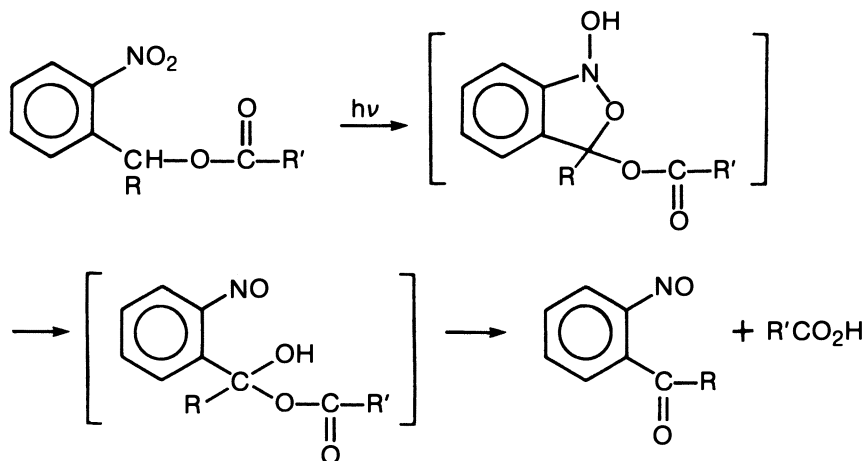
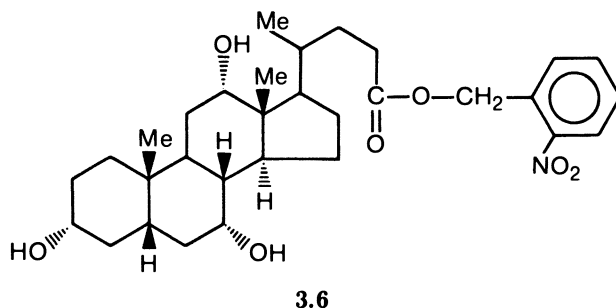


Figure 3.18. Absorbance spectra of Meldrum's diazo resist before and after exposure. (Reproduced with permission from reference 37. Copyright 1981 Institute of Electrical and Electronics Engineers.)



Scheme 3.2. Photochemical decomposition of 5-diazo-Meldrum's acid.



Scheme 3.3. Photochemical decomposition of o-nitrobenzyl ester.

weight reduction, factors controlling solvent mobility in the PMMA matrix strongly affect the dissolution kinetics of PMMA (51, 52). Ouano (51) found that the increase in the dissolution rate (S) with decreasing molecular weight (MW) is much faster in electron-beam-exposed PMMA film than in unexposed films. The slopes of the $\log S$ - $\log MW$ plots for electron-beam-exposed PMMA and unexposed PMMA are reported to be 2 and 0.5, respectively, in amyl acetate. The slope for DUV-exposed PMMA has been reported to be 1.7 in methyl isobutyl ketone (MIBK) (53). The greatly increased dissolution rate of the exposed film compared to unexposed film of the same molecular weight has been ascribed to the formation of increased free volume or density reduction due to gaseous product generation during the radiochemical degradation of PMMA and a corresponding increase in the rate at which the developer solvent diffuses into the films in the exposed regions.

PMMA offers several advantages as a resist. These include extremely high resolution, ease of handling, excellent film-forming characteristics, wide processing latitude, and ready availability. Unfortunately, PMMA is a rel-

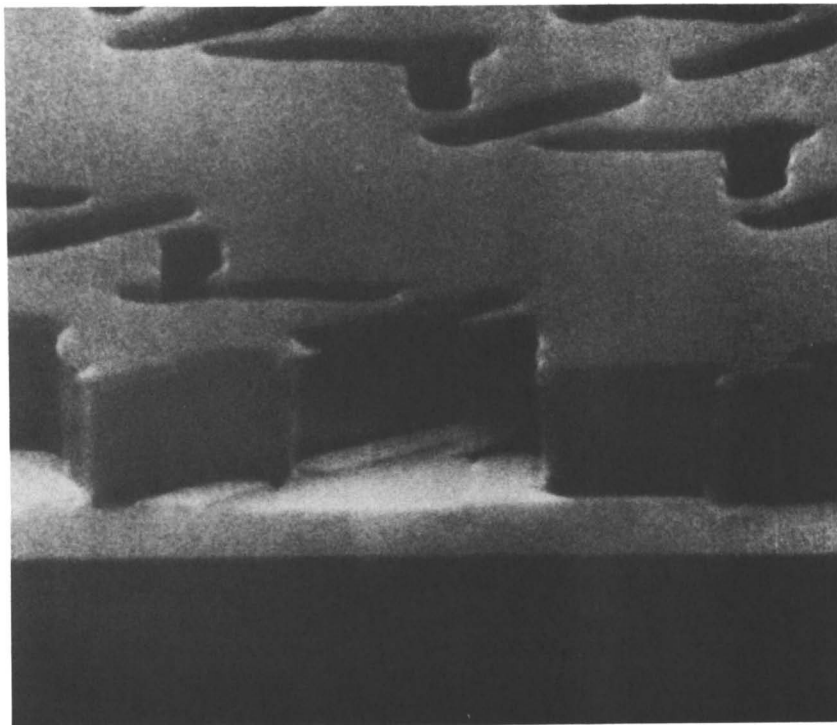
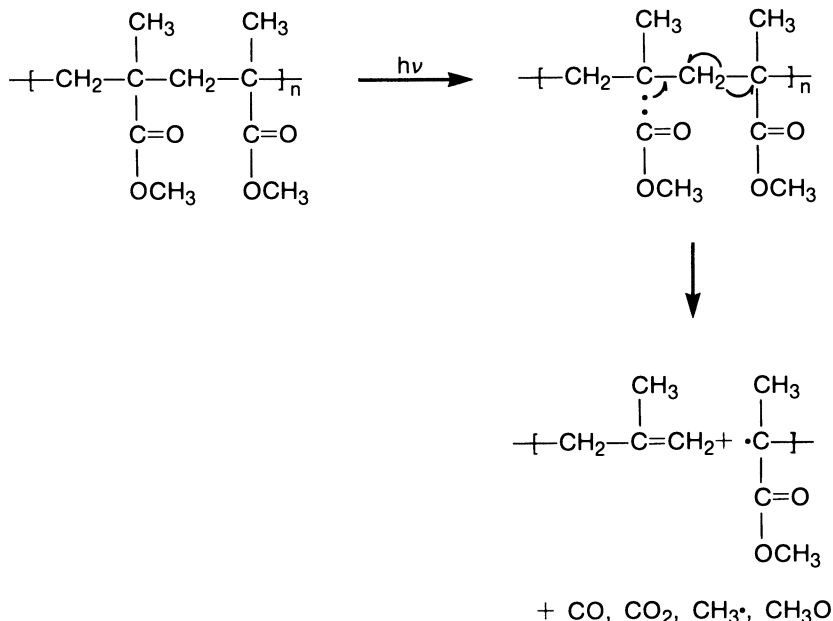


Figure 3.19. Y-I bars (Y- and I-shaped patterns) ($0.5 \mu\text{m}$) separated by $0.25\text{-}\mu\text{m}$ gaps, printed in $1.78 \mu\text{m}$ of PMMA2041. (Reproduced with permission from reference 8. Copyright 1975 American Institute of Physics.)

atively insensitive material and requires $0.5\text{--}1.0 \text{ J/cm}^2$ of DUV dose for workable processing. Consequently, many analogs of PMMA have been evaluated as DUV resists. The goal of these studies has been to preserve the desirable properties of PMMA while improving its sensitivity.

Table 3.1 summarizes the lithographic properties of methacrylate polymers (54). These polymethacrylates all exhibit similar UV absorptions with optical densities of $0.27\text{--}0.47 \mu\text{m}^{-1}$ at 215 nm , which is considerably less than that of AZ1350J in the near-UV region ($0.87 \mu\text{m}^{-1}$ at 405 nm). This low absorption represents inefficient use of flux and is one reason for the low sensitivity of the system.

Poly(glycidyl methacrylate) (PGMA), a well-known negative electron beam resist first reported by Hirai et al. (55), actually functions as a positive-tone resist upon DUV exposure (Table 3.1) (56). The epoxide functionality responsible for cross-linking under electron beam exposure does not absorb in the DUV region, and the response of PGMA to DUV radiation is determined by the absorption due to the $n - \pi^*$ transition of the carbonyl chromo-



Scheme 3.4. Mechanism of radiation-induced chain scission in PMMA.

Table 3.1. Polymethacrylate Positive DUV Resists

<i>Resist</i>	<i>Ester Group</i>	α (μm^{-1}) ^a	<i>Sensitivity</i> (J/cm^2)
Poly(methyl methacrylate) (PMMA)	−CH ₃	0.42	0.6
Poly(glycidyl methacrylate) (PGMA)	$\begin{array}{c} \text{---} \text{CH}_2 \text{---} \text{CH} \text{---} \text{CH}_2 \\ \quad \quad \quad \\ \quad \quad \quad \text{O} \end{array}$	0.33	0.8
Poly(butyl methacrylate) (PBMA)	<i>n</i> -butyl/isobutyl (50/50)	0.29	0.5
Poly(fluorobutyl methacrylate) (FBM)	−CH ₂ CF ₂ CFHCF ₃	0.27	0.094

^aThe symbol α is the absorption coefficient at 215 nm.

phore that leads to main-chain scission. Among the polymethacrylates, FBM, a poly(fluorobutyl methacrylate)-based resist, seems to be the most sensitive to DUV (54) as well as to electron beam and X-ray radiation (57). This material is commercially available from Daikin Kogyo, Japan.

Table 3.2 summarizes a variety of the methyl methacrylate (MMA) copolymers developed as DUV resists. Chandross et al. (41, 61), Wilkins et al. (58), and Reichmanis et al. (59, 60) reported that incorporation of 3-oximino-2-butanone methacrylate into the PMMA structure [P(MMA-OM)] improves both the absorption characteristics of the polymer in the 220–260-

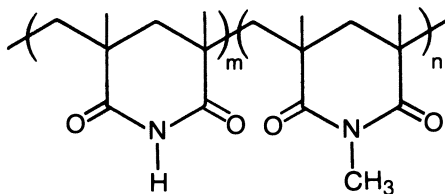
Table 3.2. MMA Copolymers as Positive DUV Resists

Resist	Comonomer	RS	Comments	Effective Spectral Range (nm)	Reference
P(MMA-MA) GCM	Methacrylic acid Glycidyl methacrylate	0.85 2	α (215 nm) = $0.47 \times \mu\text{m}^{-1}$ MMA/GMA = 70/30	200-240 200-240	54 56
P(MMA-OM)	3-Oximino-2-butanone methacrylate	50	$\lambda_{\text{max}} = 215$ nm MMA/OM = 63/37	240-270	58
P(MMA-OM- MAN)	3-Oximino-2-butanone methacrylate, methacrylonitrile	85	$\lambda_{\text{max}} = 220$ nm MMA/DM/MAN = 69/16/15	240-270	59
P(MMA-I)	Indenone	60	MMA/I = 97/3	230-300	62
P(MMA-PhIPK)	Phenyl isopropenyl ketone	110	$\lambda_{\text{max}} = 240, 280$ nm MMA/PhIPK = 72/28	220-360	71

NOTE: RS denotes the sensitivity relative to PMMA, and α denotes the absorption coefficient.

nm range and provides an alternate path for scission and therefore leads to enhanced sensitivity. P(MMA-OM) (63:37) is 50 times more sensitive than PMMA. Incorporation of methacrylonitrile (MAN) into P(MMA-OM) results in further increase in the sensitivity (41, 59–61). P(MMA-OM-MAN) is 85 times more sensitive than PMMA to DUV radiation. When sensitized with *tert*-butylbenzoic acid, it requires an exposure dose of less than 30 mJ/cm² at 240 nm (61). Copolymers of indenone with MMA, also developed by Chandross et al. (41, 61, 62), have a strong UV absorption in the 230–330-nm region and exhibit a monochromatic sensitivity of 60 mJ/cm² at 3% indenone concentration. The high sensitivity is explained in terms of the steric strain present in the cyclopentanone moiety. Resolution of 0.75- μ m lines and spaces has been achieved in the indenone copolymers by using a modified Perkin-Elmer Model 111, 1:1 projection printer.

Poly(dimethyl glutarimide) (PMGI) (structure 3.7) was shown by Hiraoaka (63) to undergo molecular weight reduction upon irradiation with a sensitivity comparable to PMMA. This polymer is sensitive to DUV radiation below 280 nm; soluble in aqueous base; resistant to common organic solvents; and thermally stable to ca. 185 °C, which renders the material very attractive as a thick planarizing layer in the exposure-PCM scheme as will be discussed in a later section. This material is being evaluated for commercialization by Shipley Company (64, 65).



Another important class of degrading DUV positive resists is based on isopropenyl ketone polymers (Table 3.3). Tsuda et al. (66) reported the use of poly(methyl isopropenyl ketone) (PMIPK) as a positive DUV resist. This polymer exhibits a weak absorption centered at 285 nm due to the carbonyl chromophore and is about 7 times more sensitive than PMMA. An exposure time of 28 s for 1- μ m-thick PMIPK films was obtained on a Canon PLA520FA contact printer equipped with a CM290 cold mirror (67). Addition of sensitizers such as 3,4-dimethoxybenzoic acid results in a threefold increase in sensitivity (53, 66, 67). PMIPK and sensitized PMIPK are commercially available under the trade names of ODUR1010 and ODUR1013 and 1014 from Tokyo Ohka Kogyo, in Japan. MacDonald et al. (68, 69) found that the quantum yield of chain scission at 313 nm in films of poly(isopropenyl *tert*-butyl ketone) (PIPTBK) is 12 times higher than that of PMIPK. In PIPTBK,

the carbonyl group is located between two quaternary centers. Thus, the Norrish Type I α -cleavage on either side of the carbonyl carbon generates a stable tertiary radical as depicted in Scheme 3.5. This result should be contrasted with the situation in PMIPK, where α -cleavage yields either a tertiary butyl or methyl radical. As the stability of these species is significantly different, cleavage only occurs to generate the tertiary radical. Thus, the replacement of the methyl in PMIPK by a tertiary butyl group increases the propensity for the Norrish Type I photochemical degradation, which is a predominant pathway in the solid state (70).

Aromatic groups provide a convenient chromophore for UV absorption. Copolymers of isopropenyl phenyl ketone (IPPhK) with MMA show spectral sensitivity up to the mid-UV range (Table 3.3) (71). P(IPPhK-MMA) (28:72) is 10 times more sensitive than PMIPK when exposed to the full output of a Xe-Hg lamp.

Poly(butene-1 sulfone) (PBS), a sensitive, positive, electron beam resist, is highly sensitive to 185-nm radiation (Table 3.4) (9). However, PBS does not absorb above 200 nm, and the sensitization has not been successful. Incorporation of pendant aromatic rings into the polysulfone structure extends the photosensitivity to the DUV and mid-UV regions (72). Himics and Ross (73) reported that carbonyl-containing poly(olefin sulfones) such as poly(5-hexen-2-one sulfone) are sensitive to UV-induced degradation and

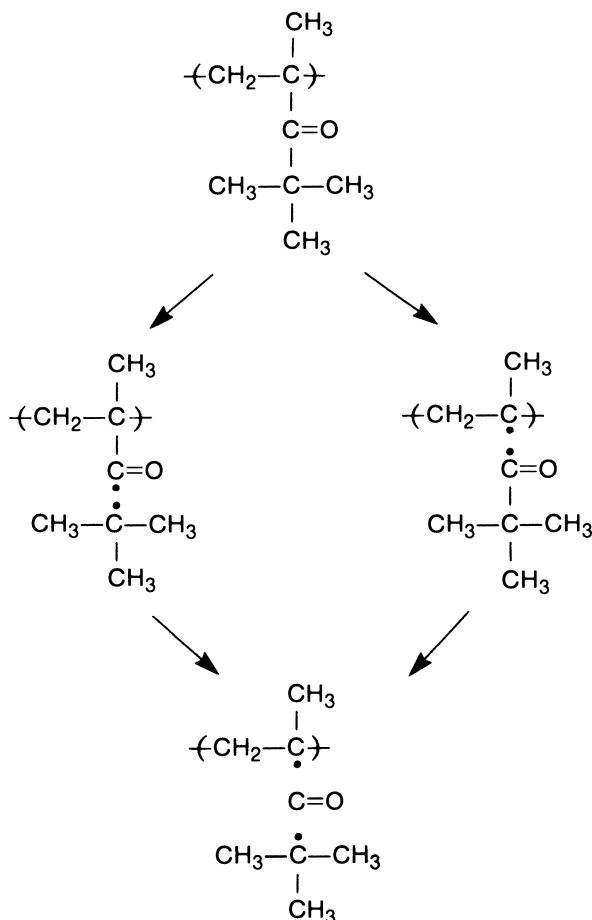
Table 3.3. Poly(isopropenyl ketones) as Positive DUV Resists

<i>Resist</i>	<i>RS</i>	<i>Comments</i>	<i>Reference</i>
Poly(methyl isopropenyl ketone) (PMIPK)	1	ODUR1010 (Tokyo Ohka)	66
	3	PMIPK + 3,4-dimethoxy benzoic acid	66
	3	PMIPK + sensitizer (ODUR1013)	53
Poly(isopropenyl <i>tert</i> -butyl ketone) (PIPTBK)		Φ (scission)(solid) = 0.29 at 313 nm 12 times higher than PMIPK	68, 69
Poly(phenyl isopropenyl ketone- <i>co</i> -MMA) [P(PhIPK-MMA)]	10	Copolymer with MMA(28:72)	71

NOTE: RS denotes the relative sensitivity to PMIPK.

Table 3.4. Poly(olefin sulfones) as Positive DUV Resists

<i>Resist</i>	<i>Effective Spectral Range (nm)</i>	<i>Sensitivity (mJ/cm²)</i>	<i>Reference</i>
Poly(butene-1 sulfone) (PBS)	180–200	5 (at 185 nm)	9
Poly(styrene sulfone) (PSS)	240–280	1000 (at 265 nm)	72
Poly(styrene- <i>co</i> -acenaphthalene sulfone)	250–300	500 (200–400 nm)	72



Scheme 3.5. Norrish Type I cleavage in PIPTBK.

that the sensitivity can be increased by addition of certain photosensitizers (e.g., benzophenone).

The incorporation of aromatic groups into DUV resist systems also offers an increase in dry etch resistance. As the minimum feature size of semiconductor devices shrink, anisotropic dry etching is becoming more and more important in device fabrication. However, positive resist materials that efficiently undergo main-chain scission upon irradiation generally lack dry etch durability. This dichotomy of performance requirements is most commonly circumvented only in two-component resists, but recently, 1:1 alternating copolymers of styrene and olefins that are tri- or tetrasubstituted with electron-withdrawing groups (74) have been shown to undergo main-chain scissioning reactions upon DUV or electron beam irradiation with a sensi-

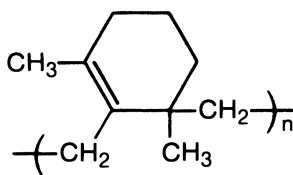
tivity comparable to that of PMMA, yet these polymers are as stable in plasma environments as polystyrene (75).

3.2.2 Negative Resists

3.2.2.1 AZIDE SENSITIZER SYSTEMS

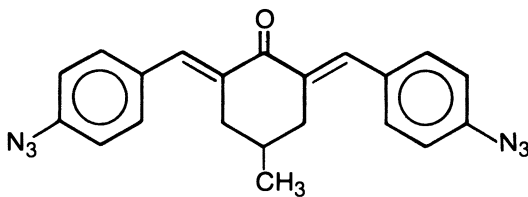
3.2.2.1.a Azide-Cyclized Polyisoprene Photoresists

Photosensitive systems composed of photoactive aromatic azide compounds and a variety of host polymers have been well known since the 1930s (1a). Negative photoresists comprising an azide and a cyclized *cis*-1,4-polyisoprene (structure 3.8) as a host polymer, such as Kodak's KTRF, have been



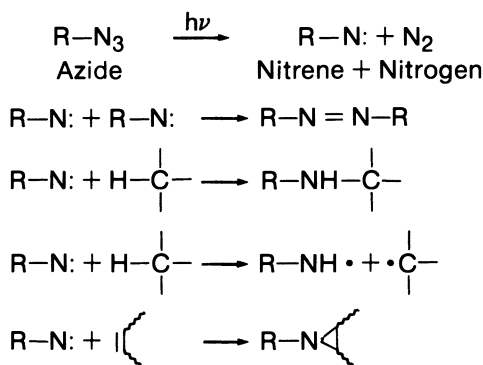
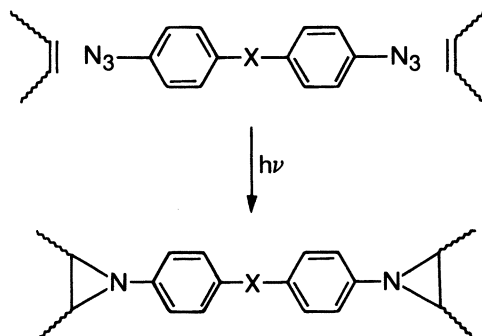
3.8

widely used in the microelectronics industry. The most commonly used azide sensitizer for conventional near-UV lithography is 2,6-bis(4'-azidobenzal)-4-methylcyclohexanone (structure 3.9).



3.9

Cyclized polyisoprene sensitized with an aromatic bisazide generates an insoluble, three-dimensional network via cross-linking upon irradiation. The photoinduced reactions associated with the generation of the network are shown in Scheme 3.6. The primary event is the decomposition of the arylazide in the excited state into a reactive nitrene intermediate that can undergo a variety of reactions. The nitrene reactions include nitrene-nitrene coupling to form azo dyes, insertion into carbon-hydrogen bonds to form secondary amines, abstraction of hydrogen from the rubber backbone to form an imino radical and a carbon radical that can subsequently undergo coupling reactions, and insertion into the double bond of polyisoprene to form three-membered aziridine linkages (Scheme 3.6).



Scheme 3.6. Crosslinking reactions in bisarylazide-rubber resists.

The cyclized rubber-bisazide formulations offer high sensitivity, ease of handling, and wide process latitude. However, the resolution of these systems is limited by relatively low contrast and the swelling-induced deformation of resist patterns during development. Although the cross-linking reaction renders the polymer insoluble in the developer, the cross-linked polymer still has an affinity for the developer solvent. Therefore, the cross-linked regions absorb solvent during development. The resulting increase in volume, or swelling, causes distortions of fine patterns $< 2 \mu\text{m}$ in the form of “bridging” or “snaking” (Figure 3.20).

Several bisazides with absorption maxima between 240 and 290 nm have been examined as DUV sensitizers for cyclized polyisoprene (76). The sensitivity of DUV resist formulated with cyclized polyisoprene and 1 wt % of 3,3'-bisazidophenyl sulfone (structure 3.10) is 75 times higher than that of PMMA. These azide DUV resists suffer from the resolution limit imposed by low contrast and the swelling phenomenon, which is as expected from the preceding discussion.

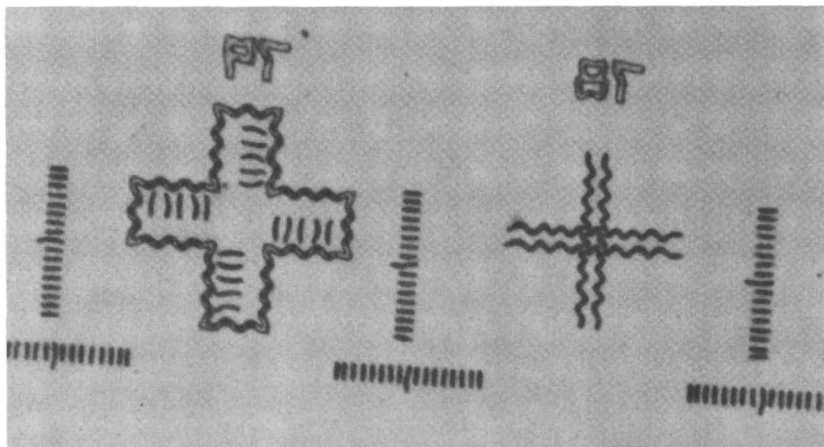
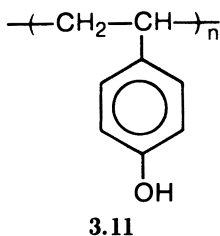
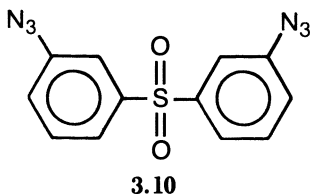


Figure 3.20. Swollen images in a cross-linking negative resist. (Reproduced with permission from reference 105. Copyright 1986 Electrochemical Society.)

3.2.2.1.b Azide-Phenolic Resin System

A novel, nonswelling DUV resist was developed by Iwayanagi et al. (77). This resist, known as MRS (micro resist for shorter wavelengths), consists of poly(*p*-vinylphenol) (structure 3.11), an alkaline-soluble phenolic resin, and an azide (structure 3.10).



Dissolution inhibition occurs upon exposure, and the unexposed portion of the resist film is dissolved in an aqueous alkali solution in an etching-type dissolution that is devoid of swelling (78, 79). Because the combined absorption of the azide and the resin is quite intense in the DUV region, as shown in Figure 3.21, the photochemical reaction leading to the decrease in solubility occurs mainly in the upper regions of the film. This situation is shown in Figure 3.22a, where the resist was exposed in the UV-2 mode (220–290 nm) on a Perkin-Elmer M500 projection printer (80). The upper layers of the exposed resist film develop slowly, and the unexposed lower levels develop at a constant rate. The insolubilized surface layer of the exposed areas acts as a mask while the alkaline developer removes unexposed

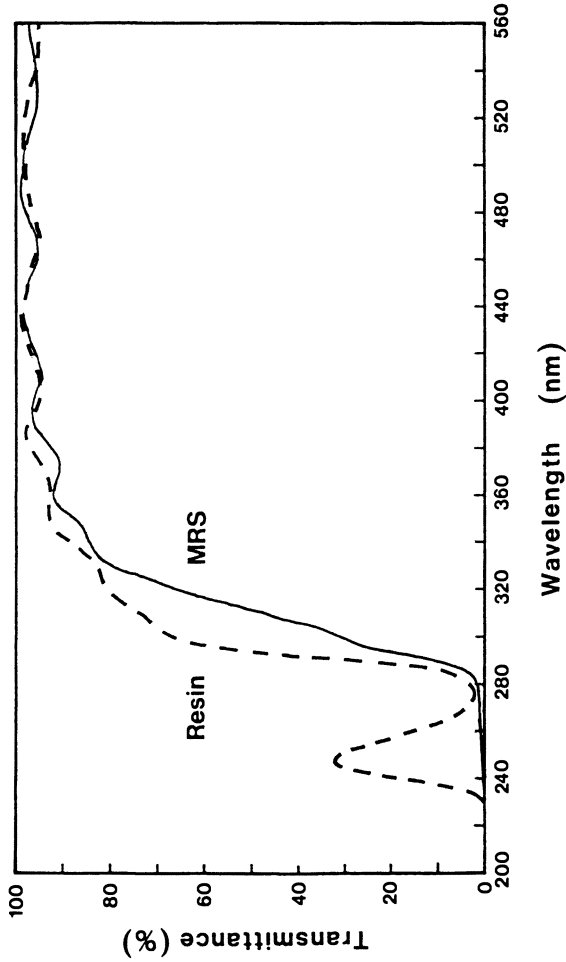
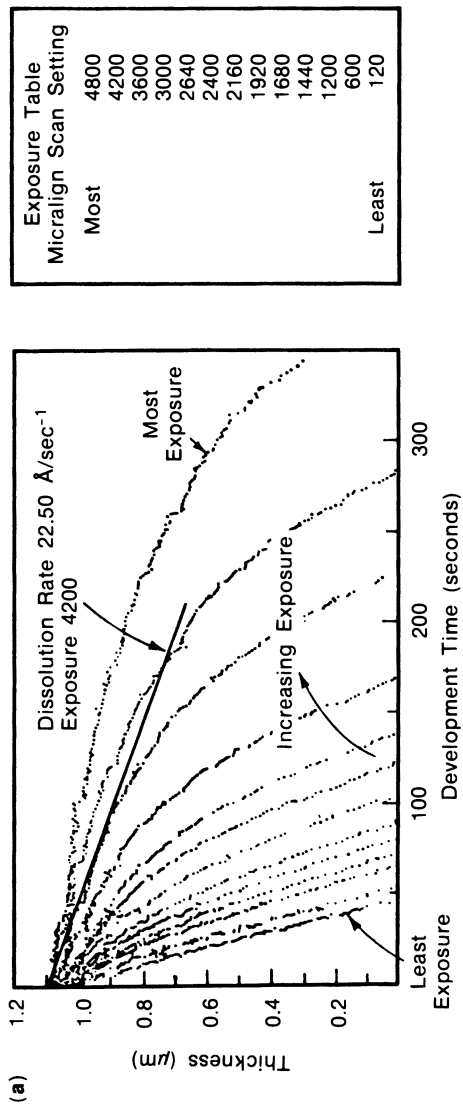


Figure 3.21. Spectral transmittance of a 1- μm -thick azide-phenolic resin photoresist. (Reproduced with permission from reference 87. Copyright 1985 Society of Photo-Optical Instrumentation Engineers.)



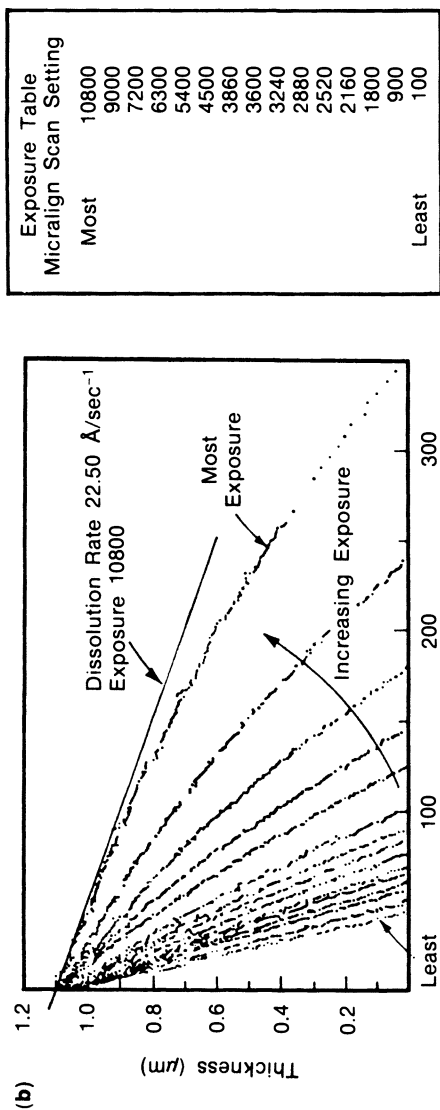


Figure 3.22. Resist thickness versus development time of RD2000N in MF312-water (1:4): (a) UV-2 mode and (b) UV-3 mode. (Reproduced with permission from reference 80. Copyright 1983 Society of Photo-Optical Instrumentation Engineers.)

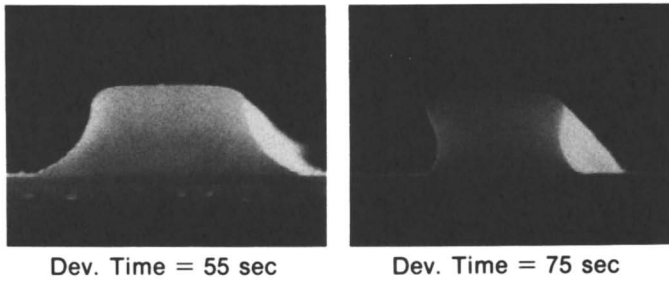
areas in an etching-type development process. Consequently, resist profiles change from overcut to undercut with increasing development time. The resist profiles calculated by the SAMPLE simulation are compared in Figure 3.23 with SEMs of resist images obtained by DUV projection printing (81).

The resist responds to mid-UV as well as DUV radiation. Figure 3.22b indicates that the exposure in the UV-3 mode (290–340 nm) results in less undercutting because of the higher transparency in the mid-UV range (80). However, the resist is less sensitive to the mid-UV than to the DUV by a factor of 2. Scanning exposure times required for MRS are ca. 20 and 40 s in the UV-2 and UV-3 mode, respectively, on a Perkin–Elmer M500 printer. To summarize, the resist offers high sensitivity and nonlinear dissolution kinetics that lead to a high propensity for undercut profiles when exposed to the DUV radiation; the resist offers linear dissolution kinetics and low sensitivity in the UV-3 mode.

One possible solution to this dichotomy is the replacement of the commercial phenolic resin with a resin more transparent in the DUV region. One such example is an acrylic acid-based resin (82), which lacks dry etching resistance. Another solution would be to expose the MRS resist simultaneously to both DUV and mid-UV radiation without any filter, which leads to high-resolution surface imaging due to the dominant DUV exposure of the surface and high aspect ratio imaging due to the deep penetration of the mid-UV light (Figure 3.24) (83, 84). This mode of exposure offers an added advantage of decreased exposure time (ca. 15 s on a Perkin–Elmer M500 scanner). An SEM photograph of 1- μm lines and spaces obtained by the broad-band exposure of MRS is given in Figure 3.25 (78). Lin (83) demonstrated the different responses of the MRS resist to monochromatic DUV KrCl (222 nm) and mid-UV XeCl (308 nm) excimer laser exposures (see Section 3.4.2).

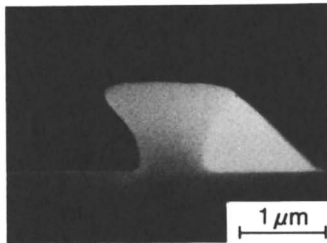
The undercut profile available from DUV exposure of MRS is, however, preferred over the overcut profile for anisotropic dry etching on stepped surfaces as illustrated in Figure 3.26 (83, 85, 86). In this application, the dimension of etched patterns is determined by the top dimension of the imaged resist; thus, the topography effect is eliminated. In fact, the top edge of the undercut MRS resist serves as a mask for anisotropic reactive ion etching (RIE) as shown in Figure 3.27, where 1- μm -tall aluminum patterns with vertical sidewalls are obtained. The MRS resist is currently being used in a 1.5- μm aluminum metalization process combining the Perkin–Elmer M500 projection printing with RIE (87).

The decrease in solubility upon exposure in this type of resist was first ascribed to the formation of a secondary amine generated from nitrene insertion into C–H bonds of the polymer (see Scheme 3.6) (88). However, gel permeation chromatographic analyses revealed that the molecular weight of poly(*p*-vinylphenol) increased upon irradiation in the presence of the azide. Hydrogen abstraction from the polymer by nitrene and subsequent polymer



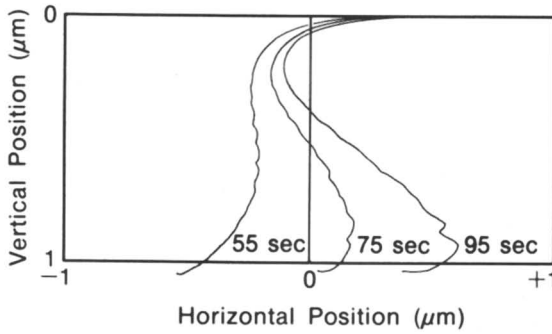
Dev. Time = 55 sec

Dev. Time = 75 sec



Dev. Time = 95 sec

(a) Experiment



(b) Simulation

Figure 3.23. Cross sectional view of MRS resist as a function of development time: (a) experiment and (b) simulation. (Reproduced with permission from reference 81. Copyright 1982 Institute of Electrical and Electronics Engineers.)

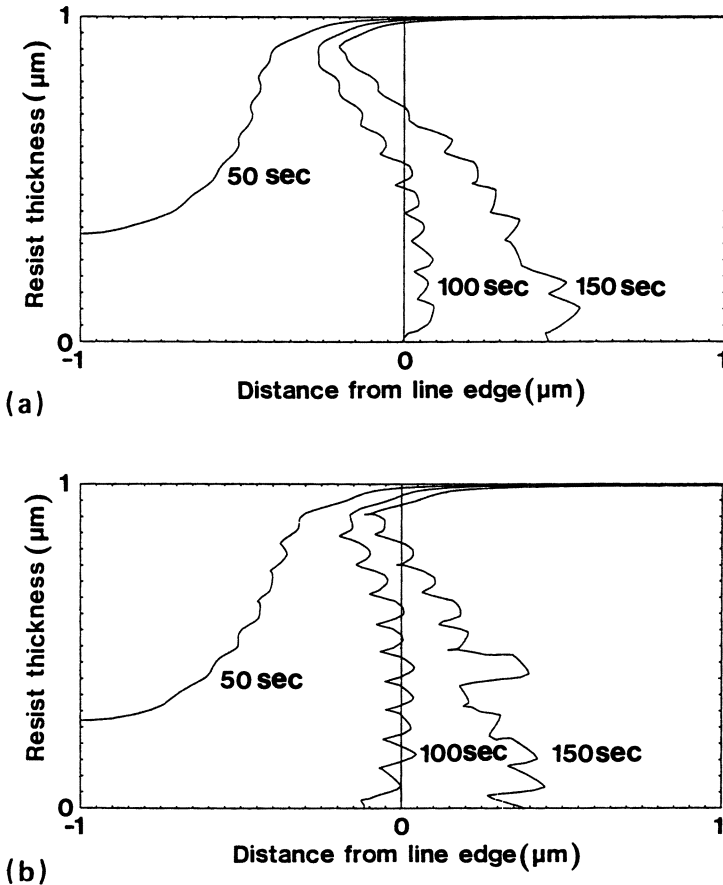


Figure 3.24. Simulated MRS profiles: (a) The intensity ratio of 256–300-nm radiation is 1:1. (b) The intensity ratio is 1:3. (Reproduced with permission from reference 84. Copyright 1983 North-Holland.)

radical recombination results in an increase in the molecular weight of the polymer, rendering the exposed areas less soluble in aqueous base solutions. The rapid decrease in the dissolution rate of poly(*p*-vinylphenol) in alkaline solution with increasing molecular weight has been separately ascertained (89).

Several DUV resists based on phenolic resins sensitized with azide compounds are now commercially available from Hitachi Chemical (RD2000N) (90), Hunt Chemical (WX303) (91), and Tokyo Ohka Kogyo (ODUR120).

3.2.2.2 NEGATIVE RESISTS BASED ON POLYSTYRENE DERIVATIVES

Incorporation of aromatic rings into polymer structures results in improvement in dry etch resistance (43, 44). Consequently, negative resists based

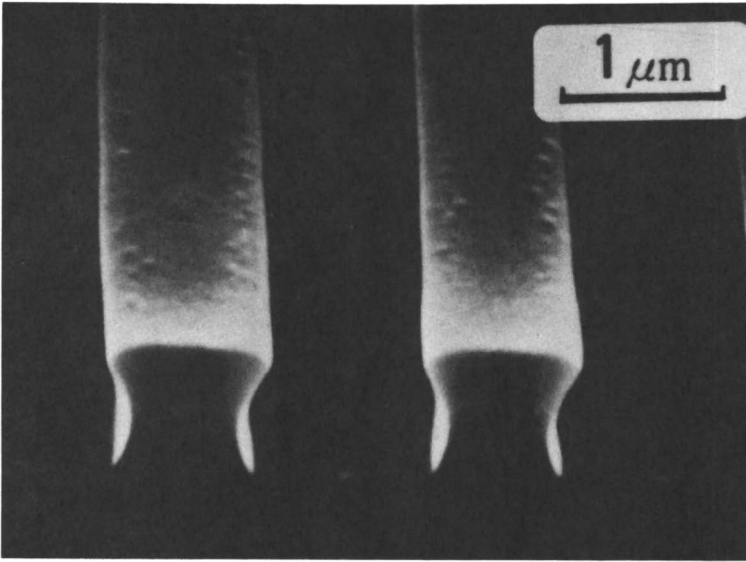


Figure 3.25. SEM of 1- μm lines and spaces printed in MRS resist by broadband exposure. (Reproduced with permission from reference 78. Copyright 1981 Institute of Electrical and Electronics Engineers.)

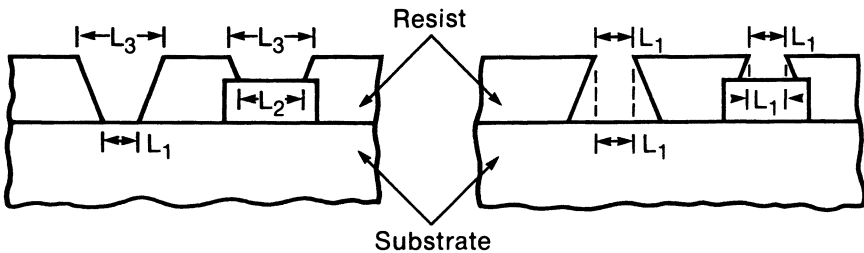


Figure 3.26. Line width variation caused by overcut resist profiles. This figure shows images printed in a resist with (left) overcut and (right) undercut resist profiles. The target etch dimension is L_1 . In the left figure, topographic features result in variation in line width $L_2 > L_1$. In the figure on the right, with undercut profiles, the anisotropically etched image is controlled by the dimension of the opening at the top of the resist. Hence, both etched dimensions are the same, L_1 . (Reproduced from reference 83. Copyright 1983 American Chemical Society.)

on cross-linking polymers with pendant aromatic groups have been developed primarily for dry etching applications in electron beam lithography (92). The incorporation of aromatic rings into polymers provides not only dry etching resistance but also absorption of DUV and mid-UV radiation due to the π - π^* transitions of the aromatic compounds as mentioned in section 3.1.2. The DUV lithographic properties of cross-linking polystyrenes are listed in Table 3.5.

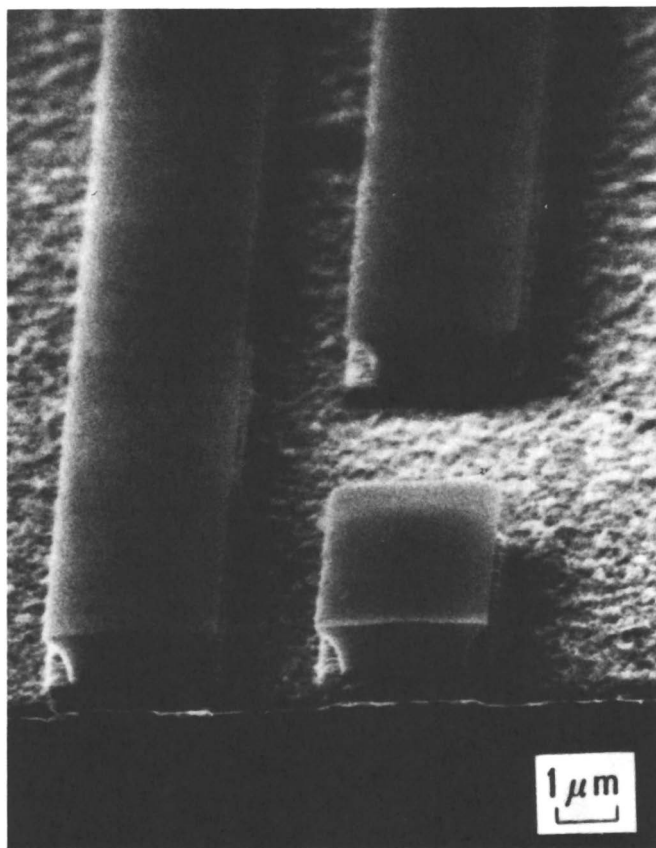


Figure 3.27. Reactive ion etching with MRS resist as the mask. (Reproduced with permission from reference 87. Copyright 1985 Society of Photo-Optical Instrumentation Engineers.)

Table 3.5. Polystyrene-Based Cross-Linking Negative DUV Resists

<i>Resist</i>	$M_w \times 10^4$	<i>Comments</i>	<i>Reference</i>
Chloromethylated polystyrene (CMS)	1.8–56	RS = 3.3–150, chloromethylation 0.13–0.98	93
Chlorinated poly(<i>m,p</i> -methylstyrene) (<i>m-/p</i> -isomer 2:1) (CPMS)	3–22	4–0.8-s exposure times for a contact printer, chlorine content ~ 20 unit%	97
Poly(4-chlorostyrene) (PCS)	70	50 mJ/cm ² , α (245 nm) = 0.21 μm^{-1}	95

NOTE: Abbreviations and symbols are as follows: M_w denotes the weight-average molecular weight, RS denotes the relative sensitivity to PMMA, and α denotes the absorption coefficient.

Polystyrene, one of the simplest vinyl polymers with a pendant benzene ring, is a negative-working resist but is much less sensitive than PMMA (93). Chloromethylation or chlorination of polystyrene has produced a class of negative DUV resists that exhibits very high sensitivity (Table 3.5). For example, chloromethylated polystyrene (CMS) with a molecular weight of 1.8×10^5 is reported to be 40 times more sensitive than PMMA (93). Polystyrene has a weak absorption at about 250 nm and a strong absorption below 220 nm. The absorption is enhanced and shifted to longer wavelength by the introduction of the chloromethyl group into the benzene ring. The absorption in the DUV region increases as the extent of chloromethylation increases, and, finally, a new peak appears at 230 nm. Increasing the extent of chloromethylation is accompanied by a deterioration in resolution, which is attributed to inevitable overexposure of the top layer of the resist film when adequate dose is delivered to ensure cross-linking of the bottom layer because of the strong absorption of the chloromethylated benzene chromophore. The DUV sensitivity of CMS increases with increasing molecular weight; its contrast decreases with increasing M_w/M_n (ratio of weight-average molecular weight to number-average molecular weight) as has been reported for electron beam and X-ray exposures (94). This class of cross-linking polymers suffers from resolution limitations due to the swelling during development. However, use of low-dispersity polymers (93, 95) and judicious choice of developer solvents (96) can minimize the swelling. A typical example is given for chlorinated polymethylstyrene (CPMS) in Figure 3.28 (97).

To elucidate the mechanism of cross-linking in CMS, pulse radiolysis studies (98) and low-temperature electron spin resonance (ESR) studies (99)

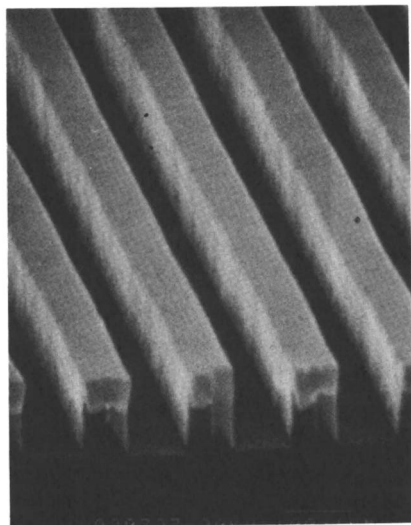
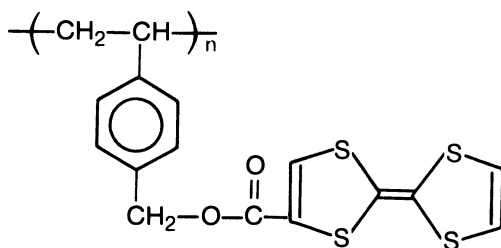


Figure 3.28. SEM of 0.8- μm lines and spaces printed in a 1- μm CPMS resist. (Reproduced with permission from reference 97. Copyright 1982 Society of Photographic Scientists and Engineers.)

on substituted polystyrene model compounds have been carried out. On the basis of their ESR studies, Tanigaki et al. (99) proposed new resist materials: a blend of poly(*p*-methoxystyrene) and poly(*p*-chloromethylstyrene) and a nonswelling, aqueous base-developable negative resist consisting of poly(*p*-hydroxystyrene) and a chlorine-releasing compound. A similar study was reported by MacDonald et al. (100).

Polystyrene-tetrathiofulvalene (PSTTF) (structure 3.12) is a novel negative resist developed by Hofer et al. (101) that has high contrast and is nonswelling. This resist has introduced a new concept in resist design. The differential dissolution is achieved not through generation of a three-dimensional, cross-linked network, but rather through a change in the polarity of pendant groups.



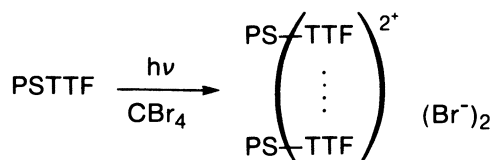
3.12.

Exposure of PSTTF sensitized with a perhaloalkane such as carbon tetrabromide results in generation of dimeric tetrathiofulvalene bromide salts (Scheme 3.7) that are polar in nature and, therefore, are insoluble in nonpolar organic solvents (102).

Consequently, development with a nonpolar solvent selectively dissolves the unexposed, nonpolar polymer, providing high-resolution negative patterns with no evidence of swelling-induced distortion. The PSTTF system is reported to show good sensitivity to Al K α X-ray (50 mJ/cm²) and electron beams (10 μ C/cm²) (101). The DUV lithographic performance of PSTTF has not yet been published.

3.2.3 Dual-Tone Resists

This section discusses recent examples of application of the design concept embodied in the PSTTF resist (i.e., differential solubility generation through



Scheme 3.7. Imaging mechanism of PSTTF resist.

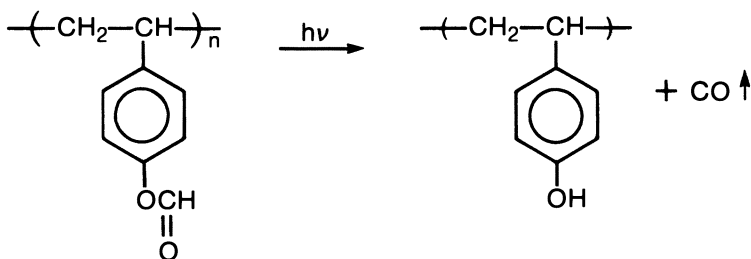
alteration of the polarity of polymer side-chain groups rather than through the molecular weight change via backbone scissioning or cross-linking). These systems do not exhibit resolution loss due to swelling during development.

One such DUV resist employs the photo-Fries rearrangement as a mechanism for achieving the desired change in side-chain polarity. This system is based on poly(*p*-formyloxystyrene) (103–105) that undergoes a Fries-like homolysis and decomposition upon exposure to DUV radiation to produce poly(*p*-hydroxystyrene) and carbon monoxide in the exposed areas (Scheme 3.8). The phenolic photoproduct is soluble in polar solvents such as alcohol or aqueous base because of the acidity of the phenolic functionality, whereas the formyl ester precursor in the unexposed areas is completely insoluble in these solvents. Consequently, development in polar solvents generates a positive-tone image of the mask. Conversely, the formyl ester polymer is soluble in nonpolar solvents such as chlorobenzene or anisole, in which the phenolic photoproduct is completely insoluble. Therefore, development in these nonpolar solvents generates a negative image of the mask.

The SEMs shown in Figure 3.29 were made from a single wafer of poly(*p*-formyloxystyrene) that had been exposed on a Perkin–Elmer M500 scanner in the UV-2 mode and then broken in half. One half was developed in a polar solvent to generate a positive-tone image, whereas the other was developed in a nonpolar solvent to produce a negative-tone image.

The avoidance of swelling during processing is a necessary but not sufficient characteristic of a viable resist system for use in micrometer and submicrometer lithography. For such systems to have practical utility, they must also function with extremely high sensitivity to maximize productivity. The efficiency of crucial photochemical transformations is characterized by the quantum yield for the process expressed as molecules transformed per photons absorbed. The quantum yield of typical diazonaphthoquinones is from 0.2 to 0.3. Thus, three or four photons are required to transform a single molecule of sensitizer. This places a fundamental limit on the photosensitivity of such systems.

To circumvent this intrinsic sensitivity limitation that quantum efficiency



Scheme 3.8. Photo-Fries degradation.

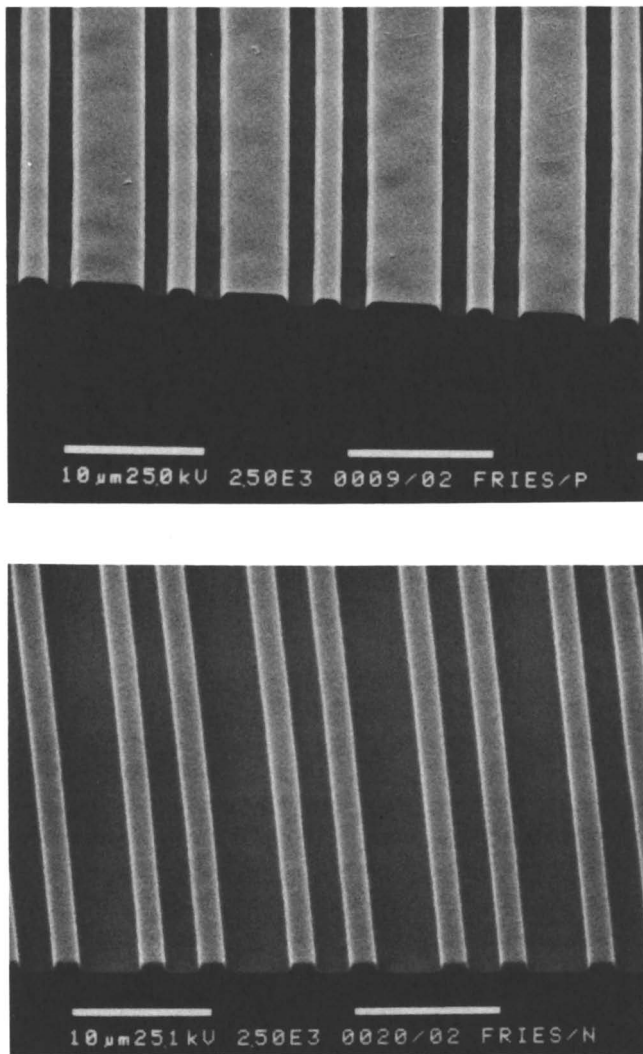


Figure 3.29. (top) Positive and (bottom) negative images projection printed in a poly(p-formylloxystyrene) resist. (Reproduced from reference 103. Copyright 1984 American Chemical Society.)

imposes on systems that consume at least one photon for every productive chemical transformation, Ito et al. (105–108) designed resist systems that incorporate “chemical amplification”. In such systems, a single photoevent initiates a cascade of subsequent chemical reactions that ultimately express the intended function. They (105–108) designed new resist materials by combining chemical amplification to provide very high sensitivity and side-chain modification to allow processing without resolution loss due to swelling.

These systems are based on acid-catalyzed thermolysis of side-chain protecting groups. Examples of polymers that function in this fashion are listed in Chart 3.1.

The tertiary butyl ester and carbonate groups are particularly useful in this application because they are sensitive to $A_{AL}-1$ hydrolysis that does not require a stoichiometric amount of water. These materials undergo acid-catalyzed thermolysis. Consequently, a resist system can be formulated by casting these polymers from solutions that also contain a substance that

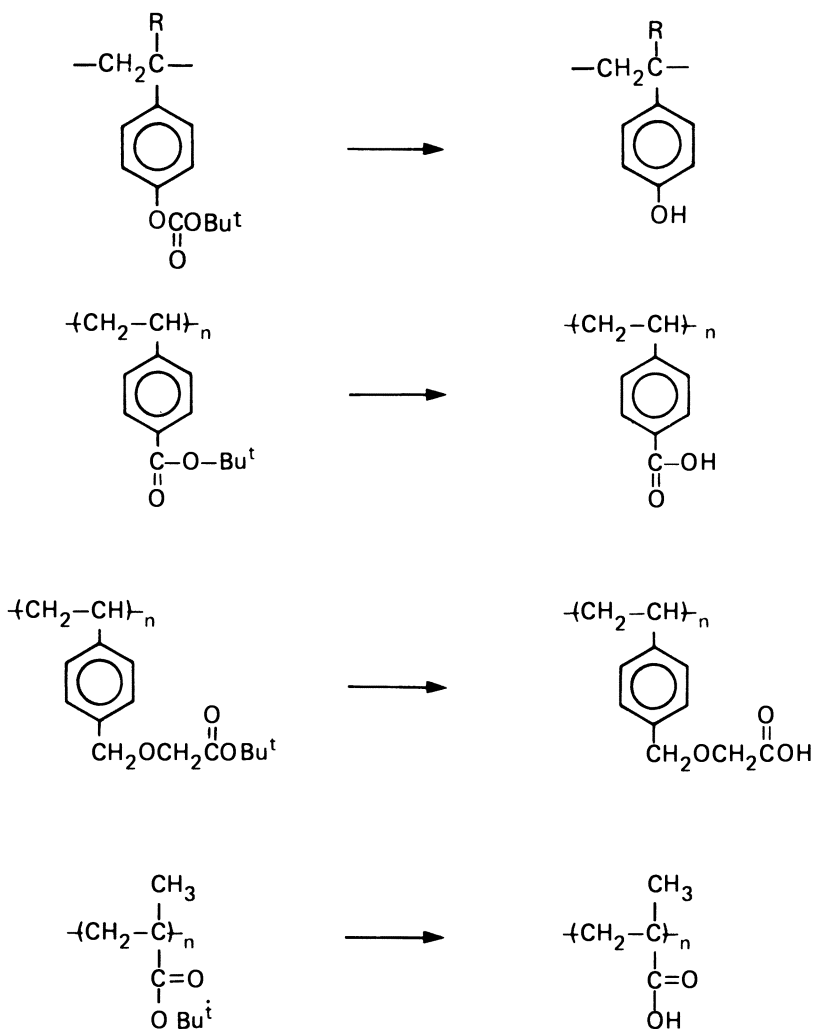


Chart 3.1. Tertiary butyl ester polymers useful in designing positive-negative resists incorporating chemical amplification.

produces strong acid upon radiolysis. Exposure creates local concentrations of strong acid such that heating the samples to an appropriate temperature after exposure causes acid-catalyzed thermolysis in the regions of the film where the photogenerated catalyst is present but no reaction in the unexposed regions of the film.

Examples of such photochemical acid generators are shown in Chart 3.2. These onium salts, which are cationic photoinitiators originally developed for curing of epoxy resins (109), can be used to formulate cross-linking negative resist materials (108), are very sensitive to electron beam and X-ray (105, 107, 108) radiation, and can be sensitized to longer wavelength radiation (108, 110, 111).

Like the poly(*p*-formyloxystyrene) resist, the overall reaction in the tertiary butyl ester resists involves generation of a large change in the polarity of the side chain. Hence, these materials can be developed as either positive- or negative-tone resists simply by appropriate choice of the developer. However, whereas one or more photons are required for each side-chain transformation in poly(*p*-formyloxystyrene), the photogenerated acid is a catalyst and is not consumed in the thermolysis reaction. Hence, the quantum yield for side-chain deprotection is the product of the quantum efficiency of acid generation multiplied by the catalytic chain length. These systems demonstrate gain and are as much as 2 orders of magnitude more sensitive than conventional resist systems. SEMs of positive and negative patterns generated in one of the tertiary butyl ester resists by projection printing on a Perkin-Elmer M500 aligner are provided in Figure 3.30.

In addition to the polarity change, the tone of certain resist materials may be reversed simply by changing the wavelength of exposure. For example, copolymers of methacrylonitrile and methacrylic acid undergo main-chain scission when exposed to DUV radiation to provide positive-tone im-

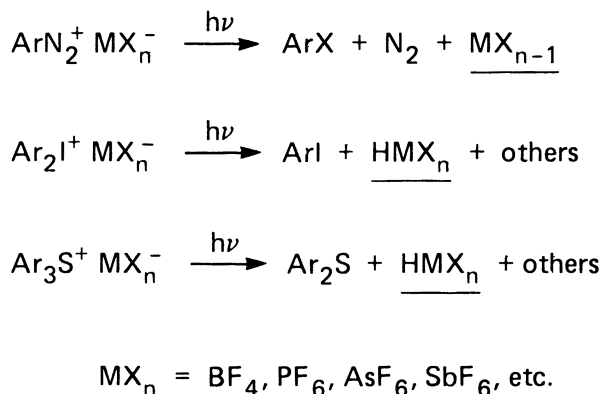


Chart 3.2. Photochemistry of onium salt cationic photoinitiators.

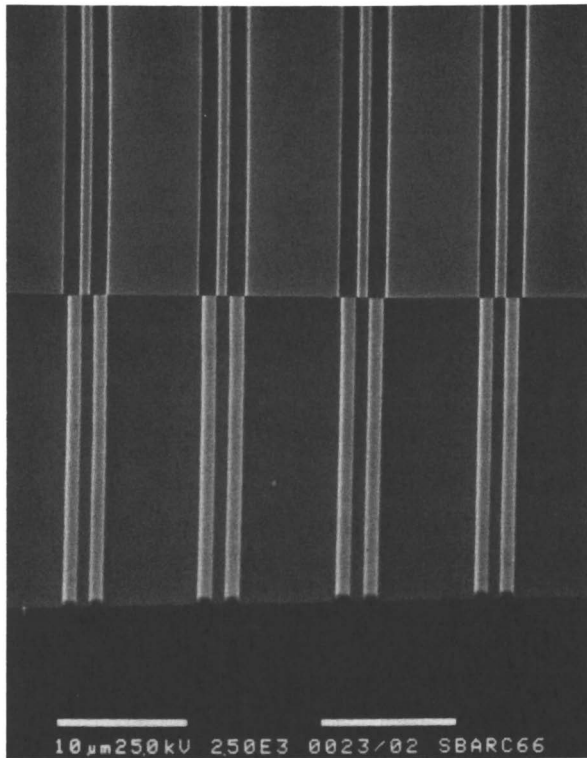
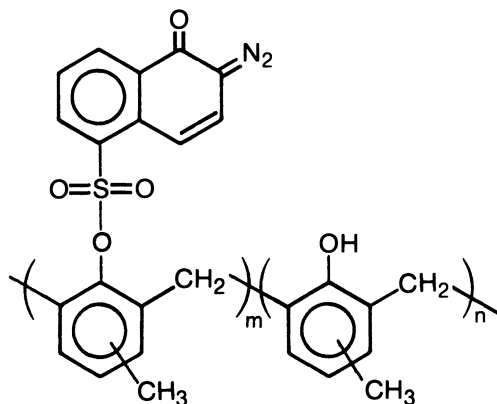


Figure 3.30. SEMs of (top) positive and (bottom) negative 1- μm images projection printed in a tertiary butyl ester-onium salt resist. (Reproduced with permission from reference 105. Copyright 1986 Electrochemical Society.)

ages of the mask. Exposure to mid-UV radiation produces negative-tone images because, at this longer wavelength, cross-linking occurs through hydrogen-transfer reactions (112). These copolymers do not have significant DUV absorption prior to prebake but exhibit a broad UV absorption centered at 246 nm after prebake at 130 °C due to some cyclization reactions (112). Therefore, the 130 °C prebake is essential for imparting DUV sensitivity.

A DUV resist based on a diazonaphthoquinone sulfonate of a cresol novolac resin (low molecular weight resist [LMR]; structure 3.13) was shown to be a cross-linking negative resist (113). Because of the very high absorbance of the resist film in the DUV region, undercut profiles, which are used in metal lift-off processes, are typically obtained. The developer for LMR is a mixture of neutral organic solvents. Exposure of LMR to near-UV light results in positive-tone imaging. Although the mechanism for the photochemically induced insolubilization is ascribed to a cross-linking reaction, the polarity change may be responsible for the dissolution differentiation.



3.13

3.2.4 Dry-Developable Resists

Dry-developing resist systems have been sought for some time. The interest in such materials throughout the semiconductor industry stems from the potential they provide for higher throughput and higher yields, and from the consideration of the environmental hazards and waste disposal problem associated with handling large volumes of developer solvents. The higher yields result from both a reduction in process steps and the fact that such materials provide the potential for carrying out exposure, development, and pattern transfer under high vacuum, thereby reducing defects due to atmospheric contaminants and the development process.

3.2.4.1 PLASMA-DEVELOPABLE RESISTS

With the advent of plasma and RIE procedures for the transfer of resist images into substrates, an effort on the part of resist chemists evolved to use these new techniques in the generation of primary resist images. In 1979, Smith et al. (114) described the development of a system called PDP (plasma-developable photoresist) based on the use of a material, the structure of which has not yet been divulged. In this process, the resist is coated in the usual fashion and exposed. The exposed film is then subjected to a baking cycle that produces a relief image (partial thermal development) of negative tone. This relief structure is then transferred into the underlying substrate by RIE to produce a negative-tone relief image of the mask (Figure 3.31).

An X-ray resist system that functions in a fashion analogous to PDP has been described in detail (115, 116). This system is based on poly(2,3-dichloropropyl acrylate) as a host polymer and an organometallic monomer, which is generally a silicon-containing material. Exposure of the resist film to X-ray radiation results in radical-initiated cross-linking of the polymer and incorporation of the silicon-containing monomer into the network (fixing). The resulting film is then heated to remove the unreacted organometallic

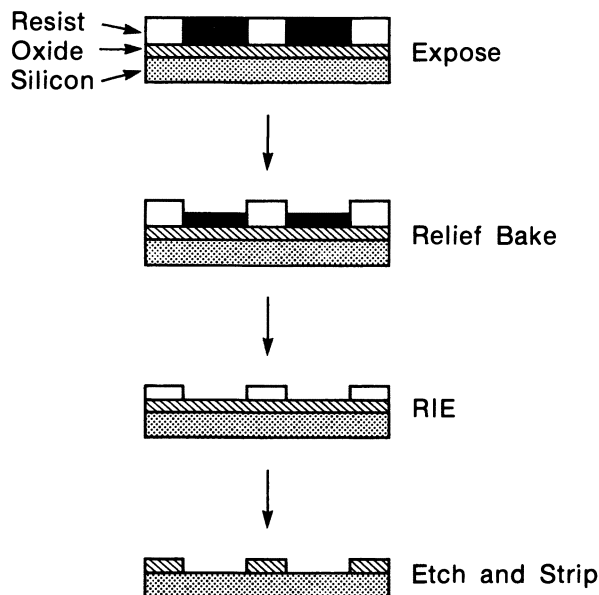


Figure 3.31. A schematic representation of the plasma-developable photoresist (PDP) process.

monomer except in those areas where it has been covalently incorporated into the film through the radiochemical reaction. The developing step involves exposure of the baked film to an oxygen plasma. Interaction of the organometallic group with the plasma generates a refractory metal oxide that acts as an etch barrier in those areas where it is still present within the film. In areas where the metallic species is absent, the organic material is rapidly removed by the oxygen plasma. The consequence of this process is generation of a dry-developed, negative-tone relief image (Figure 3.32). This scheme was later extended to the design of plasma-developed negative photoresists using *N*-vinylcarbazole and a quinone sensitizer (116).

Another class of interesting plasma-developable resists is based on a host polymer and an organic small molecule (117–119). The optical resist consists of bisarylazide and an aliphatic matrix resin such as poly(methyl isopropenyl ketone). Optical exposure of the resist results in nitrene formation, as described previously (Section 3.2.2.1), and subsequent covalent bonding of the aromatic materials into the aliphatic matrix network. After exposure, the resist films are heated, and the undecomposed arylazide is driven out of the film. Negative-tone relief-image formation is achieved by plasma development of the baked films in an appropriate gas mixture chosen to optimize the difference in etch rate between aliphatic and aromatic organic compounds (Figure 3.33). The system has been applied to both electron beam and synchrotron X-ray lithography (120).

Meyer et al. (121) described a positive-tone, plasma-developable, DUV

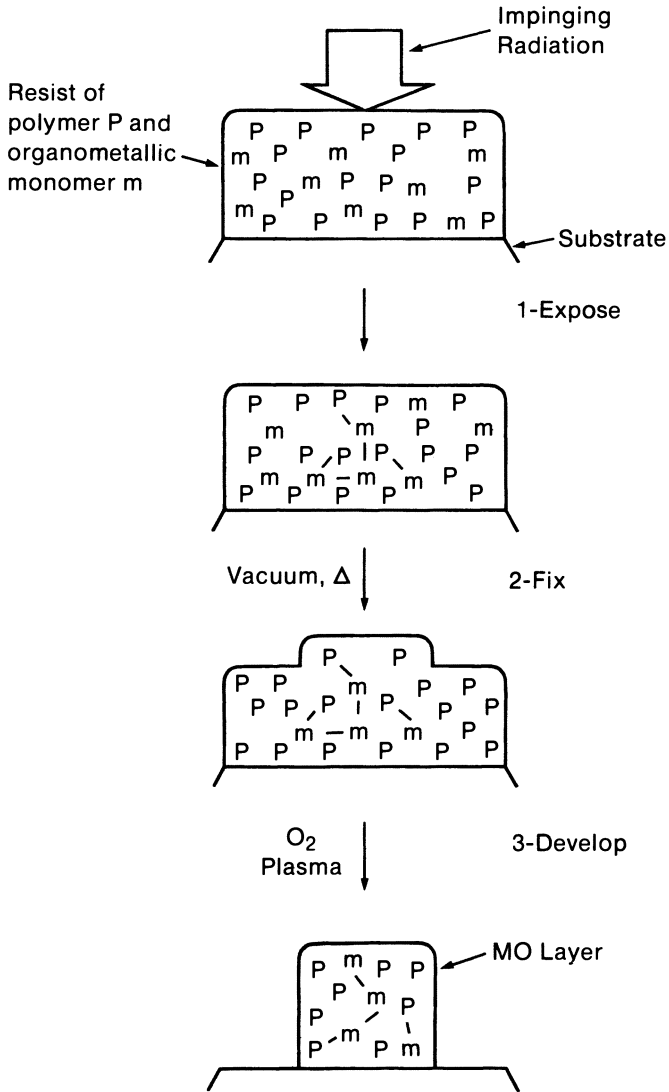
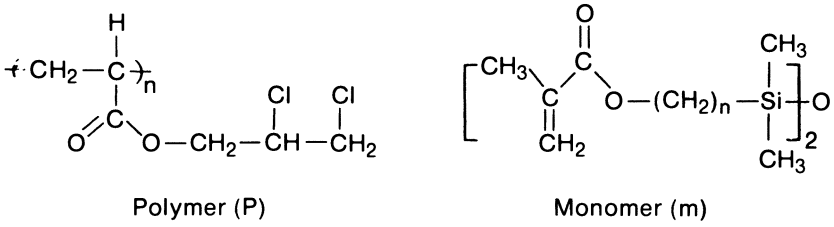


Figure 3.32. Schematic of the plasma-development process.

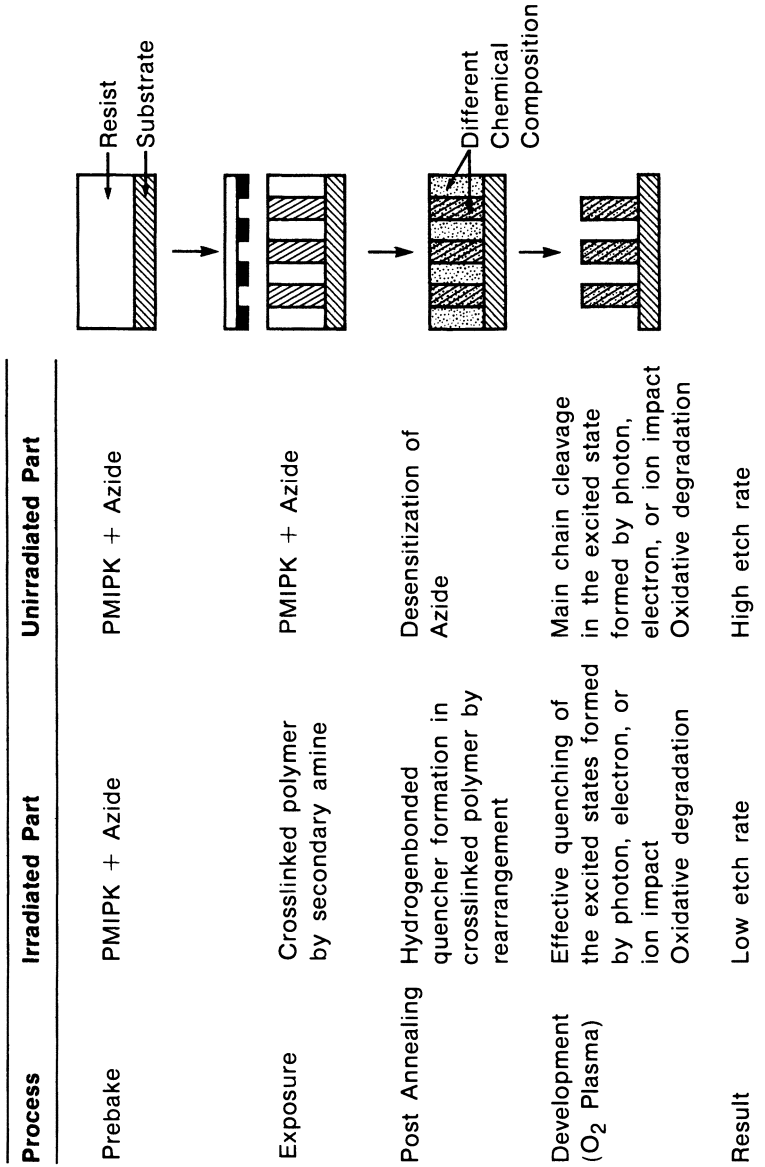


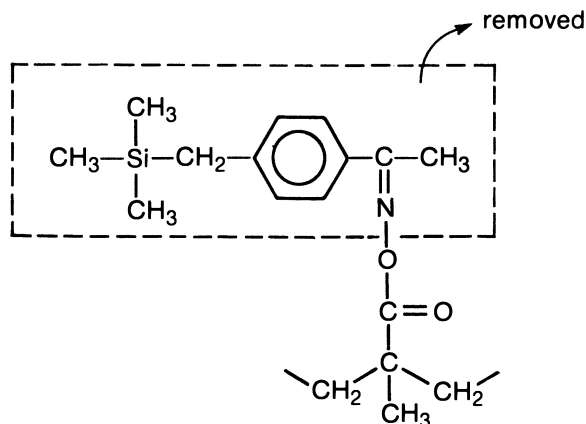
Figure 3.33. Schematic and mechanistic representation of plasma development of a PMIPK-azide resist.

resist based on an acrylic copolymer containing silicon side groups that can be cleaved from the main chain of the polymer by exposure to UV light. In a subsequent bake step, these photochemically generated, volatile, silicon-containing species are removed from the exposed regions. The oxygen plasma etch rate is higher in the exposed areas than the unexposed areas still containing the polymer-bound silicon species. The higher etch rate generates a positive-tone relief image (Scheme 3.9).

We reviewed plasma-developable resist systems designed on the basis of the use of an organic film containing a uniform distribution of an organo-metallic or organic etch barrier precursor, which is removed specifically from either exposed or unexposed regions after exposure. Another approach to designing plasma-developable resists is to coat the substrate with an organic film that lacks a metallic component and, in a subsequent step, to introduce a metallic species into selected areas of the film.

A conceptually simple example of this approach was described by Venkatesan et al. (122). In this scheme, a focused indium ion beam was used to write a pattern onto the surface of an organic polymer. When the ion-implanted resist was subjected to oxygen RIE, the surface of the ion-implanted regions was oxidized to indium oxide, which functions as an etch barrier, whereas the areas that were not implanted with indium ions were etched to the substrate (Figure 3.34). This same approach toward the design of negative resists was described by Kuwano (123), who used a focused gallium ion beam and PMMA. In this work, the PMMA layer can be dry developed with an oxygen-fluorocarbon plasma because both gallium fluoride and gallium oxide are nonvolatile materials.

Taylor et al. (124) described a process in which a bisazide-polyisoprene resist is exposed to UV light and, in a subsequent step, treated with an



Scheme 3.9. Photochemical elimination of a Si-containing side group for positive-tone plasma development.

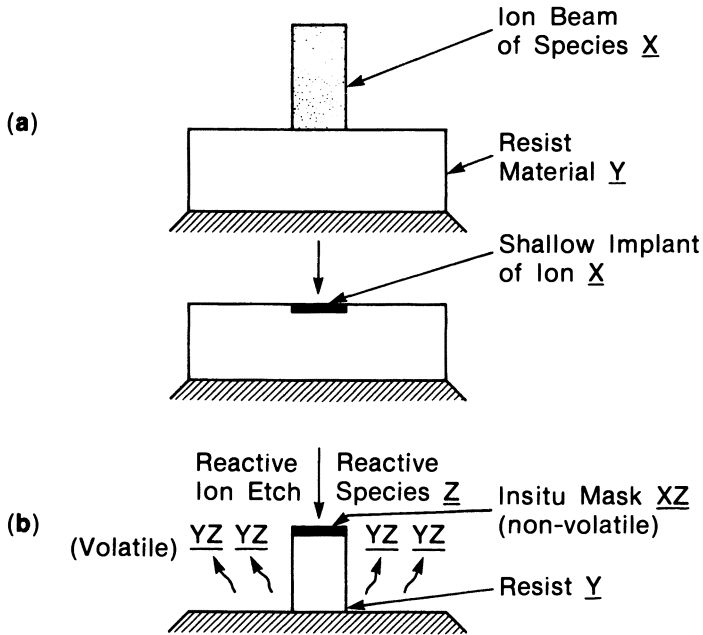


Figure 3.34. Ion implantation for the design of a plasma-developable negative resist. (Reproduced with permission from reference 122. Copyright 1981 American Institute of Physics.)

inorganic halide such as SiCl_4 (124). Silicon is reported to be predominantly incorporated into the unexposed regions (125), and accordingly, this system yields a positive-tone image when developed in an oxygen plasma. Stillwagon et al. (126) extended this scheme to a variety of polymer systems in conjunction with TiCl_4 and found that the reactivity is markedly dependent on humidity.

MacDonald et al. (127) used the positive-negative working resist systems described in Section 3.2.3 in the design of plasma-developable, UV-sensitive resists. The polymers shown in Chart 3.1 undergo a significant change in chemical reactivity as well as in polarity upon irradiation. In these systems, reactive phenolic hydroxyl or carboxylic acid groups are deprotected as a result of exposure and baking. This difference in chemical reactivity between the protected and unprotected areas can be converted into a differential etch rate by allowing the exposed portions of the polymer to react with an appropriate organometallic reagent. For example, chlorotrimethylsilane, hexamethyldisilazane (HMDS), and bis(trimethylsilyl)acetamide react with phenolic hydroxyls, carboxylic acids, and other nucleophilic species to form the corresponding trimethylsilyl derivatives. These silylating reagents do not react with such compounds as esters and carbonates. Thus, when the exposed and silylated film is subjected to oxygen RIE, a negative image of

the mask results (Figure 3.35). Figure 3.36 shows typical SEMs of the relief images obtained by exposing a 1- μm -thick resist film on a Perkin-Elmer M500 scanner in the UV-2 mode, silylating with HMDS vapor, and then developing with oxygen RIE. As is the case with the resist based on the interfacial cationic polymerization technique that will be described, the systems employing onium salts are very sensitive to DUV, electron beam, and X-ray irradiation because of chemical amplification. Also, these systems can be readily applied to near-UV lithography by dye sensitization.

Because of the high differential oxygen etch rate between the exposed and the unexposed regions generated by silylation, this system does not lose significant film thickness in the exposed and silylated regions during the oxygen RIE development step. Because of this property, this process can

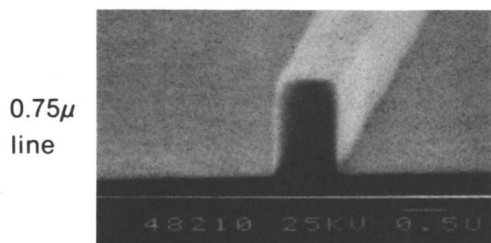
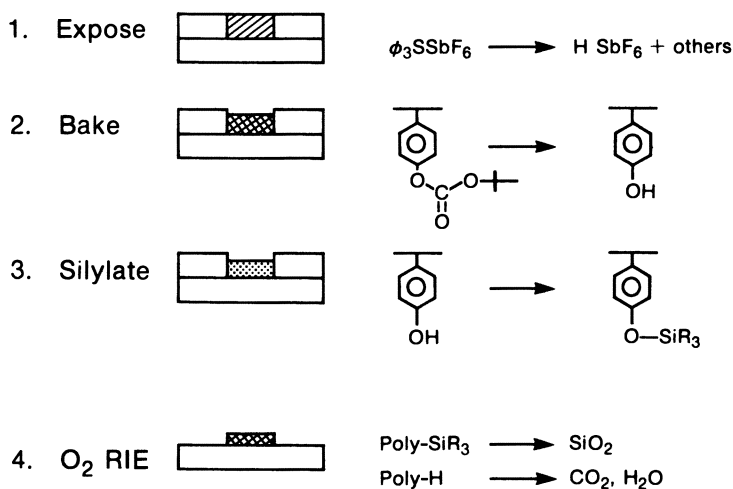


Figure 3.35. Negative plasma-development process via selective silylation of a positive-negative resist.

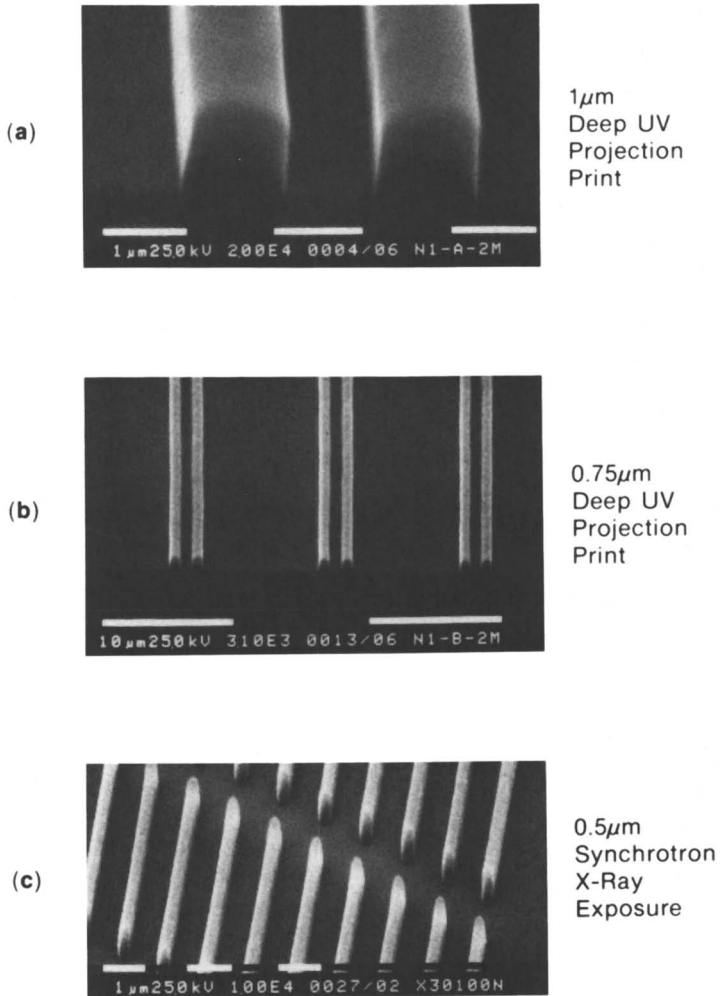


Figure 3.36. SEMs of dry-developed images generated by the process shown in Figure 3.35: (a) $1.0\text{-}\mu\text{m}$ images printed with a Perkin-Elmer M500, UV-2 mode; (b) $0.75\text{-}\mu\text{m}$ images printed with a Perkin-Elmer M500, UV-2 mode; and (c) $0.5\text{-}\mu\text{m}$ images proximity printed with a synchrotron X-ray source. (Reproduced with permission from reference 127. Copyright 1985 Society of Plastics Engineers.)

be extended to a bilayer, dry-developed scheme. In this extension, the oxygen RIE not only dry develops the relief image in the photosensitive layer, but also transfers that image into the underlying planarizing layer as shown in Figure 3.37.

A positive resist can be designed in an analogous fashion by simply changing the system such that the starting, unexposed film contains a functionality that will undergo silylation, whereas radiolysis of the film destroys this reactivity. For example, the carboxylic acid group in poly(methacrylic acid) can be silylated to form a trimethylsilyl ester, but upon ion beam exposure, this polymer undergoes decarboxylation to yield an unreactive species. Because treatment with a silylating reagent results in silicon being incorporated only in the unexposed regions, this process generates positive images by oxygen RIE development (127).

Postirradiation radical grafting reactions have been applied to the design of plasma-developable, negative electron beam resists (128). In this scheme, a polymer film is exposed to an electron beam to generate polymeric radicals in the matrix, which, when exposed to organometallic monomers, initiate radical polymerization of the monomer to form a graft polymer in the exposed areas. Oxygen plasma etches the organic polymer in the unexposed regions faster than the polymer grafted with organometallic side chains, and negative images result.

Radical reactions are sensitive to oxygen. To avoid quenching of radicals by ambient oxygen, Hult et al. (129, 130) used cationic polymerization in the design of plasma-developable, negative-resist systems. In this scheme (Figure 3.38), one of the onium salt cationic photoinitiators described previously (Chart 3.2) is coated directly on substrates or with a radiation-inert matrix polymer. DUV irradiation results in the formation of strong acids in the exposed areas. Treatment of the irradiated film with an organometallic monomer that undergoes cationic polymerization in the vapor phase or in solution results in deposition of organometallic polymer only in the exposed areas where the photochemically generated acid initiates the cationic polymerization. A subsequent oxygen plasma development generates negative relief images as shown in Figure 3.38. The organometallic polymer is not grafted onto the host polymer in this case.

3.2.4.2 SELF-DEVELOPING RESISTS

The first example of formation of a resist relief image in the absence of a wet developing step was reported by Bowden and Thompson in 1974 (131). They reported that exposure of certain poly(olefin sulfones) to electron beam radiation resulted in spontaneous relief image formation. When the films were cast thin enough and the substrates were heated above 90 °C, clean images were produced in the resist film by exposure alone. They termed this phenomenon "vapor development".

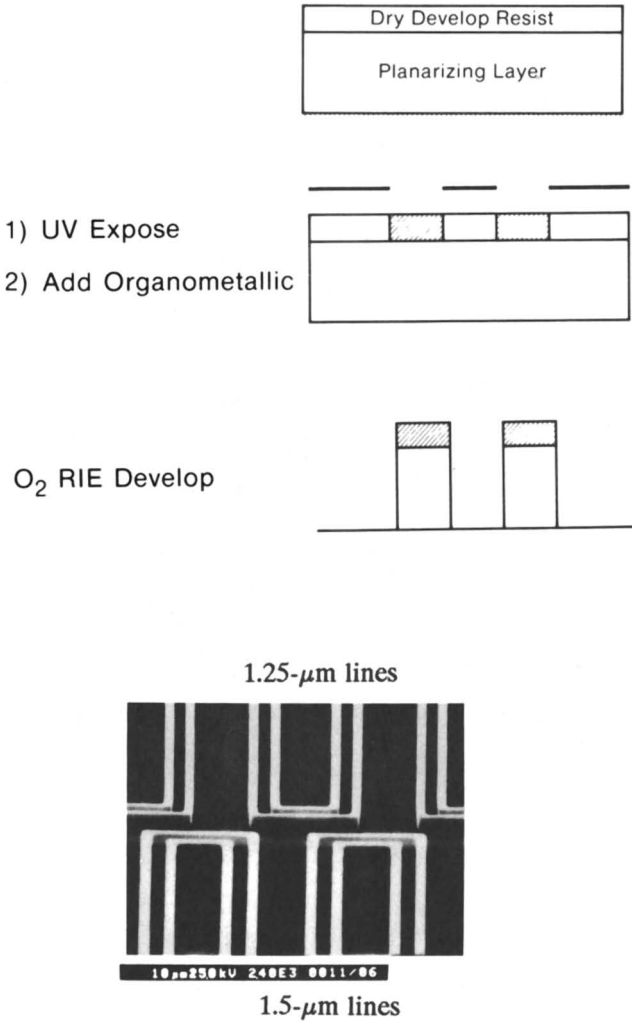


Figure 3.37. *Bilayer negative dry-development scheme. The SEM shows the final image obtained by the bilayer process with a Perkin-Elmer M500 in the UV-2 mode. (Reproduced with permission from reference 127. Copyright 1985 Society of Plastics Engineers.)*

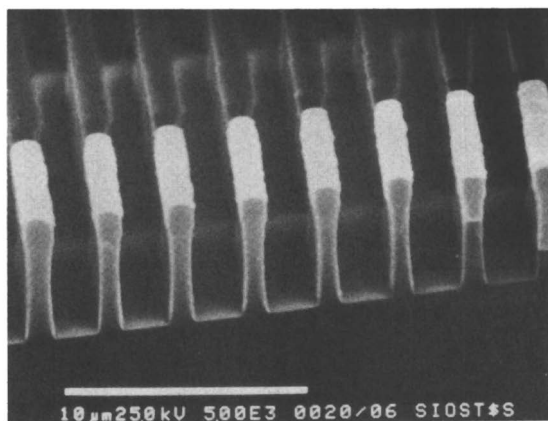
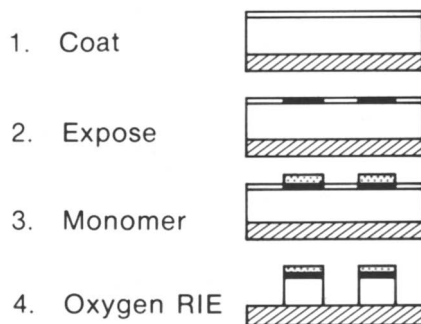


Figure 3.38. Bilayer dry process using photoinitiated interfacial polymerization of a Si-containing monomer.

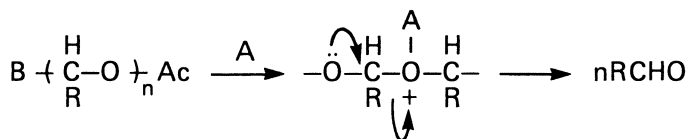
Ito and co-workers (105, 107, 108) reported a new positive-tone, dry-developing resist system incorporating two stages of chemical amplification. The polymer upon which the system is based is a polyaldehyde. Aldehydes undergo anionic and cationic polymerization in a reversible equilibrium reaction. Many of these systems have ceiling temperatures well below room temperature, and the polymerization reactions must be carried out at cryogenic temperatures. If the polymer is isolated or the reaction is warmed, the product rapidly depolymerizes to the monomer. If, however, these polymers are end-capped by acylation or alkylation prior to isolation or warming, they are often quite thermally stable. Aromatic polyaldehydes such as polyphthalaldehyde are highly soluble in common casting solvents unlike their aliphatic counterparts. A formulation consisting of the end-capped polyphthalaldehyde, sensitized by addition of onium salt cationic photoinitia-

tors (109), has allowed imaging of 1- μm -thick films at extremely low doses of DUV, electron beam, and X-ray radiation to produce clean relief patterns spontaneously upon exposure without development by solvent, plasma, or heating. Ito and Willson termed this dry-development phenomenon "self-development," in order to distinguish it from the vapor development of polysulfones, which requires simultaneous heating, and from dry development using plasma.

The mechanism by which this system functions involves radiochemical generation of a strong acid that catalyzes cleavage of the polyacetal main chain (Scheme 3.10). Because the acid is not consumed in the acidolysis reaction, a single molecule of acid is capable of cleaving many chains, thus producing one stage of chemical amplification. The second stage of amplification is achieved because a single cleavage of the polyacetal chain reestablishes the equilibrium, and the polymer simply "unzips" into the monomer at a temperature above the ceiling temperature. Under the conditions of exposure, especially under high vacuum, the monomer is volatilized, and spontaneous relief image formation results. Optical micrographs of the self-developed images are shown in Figure 3.39.

The intrinsic radiation sensitivity of polyphthalaldehyde is low in the absence of the acid generators, but films of the polymer subjected to electron beam, X-ray, and DUV exposure exhibit spontaneous high-resolution relief image formation without a development step (107). Unfortunately, exposure of the polymer alone does not provide clean self-development under these radiation conditions. However, high-power excimer laser radiation (in this case, KrF) of the polymer film results in clean, spontaneous self-development to the substrate as shown in Figure 3.40 (105). Several polymers such as nitrocellulose (132) and certain polysilanes (133, 134) were shown to exhibit self-development under similar exposure conditions. Polymethacrylates were also shown to be directly engraved by synchrotron X-ray (135) or DUV irradiation (136, 137). Direct photoengraving of PMMA requires very high doses of radiation at the fluence available from discharge lamps.

Organic materials strongly absorb below 200 nm. Excimer lasers with a wavelength below 200 nm have been shown to "ablatively" decompose organic polymers into small fragments that are expelled out of the film during exposure. This process will be discussed later (*see* Section 3.4.4).



Scheme 3.10. Acid-catalyzed depolymerization of polyaldehyde.

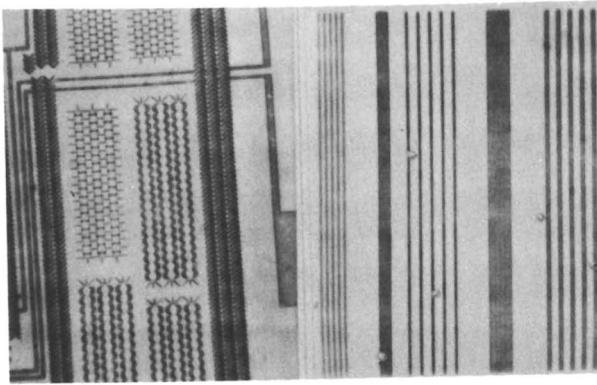
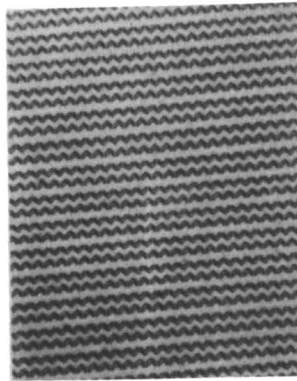
Al-K α X-Ray20 keV E-Beam
 $1 \mu\text{C}/\text{cm}^2$ 254 nm Deep UV
 $2.4 \text{ mJ}/\text{cm}^2$

Figure 3.39. Optical micrographs of self-developed images of a polyphthalaldehyde-onium salt resist. (Reproduced with permission from reference 105. Copyright 1986 Electrochemical Society.)

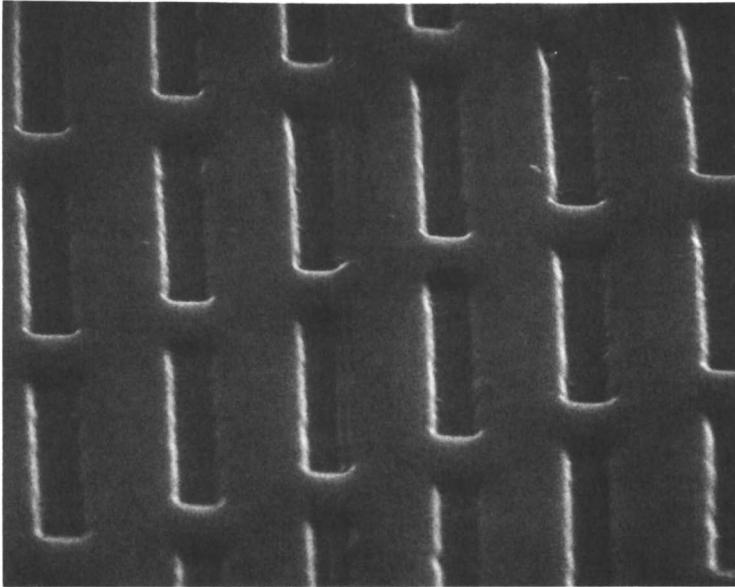


Figure 3.40. SEM of positive image self-developed in polyphthalaldehyde by a KrF excimer laser. (Reproduced with permission from reference 105. Copyright 1986 Electrochemical Society.)

3.2.4.3 THERMALLY DEVELOPABLE RESISTS

The third class of dry-developable resists involves heating the exposed resist films in a development step. This development method does not require expensive etching tools, is therefore economical, and could alleviate the potential problem of exposure tool contamination associated with the self-developing resist systems. Many of the plasma-developable resist systems involving a relief-bake step, as discussed in Section 3.2.4.1, have the thermal development characteristics to a certain extent. In the thermally developable resist scheme, development is minimal during irradiation but completed to the substrate upon postbaking.

The first example designed on the basis of this concept is poly(olefin sulfones) sensitized with pyridine *N*-oxides (138). Positive-tone relief images were obtained upon postbaking at 100 °C because of depolymerization of poly(butene-1 sulfone) initiated by energy transfer from the sensitizer.

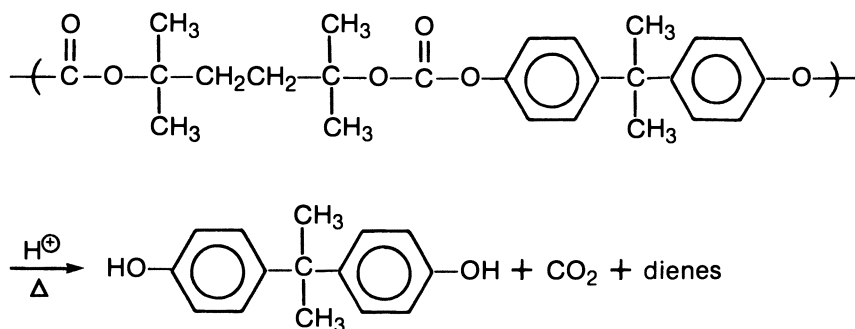
Another example is thermally depolymerizable polycarbonates that are sensitized with onium salt cationic photoinitiators (139). As discussed previously (Section 3.2.3), one of the positive–negative resists based on polystyrene with pendant tertiary butyl carbonate protecting groups undergoes acid-catalyzed thermolysis to generate poly(*p*-vinylphenol), carbon dioxide, and isobutene. Therefore, if the tertiary butyl carbonate moiety is incorporated in the polymer backbone as a repeating unit, such polymers will

depolymerize upon heating by reaction with radiochemically generated acids. Such polycarbonates were prepared by phase-transfer-catalyzed polycondensation of activated carbonyloxy derivatives of tertiary or other reactive diols with simple diols such as bisphenol A. The polycarbonates are sensitive to thermolysis and decompose rapidly and smoothly to bisphenol A, carbon dioxide, and dienes when heated to ca. 200 °C. For the polycarbonate resist containing a few percent of triphenylsulfonium metal halide, exposure of the film to a very small dose of DUV radiation creates a latent image (acid formation). Upon baking after exposure, development of a visible image is instantaneous as carbon dioxide and volatile dienes are evolved (Scheme 3.11). Because bisphenol A is not very volatile at the baking temperature, full development is achieved by removal of bisphenol A by using isopropanol or aqueous base. High-resolution positive images printed in this resist on a Perkin–Elmer M500 scanner in the UV-2 mode are provided in Figure 3.41. New resist systems that undergo clean thermal development to the substrate are awaited.

3.2.5 Inorganic Negative Resists

Inorganic resist systems form another interesting class of resist materials (140, 141). The concept of using the GeSe chalcogenide glass as a resist for microelectronics was first reported by Nagai et al. (142). In subsequent papers (143, 144), they used light-induced silver migration (photodoping) for the Ag–GeSe inorganic resist systems, demonstrating that the systems can provide negative-working optical and electron beam resists with high contrast.

These workers also demonstrated other unique resist characteristics in these systems such as no swelling during development, opacity to actinic light, and resistance to various acids commonly used in microelectronic fabrication processes. Chang and co-workers studied AgCl–As₂S₃ inorganic resist systems with optical (145, 146) and X-ray exposure tools (147). They



Scheme 3.11. Acid-catalyzed thermolysis of polycarbonate.

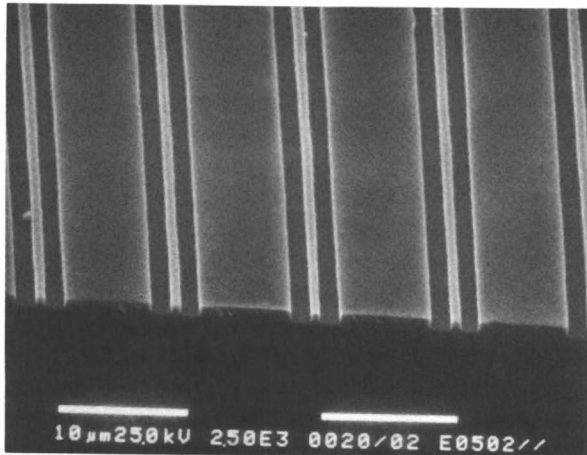
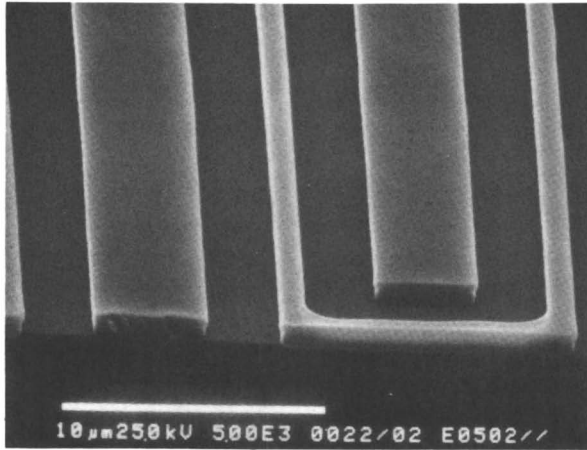
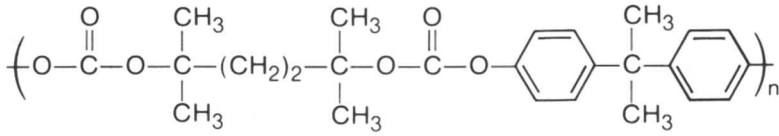
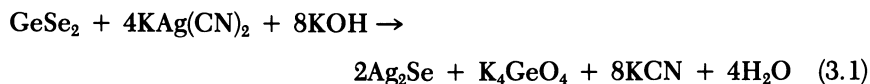


Figure 3.41. SEMs of positive images generated in a polycarbonate-onium salt resist by thermal development followed by a 2-propanol rinse (Perkin-Elmer M500, UV-2 mode).

were the first to report dry development of an As_2S_3 -based resist system (145).

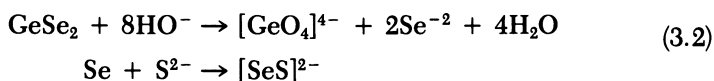
More recent work on $\text{Ag}_2\text{Se}-\text{Ge}_x\text{Se}_{1-x}$ by Tai and co-workers (140, 148–150) highlighted the value of inorganic resist systems in very large scale integration (VLSI) microlithography. In their work, the sensitized resist film was obtained by a two-stage process. $\text{Ge}_x\text{Se}_{1-x}$ chalcogenide glass was evaporated or sputtered onto the substrate followed by sensitization with $\text{KAg}(\text{CN})_2$ to yield a thin (100 Å) Ag_2Se layer on the surface of $\text{Ge}_x\text{Se}_{1-x}$ according to the following reaction:



Patterning of $\text{Ag}_2\text{Se}-\text{Ge}_x\text{Se}_{1-x}$ resists is depicted schematically in Figure 3.42. The process involves exposure (i.e., photodoping, photobleaching, and diffusion), stripping of the undoped Ag_2Se layer, and development of the unprotected $\text{Ge}_x\text{Se}_{1-x}$. In the exposure step, a latent image is formed via photodoping of Ag into a thin upper layer of the $\text{Ge}_x\text{Se}_{1-x}$. Two phenomena occur during the photodoping process.

1. Because of reduction in the concentration of the light-absorbing Ag in the Ag_2Se layer, the effective light intensity increases at the $\text{Ag}_2\text{Se}-\text{Ge}_x\text{Se}_{1-x}$ interface. This photobleaching effect enhances the image contrast.
2. A rapid diffusion of Ag in the Ag_2Se layer occurs from unexposed to exposed areas. The diffusing Ag is itself photodoped at image edges (Figure 3.43), producing an edge-sharpening effect that compensates for diffraction effects.

Development of the latent image is also a two-stage process. First, the undoped Ag_2Se layer is stripped by immersion of the wafer in a KI/KI_3 solution. Full delineation of negative patterns in the GeSe glass is accomplished by development of the unprotected $\text{Ge}_x\text{Se}_{1-x}$. The $\text{Ge}_x\text{Se}_{1-x}$ film possesses a phase-separated columnar structure consisting of 200–300-Å Ge-rich and Se-rich columns (149, 151). Two-component developer containing NaOH and a small amount of S^{2-} anion is used to delineate patterns. GeSe_2 is rapidly etched by OH^- , whereas S^{2-} slowly etches the Se-rich phase.



The Ge-rich phase of the unprotected area is quickly dissolved, allowing the Se-rich columns to be attacked from the side as illustrated in Figure

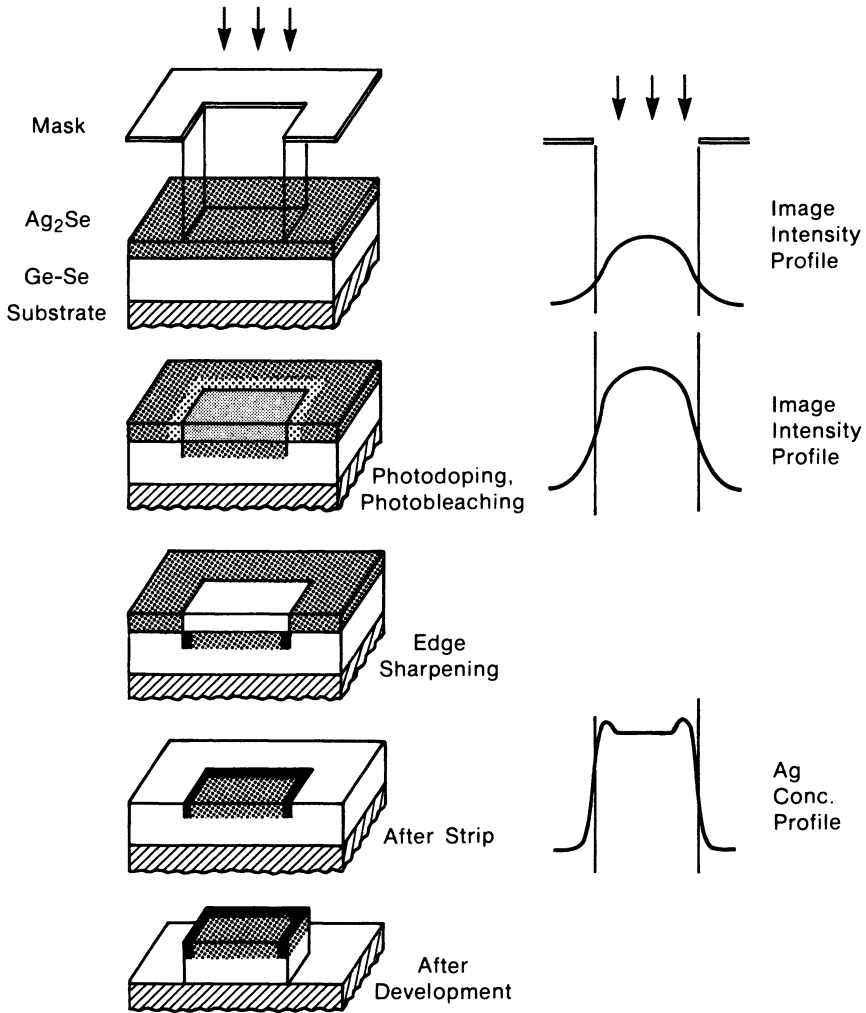


Figure 3.42. Schematic representation of imaging mechanism of $\text{Ag}_2\text{Se}-\text{Ge}_x\text{Se}_{1-x}$. (Reproduced with permission from reference 151. Copyright 1985 Society of Plastics Engineers.)

3.44 (151). The exposed areas are protected from development by the thin Ag-photodoped layer. Undercutting from the side is impeded by the relatively slow etching of the Se-rich columns. Thus, the thin latent image is transferred to the full thickness of the $\text{Ge}_x\text{Se}_{1-x}$ matrix by anisotropic, wet chemical etching. This anisotropic etching development and the unique edge-sharpening effect contribute to the exceptional lithographic performance of the $\text{Ag}_2\text{Se}-\text{Ge}_x\text{Se}_{1-x}$ resist system.

This resist exhibits a broad-band spectral response to all regions of UV

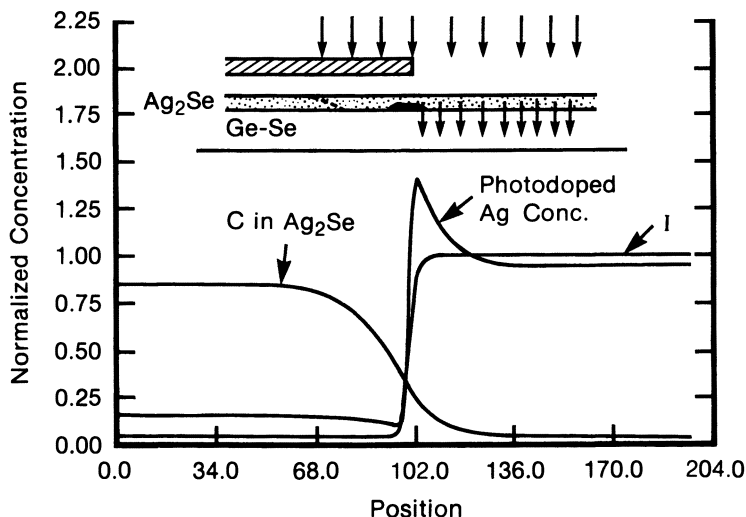


Figure 3.43. Mechanism of edge-sharpening effect. The diagram shows the profile of light intensity (I), photodoped Ag concentration in GeSe film, and the concentration of Ag remaining in the Ag_2Se layer. (Reproduced with permission from reference 149. Copyright 1982 Electrochemical Society.)

radiation and is opaque to 450 nm. Ong et al. (152) measured the sensitivity of the resist to the DUV radiation in comparison to PMMA and Hitachi Chemical RD2000N as shown in Table 3.6. This resist is 10 times more sensitive than PMMA.

Vacuum-deposited $\text{Ge}_x\text{Se}_{1-x}$ film do not smoothly cover topographic substrate surfaces. Tai et al. (140, 150, 153) combined the thin $\text{Ag}_2\text{Se}-\text{Ge}_x\text{Se}_{1-x}$ resist film with a thick planarizing organic layer to form a multilayer resist system. The resolution of the bilevel resist system is extremely high. Tai et al. (149) addressed the lithographic implications of this inorganic resist system in terms of resolution limit, field size, defocus tolerance, effects of coherency, line width control, multilevel resist compatibility, and registration accuracy. An extrapolated resolution capability of 0.25 μm has been suggested at 220 nm with a lens NA of 0.35 (152).

One problem with inorganic resist systems is that troublesome deposition techniques are required. Development of high throughput and high quality, automatic deposition equipment capable of producing defect-free GeSe films would be indispensable for the application of inorganic resist systems to device manufacturing. The Ag-doped systems are sensitive to long wavelength light; hence, their use requires special handling. There are also concerns about the potential for Ag contamination of semiconductor devices.

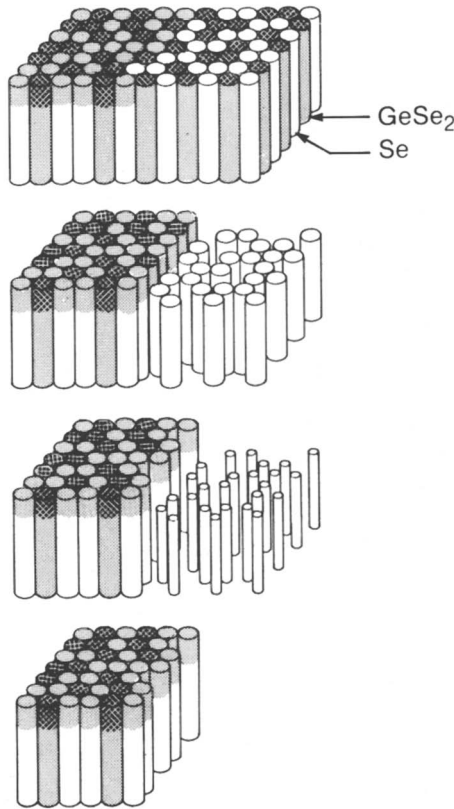


Figure 3.44. Schematic representation of anisotropic wet chemical etching of Ge_xSe_{1-x} . (Reproduced with permission from reference 151. Copyright 1985 Society of Plastics Engineers.)

Table 3.6. DUV Sensitivity of Ge_xSe_{1-x} Resist

Resist	260 nm	220 nm
Ge_xSe_{1-x}	72	48–56
RD2000N (1 μm)	48 ^a	36 ^a
PMMA (1 μm)		1500 ^b , 500 ^c

NOTE: All values are exposure energy (mJ/cm^2).

^aConditions were as follows: 120-s development in 1:4 MF312/ H_2O .

^bConditions were as follows: 60-s development in methyl isobutyl ketone.

^cConditions were as follows: 60-s development in chlorobenzene.

SOURCE: Reproduced with permission from reference 152. Copyright 1982 Electrochemical Society.

3.3 Applications

3.3.1 Multilayer Resist Systems

Although 5:1 and 10:1 reduction step-and-repeat aligners with high NA are useful in manufacturing devices with 1- μm features, the high throughput, low-NA, full-wafer 1:1 projection aligners that operate in the near-UV do not provide comparable image contrast at these dimensions. Thus, 1:1 projection aligner manufacturers have offered products operating in the mid-UV to DUV regions (Section 3.1.3.2). Even with the improved resolution available at shorter wavelengths, the utility of low-NA aligners (e.g., NA = 0.14 in the Canon MPA520, and NA = 0.16 in the Perkin-Elmer M500) at submicrometer levels is marginal. The combination of increased topography and operation so near the resolution limit seriously hampers engineers in their attempts to develop stable processes. Thus, the development of new resist materials and processes that extend the capability of UV lithography is essential.

One viable approach to the extension of photolithography to the submicrometer domain is the use of multilayer resist schemes (83, 86, 153–156). Various multilayer systems have been proposed, all of which have in common the generation of images in a thin layer of resist followed by transfer of the images into a thick, planarizing, underlying polymeric film (Figure 3.45). The planarizing layer minimizes the effects of topography and reflection. After a thin film of a resist coated on the thick planarizing layer is imaged in a standard fashion, it is used as an exposure or etch mask for patterning the bottom layer. As illustrated in Figure 3.45, the image transfer into the planarizing layer may be accomplished by DUV blanket exposure, by oxygen RIE, or by wet development. Because the image delineated in the top resist acts as a mask, always conforms to the planarizing layer, and is portable with the wafer, this sort of process has been termed “portable conformable mask” (PCM) by Lin (83, 86).

PCM systems can alleviate problems associated with topography and reflection. A thin imaging layer allows higher resolution than a thick imaging layer of the sort used in the single-layer resist process. In addition, anisotropic transfer of a top resist image into a thick planarizing layer produces high aspect ratio images in PCM systems as shown in Figure 3.45. Two important DUV applications can be found in multilayer resist systems:

- DUV flood exposure for the exposure-PCM scheme and
- DUV imaging for the RIE-PCM scheme.

3.3.1.1 DEEP-UV BLANKET-EXPOSURE-PCM SYSTEMS

DUV contact printing offers a potential for delineating submicrometer features with high aspect ratio (Figure 3.19), but suffers from mechanical defects caused by the intimate contact between a mask and a resist film. In contrast,

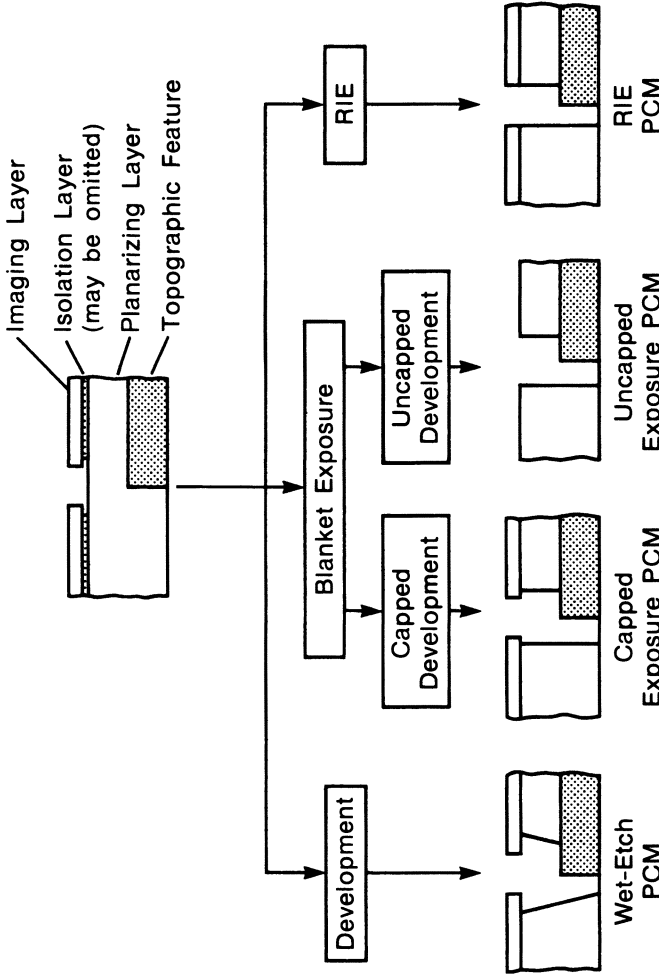


Figure 3.45. Schematic representations of multilayer resist processes. (Reproduced from reference 83. Copyright 1983 American Chemical Society.)

optical projection printing offers a freedom from such defects and a high alignment accuracy but suffers from low contrast in image intensity profiles at the resist surface caused by diffraction of light in projection optics (Figure 3.14). An elegant combination of the advantages of the two printing methods led to the exposure-PCM technique, first described by Lin (157). In this scheme, a thin resist layer that is opaque in the DUV region is spun on top of a thick, planarizing, DUV resist layer. The top layer is first imaged by an optical projection aligner and then serves as a mask for the bottom DUV resist that can now be flood exposed to DUV radiation (Figure 3.45).

Lin chose AZ1350J as a top imaging resist because of its high opacity in the DUV region (158) and PMMA as a bottom planarizing layer (157). The top layer can be imaged by electron beam exposure as well as by optical projection (159). The bottom PMMA image can be developed in chlorobenzene or toluene, with the top resist cap retained, or in MIBK, which dissolves the cap, to provide capped or uncapped structures, respectively (Figure 3.45).

The capped configuration is preferred over the uncapped one for subsequent RIE applications because PMMA has less etch resistance than aromatic materials (43, 44). On the other hand, MIBK development provides higher contrast than development in chlorobenzene or toluene. Figure 3.46 exhibits uncapped 0.85- μm lines delineated in 1.9- μm -thick PMMA. Figure 3.47 shows capped images obtained with 0.3- μm -thick AZ1350J on 2- μm -thick PMMA. The top resist layer was imaged by electron beam exposure (30 $\mu\text{C}/\text{cm}^2$) in both cases (159). Considerable effort has been devoted to the design and application of the exposure-PCM system since Lin's report. Table 3.7 summarizes the exposure-PCM systems based on the diazoquinone resist-PMMA two-layer scheme.

One problem associated with the PCM scheme is that during application of a photoresist such as AZ1350J onto a PMMA film, a thin layer of PMMA is redissolved and mixed with the photoresist so that a thin interfacial layer is formed that remains after development of the photoresist layer and inhibits proper exposure and development of the PMMA layer. Because the PMMA developer, such as chlorobenzene or toluene, used in the capped process is chosen to be a nonsolvent for the photoresist, such a solvent cannot remove the interfacial layer. Therefore, some process, like plasma treatment, is required to remove the interfacial layer prior to the blanket exposure of the bottom PMMA layer (83, 85).

MIBK used in the uncapped process dissolves the interfacial layer. However, attenuation of DUV light due to the novolac resin in the interfacial layer, coupled with the intrinsic, low sensitivity of PMMA developed in MIBK (see Table 3.6), demands prolonged blanket DUV exposure. This high dose of DUV leads to excessive cross-linking and photooxidation of the novolac resist (53, 166-169) and, consequently, to incomplete removal of the top resist during the development of PMMA in MIBK. Lin et al. (85) reported that a soak in methanol/water (1:1) prior to the MIBK development

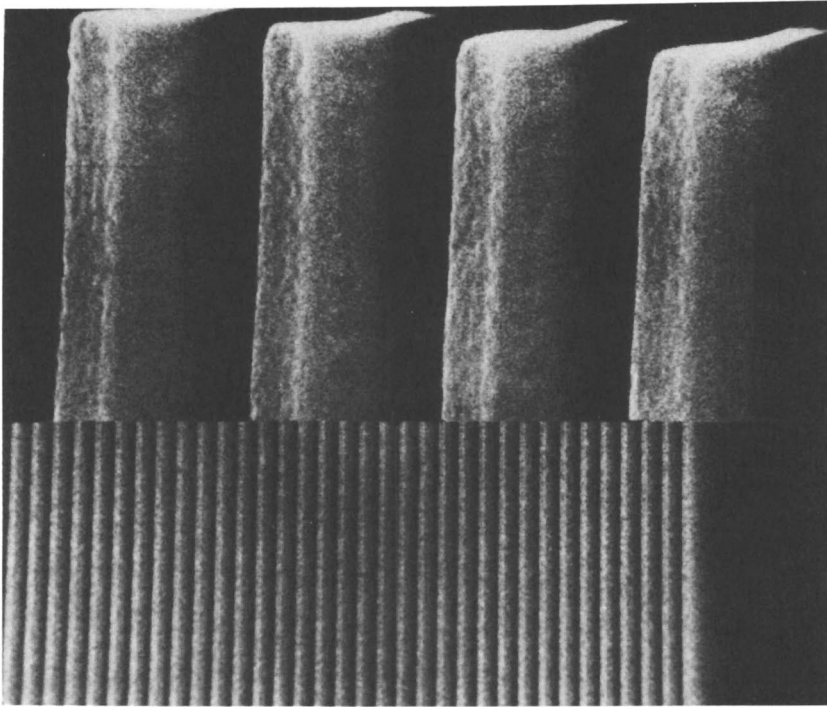


Figure 3.46. Uncapped resist image (0.8- μm lines separated by 2.4 μm) printed in 1.9- μm -thick PMMA by DUV blanket exposure with 0.2- μm -thick AZ1350J as a PCM. (Reproduced with permission from reference 159. Copyright 1979 American Institute of Physics.)

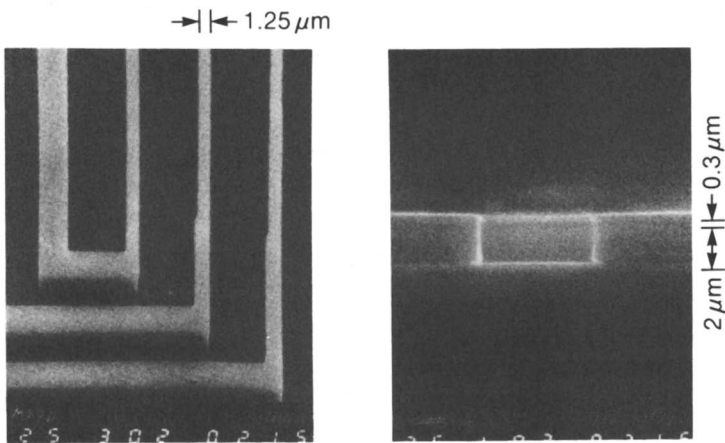


Figure 3.47. Capped resist image obtained with a DUV PCM system. (Reproduced with permission from reference 85. Copyright 1981 American Institute of Physics.)

Table 3.7. Two-Layer DUV Flood Exposure-PCM Systems

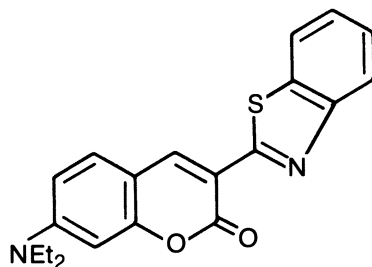
<i>Imaging Layer</i>	<i>Planarizing Layer</i>	<i>Imaging</i>	<i>Comments</i>	<i>Reference</i>
AZI350J,2400	PMMA	UV	First PCM	157
AZI350J	PMMA	E-beam	E-beam imaging	159
AZI350J	PMMA	Stepper, E-beam	Fabrication of 1- μ m MOSFET ^a	85
AZI350B	PMMA	UV	Cd lamp, acetone-based development	160
Hunt MPR	PMMA	Stepper	PMMA planarization	161
AZI350J	PMMA	Stepper	Fabrication of bubble device	162
Kodak 809	PMMA + coumarin 6	Stepper	First application to production dye in PMMA	163
AZI350J	PMMA + coumarin 30	Stepper	Submicron contact hole delineation	164
Kodak 809	PMMA + coumarin 6	Scanner, stepper	Simulation	165

^aMOSFET is metal oxide semiconductor field effect transistor.

facilitates the cap removal. Bartlett et al. (163) used Kodak 809 as the top imaging resist and removed it in a metal-free alkaline developer after blanket DUV exposure and before PMMA development in MIBK; thus, the interfacial layer problem in the uncapped process was overcome.

Wijdenes and Geomini (170) examined the effects of the phenolic resin composition, its molecular weight distribution, solvent composition, and prebake temperature on the interfacial layer formation. They found that combined use of poly(*p*-vinylphenol) (structure 3.10) as matrix resin and cyclohexanone as the casting solvent in the diazoquinone resist formulation minimizes mixing of the two layers and yields a capped PCM structure without any plasma treatment.

Another problem with the PCM process stems from reflections from substrate surfaces, which cause line width variations in the masking resist exposure. O'Toole et al. (171) demonstrated that even the PCM scheme suffers from line width variations due to reflections from the topographic structures on the wafer. They minimized the effect of the reflected light by dyeing the bottom planarizing layer in a three-layer RIE-PCM scheme. Hewlett-Packard manufactures VLSI NMOS (n-channel metal oxide semiconductor) chips in an uncapped PCM process by using Kodak 809 and a dyed planarizing layer (163, 172). A coumarin dye, coumarin 6 (structure 3.14), was chosen because this dye strongly absorbs at the imaging wave-



3.14

length, is transparent at the alignment wavelength, and does not prevent exposure of PMMA (Figure 3.48). The NMOS III chips in Hewlett-Packard's HP9000 32-bit computer are manufactured by this bilevel-dyed DUV PCM. Various modifications of the basic diazoquinone resist-PMMA combination in the bilayer blanket-exposure-PCM system have been proposed. Modified PCM systems are summarized in Table 3.8.

The bottom PMMA layer can be replaced with more sensitive DUV positive resists such as P(MMA-OM) and PMIPK (cf. Section 3.1.2) to reduce blanket-exposure time. Conventional positive photoresists are opaque enough below 250 nm to act as an excellent mask for the image transfer exposure of PMMA, which is sensitive to the DUV radiation ranging from 200 to 230 nm. On the other hand, PMIPK is most sensitive in the range

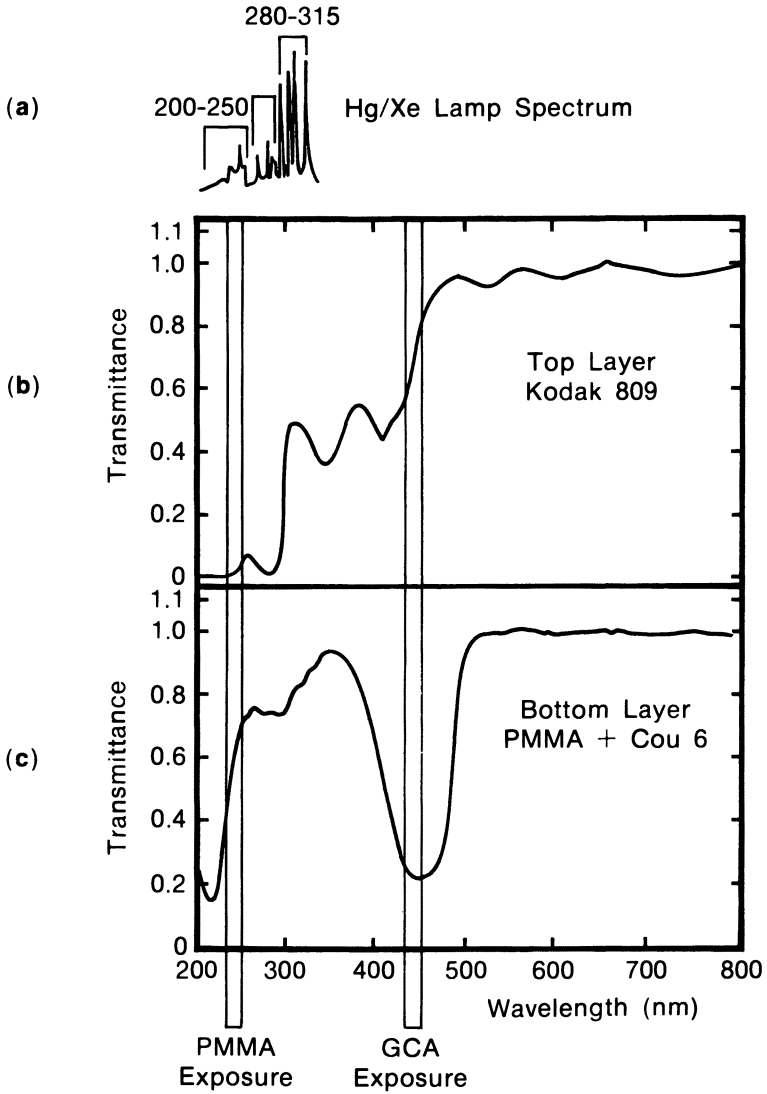
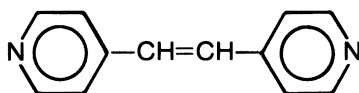


Figure 3.48. UV transmission characteristics of dyed PMMA and Kodak 809 resist as a function of wavelength. (Reproduced with permission from reference 173. Copyright 1984 Society of Photo-Optical Instrumentation Engineers.)

Table 3.8. Various Schemes of Two-Layer DUV Flood Exposure-PCM Systems

<i>Imaging Layer</i>	<i>Planarizing Layer</i>	<i>Imaging</i>	<i>Comments</i>	<i>Reference</i>
HPR204	Modified PMMA P(MMA-OM), P(MMA-OM-MAN)	UV scanner	Reduction in flood exposure time	167
Kodak 809 + dye	PMIPK + coumarin 6	Stepper	Dyes in both imaging and planarizing layers	173
PSTTF	PMMA	E-beam	Negligible interfacial layer	174
RD2000N(MRS)	PMMA	DUV scanner, DUV contact	Negligible interfacial layer	175
LMR	PMMA	DUV contact	Al lift-off	176
Ag ₂ Se/GeSe	PMMA	UV scanner, stepper	High resolution, negligible interfacial layer,	149
Microposit 1470	PMGI + coumarin 6	Stepper	Negligible interfacial layer, high thermal stability, aqueous base development	150
Photoresists	IBM terpolymer	Stepper	Higher sensitivity, higher thermal stability, mold hardening	64
				177

of 290–310 nm, where the novolac resists are transparent enough to render the mask useless for PMIPK exposure (Figures 3.10 and 3.11). Therefore, incorporation of a dye with absorption centered at about 300 nm is required to make the resist film more opaque at the wavelength of PMIPK exposure. Bispyridylethylene (structure 3.15) ($\lambda_{\max} = 300$ nm) has been found to be a good dye in Kodak 809 for this PMIPK PCM scheme as shown in Figure 3.49 (173).



3.15

Lin et al. (177) replaced PMMA with IBM terpolymer resist (a terpolymer of MMA, methacrylic acid, and methacrylic anhydride developed as an electron beam resist), which has a higher thermal stability and a higher DUV sensitivity.

Another interesting, DUV-sensitive, planarizing layer for the exposure-PCM scheme is poly(dimethyl glutarimide) (PMGI) (structure 3.7). Exposure of PMGI to DUV light or electron beam radiation results in main-chain scission; therefore, this resist is positive working.

A totally aqueous-base-developable bilayer PCM system that takes advantage of the high thermal stability, aqueous-base solubility, and high solvent resistance of PMGI has been reported (64, 65). The glass transition temperature (T_g) of PMGI is ca. 189 °C; consequently, the resist image is thermally stable to this temperature. The acidic N–H groups render PMGI soluble in aqueous base with the dissolution properties similar to those of novolac resins. This polymer is sparingly soluble in common organic solvents. This characteristic results in minimal interfacial mixing between a top imaging layer and the bottom planarizing layer. The significant absorption of PMGI in the DUV region to 280 nm necessitates the incorporation of a dye into a diazonaphthoquinone photoresist to render the imaging layer more opaque in the 250-nm region. SEMs demonstrating the thermal flow resistance and high aspect ratio PCM patterning are provided in Figures 3.50 and 3.51.

In the PCM systems just described, both top and bottom resists are positive working. Residual exposure of a bottom positive resist during UV or electron beam imaging of a positive top resist is acceptable. However, when a negative resist is used as the top layer, the residual exposure may reduce the contrast of a bottom positive resist. The several PCM systems involving the use of a negative resist as a top layer listed in Table 3.8 (imaging layers 3–6) indicate that if there is a sufficient sensitivity difference between the top and the bottom resists, the residual exposure can be tolerated.

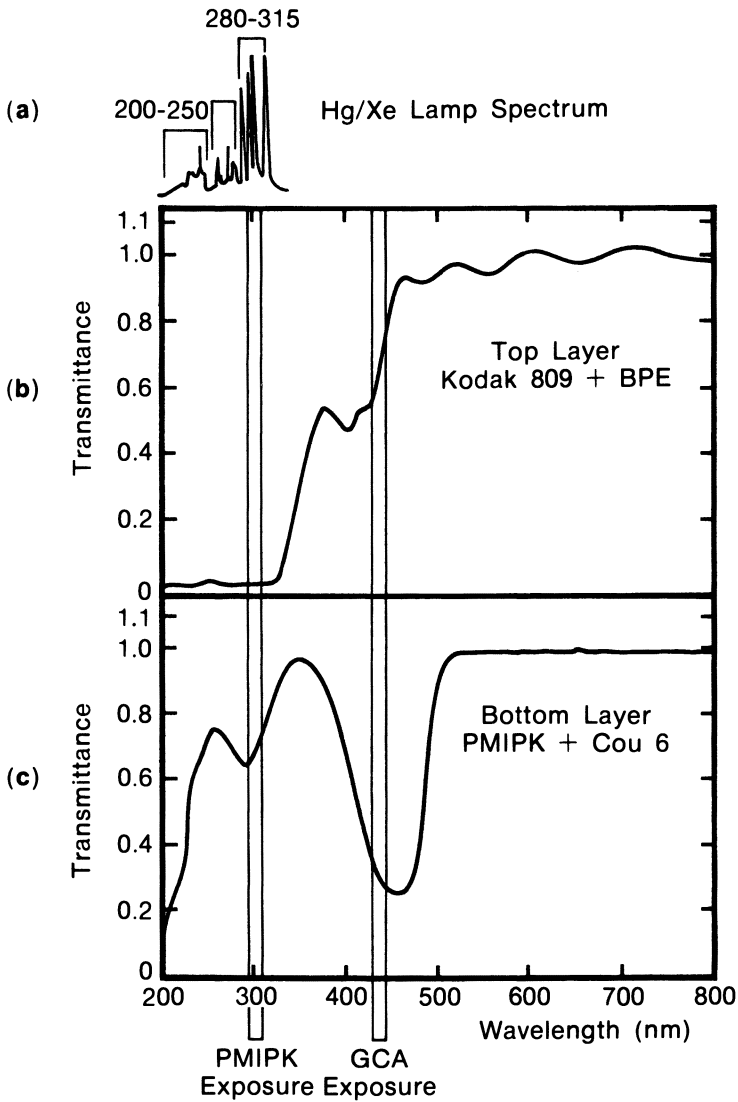


Figure 3.49. UV transmission characteristics of dyed PMIPK and dyed Kodak 809 resist in a mid-UV exposure-PCM scheme. (Reproduced with permission from reference 173. Copyright 1984 Society of Photo-Optical Instrumentation Engineers.)

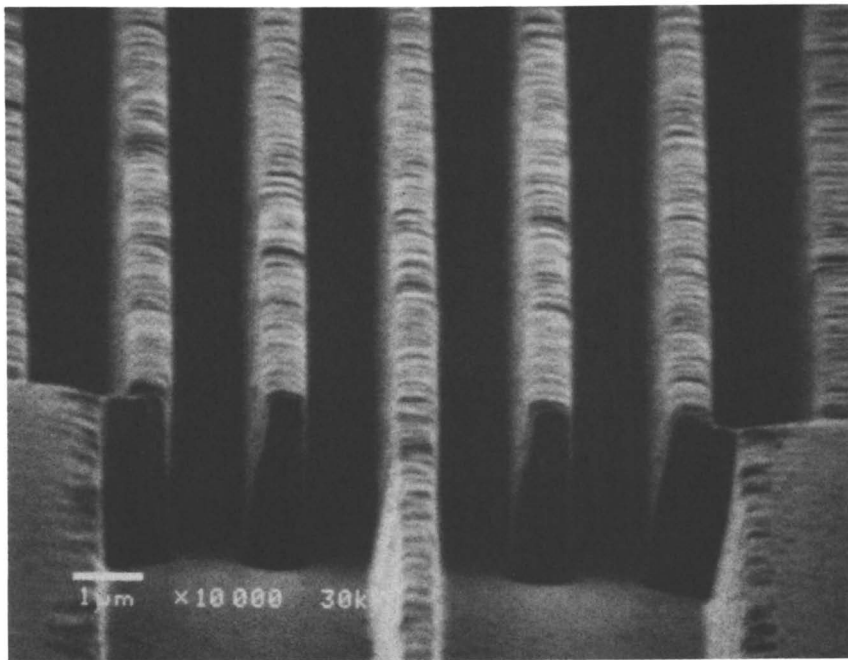


Figure 3.50. SEMs of a PMGI pattern obtained by DUV exposure. (Reproduced with permission from reference 64. Copyright 1985 Society of Photo-Optical Instrumentation Engineers.)

Lin et al. first reported a negative top resist PCM system with PSTTF (structure 3.12; Section 3.2.2.2) as an imaging layer. The PSTTF-PMMA system offers two advantages over the AZ1350J-PMMA system (174):

1. formation of a capped structure with the high-contrast development of PMMA in MIBK, and
2. no interfacial mixing.

The same advantages have been obtained with other systems that use a negative resist as an imaging layer. These systems include MRS-PMMA and Ag₂Se-GeSe-PMMA systems (Table 3.8) that are reportedly free from reflection problems due to the intense absorption of imaging UV irradiation by the top resist layer. Figure 3.52 demonstrates patterns generated in the capped PCM mode in 0.4- μm -thick MRS and 1.2- μm -thick PMMA layers coated on a 0.7- μm -stepped SiO₂ substrate (19).

An isolation layer can be incorporated between the two layers to alleviate the interfacial mixing problem. Table 3.9 summarizes such three-layer PCM systems composed of a diazoquinone resist, an isolation layer, and PMMA. The use of aluminum, amorphous silicon, and a spin-on antireflective coating

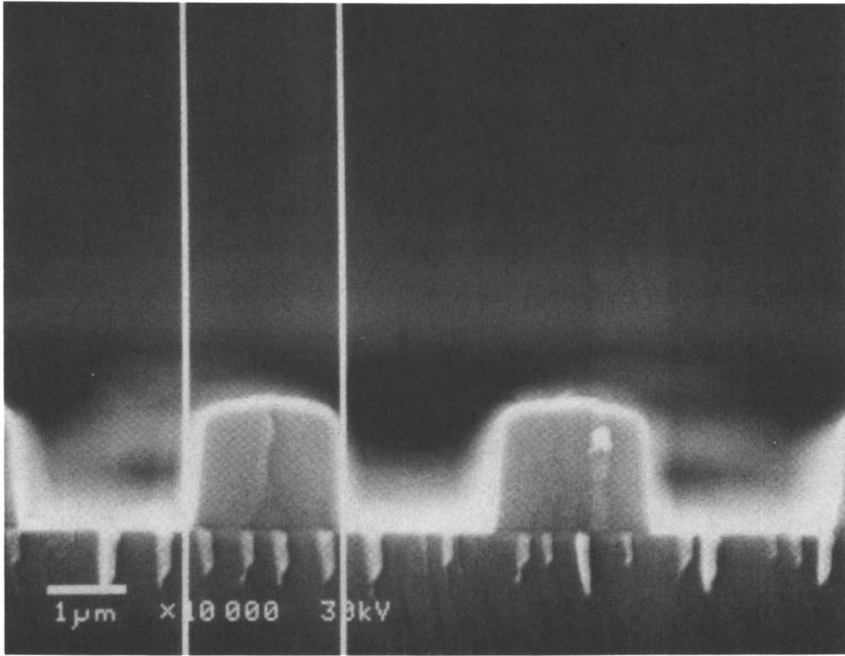
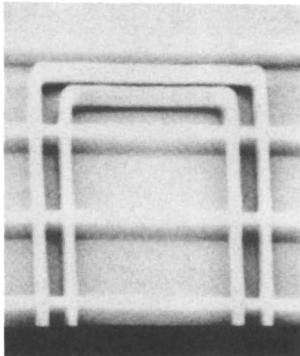
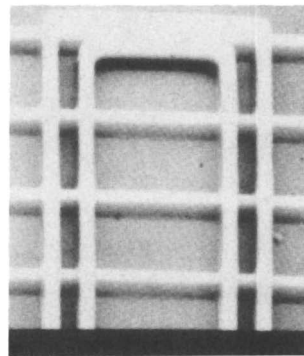


Figure 3.51. SEMs demonstrating thermal stability (180 °C) of a PMGI pattern. (Reproduced with permission from reference 64. Copyright 1985 Society of Photo-Optical Instrumentation Engineers.)



Nominal 0.75- micrometer
Lines and Spaces



Nominal 1.0- micrometer
Lines and Spaces

Figure 3.52. Patterns formed in a bilayer resist system consisting of a 1.2-μm-thick planarizing layer of PMMA and a 0.4-μm-thick RD2000N imaging resist. (Reproduced with permission from reference 19. Copyright 1984 Technical Publishing.)

Table 3.9. Three-Layer DUV Flood Exposure-PCM Systems

<i>Imaging Layer</i>	<i>Isolation Layer</i>	<i>Planarizing Layer</i>	<i>Imaging</i>	<i>Reference</i>
AZ1350J	Al	PMMA	E-beam	159
AZ1350J	a-Si ^a	PMMA	Stepper, E-beam	178
Microposit 1400-17	ARC	PMMA	Stepper	179
Kodak 820	ARC	PMMA	Stepper	180

^aa-Si is amorphous silicon.

(ARC) as the isolation layer has been reported. Attractive among the isolation materials is the ARC, because all of the layers can be obtained by spin casting. The ARC is a thin organic coating composed of a polyamic acid and dyes for near-UV projection lithography that reduces the reflection effect in diazoquinone positive resists (181). The ARC absorbs strongly at the near-UV exposure wavelength to eliminate detrimental effects of standing waves and scatterings from the surface topography in the top resist layer. The ARC layer can be etched away during the alkaline development of the top resist. Because the properly baked ARC film does not interact with either the bottom PMMA or the top photoresist, chlorobenzene development of PMMA produces a capped structure desirable for RIE processes without cumbersome plasma descumming. The major limitation of this PCM scheme seems to be the narrow process window of the ARC layer. Careful control of baking conditions is necessary to avoid severe erosion of the ARC layer during the alkaline development of the top resist layer because the ARC material is not photosensitive and is etched isotropically in base. Overbaking renders the ARC totally insoluble.

3.3.1.2 DEEP-UV IMAGING AND RIE-PCM SYSTEMS

A PCM system that uses RIE to define patterns in a thick planarizing layer was first reported by Havas for the metal lift-off process (182). Moran and Maydan (183, 184) fully demonstrated the versatility and process compatibility of this system. In the trilevel RIE-PCM system, the thin top resist is patterned in the standard fashion. The relief image is then transferred by RIE through an intermediate layer, which then serves as an oxygen RIE mask for the thick bottom layer (Figure 3.45). Hard-baked novolac resists or hard-baked polyimides are commonly used as the planarizing layer. Intermediate layers used in various trilevel systems include vacuum-deposited films of SiO₂, Si₃N₄, Si, Ge, spun-on films such as "spin-on-glass", and soluble titanium complexes. Moran and Maydan (184) demonstrated the use of electron beam, X-ray, refractive near-UV projection, and reflective near-UV projection for imaging of the top resist and addressed the benefit of the trilevel RIE scheme in each lithography technique.

DUV lithography can also benefit from the RIE-PCM scheme. Table 3.10 summarizes multilayer RIE systems that use DUV exposure to image

Table 3.10. DUV Imaging RIE-PCM Resist Systems

Imaging Layer	Planarizing Layer ^a	Comment	Reference
Ag ₂ Se/CeSe	a	Scanner(M500), 100-s exposure (UV-2), 0.75 μmL/S 200 mJ/cm ² at 254 nm	152
Poly(dimethyl diphenyl-vinyl siloxane)	a	10 mJ/cm ² at 254 nm	185
Chloromethylated polydiphenylsiloxane	a	Scanner (M500), 5 mJ/cm ² at 254 nm	186, 187
Poly(trimethylstannylstyrene-co-chlorostyrene)	a	Contact (PLA520), 60 mJ/cm ² (CM290)	188, 189
Poly(trimethylsilylstyrene-co-chloromethylstyrene)	a	Scanner (M500), 50–100 mJ/cm ² (UV-3) 0.75-μm pattern	190, 191
Aliphatic polysilane	a	Contact, 0.7-μm space pattern 0.5–3.6 J/cm ² at 260 nm	192, 193
Poly(<i>p</i> -disilanylene phenylene)	b	TiO ₂ isolation layer, contact 0.4-μm pattern	194
Poly(Si-substituted MMA-MMA-MA)	a	Spin-on-glass isolation layer, scanner (M500), 0.7-μm pattern	195
RD2000N (MRS)	b		196
RD2000N (MRS)	a		87

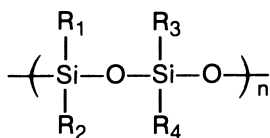
^aSymbols used are as follows: a denotes a hard-baked diazoquinone resist, and b denotes a hard-baked polyimide.

the top resist. Most of the efforts in this area have been devoted to the design of simple, bilayer RIE-PCM systems, as Table 3.10 shows.

The intermediate layer in the trilevel scheme can be eliminated if the top layer offers sufficient oxygen RIE resistance as well as imaging capability. Inorganic resist systems are quite suitable in this respect. Figure 3.53a shows profiles of 0.75- μm line and space arrays delineated in a hard-baked photoresist with $\text{Ag}_2\text{Se}-\text{Ge}_x\text{Se}_{1-x}$ a mask, which was exposed in the UV-2 mode on a Perkin-Elmer M500 scanner (152). A 50% change in exposure time of this resist still results in adequate resolution of 0.75- μm lines and spaces with reasonable line width control. Ong et al. (152) estimated that 0.65- μm line and space features could be resolved in this resist system with the scanner operating in the UV-2 mode, although 0.5- μm line and space patterns were not resolved. When the inorganic resist was exposed to the broad-band radiation, 0.75- μm features were resolved (Figure 3.53b), and the exposure time was 4 times faster than in the UV-2 mode.

Resist materials composed of organic polymers do not possess sufficient plasma etching durability to function properly as masking layers for the etching of thick planarizing polymer layers (197). To simplify the RIE-PCM scheme, various organometallic resists that offer both imaging capability and oxygen RIE resistance have been developed (Table 3.10). In general, all of the systems contain a significant weight percentage of an element that forms a refractory oxide upon reaction with oxygen plasma. When these organometallic resists are placed in an oxygen plasma, a thin layer of nonvolatile oxide is generated on the surface that is impervious to further oxygen etching (198) and acts as a mask for the anisotropic etch transfer of the top image into the thick polymer planarizing layer.

The use of organometallic polymers in the bilevel RIE-PCM scheme was first reported by Shaw et al. (185). They used polysiloxane (structure 3.16) as a negative-working electron beam imaging layer. The etch rate ratio



3.16

of AZ1350J to polysiloxane in an oxygen plasma is reported to be 50:1, indicating that only a 40-nm-thick polysiloxane layer would be sufficient to protect a 2- μm -thick novolac resist. Figure 3.54 shows high aspect ratio 0.4- μm lines imaged in the poly(dimethyl-diphenylvinylsiloxane)-hard-baked AZ1350J system. Incorporation of a chloromethyl group into the benzene ring of polydiphenylsiloxane improves the DUV sensitivity as described in the case of chloromethylated polystyrene (CMS) (see Section 3.2.2.2). A high sensitivity (10 mJ/cm^2 254 nm) has been reported for chloromethylated

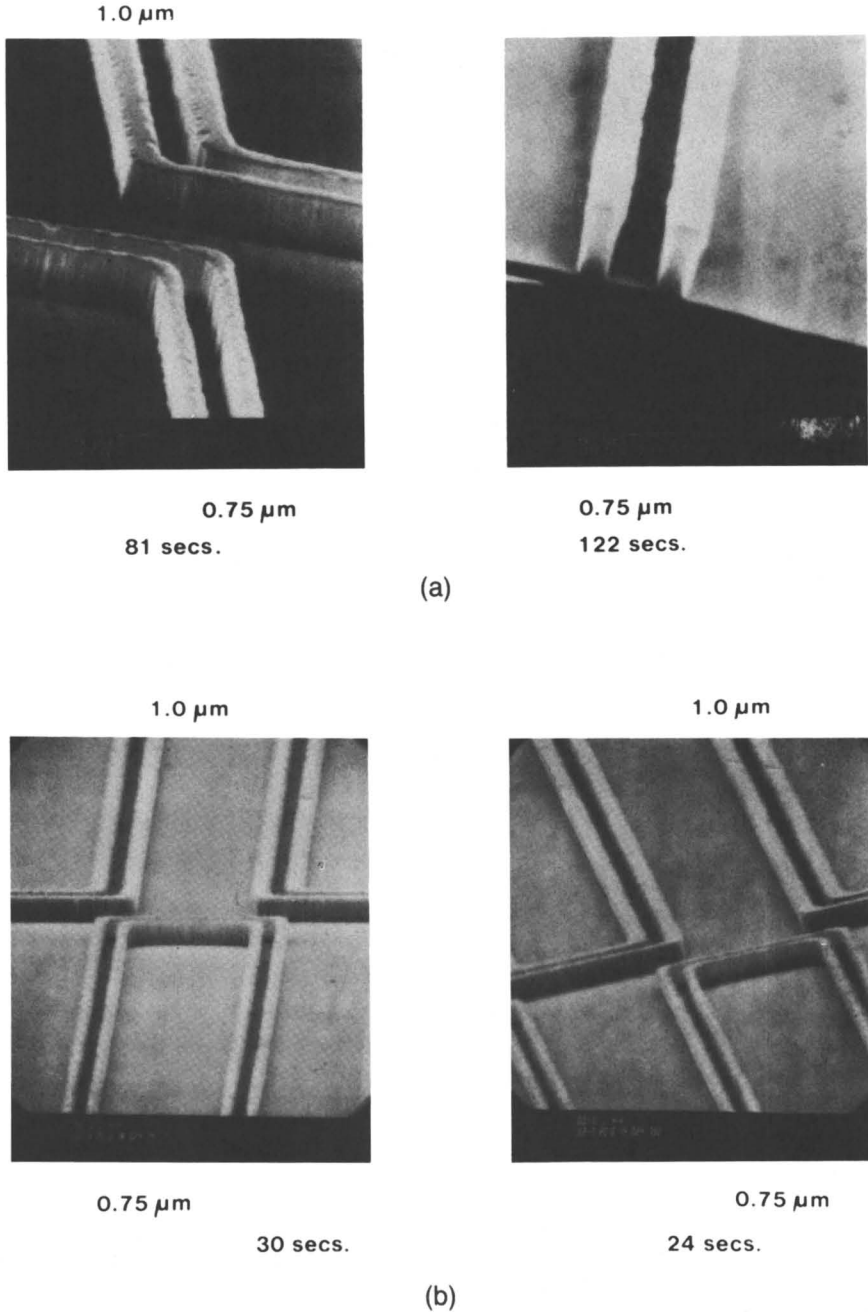


Figure 3.53. SEMs of 0.75- μm lines and spaces projection printed with a GeSe bilayer system: (a) UV-2 mode and (b) broad-band exposure. (Reproduced with permission from reference 152. Copyright 1982 Electrochemical Society.)

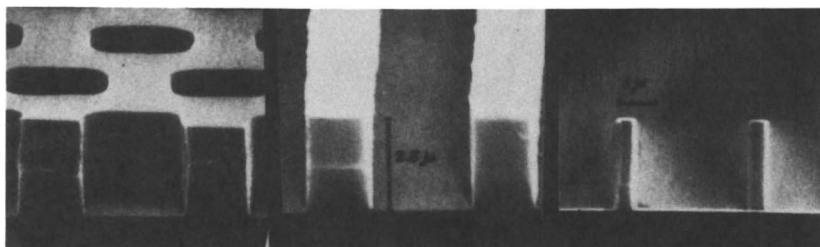
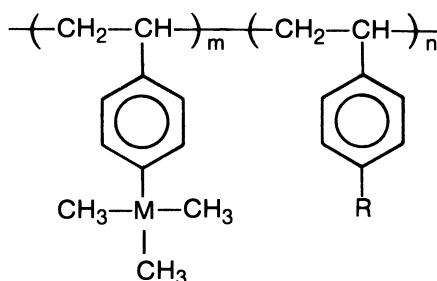


Figure 3.54. High aspect ratio images obtained by oxygen RIE pattern transfer with a polysiloxane as an etch mask. (Reproduced with permission from reference 185.)

polydiphenylsiloxane (186, 187). This material has a T_g room temperature, whereas polydimethylsiloxane is a grease at room temperature.

The high oxygen plasma resistance of trimethylsilyl- and trimethylstannylstyrene polymers has been combined with high DUV sensitivity through copolymerization with chlorinated or chloromethylated styrene polymer (188–191) to provide another example of an imageable oxygen etch barrier material. A very high sensitivity of 5.5 mJ/cm^2 254 nm has been reported for a 1:1 copolymer of trimethylstannylstyrene and *p*-chlorostyrene (189) (structure 3.17). Electron spectroscopy for chemical analysis (ESCA) (189)



M = Si or Sn

R = Cl or CH_2Cl

3.17

and Auger electron spectroscopic studies (190) showed that silicon or tin in a variety of oxidation states generates an effective oxygen etch barrier. The ESCA spectra shown in Figure 3.55 demonstrate that after oxygen RIE treatment of polytrimethylsilylstyrene, the binding energy of the Si $2p$ transition increases by 2.7 eV, indicating the formation of SiO_x , where x has a value between 1.5 and 2. MacDonald et al. (189) found that the incorporation

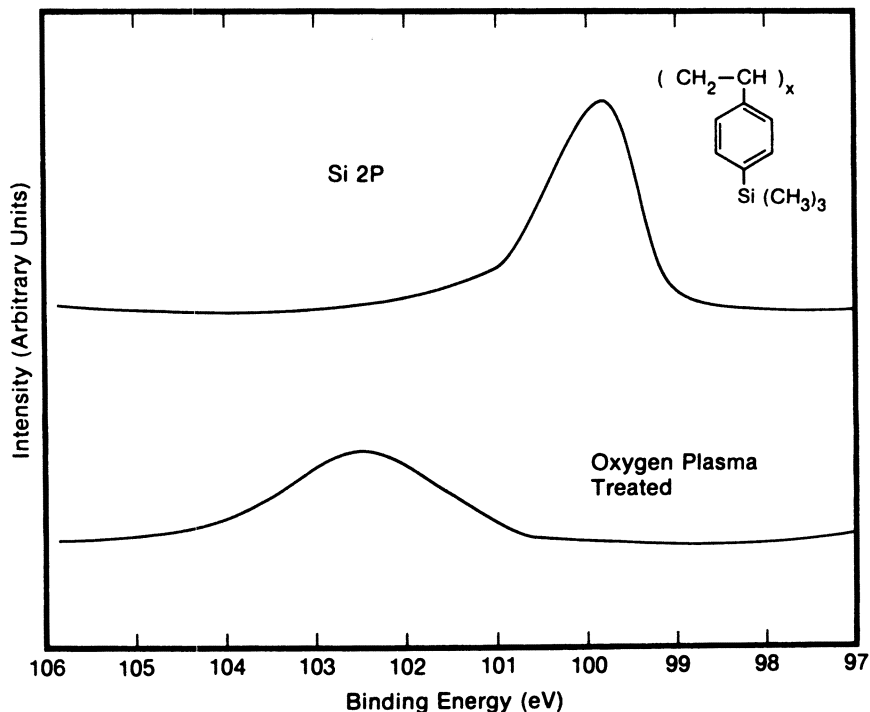


Figure 3.55. ESCA spectra of polytrimethylsilylstyrene before and after oxygen plasma treatment, showing formation of SiO_x . (Reproduced with permission from reference 189. Copyright 1983 North-Holland.)

of a small amount of Si (3 wt %) into an organic polymer has a substantial effect on the oxygen plasma etch rate, and that the incorporation of approximately 10 wt % Si is sufficient to produce an effective etch barrier. Reichmanis and Smolinsky (195) reported a similar trend in a Si-containing positive-working methacrylate resist system in which Si ranged from 0 to 17.5 wt %. Under their etching conditions, incorporation of approximately 7 wt % Si produced an effective etch barrier. These results suggest that if the Si content is above a threshold value, which is dependent on the specific etching conditions, an effective etch barrier is formed even though the bulk of the resist system is organic in nature.

Polysilanes, a class of Si-Si backbone polymers, have attracted much attention because of their lithographic potential. They have been shown to function as high-resolution, positive DUV and mid-UV resists. A unique photochemistry with high quantum yields and nonlinear photobleaching was reported by Hofer et al. (192) and by Miller et al. (193). Backbone scission of polysilanes upon irradiation leads to a decrease in chain length, an accompanying blue shift of absorption maximum, and a reduction in the extinction coefficient. The spectra in Figure 3.56 show the photobleaching and

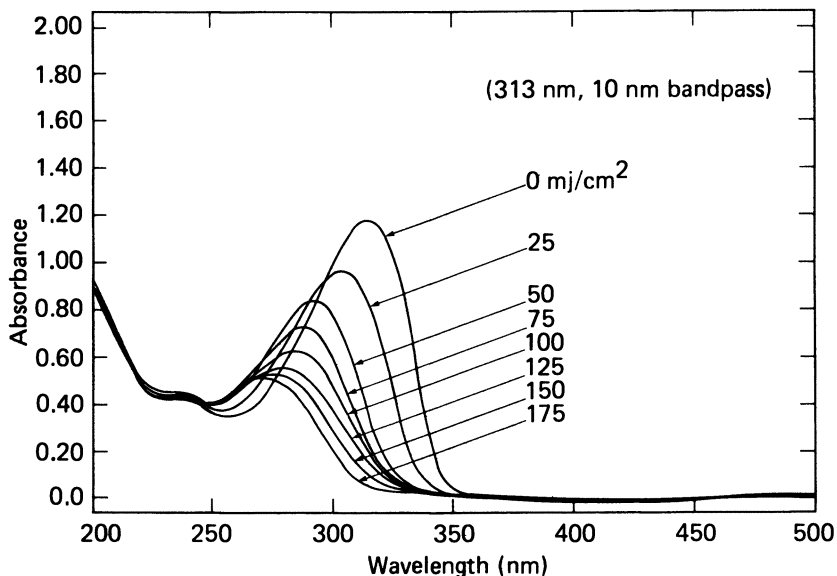
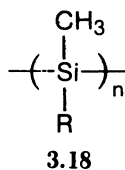
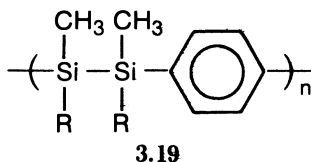


Figure 3.56. UV spectra of an aliphatic polysilane demonstrating bleaching and blue shifting. (Reproduced with permission from reference 192. Copyright 1984 Society of Photo-Optical Instrumentation Engineers.)

blue shift typically observed upon exposure of aliphatic polysilanes. The researchers used aliphatic polysilanes (structure 3.18) as a thin imaging layer



for bilevel oxygen RIE image transfer. High aspect ratio patterns imaged in an aliphatic polysilane–hard-baked photoresist system are shown Figure 3.57, where the top resist was imaged at 313 nm at a dose of 100 mJ/cm² a 1:1 projection printer (structure 3.19). Nate et al. (194) reported use of



poly(*p*-disilanylenephylene) (structure 3.19) for patterning polyimide by the bilevel oxygen RIE technique. Three-layer RIE–PCM systems obtained

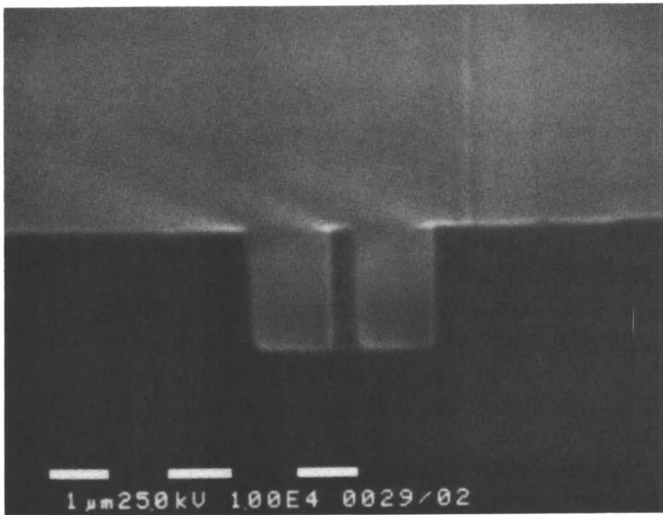
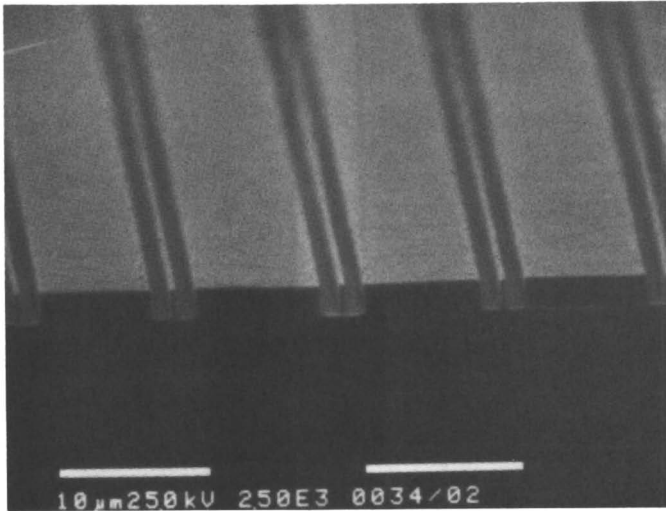


Figure 3.57. SEMs of high aspect ratio images transferred into a hard-baked photoresist by oxygen RIE after mid-UV projection printing of a 0.25- μm -thick polysilane resist. (Reproduced from reference 193. Copyright 1984 American Chemical Society.)

by using a negative DUV resist MRS as the imaging layer have been reported (Table 3.10, RD2000N) (87, 196).

Multilayer resist systems can improve the performance of optical, electron beam, X-ray, and ion beam lithography (83, 86). Whereas these schemes increase processing complexity, they appear to be gaining popularity and are currently used in several manufacturing areas. Both DUV blanket-exposure-PCM and DUV imaging and RIE-PCM schemes are strong candidates for submicrometer lithography.

3.3.2 Deep-UV Hardening

DUV blanket exposure of novolac photoresists significantly reduces thermal deformation of resist images during high-temperature treatments such as those currently practiced in semiconductor manufacturing. The DUV-hardening effect was first observed independently by van Pelt (53) and by Hiraoka and Pacansky (166, 199, 200). In the course of AZ1350J-PMMA PCM experiments, van Pelt (53) found that DUV blanket exposure rendered the photoresist insoluble in organic solvents and effectively reduced thermal flow of the resist image to 200 °C. This thermal stability of DUV-cured positive photoresists was first ascribed to the generation of indenecarboxylic acid or its salt (199, 200). Photochemical (168, 169) and processing (201, 202) studies later revealed that the thermal stability of resist patterns after DUV exposure is due to the formation of a surface skin layer of photocross-linked and photooxidized novolac resin.

Figure 3.58 (left) shows a cross section of AZ1470 photoresist images that were exposed with a low-pressure Hg lamp after normal patterning and then baked for 30 min at 180 °C. Figure 3.58 (right) shows a cross section of resist images that were irradiated with a Hg lamp by using a glass filter to remove DUV radiation. Even the standing wave patterns on the resist side wall are intact in the DUV-cured sample. Near-UV exposure ($\lambda > 300$ nm) of novolac resist patterns does not result in the formation of a cross-linked surface layer. If the DUV-hardened surface layer is removed by an oxygen plasma treatment, the underlying layers behave the same as patterns that received only near-UV exposure (201, 203).

DUV exposure of poly(*p*-substituted styrenes), such as poly(*p*-chloro-styrene), poly(*p*-chloromethylstyrene), and poly(*p*-hydroxystyrene) [poly(*p*-vinylphenol)] (structure 3.11), in air leads to photocross-linking and photooxidation. Consequently, DUV hardening is applicable to resists based on these polymers as well as novolac-based resists (168, 169).

3.4 Excimer Laser Lithography

3.4.1 Lithography with Traditional Lasers

One application of lasers to lithography is a maskless patterning technology. In this application, the spatial coherence of the laser is the essential property;

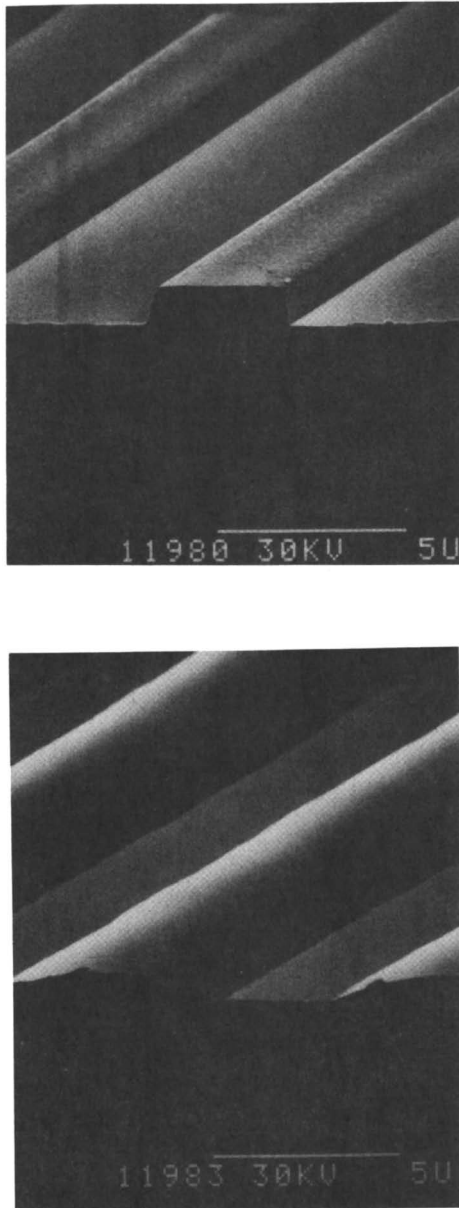


Figure 3.58. SEMs demonstrating UV hardening of a photoresist. Top, AZ1470 patterns baked at 180 °C for 30 min after exposure to a low-pressure Hg lamp containing DUV output and bottom, AZ1470 patterns under the same conditions except that the patterns were exposed through a glass filter. (Reproduced with permission from reference 201. Copyright 1982 Electrochemical Society.)

a single-mode beam allows optimal focusing of a small spot on the substrate (14). Maskless patterning of ceramic substrates for hybrid integrated circuit and wiring patterns in multilevel printed circuit boards has been reported. In these systems, a laser beam is focused onto a resist-coated wafer. The spot is blanked and scanned by precisely moving the substrate and/or optical deflection systems to delineate the desired patterns in the photoresist. Focused laser lithography is a direct-write method, similar to electron beam lithography. Such direct-write techniques have several problems:

- The laser sources have been limited to continuous wave because of the scanning nature of the exposure. Reliable continuous wave lasers currently available have limited power in the UV.
- Technical problems associated with building high-speed, two-dimensional optical deflection systems become more formidable as the resolution requirements become tighter.
- The process is serial in nature, requiring pixel-by-pixel exposure, and therefore has limited throughput.

The use of a focused UV laser beam to produce micrometer-size chemical processes on solid surfaces has been reported. These processes are initiated by the photodissociation of a molecular gas in the vicinity of the gas–solid interface. Depending on whether the active photofragment reacts with or is adsorbed on the solid, microetching or microdeposition respectively, occurs. The spatial resolution of this process is determined by

- the laser beam spot size,
- the spatial confinement of the resulting excitation, and
- the reciprocity of the surface chemical process.

Deposition and etching of Si can be accomplished at line widths $<0.4 \mu\text{m}$ (204). Practical applications of this laser microchemical processing include ohmic contact formation on p-InP (p-type indium phosphide) and hard-surface-mask repair (205). Further details on recent applications of this process can be found (204–206).

3.4.2 Contact Printing with Excimer Lasers

As mentioned in Section 3.1.2, attractive UV sources for lithography are those that produce high power and poor spatial and temporal coherence. Jain and co-workers (13–15) demonstrated that excimer lasers provide excellent quality, speckle-free images with resolution to $0.5 \mu\text{m}$ in a contact mode. The images were obtained in $1\text{-}\mu\text{m}$ -thick diazoquinone photoresists such as AZ2400 with a XeCl laser at 308 nm and a KrF laser at 248 nm

(Figure 3.59). They also showed that standing wave effects, though not totally absent, were barely noticeable despite the quasimonochromaticity of the excimer laser radiation.

Exposures of PMMA with an ArF laser at 193 nm were reported by Kawamura et al. (207). The laser beam was focused by a convex lens to increase the power density. The laser beam dose incident on the resist film was 930 mJ/cm^2 , delivered in 20 nsec. Kawamura et al. were able to image $0.5\text{-}\mu\text{m}$ lines without interference patterns.

Excimer laser lithography has been extended into the vacuum-UV (VUV) region with the use of a F_2 excimer laser operating at 157 nm and a new mask technology (208). Because the conventional mask technology using quartz substrates cannot be employed, alkaline-earth halide substrates (e.g., CaF_2) that have high transmittance at 157 nm were used to fabricate masks. As shown in Figure 3.60, the exposure was carried out either in vacuum or in a cell purged with inert gases that do not absorb light at 157 nm. PMMA and a copolymer of methyl methacrylate (MMA) and methacrylic acid, P(MMA-co-MAA), developed as an electron beam resist (209), were exposed in the 157-nm patterning experiments. The transmittance of PMMA at 157 nm decreases as the film is exposed, preventing exposure of the lower level of the PMMA film. PMMA films thicker than 100 nm were not fully developed. In contrast, P(MMA-co-MAA) becomes increasingly transparent with exposure. Features as small as $0.15 \mu\text{m}$ were generated by contact printing with use of this resist at 157 nm.

Experiments with the KrF laser (248 nm) and the inorganic resist $\text{Ag}_2\text{Se-GeSe}_2$ were reported by Polasko et al. (210). These researchers obtained well-controlled $0.5\text{-}\mu\text{m}$ line space arrays by contact printing using a

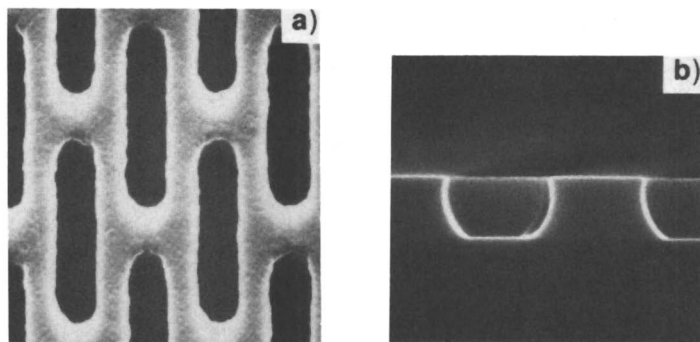


Figure 3.59. SEMs of images obtained by contact printing with excimer lasers: (a) $0.5\text{-}\mu\text{m}$ lines and spaces obtained with XeCl laser at 308 nm (two pulses, each 50 mJ/cm^2), and (b) $1.5\text{-}\mu\text{m}$ features obtained with a KrF laser at 248 nm (five pulses, each 25 mJ/cm^2). (Reproduced with permission from reference 15a. Copyright 1982 Institute of Electrical and Electronics Engineers.)

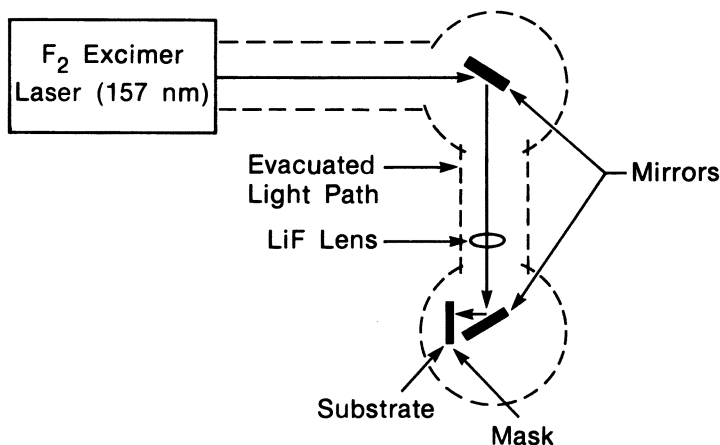


Figure 3.60. Schematic diagram of a VUV excimer laser system for contact lithography with 157-nm radiation. (Reproduced with permission from reference 208. Copyright 1983 American Institute of Physics.)

chromium-on-quartz mask. By increasing the fluence to 520 kW/cm^2 , they found that the required dose could be lowered from 130 to 5.2 mJ/cm^2 . This result signifies a 250-fold improvement relative to the value obtained with Hg arc illumination at 430 nm . Because contact printing suffers from damage to the mask and resist films resulting from frequent mask-wafer contact, projection printing systems using excimer lasers are being studied by several groups.

3.4.3 Projection Printing with Excimer Lasers

The first demonstration of projection lithography obtained with a UV laser was reported by Lacombe et al. (211). The laser they used as an illumination source was not an excimer laser but a 413-nm Kr laser with spatial coherence. Because the spatial coherence of a source depends directly on the source size (the larger the source, the less spatially coherent it is), they used a scanning laser beam system with two rotating mirrors (Figure 3.61) to reduce speckle. By scanning areas of various sizes in the entrance pupil of their projection system, they investigated the dependence of partial coherency degree, σ , on the image contrast. They were able to obtain lines as small as $0.9 \mu\text{m}$ on $0.5\text{-}\mu\text{m}$ oxide steps and on $1\text{-}\mu\text{m}$ aluminum steps (Figure 3.62) by using an experimental optical bench setup with the scanning source system and a commercial $10\times$ high-resolution lens. No speckle noise effect was observed on the resist with a coherency value of $\sigma = 0.1$.

Excimer laser projection lithography was attempted by Dubroeuq and Zahorsky (212). The image projection system having a KrF laser and a $10\times$ microscope objective lens is shown in Figure 3.63. The low divergence of

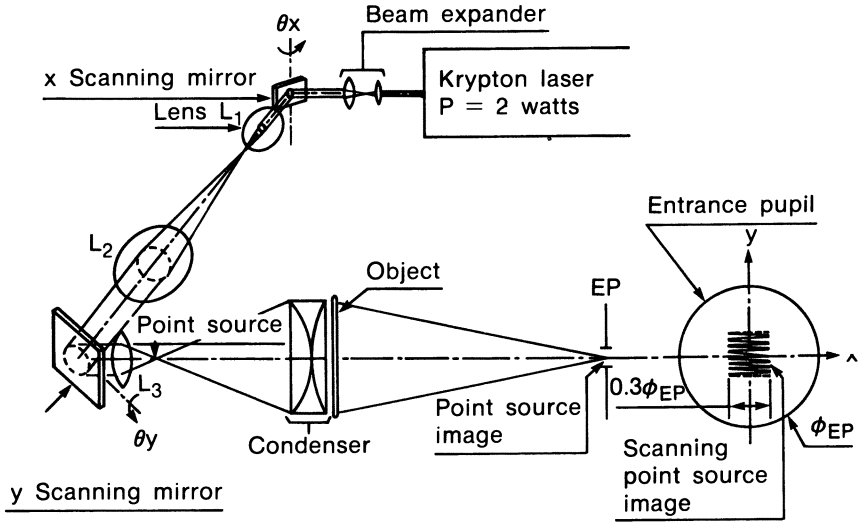


Figure 3.61. Scanning point source system. (Reproduced with permission from reference 211. Copyright 1980 Technical Publishing.)

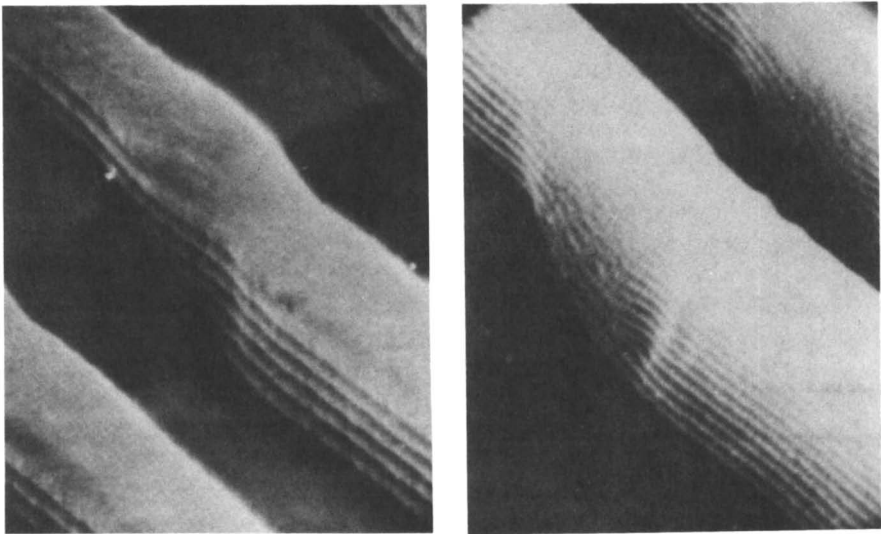


Figure 3.62. SEMs of 0.9- μm lines and spaces printed with a laser projection system in 0.7- μm -thick AZ1350H on a 0.5- μm oxide step (left) and 1.5- μm -thick AZ1350H on a 1- μm aluminum step (right). (Reproduced with permission from reference 211. Copyright 1980 Technical Publishing.)

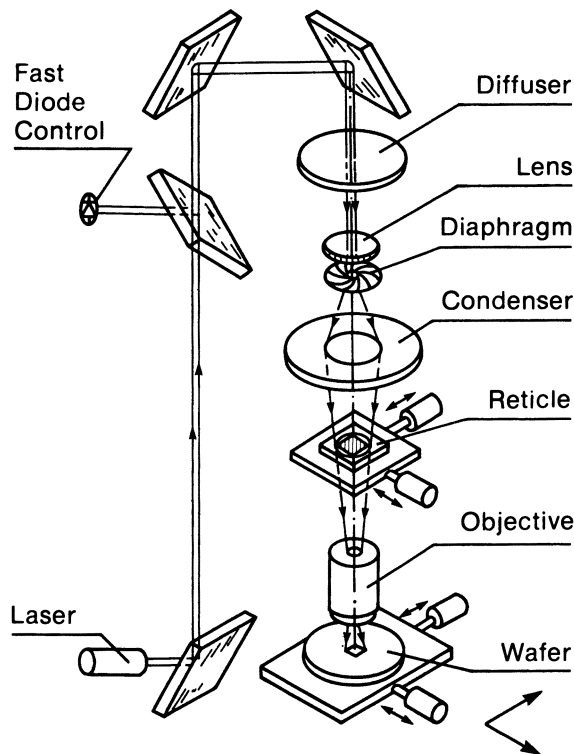


Figure 3.63. KrF excimer laser projection printing setup. (Reproduced with permission from reference 212.)

the beam is inadequate because it causes an excessive local energy density in the optics and imposes the necessity for working in a quasispatial coherent illumination mode. They placed a diffuser in front of the laser to modify the divergence. The best results were obtained with AZ2400, although the absorption at 248 nm was still significant (see Figure 3.11). Despite the fact that the 0.2-NA lens was not corrected for 248 nm, they were able to image 0.7- μm lines (Figure 3.64). The exposure dose for the resist was 150–175 mJ/cm^2 . They did not compare the laser exposure with the conventional lamp illumination in terms of the reciprocity law. Their SEM photographs show that the wall profiles are overcut and standing wave effects appear at the resist bottom and vanish at the surface. They also pointed out that the small NA value (0.2) allows printing of 1- μm lines with a depth of focus as large as 7 μm , compared to the 3.5- μm depth of focus obtained with i-line (365 nm) wafer steppers with NA = 0.35.

Pol et al. (10) developed an excimer laser-based DUV projection system by modifying a commercial step-and-repeat exposure tool (GCA model 4800 DSW). This system is equipped with a KrF (248 nm) excimer laser, an all-

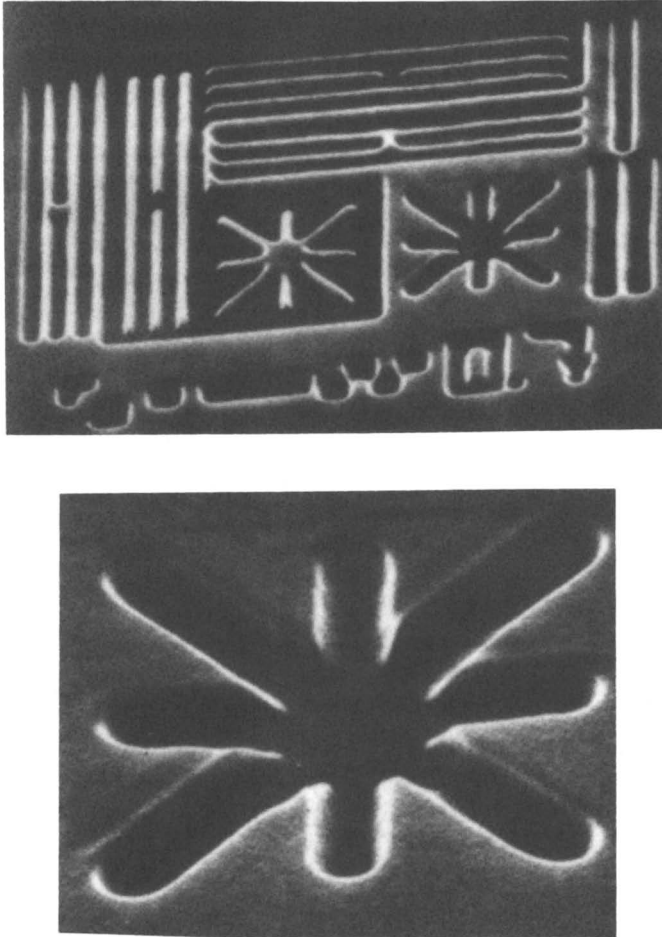


Figure 3.64. SEMs of 0.7- μm images projection printed with the experimental KrF excimer laser setup shown in Figure 3.63. (Reproduced with permission from reference 212).

quartz lens, and a laser beam scan system. The lens design with no chromatic correction imposes an extremely narrow bandwidth requirement (0.005 nm) on the light source, which has been accomplished by extending the lasing cavity beyond the excitation region and inserting two etalons, which act as narrow bandpass filters. Consequently, the exposure time for the Microposit 2400-17 resist is about 50 times longer than exposure times on current production steppers.

Jain and Kerth (213) reported results of excimer laser projection lithography that used a commercial projection printer. They demonstrated high-speed full-wafer exposures, with resolution to 1 μm , and excellent

image quality on a Perkin–Elmer model 111 full-wafer 1:1 scanning projection printer equipped with a XeCl excimer laser (308 nm). Images obtained in a diazoquinone–novolac photoresist are shown in Figure 3.65. The full exposures were achieved in 15-s scan time. This result is a fivefold improvement in the exposure time compared with a Hg lamp (14).

Kerth et al. (214) reported excimer laser (308 nm) projection lithography obtained with a modified full-field scanning projection system (Perkin–Elmer M500). The modifications included an anamorphic optical system for transforming the nearly collimated rectangular excimer laser beam into the arc shape. They obtained images of 1- μm lines with nearly vertical (85°) wall profiles.

Projection imaging with DUV (193 nm) and VUV (157 nm) excimer laser radiation was demonstrated by Ehrlich et al. (215). The optical system makes

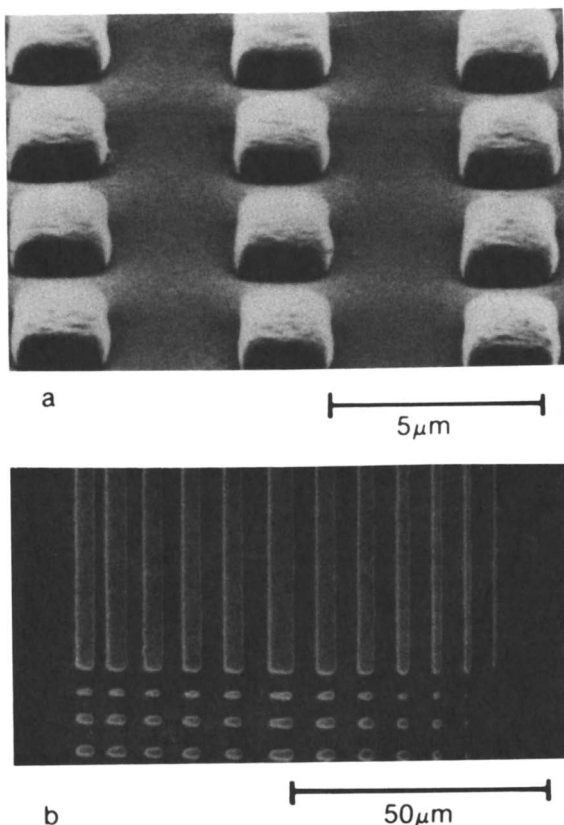


Figure 3.65. Full-wafer excimer laser projection exposure (15 s) showing (a) 2- μm squares, and (b) spaces (dark areas) 1.5–5 μm wide and lines (light areas) 1–5 μm wide. A XeCl laser was used with a commercial 1:1 projection printer. (Reproduced with permission from reference 213. Copyright 1984 Optical Society of America.)

use of a reflecting 0.5-NA microscope objective lens. They described pattern definition by exposure of multilayer organic resists, by maskless etching and doping of solids in reactive vapors, and by solid-state chemical transformations in alumina films. Well-resolved 0.4- μm lines and spaces have been achieved.

The reported results show that projection lithography with excimer lasers is quite promising. To obtain useful field size and better resolution, optical systems will have to be improved, including challenges in both condenser or coupling optics and in lens design.

3.4.4 Excimer Laser Photoetching of Organic Materials

The etching of organic materials with 193-nm ArF excimer laser radiation was demonstrated by Srinivasan and Mayne-Banton (216). Upon irradiation with the 193-nm ArF laser, organic materials undergo an ablative photo-decomposition. Andrew et al. (217) also reported the direct etching of polyimide and photoresist films with a XeCl laser. The ablation reaction can be attributed to the high absorption of almost all the incident light in a thin upper layer of the material followed by bond breaking and ejection of small molecules. The researchers concluded that etching was primarily due to a thermal process involving irradiation with the longer wavelength 308-nm XeCl laser. In both cases, a fluence threshold below which no material removal is observed was demonstrated.

Rice and Jain (218) reported the results of laser photoetching of organic materials obtained with a contact lithography apparatus equipped with an ArF excimer laser (Figure 3.66). Features as small as 0.3 μm were produced in 1- μm -thick films with no subsequent wet development steps. The intimate mask-wafer contact, however, was undesirable because it prevented volatilization of photofragments from the etched areas. Laser etching with a projection system was reported by Latta et al. (219). Their system used four planoconvex quartz elements providing a 2:1 reduction (Figure 3.67). Although it had a designed resolution of 10 μm , the on-axis performance was capable of resolving 2- μm lines at the image plane. Features ranging from 2 to 20 μm were etched in 1- μm -thick films of diazoquinone-novolac photoresists and polyimide. In both contact and projection photoetching lithography techniques, the total fluence required was in the vicinity of 1 J/cm^2 . The results of Latta et al. show significant broadening at the top of the images (Figure 3.68). Despite these engineering problems, photoetching may find use in certain areas such as resist-free patterning of cured polyimide.

3.4.5 Resist Behavior in Excimer Laser Irradiation

3.4.5.1 RECIPROCITY BEHAVIOR

An important and interesting aspect of excimer laser lithography is the effect of the large instantaneous power density on the resist sensitivity. One might

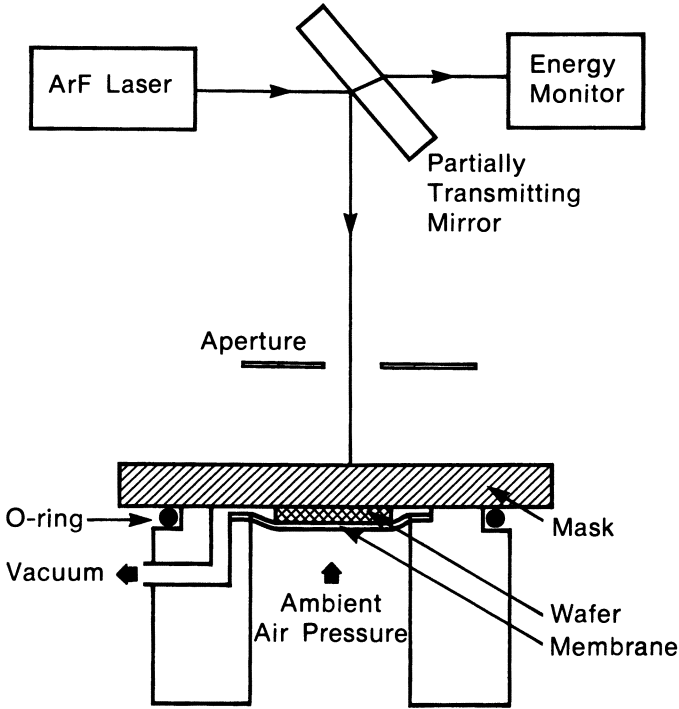


Figure 3.66. Experimental setup for contact etching at 193 nm. (Reproduced with permission from reference 218. Copyright 1984 Springer-Verlag.)

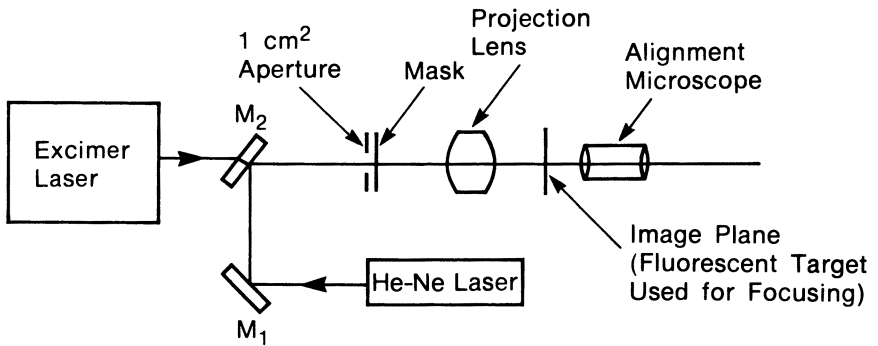


Figure 3.67. Experimental setup for projection etching at 193 nm. (Reproduced with permission from reference 219. Copyright 1984 American Institute of Physics.)

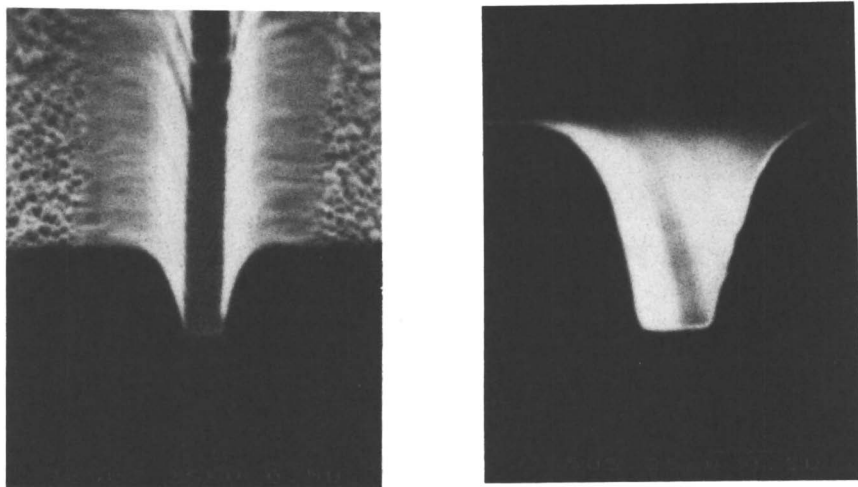


Figure 3.68. A 0.5- μm line directly photoetched in a diazonaphthoquinone-novolac positive photoresist with a 193-nm ArF excimer laser. (Reproduced with permission from reference 218. Copyright 1984 Springer-Verlag.)

expect that high-power irradiation would produce photochemical changes that differ from those produced under conventional Hg lamp illumination. Turro et al. (220) observed that the photoproducts produced by 248-nm KrF excimer laser-induced excitation of diphenyldiazomethane and tetraphenylloxirane in isoctane are different from those generated by conventional lamp excitation of the same substances. They also reported that excimer laser excitation (KrF, 248 nm; XeCl, 308 nm; or XeF, 351 nm) produced a novel, unprecedented emission from benzophenone in trichlorotrifluoroethane (Freon-113) (221). These results were attributed to reactions resulting from the high concentration of active species produced by laser illumination. On the basis of these results, one may expect resist reciprocity failure in excimer laser exposure. Studies on the reciprocity behavior of resists have been based on measurement of both bleaching and photosensitivity at various power levels (14, 15, 222, 223). The conclusion is that in the power range investigated (0.27–4.4 MW/cm²), there is no observable reciprocity failure in AZ2400 and two experimental IBM diazoquinone-novolac resists in 308-nm XeCl laser illumination (Figure 3.69). Here, bleaching was used as the response criterion (223). Photosensitivity lies between 30 and 40 mJ/cm² in the power range (8 kW/cm²–0.39 MW/cm²), as shown in Figure 3.70. This response is comparable to that observed with a conventional illumination (14). The accuracy of the experiments is such that a loss of sensitivity by a factor greater than 3 would be detectable. It is desirable to investigate the reciprocity behavior of resists through use of lithographic photosensitivity

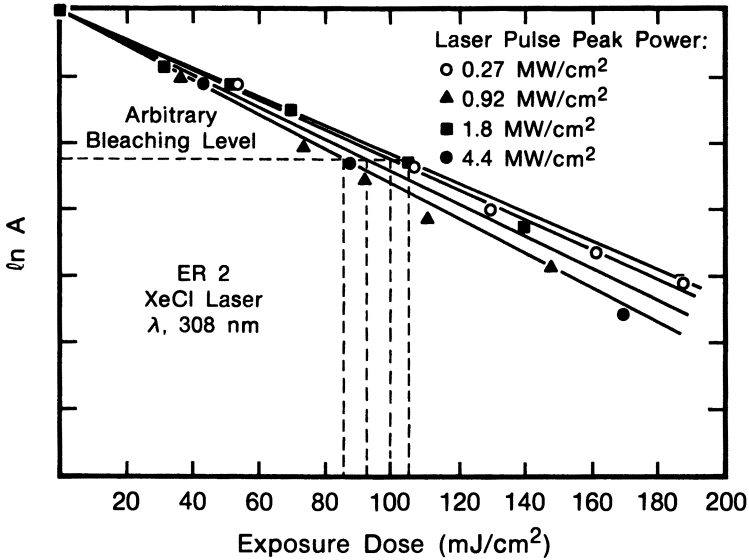


Figure 3.69. Bleaching of an experimental photoresist as a function of the integrated exposure dose for four different laser pulse peak powers. (Reproduced with permission from reference 223. Copyright 1984 Institute of Electrical and Electronics Engineers.)

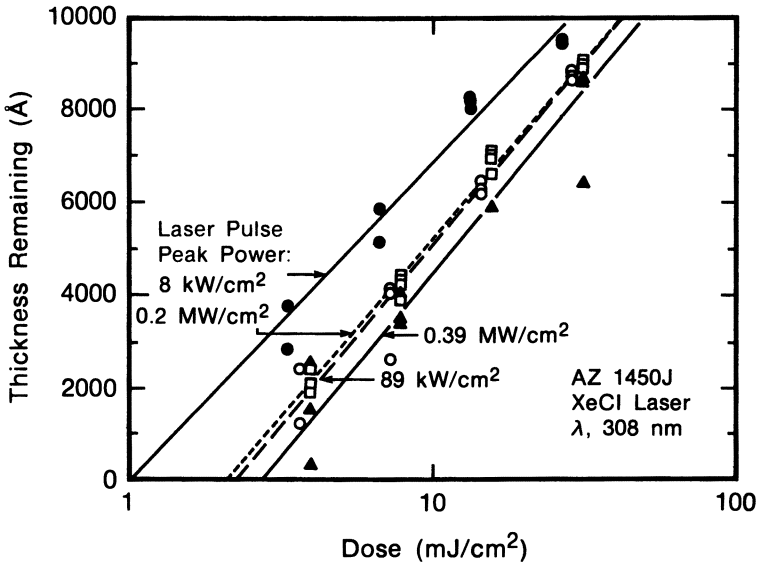


Figure 3.70. Photosensitivity of AZ1450J resist measured at different laser peak powers. (Reproduced with permission from reference 222.)

measurements rather than bleaching because sensitivity is dependent on photoproducts, whereas bleaching experiments give only the loss of photoactive compounds in the resist film without documenting the nature of the photoproducts.

A remarkable reciprocity failure was observed in the inorganic resist described in Section 3.4.2 (210). The effect of dose rate on the total dose required for response is shown in Figure 3.71, where the number of pulses required for exposure is plotted as a function of pulse energy density. As a pulse energy is increased, a drastic reduction in the required dose is observed. The reciprocity failure was attributed to a locally induced temperature rise. Further investigations are needed to clarify the reciprocity behavior of resist systems under excimer laser radiation. Multiphoton mechanistic studies are clearly warranted.

3.4.5.2 RESIST ABSORPTION CHARACTERISTICS

The absorption characteristics of resist films at the exposure wavelength of an excimer laser are important. For example, an application of conventional positive resists to 248-nm KrF excimer laser lithography is limited by ex-

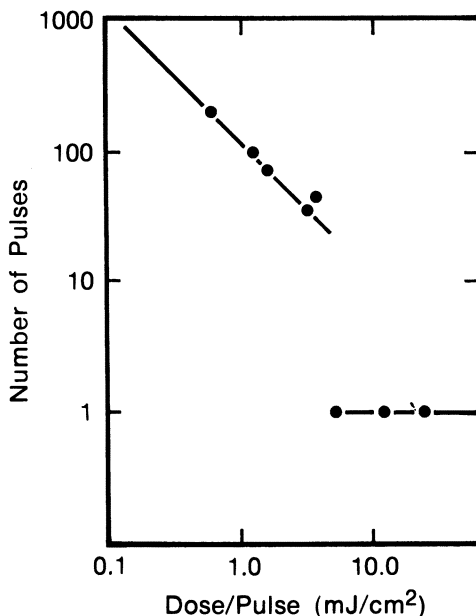


Figure 3.71. The number of 10-nm pulses required for full thickness remaining versus the dose per pulse. The discontinuity in this graph occurs at a power density and will result in an estimated maximum temperature of 140 °C. (Reproduced with permission from reference 210. Copyright 1984 Institute of Electrical and Electronics Engineers.)

posure absorption as discussed in Section 3.2.2.1. The combined absorption of the photosensitizer and the resin results in a resist film that is opaque at 248 nm (see Figures 3.10 and 3.11); hence, little or no light reaches the photosensitizer at the resist–substrate interface. Although excimer laser printing of lines down to 0.7 μm in AZ2400 has been demonstrated with KrF excimer laser projection printing, resist profiles suffered because of the high absorption (212). As mentioned in Section 3.5.2, even PMMA is sufficiently absorbing at 157 nm (F_2 excimer laser) so that severe profile degradation results (208).

Lin (83) studied the MRS resist (RD2000N) to determine the effect of optical density on performance. Resist images were delineated by 222-nm KrCl and 308-nm XeCl excimer laser radiation as shown in Figure 3.72. At 308 nm, nearly vertical resist profiles were produced. This result provides

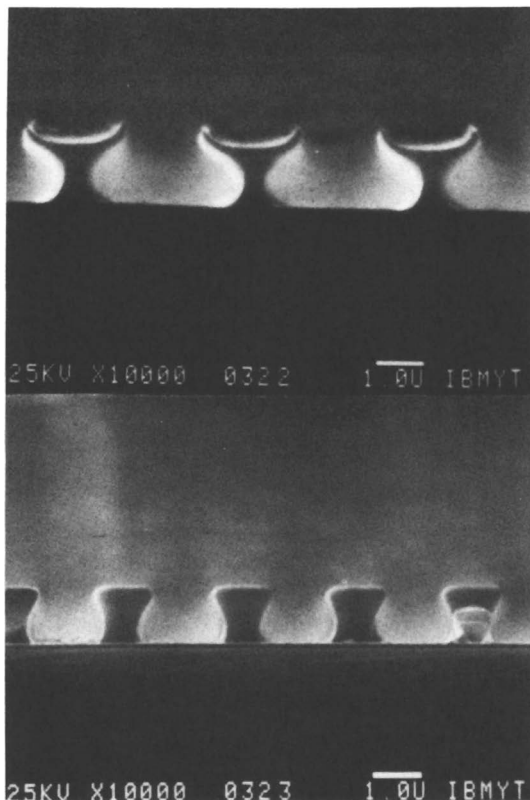


Figure 3.72. Negative image in RD2000N resist exposed with a KrCl excimer laser at 222 nm (top) and negative image in RD2000N resist exposed with a XeCl laser producing 308-nm light (bottom). (Reproduced from reference 83. Copyright 1983 American Chemical Society.)

evidence of good light penetration into the bulk of this resist. On the other hand, the images delineated at 222 nm show profiles that are extremely wide at the top and quickly become narrow with depth because of insufficient exposure in the lower layer of the resist film.

Although high photosensitivity may not be a major factor in the design of resists for excimer laser lithography, matching of the spectral characteristics of the resist and the exposure source continues to be an important challenge.

3.5 Future Projections

The future of DUV lithography is difficult to judge. We believe that DUV lithography will find a place in the manufacturing of semiconductor devices in the 0.5–1.0- μm regime and may become the dominant lithography technology of the early 1990s. The introduction of this technology seems not to be gated by material (resist) issues although much needs to be done in this area, but rather by the development of exposure systems. Until commercial DUV exposure systems are available, assessing the existing materials base is not possible in terms of critical dimension control or process bias, for example. The extent to which more complex and therefore costly multilayer processes need to be developed fully will depend on the output characteristics of the exposure tool.

The $1\times$, fully reflecting systems demand $1\times$ masks. Hence, even if the NA of such systems can be increased sufficiently to provide submicrometer printing capability in the DUV, the fabrication of full-field $1\times$ masks with accurate, defect-free submicrometer dimensions would require enormous improvements over the state of the mask-making art. Therefore, a reduction lens system of some sort will likely become the dominant approach.

Because chromatic aberration correction is so difficult to achieve in refracting lenses for DUV, such systems will undoubtedly be designed around excimer laser sources, which have the potential for providing narrow bandwidth, high-intensity radiation in the desired wavelength region. The first lenses will likely be all fused silica elements and will require spectral narrowing of the laser output. Eventually, use of fluoride optical elements may allow lens designers to work with the excimer laser output directly. Several companies are reported to be far along in the design of fused silica lenses for spectrally narrowed 248-nm excimer laser radiation, and at least one such lens has been delivered and is under evaluation. The pulsed nature of excimer lasers represents a complication for current exposure tool designs. However, with sufficient flux at the wafer plane, a "flash on the fly" system would take advantage of the narrow pulse width of the laser. Such systems could provide extremely high throughput but will appear late if at all, because they require, among other things, far more reproducible pulse-to-pulse performance from the laser than has been demonstrated.

Although an improvement in resolution resulting from the use of shorter wavelengths and higher throughput can be achieved using laser sources, use of lasers does not obviate the problems associated with the continued trend toward higher resolution and larger chip sizes. For step-and-repeat systems, there is a trade-off between resolution and field size. The last 10 years have shown a steady increase in the size and complexity of stepper lenses to overcome this difficulty. This trend will continue (19). The number of resolution elements in the field of stepper lens seems to be limited to a few times 10^8 (19, 224, 225). Today's requirements of 1.25- μm geometries and 10×10 mm chip sizes are easily met by many available lenses. However, requirements of 0.5- μm minimum geometries and 16-mm square chips, for example, amount to about 10×10^8 elements, a value which exceeds the capability of any of the current lenses.

One solution to this problem is to employ a subfield scanning (step-and-scan) system (19, 225). In such a system, the wafer area is subdivided into a number of subfields that are exposed sequentially by synchronously scanning mask and wafer through the curved zone of aberration-free imaging (Figure 3.73). A wide variety of ring-field projection systems have been proposed, including a 1:1 broadband imaging system (Figure 3.74), a 5:1 system, and a 4:1 system.

The number of resolution elements per unit area is expanded enormously by the scanning system. Such systems will easily provide the number of resolution elements required for 0.5- μm ground rules. If such systems can be developed by using DUV excimer laser sources with a moderate NA,

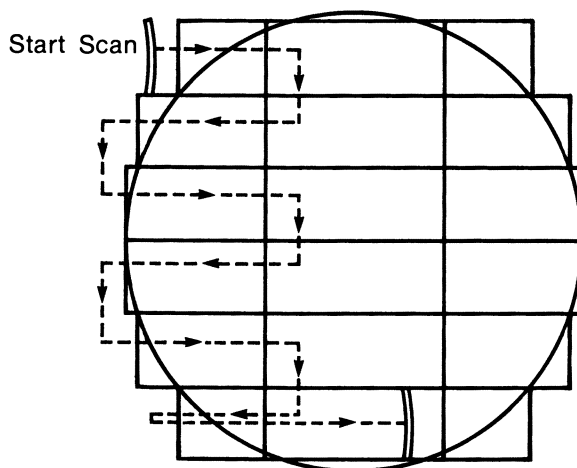


Figure 3.73. Step-and-scan principle. The wafer is exposed by synchronously scanning the mask and each wafer subfield through the illuminated zone of a ring-field imaging system. (Reproduced with permission from reference 19. Copyright 1984 Technical Publishing.)

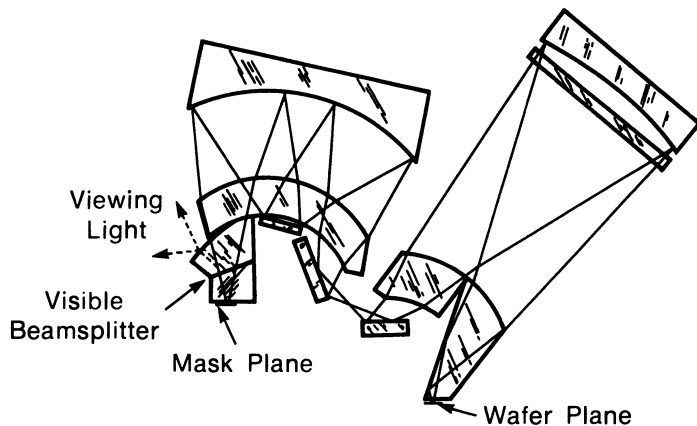


Figure 3.74. Shafer micralign-Dyson hybrid system. This 1:1, 0.33-NA ring-field imaging system has a 2-mm slit width and a spectral range that proceeds from 260 nm through the visible region. (Reproduced with permission from reference 19. Copyright 1984 Technical Publishing.)

they will certainly extend optical lithography to 0.5 μm , limited mainly by the shallow depth of focus.

Reduction in wavelength to the 193-nm excimer laser or less is possible. There have also been discussions about the use of immersion lenses. A shift to the VUV, below 200 nm, though attractive in principle, carries with it a number of new and challenging materials demands. Quartz may be useful for mask substrate and thin optical elements at 193 nm, but below this wavelength, new materials would be required. The exposure systems would have to operate in vacuo or under an inert gas fill because air absorbs at VUV wavelengths. Organic materials are generally very strongly absorbing in this spectral region because there is sufficient energy to excite $\sigma\text{-}\sigma^*$ transitions. Consequently, new resist chemistry would have to be developed to support VUV lithography. Despite these seemingly insurmountable obstacles, we expect to see serious research efforts directed toward solving the major problems of VUV lithography, and we expect the industry to abandon optical lithography only with the greatest reluctance.

Abbreviations and Symbols

ARC	antireflective coating
B	unbleachable absorbance of a resist
CMS	chloromethylated polystyrene
CPMS	chlorinated polymethylstyrene
DUV	deep-UV
ESCA	electron spectroscopy for chemical analysis
ESR	electron spin resonance

FBM	poly(fluorobutyl methacrylate)
HMDS	hexamethyldisilazane
IPPhK	isopropenyl phenyl ketone
LMR	low molecular weight resist
MAA	methacrylic acid
MAN	methacrylonitrile
MIBK	methyl isobutyl ketone
MMA	methyl methacrylate
MRS	micro resist for shorter wavelengths
NA	numerical aperture
NMOS	n-channel metal oxide semiconductor
OM	3-oximino-2-butanone methacrylate
PBS	poly(butene-1 sulfone)
PCM	portable conformable mask
PDP	plasma-developable photoresist
PGMA	poly(glycidyl methacrylate)
PIPTBK	poly(isopropenyl <i>tert</i> -butyl ketone)
PMIPK	poly(methyl isopropenyl ketone)
PMMA	poly(methyl methacrylate)
PSTTF	polystyrene-tetrathiofulvalene
RIE	reactive ion etching
SAMPLE	simulation and profiles in lithography and etching
SEM	scanning electron micrograph
UV-2	same as DUV
UV-3	same as mid-UV
UV-4	same as near-UV
VLSI	very large scale integration
VUV	vacuum ultraviolet

Acknowledgments

We thank Chizuko Iwayanagi for her skillful word processing and the Research Publications and Graphics Departments at IBM Almaden Research Center for their assistance with the manuscript preparation. Special thanks go to Bette Murray, who handled most of the administrative aspects in preparing this manuscript.

References

1. (a) DeForest, W. *Photoresist Materials and Processes*; McGraw Hill: New York, 1975; (b) *Introduction to Microlithography*; Thompson, L. F.; Willson, C. G.; Bowden, M. J., Eds.; ACS Symposium Series 219; American Chemical Society: Washington, DC, 1983; (c) Steppan, H.; Buhrand, G.; Vollman, H. *Angew.*

- Chem. Int. Ed. Engl.* **1982**, *21*(7), 455; (d) Deckert, C. A.; Ross, D. L. *J. Electrochem. Soc.* **1980**, *127*, 450.
2. (a) Broers, A. N. *Solid State Technol.* **1985**, *28*(E), 119; (b) Luman, J. *Electronics* **1977**, *52*(4), 105.
 3. (a) Chang, T. H. P.; Hatzakis, M.; Wilson, A. D.; Broers, A. N. *Electronics* **1977**, *50*(10), 89; (b) Bowden, M. J. *CRC Crit. Rev. Solid State Sci.* **1979**, *8*, 223; (c) Broers, A. N.; Chang, T. H. P. In *Microcircuit Engineering*; Cambridge University: Cambridge, England and New York, NY, 1980; p 1.
 4. Systems have been described that expose several pixels (4a,b) and many pixels (4c) at a time. However, even these systems are much less efficient than optical exposure systems in terms of wafer area exposed per unit time. (a) Pfeiffer, H. C. *IEEE Trans. Electron Devices* **1979**, *ED-26*(4), 663; (b) Moore, R. D.; Caccoma, G.; Pfeiffer, H. C.; Webber, E.; Woodart, O. *Electronics* **1981**, *54*(22), 138; (c) Bohlen, H.; Behringer, U.; Keyser, J.; Nehmiz, P.; Zapka, W.; Kucke, W. *Solid State Technol.* **1984**, *27*(9), 210.
 5. (a) Broers, A. N. *Microelectron. Eng.* **1984**, *2*, 1; (b) Emoto, F.; Gamo, K.; Namba, S.; Samoto, N.; Shimizu, R. *Jpn. J. Appl. Phys.* **1985**, *24*, L809.
 6. (a) Neureuther, A. R. In *Synchrotron Radiation Research*; Winick, H.; Doniach, S., Eds.; Plenum: New York, NY, 1980; (b) Heuberger, A. *Solid State Technol.* **1986**, *29*(2), 93.
 7. Moreau, W. M.; Schmidt, R. R. *138th Electrochemical Society Meeting Extended Abstract*; 1970; p 459.
 8. Lin, B. J. *J. Vac. Sci. Technol.* **1975**, *12*, 1317.
 9. Feldman, M.; White, D. L.; Chandross, E. A.; Bowden, M. J.; Appelbaum, J. *Proceedings, Kodak Microelectronics Seminar*; Eastman Kodak: Rochester, NY, 1975; p 40.
 10. (a) Pol, V.; Bennewitz, J. H.; Escher, G. C.; Feldman, M.; Firtion, V. A.; Jewell, T. E.; Wilcomb, B. E.; Clemens, J. T. *SPIE* **1986**, *633*, 6; (b) Pol, V. *Solid State Technol.* **1987**, *30*(1), 71.
 11. Lin, B. J. In *Fine Line Lithography*; Newman, R., Ed.; North-Holland: New York, NY, 1980.
 12. (a) Petelin, A. N.; Ury, M. G. In *VLSI Electronics: Microstructure Science*; Einspruch, N. G.; Brown, D. M., Eds.; Academic: 1984; Vol. 8, Chapter 7; (b) Phillips, R. *Sources and Application of Ultraviolet Radiation*; Academic: London, 1983.
 13. Jain, K.; Willson, C. G. U.S. Patent 4 458 994, 1984, assigned to IBM Corporation.
 14. (a) Jain, K. *Laser Appl.* **1983**, *9*, 49; (b) *Proc. Int. Nat. Conf. Microcircuit Eng.*; Cambridge, United Kingdom, 1983; p 181.
 15. (a) Jain, K.; Willson, C. G.; Lin, B. J. *IBM J. Res. Dev.* **1982**, *26*, 151; (b) Jain, K.; Willson, C. G.; Lin, B. J. *IEEE Electron Device Lett.* **1983**, *EDL-3*, 53.
 16. Karl Süß, KG-GmbH and Company, Munich, West Germany, offers their Süß MJB-3 Series aligner with an excimer laser as an optical source.
 17. (a) Kano, I.; Momose, K. *Proc. 16th Symp. Semiconductor and Integrated Circuits Technology*; Tokyo, 1979 (in Japanese); (b) Iwamatsu, S.; Asanami, K. *Solid State Technol.* **1980**, *23*(5), 81; (c) Komine, T.; Nakamura, Y. *Denshi Zairyo* **1979**, *18*(10), 40.
 18. Moller, P. *Technical Papers of the Society of Plastic Engineers Regional Technical Conference on Photopolymers*; Mid-Hudson Section, Society of Plastic Engineers: Ellenville, NY, 1973; p 56.
 19. Markle, D. A. *Solid State Technol.* **1984**, *27*(9), 159.
 20. Pacansky, J.; Lyerla, J. R. *IBM J. Res. Dev.* **1979**, *23*, 42.

21. Bruning, J. H.; Shankoff, T. A. *Proc. Microcircuit Eng.* 1979, 300.
22. Bruning, J. H. *J. Vac. Sci. Technol.* 1979, 16, 1925
23. Shankoff, T. A.; Bruning, J. H.; Johnston, R. L. *Polym. Eng. Sci.* 1980, 20, 1102.
24. Willson, C. G. *Introduction to Microlithography*; Thompson, L. F.; Willson, C. G.; Bowden, M. J., Eds.; ACS Symposium Series 219; American Chemical Society: Washington, DC, 1983; p 87.
25. McCullough, A. W. *J. Electrochem. Soc.* 1981, 128, 225.
26. Hofer, D. C.; Willson, C. G.; Neureuther, A. R.; Hakey, M. *SPIE* 1982, 334, 196.
27. Hakey, M.; Straub, W. J. *Electron. Mater.* 1982, 11, 813.
28. Voshchekov, A. M.; Hanson, R. C. *IEEE Electron Device Lett.* 1982, EDL-3, 208.
29. Babie, W. T.; Chow, M.-F.; Moreau, W. M. *Polymers in Electronics*; Davidson, T., Ed.; ACS Symposium Series 242; American Chemical Society: Washington, DC, 1984; p 41.
30. Willson, C. G.; Miller, R.; McKean, D.; Clecak, N.; Thompkins, T.; Hofer, D.; Michl, J.; Downing, J. *Polym. Eng. Sci.* 1983, 23, 1004.
31. Miller, R. D.; McKean, D. R.; Thompkins, T. L.; Clecak, N.; Willson, C. G.; Michl, J.; Downing, J. In *Polymers in Electronics*; Davidson, T., Ed.; ACS Symposium Series 242; American Chemical Society: Washington, DC, 1984; p 25.
32. *Sci. News* 1985, June 1, 341.
33. Lin, B. J. *Proceedings, 8th International Conference on Electron and Ion Beam Science and Technology*; 1978; p 320.
34. Gipstein, E.; Ouano, A. C.; Tompkins, T. J. *Electrochem. Soc.* 1982, 129, 201.
35. Oldham, W. G.; Nondgaonkar, S. N.; Neureuther, A. R.; O'Toole, M. *IEEE Trans. Electron Devices* 1979, ED-26, 717.
36. Dill, F. H.; Hornberger, W. P.; Hauge, P. S.; Shaw, J. M. *IEEE Trans. Electron Devices* 1975, ED-22, 445.
37. Grant, B. D.; Clecak, N. J.; Twieg, R. J.; Willson, C. G. *IEEE Trans. Electron Devices* 1981, ED-28, 1300.
38. Reichmanis, E.; Wilkins, C. W., Jr.; Chandross, E. A. *J. Vac. Sci. Technol.* 1980, 19, 1338.
39. Wilkins, C. W., Jr.; Reichmanis, E.; Chandross, E. A. *J. Electrochem. Soc.* 1982, 129, 2552.
40. Reichmanis, E.; Wilkins, C. W., Jr.; Price, D. A.; Chandross, E. A. *J. Electrochem. Soc.* 1983, 130, 1433.
41. Chandross, E. A.; Reichmanis, E.; Wilkins, C. W., Jr.; Hartless, R. L. *Can. J. Chem.* 1983, 61, 817.
42. Morrison, H. A. *The Chemistry of the Nitro and Nitroso Groups*; Feuer, H., Ed.; Wiley: New York, 1970; Part I, p 185.
43. Pederson, L. A. *J. Electrochem. Soc.* 1982, 129, 205.
44. Gokan, H.; Esho, S.; Ohnishi, Y. *J. Electrochem. Soc.* 1983, 130, 143.
45. Shultz, A. R. *J. Polym. Sci.* 1959, 35, 369.
46. Campbell, D. J. *Polym. Sci.* 1970, 4, 97.
47. Tsuji, K. *Adv. Polym. Sci.* 1973, 12, 131.
48. Hiraoka, H. *J. Am. Chem. Soc.* 1973, 95, 1664.
49. Hiraoka, H. *Macromolecules* 1976, 9, 359.
50. Hiraoka, H. *IBM J. Res. Dev.* 1977, 21, 121.
51. Ouano, A. C. *Polym. Eng. Sci.* 1978, 18, 306.
52. Ouano, A. C. In *Polymers in Electronics*; Davidson, T., Ed.; ACS Symposium Series 242; American Chemical Society: Washington, DC, 1984; p 79.

53. van Pelt, P. *SPIE* 1981, 275, 150.
54. Mimura, H.; Ohkubo, T.; Takeuchi, T.; Sekikawa, K. *Jpn. J. Appl. Phys.* 1978, 17, 541.
55. Hirai, T.; Hatano, Y.; Nonogaki, S. *J. Electrochem. Soc.* 1971, 118, 669.
56. Yamashita, Y.; Ogura, K.; Konishi, M.; Kawazu, R.; Ohno, S.; Mizokami, Y. *J. Vac. Sci. Technol.* 1979, 16, 2026.
57. Kakuchi, M.; Sugawara, S.; Murase, K.; Matsuzama, K. *J. Electrochem. Soc.* 1977, 124, 1648.
58. Wilkins, C. W., Jr.; Reichmanis, E.; Chandross, E. A. *J. Electrochem. Soc.* 1980, 127, 2510.
59. Reichmanis, E.; Wilkins, C. W., Jr.; Chandross, E. A. *J. Electrochem. Soc.* 1980, 127, 2514.
60. Reichmanis, E.; Wilkins, C. W., Jr. In *Polymer Materials for Electronic Applications*; Feit, E. D.; Wilkins, C. W., Jr., Eds.; ACS Symposium Series 184; American Chemical Society: Washington, DC, 1982; p 29.
61. Chandross, E. A.; Reichmanis, E.; Wilkins, C. W., Jr.; Hartless, R. C. *Solid State Technol.* 1981, 24(8), 81.
62. Hartless, R. L.; Chandross, E. A. *J. Vac. Sci. Technol.* 1981, 19, 1333.
63. Hiraoka, H. *Macromolecules* 1977, 10, 719.
64. de Grandpre, M. P.; Vidusek, D. A.; Legenza, M. W. *SPIE* 1985, 539, 103.
65. Legenza, M. W.; Vidusek, D. A.; de Grandpre, M. *SPIE* 1985, 539, 250.
66. Tsuda, M.; Oikawa, S.; Nakamura, Y.; Nagata, H.; Yokota, A.; Nakane, H.; Tsumori, T.; Nakane, Y.; Mifune, T. *Photogr. Sci. Eng.* 1979, 23, 290.
67. Nakane, H.; Yokota, A.; Nakamura, Y.; Nagata, H.; Tsuda, M. *Preprints of 2nd Technical Conference on Photopolymers*; Tokyo, 1979; p 71.
68. MacDonald, S. A.; Ito, H.; Willson, C. G.; Moore, J. W.; Gharapetian, H. M.; Guillet, J. E. In *Materials for Microlithography*; Thompson, L. F.; Willson, C. G.; Fréchet, J. M. J., Eds.; ACS Symposium Series 266; American Chemical Society: Washington, DC, 1984; p 179.
69. Ito, H.; MacDonald, S. A.; Willson, C. G.; Gharapetian, H. M.; Moore, J. W.; Guillet, J. E. *Preprints of 1st SPSJ International Polymer Conference*; The Society of Polymer Science: Kyoto, Japan, 1984; p 106.
70. Dan, E.; Somerstall, A. C.; Guillet, J. E. *Macromolecules* 1973, 6, 228.
71. Nate, K.; Kobayashi, T. *J. Electrochem. Soc.* 1981, 128, 1394.
72. Bowden, M. J.; Chandross, E. A. *J. Electrochem. Soc.* 1975, 122, 1370.
73. Himics, R. J.; Ross, D. L. *Polym. Eng. Sci.* 1977, 17, 350.
74. Hall, H. K., Jr.; Daly, R. C. *Macromolecules* 1975, 8, 22.
75. Ito, H.; Hrusa, C.; Hall, H. K., Jr.; Padias, A. B. *J. Polym. Sci. Part A: Polym. Chem.* 1986, 24, 955.
76. Iwayanagi, T.; Kohashi, T.; Nonogaki, S. *J. Electrochem. Soc.* 1980, 127, 2759.
77. Iwayanagi, T.; Kohashi, T.; Nonogaki, S.; Matsuzawa, T.; Douta, K.; Yanazawa, H. *IEEE Trans. Electron Devices* 1981, ED-28, 1306.
78. Matsuzawa, T.; Tomioka, H. *IEEE Trans. Electron Devices* 1981, EDL-2, 90.
79. Matsuzawa, T.; Tomioka, H. *IEEE Trans. Electron Devices* 1981, ED-28, 1284.
80. McCullough, A. W.; Sewell, H. *SPIE* 1983, 394, 107.
81. Matsuzawa, T.; Kishimoto, A.; Tomioka, H. *IEEE Trans. Electron Device Lett.* 1982, EDL-3, 58.
82. Yang, J.-M.; Chiong, K.; Yan, H.-G.; Chow, M.-F. *SPIE* 1984, 469, 117.
83. Lin, B. J. In *Introduction to Microlithography*; Thompson, L. F.; Willson, C. G.; Bowden, M. J., Eds.; ACS Symposium Series 219; American Chemical Society: Washington, DC, 1983; Chapter 6.
84. Matsuzawa, T.; Iwayanagi, T.; Ohbayashi, H.; Tomioka, H. *Microelectron. Eng.* 1983, 1, 185.

85. Lin, B. J.; Bassous, E.; Chao, V. W.; Petrillo, K. E. *J. Vac. Sci. Technol.* **1981**, *19*, 1313.
86. Lin, B. J. *Solid State Technol.* **1983**, *26*(5), 105.
87. Tomioka, H. *SPIE* **1985**, 593, 151.
88. Iwayanagi, T.; Hashimoto, M.; Nonogaki, S.; Koibuchi, S.; Makino, D. *Polym. Eng. Sci.* **1983**, *23*, 935.
89. Nonogaki, S.; Hashimoto, M.; Iwayanagi, T.; Shiraishi, H. *SPIE* **1985**, 539, 189.
90. Koibuchi, S.; Isobe, A.; Makino, D.; Iwayanagi, T.; Hashimoto, M.; Nonogaki, S. *SPIE* **1985**, 539, 182.
91. Toukhy, M. A.; Leonard, R. F. *SPIE* **1983**, 394, 162.
92. Bowden, M. J. In *Materials for Microlithography*; Thompson, L. F.; Willson, C. G.; Fréchet, J. M. J., Eds.; ACS Symposium Series 266; American Chemical Society: Washington, DC, 1984; p 39.
93. Imamura, S.; Sugawara, S. *Jpn. J. Appl. Phys.* **1982**, *21*, 776.
94. Imamura, S. *J. Electrochem. Soc.* **1979**, *126*, 1628.
95. Liutkus, J.; Hatzakis, M.; Shaw, J.; Paraszczak, J. *Polym. Eng. Sci.* **1983**, *23*, 1047.
96. Novembre, A. E.; Masakowski, L. M.; Hartney, M. A. *Polym. Eng. Sci.* **1986**, *26*, 1158.
97. Harita, Y.; Kamoshida, Y.; Tsutsumi, K.; Koshiha, M.; Yoshimoto, H.; Harada, K. *SPSE 22nd Symposium on Unconventional Imaging Science and Technology*; **1982**; p 34.
98. Tabata, Y.; Tagawa, S.; Washio, M. In *Materials for Microlithography*; Thompson, L. F.; Willson, C. G.; Fréchet, J. M. J., Eds.; ACS Symposium Series 266; American Chemical Society: Washington, DC, 1984; p 151.
99. Tanigaki, K.; Takeishi, K.; Ohnishi, Y. *Polym. Eng. Sci.* **1986**, *26*, 1116.
100. MacDonald, S. A.; Allen, R. D.; Clecak, N. J.; Willson, C. G.; Fréchet, J. M. J. *SPIE* **1986**, 631, 28.
101. Hofer, D. C.; Kaufman, F. B.; Kramer, S. R.; Aviram, A. *Appl. Phys. Lett.* **1980**, *37*, 314.
102. Kaufman, F. B.; Kramer, S. R. *Extended Abstracts of the Electrochemical Society Spring Meeting*; Electrochemical Society: Montreal, Canada, 1982; Abstract 270.
103. Tessier, T. G.; Fréchet, J. M. J.; Willson, C. G.; Ito, H. In *Materials for Microlithography*; Thompson, L. F.; Willson, C. G.; Fréchet, J. M. J., Eds.; ACS Symposium Series 266; American Chemical Society: Washington, DC, 1984; p 269.
104. Fréchet, J. M. J.; Tessier, T. G.; Willson, C. G.; Ito, H. *Macromolecules* **1985**, *18*, 317.
105. Willson, C. G.; Ito, H.; Fréchet, J. M. J.; Tessier, T. G.; Houlihan, F. M. J. *Electrochem. Soc.* **1986**, *133*, 181.
106. Ito, H.; Willson, C. G.; Fréchet, J. M. J. *Digest of Technical Papers of 1982 Symposium on VLSI Technology*; **1982**; p 86.
107. Ito, H.; Willson, C. G. *Polym. Eng. Sci.* **1983**, *23*, 1012.
108. Ito, H.; Willson, C. G. In *Polymers in Electronics*; Davidson, T., Ed.; ACS Symposium Series 242; American Chemical Society: Washington, DC, 1984; p 11.
109. Crivello, J. V. In *UV Curing: Science and Technology*; Pappas, S. P., Ed.; Technology Marketing Corporation: Stamford, CT, 1978; pp 23–77 and references therein.
110. Crivello, J. V.; Lam, J. H. W. *J. Polym. Sci. Polym. Chem. Ed.* **1978**, *16*, 2441.
111. Crivello, J. V.; Lam, J. H. W. *J. Polym. Sci. Polym. Chem. Ed.* **1979**, *17*, 1059.

112. Hiraoka, H.; Welsh, W. L., Jr.; Bargon, J. *J. Vac. Sci. Technol.* **1983**, *B1*, 1062.
113. Yamashita, Y.; Kawazu, R.; Kawamura, K.; Ohno, S.; Asano, T.; Kobayashi, K.; Magamatsu, G. *J. Vac. Sci. Technol.* **1985**, *B3*, 314.
114. Smith, J. N.; Hughs, H. G.; Keller, J. V.; Goodner, W. R.; Wood, T. E. *Semicond. Int.* **1979**, *2(10)*, 41.
115. Taylor, G. N.; Wolf, T. M. *J. Electrochem. Soc.* **1980**, *127*, 2665.
116. (a) Taylor, G. N. *Solid State Technol.* **1980**, *23(5)*, 73; (b) Taylor, G. N.; Wolf, T. M.; Goldrick, M. R. *J. Electrochem. Soc.* **1981**, *128*, 361.
117. Tsuda, M.; Oikawa, S.; Kanai, W.; Yokota, A.; Hijikata, I.; Uehara, A.; Nakane, H. *J. Vac. Sci. Technol.* **1981**, *19*, 259.
118. Tsuda, M.; Yokota, A.; Kashiwagi, K.; Yabuta, M.; Oikawa, S.; Kanai, W.; Nakane, H. *Jpn. J. Appl. Phys.* **1983**, *22*, 1215.
119. Tsuda, M.; Oikawa, S.; Yokota, A.; Yabuta, M.; Kanai, W.; Kashiwagi, K.; Hijikata, I.; Nakane, H. *Polym. Eng. Sci.* **1983**, *23*, 993.
120. Tsuda, M.; Oikawa, S.; Yabuta, M.; Yokota, A.; Nakane, H.; Atoda, N.; Hoh, K.; Gamo, K.; Namba, S. *Polym. Eng. Sci.* **1986**, *26*, 1148.
121. Meyer, W. H.; Curtis, B. J.; Brunner, H. R. *Microelectron. Eng.* **1983**, *1*, 29.
122. Venkatesan, T.; Taylor, G. N.; Wagner, A.; Wilkens, B.; Barr, D. *J. Vac. Sci. Technol.* **1981**, *19*, 1379.
123. Kuwano, H. *J. Appl. Phys.* **1984**, *55*, 1149.
124. Taylor, G. N.; Stillwagon, L. E.; Venkatesan, T. *J. Electrochem. Soc.* **1984**, *131*, 1658.
125. Wolf, T. M.; Taylor, G. N.; Venkatesan, T.; Kretsch, R. T. *J. Electrochem. Soc.* **1984**, *131*, 1664.
126. Stillwagon, L. E.; Silverman, P. J.; Taylor, G. N. *Technical Papers of SPE Regional Technical Conference on Photopolymers*; 1985; p 87.
127. MacDonald, S. A.; Ito, H.; Hiraoka, H.; Willson, C. G. *Technical Papers of SPE Regional Technical Conference on Photopolymers*; 1985; p 177.
128. Hattori, S.; Morita, S.; Yamada, M.; Tamano, J.; Ieda, M. *Polym. Sci. Eng.* **1983**, *23*, 1043.
129. Willson, C. G.; Hult, A.; MacDonald, S. A. *Proc. ACS Div. Polym. Mater. Sci. Eng.* **1985**, *52*, 339.
130. Hult, A.; MacDonald, S. A.; Willson, C. G. *Macromolecules* **1985**, *18*, 1804.
131. Bowden, M. J.; Thompson, L. F. *Polym. Eng. Sci.* **1974**, *14*, 525.
132. Geis, M. W.; Randall, J. N.; Deutsch, T. F.; Efremow, N. N.; Donnelly, J. P.; Woodhouse, J. D. *J. Vac. Sci. Technol.* **1983**, *B1*, 1178.
133. Hofer, D. C.; Jain, K.; Miller, R. D. *IBM Tech. Disc. Bull.* **1984**, *26*, 5683.
134. Ziegler, J. M.; HARRAH, L. A.; Johnson, A. W. *SPIE* **1985**, *539*, 166.
135. Ichimura, S.; Hirata, M.; Tanino, H.; Atoda, N.; Ono, M.; Hoh, K. *J. Vac. Sci. Technol.* **1983**, *B1*, 1076.
136. Lanagan, M.; Lindsey, S.; Viswanathan, N. S. *Jpn. J. Appl. Phys.* **1983**, *22*, L67.
137. Sugita, K.; Ueno, N.; Konishi, S.; Suzuki, Y. *Photogr. Sci. Eng.* **1983**, *27*, 246.
138. Hiraoka, H.; Welsh, L. W., Jr. In *Polymers in Electronics*; Davidson, T., Ed.; ACS Symposium Series 242; American Chemical Society: Washington, DC, 1984; p 55.
139. Fréchet, J. M. J.; Houlihan, F. M.; Bouchard, F.; Eichler, E.; Hult, A.; Allen, R.; MacDonald, S. A.; Ito, H.; Willson, C. G. *Technical Papers of SPE Regional Technical Conference on Photopolymers*; 1985; p 1.
140. Ong, E.; Tai, K. L.; Vadimsky, R. G.; Kemmerer, C. T. *SPIE* **1983**, *394*, 39.
141. Huggett, P. G.; Lehmann, H. W. *J. Electron. Mater.* **1985**, *14*, 205.
142. Nagai, H.; Yoshikawa, A.; Toyoshima, Y.; Ochi, O.; Mizushima, Y. *Appl. Phys. Lett.* **1976**, *28*, 145.

143. Yoshikawa, A.; Ochi, O.; Nagai, H.; Mizushima, Y. *Appl. Phys. Lett.* **1976**, *29*, 677.
144. Yoshikawa, A.; Ochi, O.; Nagai, H.; Mizushima, Y. *Appl. Phys. Lett.* **1977**, *31*, 161.
145. Chang, M. S.; Chen, J. T. *Appl. Phys. Lett.* **1978**, *33*, 892.
146. Chang, M. S.; Hou, T. W.; Kolwicz, K. D.; Zemel, J. N. *J. Vac. Sci. Technol.* **1979**, *16*, 1973.
147. Kolwicz, K. D.; Chang, M. J. *J. Electrochem. Soc.* **1980**, *127*, 135.
148. Tai, K. L.; Ong, E.; Vadimsky, R. G. *Proceedings, Symposium on Inorganic Resist Systems*; Doane, D. A.; Heller, A., Eds.; Electrochemical Society; 1982; p 9.
149. Tai, K. L.; Ong, E.; Vadimsky, R. G.; Kemmerer, C. T.; Bridenbaugh, P. M. *Proceedings, Symposium on Inorganic Resist Systems*; Doane, D. A.; Heller, A., Eds.; Electrochemical Society; 1982; p 49.
150. Vadimsky, R. G.; Tai, K. L.; Ong, E. *Proceedings, Symposium on Inorganic Resist Systems*; Doane, D. A.; Heller, A., Eds.; Electrochemical Society; 1982; p 37.
151. Ong, E.; Tai, K. L.; Vadimsky, R. G.; Kemmerer, C. T.; Bridenbaugh, P. M. *SPIE* **1985**, *539*, 52.
152. Ong, E.; Tai, K. L.; Vadimsky, R. G.; Kemmerer, C. T. *Proceedings, Symposium on Inorganic Resist Systems*; Doane, D. A.; Heller, A., Eds.; Electrochemical Society; 1982; p 71.
153. Tai, K. L.; Vadimsky, R. G.; Ong, E. *SPIE* **1982**, *333*, 32.
154. (a) Hatzakis, M. *Solid State Technol.* **1981**, *24*(8), 74; (b) Reichmanis, E.; Wilkins, C. W., Jr.; Ong, E. *Polym. Eng. Sci.* **1983**, *23*, 1039.
155. Ong, E.; Baker, R. M.; Hale, L. P. *J. Vac. Sci. Technol.* **1983**, *B1*, 1247.
156. Ong, E.; Hu, E. L. *Solid State Technol.* **1984**, *27*(6), 155.
157. Lin, B. J. *SPIE* **1979**, *174*, 114.
158. Lin, B. J. *J. Electrochem. Soc.* **1980**, *127*, 202.
159. Lin, B. J.; Chang, T. H. *J. Vac. Sci. Technol.* **1979**, *16*, 1669.
160. Griffing, B. F. *J. Vac. Sci. Technol.* **1981**, *19*, 1423.
161. Batchelder, T.; Takemoto, C. *Semicond. Int.* **1981**, *4*, 213.
162. Santini, H.; Viswanathan, N. S. *Proceedings, Kodak Microelectronics Seminar*; Eastman Kodak: Rochester, NY, 1982; p 47.
163. Bartlett, K.; Hillis, G.; Chen, M.; Trutna, R.; Watts, M. *SPIE* **1983**, *394*, 49.
164. Petrillo, K. E.; Chao, V. W.; Lin, B. J. *J. Vac. Sci. Technol.* **1983**, *B1*, 1219.
165. Meyerhofer, D.; White, L. K. *SPIE* **1984**, *469*, 11.
166. Hiraoka, H.; Pacansky, J. Presented at the 16th Symposium on Electron, Ion and Photon Beam Technology, Dallas, TX, 1981.
167. Ong, E.; Tai, K. L.; Reichmanis, E.; Wilkins, C. W., Jr. *Proceedings, Kodak Microelectronics Seminar*; Eastman Kodak: Rochester, NY, 1981; p 91.
168. Hiraoka, H.; Welsh, L. W., Jr. *Proceedings, 10th International Conference on Electron and Ion Beam Science and Technology*; 1982; p 171.
169. Hiraoka, H. In *Materials for Microlithography*; Thompson, L. F.; Willson, C. G.; Fréchet, J. M. J., Eds.; ACS Symposium Series 266; American Chemical Society: Washington, DC, 1984; p 339.
170. Wijdenes, J.; Geomini, M. J. H. *J. SPIE* **1985**, *539*, 97.
171. O'Toole, M. M.; Liu, E. D.; Chang, M. S. *IEEE Trans. Electron Devices* **1981**, *ED-28*, 1405.
172. Abraham, H.; Bartlett, K. G.; Hillis, G. L.; Stolz, M.; Wilson, M. S. *Hewlett-Packard J.* **1983**, *34*, 34.
173. Watts, M. P. C. *SPIE* **1984**, *469*, 2.

174. Lin, B. J.; Chao, V. W.; Kaufman, F. B.; Kramer, S. R. *Extended Abstracts of Electrochemical Society Spring Meeting*; Electrochemical Society: Montreal, Canada, 1982; Abstract 275.
175. McCullough, A. W.; Pavelchek, E.; Windischmann, H. J. *Vac. Sci. Technol.* **1983**, *B1*, 1241.
176. (a) Yamashita, Y.; Kawazu, R.; Ito, T.; Kawamura, K.; Ohno, S.; Asano, T.; Kobayashi, K.; Nagamatsu, G. *Proceedings, 27th Symposium on Semiconductors and Integrated Circuits Technology*; 1984; p 30; (b) *J. Vac. Sci. Technol.* **1985**, *B3*, 314.
177. Lin, B. J.; Chao, V. W.; Petrillo, K. E.; Yang, B. J. L. *Polym. Eng. Sci.*; **1986**, *26*, 1112.
178. Bassous, E.; Ephrath, L. M.; Pepper, G.; Mikalsen, D. J. *J. Electrochem. Soc.* **1983**, *130*, 478.
179. Lin, Y-C.; Johes, S.; Fuller, G. J. *Vac. Sci. Technol.* **1983**, *B1*, 1215.
180. Ting, C. H.; Liauw, K. L. *SPIE* **1984**, *469*, 24.
181. Brewer, T.; Carlson, R.; Arnold, J. *J. Appl. Photogr. Eng.* **1981**, *7*, 184.
182. Havas, J. *Electrochem. Soc. Extended Abstracts* **1976**, *762*, 743.
183. Moran, J. M.; Maydan, D. *J. Vac. Sci. Technol.* **1979**, *16*, 1620.
184. Moran, J. M. J.; Maydan, D. *Technical Papers of the Society of Plastic Engineers Regional Technical Conference on Photopolymers*; Society of Plastic Engineers: Ellenville, NY, 1979; p 248.
185. Shaw, J. M.; Hatzakis, M.; Paraszczak, J.; Liutkus, J. *Polym. Eng. Sci.* **1983**, *23*, 1054.
186. Morita, M.; Tanaka, A.; Imamura, S.; Tamamura, T.; Kogure, O. *Jpn. J. Appl. Phys.* **1983**, *22*, L659.
187. Tanaka, A.; Morita, M.; Imamura, S.; Tamamura, T.; Kogure, O. In *Materials for Microlithography*; Thompson, L. F.; Willson, C. G.; Fréchet, J. M. J., Eds.; ACS Symposium Series 266; American Chemical Society: Washington, DC, 1984; p 311.
188. MacDonald, S. A.; Steinmann, A. S.; Ito, H.; Lee, W.; Hiraoka, H.; Willson, C. G.; Hatzakis, M.; Shaw, J.; Paraszczak, J. *Abstracts of the 1983 International Symposium on Electron, Ion and Photon Beams*; Los Angeles, CA, 1983; p I-4.
189. MacDonald, S. A.; Ito, H.; Willson, C. G. *Microelectron. Eng.* **1983**, *1*, 269.
190. Suzuki, M.; Saigo, K.; Gokan, H.; Ohnishi, Y. *J. Electrochem. Soc.* **1983**, *130*, 1962.
191. Ohnishi, Y.; Suzuki, M.; Saigo, K.; Saotome, Y.; Gokan, H. *SPIE* **1985**, *539*, 60.
192. Hofer, D. C.; Miller, R. D.; Willson, C. G. *SPIE* **1984**, *469*, 16.
193. Miller, R. D.; Hofer, D.; McKean, D. R.; Willson, C. G.; West, R.; Trefonas, R. T., III. *Materials for Microlithography*; Thompson, L. F.; Willson, C. G.; Fréchet, J. M. J., Eds.; ACS Symposium series 266; American Chemical Society: Washington, DC, 1984; p 293.
194. Nate, K.; Sugiyama, H.; Inoue, T.; Ishikawa, M. *Extended Abstracts of the Electrochemical Society Fall Meeting*; 1984; Abstract 530.
195. Reichmanis, E.; Smolinsky, G. *SPIE* **1984**, *469*, 38.
196. Umezaki, H.; Koyama, N.; Maruyama, Y.; Sugita, Y.; Suzuki, R. *J. Electrochem. Soc.* **1985**, *132*, 2440.
197. Taylor, G. N.; Wolf, T. M. *Polym. Eng. Sci.* **1980**, *20*, 1087.
198. Taylor, G. N.; Wolf, T. M.; Moran, J. M. *J. Vac. Sci. Technol.* **1981**, *19*, 872.
199. Hiraoka, H.; Pacansky, J. *J. Vac. Sci. Technol.* **1981**, *19*, 1132.
200. Hiraoka, H.; Pacansky, J. *J. Electrochem. Soc.* **1981**, *128*, 2645.

201. Allen, R.; Foster, M.; Yen, Y.-T. *J. Electrochem. Soc.* **1982**, *129*, 1379.
202. Spiertz, E. J.; Vollenbroek, F. A.; Verhaar, R. D.; Dil, J. G. *Microcircuit Eng.* **1984**.
203. Yen, Y.-T.; Foster, M. *Proceedings, Kodak Microelectronics Seminar*; Eastman Kodak: Rochester, NY, 1982; p 125.
204. Ehrich, D. J.; Tsao, J. Y. *J. Vac. Sci. Technol.* **1983**, *B1*, 969.
205. Ehrich, D. J.; Osgood, R. M., Jr.; Deutsch, T. F. *IEEE J. Quantum Electron.* **1980**, *QE-16*, 1233.
206. Chuang, T. J. *Surf. Sci. Rep.* **1983**, *3*, 1.
207. Kawamura, Y.; Toyoda, T.; Namba, S. *J. Appl. Phys.* **1982**, *53*, 6489.
208. Craighead, H. G.; White, J. C.; Howard, R. E.; Jackel, L. D.; Behringer, R. E.; Sweeney, J. E.; Epworth, R. W. *J. Vac. Sci. Technol.* **1983**, *B1*, 1186.
209. Haller, I.; Feder, R.; Hatzakis, M.; Spiller, E. *J. Electrochem. Soc.* **1979**, *126*, 154.
210. Polasko, K. J.; Ehrich, D. J.; Tsao, J. Y.; Pease, R. F. W.; Varinero, E. E. *IEEE Trans. Electron Device Lett.* **1984**, *EDL-5*, 24.
211. Lacombat, M.; Dubroeuq, G. M.; Massin, J.; Brevignon, M. *Solid State Technol.* **1980**, *23(8)*, 115.
212. Dubroeuq, G. M.; Zahorsky, D. *Proceedings, International Conference on Microcircuit Engineering*; Grenoble, France, 1982; p 73.
213. Jain, K.; Kerth, R. T. *Appl. Opt.* **1984**, *23*, 648.
214. Kerth, R. T.; Jain, K.; Latta, M. R. *IEEE Electron Device Lett.* **1986**, *EDL-7*, 299.
215. Ehrlich, D. J.; Tsao, J. Y.; Bozler, C. O. *J. Vac. Sci. Technol.* **1985**, *B3*, 1.
216. Srinivasan, R.; Mayne-Banton, V. *Appl. Phys. Lett.* **1982**, *41*, 576.
217. Andrew, J. E.; Dyer, P. E.; Forster, D.; Key, P. H. *Appl. Phys. Lett.* **1983**, *43*, 717.
218. Rice, S.; Jain, K. *Appl. Phys.* **1984**, *A33*, 195.
219. Latta, M.; Moore, R.; Rice, S.; Jain, K. *J. Appl. Phys.* **1984**, *56*, 586.
220. Turro, N. J.; Aikawa, M.; Butcher, J. A., Jr.; Briffin, G. W. *J. Am. Chem. Soc.* **1980**, *102*, 5127.
221. Turro, N. J.; Aikawa, M.; Gould, I. R. *J. Am. Chem. Soc.* **1982**, *104*, 856.
222. Jain, K.; Rice, S.; Lin, B. J. *Polym. Eng. Sci.* **1983**, *23*, 1019.
223. Rice, S.; Jain, K. *IEEE Trans. Electron Devices* **1984**, *ED-31*, 1.
224. Ittner, G. *SPIE* **1977**, *100*, 115.
225. Bruning, J. L. *J. Vac. Sci. Technol.* **1980**, *17*, 1147.

RECEIVED for review March 31, 1987. ACCEPTED April 15, 1988.

Molecular Electronics Using Langmuir–Blodgett Films

G. G. Roberts

Department of Engineering Science, University of Oxford, Oxford OX1 3PJ
England

Langmuir–Blodgett (LB) films are monomolecular assemblies deposited one molecular layer at a time onto the surface of a suitable solid substrate. The combination of a carefully engineered molecule and a good Langmuir trough can result in high quality films displaying a high degree of structural order. Following a brief introduction to the preparation of LB films, this review describes their importance as model systems in basic research. However, the main emphasis is placed on their potential applications in the field of electronics, particularly those relying on the highly nonlinear properties of supermolecular assemblies.

THE RELATIVELY INEXPENSIVE EQUIPMENT REQUIREMENTS associated with the Langmuir-trough technique coupled with the elegance of the fundamental science involved with Langmuir–Blodgett (LB) films and their interesting applied prospects have generated considerable activity in the electronics field. The noticeable increase in the numbers of participants at relevant conferences and papers published in the learned journals testifies to the importance of the topic, whose pioneers worked in the General Electric Research Laboratories between the two world wars.

The first detailed description of sequential organic monolayer transfer was given by Langmuir and Blodgett (1, 2) in the mid-1930s and led to several simple applications of LB films including step-thickness gauges, antireflection coatings, and soft X-ray gratings. The majority of the early papers concentrated on a well-defined series of fatty acids and their salts. The subject received an impetus in the early 1960s by the work of Kuhn et al. (3), who showed how monomolecular assemblies could be used as matrices to support

0065-2393/88/0218-0225\$12.25/0
© 1988 American Chemical Society

various dye molecules and as spacers to separate donor and acceptor species. Their elegant, artificial systems were designed ingeniously to differentiate between the different interactions that could occur via photon, electron, and proton transfer. The present phase of intense activity started about 15 years ago with the synthesis of a wider range of more stable materials and a genuine appreciation of the applied prospects for LB films (4). Many of the basic principles underlying the technique can be found in the text by Gaines (5). The first two international conferences on the subject (6, 7) provide a detailed account of recent developments.

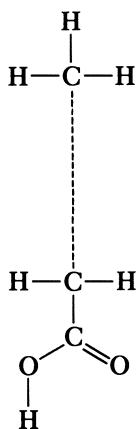
This chapter provides a brief introduction to the preparation of multilayer films; however, the main focus is on their potential applications in the field of electronics, especially in those areas that capitalize on the nonlinear properties of LB layers.

4.1 Preparation of Langmuir–Blodgett Films

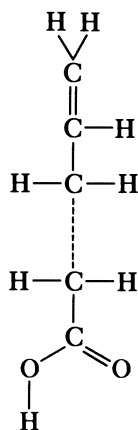
Chart 4.1 shows stearic acid, a molecule in which 16 CH_2 groups form a long hydrophobic chain. The other end of the molecule terminates in a hydrophilic carboxylic acid group. When dissolved in a suitable solvent and spread on the surface of water, molecules may be compressed with the aid of a barrier. Figure 4.1 shows a plot of the surface pressure (differential surface tension) versus area occupied per molecule for stearic acid. The monolayer undergoes a number of phase transformations during compression; the well-defined sequence can be viewed as the two-dimensional analogue of the classical transitions observed with pressure–volume isotherms.

An LB film is formed by transferring a floating monolayer onto a solid substrate; the surface pressure at which “dipping” occurs is established by the type of isotherm shown in Figure 4.1. The subphase is normally ultrapure water because it is readily available and has an exceptionally high value of surface tension. The composition of the subphase including its purity, pH, and ionic strength can have a profound influence on factors such as the solubility of the monolayer and segregation effects resulting in molecular aggregates or domains.

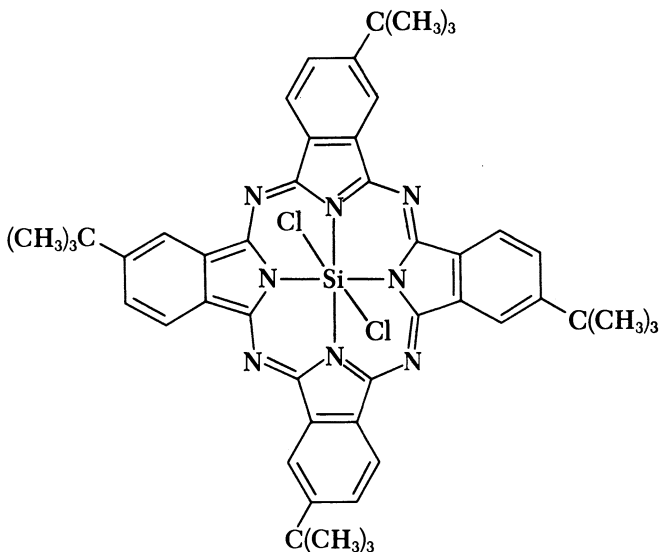
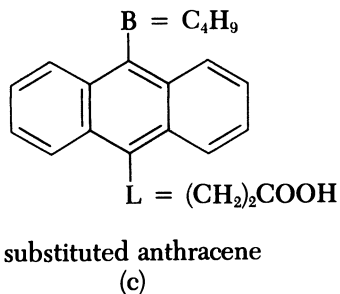
By using conventional LB film technology, the substrate is raised and lowered vertically through a compact floating monolayer; the surface pressure at which this occurs is normally just above the “knee” in the liquid-to-solid transition section of the isotherm, indicating low compressibility in the monolayer. At this stage, if conditions are carefully controlled and appropriate molecules are used, one monolayer is transferred during each excursion through the subphase surface. The most common deposition mode (Y-type) is illustrated in Figure 4.2, where the molecules can be seen to stack in a head-to-head and tail-to-tail configuration. The floating molecules on a liquid surface are shown in Figure 4.2a. With a hydrophilic substrate, no pickup occurs during the first immersion, and the first monolayer is therefore



stearic acid
(a)



ω -tricosenoic acid
(b)



substituted phthalocyanine
(d)

Chart 4.1. A selection of molecules used to form LB films: (a) a fatty acid (stearic acid), (b) ω -tricosenoic acid (ω -TA), (c) a substituted anthracene (9-butyl-10-anthrylpropionic acid), and (d) a substituted phthalocyanine (tetra-4-tert-butylphthalocyaninatosilicon dichloride).

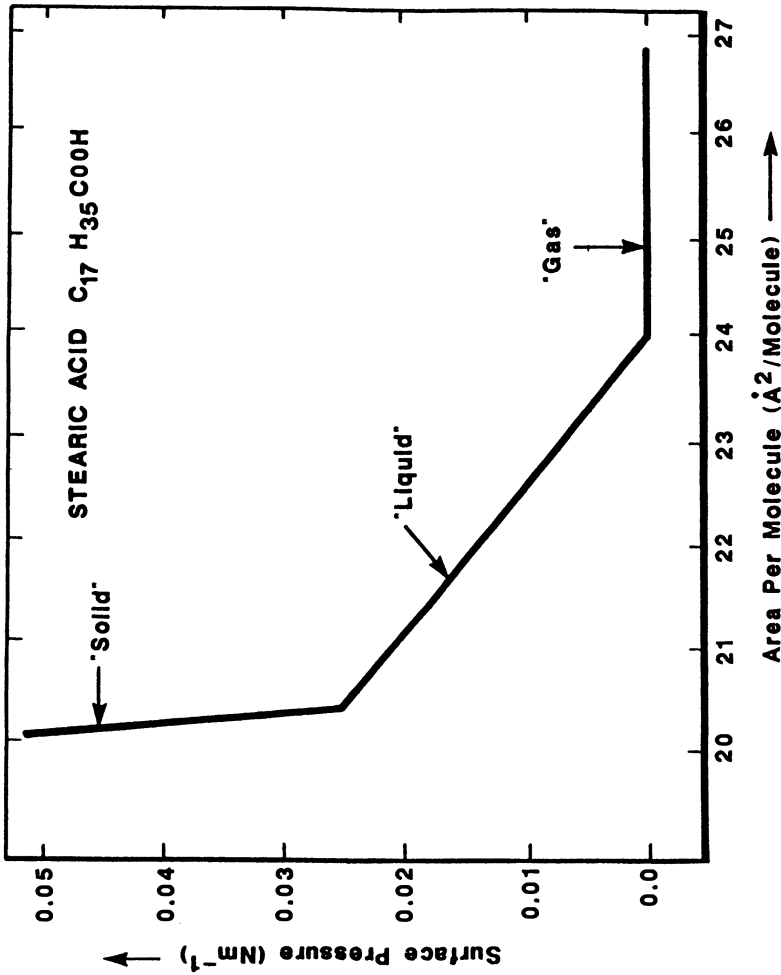


Figure 4.1. Surface pressure versus area for stearic acid.

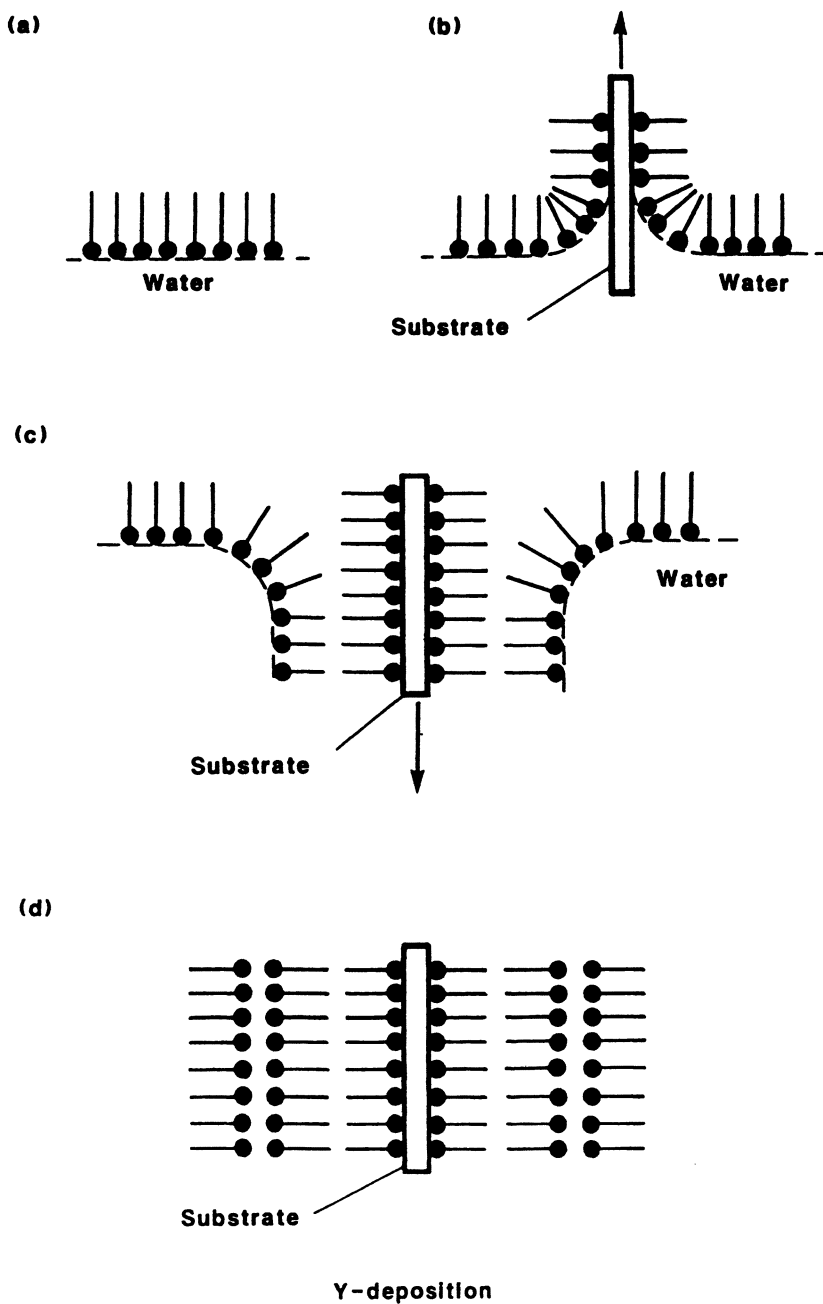


Figure 4.2. Langmuir-Blodgett film deposition (Y-type) on a hydrophilic substrate: (a) monolayer on the surface of water, (b) first layer on withdrawal, (c) second layer (second insertion), and (d) substrate with three layers (after second removal).

deposited during the first withdrawal as shown in Figure 4.2b. The surface is now hydrophobic and deposition occurs during the next immersion into the water. Thus, one monolayer coverage is obtained with each traversal through the liquid. With a hydrophobic surface such as freshly etched silicon, pickup occurs during the first insertion. Sometimes, the common Y-type deposition mode illustrated in Figure 4.2d is not followed, and one of the other two possible configurations, X- or Z-type, is observed, where transfer occurs only during immersion or withdrawal, respectively. The surface quality and chemical composition of the substrate affects the nature of the deposited layer. Provided the surface is very hydrophilic or very hydrophobic, good adhesion is normally obtained; satisfactory cohesion between adjacent monolayers is harder to achieve.

4.2 Modern Developments

4.2.1 Organic Synthesis

Generally speaking, the synthesis of suitable molecules for examination with a Langmuir trough has been made by an ad hoc procedure and has relied on the modification of known materials. For example, the alkyl group of fatty acids may be replaced by chains containing one or more double bonds. The ω -tricosenoic acid (ω -TA) molecule (8) shown in Chart 4.1, which is similar to stearic acid but contains a terminal double bond, displays all the essential film-forming qualities including solubility in convenient organic solvents, stability at the surface of water, shear resistance, stability against collapse, and suitable orientation features.

The diacetylenic acids (9, 10) have also been widely investigated because of their polymerizability. Here the interesting diacetylenic entity is normally incorporated into the structure of an alkanolic acid to give a compound such as $\text{CH}_3(\text{CH}_2)_{10}\text{C}\equiv\text{C}-\text{C}\equiv\text{C}(\text{CH}_2)_7\text{COOH}$. The topochemical polymerization proceeds within the LB layer but results in an array of two-dimensional domains whose size is influenced by material purity. Diacetylenes have also been incorporated into lipidlike molecules and polymerized as model membranes (11, 12). Because of the structural flexibility of LB films, there is likely to be continued interest in polymer LB films research, some of which will involve preformed polymers (13). However, the rigidity of many polymer films prevents this approach being used generally.

To attach long aliphatic chains to a molecule and spread a monolayer is relatively straightforward. However, this procedure may well dilute the desirable properties of the basic molecule. Moreover, for stability reasons, the presence of long side groups will severely restrict their practical applicability. Therefore, the scope of the Langmuir-trough technique would be considerably enhanced if interesting materials containing only short, stable side groups could be formed into LB films. A good example is provided by the anthracene derivative (14) shown in Chart 4.1; multilayers of excellent

quality can be obtained, even though the alkyl group contains only four aliphatic carbons and the hydrophobic group is attached to the ring structure via only two methylene groups.

Extremely robust monolayer assemblies can be constructed by using dye molecules such as the porphyrins and phthalocyanines. In general, their quality is relatively imperfect compared with those of the classic film-forming materials, but their significant advantages lie in their thermal and mechanical stabilities. An example of a substituted phthalocyanine molecule (15), which can be deposited in monolayer form, is shown in Chart 4.1.

The molecules shown in Chart 4.1 represent only a few of the materials that have been studied in LB film form. Nonetheless, a great deal more needs to be done to tap the vast wealth of opportunities available with organic systems. Inevitably, short-term opportunistic attempts will be aimed at discovering molecules for specific devices. However, a more pressing need is for a systematic approach that will yield rules governing structure-property correlations so as to enable scientists to confidently predict the molecular architecture of monolayer assemblies.

4.2.2 Langmuir Troughs

The upsurge in interest in LB films has led to greater attention being placed on trough design and control systems to meet the stringent requirements of scientists and engineers. Therefore, modern instruments are relatively sophisticated, and, for device-related work, need to be situated on anti-vibration tables in clean environments. Although it is possible to automate most features, the primary benefit at the present time lies in efficient data collection and the ease with which data can be manipulated. For example, phase transitions are more apparent when the differential of the pressure-area isotherm is plotted. Also, the deposition process can be programmed and monitored in a straightforward manner. In the example shown in Figure 4.3, the substrate is moved between different vertical limits to provide a staircaselike multilayer structure comprising 4, 8, 12, and 16 layers. In order to maintain a constant surface pressure during the Y-type dipping cycle, the film area enclosed by the barrier is reduced systematically.

A recent development in trough design could have important commercial significance. This development has arisen because of the need to produce noncentrosymmetric structures that display interesting nonlinear physical effects. The conventional Y-type films are symmetrical in character, and experience has shown that X- and Z-type layers, although nonsymmetrical, are usually imperfect. Therefore, an alternative approach to producing noncentrosymmetric structures is to use alternate layers of two different materials where the contributions of adjacent molecules do not cancel (Figure 4.4). The additions of a fixed beam and a revolving center section to an automated constant-perimeter-barrier Langmuir trough enables the formation of an alternating Y-type structure of two different molecules

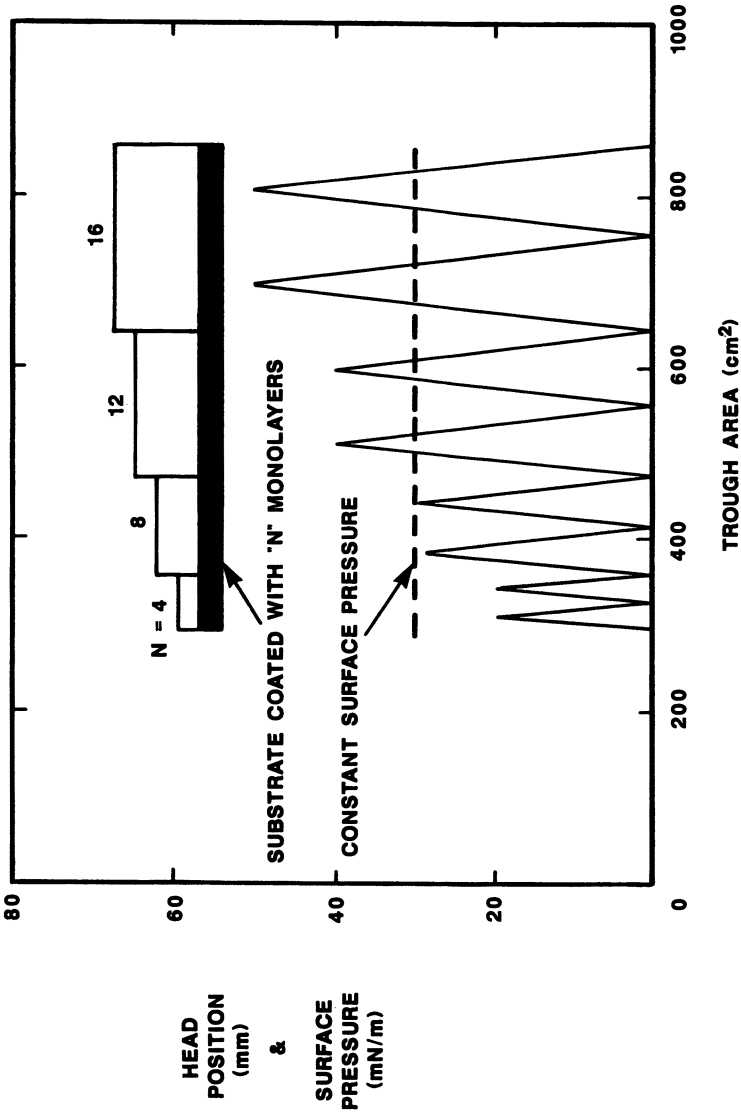


Figure 4.3. To maintain a constant surface pressure during the deposition process, the area enclosed by the barrier is reduced systematically. This schematic Y-type dipping sequence for a staircase shows a staircase structure of 4, 8, 12, and 16 monolayers. (Courtesy of Joyce-Loebel Company, Gateshead, England.)

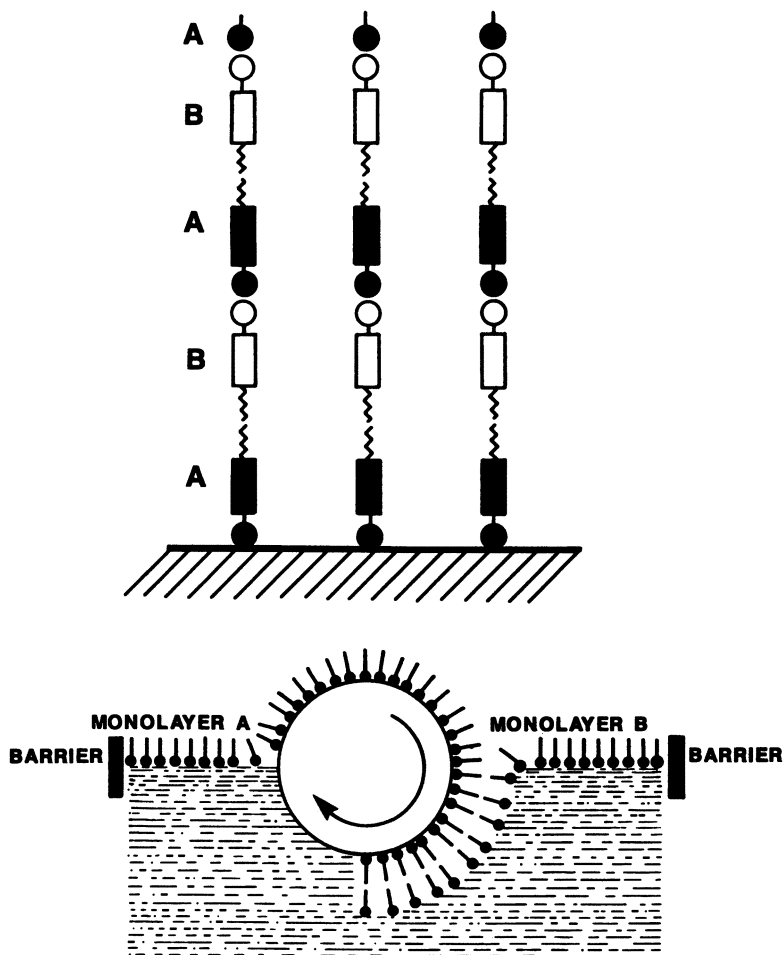


Figure 4.4. Top: A combination of two molecules A and B enables a Y-type film to be produced of noncentrosymmetric character. Bottom: A rotating substrate is used to alternately pick up different molecules from separate areas of the trough and thus form an organic superlattice.

spread in the two distinct areas of the subphase. The structural qualities of the LB films prepared in this way can be of high quality (16). Another advantage of the rotating substrate arrangement, which is conducive to fast dipping, is that the meniscus, unlike that in the vertical dipping method, is always in the same direction.

4.3 Characterization of Langmuir-Blodgett Films

Many different experimental techniques indicate that carefully prepared films of appropriately substituted molecules possess a high degree of struc-

tural order. The surface quality and chemical composition of the substrate can have a profound effect on the nature of the deposited layers. However, as in the case of the spread monolayer, researchers have frequently ignored the underlying science and have arrived at empirical procedures for preparing specimens. Naturally, the quality of the floating layer is important and needs to be characterized, as does the interface between the first deposited layer and the substrate. A popular objective in studies of floating monolayers is to monitor a physical parameter during compression of the film and thus correlate phase transitions in the pressure–area isotherm with effects such as the formation of aggregates. For example, Raman spectroscopy (17) can provide evidence of molecular orientation, and fluorescence microscopy (18) can be used to illustrate the change in texture of a monolayer due to dendrite formation.

Electron diffraction was first used to study LB films over 50 years ago, but only recently have the packing arrangements of molecules in multilayer films been investigated in detail. For example, transmission electron diffraction has provided evidence that epitaxial growth occurs under certain conditions where the multilayer film assumes the structural order present in the first layer. Very few experiments have been concerned with films constituting fewer than 10 monolayers, and little attention has been paid to the structure of the initial few monolayers deposited onto a substrate. In these situations, reflection high-energy electron diffraction (RHEED) is particularly convenient because it is nondestructive and permits a rapid identification of the film structure to be achieved with minimal sample preparation. A RHEED pattern from a molecule specially designed for nonlinear optics applications (19) is illustrated in Figure 4.5. The electron microscope can also be used in transmission; the first direct image of an LB film was reported by Fryer et al. (20) for a single monolayer of a substituted phthalocyanine. The structure exhibited in Figure 4.6 is for a single monolayer of tricosenoic acid (21).

X-ray diffraction techniques have been used extensively to determine the monolayer thicknesses of LB films. Because the scattering of X-rays from carbon and hydrogen atoms can be assumed to be very small compared to that from heavier metal ions incorporated in a film, the lattice spacing normal to the film corresponds to the distance between adjacent planes containing metal ions. Some workers have noted X-ray d spacings that are significantly less than those expected from consideration of the molecular length; such evidence normally points to a tilt in the hydrocarbon chain. For example, the long-axis molecular tilt angle in films of the anthracene compound shown in Chart 4.1 is 60° , and the molecules in consecutive layers appear to interpenetrate (14). Neutron diffraction and reflection measurements have also been reported (22, 23). The precise regularity of the layer spacing and the finite number of layers enables a precise quantitative fit to be obtained. Optical techniques were applied by Blodgett and Langmuir (24) to determine

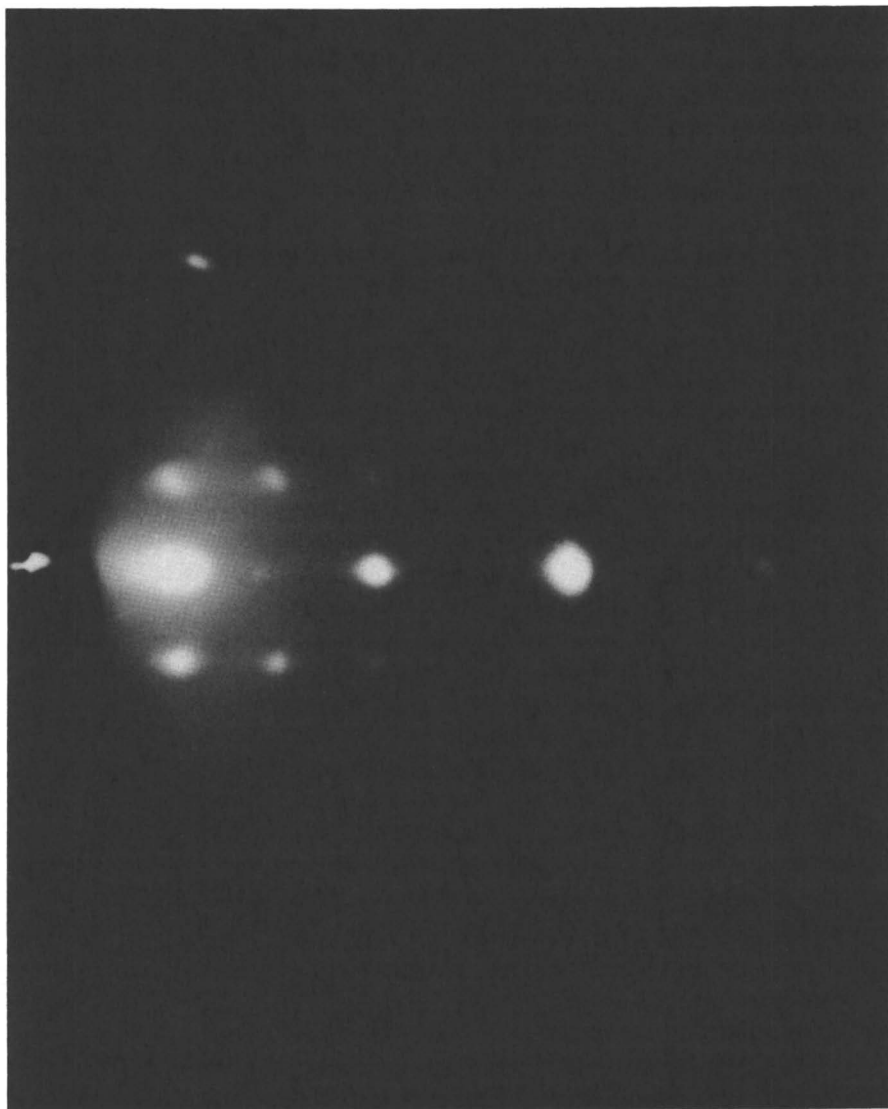


Figure 4.5. An 80-keV reflection high-energy electron-diffraction (RHEED) pattern from a single layer of the nitrostilbene molecule shown in Structure 4.1b. The substrate is {111} silicon.

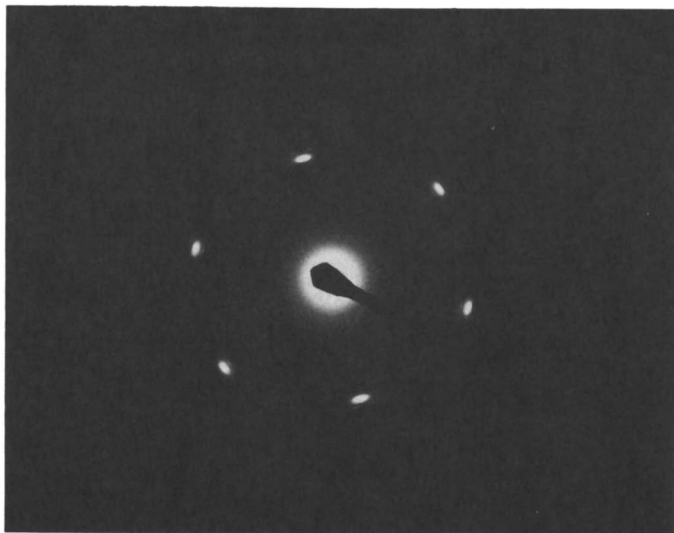


Figure 4.6. A 100-keV transmission-electron-diffraction pattern of a single monolayer of tricosenoic acid. (See reference 21.)

the optical constants of fatty acid salt monolayers; they showed how the refractive index could be modified by skeletonizing the films and adjusting the salt-acid ratio. Modern methods allow thickness determinations to be measured routinely by using ellipsometry, and, by using intensity variations, the lateral heterogeneity from domains larger than the wavelength of light can be established. Very thick films can be used to determine both the thickness and the refractive index by studying multimode propagation in a waveguide configuration. For example, Walpita and Pitt (25) measured the waveguiding characteristics of more than 200 layers of cadmium stearate and similar data have been reported for a diacetylene polymer by Chen et al. (26).

Surface analytical techniques such as Auger electron spectroscopy (27), X-ray photoelectron spectroscopy (28), and secondary-ion mass spectrometry (29) have been used to study LB films. Synchrotron radiation is a particularly powerful probe enabling X-ray near-edge structure and extended X-ray absorption fine structure to be measured. Angle-resolved photoemission studies (30) confirmed the existence of a one-dimensional energy band along the $(\text{CH}_2)_x$ chain in a fatty acid salt film.

Infrared spectroscopy is a powerful tool to study LB films. With modern instruments such as Fourier transform spectrometers, detailed information can be obtained about functional groups and their orientation. For example, IR spectroscopy can be used (1) to show that the simple acid salts are inclined at only a few degrees from the normal to the substrate surface (31) and to

study polymerization processes (32). Raman spectroscopy can also provide similar data, but, being an inherently weak process, sensitivity is limited.

Modern enhancement techniques enable the signal-to-noise ratio to be increased by interactions with surface plasmons (33) or surface effects (34). Inelastic tunneling spectroscopy (35), Brillouin scattering (36), and photoacoustic spectroscopy (37) have also been used to explore the vibrational modes in LB films.

During the next few years, scientists will devise new and improved methods of characterizing monomolecular assemblies. A great deal needs to be learned about the ordering of monolayers, and techniques such as scanning tunneling microscopy may provide some of the answers.

The four separate diagrams in Figure 4.7 all describe results for fatty

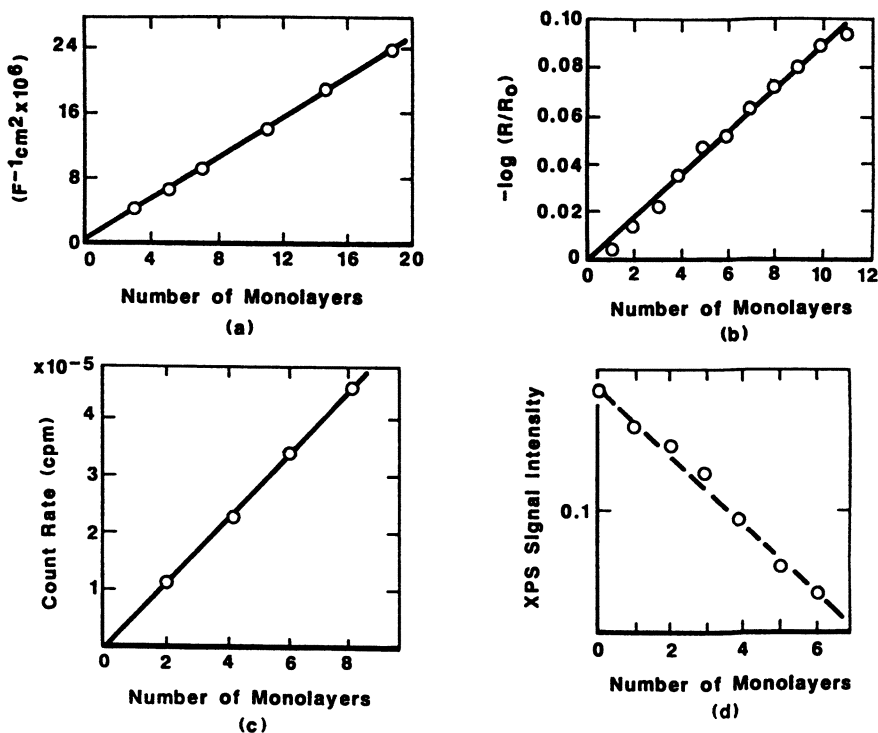


Figure 4.7. These diagrams are designed to emphasize the reproducibility of various physical parameters in monolayer assemblies of different thicknesses: (a) reciprocal capacitance per unit area versus number of monolayers of cadmium arachidate on an aluminum substrate (see reference 38), (b) absorption intensity versus number of monolayers for the symmetric carboxylate stretching mode of cadmium arachidate at 1432 cm^{-1} (see reference 39), (c) count rate of ^{14}C rays versus number of layers of barium stearate labeled with ^{14}C (see reference 40), and (d) X-ray photoelectron signal (XPS) intensity versus number of layers of cadmium dimethylarachidate on silver (see reference 28).

acids or their derivatives and are designed to emphasize the reproducibility of various physical parameters from one monolayer to the next. Figure 4.7a shows the capacitance (C) as a function of film thickness for cadmium arachidate deposited onto aluminum (38). The linear dependence of C^{-1} versus the number of monolayers demonstrates clearly the repeatability of the dielectric thickness of each monolayer. In Figure 4.7b, a band in the IR reflection spectrum of the same material has been used to demonstrate the uniformity of successive monolayers (39). Figure 4.7c is based on experiments using barium stearate as the absorber for L-shell Auger electrons (40). By labeling the molecules in these overlays with ^{14}C and examining their autoradiographs, the uniformity of the deposition process may be confirmed by plotting the count rate of ^{14}C rays versus the number of monolayers. The final diagram in the set (Figure 4.7d) illustrates another powerful tool for investigating organic coatings on metals. In this case, different thicknesses of cadmium dimethylarachidate have been used to attenuate the substrate X-ray photoemission signal (28).

4.4 Langmuir–Blodgett Films as Model Systems in Basic Research

One of the principal virtues of LB films is their usefulness in fundamental research. Many areas of science can benefit from investigations of model systems based on monomolecular assemblies. These areas include

- energy transfer in complex monolayers,
- biological membranes, and
- metal ion incorporation.

4.4.1 Energy Transfer in Complex Monolayers

The Langmuir-trough technique provides a method of constructing simple artificial systems of cooperating molecules on a substrate. Kuhn has been the pioneer in this field. The elegance of his work and that of his colleagues is evident in their reviews of the subject. These reviews describe the use of LB films to investigate intermolecular interactions and various photo-physical and photochemical processes. An example of this research (41), designed to investigate the Forster type of energy transfer from a sensitizing molecule, S, to an acceptor molecule, A, is given in Figures 4.8 and 4.9. If S is a compound that absorbs in the UV part of the spectrum and fluoresces in the blue, and A absorbs in the blue and fluoresces in the yellow, then interesting effects are observed when the system is irradiated with UV light. If there is a sufficient distance between S and A, as in Figure 4.8a, the fluorescence of S appears because A does not absorb UV radiation. However,

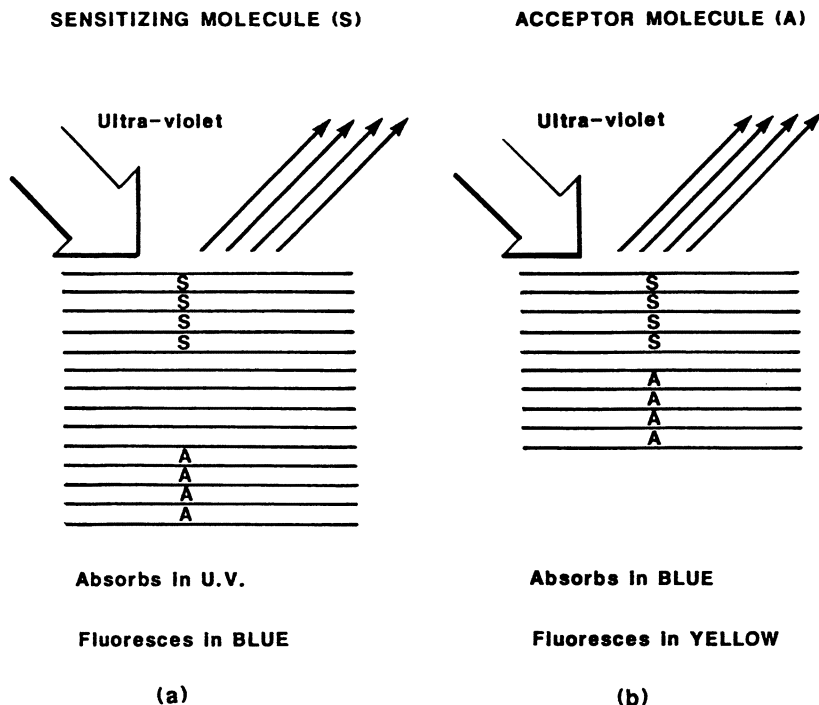


Figure 4.8. Schematic diagram showing basis of experiments designed to investigate energy transfer from a sensitizing molecule (S) to an acceptor molecule (A). The number of monolayers separating the two species governs the spectral response of the fluorescence spectrum. (a) The acceptor molecule does not absorb the UV radiation. (b) The separation distance is sufficiently small for the excitation energy of S to be transferred to A.

below a certain threshold distance, as in Figure 4.8b, the excitation energy of S is transferred to A, and the yellow fluorescence of A is expected. Similar experiments based on fluorescence quenching indicate that the rate constant of the electron transfer decreases exponentially with increasing barrier thickness separating a donor chromophore and an electron acceptor. In the example shown in Figure 4.9, *N,N'*-dioctadecylthiacyanine has been used in conjunction with a viologen acceptor layer to observe the steady fluorescence intensities of the cyanine dye monolayer in the absence (I_0) and in the presence (I) of the acceptor layer. The quantity, $(I_0/I) - 1$, is proportional to the rate constant of the electron transfer. Its linear dependence with d , the distance between the chromophores, is evidence of electron tunneling. In a similar series of experiments, the energy-transfer mechanism responsible for spectral sensitization has been investigated.

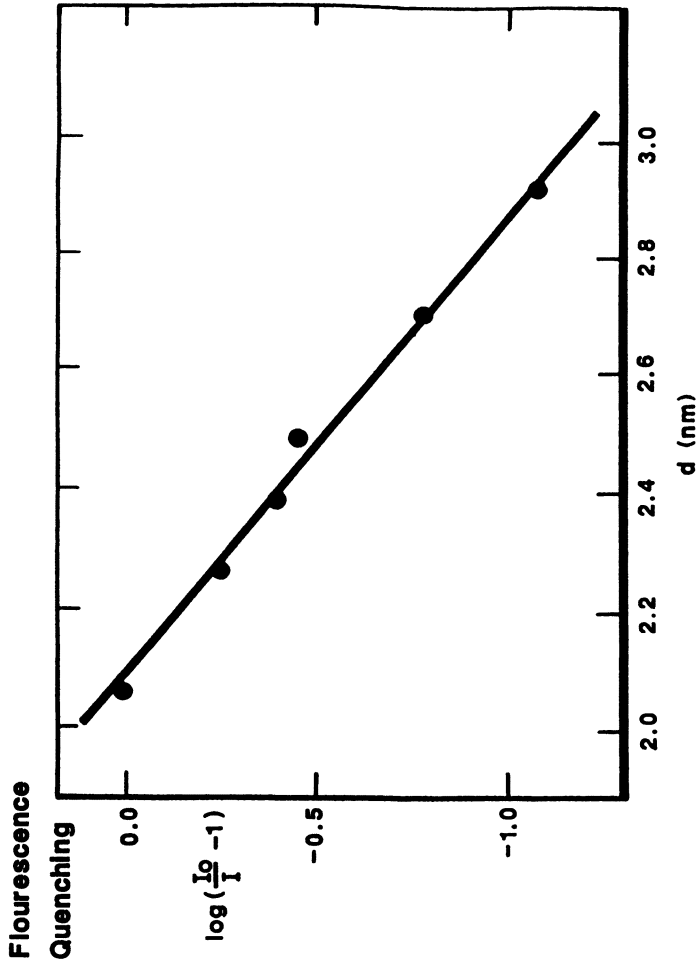


Figure 4.9. The fluorescence intensity (I_0) of a donor dye is reduced to a value I in the presence of an acceptor dye. The logarithm of $(I_0/I) - 1$ is shown as a function of d , which is the spacing between the donor and acceptor planes (see reference 41).

4.4.2 Biological Membranes

The physical structure and chemical nature of classical LB films gives them a close resemblance to naturally occurring biological membranes. For example, because the two ends of a lipid molecule have incompatible solubilities, they spontaneously organize in the form of a bilayer, or essentially a two-layer LB film. Scientists have suggested that they might provide a suitable model of the lipid membrane for probing the cooperative interactions between its constituents. However, caution must be exercised in assessing the biological relevance of this type of work and associated studies aimed at incorporating ionophores into phospholipid layers.

Much of this research is targeted at novel integrated solid-state devices incorporating biological molecules such as enzymes, but in some cases, LB films have been used to facilitate physical studies of biological molecules (e.g., to measure the ionic permeability of reconstituted membranes). Supramolecular structures have also been designed to mimic the primary process in photosynthesis and for achieving an efficient photoinduced charge separation by appropriate modeling of potential profiles. Chlorophyll has been studied in this context. Some of the results may have relevance to solar photochemical conversion devices (42).

4.4.3 Metal Ion Incorporation

The addition of divalent ions into the liquid subphase in a Langmuir trough can increase the shear resistance and cohesion of the monolayer. For this reason, studies of fatty acid salts are more common than on their acids. By adjusting the pH of the subphase, multilayers containing metal ions separated by the width of an integral number of monolayers (for Y-type deposition, two monolayers) can be assembled. The ability to do this has been capitalized upon in several fundamental investigations, three of which will be mentioned here. The first of these relates to two-dimensional magnetic monolayers involving iron or manganese ions. Using electron spin resonance, Pomerantz (43) demonstrated that at temperatures near 2 K, the resonance field and line shapes are affected. This result signals the rapid development of a large internal magnetic field. Pomerantz's results have been interpreted in terms of a predominantly antiferromagnetic state but with a weak ferromagnetic component. Further experiments are required to clarify magnetic ordering in two-dimensional space.

In the area of surface science, X-ray photoemission is now used extensively to study organic materials on surfaces. In such experiments, establishing electron mean free path lengths as a function of kinetic energy is important. An example of this type of investigation in LB films is illustrated in Figure 4.7d. Generally, the mean free paths for ordered multilayers are significantly longer than those for conventionally produced polymers (28).

A third example of the usefulness of the Langmuir-trough technique to

provide matrices containing regularly spaced metal ions lies in radioactivity. Mori et al. (40) used radioactive stearate monolayers, in which some of the hydrogen atoms had been replaced by nuclides, such as ^{51}Cr , ^{54}Mn , ^{55}Fe , ^{57}Co , ^{65}Zn , and ^{109}Cd , to produce dilute and standard radioactive sources. By labeling the molecules with ^{14}C and examining autoradiographs, they were able to confirm the uniformity of the deposition process as shown in Figure 4.7c. Using conventional monolayers with well-controlled dimensions as overlays, they were also able to demonstrate that Auger electrons from the L shell with an energy of approximately 0.5 keV are almost completely absorbed by 15 monolayers of barium stearate. Experiments of this kind are of importance in fields such as medical physics and upper atmosphere science.

4.5 Promising Applied Research Areas for Langmuir-Blodgett Films

Despite the increased activity during the past 10 years, no important commercial venture based on LB films has been started. However, the level of financial investment, even in the general field of organic molecular solids, is still a small fraction of the sum devoted to inorganic materials. When an institution decides to invest in an expensive item such as molecular beam epitaxial-growth equipment, it invariably ensures that a reasonable number of workers are associated with the project. Langmuir troughs are relatively inexpensive, and normally much smaller size teams are involved. This factor, coupled with the difficulty of organizing interdisciplinary teams, probably accounts for the current situation. A comparison can be made between the present situation for LB films and that which existed 15 years ago for liquid crystals. At that time, when the display application was clearly appreciated, a large amount of background knowledge of structure-property relationships was available. This knowledge base enabled applied scientists to replace deficient materials by more desirable, tailored structures that had already been thoroughly investigated by chemists engaged in pure research programs. The situation is totally different for LB films; hence, technical progress should not be expected to take place at the same dramatic rate as occurred for liquid crystals.

Until recently, industry has had a suspicious view of organic solids on account of their inherent stability compared with their inorganic counterparts. However, spectacular advances in liquid crystal displays, organic photoconductors, and piezoelectric polymers have given industry more confidence in such materials. Nevertheless, the average industrialist will seek an order-of-magnitude improvement in device performance if a new technique such as the Langmuir trough is to be introduced. Thus, for commercial applications, the LB films will need to be an essential, integral part of the device. That is, one must capitalize on their unique features such as

the degree of control over the molecular architecture, their thinness, or the selective way in which they might react with the environment.

Now that a commitment has been made to the subject, with higher levels of funding and personnel being made available, at least one innovative application is likely to emerge. When this happens, a need will arise to produce a specially designed trough capable, for example, of coating a moving belt or multiple wafers of silicon. No difficulties are envisaged in constructing continuous fabrication equipment, and substantial progress has already been made in this direction.

Langmuir-Blodgett films may have value in many applied areas of traditional interest to the industrial chemist, such as adhesion, encapsulation, and catalysis. The permeability characteristics of monolayer assemblies may also find application as synthetic membranes for ultrafine filtration, gas separation, and reverse osmosis. For example, Albrecht et al. (44) proved the efficiency of polymeric diacetylene monolayers on semipermeable supports in reducing the flow of CH_4 . One interesting possibility lies in using LB monolayers as lubricants in magnetic tape technology. Unpublished reports have indicated that frictional coefficients can be reduced markedly when the tape is coated with a few monolayers. In applications such as those listed previously, difficulties may well be encountered with the mechanical stability of the films. To date, relatively little research has been carried out in this area.

The long-term interest, as far as the applied physicist is concerned, lies in the possible uses of supermolecular assemblies for memory storage, molecular switching, and superconducting devices. However, at the present time, potential improvement areas are where monomolecular films show most promise and where the prospects of commercial exploitation seem reasonable in the medium term. A few of these areas are described in this section; most of the illustrations are based on work carried out in my research laboratories. These potential improvement areas are grouped into three categories, but most of the emphasis is placed on utilizing the nonlinear properties of LB films.

4.5.1 Nonlinear Physics

Many organic molecules possess very high nonlinear coefficients. Therefore, if LB films with the required architecture can be formed, these could form the basis of novel devices. To avoid the symmetry inherent with conventional Y-type deposition, X- and Z-type films have been studied. Some of these films displayed a permanent polarization with a strong component in a direction perpendicular to the substrate. However, films produced in this way, with their dipoles supposedly aligned in a common direction, are invariably of poorer quality than Y-type layers. A possible method of improving the structure is to use electric or magnetic fields to help align the molecules,

but efforts to orient films on the subphase and substrate have met with only limited success. The problem can be overcome by using organic superlattices based on alternating layers of two different materials (Figure 4.4). A good example is given in Figure 4.10, which shows a superlattice comprising acid and amine molecules whose dipole moments are in opposite senses, but when deposited in Y-type LB film form, are aligned in the same direction. Two areas of particular interest that would capitalize on this feature of organic superlattices are pyroelectricity and optoelectronics. Each of these areas will now be considered. The acoustoelectric opportunities are mentioned in the section devoted to sensor-type applications.

4.5.1.1. PYROELECTRIC DEVICES

When the centers of positive and negative charge in a crystalline material do not coincide, then a spontaneous polarization exists across it. If this

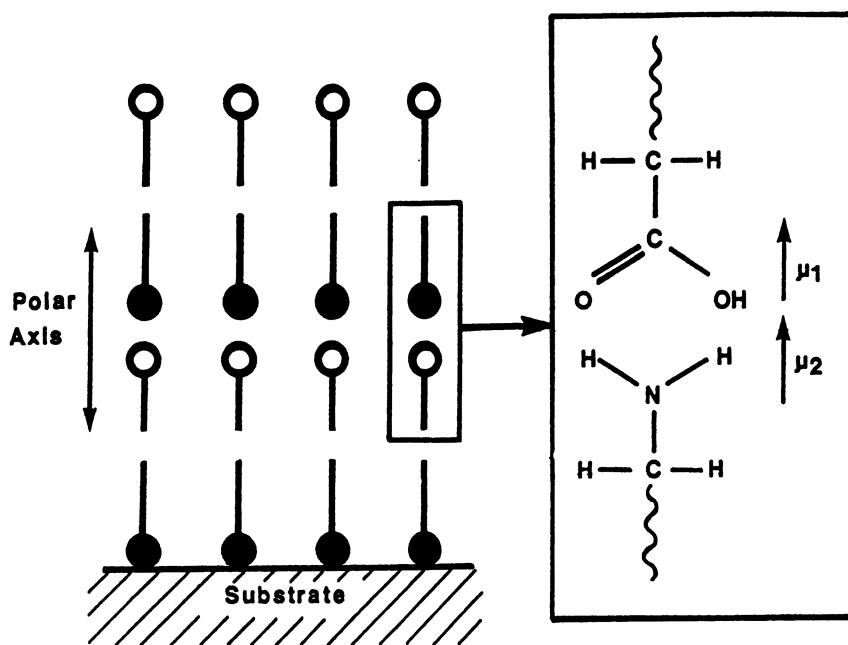


Figure 4.10. Left: An organic superlattice with a unique polar axis. The two types of molecules involved could be a fatty acid and a fatty amine. The insert is designed to show that these two materials have dipole moments in opposite senses with respect to the hydrophobic chain. Thus, the Y-type film has a resultant dipole moment.

polarization is temperature dependent, the crystal develops an electric charge on its surface and exhibits the pyroelectric effect. Devices based on pyroelectricity thus respond to a rate of change of temperature rather than to changes of temperature as in a semiconductor type of thermal detector. This response gives them inherent advantages, but their full potential has yet to be realized. For applications where both high speed and sensitivity are required, conventional materials have been unsuccessful. This failure can be attributed partly to the fact that conventional materials have not been available in very thin films. For device applications, a thin-film geometry is preferred because one can then form large area imaging devices directly on microelectronic amplifying circuits. The pyroelectric properties of inorganic materials such as the titanates tend to be offset by their high relative permittivities, and pyroelectric organic single crystals such as triglycine sulfate cannot be produced as thin films. Thus, the future development of relatively cheap thermal imaging systems with reasonable performance and an optimum thickness of approximately 0.5 μm requires a materials breakthrough. Some research effort is being given to ferroelectric liquid crystals (45), but difficulties with encapsulating such materials in low thermal capacity structures are likely to hinder such developments. On the other hand, the opportunities for depositing highly anisotropic pyroelectric LB films onto reticulated silicon substrates seem good. These assemblies would be inherently polar and would not require "poling", as do conventional pyroelectric polymers such as poly(vinyl difluoride) (PVDF).

The first report of pyroelectric behavior in LB films was by Blinov et al. (46). Electroabsorption studies were made to confirm the orientation of the azocompound monolayers used in their work. No detailed results are presented in their paper, but pyroelectric coefficients approximately one order of magnitude less than those for PVDF are reported for X- and Z-type structures.

The pyroelectric coefficient (p) is a useful parameter with which to compare different materials. If the thin film acts as a dielectric in a capacitor, and an external resistance is connected between the electrodes, then a pyroelectric current (I) flows in the circuit. This situation can be expressed as

$$I = pA \frac{dT}{dt} \quad (4.1)$$

where dT/dt is the rate of change of temperature, and A is the cross sectional area of the device. The pyroelectric coefficient is a measure of the current generated by a specific rate of change of temperature. However, the induced voltage (V) is a more useful parameter in an IR detection system. For an

incremental change in temperature, dT generates a charge $dQ = pAdT$. Therefore, when $dQ = CdV$,

$$\frac{dV}{dT} = \frac{pd}{\epsilon A} \quad (4.2)$$

where ϵ is the permittivity and d is the pyroelectric material thickness. The quantity (p/ϵ) is a useful figure of merit for a pyroelectric material. Table 4.1 lists this parameter for a number of different materials.

The potential across a film is clearly dependent on the amount of surface charge. Thus, if the polarization of the film is constant throughout the sample, the magnitude of V should increase in proportion to the number of layers deposited. Moreover, the sign of this increase in surface potential should be reversed by inverting the polar axis. This result occurs when organic superlattices are prepared by using the alternate-layer trough described previously. Figure 4.11 shows the surface potential as a function of number of layers for two complementary orientations of the polar axis of the molecular structure illustrated in Figure 4.10. The top half corresponds to the case where the amine layer is deposited first. The surface potential steps are of different sign when the acid layer is deposited first. These experiments confirm that a thin film with a unique polar axis has been assembled. Using dynamic and static detection techniques, Christie et al. (47) showed that this combination of simple molecules is pyroelectric with $p \sim 1 \text{ C cm}^{-2} \text{ K}^{-1}$. More recent results, involving a system where proton transfer occurs from the acid to the amine, have yielded higher values. Therefore, even when standard materials are used, figures of merit comparable with those of the best alternatives can be achieved.

However, the exploitation of pyroelectric LB films depends not only on the figures of merit listed in Table 4.1, but also on the ability to deposit such layers successfully on surfaces with low thermal mass. A substrate imposes two constraints on the pyroelectric response of a film. Not only does it provide an undesirable heat sink and reduce the excess temperature of

Table 4.1. Pyroelectric Coefficients and Figures of Merit for a Selection of Different Materials

<i>Material</i>	<i>Form</i>	<i>Pyroelectric Coefficient</i> ($\text{nC cm}^{-2} \text{ K}^{-1}$)	<i>Relative Permittivity</i>	p/ϵ ($\text{nC cm}^{-2} \text{ K}^{-1}$)
Lithium tantalate	Bulk crystal	19.0	46.0	0.41
Triglycine sulfate	Bulk crystal	30.0	50.0	0.60
Strontium barium niobium oxide	Ceramic	85.0	607.0	0.14
Poly(vinyl difluoride)	Polymer film	3.0	10.0	0.30
Phenylbenzoate ester	Liquid crystal	0.7	4.0	0.18 ^a
Acid/amine superlattice	LB film	1.0	2.5	0.40

^a This value is 5 °C from the Curie point.

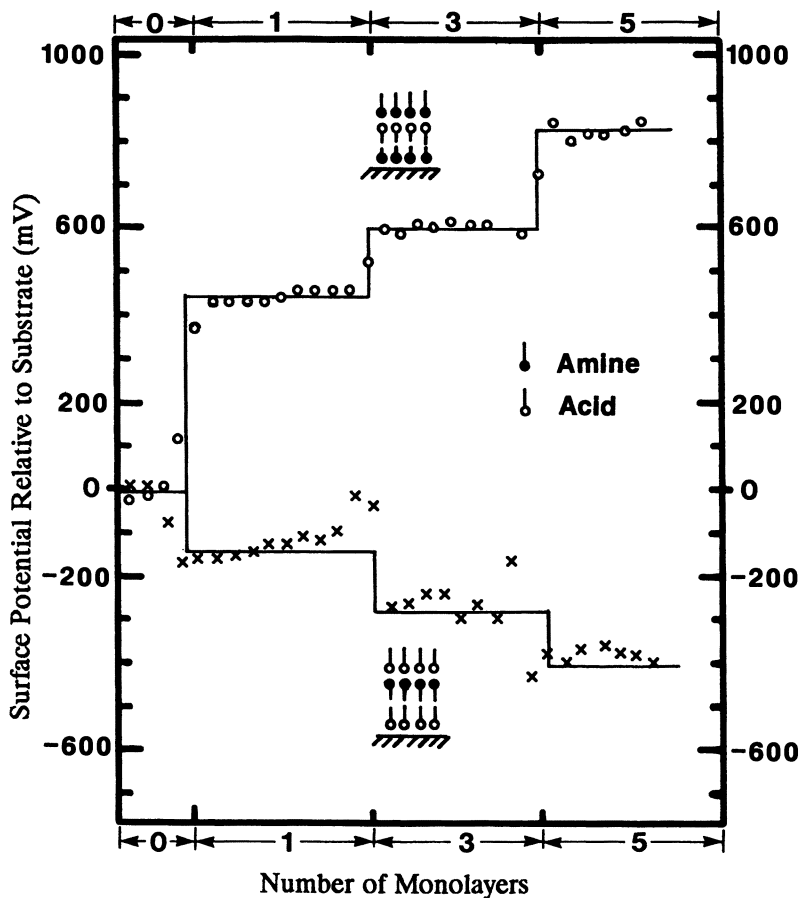


Figure 4.11. Surface potential of ω -TA-docosylamine alternate layers as a function of the number of layers for two complementary orientations of the polar axis. (Reproduced with permission from reference 47. Copyright 1986 American Institute of Physics.)

the pyroelectric layer (thermal clamping), but it also limits a secondary pyroelectric contribution due to temperature-dependent volume changes (mechanical clamping). Reticulated substrates with appropriate thermal expansion coefficients will be required to fully exploit the advantages of using optimum-thickness ($\sim 0.5 \mu\text{m}$) pyroelectric supermolecular assemblies. Noise considerations also dictate that the pyroelectric thin film material must exhibit low dielectric loss.

4.5.1.2 OPTOELECTRONIC DEVICES

Although many of the potential optical applications of LB films are in transmission optics, employing the linear response properties of molecules, the

most exciting applications are perceived in the area of nonlinear optics. Functions such as second harmonic generation and parametric amplification can be obtained by using inorganic single-crystal materials such as lithium niobate, but recently, organic crystals such as 3-methyl-4-nitroaniline have been shown to possess exceptionally large second-order electrooptic coefficients (48).

Similarly, cubic effects such as four-wave mixing, phase conjugation, and optical bistability form the basis of optical functions of strategic importance. In this case, materials such as polyacetylene could, in principle, compete effectively with inorganic solids such as gallium arsenide.

The macroscopic polarization (P) of a solid comprising many individual molecules may be expressed as

$$P = P_0 + \chi_1(E) + \chi_2(E^2) + \chi_3(E^3) + \dots \quad (4.3)$$

where P_0 is a constant, E is the electric field, and χ_n is the n th order susceptibility tensor. In this equation, χ_2 and χ_3 are responsible for the second and third harmonic generation, respectively. When an individual molecule is involved, the polarizing effect can be expressed in terms of an induced dipole moment (μ) and a series of polarizabilities. That is,

$$\mu = \alpha E + \beta E^2 + \gamma E^3 + \dots \quad (4.4)$$

where the coefficients α , β , and γ are tensor quantities.

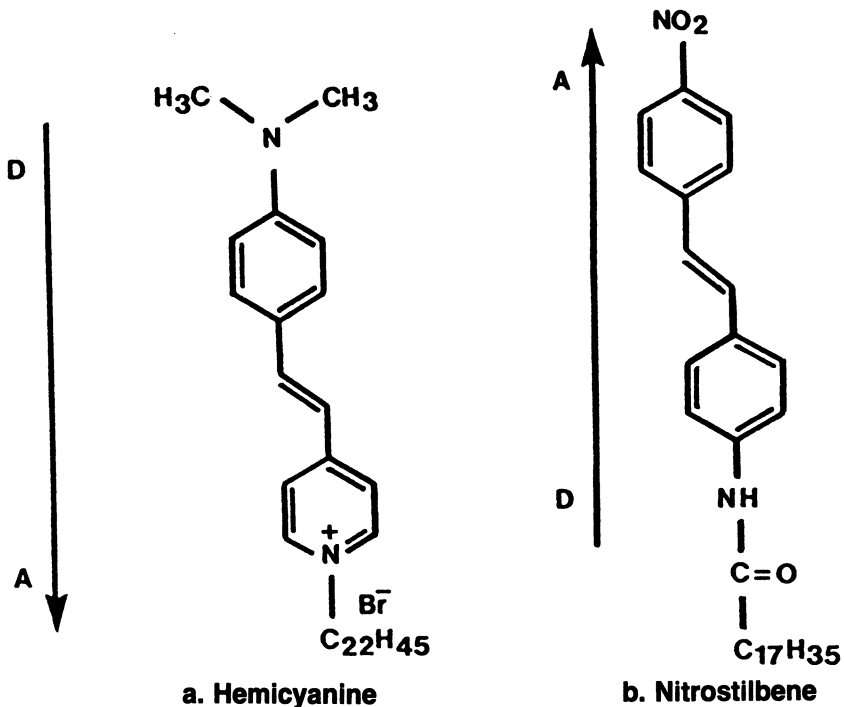
The basic molecular properties that give rise to high values of the hyperpolarizabilities, such as β and γ , are reasonably well understood in organic solids. For quadratic molecular effects, conjugation and intramolecular charge transfer are important. Cubic-nonlinearity-related effects are enhanced in one-dimensional conjugated structures, but no charge-transfer-induced asymmetry is required.

Thus, in both cases, the molecular unit can be "tailored" to meet a specific requirement. A second crucial step in engineering a molecular structure for nonlinear applications is to optimize the crystal structure. For second-order effects, a noncentrosymmetrical geometry is essential. Anisotropic features, such as parallel conjugated chains, are also useful for third-order effects. An important factor in the optimization process is to shape the material for a specific device so as to enhance the nonlinear efficiency of a given structure. A thin-film geometry is normally preferred because nonlinear interactions, linear filtering, and transmission functions can be integrated into one precise monolithic structure.

In all stages of the process of designing nonlinear organic integrated devices, LB film techniques appear to offer considerable advantages. Several researchers are currently substituting organic molecules with appropriate side groups to enable LB film deposition to occur. In many cases, nonlinear coefficients comparable to those of inorganic materials have been achieved.

However, other considerations are also involved if LB films are to compete effectively with materials such as lithium niobate and gallium arsenide. Molecular engineering will also be required to cater to needs such as phase matching, suitable spectral response and refractive index, good optical damage threshold, low scattering coefficients, and mechanical stability before practical objectives can be accomplished.

To illustrate the potential of LB films in nonlinear optics, two examples will be given to illustrate both quadratic- and cubic-order effects. The motivation for the first example came from early accounts of nonlinearity in a specific merocyanine dye molecule (49). No good crystals of this material are available, but an extremely large value of β was predicted on the basis of measurements with powdered samples. The reliability of such data is not high because powder efficiency is a function of particle size distributions. The initial experiments were with a simple merocyanine dye alternated with ω -TA. However, the best results (50) were obtained by using organic superlattices based on the two molecules shown by Structures 4.1a and 4.1b.



Structures 4.1a and 4.1b. These two molecules, one (a) a hemicyanine and the other (b) a nitrostilbene dye, can be used to form an organic superlattice displaying a high coefficient for second harmonic generation (see reference 50).

As in the case of the acid-amine structure described previously, the two molecules, when deposited in alternate-layer form, have their dipoles mutually aligned and produce a highly noncentrosymmetric structure ideal for second harmonic generation. The insert in Figure 4.12 shows that the non-linear response of a hemicyanine-nitrostilbene layer is greater than that expected from the simple addition of contributions arising from the individual (separated) monolayers. The coefficient for second harmonic generation, β , of the alternate layer structure is approximately 5 times the average value of the same parameter measured for hemicyanine and nitrostilbene. This

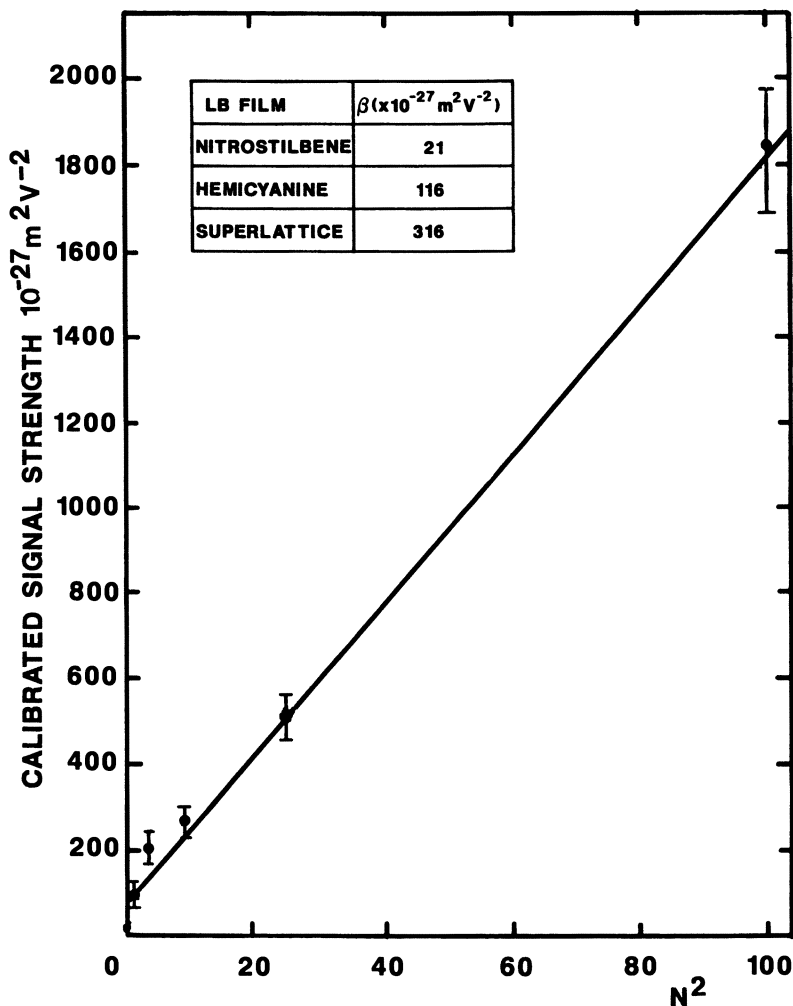


Figure 4.12. Second harmonic generation signal strength versus the square of the number of bilayers based on the two molecules shown in Structures 4.1a and 4.1b.

superadditive effect is best explained in terms of improved film structure with adjacent molecules influencing each other to orient more vertically with respect to the substrate. However, synergistic interactions between the dipoles and aggregation may also be responsible.

This interesting result, when translated into macroscopic terms, gives a χ_2 value 50 times greater than that of lithium niobate. Figure 4.13 also

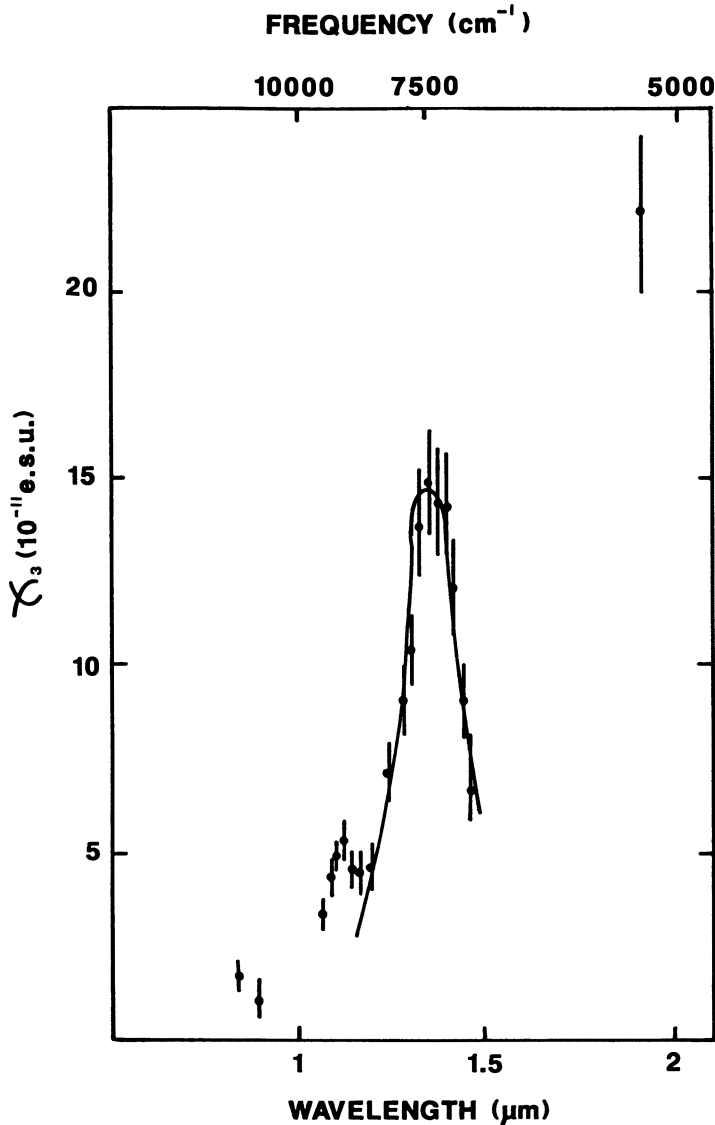


Figure 4.13. Cubic susceptibility measured as a function of wavelength for 78 layers of polydiacetylene. (Reproduced with permission from reference 51. Copyright 1985 Elsevier Sequoia.)

shows that the second harmonic power increases quadratically with the number of deposited bilayers; this dependence on the areal density of the dye is to be expected for a film that is thin compared with the incident wavelength but is rarely observed in practice.

The fundamental properties of a high χ_3 material may be very different from those required for second harmonic generation. A favorable structure for the enhancement of cubic susceptibilities is a one-dimensional conjugated periodic system. A good example is polydiacetylene with a diacetylene monomer: bis(*p*-toluenesulfonate)-2,4-hexadiyne-1,6-diol, which is abbreviated PTS-PDA. The cubic susceptibility parallel to the polymer chains in bulk single crystals of this material is approximately 13 times the value of χ_3 for gallium arsenide. The tensor coefficients perpendicular to the polymer chain are similar to those in the monomer crystal. This similarity reflects the high anisotropy of the structure. These encouraging results have prompted several research groups to study third harmonic generation in diacetylene-based LB films. Early measurements indicated χ_3 values approximately 2 orders of magnitude lower than those reported for PTS-PDA. More recent data (51) are shown in Figure 4.13, which presents the cubic susceptibility as a function of wavelength. Of special interest is the resonance observed at $\lambda = 1.35 \mu\text{m}$, as this can be used for high-powered laser conversion. At this wavelength, the measured value of the cubic susceptibility is only a factor of 6 less than that observed for single crystals of PTS-PDA and is larger than that of gallium arsenide.

A systematic approach to the synthesis of novel molecules may yield significantly higher coefficients for both second and third harmonic generation. However, it is generally accepted that LB films, because of their anisotropy, have a better chance of displacing inorganic materials in second-order rather than third-order applications. For this to happen, optical devices requiring only a few monolayers of materials that display little scattering must be designed.

4.5.2 Enhanced Device Processing

Inorganic semiconductors, especially silicon and gallium arsenide, are likely to dominate transistor technology for at least the next decade. With the advent of low-dimensional structures produced by MBE (molecular beam epitaxy) and MOCVD (organometallic chemical vapor deposition), one can foresee interesting new high-frequency devices relying on both high-mobility electrons and short interelectrode spacings. LB films are unlikely to perform an active role in conventional semiconductor circuits and devices. However, there may be interesting niches for them as passive layers. The majority of high quality LB films are invariably excellent insulators; some, such as ω -TA, can effectively seal the surface of etched silicon against the atmosphere and thereby greatly retard the development of interface states (52). Related

work also proves that even a single monolayer is very often sufficient to increase the breakdown strength of “leaky” oxide films. Three of the more interesting applied areas where the LB film contributes a useful, passive role are

- electron beam lithography,
- semiconductor barrier height modification, and
- tunneling devices.

4.5.2.1 ELECTRON BEAM LITHOGRAPHY

In integrated circuit technology, the quest for faster speeds and larger memories has led to a gradual refinement of microlithographic methods for producing smaller and more closely spaced circuit elements. Submicron resolution is now required, and this has necessitated a move away from conventional photolithography to techniques involving electron or ion beams and X-rays. The main disadvantage of electron beam systems lies with their scattering characteristics; this disadvantage enforces the requirement that the resist materials be pinhole free and less than 1 μm thick. Conventional spin-coated polymers display unacceptably large pinhole densities and variations of thickness. However, LB films have already demonstrated their capability in this regard. There are good examples of both positive and negative resists, but the best material reported to date is the ω -TA molecule shown in Chart 4.1 (8). In purified form, this material has adequate sensitivity, may be deposited at a rate of 0.5 cm^{-1} to produce uniform coatings in the range 30–90 nm, and has been shown to be capable of a line resolution of 60 nm. The main property that requires some improvement is the etch resistance during plasma processing.

4.5.2.2 SEMICONDUCTOR BARRIER HEIGHT MODIFICATION

Probably the most important role for an LB film in semiconductor technology is the ability of an oriented monolayer to change the effective barrier height at a semiconductor surface. Researchers at the University of Durham first demonstrated the effect on cadmium telluride and showed how it could be used to improve the efficiency of a photovoltaic diode (53). Similar effects have now been confirmed on a variety of materials including ZnSe, InP, GaP, GaAs (54), and related group III–group V semiconductor alloys. The control afforded by the Langmuir–Blodgett technique permits the degree of band bending to be adjusted to suit the particular application (e.g., the increase in efficiency of an electroluminescent diode). In most applications, robust monolayers of phthalocyanine, which can withstand the large current densities involved, have been used. Figure 4.14 shows data for gallium phosphide (55, 56). For convenience, the error bars have been removed.

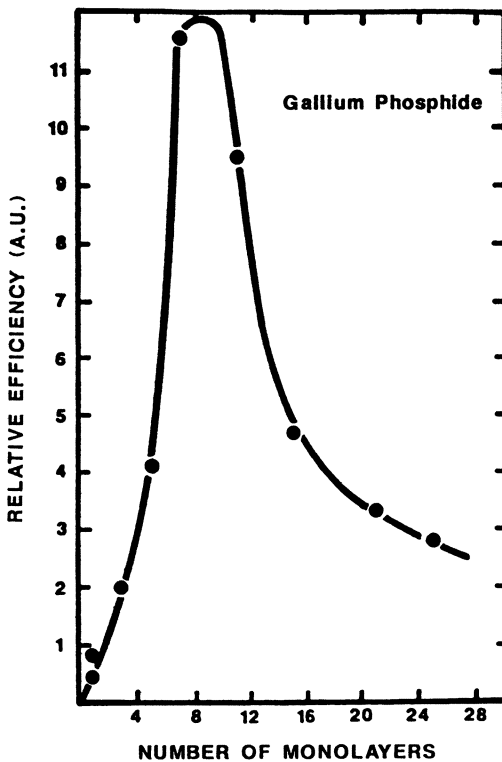
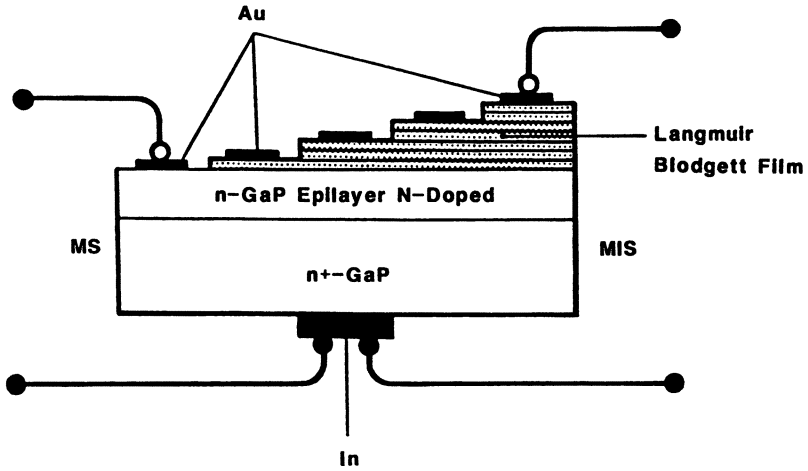


Figure 4.14. Top (not to scale): An Au-LB film-GaP structure. The semiconductor-organic film interface is common to all four devices. Bottom: A plot of the electroluminescent efficiency versus the number of monolayers of substituted phthalocyanine (see reference 55).

The LB thickness required to optimize the electroluminescence efficiency is found to be approximately 21 nm. This value is determined by the ability of minority carriers to cross the semi-insulating phthalocyanine film. Similar results have recently been achieved by using zinc selenide layers grown with MOCVD (57). Blue electroluminescence is observed, provided the organic film is present.

A surface layer on a semiconductor can be produced by many methods. However, experience has shown that when an energetic process such as evaporation, sputtering, or growth from a plasma is used to deposit a thin film onto a semiconductor, a surface-damaged layer is produced that invariably dominates the electrical characteristics of the junctions so formed. However, the Langmuir-trough technique, being a low-temperature deposition process, provides a means of circumventing this particular difficulty. On the other hand, how the substrate is prepared before dipping is of considerable importance in determining the quality of the interface produced. That is, the nascent "oxide" layer formed during the etching procedure remains relatively undisturbed, and this layer can play a vital role even after it has been coated with an LB film. For this reason, a systematic study of the surface chemistry of the semiconductor substrates should be carried out first.

4.5.2.3 TUNNELING DEVICES

Figures 4.8 and 4.9 show how the fine control of thickness available with monomolecular films has been utilized to great advantage in fundamental research, even to dimensions as low as 1 nm. Some researchers have highlighted the benefits of the trough technique to produce tailored materials that might control the critical current, switching speeds, and energy gap parameters in low-temperature devices such as SQUIDS (superconducting quantum interference devices). Certain semiconductor devices (e.g., a floating-gate transistor or a switching structure) also require a uniform, ultrathin insulating film of less than 10-nm thickness.

The result shown in Figure 4.15 is for a bistable switch based on a metal-thin insulator-n-p+ structure. Potential applications of these MISS (metal insulator double semiconductor) devices, if a reproducibly thin, high quality semi-insulating layer can be found, include memories and shift registers. With silicon, oxide layers approximately 3 nm thick can be used, although they are difficult to grow uniformly. For high-mobility group III-V compounds, the difficulties are more severe owing to the lack of a suitable native oxide. However, the current-voltage characteristics shown have been obtained by using GaAs as the semiconductor and the ω -TA molecule shown in Chart 4.1 as the insulator (59). Operation for 10^7 cycles at 100 Hz does not degrade the switching characteristics, which are insensitive to illumination and temperature.

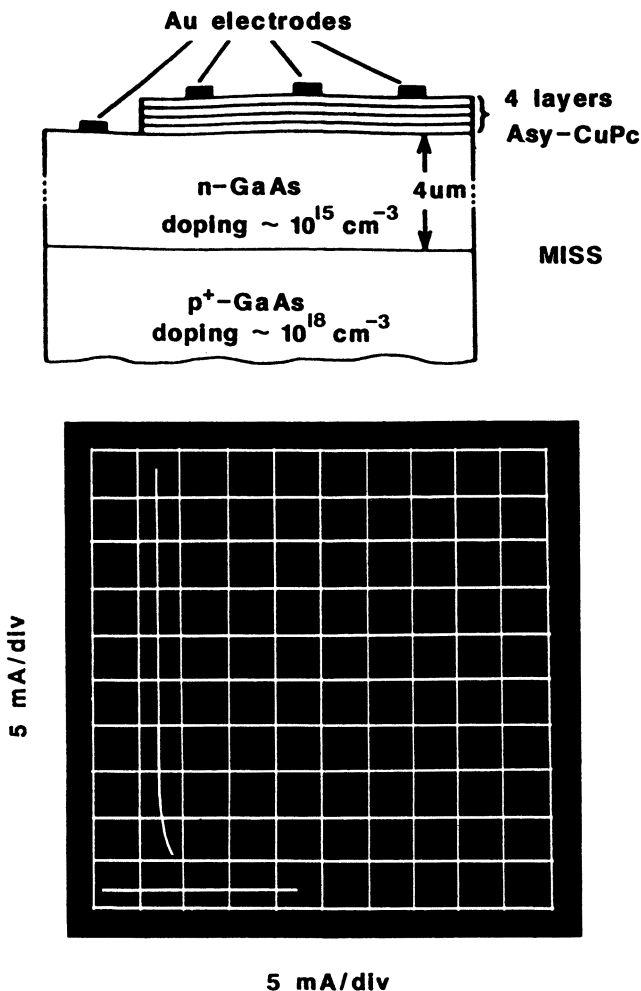


Figure 4.15. Top: Cross section of a MISS diode. The device can be regarded as a reverse-biased metal-insulator-semiconductor diode in series with a forward-biased n - p^+ junction. It then exhibits two stable states separated by an unstable negative resistance region. Bottom: Current-voltage characteristics for a GaAs- ω -TA MISS device. The LB film thickness is approximately 9 nm (see reference 59).

4.5.3 Sensors and Transducers

The fact that organic compounds normally respond more positively than inorganic materials to external stimuli such as pressure, temperature, or radiation provides a means of making sensitive transducers. Moreover, by controlling the architecture of the LB film, the interactions can be designed to be of a lock-key type; thus, the selectivity of the device can be enhanced.

Another advantage of ultrathin organic films is their fast response and recovery times because so little material is present.

The amplifying features of an electronic device can be combined with the attributes of an LB film to form sophisticated microsensors. However, optical and acoustic devices frequently show interesting threshold or resonance effects that can also form the basis of useful sensors. In this section, detailed results are presented only for acoustoelectric devices.

4.5.3.1 SEMICONDUCTOR DEVICES

The good insulating properties of LB films suggest their possible use in field-effect devices, not so much to compete with existing semiconductor technology, but to capitalize on the advantages of being able to incorporate an organic layer within a semiconductor structure. Figure 4.16 shows schematic

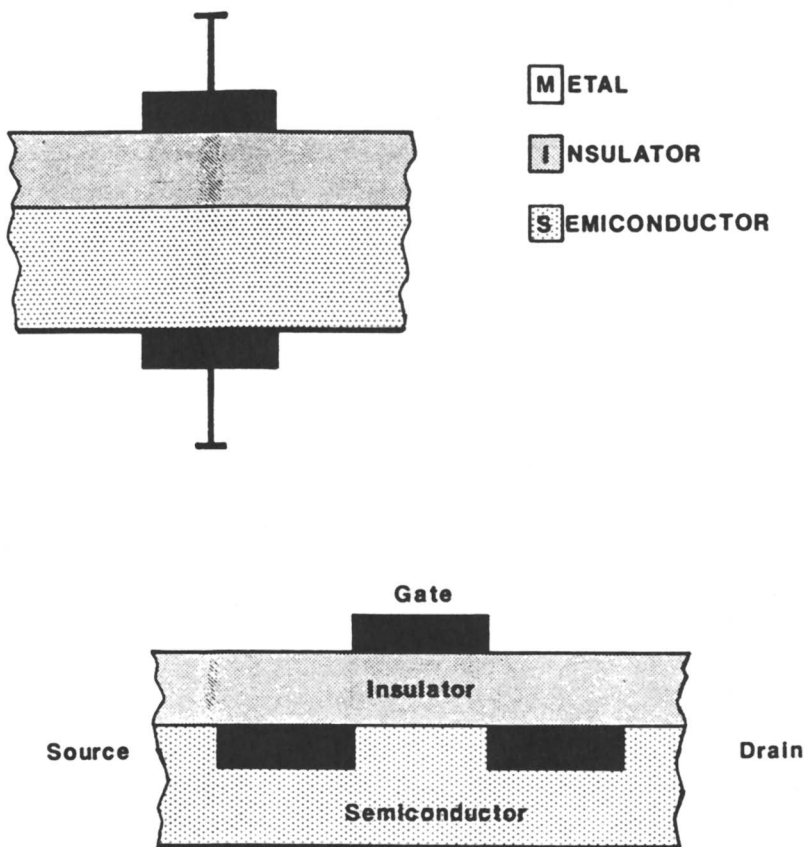


Figure 4.16. Schematic diagrams (not to scale) showing (top) a metal-insulator-semiconductor (MIS) that forms an integral part of the field-effect transistor (bottom).

diagrams of both a field-effect transistor (FET) and the "heart" of this device, which is the metal-insulator-semiconductor (MIS) diode. Conventionally, these devices are made by using inorganic materials; silicon holds a preeminent position, mainly because of the insulating qualities of its native oxide. The first transistor incorporating LB monolayers as the insulator was obtained several years ago (60) with the type of three-terminal device (Figure 4.16) based on indium phosphide and cadmium stearate. Roberts et al. (60) showed that the channel conductivity between the source and the drain could be modulated by the action of a gate electrode. Subsequently, other semiconductors have been used, and results have confirmed the ease with which a range of single-crystal surfaces can be accumulated, depleted, or inverted with an applied voltage. In all cases, the LB film is deposited on top of a nascent "oxide" layer, and the insulation is provided essentially by a double dielectric structure.

Following the nonlinear physics work described earlier, pyro- or piezo-FETs based on insulating LB films with an in-built polarization, or field-effect devices incorporating biological membranes, can be envisaged. Furthermore, the discussion of microelectronic LB film based on sensors does not have to be confined to MIS or FET structures. For example, the switching voltage of the bistable switch described in Figure 4.15 or the characteristics of a gate-controlled diode could be made very sensitive to a change in ambient conditions (61).

4.5.3.2 OPTICAL SENSORS

One area that is receiving particularly strong attention is that of surface plasmon resonance (SPR) (62). The principle of this optical detection method is illustrated in Figure 4.17. A surface plasmon is a surface charge density wave at a metal surface. If the metal is sandwiched between two materials of different dielectric constants, then resonances can occur. This phenomenon is observed as a very sharp minimum of the light reflectance when the angle of incidence (θ) is varied. The resonance angle is ultrasensitive to variations in the refractive index of the medium adjacent to the metal film. For example, the small change in an organic material due to gas absorption can easily be monitored even for concentrations in the parts-per-billion range. In a practical situation, one normally selects an angle of incidence approximately halfway down the reflectance minimum curve when no special gas is present; the change in intensity of the reflected light is then monitored at a constant angle.

Widespread interest has arisen in the potential of LB films as biosensors because many believe that the incorporation of biological molecules such as enzymes will lead to novel devices. Some are exploring the deposition of biologically active molecules onto the gate electrodes or oxides of field-effect transistors, but optical sensors, probably based on fiber optics, are the most favored technique. In all cases, the aim is to couple the specificity of inter-

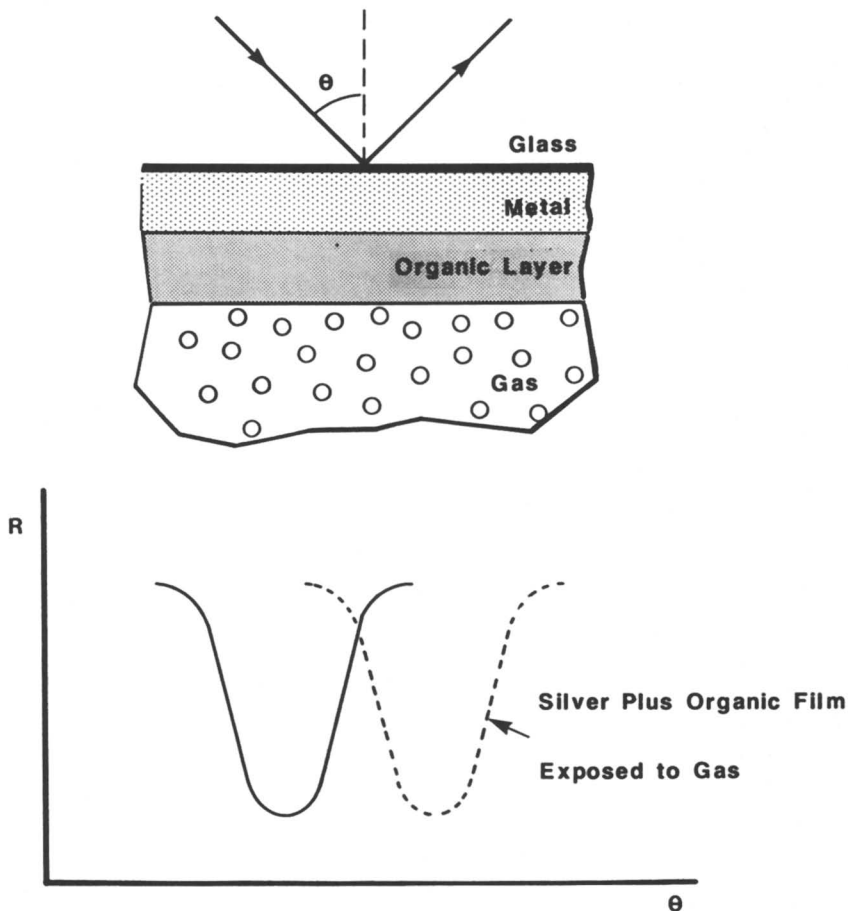


Figure 4.17. Schematic diagrams illustrating the basis of the surface plasmon resonance technique. Top: A beam of radiation striking the back surface of a glass prism coated with a metal film (usually evaporated silver). The reflected intensity and angle of reflection are extremely sensitive to variations in the dielectric on the metal surface. Bottom: Shift in the R vs. θ plot when the organic film is exposed to a gas.

action of chemical or biochemicals with proteins or enzymes (e.g., the change in their molecular conformation) with the sensitivity and signal transduction properties of the device. Stability and lifetime may be problem areas, and, for this reason, cross-linked polymers are being explored as the hosts for the active species.

4.5.3.3 ACOUSTOELECTRIC DEVICES

When materials are added or removed from a vibrating body, its resonant frequency is changed. This phenomenon has been used for mass determi-

nation, normally with a resonator made of piezoelectric quartz cut with a specific crystallographic orientation. A more sophisticated acoustoelectric microgravimetric sensor is a surface acoustic wave (SAW) structure. Such devices had a great impact in the field of signal processing, especially as filters and delay lines. The absorption of a gas introduces minute changes in the mass of a sensing layer. Thus, both bulk quartz oscillators and SAW devices can form the basis of gas detectors.

4.5.3.4 QUARTZ OSCILLATOR

Traditionally, the most common technique to check the reproducibility of LB film monolayer deposition has been the capacitance method, where the aim is to produce good linear plots of inverse capacitance versus number of layers (Figure 4.7a). However, this technique involves evaporating metal contacts onto the organic film and possibly damaging the surface region. The use of simple quartz oscillators circumvents this difficulty (63). Typical results for piezoelectric crystals loaded with LB films of ω -TA and *t*tb PcSiCl_2 , are shown in Figure 4.18. The reproducibility of the dipping process is confirmed by the linear relationship between the change in the resonant frequency (Δf) and *N*, which is the number of monolayers. The resolution of the measurement system used was 0.1 Hz. This resolution enables single monolayer films to be detected with little difficulty. The responses to ammonia and hydrogen sulfide of quartz crystals coated with five-monolayer-thick films of ω -TA are shown in Figure 4.19. In all cases, the coatings responded reversibly to the presence of gases at room temperature; the lowest detection limit using the single crystal resonators was approximately 1 ppm. These results demonstrate that Δf varies approximately linearly with gas concentration in the range 5–100 ppm. The magnitude of the responses for both gases was the same for both three- and five-layer films, a result suggesting that the coated crystals are responding principally to surface adsorption. These results were obtained for an LB film material developed for applications other than sensors. Nevertheless, they demonstrate the enormous potential of the technique using specially tailored receptor molecules for specific target gases. In a practical device, a differential sensing system would be preferable over one using a single crystal oscillator as described here. That is, the gas-sensitive coated crystal would be examined in conjunction with an identical reference uncoated crystal.

4.5.3.5 SURFACE ACOUSTIC WAVE OSCILLATOR

The most common SAW devices are based on quartz or lithium niobate. Eventually, piezoelectric LB films may be used to launch the surface waves. To date, however, the reported values of the piezoelectric coefficients in monolayers are too small (64). In SAW devices, input and output interdigitated electrodes are defined with lithography. These electrodes perform

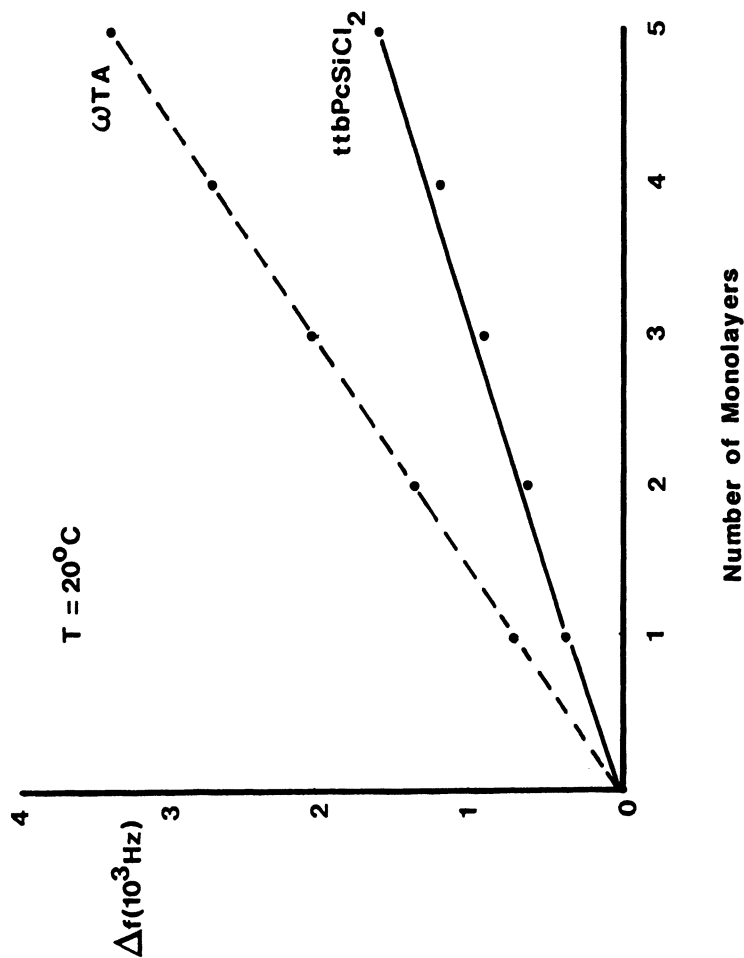


Figure 4.18. The change in resonance frequency of 18-MHz piezoelectric quartz crystals coated with LB films of different thicknesses. The molecular structures of the organic films are shown in Figures 4.2b and 4.2d.

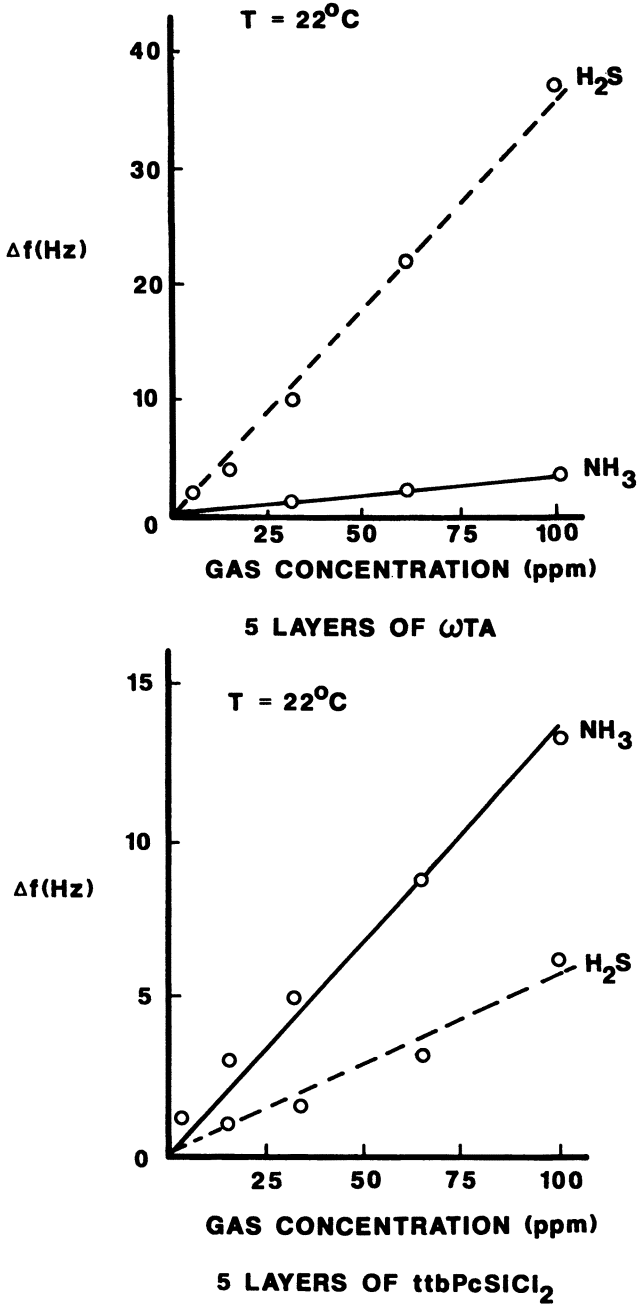


Figure 4.19. Response characteristics of (top) a substituted phthalocyanine-coated (see Chart 4.1d) quartz crystal and (bottom) ω -TA to hydrogen sulfide and ammonia.

the conversion between electric and acoustic energy. The single-crystal surface region between the transducers serves as a propagation path for acoustic waves and thus forms a delay line. Figure 4.20 shows a dual line configuration specially designed for sensing purposes. Basically, the device comprises two identical SAW oscillators positioned alongside each other. The hatched regions are earth-shielded to minimize reflections and cross-talk between the two oscillators. The selective coating is placed in the propagation path of one of the oscillators; thus, the delay time is affected. The relative shift in frequency between the two oscillators is measured by first using a mixer circuit to obtain the difference frequency and then passing the resulting signal through a low-pass filter. The change in frequency (Δf) between the two channels is then directly attributable to the sensor layer. Other extraneous effects, such as those due to temperature changes, are eliminated or very much reduced. Other geometries (e.g., a SAW resonator) are also possible.

This delay line has provided results for both insulating and semiconducting LB films. Figure 4.21 shows results for a substituted phthalocyanine molecule deposited onto a lithium niobate device. As expected, the velocity change Δv scales almost perfectly with the number of deposited layers. Similar data for insulating LB films also yield straight line graphs; thus, the change is governed purely by simple microgravimetric effects. Therefore, a SAW device provides essentially the same information as that obtained with single-crystal resonators. However, they do offer increased sensitivity because even with single monolayers, frequency changes in excess of 1 kHz are observed.

Contrasting results are obtained when a more conducting LB film (66) is deposited onto the SAW device. Additional effects are introduced as a result of interactions between the SAW and mobile charges in the organic layer. Figure 4.22 shows the fractional velocity change observed for different numbers of layers of a substituted pyridinium tetracyanoquinodimethane (Py-TCNQ). The shape of the characteristic is quite different to that shown in Figure 4.21. By subtracting the component due to mass-loading effects, the conductivity of the surface film can be measured. For films of different thickness, a conductivity of approximately $0.5 \Omega^{-1} \text{ cm}^{-1}$ is obtained. Such an experiment is difficult to achieve by means other than the Langmuir trough because for films thicker than a few tenths of a nanometer, mass loading effects dominate those due to the electric field.

The ability to separate electric field and mass loading effects when the devices are exposed to gases means that much more selectivity is possible. Other device geometries (e.g., a SAW resonator) could also be used to similar effect. In conclusion, the combination of a device capable of measuring mass changes as low as femtograms per square centimeter, and the ability to detect minute changes in the electrical characteristics of a monolayer, provide support for sensors based on SAW devices and LB films. For sensors,

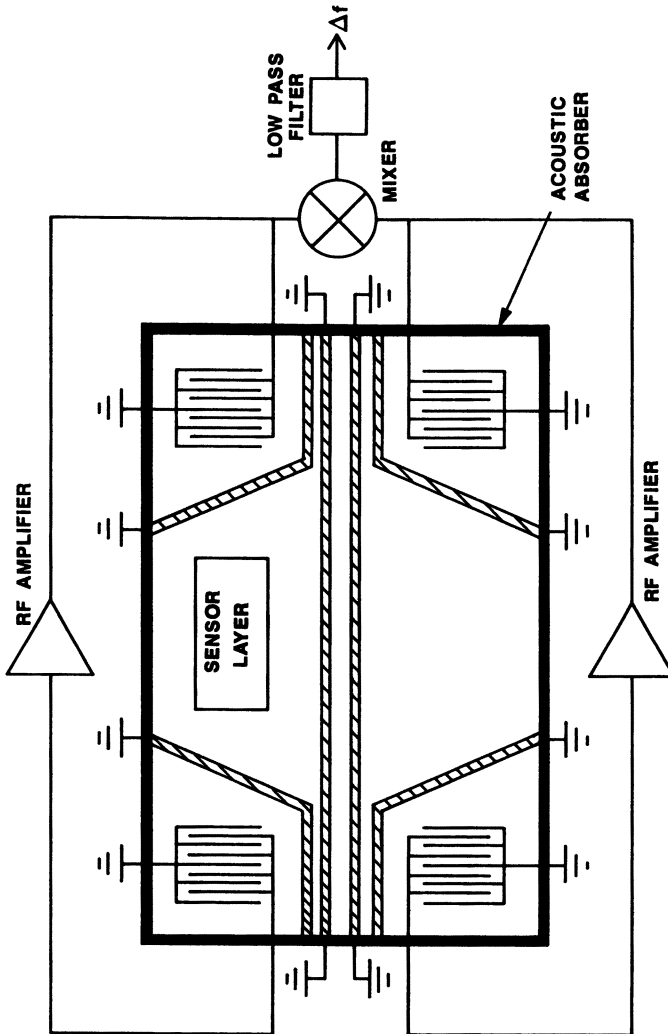


Figure 4.20. A SAW dual delay line oscillator. The sensitive layer is placed in the propagation path of one of the two SAW devices. The difference in frequency (Δf) between the two channels provides a direct result of the mass loading and electric field effects associated with the sensor layer. (Reproduced with permission from reference 65.)

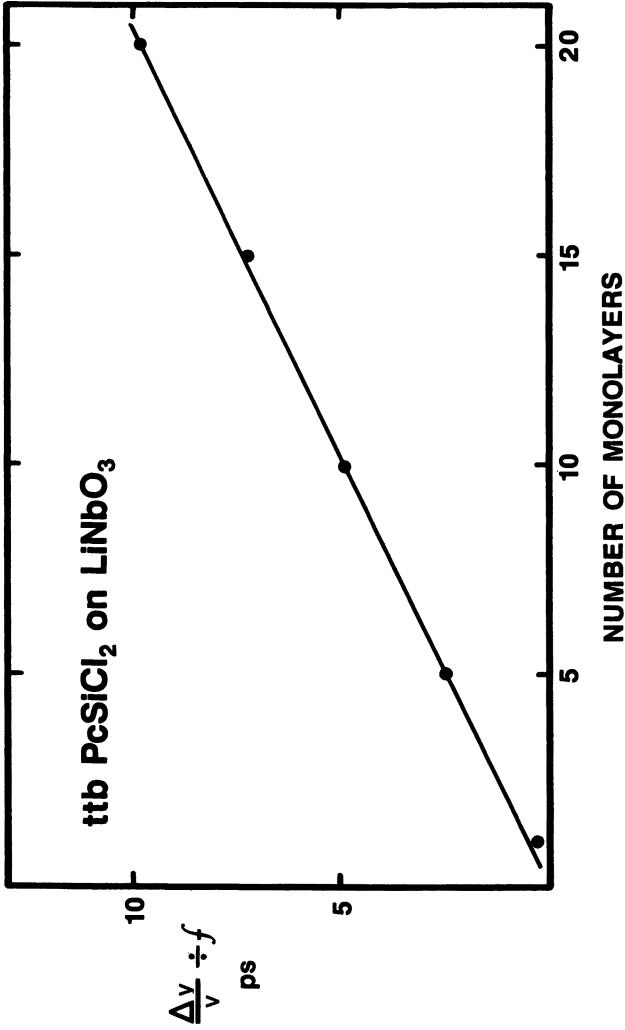


Figure 4.21. Fractional change in velocity divided by resonant frequency for a lithium niobate dual delay line SAW device coated with different multilayer thicknesses of the molecule shown in Chart 4.1d.

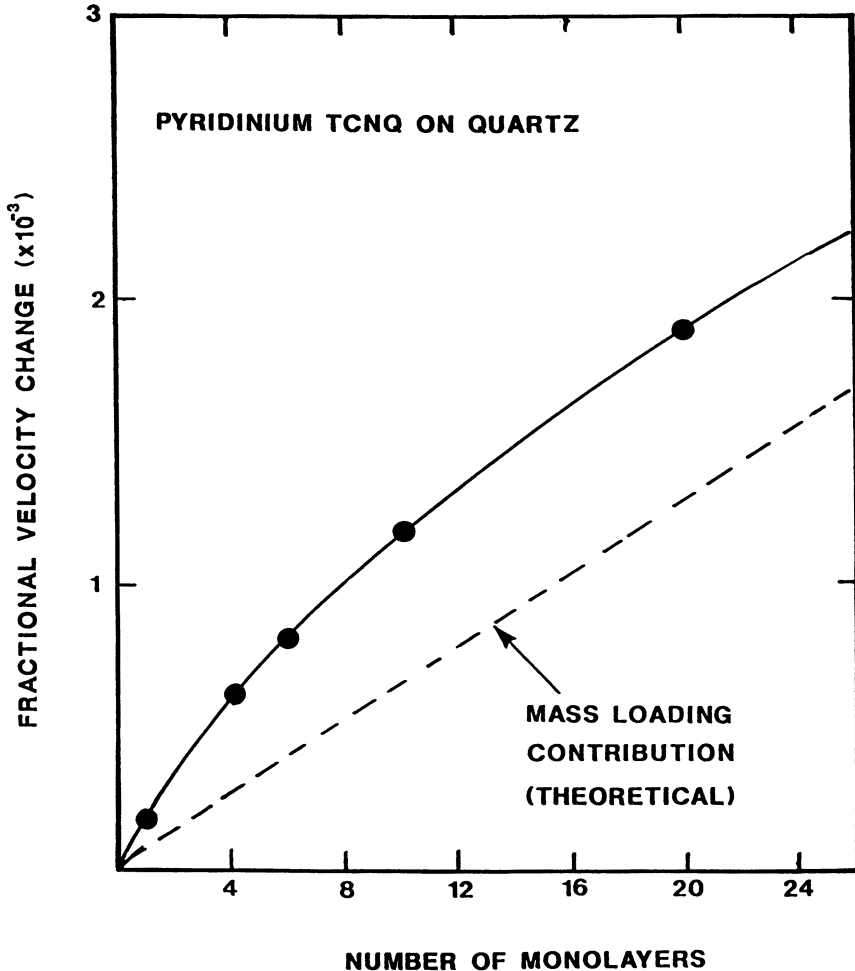


Figure 4.22. Fractional change in velocity in a quartz dual delay SAW device coated with N monolayers of Py-TCNQ. The full curve shows the computer fit to the experimental points by using a resistivity of $2 \Omega \text{ cm}$.

the selective and sensitive layer needs to be exposed to the environment. The formation of robust films is, therefore, essential for this application.

4.6 Molecular and Supramolecular Electronics

Several research areas have been discussed where a tangible benefit results in using monomolecular assemblies rather than organic or inorganic thin films deposited by other means. Organic films can be produced in many

ways, and the onus will be on the LB enthusiasts to demonstrate the special advantages gained from their technique for a particular application. This proof will probably occur, but it will require the combined efforts of high caliber teams with knowledge of physics, chemistry, electronics, and biology. The ability of the synthetic chemist to manipulate the molecular architecture of a material to optimize a specific physical parameter or figure of merit will be vital. However, the role of the physicist or engineer in identifying the targets and guiding the main thrust of the research program will also be essential. Industry is already able to organize interdisciplinary activities. The relatively inexpensive equipment requirements associated with the Langmuir-trough technique coupled with the elegance of the fundamental science and the interesting applied prospects for LB films provide an excellent opportunity for the academic community to similarly breakdown the traditional barriers between disciplines. At the present time, nonlinear optics, thermal imaging, sensors, and optical storage are the areas most likely to benefit from LB film technology.

Only a modest diminution in the size of electronic circuit components is required before the scale of individual molecules is reached. In fact, many existing circuit elements could already be accommodated within the area occupied by a leukemia virus. To achieve switching on a molecular scale, the requirements of reliability and testing of complex structures suggest a systems approach rather than the traditional one that uses the properties of individual circuit elements. Sequential designs, because of their vulnerability, will likely be abandoned in favor of supermolecular arrays acting as concurrent processor networks.

Three-dimensional integration is extremely difficult to obtain with silicon technology, and chemically nonspecific methods such as molecular beam epitaxy are relatively crude. A self-assembly technique is a far more attractive alternative if regular, three-dimensional, ordered structures are required. This requirement involves the construction of unique assemblies whose architectures depend on the shapes and charge distributions of the units from which they are built as distinct from the methods used to assemble them. Organic monomolecular films deposited by using the Langmuir-trough technique are associated with a considerable degree of self-assembly. Therefore, in the long term, LB films may well be viewed as having contributed toward the ambitious goal of a supermolecular information processor.

Pursuing this target should serve to enumerate technologies and identify areas of basic scientific research that would otherwise remain dormant and unexplored. Far simpler but novel devices based on organic molecular materials should appear as a result of this research effort. Langmuir-Blodgett films will most likely play a key role in helping scientists identify basic physical phenomena in supermolecular assemblies and at the same time enable engineers to become more familiar with devices incorporating organic films.

Abbreviations and Symbols

α	tensor quantity
β	tensor quantity ϵ permittivity
γ	tensor quantity
λ	wavelength
μ	individual dipole moment
ω -TA	ω -tricosenoic acid
A	cross sectional area
C	capacitance
d	distance between chromophores
E	electric field
f	frequency
FET	field-effect transistor
I_0	fluorescence intensity in the absence of an acceptor layer
I	1. fluorescence intensity in the presence of an acceptor layer 2. pyroelectric current
LB	Langmuir–Blodgett
MBE	molecular beam epitaxy
MIS	metal-insulating semiconductor electrode
MISS	metal-insulating double semiconductor
MOCVD	organometallic chemical vapor deposition
p	pyroelectric coefficient
P	macroscopic polarization of a solid
PTS-PDA	bis(<i>p</i> -toluenesulfonate-2,4-hexadiyne-1,6-diol
PVDF	poly(vinyl difluoride)
Py-TCNQ	pyridinium tetracyanoquinodimethane
Q	charge
RHEED	reflection high-energy electron diffraction
S	sensitizing molecule
SAW	surface acoustic wave
SPR	surface plasmon resonance
SQUIDS	superconducting quantum interference devices
V	voltage

Acknowledgments

I am indebted to my colleagues and former colleagues at the Universities of Durham and Oxford for their important contributions to the research described in this chapter. I thank, in particular, M. C. Petty and B. Holcroft. The LB film research work at the Department of Engineering Science at Oxford University is financed by Thorn EMI plc.

References

1. Langmuir, I. *J. Chem. Phys.* **1933**, *1*, 756
2. Blodgett, K. B. *J. Am. Chem. Soc.* **1935**, *57*, 1007
3. Kuhn, H.; Möbius, D.; Bücher, H. *Phys. Methods Chem. Part 3B* **1972**, *1*, 577
4. Roberts, G. G. *Adv. Phys.* **1985**, *34*, 475
5. Gaines, G. L. *Insoluble Monolayers at Liquid-Gas Interfaces*; Interscience: New York, 1966
6. Roberts, G. G.; Pitt, C. W. *Thin Solid Films* **1983**, *99*
7. Gaines, G. L. *Thin Solid Films* **1985**, *132-134*
8. Barraud, A.; Rosilio, C.; Ruaudel-Teixier, A. *Thin Solid Films* **1980**, *68*, 91
9. Tieke, B.; Wegner, G.; Naegele, D.; Ringsdorf, H. *Angew. Chem. Int. Ed. Engl.* **1976**, *15*, 764
10. Bäessler, H. *Adv. Polym. Sci.* **1984**, *63*, 1
11. Hupfer, B.; Ringsdorf, H. *Chem. Phys. Lipids* **1982**, *33*, 263
12. Albrecht, O.; Johnston, D. S.; Villaverde, C.; Chapman, D.; *Biochim. Biophys. Acta* **1982**, *165*, 687
13. Tredgold, R. H.; Winter, C. S. *Thin Solid Films* **1983**, *99*, 81
14. Vincett, P. S.; Barlow, W. A.; Boyle, F. T.; Finney, J. A.; Roberts, G. G. *Thin Solid Films* **1979**, *60*, 265
15. Hua, Y. L.; Roberts, G. G.; Ahmad, M. M.; Petty, M. C.; Hanack, M.; Rein, M. *Philos. Mag.* **1986**, *53*, 105
16. Holcroft, B.; Petty, M. C.; Roberts, G. G.; Russell, G. J. *Thin Solid Films* **1985**, *134*, 83
17. Takenaka, T.; Fukuzaki, H. *J. Raman Spectrosc.* **1979**, *8*, 151
18. Losche, M.; Rabe, J.; Fischer, A.; Rucha, B. U.; Knoll, W.; Muhwald, H. *Thin Solid Films* **1984**, *117*, 269
19. Neal, D. B.; Russell, G. J.; Petty, M. C.; Roberts, G. G.; Ahmad, M. M.; Feast, W. J. *J. Mol. Electron.* **1986**, *2*, 135
20. Fryer, J. R.; Hann, R. A.; Eyres, B. L. *Nature* **1985**, *313*, 382
21. Heard, D.; Goring, M. J.; Roberts, G. G. *Thin Solid Films* (to be published)
22. Nicklow, R. M.; Pomerantz, K.; Segmuller, A. *Phys. Rev. B* **1981**, *23*, 1081
23. Highfield, R. R.; Thomas, R. K.; Cummins, P. G.; Gregory, D. P.; Mingsins, J.; Hayter, J. B.; Scharpf, O. *Thin Solid Films* **1983**, *99*, 165
24. Blodgett, K. B.; Langmuir, I. *Phys. Rev.* **1937**, *51*, 964
25. Walpita, L. M.; Pitt, C. W. *Electron. Lett.* **1977**, *13*, 210
26. Chen, Y. J.; Tripathy, S. K.; Carter, G. M. *Mol. Cryst. Liq. Cryst.* **1984**, *106*, 403
27. Barraud, A.; Rosilio, C.; Ruaudel-Teixier, A. *Thin Solid Films* **1980**, *68*, 7
28. Brundell, C. R.; Hopster, H.; Swalen, J. D. *J. Chem. Phys.* **1979**, *70*, 5190
29. Laxpuber, L.; Mohwald, H.; Hashmi, M. *Int. J. Mass Spectrom. Ion Phys.* **1983**, *51*, 93
30. Ueno, N.; Gadeke, W.; Koch, E. E.; Engelhardt, R.; Duddles, R.; Laxhuber, L.; Mohwald, H. *J. Mol. Electron.* **1985**, *1*, 19
31. Chollet, P. A. *Thin Solid Films* **1978**, *52*, 343
32. Barkar, M.; Lando, J. B. *Thin Solid Films* **1983**, *99*, 119
33. Knoll, W.; Philpott, M. R.; Swalen, J. D.; Firlando, A. *J. Chem. Phys.* **1982**, *77*, 2254
34. Aroca, R.; Jennings, C.; Kovacs, G. J.; Loutfy, R. O.; Vincett, P. S. *J. Chem. Phys.* **1985**, *89*, 4051
35. Ginnai, T. M.; Oxley, D. P.; Pritchard, R. G. *Thin Solid Films* **1980**, *68*, 241

36. Zanoni, R.; Naselli, C.; Bell, J.; Stegeman, B.; Sprague, R.; Seaton, C.; Lindsay, S., *Thin Solid Films* **1985**, *134*, 179
37. Caufall, H. *Appl. Phys. Lett.* **1983**, *44*, 59
38. Roberts, G. G.; Vincett, P. S.; Barlow, W. A. *J. Phys. C* **1978**, *11*, 2077
39. Allara, D.; Swallen, J. D. *J. Phys. Chem.* **1982**, *86*, 2700
40. Mori, C.; Noguchi, H.; Mizuno, M.; Watanabe, T. *Jpn. J. Appl. Phys.* **1980**, *19*, 725
41. Möbius, D. *Acc. Chem. Res.* **1981**, *14*, 63
42. Flanagan, M. T. *Thin Solid Films* **1983**, *99*, 133
43. Pomerantz, M. *Phase Transitions in Surface Films*; Plenum: New York, **1980**; p 317
44. Albrecht, O.; Laschewsky, A.; Ringsdorf, H. *J. Membr. Sci* **1985**, *22*, 187
45. Glass, A. M.; Patel, J. S.; Goodby, J. W.; Olson, D. H.; Geary, J. M. *J. Appl. Phys.* **1986**, *60*, 2778
46. Blinov, L. M.; Davydora, N. N.; Lazarev, V. V.; Yudin, S. G. *Sov. Phys. Solid State* **1982**, *24*, 1523
47. Christie, P.; Roberts, G. G.; Petty, M. C. *Appl. Phys. Lett.* **1986**, *48*, 1101
48. Zyss, J. *J. Mol. Electron.* **1986**, *2*.
49. Dulcic, A.; Flytzanis, C. *Opt. Commun.* **1978**, *25*, 402
50. Neal, D. B.; Petty, M. C.; Roberts, G. G.; Ahmad, M. M.; Feast, W. J.; Girling, I. R.; Cade, N. A.; Kolinsky, P. V.; Peterson, I. R. *Electron. Lett.* **1986**, *22*, 460
51. Kajzar, F.; Messier, J. *Thin Solid Films* **1985**, *132*, 11
52. Roberts, G. G.; Petty, M. C.; Caplan, P. J.; Poindexter, E. H. *Proceedings of the INFOS (Insulating Films on Semiconductors) 83 Conference*; Verwey, J., Ed.; North Holland: Amsterdam, **1983**; p 141
53. Dharmadasa, I. M.; Roberts, G. G.; Petty, M. C. *Electron. Lett.* **1980**, *16*, 201
54. Winter, C. S.; Tredgold, R. H.; Hodge, P.; Koshdel, E. *Proc. IEE Part I* **1984**, *131*, 125
55. Batey, J.; Roberts, G. G.; Petty, M. C. *Thin Solid Films* **1983**, *99*, 283
56. Petty, M. C.; Batey, J.; Roberts, G. G. *Proc. IEE Part I* **1985**, *132*, 133
57. Hua, Y. L.; Petty, M. C.; Roberts, G. G.; Ahmad, M. M.; Yates, H. M.; Maung, N. J.; Williams, J. O. *Electron. Lett.* **1987**, *23*, 231
58. Larkins, G. L.; Thompson, E. D.; Ortiz, E.; Burkhart, C. W.; Lando, J. B. *Thin Solid Films* **1983**, *99*, 277
59. Thomas, N. J.; Petty, M. C.; Roberts, G. G.; Hall, H. Y. *Electron. Lett.* **1984**, *20*, 838
60. Roberts, G. G.; Pande, K. P.; Barlow, W. A. *Proc. IEE Part I* **1978**, *2*, 169
61. Roberts, G. G.; Petty, M. C.; Baker, S.; Fowler, M. T.; Thomas, N. J. *Thin Solid Films* **1985**, *132*, 113
62. Nylander, C.; Liedberg, B.; Lind, T. *Sens. Actuators* **1982**, *3*, 79
63. Ross, J.; Roberts, G. G. *Proceedings of 2nd International Meeting on Chemical Sensors*; Bordeaux, **1986**; p 704
64. Novak, V. R.; Myagkov, I. V. *Sov. Tech. Phys. Lett.* **1985**, *11*, 159
65. Roberts, G. G.; Holcroft, B.; Ross, J.; Huang, F.; Barraud, A. *J. Polym. Sci.* **1987**, *19*, 401
66. Ruandel-Teixier, A.; Vandevyver, M.; Barraud, A. *Mol. Cryst. Liq. Cryst.* **1985**, *120*, 319.

RECEIVED for review April 15, 1987. ACCEPTED January 20, 1988.

Progress Toward Processable, Environmentally Stable Conducting Polymers

Gregory L. Baker

Bell Communications Research, 331 Newman Springs Road, Red Bank, NJ
07701-7020

The progress toward the development of tractable, environmentally stable conducting polymers is reviewed. Many of the difficulties in developing such materials are a direct result of the high reactivity of the electronic states responsible for high conductivity. Although conducting polymers based on polyenes are generally unstable, environmentally stable substituted polythiophenes, polypyrroles, and poly(arylene vinylene)s have been prepared. Efforts to synthesize tractable conducting polymers have yielded a rich variety of blends, random copolymers, and graft and block copolymers with enhanced processability. The use of soluble precursor polymers has been an especially effective strategy for the preparation of dense anisotropic conducting polymer films.

THE IDEA THAT ORGANIC POLYMERS could be made electrically conductive has stimulated research for more than 20 years (1). Indeed, the first measurements of the conductivity of poly(acetylene) appeared in 1961 (2), only 3 years after Natta's report of the synthesis of polyacetylene (3). Although extensive conjugation was generally considered to be required in an effective organic conductor (or superconductor) (4), the need for the oxidation or reduction of the conjugated system was not fully appreciated. Early work (1) was hampered by the lack of a general theory, or a successful organic conductor to use as a model for the preparation of new materials. Equally important, the intractability of the existing materials, often referred to as "brick dust", discouraged characterization efforts.

0065-2393/88/0218-0271\$07.50/0
© 1988 American Chemical Society

A materials breakthrough led to the current high interest in conducting polymers. Polyacetylene, previously known only as an intractable powder, was prepared as shiny free-standing films (5). The later observation that the controlled oxidation or reduction of polyacetylene films led to highly conducting materials (6) sparked tremendous interest in conducting polymers and their applications (Figure 5.1). This interest was inspired partly by the belief that a polymer with the conductivity of a metal and the physical characteristics of conventional thermoplastics (the "ideal" conducting polymer) would soon be available. Proposed uses for these materials included lightweight conductors, battery electrodes, solar cells, semiconductors, and the basic material for molecular-sized electronic devices. The implementation of conducting polymers in these applications has lagged behind the early predictions of widespread near-term use. This delay can be traced to the difficult problem of preparing stable, tractable conducting polymers for general use.

Although the ideal conducting polymer has yet to be synthesized, spectacular improvements in the conductivity and tractability of conducting organic polymers have been reported. Two principal goals have guided synthetic chemists:

1. the preparation of heat- or solution-processable conducting polymers, and

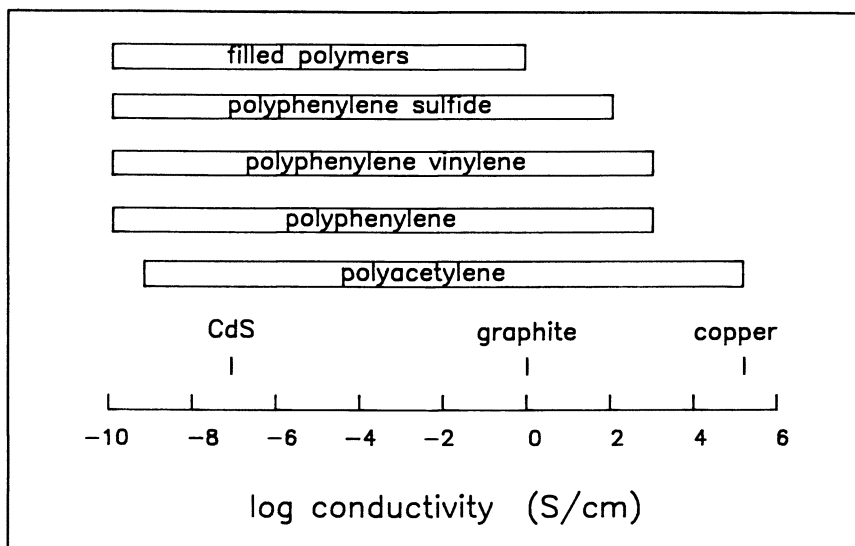


Figure 5.1. Polymers with very different chemical structures can be converted from insulators to conducting materials by controlled oxidation or reduction. The conductivity of the conducting polymer may be as much as 10^{12} times as large as the pristine polymer.

2. the preparation of materials with minimal defects and a high degree of chain alignment.

Processability has obvious benefits, and samples with fewer defects or aligned chains can have significantly higher conductivities and stabilities relative to disordered materials. The most dramatic example of such benefits was the preparation of polyacetylene by using a modified catalyst (7, 8). The resulting material was in many ways spectroscopically identical to that made from standard preparations of polyacetylene, except that it contained few sp^3 defects. The resulting conductivities for iodine-doped samples of stretch-aligned polyacetylene were 1.5×10^5 S/cm, and the electrical anisotropies were around 1000. Accompanying the increase in conductivity was an increase in the environmental stability of the doped polymer. Significant progress has also been reported in making tractable conducting polymers. Solutions of conducting polymers in both their neutral and doped states have been prepared, and even water-soluble conducting polymers have been synthesized. Latexes are now available that dry to yield conductive films.

In this chapter, the progress toward making conducting organic materials tractable and stable enough for electronic applications is reviewed. Because the general field of conducting polymers has been reviewed many times (9, 10), this chapter will focus almost entirely on the issues of stability and tractability by using the literature references available in June 1987. Because of the breadth of the field, not all materials popularly described as conducting polymers are included in this review. For example, the area of conducting composites is not comprehensive because a good review of composites should also include polymers filled with carbon black, metal particles, and inorganic fillers. Inorganic and organometallic conductors (e.g. the phthalocyanines) are beyond the scope of this review and will not be covered.

This chapter will first review the electronic states responsible for high conductivity in organic polymers (11) to provide insight into the design of stable organic conductors. Next, the efforts to impart environmental stability to the polymers will be described. Finally, the principal efforts toward the preparation of tractable conducting polymers will be discussed.

5.1 Electronic States of Conducting Polymers

Although the exact mechanisms by which charge is transported in conducting polymers are still disputed (12, 13), it is still useful to examine the simple one-electron model for the electronic states formed in organic polymers upon oxidation or reduction (*doping*). (Detailed discussions of this model can be found in reference 9.) These states are not necessarily synonymous with their being charge carriers, but they do represent the chemistry of doping. The model also provides guidelines for the synthesis of new conducting polymers and illustrates why most conducting polymers have limited stability.

For this exercise, conjugated polymers can be divided into two groups: those with degenerate ground states such as *trans*-polyacetylene and poly(phenylene methine), and those without degenerate ground states, such as nearly all other conducting polymers (Figure 5.2). On an infinite polyene chain, the transposition of single and double bonds yields energetically equivalent structures. This situation is to be contrasted with poly(*p*-phenylene), where a similar transposition leads to the formation of a quinoid structure of significantly higher energy. This difference leads to qualitatively different electronic structures for the two polymers.

The reduction (oxidation) process (Figure 5.3) consists of adding (removing) one electron to the polymer chain, which causes the injection of states from the top of the valence band and bottom of the conduction band into the gap. This radical anion (cation), commonly termed a *polaron*, carries both spin and charge. Addition (removal) of a second electron forms a second polaron, which can lower the total energy of the system through dimerization and yield a *bipolaron*. In the special case of polymers with degenerate ground states, the excitations can further lower their energy by separating to yield two independent states (*solitons*) at one-half of the gap energy. This separation is possible because a polyene segment of equivalent energy is formed between the charges as they separate.

In polymers with nondegenerate ground states, the chemistry is similar, but pairs of solitons cannot completely separate because a polymer segment of higher energy would form between the charges. Thus, for poly(*p*-phenylene) (Scheme 5.1), the formation of the less stable quinoid structure acts as a restraint to the development of independent soliton pairs, and instead, a bipolaron results. The signature of the bipolaron is the presence of three electronic transitions with energies less than the gap energy, whereas the soliton exhibits only one electronic transition. Electronic structures similar

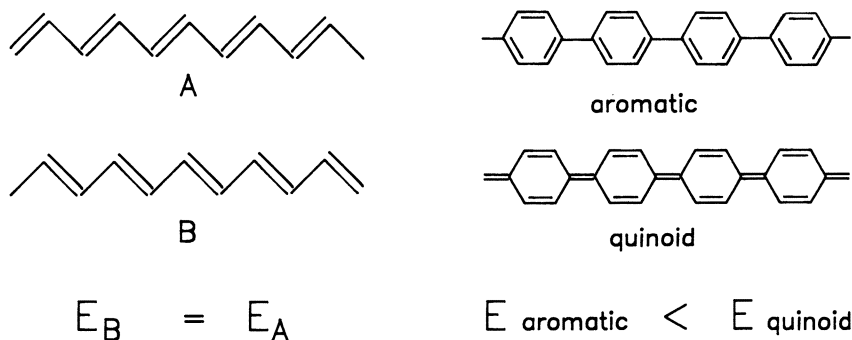


Figure 5.2. A, Poly(*p*-phenylene) and B, *trans*-polyacetylene. These compounds are, respectively, prototypes for polymers with nondegenerate (aromatic structure) and degenerate (quinoid structure) ground states. The symbol E denotes the energy.

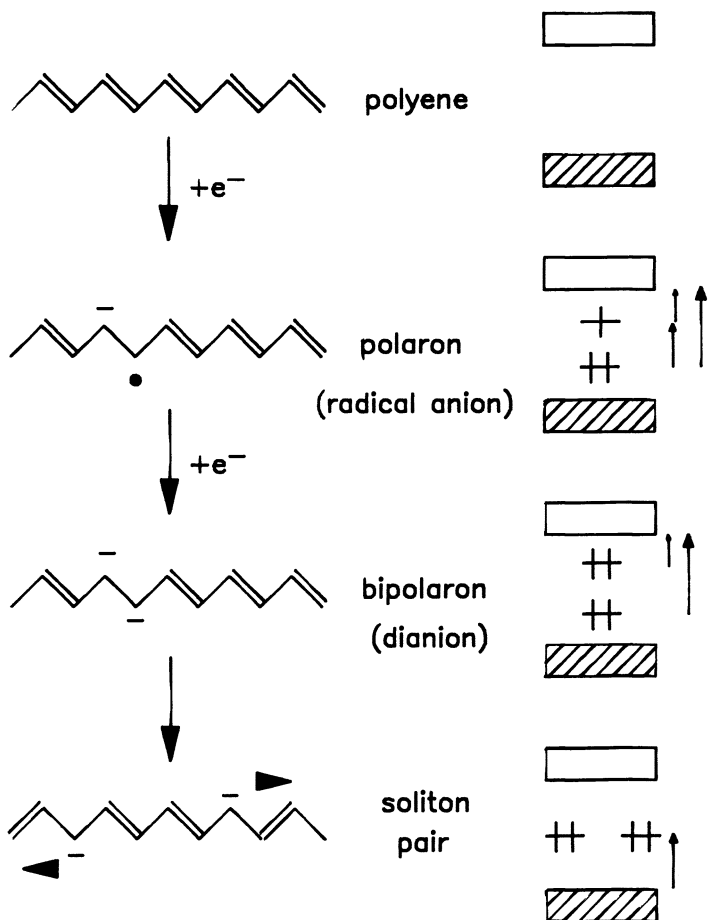
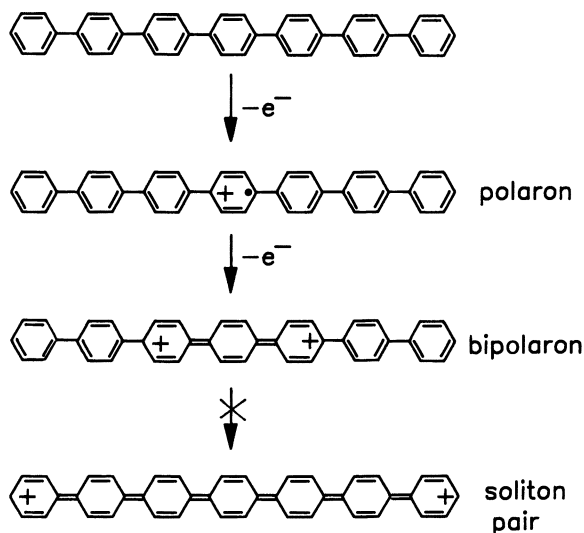


Figure 5.3. The reduction (doping) of *trans*-polyacetylene. In the ideal case, the mobility of the charged states allows the bipolaron to collapse into a pair of solitons.

to that of poly(*p*-phenylene) are expected for most conducting polymers because few have the degenerate ground state required for soliton formation. The presence of these excitations has been experimentally confirmed in polyphenylene (14), polypyrrole (15), polythiophene (16), and other conducting polymers.

Although the simple one-electron model as described here (electronic correlations, screening, or counterion effects have not been considered) is inaccurate in the detailed description of the electronic states of conducting polymers, it is useful to consider the problem of environmental stability in light of the types of electronic states formed on doping. In this chapter, the term *stability* is narrowly defined as the maintenance of conductivity. Be-



Scheme 5.1. The oxidation (doping) of poly(p-phenylene). The bipolaron is the final oxidation product in poly(p-phenylene) and other polymers with nondegenerate ground states.

cause conductivity is related to the number and type of doping sites in the polymer, stabilization becomes an effort to minimize doping site loss by chemical degradation or doping site quenching by such contaminants as O_2 or water.

If a polaron, soliton, or bipolaron is considered to be confined to an oligomeric conducting polymer chain, then for a polymer such as polyacetylene, the high chemical reactivity of oxidation or reduction sites would result in their having an extremely limited lifetime outside the friendly confines of the dry box. What then allows such states to persist in their polymeric analogues and be responsible for the high conductivity of doped polymers? The answer can be a combination of several factors. For small molecules (H_2O , O_2), stability may be a consequence of their much slower diffusion rates in the polymer matrix. This effect can be exploited by barrier layers that encapsulate the polymer or by improved, denser morphologies that minimize the surface area. For example, simply pressing polyacetylene films (17) had a significant stabilizing effect. Low-density polyacetylene films ($\rho \sim 0.5 \text{ g/cm}^3$) pressed at $1.3 \times 10^5 \text{ psi}$ resulted in a six-fold reduction in surface area and an oxidation rate 5.6 times less than unpressed films. The diffusion rate of iodine into and out of pressed films was reduced by compacting the samples.

If, however, instability is related to the propensity of the doping sites to undergo further chemical transformations, then those sites must be immobilized in the conducting polymer. The reaction of bromine with solid

polyacetylene (18) and soluble polyacetylene block copolymers (19) illustrates the stabilizing effect of the crystalline matrix of polyacetylene. In the soluble material, bromine added to the double bonds to yield a saturated nonconducting product, but in crystalline polyacetylene, the polymer became conductive. The difference in the behavior of the two polymers was a matter of kinetics. With time, bromine added across the double bonds in solid polyacetylene (18) as well, yielding the brominated polymer. Thus, the effect of the stiff polymeric matrix of polyacetylene was to stabilize those oxidation sites responsible for conductivity.

The implication that flexible polymers should be poor candidates for conducting polymers is not necessarily true. Flexible polymers have been converted to conducting polymers via carbon-carbon bond formation, which transforms the flexible polymer to a rigid, conductive polymeric material. The oxidation of poly(phenylene sulfide) by AsF_5 may be such an example. The detection of a variety of fused-ring structures (20, 21) in the oxidized product suggests a series of acid-catalyzed rearrangements that convert the processable polymer into a rigid, cross-linked but conductive polymeric material (Chart 5.1). Further rearrangements are limited by the rigidity of the matrix that immobilizes the doping sites. Carried to its extreme, oligomers of polyphenylene (terphenyl and biphenyl) are converted to intractable conducting polyphenylenes upon treatment with AsF_5 (22).

The preferred route to stable conducting polymers is to engineer stability into the monomer unit. Thus, although both neutral and doped polyenes are unstable toward molecular oxygen, doped polypyrrole and

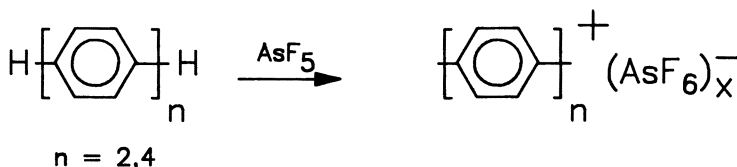
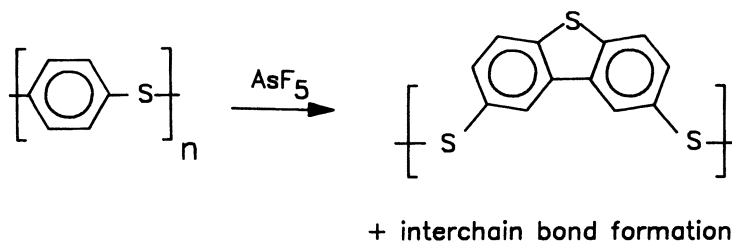


Chart 5.1. Oxidizing dopants can convert flexible polymers or monomers to rigid conducting materials.

polythiophenes are robust and reflect the increased stability of the heterocyclic monomer units toward oxidation. Variations in stability are reflected in the difference in the oxidation and reduction potentials of conducting polymers (23).

5.2 Stabilization of Conducting Polymers

In a practical sense, the stability or instability of a conducting polymer can only be defined with respect to its intended use. Materials with limited environmental stability might be useful for applications requiring moderate conductivities such as antistatic packaging ($<10^{-2}$ S/cm), whereas an application such as the electrode for a rechargeable battery has a different set of requirements. Various methods have been explored by which the stability of conducting organic polymers might be improved. Among these methods are encapsulation techniques, the use of barrier resins, sacrificial layers, and the traditional antioxidants useful for the stabilization of organic polymers. These methods are all aimed at reducing the sensitivity of the conducting polymer to the environment; inherent thermodynamic instabilities of conducting polymers are unaffected by such schemes.

5.2.1 Encapsulation Techniques

Polyacetylene and a variety of polyacetylene copolymers were found to be partially stabilized by encapsulation in oxygen barriers such as glass and several organic polymers. Iodine-doped polyacetylene was unstable when silicone rubber, polyethylene, polyurethanes, or epoxy resins were employed as the barrier (24). Only glass proved effective; the other materials were only slightly better than no barrier at all. When an iodine-doped polyacetylene sample having an initial conductivity of 300 S/cm was totally encased in a thick (400 μm) epoxy matrix (25) and the conductivity was monitored externally by using a microwave technique, the conductivity decreased by a factor of 10 in 50 days but then remained stable for up to 250 days. This enhancement in stability was thought to be a result of the sample's total encasement in the epoxy matrix; no electrical leads led from the polyacetylene to the outside environment.

Much better stability was reported for AsF_5 -doped polyacetylene coated with poly(*p*-xylylene) (26), which is an excellent barrier toward oxygen and water. Samples having conductivities of 260 S/cm were coated by vacuum deposition; thus, the initial concentration of oxygen in the sample was low. After 24 h in air, a conductivity loss of 10% was observed for treated films, whereas the conductivity of uncoated control samples decreased by a factor of 3. After 1 month, the coated samples had a conductivity of 150 S/cm, whereas that of the control was only 11 S/cm. From isothermal aging studies, the poly(*p*-xylylene) coating was found to increase the first-order activation energy for conductivity loss by 2.4 Kcal/mol, from 17.2 to 14.8. These data

underestimate the efficacy of poly(*p*-xylylene) encapsulation because AsF₅-doped polyacetylene degrades even in the absence of air and moisture (27, 28).

5.2.2 Chemical Stabilization

The utility of classical antioxidants such as hindered amines, phenols, and nitrones for the stabilization of pristine polyacetylene (29), poly(methyl acetylene) (30), and poly(1,6-heptadiyne) (31) has been examined. Poly(methyl acetylene), although dopable to only low conductivities (10⁻⁵ S/cm), has similar oxidative behavior to polyacetylene and serves as a good model for other polyenes. In general, the improvement in stability of poly(methyl acetylene) was limited, but combinations of hindered phenols and hydroperoxide scavengers resulted in a factor of 5 decrease in the oxidation rate (30) as monitored by the appearance of IR absorption bands attributable to carbonyl groups. These degradation rates are still too high for the use of these polyenes in an unprotected environment. The compatibility of such stabilizers with the dopants commonly used for polyacetylene was not studied.

The addition of *N*-bromosuccinimide (NBS) to pristine polyacetylene stabilized the undoped polymer (32). The enhanced stability was attributed to the reaction of NBS with the numerous free radicals found in polyacetylene, as evidenced by the decreased rate of oxygen uptake in treated samples and increased final conductivities for iodine-doped polyacetylene. The conductivity of the undoped polymer rose from 10⁻⁵ S/cm for untreated samples to greater than 10⁻⁴ S/cm for NBS-treated samples. A slight amount of Br₃⁻ was detected in treated samples; this finding indicates that some doping accompanies the treatment. The stability of doped polymer samples was not significantly improved by this treatment.

The reaction of dienophiles with polyacetylene (33) was investigated for limiting the decomposition of the polyene. Previously, intermolecular Diels–Alder reactions involving *cis* bonds were believed to form cross-links and render polyacetylene intractable, and that their elimination would lead to soluble products (34). No reaction of maleic anhydride or benzoquinone with polyacetylene was observed. In contrast, a second study (35) described the successful formation of the Diels–Alder adduct of maleic anhydride with remnant *cis* bonds in thermally isomerized samples of *trans*-polyacetylene. These data were used to support the notion that the thermal isomerization process used to convert *cis*-polyacetylene to the *trans* isomer does not go to completion. Unfortunately, the effect of this transformation on the tractability or stability of the polymer was not noted.

The choice of counterion (anion or cation) has a major effect on the stability of conducting polymers. The stability of donor- (36) and acceptor-doped (37, 38) polyacetylenes, polypyrrole (39), poly(alkylthiophene)s (40), and other polymers (40) has been studied by using thermogravimetric anal-

yses and isothermal aging techniques. In air, the perchlorate and tetrafluoroborate salts of polypyrrole decomposed and lost conductivity above 150 °C (41), but poly(pyrrole) *p*-toluenesulfonate remained stable to 280 °C. A kinetic analysis (39) of the decay in conductivity for poly(pyrrole) *p*-toluenesulfonate showed that after 3 years at room temperature in air, the conductivity should decrease to one-tenth of its initial value of ~100 S/cm.

Postsynthesis treatment of poly(pyrrole) benzenesulfonate with aqueous sodium hydroxide (32) significantly enhanced the long-term environmental stability of polypyrrole. Electropolymerized films with an initial conductivity of ~100 S/cm were treated with solutions of aqueous NaOH ranging from 0.1%–20% in concentration. The treatment (the exchange of the benzenesulfonate counterion for hydroxide) caused a drop in conductivity of nearly 100 S/cm for samples treated with 20% NaOH, but significant improvements in long-term environmental stability were gained. Thus, a sample treated with a 1% NaOH solution for 240 min had a conductivity of 90 S/cm immediately after treatment, and ~80 S/cm after more than 100 days at 140 °C. A similar stabilizing effect was observed for samples treated with H₂SO₄ (42) except that no drop in conductivity occurred during ion exchange. The permeability of treated films toward oxygen and water decreased after treatment. This result is consistent with the proposal that the shrinkage of treated films that accompanies the anion exchange protects them from degradation by oxygen and water vapor.

Pyrrole has been electropolymerized in aqueous solution in the presence of sulfonated cobalt phthalocyanine (43, 44). Although the electropolymerized film was not highly tractable, it was more stable than polypyrrole itself, and the conductivity of the composite increased from 4 S/cm to greater than 400 S/cm during a 2-month exposure to air. In addition, the electrochromic behavior was modified compared to poly(pyrrole) perchlorate. Poly(pyrrole) perchlorate is black when oxidized and semitransparent when reduced, but four distinct colors were observed for the poly(pyrrole) phthalocyanine polymer: yellow-green, dark blue, violet, and red-brown. The colors result from the various oxidation states of the phthalocyanine ring, which is electrochemically coupled to polypyrrole. The phthalocyanine moiety appears to be coordinated to the pyrrole ring through the pyrrole nitrogen because the addition of a methyl group to pyrrole, which would hinder complexation of the pyrrole to cobalt, leads to electrochemistry analogous to polypyrrole alone and the loss of phthalocyanine during electrochemical cycling.

An interesting composite material has been prepared by the electropolymerization of pyrrole on polyacetylene electrodes (45). Because oxidized polypyrrole is far more stable in air than polyacetylene, the resulting composite has the stability of polypyrrole. With different synthetic conditions, either a thin layer of polypyrrole was deposited over individual fibrils of the polyacetylene film or a dense polypyrrole film coated the entire film. When the dense polypyrrole film covered the entire polyacetylene film, the interior

of the film slowly degraded, leaving highly conducting polypyrrole surfaces and a poorly conducting polyacetylene interior.

5.3 Tractability Improvements

Without tractability, the applications for conducting polymers would be limited. Many approaches to making tractable materials have been explored, including

- the preparation of blends, dispersions, and composites;
- the synthesis of random, graft, and block copolymers;
- the use of precursor polymers that can be converted to conducting polymers; and
- the use of exotic solvents like molten iodine that render some conductive polymers soluble.

Some of these approaches have yielded tractable conducting polymers; others have resulted in poorly conducting but unique and interesting materials. This section details these efforts.

5.3.1 Polymer Dispersions, Composites, and Blends

Suspensions of polyacetylene were prepared as burrs or fibers (46) by using a vanadium catalyst. When the solvent was removed, films of polyacetylene were formed with densities greater than that prepared by the Shirakawa method. These suspensions were mixed with various fillers to yield composite materials. Coatings were prepared by similar techniques. Blends of polypyrrole, polyacetylene, and phthalocyanines with thermoplastics were prepared (47) by using the compounding techniques typically used to disperse colorants and stabilizers in conventional thermoplastics. Materials with useful antistatic properties were obtained with conductivities from 10^{-9} to 10^{-7} S/cm. The blends were transparent and had colors characteristic of the conducting polymer. For example, plaques containing *trans*-polyacetylene had the characteristic violet color exhibited by thin films of solid *trans*-polyacetylene.

Polyacetylene latexes (48) have been prepared by polymerizing acetylene in the presence of poly[(*tert*-butylstyrene)-*b*-(ethylene oxide)]. The use of a tetrahydrofuran/cyclohexane (THF/cyclohexane) solvent combination led to the formation of a stable dispersion of nearly uniform spherical polyacetylene particles 40–200 nm in diameter. The block copolymer was separated from the polyacetylene by several wash cycles with a good solvent for the block copolymer (cyclohexane), and after removing the solvent, a polyacetylene powder was obtained. On the basis of nitrogen adsorption

measurements of the surface area of the particles, the particles were concluded to be nonporous. Pressed pellets of the powdery product had conductivities of 10^{-5} S/cm, but no results for doped polymers were reported.

Suspensions of polypyrrole were prepared by the FeCl_3 oxidation of pyrrole in an aqueous solution of methylcellulose (49). The product was dried and yielded films with conductivities of 0.2 S/cm. Scanning electron microscopy revealed globular polypyrrole embedded in the methylcellulose matrix. After several months, these suspensions remained stable with no detectable precipitation. Similarly, the electropolymerization of 3-methylthiophene in solutions of poly(methyl methacrylate) and poly(vinyl chloride) was reported (50, 51).

Early work on the electropolymerization of pyrrole (52) showed that variations in the counterion used in the polymerization would not only affect the stability of the polymer, but the mechanical properties of the polymer might also be improved. Thus, films of poly(pyrrole) *p*-toluenesulfonate prepared in wet acetonitrile were flexible (53) and could be elongated 60% without fracturing. Polymerizations in the presence of *n*-alkylsulfate and *n*-alkylsulfonate counterions (54) led to the formation of layered materials composed of alternating regions of surfactant and conducting polypyrrole. Polymeric counterions such as sulfonated polystyrene (55) could also be employed. The solvent chosen for such polymerizations (55, 56) and the particular polymeric counterion (56) had a large effect on the conductivity and tractability of the product. Thus, pyrrole electropolymerized in the presence of a sulfonated styrene and hydrogenated butadiene triblock copolymer (56) yielded flexible polymers that were melt pressed to form conducting polymer plaques. The elastomeric properties of the triblock copolymer were retained in the polypyrrole product, but the conductivities were only 5×10^{-3} S/cm after melt pressing.

The electropolymerization of pyrrole in a polymeric latex dispersion yielded a modified latex (57) that dried to give conductive films. Although the conductivity was not exceptionally high (1 S/cm for 10%–20% pyrrole content and 10^{-3} S/cm for 1% pyrrole content), the ease in handling the conductive material makes it attractive for the preparation of conductive coatings. Similarly, pyrrole was chemically polymerized with H_2SO_4 and FeCl_3 in polystyrene latexes (58). The sulfonic acid and carboxylic acid groups in the latex provided the counterions for the doped polypyrrole, which uniformly coated the latex particles. The dried latex formed conducting films with conductivities as high as 2.5×10^{-1} S/cm when the pyrrole content of the modified latex was nearly 50%.

The polymerization of intractable conducting polymers within tractable polymers has been investigated as a route to potentially useful composite materials. In an early example (59), low-density polyethylene was swollen with catalyst at 70 °C, and after exposure to acetylene gas, polyacetylene–polyethylene composites containing 1%–18% polyacetylene were ob-

tained (60). The composites were treated with iodine to yield materials with conductivities of 5–10 S/cm. Interestingly, the maximum conductivity could be obtained with as little as 2%–4% polyacetylene. TEM studies showed that the polyacetylene formed irregular aggregates within the insulating matrix. This result suggests a percolation mechanism for the conductivity. Some improvement in stability resulted from the encapsulation of these conductive aggregates, but the improvement was not enough to allow the use of these materials under ambient conditions.

This *in situ* polymerization of acetylene was extended to elastomers such as polybutadiene (61); block copolymers of styrene and diene (62); and terpolymers of ethylene, propylene, and diene (63). On doping, these materials retained flexibility while achieving conductivities as high as 100 S/cm. Composites containing 30% polyacetylene became brittle when exposed to air and were composed of continuous regions of both elastomer and polyacetylene. Stretching these materials before doping increased the crystallinity of the polyacetylene and improved the conductivity of the doped composite. For a polybutadiene composite containing 40% polyacetylene, the conductivity of the stretched material after iodine doping improved from 15 to 575 S/cm (61). No increased stability toward oxygen or moisture was afforded by the elastomeric matrix.

Composites of polypyrrole and poly(vinyl chloride) have been prepared by several groups (64–67). Polythiophene–poly(vinyl chloride) composites have also been prepared (68). The electropolymerization of pyrrole on poly(vinyl chloride)-coated electrodes yielded composites with mechanical properties (tensile strength, percent elongation at break, percent elongation at yield) similar to poly(vinyl chloride) (65) but with a conductivity of 5–50 S/cm, which is only slightly inferior to polypyrrole (30–60 S/cm) prepared under similar conditions. In addition, the environmental stability was enhanced. Morphological studies (69) showed that the polypyrrole was not uniformly distributed in the film and had polypyrrole-rich layers next to the electrode. Similarly, poly(vinyl alcohol) (70) poly[(vinylidene chloride)-*co*-(trifluoroethylene)] (69) and brominated poly(vinyl carbazole) (71) have been used as the matrix polymers. The chemical polymerization of pyrrole in a poly(vinyl alcohol) matrix by ferric chloride and potassium ferricyanide also yielded conducting composites with conductivities of ~10 S/cm (72–74).

An established technique for preparing soluble derivatives of intractable polymers is to add solubilizing substituents to the monomer. Thus, insoluble polyphenylenes have been rendered soluble (75) in common solvents such as chloroform by phenyl substitution. Similarly, a wide range of substituted pyrroles and thiophenes have been investigated to improve the tractability of these relatively stable conducting polymers. The chemical and electropolymerization of *N*-substituted pyrroles (76) gave polymers with substantially decreased conductivities, generally by a factor of 10^3 compared to polypyrrole. However, monomers substituted at the 3 and 4 positions of

pyrrole with alkyl or alkoxy groups were electropolymerized to give soluble processable polymers (77).

The same type of structure modifications have been applied to polythiophenes with impressive results. Early work (78) suggested that poly(3-methylthiophene) would be far more tractable than polythiophene itself, and the optical absorption spectrum of the polymer indicated that the addition of the methyl group had not significantly affected the electronic properties. The increased tractability of such derivatives was demonstrated by the electropolymerization of 3-methoxythiophene (79). The neutral polymer was soluble in acetonitrile, acetone, and methylene chloride, whereas both the oxidized and neutral forms of poly(3-methoxythiophene) were soluble in dimethylformamide. A variety of tractable 3-alkyl-substituted polythiophenes were subsequently reported (80–83). The solubility of these polymers improved with increases in the length of the alkyl group in the order *n*-butyl > ethyl >> methyl (80, 81). The *n*-hexyl, *n*-octyl, *n*-dodecyl, *n*-octadecyl, and *n*-eicosyl derivatives have been synthesized as well as random copolymers of 3-alkylthiophenes. The polymers were soluble in common organic solvents such as THF, chloroform, and xylene. Disubstituted polymers (e.g., the 3,4-dimethyl derivative) were less soluble. Films cast from solution and doped with iodine and FeCl₃ yielded conductivities as high as 50 S/cm. Poly(alkylthiophenes) could also be oxidized in solution with nitrosyl salts to give stable conducting polymer solutions, and on drying, conducting polymer films. Films cast from conducting polymer solutions were more brittle than films that had been oxidized in the solid state. By incorporating sulfonic and carboxylic acids in the alkyl substituent of the 3-alkylthiophenes, water-soluble polythiophenes (84, 85) were prepared (Figure 5.4). These polymers contain counterions for the oxidized polymer as a part of the polymer structure, and thus have been termed “self-doped” conducting polymers. The conductivities of doped polymers that had been cast from water were as high as 10 S/cm, but losses in conductivity were observed for thoroughly dried films.

5.3.2 Random Copolymers

A variety of copolymers of acetylene and other alkynes have been prepared. Copolymers of acetylene and methylacetylene (86), a soluble polyene, were more tractable than polyacetylene itself, but as the fraction of methylacetylene in the copolymer increased, both the tractability and the final conductivity of the iodine-doped polymer decreased. At an acetylene mole fraction of 0.5, the copolymer was insoluble, and the final conductivity had fallen from greater than 100 to 1 S/cm. Some plasticization remained, however, and the polymer could be stretched to elongation ratios as high as 7. Copolymers of acetylene and phenylacetylene containing 26% acetylene were soluble in methylene chloride (24). Like methylacetylene copolymers,

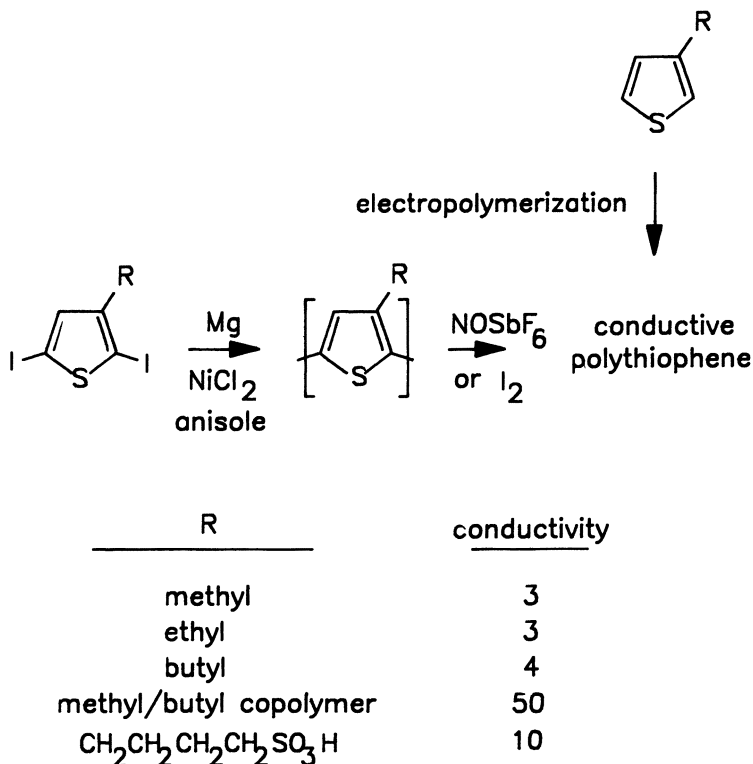


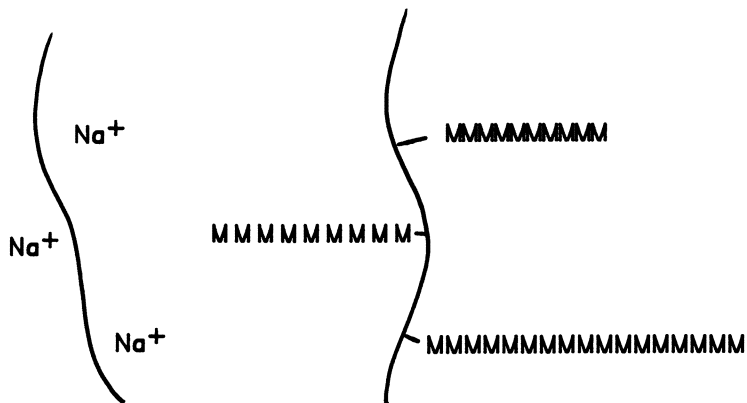
Figure 5.4. Poly(3-alkylthiophene)s are more stable than polythiophene and have excellent tractability and good conductivities.

the conductivities of the doped copolymers were much less than homopolyacetylene.

5.3.3 Graft and Block Copolymers

Graft and block copolymerization is a slightly different approach to the solubilization of intractable polymers. Instead of building flexibility into the polymer backbone, polymeric solubilizing groups are attached to the chain. In both graft and block copolymers, the integrity of the backbone of the conjugated polymer is maintained to a much higher degree than in random copolymers. This is important for conjugated polymers because the disruption of conjugation usually leads to the degradation of the desirable electronic properties of the polymer.

Sodium-reduced polyacetylene was functionalized in two separate examples. In the first example (87), the doped polymer was used to initiate the polymerization of ethylene oxide from fibrillar films of polyacetylene (Figure 5.5). The product did not become appreciably soluble, and poly-



M= methyl methacrylate, ethylene oxide

Figure 5.5. Graft copolymers can be formed by using doped polymers as the initiation site.

merization of ethylene oxide by electron transfer from the reduced polymer was a significant competitor to graft formation. In a similar experiment (88), methyl methacrylate was added to sodium-doped polyacetylene, and a blue fraction soluble in THF was obtained. The soluble fraction had an electronic absorption spectrum similar to *trans*-polyacetylene but shifted slightly to higher energies. The shift was attributed to a disruption of the conjugated backbone as a result of the formation of poly(methyl methacrylate) grafts. The electrical properties of these products were not reported.

The inverse of this procedure has received more attention. In these experiments, the conductive polymer or incipient conducting polymer is polymerized from multiple catalytic sites on a soluble substrate polymer. Alternatively, conducting segments can be bonded to a polymer chain by standard chemical techniques. Stable catalyst sites have been generated on pendant olefins in polybutadiene with the $\text{Ti}(\text{OCH}_2\text{CH}_2\text{CH}_2\text{CH}_3)_4/\text{Al}(\text{CH}_2\text{CH}_3)_3$ catalyst typically used to prepare polyacetylene (Figure 5.6). With the addition of acetylene, graft copolymers (89) were formed that were handled as solutions. Although solubility for the polyacetylene fraction was claimed, much of the characterization data presented for the copolymers [UV-visible radiation absorption (89), photo-induced absorption (90), and morphology (91)] was more typical of solid polyacetylene and significantly differed from other preparations of soluble copolymers. The products were probably best described as stabilized suspensions of polyacetylene (92). Lithiation of polybutadiene followed by the addition of $\text{Ti}(\text{OCH}_2\text{CH}_2\text{CH}_2\text{CH}_3)_4$ allowed the preparation of comb-like graft copolymers (93, 94). These materials differed in that TEM micrographs of the copolymers showed small,

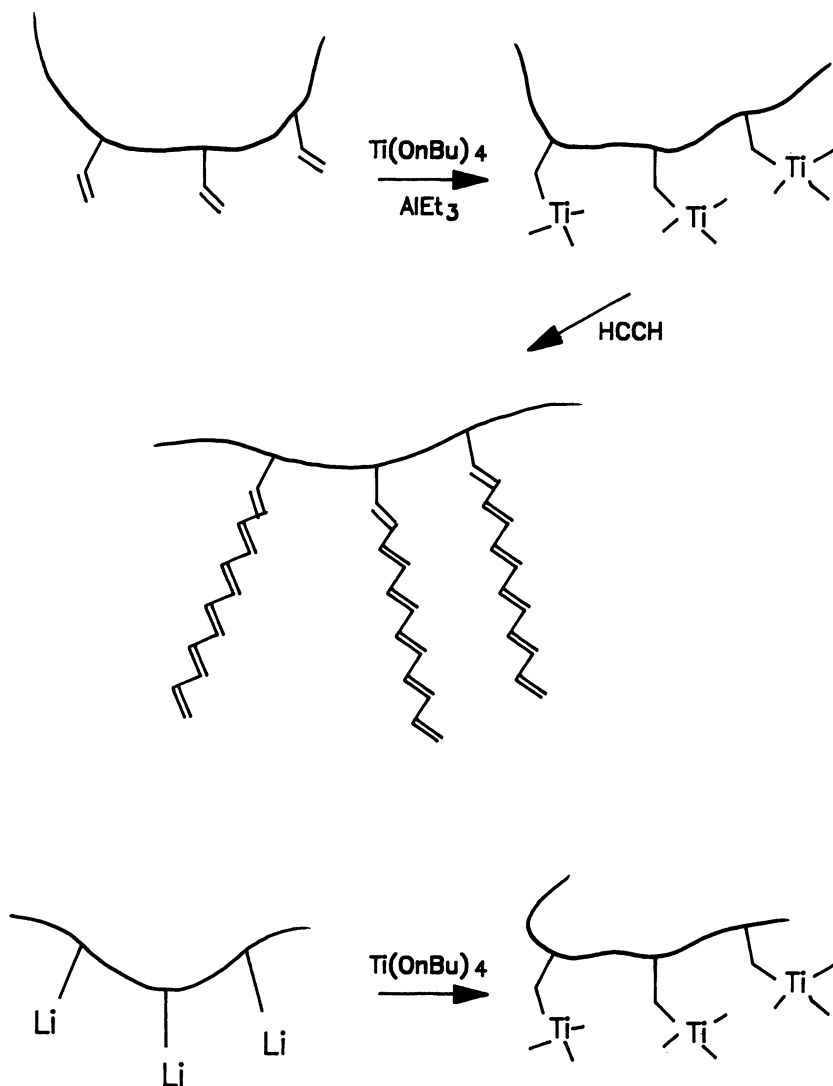


Figure 5.6. Synthesis of graft copolymers containing polyacetylene. Active catalysts for acetylene polymerization are generated on the polymer backbone, and the polyacetylene grows from the backbone.

spherical microdomains of polyacetylene embedded in the polybutadiene matrix. The conductivity of iodine-doped samples was 10^{-3} S/cm.

Cross-linked poly(pyrrole-*g*-styrene) copolymers were prepared by the electropolymerization of pyrrole in the presence of polystyrene-bound pyrrole (95). Films grown from 1:1 mixtures of pyrrole and the pyrrole-func-

tionalized polystyrene were brittle and had conductivities of 5×10^{-2} S/cm, whereas those grown from 6:1 mixtures yielded copolymers with properties typical of polypyrrole and conductivities of 0.4 S/cm. Other characteristics of the copolymers were not reported.

Three different routes to polyacetylene block copolymers have been developed. In the first method (19), acetylene is polymerized in the presence of a second polymer functionalized with epoxides, aldehydes, or ketones that react with growing polyacetylene chains (Figure 5.7). Thus, the growing chains are simultaneously terminated and bound to the second polymer by the formation of carbon-carbon bonds. By adjusting the relative amounts of monomer and termination sites, the molecular weight of the polyene segments can be controlled. Polyacetylene block copolymers with polystyrene, polybutadiene, or polyisoprene have been prepared. When the polyene block is short, dark-purple solutions of the copolymer in common organic solvents are obtained. Light scattering results (96) suggested that these solutions were actually micellar aggregates of copolymers; the polyacetylene portion was arranged as an elongated and amorphous core.

Copolymers with longer polyene segments were found to be insoluble in the reaction solvent (toluene). In these materials, the polyacetylene fraction was crystalline (97). Copolymers with a low acetylene content were composed of a variety of isolated crystalline structures within an amorphous matrix, whereas those containing 50% or more polyacetylene had a morphology that resembled fibrillar polyacetylene. Dried copolymer solutions and suspensions gave blue films with the mechanical properties characteristic of the carrier polymer. No increase in environmental stability was observed.

The second route (87, 98) to block copolymers is the "anion to Ziegler-Natta transformation" reaction. Living anionic polymerizations (polymerizations that do not terminate) of styrene and isoprene are treated with

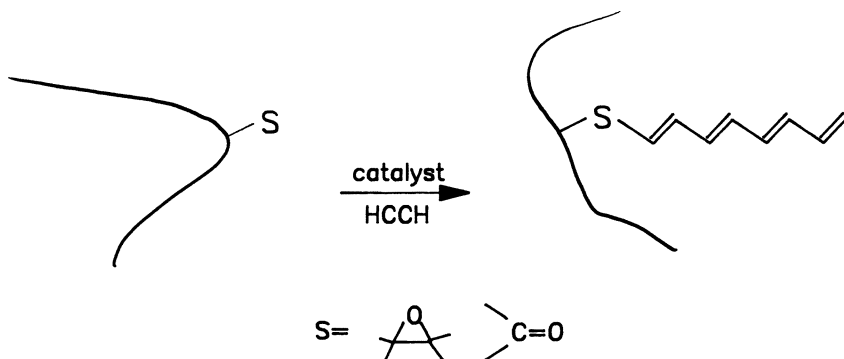


Figure 5.7. Synthesis of block copolymers via termination reactions. Control over the molecular weight of the polyacetylene segment is afforded by varying the ratio of monomer to terminating groups (S).

$\text{Ti}(\text{OCH}_2\text{CH}_2\text{CH}_2\text{CH}_3)_4$ to yield polymer solutions catalytically active toward acetylene polymerization (Figure 5.8). Blue solutions, characterized by gel permeation chromatography and radioisotopic labeling studies, are formed (99). This procedure was recently repeated by using CoCl_2 as the transition metal (100).

The properties of such apparently soluble materials differed greatly from those containing stabilized polyacetylene crystallites. Attempts to dope the soluble copolymers yielded materials with low conductivities, and chemistry typical of solution chemistry (bromination) was observed rather than the formation of a stable bromine-doped polyacetylene phase. A poly(isoprene-*b*-acetylene) copolymer oxidized with iodine gave conductivities as high as 1–10 S/cm, but the characterization of the copolymer was insufficient to unambiguously identify it as a soluble copolymer. On the basis of previously reported work, this material is likely to correspond to a stabilized suspension rather than a solution.

The third route involves metathesis polymerization of cyclooctatetraene with tungsten catalysts, yielding polyacetylene as an insoluble film along with oligomers (101). By first polymerizing cyclooctene and then adding cyclooctatetraene, a soluble, red block copolymer was obtained. On the basis of the visible absorption spectrum, at least two or three cyclooctatetraene units were concluded to have been added to the polymer chain forming a short polyacetylene block. No conductivity data were reported for this copolymer.

5.3.4 Precursor Polymers

One of the most innovative and useful techniques for the preparation of conducting polymers has been the synthesis of highly soluble precursor polymers that can be easily handled in solution, purified, and then later converted to the less tractable conducting polymer. The first example of such an approach was the dehydrohalogenation of poly(vinyl chloride) (102). This reaction, like most elimination reactions on polymers, rarely goes to completion and is not well suited for the synthesis of useful conducting

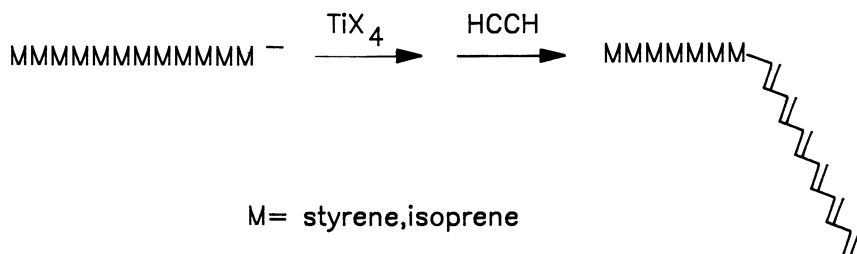


Figure 5.8. Synthesis of block copolymers via the “anion to Ziegler–Natta transformation” scheme.

materials. Recently several elimination schemes have yielded high quality conducting polymers from tractable precursors.

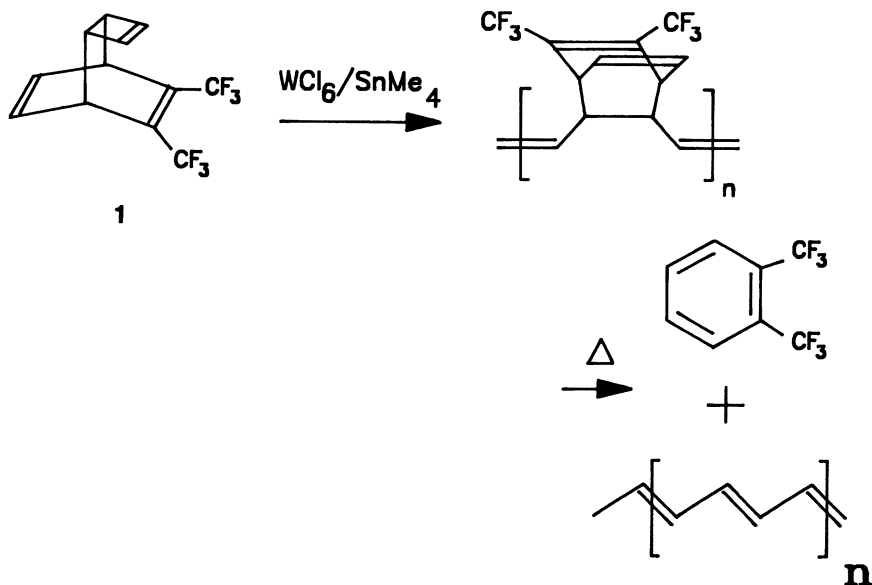
The Durham route to polyacetylene (103, 104) involves the metathesis polymerization of **1** to give a soluble but thermally unstable high polymer (Scheme 5.2). Slowly at room temperature, or more rapidly at 80 °C, the polymer undergoes a retro-Diels–Alder reaction. This reaction results in elimination of a substituted benzene and formation of amorphous polyacetylene. An enormous weight loss accompanies the conversion, but high-density films were produced with no apparent voids. The kinetics of the transformation reaction were extensively studied (105).

By choosing the appropriate monomers (106), the temperature at which the retro-Diels–Alder reaction takes place can be controlled (Scheme 5.3). When **1** and **2** were copolymerized, the precursor polymer became thermally stable at room temperature (79) yet still could be converted to polyacetylene at 80 °C. Long runs of polyenes that would make the polymer intractable were avoided by the inclusion of the saturated 2 + 2 photoproduct, which is stable at room temperature. At higher temperatures, the diene was regenerated, and the conversion to polyacetylene proceeded to completion. The diene regeneration and the retro-Diels–Alder reaction are so highly exothermic that the homopolymer of **2** can char during the transformation.

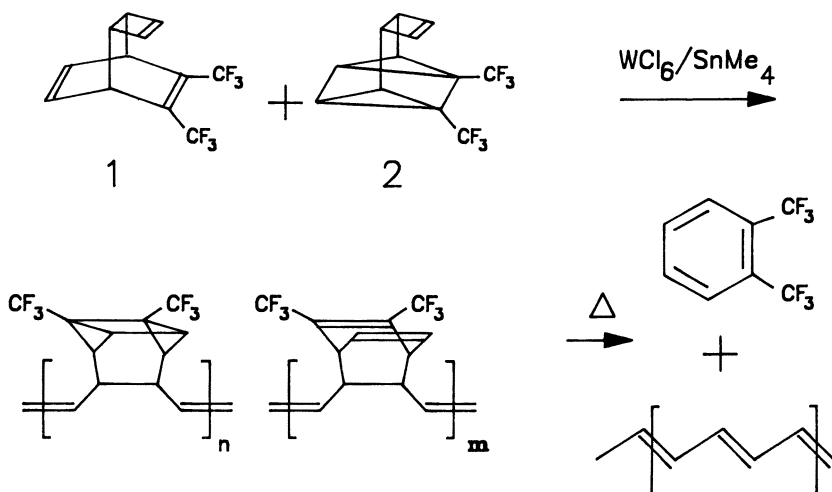
A triumph of the Durham route was the preparation of oriented crystalline polyacetylene (107–109) by stretch orientation of the polymer during the transformation reaction. This material has highly anisotropic optical properties, but the anisotropy of the conductivity of the doped polymer was low. Oriented fibers as well as films were prepared.

Similar success was reported in the synthesis of poly(phenylenevinylene) by an indirect route (110–112). Previous routes to poly(phenylenevinylene) yielded intractable materials that when oxidized gave conductivities as high as 1 S/cm (113). By eliminating HCl or HBr and dimethyl sulfide from poly(*p*-xylene- α -dimethylsulfonium halide) in a thermal treatment, high quality poly(phenylenevinylene) was prepared (110, 112) analogously to the Durham route to polyacetylene (Scheme 5.4). The poly(phenylenevinylene) could also be stretch aligned during the transformation reaction to yield highly oriented films, with conductivities of 2780 S/cm after doping with iodine. The anisotropy of the conductivity was 100 for films at a draw ratio of 10.

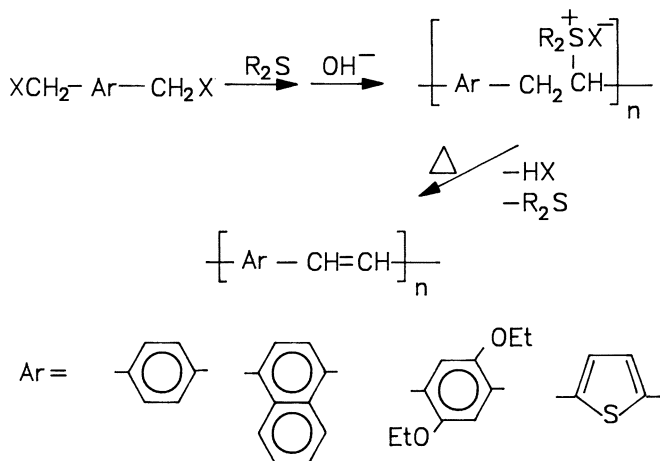
Alkoxy-substituted poly(phenylenevinylene)s have been prepared by the identical route (114, 115). As the substituents of the aromatic ring were varied, significant changes in conductivity of the AsF₅-doped polymer were noted. The polymers with the highest conductivities (200 S/cm) were substituted with methoxy or ethoxy groups at the 2 and 5 positions. Although AsF₅-doped polymers are unstable in air, iodine-doped derivatives of dialkoxy poly(phenylenevinylene)s are stable. Copolymers that contained 12%–53% of the dialkoxy unit were stretch-oriented and doped with iodine



Scheme 5.2. Synthesis of polyacetylene by the Durham route. The precursor polymer is soluble and can be processed prior to conversion to polyacetylene.



Scheme 5.3. A revised synthesis of polyacetylene by the Durham route. When 2 is included in the polymer, the conversion to polyacetylene first requires that the diene be generated (at $\sim 80^\circ\text{C}$) before the retro-Diels-Alder reaction can occur.



Scheme 5.4. Synthesis of poly(arylene vinylene)s obtained by the elimination of small molecules from a precursor polymer.

and yielded conductivities ranging from 300 to nearly 700 S/cm (116). A copolymer with an initial conductivity of 428 S/cm was unchanged after 6 months in ambient air.

Poly(arylenevinylene)s based on naphthalene (117) and thiophene (118, 119) have been reported. When naphthalene was substituted for benzene in the polymer structure, the resulting conductivity for the AsF₅-oxidized polymer was 10⁻² S/cm. Orientation of the polymer via stretch alignment has not been reported. The thiophene derivative, however, was stretch aligned (118) and doped with iodine and FeCl₃. Conductivities of 2700 were obtained with iodine-doped samples having elongation ratios of 6. The anisotropy of the conductivity was 35.

5.3.5 Exotic Solvents

Although organic solvents are generally nonsolvents for conducting polymers, solutions of conducting polymers have been prepared (120). Mixtures of AsF₅ and AsF₃ were shown to dissolve polyphenylene, poly(phenylene oxide), and other polymers. The AsF₅-oxidized polymers were stabilized in AsF₃, and electrically conductive films were cast from the polymer solutions. The conductivities observed were substantially improved relative to polymers prepared by solid-state doping reactions. Thus, the conductivity of poly(phenylene oxide) improved from <10⁻³ S/cm for solid-state doping to 100 S/cm for solution-cast films. Once cast, the films underwent additional chemical modification and became insoluble.

An extension of this method is the simultaneous oxidative polymerization and solubilization of polymers in AsF₅/AsF₃ mixtures. Polythiophene,

poly(3-methylthiophene), polypyrrole, polyphenylene, and copolymers of polyphenylene and poly(phenylene sulfide) have been prepared by this method (120). In related experiments (121), the polymerization of acetylene was carried out in $\text{AsF}_5/\text{AsF}_3$ mixtures. Soluble materials are obtained from these polymerizations, but little characterization of the polymer microstructure has been reported. Molten iodine has also been reported to act as a polymerization catalyst and solvent for carbazole (122). Films cast from solution were reported to have conductivities of 1 S/cm.

5.4 Outlook

The development of tractable, stable conducting polymers has taken considerable effort, and the development of a single, general-purpose conducting polymer may not be its logical result. Instead, conducting polymers will probably be tailored to match the stability and processability requirements of applications on a case by case basis. This means that opportunities will arise for a wide range of conducting polymers, and that opportunities will arise for chemists intent on improving the performance of existing conducting polymers.

References

1. Rembaum, A.; Landel, R. F. *J. Polym. Sci. Polym. Symp.* **1977**, *17*.
2. Hatano, M.; Kambara, S.; Nakada, I. *J. Polym. Sci.* **1961**, *51*, 526.
3. Natta, G.; Mazzanti, G.; Corradini, P. *Atti. Acad. Naz. Lincei, Rend. Cl. Sci. Fis. Mat. Nat.* **1958**, *8*, 3.
4. Little, W. A. *Phys. Rev.* **1964**, *134*, 1416.
5. Ito, T.; Shirakawa, H.; Ikeda, S. *J. Polym. Sci., Polym. Chem. Ed.* **1974**, *12*, 11.
6. Shirakawa, H.; Louis, E. J.; MacDiarmid, A. G.; Chiang, C. K.; Heeger, A. J. *J. Chem. Soc. Chem. Commun.* **1977**, 578.
7. Naarmann, H. *Synth. Met.* **1987**, *17*, 223.
8. Basescu, N.; Liu, Z.-X.; Moses, D.; Heeger, A. J.; Naarmann, H.; Theophilou, N. *Nature* **1987**, *327*, 403.
9. *Handbook of Conducting Polymers*; Skotheim, T. A., Ed.; Marcel Dekker: New York, 1986.
10. Reynolds, J. R. *J. Mol. Electron.* **1986**, *2*, 1.
11. Bredas, J. L.; Street, G. B. *Acc. Chem. Res.* **1985**, *18*, 309.
12. Ehinger, K.; Roth, S. *Philos. Mag.* **1986**, *53*, 301.
13. Heeger, A. J. *Polym. J.* **1985**, *17*, 201.
14. Crecelius, G.; Stamm, M.; Fink, J.; Ritsko, J. J. *Phys. Rev. Lett.* **1983**, *50*, 1498.
15. Scott, J. C.; Pfluger, P.; Krounbi, M. T.; Street, G. B. *Phys. Rev. B.* **1983**, *28*, 2140.
16. Chung, T. C.; Kaufman, J. H.; Heeger, A. J.; Wudl, F. *Phys. Rev. B* **1985**, *30*, 702.
17. Chen, S.-A.; Chan, W.-C.; Li, L.-S. *Angew. Makromol. Chem.* **1987**, *148*, 87.
18. Shirakawa, H.; Sasaki, T.; Ikeda, S. *Chem. Lett.* **1978**, 1113.

19. Baker, G. L.; Bates, F. S. *Macromolecules* 1984, 17, 2619.
20. Shacklette, L. W.; Elsenbaumer, R. L.; Chance, R. R.; Eckhardt, H.; Frommer, J. E.; Baughman, R. H. *J. Chem. Phys.* 1981, 75, 1919.
21. Elsenbaumer, R. L.; Shacklette, L. W. *J. Polym. Sci. Polym. Phys. Ed.* 1982, 20, 1781.
22. Shacklette, L. W.; Eckhardt, H.; Chance, R. R.; Miller, G. C.; Ivory, D. M.; Baughman, R. H. *J. Chem. Phys.* 1980, 73, 4098.
23. Tourillon, G.; Garnier, F. J. *Electrochem. Soc.* 1983, 130, 2042.
24. Deits, W.; Cukor, P.; Rubner, M.; Jopson, H. *Synth. Met.* 1982, 4, 199.
25. Pekker, S.; Bellec, M.; Le Cleach, X.; Beniere, F. *Synth. Met.* 1984, 9, 475.
26. Osterholm, J. E.; Yasuda, H. K.; Levenson, L. L. *J. Appl. Polym. Sci.* 1982, 27, 931.
27. Seeger, K.; Gill, W. D.; Clarke, T. C.; Street, G. B. *Solid State Commun.* 1978, 28, 873.
28. Inoue, T.; Osterholm, J. E.; Yasuda, H. K.; Levenson, L. L. *Appl. Phys. Lett.* 1980, 36, 101.
29. Yang, X.-Z.; Dickinson, L. C.; Chien, J. C. W. *Polym. Prepr. Am. Chem. Soc. Div. Polym. Chem.* 1983, 24(2), 155.
30. Chien, J. C. W.; Dickinson, L. C.; Yang, X. *Macromolecules* 1983, 16, 1287.
31. Pochan, J. M.; Gibson, H. W.; Harbour, J. *Polymer* 1982, 23, 435.
32. Munstedt, H.; Naarmann, H.; Kohler, G. *Mol. Cryst. Liq. Cryst.* 1985, 118, 129.
33. Wilhelm, D.; Strohmaier, D.; Kleeberg, W. *Angew. Makromol. Chem.* 1986, 141, 141.
34. Enkelmann, V.; Muller, W.; Wegner, G. *Synth. Met.* 1979, 1, 185.
35. Gibson, H. W.; Weagley, R. J.; Mosher, R. A.; Kaplan, S.; Prest, Jr., W. M.; Epstein, A. J. *Br. Polym. J.* 1986, 18, 115.
36. Elsenbaumer, R. L.; Delannoy, P.; Miller, G. G.; Forbes, C. E.; Murthy, N. S.; Eckhardt, H.; Baughman, R. H. *Synth. Met.* 1985, 11, 251.
37. Elsenbaumer, R. L.; Miller, G. G.; Khanna, Y.; McCarthy, E.; Baughman, R. H. *Electrochem. Soc. Extended Abstr.* 1985, 1, 118.
38. Druy, M. A.; Rubner, M. F.; Walsh, S. *Synth. Met.* 1986, 13, 207.
39. Samuelson, L. A.; Druy, M. A. *Macromolecules* 1986, 19, 824.
40. Elsenbaumer, R. H.; Maleysson, C.; Jen, K. Y. *Polym. Mater. Sci. Eng.* 1987, 56, 54.
41. Salmon, M.; Diaz, A. F.; Logan, A. J.; Krounbi, M.; Bargon, J. *Mol. Cryst. Liq. Cryst.* 1982, 83, 265.
42. Munstedt, H. *Polymer* 1986, 27, 899.
43. Skotheim, T.; Rosenthal, M. V.; Linkous, C. A. *J. Chem. Soc. Chem. Commun.* 1985, 612.
44. Rosenthal, M. V.; Skotheim, T. A.; Linkous, C. A. *Synth. Met.* 1986, 15, 219.
45. Ahlgren, G.; Krische, B. *J. Chem. Soc. Chem. Commun.* 1984, 946.
46. Hocker, J.; Schneider, G. *J. Phys. Colloq. C3* 1983, 44, 147.
47. Wessling, B.; Volk, H. *Synth. Met.* 1986, 15, 183.
48. Edwards, J.; Fisher, R.; Vincent, B. *Makromol. Chem. Rapid Commun.* 1983, 4, 393.
49. Bjorklund, R. B.; Liedberg, B. *J. Chem. Soc. Chem. Commun.* 1986, 1293.
50. Roncali, J.; Garnier, F. J. *Chem. Soc. Chem. Commun.* 1986, 783.
51. Roncali, J.; Mastar, A.; Garnier, F. *Synth. Met.* 1987, 18, 857.
52. Diaz, A. F.; Hall, B. *IBM J. Res. Dev.* 1983, 27, 342.
53. Wynne, K. J.; Street, G. B. *Macromolecules* 1985, 18, 2361.
54. Wernet, W.; Monkenbusch, M.; Wegner, G. *Makromol. Chem. Rapid Commun.* 1984, 5, 157.

55. Glatzhofer, D. T.; Ulanski, J.; Wegner, G. *Polymer* **1987**, *28*, 449.
56. Bates, N.; Cross, M.; Lines, R.; Walton, D. *J. Chem. Soc. Chem. Commun.* **1985**, 871.
57. Jasn, S. J.; Chiklis, C. K. *Synth. Met.* **1986**, *15*, 175.
58. Yassar, A.; Roncali, J.; Garnier, F. *Polym. Commun.* **1987**, *28*, 103.
59. Galvin, M. E.; Wnek, G. E. *Polymer* **1982**, *23*, 795.
60. Galvin, M. E.; Wnek, G. E. *J. Polym. Sci. Polym. Chem. Ed.* **1983**, *21*, 2727.
61. Rubner, M. F.; Tripathy, S. K.; Georger, Jr., J.; Cholewa, P. *Macromolecules* **1983**, *16*, 870.
62. Lee, K. I.; Jopson, H. *Polym. Bull.* **1983**, *10*, 105.
63. Lee, K. I.; Jopson, H. *Makromol. Chem. Rapid Commun.* **1983**, *4*, 375.
64. Niwa, O.; Tamamura, T. *J. Chem. Soc. Chem. Commun.* **1984**, 817.
65. De Paoli, M.-A.; Waltman, R. J.; Diaz, A. F.; Bargon, J. *J. Chem. Soc. Chem. Commun.* **1984**, 1015.
66. Wang, T. T.; Tasaka, S.; Hutton, R. S.; Lu, P. Y. *J. Chem. Soc. Chem. Commun.* **1985**, 1343.
67. Niwa, O.; Hikita, M.; Tamamura, T. *Makromol. Chem., Rapid Commun.* **1985**, *6*, 375.
68. Niwa, O.; Tamamura, T. *Synth. Met.* **1987**, *20*, 235.
69. Niwa, O.; Kakuchi, M.; Tamamura, T. *Macromolecules* **1987**, *20*, 749.
70. Lindsey, S. E.; Street, G. B. *Synth. Met.* **1984**, *10*, 67.
71. Niwa, O.; Hikita, M.; Tamamura, T. *Appl. Phys. Lett.* **1985**, *46*, 444.
72. Ojio, T.; Miyata, S. *Polym. J.* **1986**, *18*, 95.
73. Pron, A.; Fabianowski, W.; Budrowski, C.; Raynor, J. B.; Zucharski, Z.; Suwalski, J.; Lefrant, S.; Fatseas, G. *Synth. Met.* **1987**, *18*, 49.
74. Pron, A.; Zagorska, M.; Fabianowski, W.; Raynor, J. B.; Lefrant, S. *Polym. Commun.* **1987**, *28*, 193.
75. Rakutis, R. A.; Mukamol, H.; Harris, F. W. *Macromolecules* **1968**, *1*, 431.
76. Diaz, A. F.; Kanazawa, K. K. *Chem. Scr.* **1981**, *17*, 145.
77. Traynor, L. U.S. Patent 4 487 667, 1984.
78. Yamamoto, T.; Sanechika, K.; Yamamoto, A. *Bull. Chem. Soc. Jpn.* **1983**, *56*, 1497.
79. Blankespoor, R. L.; Miller, L. L. *J. Chem. Soc. Chem. Commun.* **1985**, 90.
80. Elsenbaumer, R. L.; Jen, K. Y.; Oboodi, R. *Synth. Met* **1986**, *15*, 169.
81. Elsenbaumer, R. L.; Jen, K. Y.; Miller, G. G.; Shacklette, L. W. *Synth. Met.* **1987**, *18*, 277.
82. Sato, M.; Tanaka, S.; Kaeriyama, K. *J. Chem. Soc. Chem. Commun.* **1986**, 873.
83. Hota, S.; Rughooputh, S. D. D. V.; Heeger, A. J.; Wudl, F. *Macromolecules* **1987**, *20*, 212.
84. Patil, A. O.; Ikenoue, Y.; Basescu, N.; Colaneri, N.; Chen, J.; Wudl, F.; Heeger, A. J. *Synth. Met.* **1987**, *20*, 151.
85. Patil, A. O.; Ikenoue, Y.; Wudl, F.; Heeger, A. J. *J. Am. Chem. Soc.* **1987**, *109*, 1858.
86. Chien, J. C. W.; Wnek, G. E.; Karasz, F. E.; Hirsch, J. A. *Macromolecules* **1981**, *14*, 479.
87. Dandreaux, G. F.; Galvin, M. E.; Wnek, G. E. *J. Phys. Colloq. C3* **1983**, *44*, 135.
88. Kminek, I.; Trekoval, J. *Makromol. Chem. Rapid Commun.* **1984**, *5*, 53.
89. Destri, S.; Catellani, M.; Bolognesi, A. *Makromol. Chem. Rapid Commun.* **1984**, *5*, 353.
90. Dorsinville, R.; Tubino, R.; Krimchansky, S.; Alfano, R. R.; Birman, J. L.; Bolognesi, A.; Destri, S.; Catellani, M.; Porzio, W. *Phys. Rev. B* **1985**, *32*, 3377.

91. Bolognesi, A.; Catellani, M.; Destri, S.; Porzio, W.; Meille, S.; Pedemonte, E. *Makromol. Chem.* **1986**, *187*, 1287.
92. Porzio, W.; Bolognesi, A. Catellani, M.; Destri, S.; Meille, S. V.; Pedemonte, E. *Mol. Cryst. Liq. Cryst.* **1985**, *117*, 71.
93. Bolognesi, A.; Catellani, M.; Destri, S. *Mol. Cryst. Liq. Cryst.* **1985**, *117*, 29.
94. Bolognesi, A.; Catellani, M.; Destri, S.; Porzio, W. *Polymer* **1986**, *27*, 1128.
95. Nazzal, A. I.; Street, G. B. *J. Chem. Soc. Chem. Commun.* **1985**, 375.
96. VanNice, F.; Bates, F. S.; Baker, G. L.; Carroll, P. J.; Patterson, G. D. *Macromolecules* **1984**, *17*, 2626.
97. Baker, G. L.; Bates, F. S. *Mol. Cryst., Liq. Cryst.* **1985**, *117*, 15.
98. Aldissi, M. *Synth. Met.* **1986**, *13*, 87.
99. Galvin, M. E.; Wnek, G. E. *Polym. Bull.* **1985**, *13*, 109.
100. Armes, S.; Vincent, B.; White, J. W. *J. Chem. Soc. Chem. Commun.* **1986**, 1525.
101. Korshak, Y. V.; Korshak, V. V.; Kanischka, G.; Hocker, H. *Makromol. Chem. Rapid Commun.* **1985**, *6*, 685.
102. Marvel, C. S.; Sample, J. H.; Roy, M. F. *J. Am. Chem. Soc.* **1939**, *61*, 3241.
103. Edwards, J. H.; Feast, W. J. *Polymer* **1980**, *21*, 595.
104. Edwards, J. H.; Feast, W. J.; Bott, D. C. *Polymer* **1984**, *25*, 395.
105. Foot, P. J. S.; Calvert, P. D.; Billingham, N. C.; Brown, C. S.; Walker, N. S.; James, D. I. *Polymer* **1986**, *27*, 448.
106. Feast, W. J.; Winter, J. N. *J. Chem. Soc. Chem. Commun.* **1985**, 202.
107. White, D.; Bott, D. C. *Polym. Commun.* **1984**, *25*, 98.
108. Leising, G. *Polym. Bull.* **1984**, *11*, 401.
109. Leising, G. *Polym. Commun.* **1984**, *25*, 201.
110. Wessling, R. A.; Zimmerman, R. G. U.S. Patent 3 706 677, 1972; U.S. Patent 3 401 152, 1968.
111. Murase, I.; Ohnishi, T.; Noguchi, T.; Hirooka, M.; Murakami, S. *Mol. Cryst. Liq. Cryst.* **1985**, *118*, 333.
112. Karasz, F. E.; Capistran, J. D.; Gagnon, D. R.; Lenz, R. W. *Mol. Cryst. Liq. Cryst.* **1985**, *118*, 327.
113. Gourley, K. D.; Lillya, C.; Reynolds, J. R.; Chien, J. C. W. *Macromolecules* **1984**, *17*, 1025.
114. Murase, I.; Ohnishi, T.; Noguchi, T.; Hirooka, M. *Polym. Commun.* **1985**, *26*, 362.
115. Antoun, S.; Gagnon, D. R.; Karasz, F. E.; Lenz, R. W. *Polym. Bull.* **1986**, *15*, 181.
116. Han, C.-C.; Lenz, R. W.; Karasz, F. E. *E. Polym. Commun.* **1987**, *28*, 261.
117. Antoun, S.; Gagnon, D. R.; Karasz, F. E.; Lenz, R. W. *J. Polym. Sci. Polym. Lett. Ed.* **1986**, *24*, 503.
118. Murase, I.; Ohnishi, T.; Noguchi, T.; Hirooka, M. *Polym. Commun.* **1987**, *28*, 229.
119. Jen, K.-Y.; Jow, R.; Eckhardt, H.; Elsenbaumer, R. L. *Polym. Mat. Sci. Eng.* **1987**, *56*, 49.
120. Frommer, J. E. *Acc. Chem. Res.* **1986**, *19*, 2.
121. Aldissi, M.; Liepins, R. *J. Chem. Soc. Chem. Commun.* **1984**, 255.
122. Jenekhe, S. A.; Wellinghoff, S. T.; Reed, J. F. *Mol. Cryst. Liq. Cryst.* **1984**, *105*, 175.

RECEIVED for review April 15, 1987. ACCEPTED April 4, 1988.

Polymers in Nonlinear Optics

David Williams

Corporate Research Laboratories, Eastman Kodak Company, Rochester,
NY 14650

The delocalized pi electronic structures exhibited by organic aromatic and polyenelike structures lead to extremely large and potentially useful second- and third-order nonlinear coefficients. Research on the fundamental aspects of these processes has enhanced the understanding of their origins, and new approaches for combining the various properties required for practical application have been identified. Among these approaches are poled polymer films, organic crystals grown in thin-film formats, and mono-multilayer assemblies fabricated by the Langmuir-Blodgett deposition technique. In this chapter, the fundamental concepts of nonlinear optics are reviewed with particular emphasis on second-order processes and materials designed to exhibit them. Electric field poling as a method for removing the orientational averaging of polymer films and considerations for the use of poled films and Langmuir-Blodgett multilayers in waveguide formats are discussed.

I NTEREST IN THE NONLINEAR OPTICAL PROPERTIES of organic and polymeric materials has been spawned in recent years by the recognition that these materials may have unique applications as active components in the rapidly expanding optical communication and optical information processing fields (1-3). The cost-performance advantages of technology using these materials over more conventional inorganic single-crystal technology have been recognized, but significant advances in the design, synthesis, and processing of these polymers and in condensed-matter physics must take place before these advantages can be realized.

Nonlinear optics is concerned with the interaction of electromagnetic fields, generally in the optical frequency range, with a medium, resulting in the alteration of the phase, frequency, or other propagation characteristics

0065-2393/88/0218-0297\$09.50/0
© 1988 American Chemical Society

of the incident light. Interesting and useful phenomena involving organic crystalline and polymeric systems have been demonstrated and studied in recent years, but the incorporation of the properties required for broad-scale technological utility is far from reality today.

The complexity of the task can be appreciated by comparing the requirements for a nonlinear optical polymer for integrated optics applications with those for other polymer thin-film technologies. In general, all the requirements for high-quality thin films used in photoresist applications, for example, film-forming qualities, adhesion, freedom from defects, thermal stability, and patternwise delineation capability, must be combined in a single material with sophisticated electronic properties similar in complexity to those found in organic photoconductors. In addition, for second-order nonlinear effects, polar symmetry and extremely uniform birefringence must be imparted to the thin film.

In this chapter, the current state of understanding of second-order nonlinear optical properties in organic materials, thin films, including Langmuir-Blodgett films, and polymers will be reviewed. Brief mention will be made of third-order nonlinear effects in polymer films. Recent progress in that area warrants a separate review. Particular attention will be paid to a qualitative discussion of concepts to encourage interested readers to consult the extensive body of literature that describes the mathematics and physical chemistry required for performing and interpreting experiments in this field.

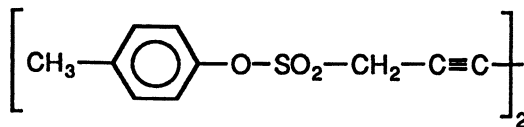
6.1 Origin of Nonlinear Effects

The starting point for nonlinear optics is the constitutive relationship between the polarization induced in a molecule (p) and the electric field components of incident electromagnetic waves (E). With the electric dipole approximation that ignores magnetic dipoles and higher order multipoles

$$p = \alpha \cdot E + \beta \cdots EE + \gamma \cdots EEE + \cdots \quad (6.1)$$

Since p and E are vector quantities, α , β , γ , etc., are tensors. For example, the electric field vector in the first term will have three components in the molecular coordinate system. Each electric field component can contribute to polarization along each of the three directions in the molecular coordinate system. This triple contribution of electric field components leads to a total of nine elements to the second rank polarizability tensor. Similarly, there are 27 components to the β tensor and 81 components to γ . Molecular symmetry generally reduces these tensors to only a few independent elements. Unless the molecular coordinate system lacks an inversion center, the form of the odd-rank tensors such as β will lead to zero induced polarization in this representation of optical nonlinearities. For molecules such as benzene and polymers such as poly[bis(p -toluenesulfonate)diacetylene]

(PTS; structure 6.1), α and γ will be nonzero but β will be zero because of inversion symmetry. For molecules such as *p*-nitroaniline and polymer chains such as isotactic polyphenylacrylate, β , as well as α and γ , is nonzero.



6.1

A similar expression can be written for the polarization induced in an ensemble of molecules in the liquid, solid, or gas phase. In this case, with the electric dipole approximation, the polarization P is written as

$$P = \chi^{(1)} \cdot E + \chi^{(2)} \cdot EE + \chi^{(3)} \cdot \dots EEE + \dots \quad (6.2)$$

The coefficients $\chi^{(1)}$, etc., are tensors with similar meanings in relation to the molecular quantities, except that they describe the polarization induced in the ensemble. From the properties of third-rank tensors, it follows that the contribution of $\chi^{(2)}$ to nonlinear polarization is zero in centrosymmetric crystals, isotropic gases, liquids, glassy polymers, etc. On the other hand, films of PTS, polyacetylene, polypyrrole, etc., can have substantial values of $\chi^{(1)}$, $\chi^{(3)}$, etc. For a polymeric material or any isotropic medium to exhibit a value of $\chi^{(2)}$ greater than that resulting from magnetic dipolar and higher order electric multipolar contributions, asymmetry must be induced in the medium. In general, for polymeric materials, asymmetry is induced by the generation of a polar axis in the medium through electric field poling.

The electric field components in equations 1 and 2 can be associated with the same or with different frequency components and, in some situations, can resonate with electronic or vibrational oscillations in the medium. This situation has led to a shorthand notation to describe the interactions leading to the various nonlinear effects of interest. Various susceptibility functions corresponding to the $\chi^{(2)}$ and $\chi^{(3)}$ effects of interest and their shorthand representation are listed in Table 6.1.

6.1.1 Effects Occurring through $\chi^{(2)}$

Several useful effects occurring through $\chi^{(2)}$ are illustrated in Figure 6.1. Second harmonic generation (SHG) can be viewed as the combination of two photons at frequency ω to produce a new one at 2ω . This process occurs because the nonlinear polarization which is created in the medium contains a Fourier component at 2ω which acts as a source of electromagnetic radiation at 2ω . As the electromagnetic wave at ω and the bound harmonic wave at 2ω induced by the nonlinear polarization propagate through the medium,

Table 6.1. Electric Susceptibility Functions $\chi^{(2)}$ and $\chi^{(3)}$ for Various Types of Interacting Field Components, Terminology, and Applications

<i>Susceptibility</i>	<i>Effect</i>	<i>Application</i>
$\chi^{(2)}(0; \omega, \omega)$	Optical rectification	Hybrid bistable device
$\chi^{(3)}(-\omega; \omega, 0)$	Electrooptic (Pockels) effect	Modulators, variable-phase retarders
$\chi^{(2)}(-2\omega; \omega, \omega)$	Frequency doubling	Harmonic generation
$\chi^{(2)}(-\omega_a; \omega_a, \omega_b)$	Frequency mixing	Parametric amplifiers, IR up conversion
$\chi^{(3)}(0; 0, 0, 0)$	Dielectric saturation	Poling
$\chi^{(3)}(0; 0, -\omega, \omega)$	Second-order optical rectification	
$\chi^{(3)}(-\omega; \omega, 0, 0)$	Quadratic electrooptic effect	Variable-phase retardation, liquid-crystal displays
$\chi^{(3)}(-\omega_a; \omega_a, \omega_b, -\omega_b)$	AC electrooptic effect, AC Kerr effect, Brillouin scattering, Raman scattering,	High-speed optical gates
$\chi^{(3)}(-\omega_a; \omega_a, \omega_b, -\omega_b)$	Two-photon absorption	
$\chi^{(3)}(-\omega; \omega, \omega, -\omega)$	Self-focusing, degenerate four-wave mixing, optical Kerr effect	Optical bistability, phase conjugation, optical transistors, image processing
$\chi^{(3)}(-3\omega; \omega, \omega, \omega)$	Frequency tripling	Deep-UV conversion

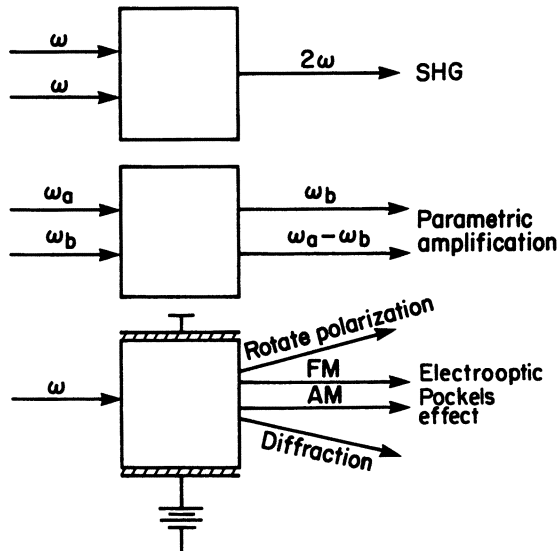


Figure 6.1. Nonlinear optical effects occurring through $\chi^{(2)}$.

their amplitudes can change periodically, depending on the phase relationship between them. As these waves exit the medium, the nonlinear interaction is terminated, and the relative intensities at the fundamental and harmonic frequencies are determined at that point. If the bound wave travels through the nonlinear medium in phase with the fundamental wave, the harmonic field can build up considerable amplitude (4).

Frequency mixing occurs when the incident fields ω_a and ω_b are different. In this case, beat frequencies occur in the polarization at $\omega_a \pm \omega_b$. Again the electric field distributions are determined by the magnitude of the nonlinear coefficient, the path length over which the interaction occurs, and the phases of the waves. The case of frequency difference mixing $\omega_a - \omega_b$ is particularly interesting. If ω_a is the more intense "pump" wave and ω_b is the weak "idler" wave, the nonlinear interaction leads to the splitting of ω_a into two lower frequency photons and the amplification of ω_b (5). This parametric amplifier is potentially extremely useful in spectroscopy for detecting weak signals and in optical communications for detecting repeaters (6).

The linear electrooptic or Pockels effect occurs from the interaction between an optical field and a direct-current (dc) field in the nonlinear medium, altering the propagation characteristics of light in a medium. The propagation characteristics are described by an ellipsoid with components along the principal dielectric axes $1/n_x^2$, $1/n_y^2$, and $1/n_z^2$. Depending on the symmetry of the medium, the application of an electric field can change these values, which can be used to rotate polarization, achieve frequency or amplitude modulation, or diffract light, if a periodic refractive index modulation can be achieved. Complete discussions of these effects and devices using them can be found in the literature (7-9).

6.1.2 Effects Occurring through $\chi^{(3)}$

Several nonlinear effects occurring through $\chi^{(3)}$ are illustrated schematically in Figure 6.2. The first of these is third harmonic generation (THG). Similar to SHG, this effect arises from a Fourier component of the nonlinear polarization at 3ω acting as a source of electromagnetic radiation. As with SHG, the magnitude of the field at 3ω depends on the magnitude of the coefficient, the interaction, and the phases of the interacting field components.

A major difference between even- and odd-order nonlinear interactions is that a response can occur at the fundamental frequency in media exhibiting odd-order responses. Thus, a variety of interesting and useful phenomena occur through $\chi^{(3)}$. One such effect is optical bistability resulting from light-intensity-induced changes in the refractive index of the medium in a resonant cavity (10), which in turn affects beam propagation in the cavity. In this case, the cavity is formed from a nonlinear medium designed to be an integral number of wavelengths of the incident radiation in length, with partially reflecting front and rear faces. Destructive interference in the cavity results in low transmission through the device. As the light intensity increases, the

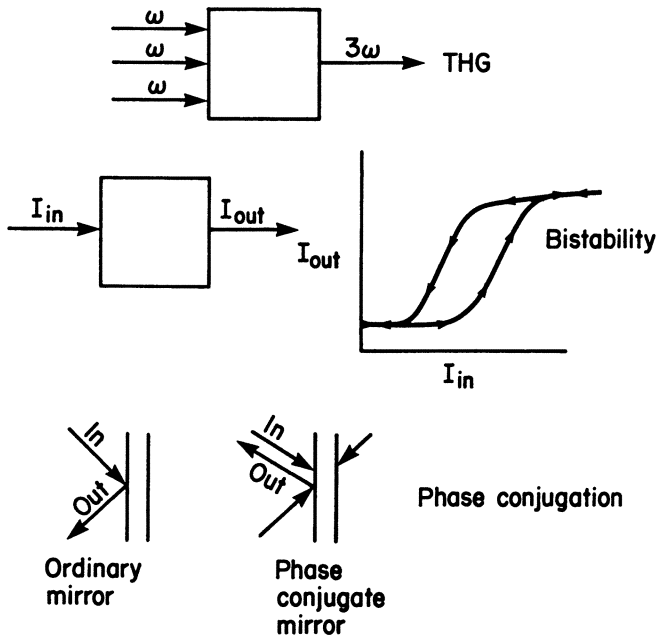


Figure 6.2. Nonlinear optical effects occurring through $\chi^{(3)}$.

electric field amplitude in the sample increases and alters the refractive index of the medium. For a properly designed cavity, the resulting phase shift tunes the cavity to a resonance, and the cavity becomes transmitting. This characteristic of highly nonlinear transmission versus light intensity results in hysteresis and bistable behavior. Variations of this effect have been investigated, including the optical analogue of a transistor in which a weak beam is used to control the transmission characteristics of an intense beam (10).

The third effect illustrated in Figure 6.2 is optical phase conjugation. An overview of this effect was published recently by Pepper (11). This effect results from a degenerate four-wave mixing process by which two beams interfere to form a phase grating, and the complex conjugate of the phase front of the incoming beam is created as an outgoing beam. The significance of the complex conjugate is that the phase front of the outgoing beam propagates as if it were time reversed relative to the incoming beam. Thus any loss in information because of phase shifts or aberrations in the incoming optical path is recovered in the outgoing path. In addition, electric field amplitudes can be altered in the nonlinear medium, and these alterations result in the amplification of the phase conjugate beam.

With an ordinary mirror, the image is reflected rather than redirected. Phase conjugate mirrors can be constructed to provide a number of lensless imaging and image-processing functions. Current values of electronic nonlinearities in polymers require laser power densities in the range of kilowatt per square centimeter in order for these effects to be manifested. Photo-refractive materials such as BaTiO₃ crystals have been used to demonstrate these effects at a power density of approximately 10 mW/cm² (12).

6.2 Microscopic Origin of Second-Order Nonlinearities

Rewriting equation 1 for the *i*th Cartesian component of the induced polarization in a molecule, one obtains

$$p_i = \alpha_{ij}E_j + \beta_{ijk}E_jE_k + \gamma_{ijkl}E_jE_kE_l + \dots \quad (6.3)$$

Understanding the electronic origins of β in a molecule begins with an analysis of the dynamic behavior of electrons in the molecule under the action of an electromagnetic field in the frequency range above vibrational and rotational modes and below electronic resonances. Under this influence, the state of the electrons in a molecule will be perturbed and oscillating currents will be induced in the molecule. A quantum mechanical expression can be obtained for computing the dipolar contributions to the current density induced in the molecule by the perturbing field and collecting terms of appropriate order. Ward (13) has expressed the perturbation to the Hamiltonian as

$$H' = -e(E^\omega \cdot r) \sin \omega t \quad (6.4)$$

where e is the electronic charge, E^ω is the field amplitude at frequency ω , and r is a coordinate associated with the position of the electrons and is calculated from

$$r = \sum_a r_a \quad (6.5)$$

in which a is summed over all electrons, and

$$er = \mu \quad (6.6)$$

The result is a perturbation expression for the components of the hyperpolarizability tensor which can be written as

$$\beta_{ijk} = \frac{1}{4^2} \sum_{e,e'} \sum_p \frac{\langle g | \tilde{\mu}_i | e \rangle \langle e | \tilde{\mu}_j | e' \rangle \langle e' | \tilde{\mu}_k | g \rangle}{(\omega_{e,g} - 2\omega)(\omega_{e',g} - \omega)} \quad (6.7)$$

In equation 7, the sums run over all excited states of the molecule and the sum over p generates three distinct terms by permutting $(-2\omega, i)$, (ω, j) , and (ω, k) . The operator $\hat{\mu}_i$ is defined as

$$\langle V | \hat{\mu}_r | W \rangle = \langle V | \hat{\mu}_r | W \rangle - \delta_{vw} \langle g | \hat{\mu}_r | g \rangle \quad (6.8)$$

where $\hat{\mu}_r$ is the dipole moment operator, $\omega_{e,g} = \omega_e - \omega_g$, and $\omega_{e',g} = \omega_{e'} - \omega_g$. When $V = W$ (diagonal terms), the matrix element is the difference between excited-state and ground-state dipole moments. When V is not equal to W (nondiagonal terms), there is a transition moment between excited states (14). To use this expression, it is essential to have good excited-state eigenfunctions for the molecule, and this requirement is far from a trivial matter. Garito and coworkers (15, 16) used a spectroscopically parameterized version of complete neglect of differential overlap (CNDO/S) with configuration interaction from all singly excited states to describe the excited state eigenfunctions of a number of substituted benzenes and obtained good agreement with experimental results. More recently, Docherty et al. (17) reparameterized CNDO/S by correlating computed and measured dipole moments and transition wavelengths for a series of organic conjugated molecules and obtained excellent agreement between measured and calculated values of β . Experimental determinations of β by electric-field-induced second harmonic generation give the vector component of β in the direction of the molecular dipole (x direction), and this quantity is related to the Cartesian components in equation 7 by

$$\beta_{\text{vec}} = \beta_{\text{xxx}} + (\beta_{\text{xyy}} + \beta_{\text{zzz}} + 2\beta_{\text{yyx}} + 2\beta_{\text{zzx}}) \quad (6.9)$$

For molecules with intense intramolecular charge-transfer transitions, β_{xxx} is by far the largest component of the hyperpolarizability, so

$$\beta_{\text{vec}} \sim \beta_{\text{xxx}} \quad (6.10)$$

Some interesting points can be made from Figure 6.3, for which the data of Docherty et al. (17) have been used and which shows the plot of the contributions of various excited states in the sum over states indicated in equation 7 to β_{vec} for 4-amino-4'-nitro-*trans*-stilbene. First, most of the nonlinearity occurs because of the charge-transfer resonance associated with the lowest optical transition in the molecule. Second, the seventh excited state drastically reduces the nonlinearity of the molecule. Careful examination of the matrix elements is required to determine whether this reduction is caused by reverse charge transfer or by an unfavorable transition moment between two of the low-lying excited states. Third, the calculation converges with inclusion of only a fraction of the total number of excited states included in the calculation. Judicious use of the last observation could save tremendous amounts of computer time in evaluating classes of similar molecules.

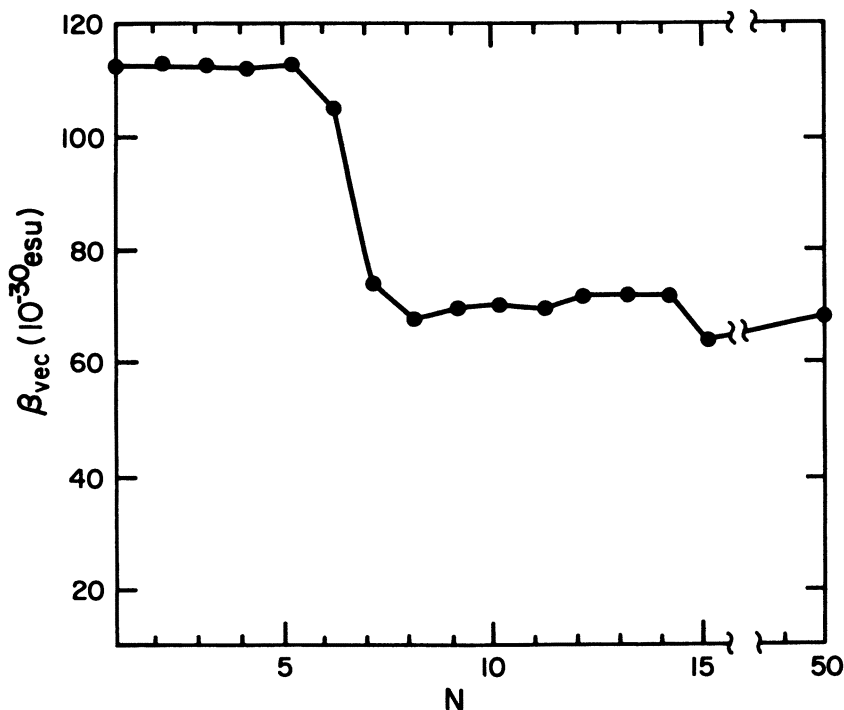
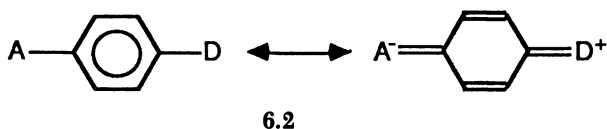


Figure 6.3. β_{vec} for 4,4'-N,N-dimethylaminonitrostilbene calculated by the excited-state perturbation method with CNDO/S-CI basis set versus the number of states (N) included in summation in equation 7. Data taken from Doherty *et al.* (17).

By carrying this observation to its extreme, a relatively simple two-level model can be developed that is useful for conceptualizing trends that influence β . If we assume a model with a nonpolar ground state and a polar lowest excited state coupled by charge-transfer resonance (structure 6.2), equation 6.7 simplifies to



$$\beta_{vec} = \frac{3e^2\hbar^2}{2m} F(\omega) f \Delta\mu_{e,g} \quad (6.11)$$

where

$$F(\omega) = \frac{W}{[W - (2\hbar\omega)^2][W^2 - (\hbar\omega)^2]} \quad (6.12)$$

In equation 12, W is the energy of the optical transition, f is the oscillator strength, and $\Delta\mu_{e,g}$ is the difference between ground-state and excited-state dipole moments. Increases in the electron-donating ability of the donor substituent and the electronegativity of the acceptor should increase both $\Delta\mu_{e,g}$ and f to a point that should have a favorable impact on β . Beyond that point, further increases in polarity will result in decreases in both F and $\Delta\mu_{e,g}$, and β will become smaller.


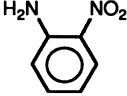
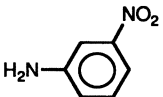
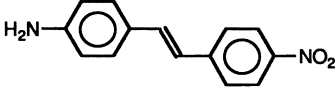
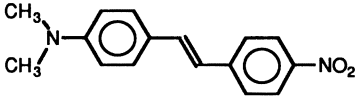
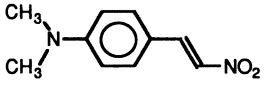
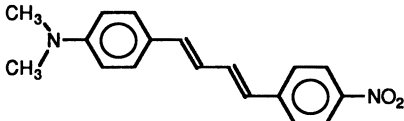
If we could continually vary the polarities in this simplified picture, we would see β going through zero to large negative values for appropriate combinations of highly polar ground states with less polar excited states. Increasing the conjugation length should also have a favorable impact. The two-level model was applied extensively to *p*-disubstituted benzenes (18, 19) and stilbene derivatives (20, 21) to illustrate the qualitative trends in the charge-transfer contribution to β_{vec} . The model appears to be most applicable when the primary electronic transition contributing to the enhancement in β arises from an intense low-lying charge-transfer transition well removed from other optical transitions in the molecule.

Table 6.2 lists values of β_{vec} obtained from the two-level model and compares them with published experimental values (17, 19, 20, 22, 23). The effect of the resonance interaction between amino and nitro substituents is clearly predicted by the model and confirmed experimentally. The agreement is far from quantitative, but qualitative trends can be seen. Increasing the conjugation length results in a gain in β by approximately 1 order of magnitude. The effects of increasing the charge density on the nitrogen atom by methyl substituent are both predicted and observed and are consistent with physical organic chemistry principles. The addition of ethylenic double bonds also results in a considerable increase in β . The numbers in parentheses were obtained by the method of excited-state perturbation sum over states described earlier. The numbers are considerably lower than the experimental values and smaller than those obtained by the two-level model. Nevertheless, the method of sum over states provides greater physical insight on the effects of structural variation on β .

6.3 Relationship between Microscopic and Macroscopic Nonlinearities

In experiments designed to measure nonlinear optical effects and in applications of these effects, the important properties are those of an ensemble of molecules. The observed nonlinear property is characteristic of the orientation of the molecules and corrections to incident electric field components caused by fields arising from charges on neighboring molecules. In the case of isotropic media, $\chi^{(1)}$ and $\chi^{(3)}$ are readily related to the molecular

Table 6.2. Values of β Computed from the Two-Level Model and Method of Sum Over States (in parentheses) Compared with Experimentally Obtained Values

<i>Molecule</i>	$\beta_{two\ level} (10^{-30}\ esu)$	$\beta_{exp} (10^{-30}\ esu)$
	19.6	16.2 ²² - 34.5 ¹⁹
	10.9	10.2 ¹⁹
	4	6 ²³
	227 (69.1) ¹⁷	225 - 295 ²³
	383	450 ²³
	217 (126) ¹⁷	180 - 260 ²³
	715 (355) ¹⁷	470 - 790 ²³

quantities α and γ by equations 13 and 14

$$\chi^{(1)} = N\alpha F^2(\omega) \quad (6.13)$$

$$\chi^{(3)} = N\gamma F(\omega_1)F(\omega_2)F(\omega_3)F(\omega_4) \quad (6.14)$$

where N is the number density of molecules and $F(\omega)$ is a local field factor providing a correction to fields incident on the medium for the reasons just described. For the sake of simplicity, α and γ are assumed to be orientational averages of the tensor quantities in equation 1 so that expressions 13 and 14 apply only to isotropic media. Local field factors are commonly estimated from the Onsager expression

$$F(\omega_i) = (\epsilon_\infty^1 + 2)\epsilon_\omega / (\epsilon_\infty^1 + 2) \quad (6.15)$$

where ϵ_ω and ϵ_∞ are the dielectric constants at frequency ω and the optical frequency limit (24), respectively. Because $\chi^{(2)}$ is zero in isotropic and centrosymmetric media, an orientational factor $O(\Omega)$ must be included in the relationship between the elements of the $\chi^{(2)}$ and β tensors

$$\chi^{(2)} = N\beta F(\omega_1)F(\omega_2)F(\omega_3)O(\Omega) \quad (6.16)$$

In the following discussion, expressions are developed for relating $\chi^{(2)}$ tensor components to the molecular tensor components for crystals, oriented polymers, and Langmuir–Blodgett films. The situation for crystals is illustrated schematically in Figure 6.4. In this figure, two molecules of different orientation are depicted as occupying the unit cell. The molecular Cartesian coordinates are designed as x , y , z , x' , y' , and z' and the crystal coordinates are X , Y , and Z . By assuming that the macroscopic nonlinearities arise primarily from intramolecular processes, the expression describing the mapping of β_{ijk} onto the crystal coordinate system is (25)

$$\chi_{ijk}^{(2)} = 2NF_I(2\omega)F_j(\omega)F_k(\omega) \sum_{s=1}^n \{ \cos [I, i(s)] \cos [J, j(s)] \cos [K, k(s)] \beta_{ijk}(s) \} \quad (6.17)$$

The summation over s ($n = 2$ in the case of the example) indicates the importance of orientation in the unit cell on the magnitude of $\chi^{(2)}$. Even large values of β in noncentrosymmetric space groups can result in small values of $\chi^{(2)}$ depending on the details of orientation. Oudar and Zyss (25, 26) have analyzed the orientational dependence of molecules in all the polar crystallographic point groups. The maximum value of $\chi^{(2)}$ that can be obtained for a properly phase matched interaction for optimal molecular orientation in that space group is listed in Table 6.3. The values are relative to an

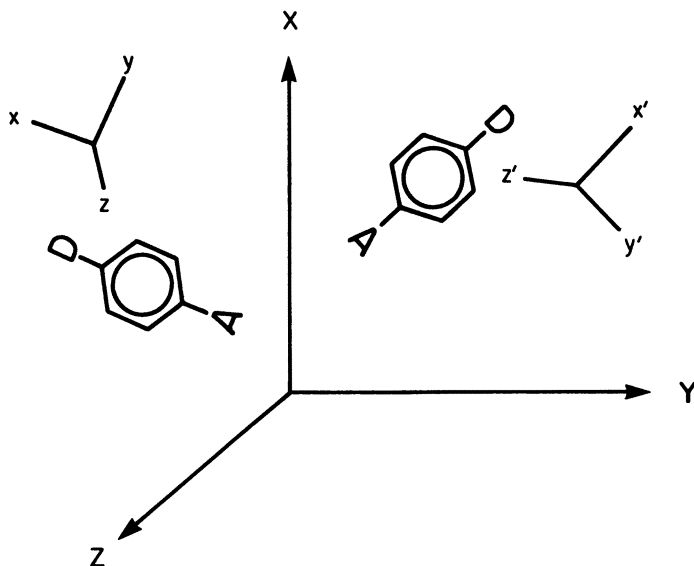


Figure 6.4. Molecular and crystal frames of reference for a noncentrosymmetric crystal.

Table 6.3. Polar Point Groups and Maximum Fractional Value of the Rigid Oriented Gas $\chi^{(2)}$ for a Phase-Matched Interaction for Optimum Molecular Orientation in the Unit Cell

<i>Point Group</i>	$\chi_{max}^{(2)}$
1, 2, m, mm2	0.38
62 M, 6, 3, 3 M, 32	0.25
222, 6 mm, 6, 4 mm, 42 M, 23, 43 M	0.19

NOTE: Point group 4 showed no phase-matched interaction.

SOURCE: Refs. 25 and 26.

oriented gas in which all molecules are pointed along the x axis, assuming that phase matching could be achieved. This assumption is generally not possible for π electronic systems in the visible and near-IR regions of the spectrum.

The previous discussion illustrates the difficulties in crystal engineering as an approach to the development of new nonlinear materials. With polymers, the situation is, conceptually at least, straightforward, and the problems that must be overcome are subject to analysis. The approach is to apply an external alignment field to polymer (or prepolymer) in a softened state and to fix the orientation with one of a variety of processing approaches. This approach is illustrated schematically in Figure 6.5, which shows how

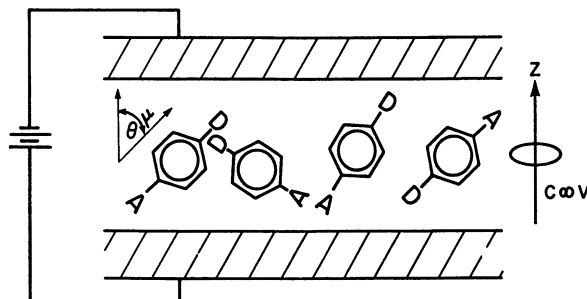


Figure 6.5. Poling a polymer film.

a film containing nonlinear chromophores is poled in the direction perpendicular to the film.

Polar alignment resulting from this process establishes $C_{\infty v}$ symmetry in the medium. There are two unique directions in the point group, the polar direction X and the direction perpendicular and cylindrically symmetric with respect to the X direction. When the common assumption that frequencies and the Cartesian axes along which they are applied can be freely interchanged in lossless media is invoked, only two nonequivalent tensor components exist.

$$\chi_{XXX}^{(2)} = N\beta_x f_X(2\omega)[f_X(\omega)]^2 \langle \cos^3 \theta \rangle \quad (6.18)$$

$$\chi_{XYX}^{(2)} = N\beta_x f_X(2\omega)[f_X(\omega)]^2 \langle (\cos \theta)(\sin^2 \theta) \rangle \quad (6.19)$$

In these equations, β is assumed to be equal to $\beta_x = \beta_{\text{vec}} \sim \beta_{\text{xxx}}$, and the orientation factor can be expressed in terms of average values of the molecular x axis which is parallel with the dipole moment with the poling direction X . Inspection of these expressions shows that a high degree of polar ordering favors $\chi_{XXX}^{(2)}$. For complete ordering of molecules, $\chi_{XYX}^{(2)}$ approaches zero. These observations have general implications for the types of nonlinear devices and waveguided structures that can be fabricated from such structures. These issues are discussed later in the chapter.

The analysis for polymers oriented perpendicularly to the plane of the film is readily extended to X - or Z -type Langmuir-Blodgett films. This analysis is illustrated schematically in Figure 6.6. When the chromophore dipole is parallel to the long axis of the amphiphilic unit, $C_{\infty v}$ symmetry is assumed and equations 18 and 19 are applied. For near-perfect orientation,

$$\chi_{XXX}^{(2)} \sim N\beta_x f_X(2\omega)^2 f_X(\omega) \quad (6.20)$$

and

$$\chi_{ZYX}^{(2)} \sim 0 \quad (6.21)$$

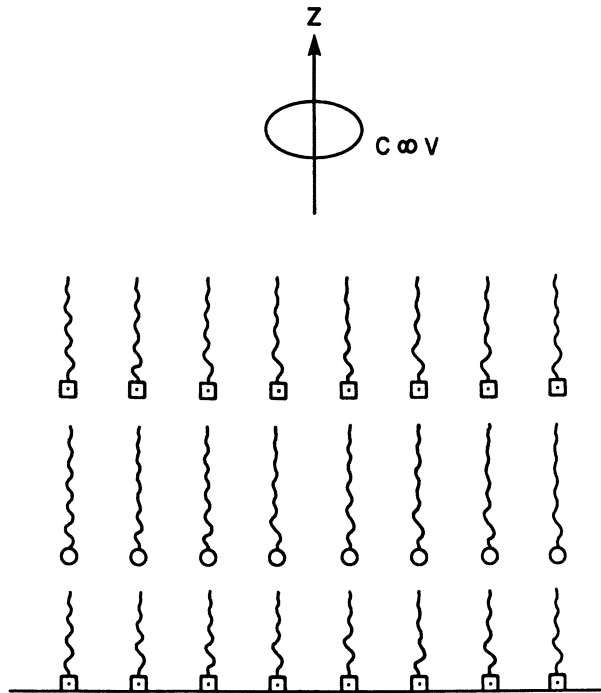


Figure 6.6. Langmuir-Blodgett alternating multilayer with $C_{\infty v}$ symmetry.

In general, perpendicular alignment is not observed, but rather, some degree of tilt within a domain structure in the film is observed. Thus cylindrical symmetry and values of tensor components significantly different from those of the idealized case are usually observed. The applications for oriented polymer films and Langmuir-Blodgett (LB) films will therefore be quite similar.

6.4 Recent Results for Polymers and LB Films

Values of $\chi^{(2)}$ for various types of materials are expressed as ranges in Figure 6.7, with the largest reported values to date indicated. My opinion is that uniquely useful applications for organic materials will require a $\chi^{(2)}$ of 10^{-7} esu or greater. In addition, a variety of additional application-dependent properties and attributes must be present in a material. Some of the important ones that must be considered are

- uniform birefringence,
- minimized scattering losses,
- transparency,

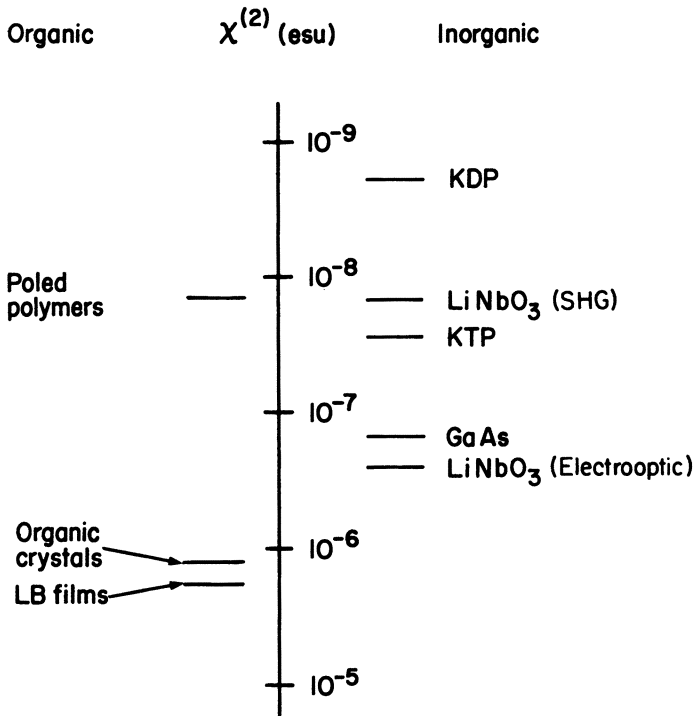


Figure 6.7. Upper limits of $\chi^{(2)}$ values reported for second harmonic generation of poled polymers, crystals, and LB films compared with those of inorganic crystals. Also noted is $\chi^{(2)}$ for the linear electrooptic effect in LiNbO₃.

- stability in ambient and operating environments,
- dimensional stability,
- thickness control, and
- processability.

At this time, molecularly doped poled polymers appear to fall somewhat short in the magnitude of the nonlinear coefficient (27, 28). As will be shown in the following paragraph this fact is primarily due to the competition between molecular orientation and thermal randomization. This competition emphasizes the importance of having a high concentration of dopant molecules and favorable thermodynamic factors to suppress thermal-randomization effects.

There are reports of a number of single crystalline materials with exceptionally large nonlinear coefficients, exceeding those for the best inorganic materials. Although impressive progress has been made in growing crystals in formats suitable for waveguide nonlinear optics (29), lack of control of crystal orientation has remained a source of difficulty and has limited this approach.

On a conceptual level, the ideal format for thin-film materials for nonlinear optics is the Langmuir–Blodgett film. Molecularly engineered chromophores with large hyperpolarizabilities can, in principle, be incorporated at high concentration, with well-defined orientations into films having thicknesses defined by molecular resolution. Extremely large resonantly enhanced values of $\chi^{(2)}$ have been reported in LB films several layers thick (30, 31); thus the considerable promise of this approach is established.

6.5 Poled Polymers

The use of molecularly doped poled polymers for second-order nonlinear optics was first explored by Meredith et al. (27).

6.5.1 Polar Alignment

Polar alignment can be described physically through a knowledge of the orientational distribution function $f(\theta)$ (32). A related quantity that can be expressed as a single number is the order parameter. The order parameter describing the induced polar alignment G is given by

$$G = \langle \cos \theta \rangle = \langle i \cdot I \rangle = \frac{\int_0^\pi f(\theta) \cos \theta \sin \theta d\theta}{\int_0^\pi f(\theta) \sin \theta d\theta} \quad (6.22)$$

where i and I are unit vectors parallel to the i th component of the molecular dipolar and the I th component of the field, respectively. The quantity $f(\theta)$ is given by

$$f(\theta) = e^{-U(\theta)/kT} \quad (6.23)$$

where $U(\theta)$ is the potential energy as a function of θ . In an isotropic medium

$$f(\theta) = e^{\mu E \cos \theta / kT} \quad (6.24)$$

In an anisotropic medium such as a nematic mesophase or a uniaxially stretched medium film, $f(\theta)$ is given by

$$f_n(\theta) = e^{(-U_n(\theta) + \mu E \cos \theta) / kT} \quad (6.25)$$

Therefore, an appropriately designed anisotropic medium could enhance (or retard) polar alignment.

In a nematic environment, $U_n(\theta)$ is given by (35)

$$U_n(\theta) = -\frac{\epsilon_\perp}{8\pi} E^2 - \frac{\epsilon_a}{8\pi} (N \cdot E)^2 \quad (6.26)$$

where N is the nematic director axis, ϵ_{\perp} is the component of the dielectric constant parallel to N , and ϵ_a is the dielectric anisotropy ($eS - e_{\perp}$).

Substituting equations 24–26 into equation 22 leads to expressions for $\langle \cos \theta \rangle$. For an isotropic environment and $\mu E/kt \ll 1$,

$$\langle \cos \theta \rangle_{\text{isotropic}} = \mu E/3kT \quad (6.27)$$

Assuming a sharply peaked nematic environment allowing orientation parallel or antiparallel to N , that is, the Ising model, yields

$$\langle \cos \theta \rangle_{\text{Ising}} = \mu E/kT \quad (6.28)$$

A general expression can be written for large fields and/or dipoles

$$\langle \cos \theta \rangle = \coth a - \frac{1}{a} = L(a) = \frac{1}{3a} - \frac{1}{45a^3} + \frac{2}{945a^5} - \frac{2}{9450a^7} + \dots \quad (6.29)$$

where $a = \mu E/kt$. This expression is identical to that derived by Langevin (36) to describe the behavior of magnetic dipoles in a directing field. For small fields, equation 29 is equivalent to equation 27, but for large fields (dipoles), the expression predicts saturation behavior. Substitution of these results into equations 18 and 19 gives the $\chi^{(2)}$ values listed in Table 6.4. These results demonstrate that only one tensor component will be significant in highly poled polymer films or in perfectly oriented X or Z Langmuir–Blodgett films. This property has important consequences for the types of applications for these materials.

6.5.2 Examples of Behavior of Poled Polymer Films

For the remainder of this section, three examples illustrating the behavior predicted in Table 6.4 are discussed. Singer et al. (28) have extensively investigated field-induced alignment for the azo dye Disperse Red I in polymethyl methacrylate (PMMA). Using a dopant molecule number density of $2.74 \times 10^{20}/\text{cm}^3$, they showed the reasonably linear behavior of $\chi_{XXX}^{(2)}$ with poling field when the film was poled above its T_g and quenched in the

Table 6.4. Expressions for Estimating Values of $\chi_{XXX}^{(2)}$ and $\chi_{YXX}^{(2)}$ in Various Environments

Parameter	Isotropic	Ising	Saturation
$\chi_{XXX}^{(2)}$	$\frac{fN\mu E\beta_z}{5kT}$	$\frac{fN\mu E\beta_z}{kT}$	$fN\beta_z$
$\chi_{YXX}^{(2)}$	$\frac{fN\mu E\beta_z}{15kT}$	Small	Small

presence of a field. The measured value of the coefficient agrees well with that predicted from the model for a poled isotropic system in Table 6.4 and gave a value of 3×10^{-6} esu at a poling field of 0.6×10^6 V/cm. The poling process is illustrated schematically in Figure 6.8.

An earlier study of the molecularly doped polymer liquid crystalline system shown in Figure 6.9 revealed more complex behavior (27, 32). In this study, the amount of induced nonlinearity was path dependent, with the largest observed value occurring when poling was done near T_g ($\sim 25^\circ\text{C}$). The host polymer exhibits a nematic-to-isotropic transition at $T_i = 100^\circ\text{C}$ and a nematic texture between T_g and T_i . Poling at 50°C produces a decrease in $\chi_{xxx}^{(2)}$ of approximately 1 order of magnitude. The $1/T$ dependence predicted by the model would account for only a small portion of that decrease. Nevertheless, the observed value of $\chi^{(2)}$ for a sample with $N = 4.4 \times 10^{-19}/\text{cm}^3$ and a poling field of 0.013×10^6 V/cm was 6×10^{-9} esu and agrees well with the predicted value.

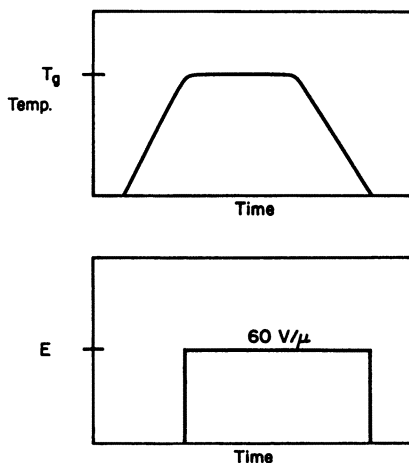
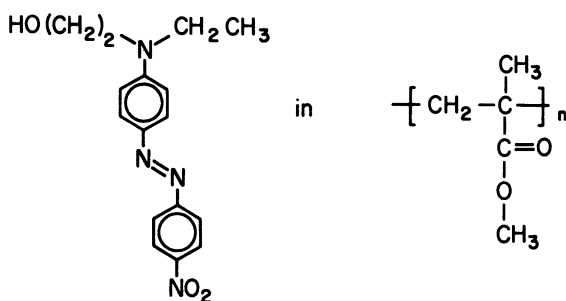


Figure 6.8. Poling profile for the dye Disperse Red I in PMMA (28).

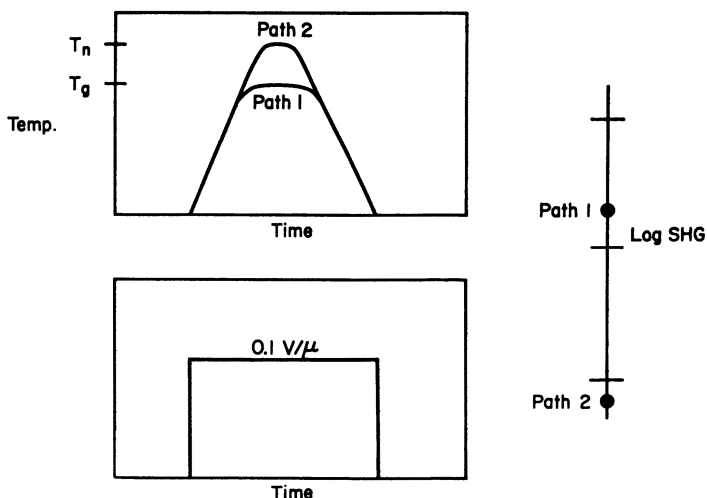
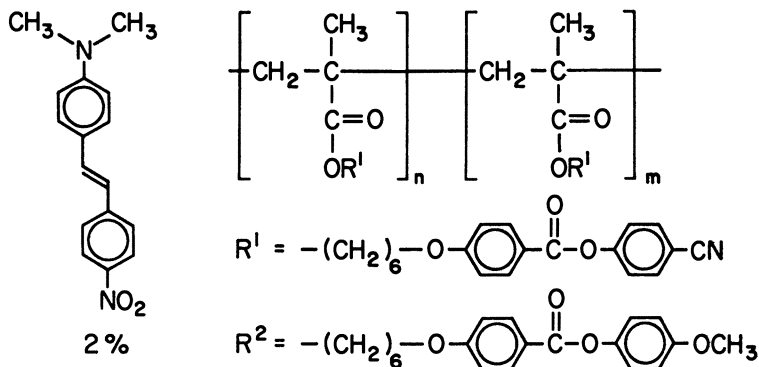


Figure 6.9. Poling profile for 4,4'-N,N-dimethylaminonitrostilbene in a liquid crystalline thermoplastic polymer (27).

These results point out the value of the weak cooperative interaction between the dopant molecules and the anisotropic liquid crystalline environment. The reason for the sharp drop in $\chi^{(2)}$ with increasing temperature in the nematic region is unclear at this point. Competing equilibria involving molecular association combined with temperature-dependent relaxation processes may have something to do with it. These effects were not observed in the isotropic system discussed earlier.

If the concentration is increased by 10 times without disrupting the nematic order and the high poling fields employed by Singer et al. (28) are used, values of $\chi^{(2)}$ greater than 10^{-7} esu might be obtained by this approach,

which would enable the use of this material for many devices and applications of second-order nonlinear phenomena.

Another way to take advantage of cooperative phenomena to achieve enhanced polar alignment is illustrated in Figure 6.10. In this approach, a solution of γ -polybenzyl-L-glutamate (PBG) is subjected to an electric field and second harmonic generation is monitored (33). Because the individual repeat units of the polymer chain are noncentrosymmetric and rigidly coupled to each other through hydrogen bonding, an extended polar polymer chain is obtained. The figure shows that the alignment is approaching saturation. Extension of the concept to chains with higher nonlinearity per repeat unit could result in very large values of $\chi^{(2)}$. For PBG, the behavior predicted in Table 6.4 (near saturation) is observed and corresponds to a chain dipole moment of 6000 D.

The Langmuir-Blodgett deposition technique shows excellent promise for the assembly of films with noncentrosymmetric ordering and $C_{\infty v}$ symmetry. A system that was reported recently (31) is shown in Figure 6.11. In this system, monolayers of the hemicyanine dye and the nitrostilbene

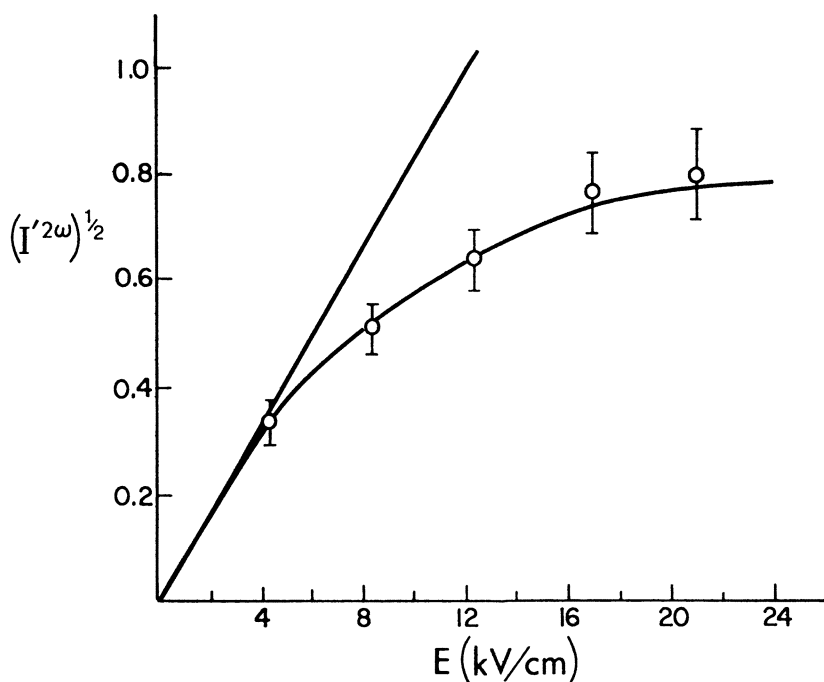


Figure 6.10. Square root of second harmonic intensity (O) versus electric field for γ -polybenzyl-L-glutamate (33). The curved line is the best fit to equation 28, and the straight line is the extrapolation of the low-field value obtained from $\chi_{xxx}^{(2)}$ in Table 6.4.

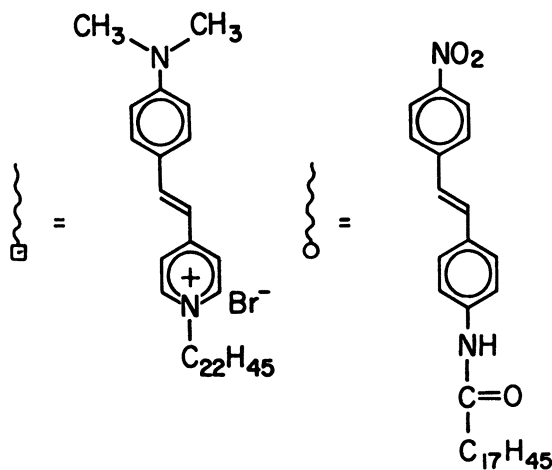
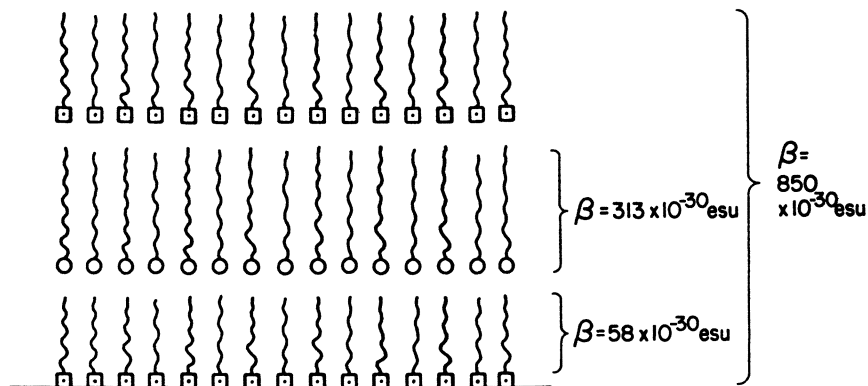


Figure 6.11. Langmuir-Blodgett alternate multilayers with hyperpolarizabilities associated with the individual layers and the multilayer according to Neal *et al.* (31).

derivative were alternatively transferred to a glass slide to build up multilayer structures. If the deposited chromophores had perfect perpendicular alignment with respect to the plane of the film, values of $\chi_{XXX}^{(2)}$ and $\chi_{ZXX}^{(2)}$ similar to those reported in Table 6.4 for saturation alignment would be expected. An analysis of signals obtained by second harmonic generation techniques (31) produced the values of β shown in the figure, with the average polar angle relative to the substrate normal of 23° in a bilayer of the two components. For monolayer films of the nitrostilbene derivative and hemicyanine dye, individual angles of 30° and 24° , respectively, were obtained. The bilayer structure seems to reinforce the perpendicular alignment in the film. For a five-layer film with hemicyanine at the bottom and top

layers, one can estimate that $\chi_{XXX}^{(2)} \sim 3\chi_{XTY}^{(2)} \sim \chi_{YYX}^{(2)} > 10^{-6}$ esu, which has important implications for waveguide design, which is discussed later.

A variety of additional properties and requirements must be demonstrated before such films are useful for devices. Waveguide designs require layers in the 0.1- to 1- μm thickness range. The films must be thermally stable, a property that is not a trivial matter for these waxy materials. It must also have photochemical and chemical stability in the environment in which it is used. The solution to these problems will require significant advances in synthetic and polymer chemistry.

6.6 Polymers and LB Films in Waveguides

6.6.1 Waveguides

A potentially important application of poled polymer films and LB multilayers, assuming they can be made with sufficient quality and stability, is in waveguide nonlinear optics. The work done in the field of second- and third-order nonlinear effects in waveguides was recently reviewed by Stegeman and Seaton (34). The advantages of waveguides are that beams can be confined to regions of the order of the wavelength of light and that very large intensities can be achieved with small total powers. Diffractionless propagation occurs in the film for distances limited only by the absorption and scattering losses in the film. In this section, I will discuss some of the general features of simple planar waveguides and illustrate their utility for second harmonic generation.

The main features of a planar waveguide are illustrated in Figure 6.12. The waveguide is formed by sandwiching layers of high-refractive-index material between two layers of material with lower refractive index. In this case $\eta_2 > \eta_1 \sim \eta_3$. The spatial distribution of optical energy propagating in the z direction in the waveguide is referred to as a mode. An equivalent mathematical definition of a mode is an electromagnetic wave which is a

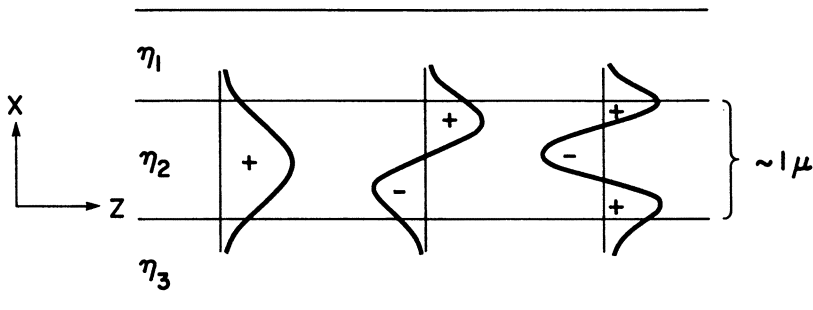


Figure 6.12. X electric field distributions in TM modes in a symmetric waveguide where $\eta_1 = \eta_3 < \eta_2$.

solution to Maxwell's equations. The boundary conditions imposed on the solution to Maxwell's equations permit only discrete modes to occur (37).

A particular set of modes referred to as TM modes is illustrated in Figure 6.12. In this figure, the curves represent the electric field intensity distribution along the x direction in the waveguide. The TM_0 mode has the highest propagation momentum in the waveguide and hence the lowest phase velocity of the guided modes. The higher order modes have high phase velocities. Therefore, the effective refractive index in the waveguide is larger for the higher order modes. Alternatively, the modes can be viewed as interference conditions resulting from light rays that are totally internally reflected from the refractive index discontinuities in the waveguide and the curves represent standing-wave intensities resulting from the multiple internal reflections.

Hypothetical refractive index dispersion curves for TM-guided modes at ω and 2ω in an isotropic medium are shown in Figure 6.13 (38). The effective refractive index depends on both guide thickness and wavelength. In ordinary bulk media such as liquids or crystals, the refractive index dispersion is a function of only the wavelength and is independent of the geometry of the medium. Therefore, by adjusting either the thickness or the wavelength, it is possible to find two modes with exactly the same effective refractive index at the fundamental and harmonic frequencies. In other words, the modes are phase matched because the optical phase velocities are identical.

Depending on factors discussed as follows, this matching of modes can lead to an extremely efficient second harmonic generation. Figure 6.14 shows a hypothetical plot of phase-matching thickness versus waveguide thickness,

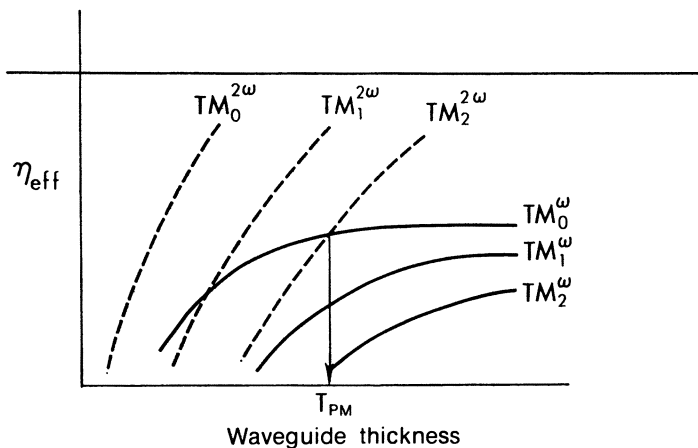


Figure 6.13. Effective refractive index in a waveguide versus thickness for various modes at the fundamental (ω) and harmonic (2ω) frequencies. A phase match thickness (T_{pm}) for $TM_0^\omega \rightarrow TM_2^{2\omega}$ conversion is indicated (40).

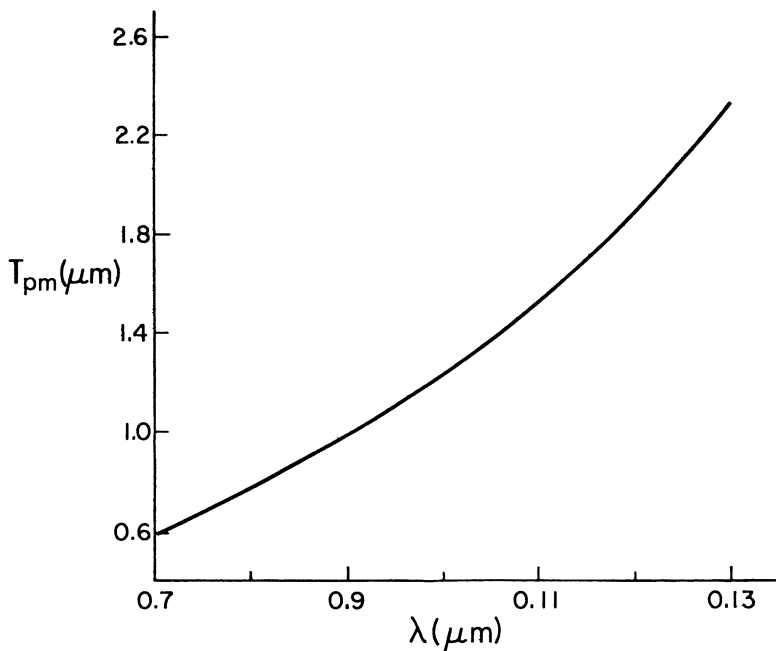


Figure 6.14. Wavelength dispersion of the phase-matching thickness T_{pm} (40).

emphasizing that layer thickness control can be used to tune the waveguide to a particular laser source (38).

6.6.2 SHG in Waveguides versus Bulk

For focused beams incident on a crystal, the optimum harmonic conversion efficiency is given by (39)

$$\eta_{\text{crystal}} = \frac{\omega^2}{n^3} \left(\frac{\mu_0}{\epsilon_0} \right)^{3/2} [\chi^{(2)}]^2 \lambda^{-1} L P^{(\omega)} F \left(\frac{\Delta k L}{2} \right) \quad (6.30)$$

where λ , ω , and n are the wavelength, frequency, and refractive index of the fundamental beam, respectively; $P^{(\omega)}$ is the power; Δk is the momentum difference at the fundamental and harmonic frequencies; L is the interaction length; and $F(\Delta k L/2)$ is a phase mismatch factor defined as $F(X) = \sin^2 X/X^2$ with $X = \Delta k L$. The quantity $\Delta k L$ is a phase angle $\Delta\phi$. $F(X)$ is zero at $\Delta k = 0$ and a maximum at $\pi/2$.

At the top of Figure 6.15, the refractive index dispersion associated with an optical transition at a frequency greater than 2ω is schematically illustrated. The difference in refractive index $\Delta\eta$ produces a phase difference $\Delta\phi$ after the waves have traversed a distance L . Phase-matched versus non-

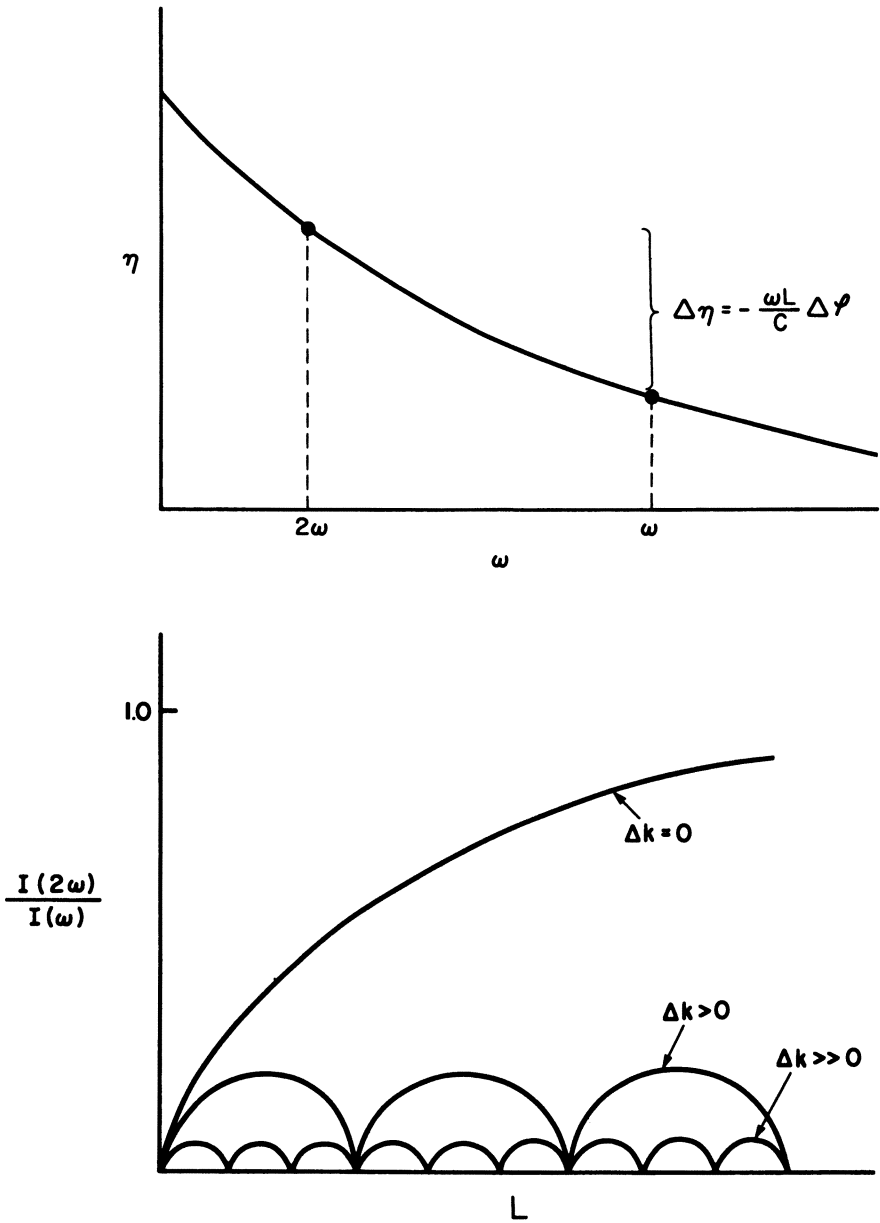


Figure 6.15. Refractive index dispersion and harmonic conversion efficiency versus interaction length for various degrees of phase mismatch Δk .

phase-matched harmonic generation is illustrated at the bottom of Figure 6.15. In this figure, for a given amount of phase mismatch Δk , the amount of power at the harmonic frequency relative to that at the fundamental frequency will be determined by the path length traveled in the crystal, and only the last coherence length before the interface at which the waves leave the nonlinear medium is important.

The characteristic oscillation length is referred to as the coherence length L_C . For phase-matched harmonic generation, the conversion of fundamental beams to harmonic beams is determined by the interaction length. Other factors, such as diffraction, lack of colinearity of propagation of fundamental and harmonic beams in birefringent media, and depletion of fundamental beam power, ultimately limit the conversion efficiency.

In a waveguide, the conversion efficiency is given by (29)

$$\eta_{\text{wg}} = \frac{\omega^2}{n^3} \left(\frac{\mu_0}{\epsilon_0} \right)^{3/2} [\chi^{(2)}]^2 a^{-1} I_R F \left(\frac{\Delta k L}{2} \right) \quad (6.31)$$

where a is the waveguide thickness, I_R is an overlap integral defined as

$$I_R = \int P_{\text{NL}} E_m^{2\omega} d\sigma \quad (6.32)$$

where P_{NL} is the nonlinear polarization, $E_m^{2\omega}$ is the harmonic field distribution, and σ is the cross-sectional coordinate. I_R is optimal at $1/a$. Under these conditions

$$\eta_{\text{wg}} / \eta_{\text{crystal}} \sim L / \lambda \quad (6.33)$$

In practical situations, the advantage of the waveguide will be determined primarily by the coherence length (or degree of phase mismatch) within the waveguide. As previously mentioned, the effective refractive index for a guided mode is thickness dependent so that the thickness, as well as its uniformity over the length of the waveguide, will determine the phase mismatch.

To assess the potential impact of polymeric and LB films on waveguide design and performance for SHG, I have examined the limitations imposed by phase-matching requirements on the interaction length needed to achieve a desired degree of conversion efficiency.

Figure 6.16 shows a plot of $f(\Delta k L)$ versus Δk for various interaction lengths. The plot shows that for a particular degree of phase mismatch Δk the impact of $f(\Delta k L)$ is far less if the needed degree of conversion can be achieved in 0.05 cm (for example) rather than in 1 cm. According to equation 32, an approximately $\times 4.5$ increase in nonlinear coefficient would be required to enable a degree of conversion in the 0.05-cm waveguide similar to that achieved in the 1-cm waveguide. Thus waveguide thickness tolerances

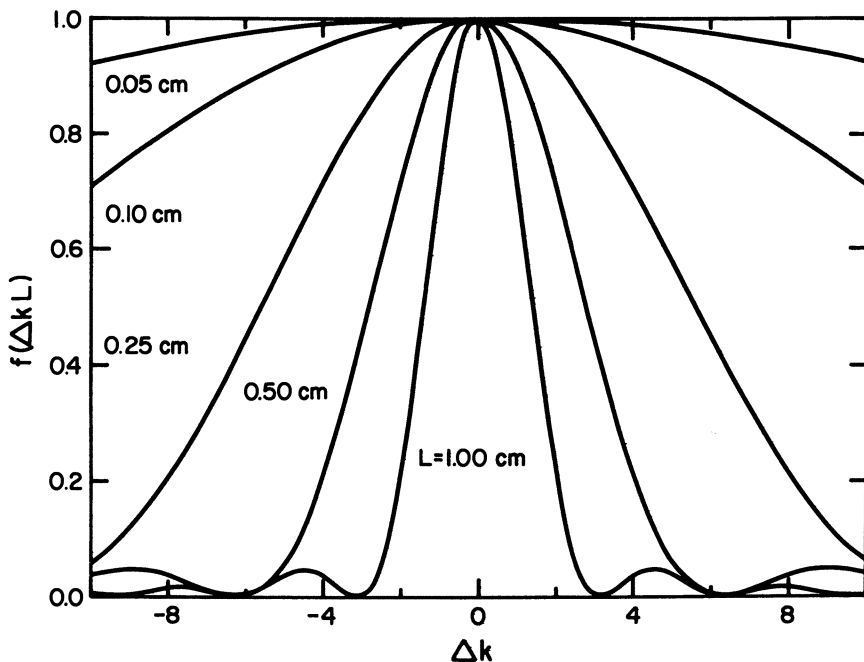


Figure 6.16. Phase mismatch factor $f(\Delta kL)$ versus degree of phase mismatch Δk for various interaction lengths L .

and refractive index inhomogeneity requirements could be greatly eased with the material of higher nonlinearity, assuming other factors are equal. To further illustrate the point, a plot of η_{wg} versus L for various nonlinear coefficients is shown in Figure 6.17. The input power is 10 mW, and the overlap integral is assumed to be optimized.

As the figure indicates, a material with $\chi^{(2)} \sim 10^{-6}$ could provide 10% conversion efficiency in $\sim 150 \mu\text{m}$. For a material like LiNbO_3 with $\chi^{(2)} \sim 3.1 \times 10^{-8}$ esu, waveguiding lengths of ~ 1 cm or so are anticipated. On the other hand, higher incident powers could achieve larger conversion efficiencies, with the power requirement proportional to $[\chi^{(2)}]^{-2}$. Crystals of *N*-(4-nitrophenyl)-*L*-prolinol (NPP) have a phase-matchable second-order coefficient of 3.94×10^{-7} esu, and investigations of these materials in waveguided formats are underway (29). If appropriate orientation and geometrical control can be achieved, highly efficient devices can be designed.

For organic materials, a figure of merit for η according to equations 30 and 31 is $\chi^{(2)}/n^3$. Organic materials typically have refractive indices of ~ 1.5 , whereas LiNbO_3 , which is more commonly used for waveguide nonlinear processes, has a refractive index of 2.24. The low refractive index of organic polymeric materials is therefore an additional benefit for parametric processes.

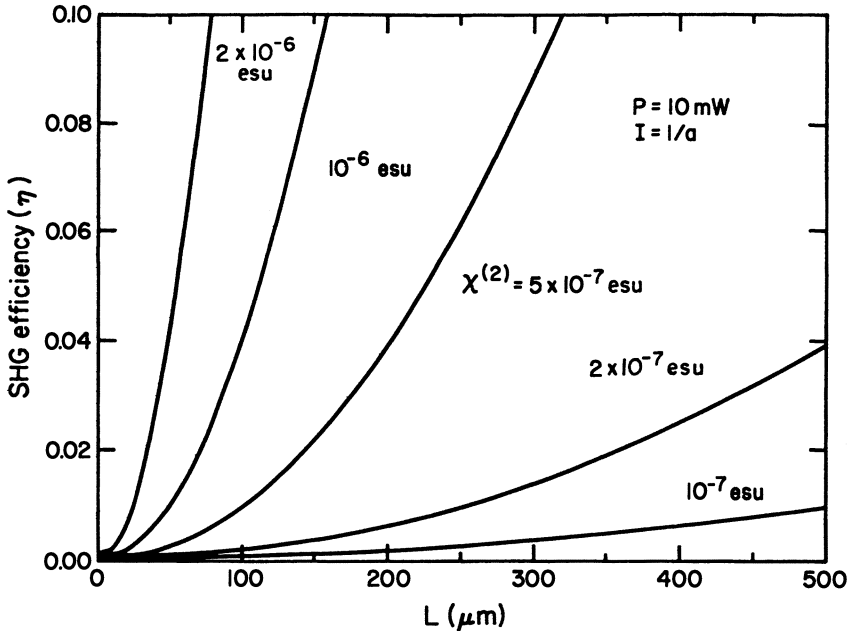


Figure 6.17. Harmonic conversion efficiency in a waveguide under phase-matched conditions versus path length for various values of $\chi^{(2)}$ at a 10-mW input power and for the optimum value of the overlap integral as explained in the text.

A final point concerning harmonic generation in waveguides relates to the design of the waveguide itself. Waveguide dispersion as illustrated in Figure 6.13 suggests that it is, in general, not possible to achieve phase matching between harmonic and fundamental beams in the same guided mode. Figure 6.13 indicates that for this hypothetical example phase matching occurs for several combinations of thickness (t) and wavelength (λ). The spatial distributions of electric fields for the TM_0 and TM_1 modes (point 1) indicate that the overlap integral between these two modes should be zero. In Figure 6.13 also, a second phase-matching point (2) exists for TM_0^o and TM_2^o . Although the overlap integral is nonzero, the negative lobe in TM_2 reduces the efficiency of the interaction considerably.

It is also necessary that there be an effective nonlinear coefficient $\chi^{(2)}$ that couples the two modes. As I indicated earlier, poled polymer films and X- or Z-oriented LB films should have large $\chi_{XXX}^{(2)}$ values that are optimum for interactions involving TM modes which contain E_x components. By using multilayer waveguides, it is possible to devise approaches that avoid the spatial concentration of field distributions between low-order modes. One such approach is illustrated in Figure 6.18, with X- or Z-deposited LB films. In this figure, the polar orientation is reversed at the node of the TM_1 mode.

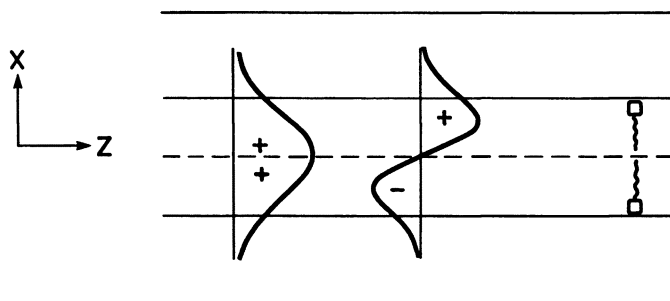


Figure 6.18. $TM_0 \rightarrow TM_1$ conversion in a multilayer LB waveguide with the direction of alignment reversed at the node of the TM_1 mode.

Because β has a sign associated with it, the electric field sign should also be reversed and the effective overlap integral would be large.

Another way to achieve large harmonic conversion efficiencies is to phase match the zeroth order TM and TE modes. The overlap integral would, in principle, be quite large, but a large off-diagonal coefficient coupling the two polarization directions would also be required. Figure 6.13 illustrates TM dispersion curves in an isotropic medium for simplicity, but in birefringent media, the situation is considerably more complex (40). Under these circumstances, the TM modes split into six branches and the TE modes that were not shown split into an additional three branches. Because the dispersion of TE modes tends not to significantly depart from that for the TM modes in isotropic media, a $TM_0^\circ - TE_0^{2\omega}$ crossing point does not exist and phase matching cannot be achieved.

In anisotropic media, the splittings described lead to significantly different dispersion behaviors for TM and TE modes and a waveguide thickness is more likely to exist where η_{eff} for the two polarizations is equal and phase matching occurs. As mentioned, an off-diagonal tensor element is required to couple the two polarizations. Analysis of equation 9 shows that a polar tilt angle of 66° from the waveguide normal would maximize $\chi_{XY}^{(2)}$.

In the hemicyanine–nitrostilbene system described earlier (31) (Figure 6.11), the off-diagonal tensor elements are large, indicating a substantial average tilt in the molecular axis relative to the direction perpendicular to the film plane, and thus, this system might be conducive to phase matching between the TM° and TE° modes, assuming other fabrication requirements for waveguides are achieved.

6.7 Issues for Polymers and LB Films

Organic materials, in particular polymers and LB films, have important characteristics that may warrant their use in integrated optical and other

thin-film optical technologies. Before these applications can be realized, considerable effort will be required to develop a technologically useful material(s). Some of the issues that must be addressed in chemical and materials research are outlined in the following section.

6.7.1 New Chromophore Design and Synthesis

The hyperpolarizabilities of a number of organic chromophores have been reported (17, 19, 20, 22, 23), and many of them are quite large and would be suitable for use in devices if they could be aligned at high density in the solid state. Some of the issues that must be considered are the following.

- The chromophore must be stable in the environment under which it will be used.
- The chromophore must be transparent in the appropriate spectral region for the desired application (for second harmonic generation of 825-nm laser diodes, transparency at 412 nm is essential, but this generally occurs at the expense of β).
- β should be as large as possible per unit of molecular volume (if increasing the size of the chromophore does not produce a disproportionately large increase in β , an alternative molecular design and synthetic strategy should be pursued).
- The chromophore should be compatible with other synthetic strategies that might be needed for monomer design and polymer formation.
- High concentrations of chromophore per unit volume in the solid is essential because $\chi^{(2)} \propto \beta/N$.

6.7.2 High Degree of Polar Order

A high degree of polar order, in general, leads to high values of the $\chi_{xxx}^{(2)}$ coefficient. The usefulness of maximizing this coefficient is application dependent. Whereas a large off-diagonal tensor component, for example, $\chi_{xy}^{(2)}$, might be more useful for SHG with birefringent phase matching or maximizing a waveguide nonlinear interaction between modes of different polarization, it is also true that waveguide structures can be designed to produce a similar end result with $\chi_{xxx}^{(2)}$.

The main issues that need to be considered in the approach with molecularly doped polymer are concentration of dopant molecules that must be maximized, electric fields required for poling, retention of field-induced alignment, and compatibility of poling with device concepts.

For LB multilayers, the main issue is the control of film symmetry through deposition characteristics. Polar alignment can be achieved through molecular design and synthesis.

6.7.3 Minimal Scattering

For a various reasons, light scattering losses can limit the utility of an otherwise potentially promising material. Partial crystallinity in polymer films, incompatibility in multicomponent systems, strain birefringence from the fabrication process, and broad molecular weight distributions leading to segregation are all potential contributors to light scattering.

In LB films, the formation of domains with different horizontal orientation components can lead to substantial scattering losses. This problem might worsen as the individual molecules or groups of molecules deviate from perfect vertical alignment.

6.7.4 Thickness Control

For polymers and LB films to be useful for waveguide applications, it is necessary to have excellent thickness control at the deposition stages or to achieve thickness control through subsequent processing steps. Absolute control of thickness is necessary for tuning the waveguide modes to specific modes and phase matching. Control over thickness variations at the dielectric interfaces is required because thickness variations translate to effective refractive index variations which lead to scattering losses or coupling out of the waveguide.

6.7.5 Patternwise Delineation

Patternwise delineation must be achieved for waveguide-based devices. It should be possible to form a precise, high-quality dielectric boundary between the linear and nonlinear regions of the device and to accurately define shapes and patterns.

For polymer films, orientation might be followed by photocross-linking and pattern development on the basis of differential solubility. This approach may be problematic because of strains resulting from photocross-linking or the quality of interfaces, vertical sidewalls, etc., that can be achieved. Deposition of image-forming layers above combined with dry processing, for example, reactive-ion etching, is also another possible approach.

The same issues apply to LB films. Flexibility of chemical design and the order that can be achieved in these films could lead to relatively straightforward approaches to patternwise delineation.

References

1. *Nonlinear Optical Properties of Organic Materials*; Williams, D. J., Ed.; ACS Symposium Series 253; American Chemical Society: Washington, DC, 1983.
2. Williams, D. J. *Angew. Chem. Int. Ed. Eng.* **1984**, *23*, 690.
3. *Nonlinear Optical Properties of Organic Molecules and Crystals*; Chemla, D. S.; Zyss, J., Eds.; Academic: Orlando, FL, 1987.
4. Zernike, F.; Midwinter, J. E. *Applied Nonlinear Optics*; John Wiley: New York, 1973; p 54–72.
5. Zernike, F.; Midwinter, J. E. *Applied Nonlinear Optics*; John Wiley: New York, 1973; p 153–176.
6. Ledoux, I.; Zyss, J.; Migus, A.; Etchepare, G.; Grillon, G.; Antonetti, A. *Appl. Phys. Lett.* **1986**, *48*, 1564.
7. Hunsberger, R. G. *Integrated Optics: Theory and Technology*; Springer-Verlag: Berlin, 1982; p 120–157.
8. Yariv, A. *Quantum Electronics*; John Wiley: New York, 1975; p 327–370.
9. Goldstein, R. *Laser Appl.* **1986**, *67*.
10. Gibbs, H. M.; McCall, S. L.; Venkaterson, T. N. C. *Opt. Eng.* **1980**, *19*, 463.
11. Pepper, D. M. *Sci. Am.* **1986**, *254*(1), 74.
12. Feinberg, J.; Heiman, D.; Tanguay, A. R., Jr.; Hellwarth, R. W. *J. Appl. Phys.* **1980**, *51*, 1297.
13. Ward, J. *Rev. Mod. Phys.* **1965**, *37*, 1.
14. Flytzanis, C. In *Quantum Electronics*; Rabin, H.; Tang, C. L., Eds.; Academic: New York, 1975; Vol. 1, Part A, p 74.
15. Lalama, S. J.; Garito, A. F. *Phys. Rev. A* **1979**, *208*, 1179.
16. Garito, A. F.; Teng, C. G.; Wong, K. Y. *Mol. Cryst. Liq. Cryst.* **1984**, *106*, 219.
17. Docherty, V. J.; Pugh, D.; Morley, J. O. *J. Chem. Soc. Faraday Trans.* **1985**, *81*, 1179.
18. Levine, B. F. *Chem. Phys. Lett.* **1976**, *37*, 516.
19. Oudar, J. L.; Chemla, D. S. *J. Chem. Phys.* **1977**, *66*, 2664.
20. Dulcic, A.; Dauteret, C. *J. Chem. Phys.* **1978**, *69*, 3453.
21. Dulcic, A.; Flytzanis, C.; Tang, C. L.; Pepen, D.; Fitzon, M.; Hoppilliard, Y. *J. Chem. Phys.* **1981**, *74*, 1559.
22. Teng, C. C.; Garito, A. F. *Phys. Rev. B* **1983**, *28*, 6766.
23. Oudar, J. L. *J. Chem. Phys.* **1977**, *67*, 446.
24. Onsager, L. *J. Am. Chem. Soc.* **1936**, *58*, 1486.
25. Oudar, J. L.; Zyss, J. *Phys. Rev. A* **1982**, *26*, 2016.
26. Zyss, J.; Oudar, J. L. *Phys. Rev. A* **1982**, *26*, 2025.
27. Meredith, G. R.; Van Dusen, J. G.; Williams, D. J. *Macromolecules* **1982**, *15*, 1385.
28. Singer, K. D.; Lalama, S. J.; Sohn, J. E. *SPIE Integrated Optical Circuit Eng. II* **1985**, *578*, 130.
29. Ledoux, I.; Josse, D.; Vidakovic, P.; Zyss, J. *Opt. Eng.* **1986**, *25*, 202.
30. Girling, I. R.; Kolinsky, P. V.; Cade, N. A.; Earls, J. D.; Peterson, I. R. *Opt. Commun.* **1985**, *55*, 289.
31. Neal, D. B.; Petty, M. C.; Roberts, G. G.; Ahmad, M. M.; Feast, W. J.; Girling, I. R.; Cade, N. A.; Kolinsky, P. V.; Peterson, I. R. *Electron. Lett.* **1986**, *22*, 460.
32. Williams, D. J. In *Nonlinear Optical Properties of Organic Molecules and Crystals*; Chemla, D. S.; Zyss, J., Eds.; Academic: Orlando, FL, 1987; Vol. 1, p 405.
33. Levine, B. F.; Bethea, C. G. *J. Chem. Phys.* **1976**, *65*, 1979.
34. Stegeman, G. I.; Seaton, C. T. *J. Appl. Phys.* **1985**, *58*, 1257.

35. de Gennes, P. G. In *The Physics of Liquid Crystals*; Clarendon: Oxford, 1974, p 97.
36. Langevin, P. J. *Phys.* **1905**, *4*, 678.
37. Hunsberger, R. G. *Integrated Optics: Theory and Technology*; Springer-Verlag: Berlin, 1982; p 31-69.
38. Jain, K.; Hewig, G. H. *Opt. Commun.* **1981**, *36*, 483.
39. Zyss, J. J. *Mol. Electron.* **1985**, *1*, 25.
40. Zyss, J.; Chemla, D. S. In *Nonlinear Optical Properties of Organic Molecules and Crystals*; Chemla, D. S.; Zyss, J., Eds.; Academic: Orlando, FL, 1987; Vol. 1, p 166.

RECEIVED for review April 15, 1987. ACCEPTED November 2, 1987.

Polymers in Optical Recording

James M. Pearson

Corporate Research Laboratories, Eastman Kodak Company, Rochester, NY 14650

Optical information storage, which has been a dream since the discovery of the laser, is now becoming a commercial reality. Read-only consumer products (video and digital audio disks) have provided a solid technological base for the development and introduction of the more sophisticated write-once and erasable recording systems. This chapter will review the current status of polymeric materials as substrates, protective layers, and active recording media in laser recording.

OPTICAL INFORMATION RECORDING AND RETRIEVAL have been a dream since the invention of the laser 20 years ago. It is only now becoming a commercial reality. Read-only consumer products such as the optical video disk and the digital audio disk have established a disk manufacturing and peripherals technological base that has accelerated the development of more sophisticated write-once and reusable recording systems. The availability of small GaAlAs semiconductor diode lasers having adequate power and stability has enabled the design and construction of the compact lightweight optical heads required by the technology. In addition, these lasers have also defined the wavelength region for recording, reading, and erasing and the sensitivity parameters required of the media.

The challenge to find appropriate recording media has proven to be a significant one. Appropriate recording media must have high marking sensitivity in the near-IR region of the spectrum coupled with long-term stability for write-once media and facile, rapid, and multicycle reversal for reusable materials. At present, the opportunity for polymer-based recording materials appears to be in the write-once arena. In "ablative" (pit forming) write-once systems, marking occurs by a thermal process, and low-melting, low-vaporization, low-flow-temperature materials with low thermal conductivity are

0065-2393/88/0218-0331\$06.75/0
© 1988 American Chemical Society

desirable. Organic and polymeric materials are, therefore, ideally suited for this mode of recording (1).

Polymer materials are also the leading candidates for disk substrates and for a number of disk packaging and protective configurations. Injection molding of video and compact disks has demonstrated that this technology has the potential for producing the more complex and demanding substrates required for recording systems. Advances in materials and processing will be necessary, but the appropriate research and development efforts appear to be in place, and recent disclosures suggest that success is imminent.

This chapter will review the present position and opportunities for polymeric materials in write-once and reversible optical recording. At present, no consensus has been reached on the optimal recording or disk substrate materials. Several alternatives are still being actively investigated.

7.1 Functional Performance Criteria

A summary of some typical performance requirements for a write-once medium is presented in Table 7.1. The material must be capable of producing well-defined micrometer-sized marks virtually instantaneously with a focused solid-state diode laser. For an optical system operating at a wavelength of ~ 800 nm with a numerical aperture of ~ 0.5 , this will enable a storage density of about 10^8 bits/cm². The medium should exhibit a marking sensitivity at 820 nm of better than 20-mW incident pulse power for 50-ns pulses, corresponding to a 10-Mbits/s recording rate. Threshold sensitivity should be in the 1–5-mW range.

The actual marking event should be rapid enough to allow for immediate read after writing, or direct read after write (DRAW). This capability will eliminate any type of postprocessing to create a detectable image and any slow image-forming chemistries. The DRAW feature employs a read-only laser that is mounted on the optical head unit along with the recording laser. The read spot trails the write spot by several micrometers and verifies the

Table 7.1. Performance Criteria for Write-Once Media

<i>Characteristic</i>	<i>Criterion</i>
Resolution	$\leq 1 \mu\text{m}$
Recording rate	≥ 10 Mbits/s
Sensitivity	$\leq 10^{-2}$ J/cm ²
Threshold sensitivity	≥ 1 mW
CNR ^a	> 50 dB
Packing density	$\geq 10^8$ bits/cm ²
Real-time recording	DRAW ^b
Areal defect density	$\leq 10^{-5}$ (uncorrected)
Stability	10 years

^a The abbreviation CNR stands for carrier-to-noise ratio.

^b The abbreviation DRAW stands for direct read after write.

accuracy of the recorded data. Inaccurate data, resulting from physical defects in the medium or erroneous signals, are then instantly rerecorded in a specially reserved sector area on the disk. This concept is critical in reducing the disk intrinsic defect level, which is a complex function of a number of system parameters, from a fabricated value of 10^{-4} – 10^{-6} to a corrected level of 10^{-12} as required by the technology.

To read out the recorded information with an adequate carrier-to-noise ratio (CNR), the medium must exhibit threshold recording behavior. The power level of the read beam can then be set at some value below threshold to guarantee nondestructive playback. For a variety of write-once media, the read power appears to be generally 3–5 times lower than the recording power.

The performance criteria in Table 7.1 are also generally applicable for the recording component of reversible (erasable) media. This type of medium must also undergo rapid, laser-induced reversibility from its marked state to its original state and be capable of a large number of switching cycles. Practical devices will probably require single-pass laser erasure using pulses in the microsecond to nanosecond time domain, and the ability to support as many as 10^6 erase–record cycles. Industry standards have not yet been established for these reversible systems.

7.2 Substrates

The technological base established by consumer video and digital audio disk products has created a solid foundation on which to build the advanced technology required for the more complex write-once and erasable systems. The demanding mechanical and optical requirements for these substrates severely limit the choice of polymers (2). Acrylics and polycarbonates appear to be the leading candidates for transparent disks; a number of other polymers (e.g., thermosetting resins and polyolefins) are reported to be under consideration (3). Injection molding and the 2P process (4) are the techniques presently employed to manufacture disks. Because both processes are ideally suited for introducing grooves and information marks directly into the surface of a disk, they are likely to continue to be the manufacturing methods of choice.

Detailed information on materials and fabrication equipment and processes is difficult to obtain. Competition is intense, largely owing to the staggering growth projections for disks, and only limited technical data are available. Nevertheless, a reasonable picture of the state of the art of both materials and process technology can be constructed.

7.2.1 Materials

Some of the key material requirements for optical disk substrates are mechanical integrity, dimensional stability over a range of temperatures and

humidities, good processability, high optical clarity, and low birefringence. One of the primary challenges facing the polymer manufacturer is the removal of particulate contaminants down to micrometer dimensions from the product. Also, the use of the standard additive approach to control physical properties may not be appropriate for this application where exudates are likely to be highly undesirable and the optical properties of the addenda become important. This possibility will necessitate property control via polymer structure modification. A comparison of a number of important properties for some candidate materials is provided in Table 7.2. The actual choice of substrate material will ultimately depend on factors such as cost, volume, performance requirements, and disk configuration. As has been the case for magnetic technology, particular materials will be suited for particular market segments and applications.

7.2.1.1 POLYCARBONATES

Several companies currently supply special-grade polycarbonates for injection molding of optical disks. Improvements in material purity and cleanliness over standard-grade polymers have been achieved through rigid process control and quality control procedures.

To improve processability, lower molecular weight resins ($M_n < 20,000$) with higher melt-flow indices (50–60 g/10 min compared with standard resin values <20 g/10 min at operating temperature) have been designed. Resin manufacturers appear to have been successful in reducing molecular weight without sacrificing impact strength. The ability to mold at higher temperatures to improve melt-flow response also appears to have been achieved with these resins. Higher thermal stability has most likely been attained by polymer end-capping rather than by conventional heat-stabilizer additives.

7.2.1.2 POLYACRYLICS

Acrylics are logical candidates for optical disks because of their outstanding optical properties (high transmission and low birefringence) and superior

Table 7.2. Selected Physical Properties of Substrate Polymers

<i>Property</i>	<i>PC</i>	<i>PMMA</i>	<i>Epoxy</i>
Transmittance (% at 830 nm)	90	92–93	92
Refractive index	1.58	1.49	1.51
Birefringence (nm at 830 nm)	20–30	<20	<5
T_g (°C)	150	100	125
Thermal expansion coefficient (°C)	$6-7 \times 10^{-5}$	7.6×10^{-5}	6.6×10^{-5}
Rockwell hardness (M scale)	75	90	90
Izod impact strength (kg · cm/cm)	1–2	1.6	1.6
H ₂ O absorption (%)	0.25	0.54	0.30

NOTE: Abbreviations are as follows: PC is bisphenol-A-polycarbonate, and PMMA is poly(methyl methacrylate). The structure of the epoxy resin is unknown.

molding characteristics. Optical-disk-grade acrylic polymers are now available. In addition to molding resins, acrylics are also available in sheet form that can be used with a surface-embossing process or the 2P process to fabricate preformatted disks.

The primary disadvantages cited for acrylic disks are lower impact strength, lower heat-distortion temperature, and high moisture absorption leading to warping. Copolymers are being evaluated to determine if they can eliminate or minimize these problems. Acrylics offer benefits in material cost and molding performance. Their superior melt-flow properties are claimed to provide higher molding rates with improved process throughput.

7.2.1.3 OTHER POLYMERS

A few other polymers are being investigated for optical disk substrates. A thermosetting epoxy resin with good mechanical and optical properties has been disclosed (5). Filling a prepatterned mold with liquid monomer and polymerizing photochemically or thermally will ensure a low level of birefringence in the disk, but details of the process are not yet available. Low birefringence substrates manufactured from a blend of polycarbonate and polystyrene and from a moisture-insensitive acrylic polymer have also been claimed (6).

7.2.2 Disk Fabrication

Perhaps one of the most difficult technical problems in the manufacture of optical disk substrates is achieving the high optical quality demanded of the component. In a number of device configurations, recording and reading through the substrate is necessary. Imperfections that interfere with the passage of the laser beam through the disk (e.g., scattering sites, absorption, or refraction centers) will adversely affect performance. The polymer supplier has the responsibility for product quality issues such as particulates, occlusions, color, and transparency. The disk manufacturer must also maintain extremely high levels of cleanliness and has the additional challenge of producing a completely isotropic element free of polymer-chain orientation effects. It is no simple task to produce thin, 1–3-mm disk structures in the 4–12-in.-diameter range, either from cast sheets or by molding, which are truly amorphous. Orientation of optically anisotropic polymer chains during formation will result in birefringent domains within an isotropic matrix. These domains produce aberrations in the laser beam with a corresponding loss of signal quality. Another approach to controlling birefringence is to use polymer mixtures. Polymers having negative and positive segmental polarizabilities [e.g., polystyrene (–) and polycarbonate (+) and poly(methyl methacrylate) (–) and poly(vinylidene fluoride) (+)] can be blended at some ratio to achieve zero birefringence by a compensation mechanism (7, 8). Polymer compatibility at a molecular level is necessary for this approach to

be effective, and the polymers must obviously remain compatible throughout the processing cycle. This approach is being pursued to produce extremely low birefringence disks for erasable recording (5).

Significant progress has been achieved in both materials and fabrication processes for making high optical quality substrates. State-of-the-art molding and photopolymer replicating technology allow micrometer-sized marks to be transferred into the surface of a polymer disk with a precision of a few hundred angstroms. The surface details in a prepatterned disk are shown in Figure 7.1. Because the optical demands for write-once and erasable substrates will be even more stringent, further technological advances will have to be achieved.

At this time, two disk production methods appear to be commercially viable: injection molding and a 2P replication process.

7.2.2.1 2P REPLICATION PROCESS

In the 2P process (4), a thin photopolymerizable liquid layer is cured in situ between a smooth substrate (cut from a polymer sheet or molded) and a master and stripped off to effect pattern transfer. The liquid layer ensures accurate, defect-free replication. Examples of solvent-free formulations include multifunctional acrylates with adhesion, wetting, and release agents. Free radical and cationic polymerization processes have been described (9). At the present disk volume levels, this method is claimed to be cost competitive with injection molding.

7.2.2.2 INJECTION MOLDING

The polymer grades of polycarbonate and acrylic designed specifically for molding optical disks have high cleanliness levels, low melt viscosity, and

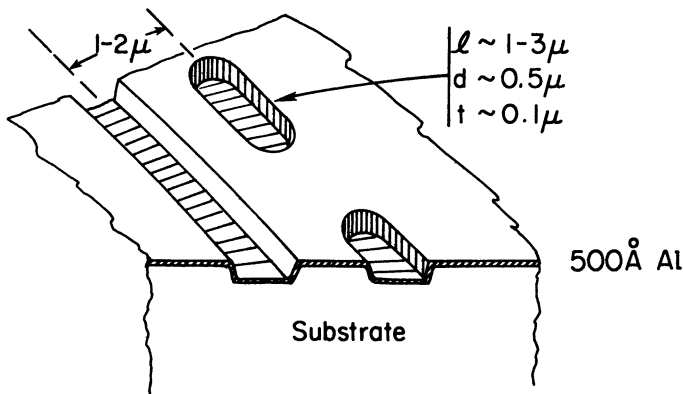


Figure 7.1. Surface details in a prepatterned optical disk. The abbreviations l , d , and t refer to length, width, and thickness, respectively.

high melt flow to facilitate delivery of a stress-free melt to the mold. Equipment suppliers have responded with systems having improved mold design and clamping to give higher precision and flatness control. Specifications for disk surface flatness and parallelism will remain extremely tight until existing disk focus and tracking systems are improved. At least four different techniques are being used to reduce birefringence levels and improve dimensional stability: starved feed injection, injection-compression molding (referred to as "coining" in the industry), precise injection profiling, and rapid heating plasticating screw injection. Further advantages have been achieved by using modular construction with computer process control.

Through more accurate metering and temperature control and reduced barrel residence time, resin degradation effects have been minimized and melt uniformity has been improved. The issue of straight injection versus injection-compression molding is still open. In injection-compression molding, the mold assembly is compressed following the injection stroke to compensate for resin shrinkage. Those equipment manufacturers using the method claim better part flatness and pattern transfer. With all the equipment available today, single-cavity molds are being used.

The most significant change in molding technology is the need for high levels of cleanliness in materials, equipment, and environment. Molding has to be conducted in class 100 clean-room facilities or better. This requirement is more familiar to the semiconductor industry. The use of robots in disk transfer, finishing, packing, and testing to minimize human source contamination is likely to increase as the technology grows.

Takeshima and Funakoshi (10) published the most detailed analysis of molecular orientation in injection-molded polycarbonate disks. Birefringence, heat-shrinkage, and laser Raman spectroscopic measurements enabled them to profile the molecular orientation (birefringence) in both the radial and depth dimensions of a molded disk 300 mm in diameter and 1.5 mm thick. Figure 7.2 shows that the birefringence decreases with distance (L) from the gate and that increasing the barrel temperature, T_c (the temperature of the molten resin), decreases the overall value. Heat-shrinkage measurements on specimens cut from disks confirm these observations.

The orientation distribution across the disk thickness and as a function of distance from the gate is shown in Figure 7.3. The Raman peak intensity ratio $I(635\text{ cm}^{-1})/I(703\text{ cm}^{-1})$ is a measure of the degree of molecular orientation. The asymmetry found in some of these plots (evident in Figure 7.2) is believed to result from nonuniformities (e.g., flow, pressure, and temperature) in the molding process. The disk cross-section consists of three orientation zones: a skin (surface) zone and a core zone, where the degree of orientation is low and independent of molding conditions, and an intermediate shear zone, where the orientation is higher and determined by molding conditions. These findings can be rationalized. Polymer in contact with the mold wall solidifies rapidly, freezing the chains in a state of random

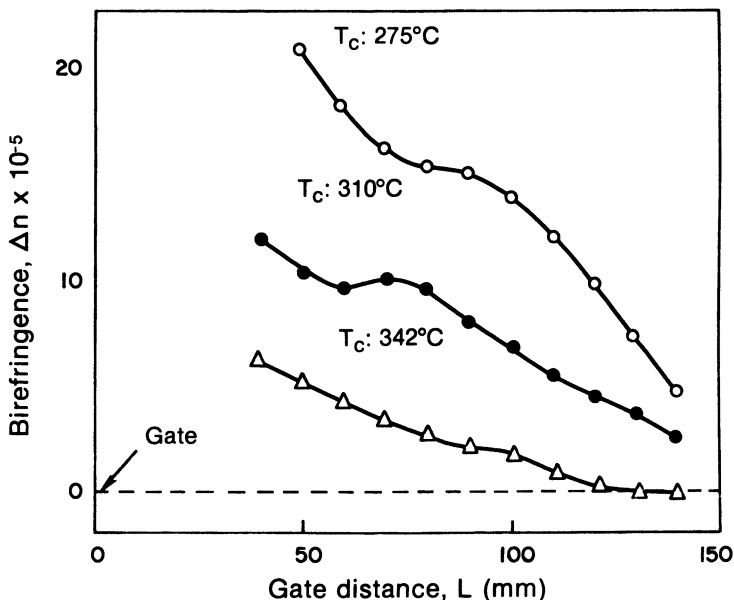


Figure 7.2. Birefringence distribution along the diameter of an injection-molded polycarbonate disk. (Reproduced with permission from reference 10. Copyright 1986 John Wiley and Sons.)

orientation. Material in the center cools at the slowest rate, enabling the chains to undergo partial to complete relaxation into a disordered state. Between these two zones, the polymer is exposed to the highest shear stress levels, and cooling is relatively rapid. The result is freezing in the chain orientation. These events occur during the cooling cycle, and the chain-orienting forces arise from backflow rather than inflow shear strain. Any orientation introduced during mold filling is believed to relax out rapidly within the hot, molten resin. Annealing of molded disks above the glass transition temperature ($T_g - 160^\circ\text{C}$, 7 h) reduces the orientation (birefringence) to very low levels, but this is not a practical production process.

7.3 Media Protection Schemes

Optical disk media must be protected from physical and environmental damage and from particulate contamination. Favored protective schemes include encapsulation and air-sandwich structures. Both systems are designed to keep dust particles away from the plane of focus at the recording surface, thereby reducing impact on signal quality. The two configurations are shown in Figure 7.4 along with a related cover-sheet structure.

Encapsulation is achieved by solvent coating a relatively thick (milli-

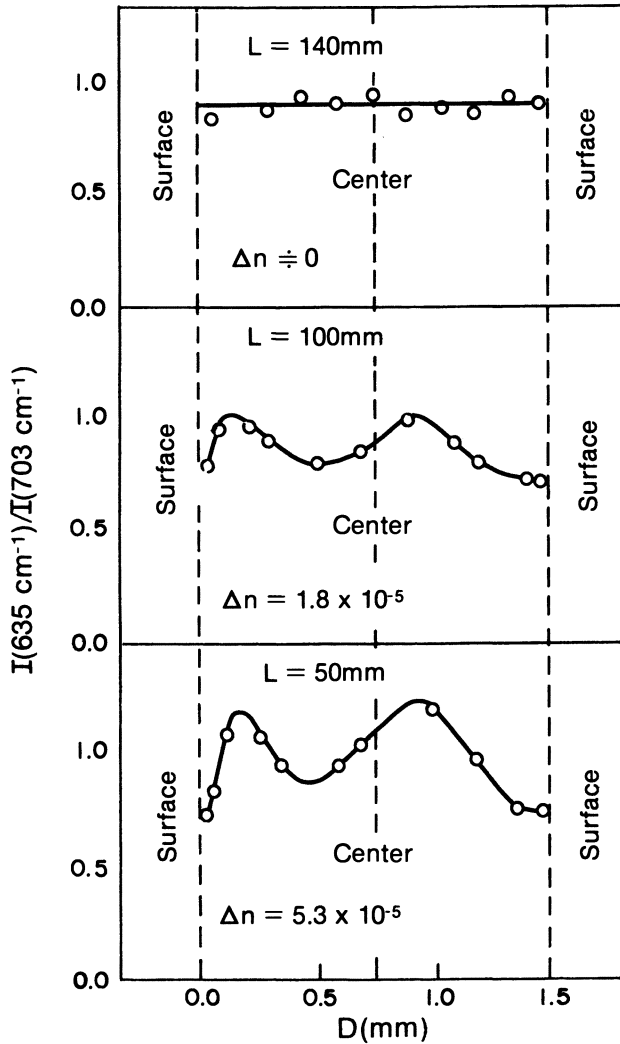


Figure 7.3. Change in birefringence [as measured by the relative Raman intensity ratio $I(635\text{ cm}^{-1})/I(703\text{ cm}^{-1})$] across an injection-molded polycarbonate disk cross-section (D) as a function of distance (L) from the gate. (Reproduced with permission from reference 10. Copyright 1986 John Wiley and Sons.)

meters) polymer film directly over the recording layer. The chemical and physical properties of the polymer are important, and choice of solvent is critical for organic-type recording media. Because the encapsulant layer becomes part of the optical write and read path, the layer must be transparent and birefringence free. Coating films of this thickness, uniformity, and optical quality is not a simple task. For ablative recording, in-contact overcoats can

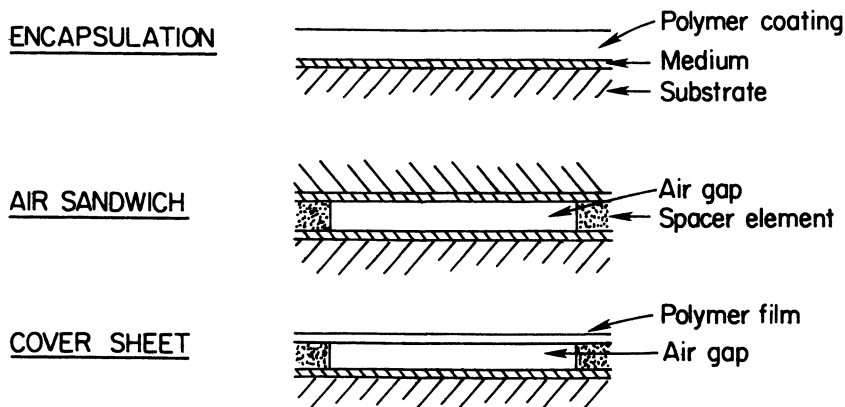


Figure 7.4. Optical disk protection schemes.

degrade writing performance significantly (2). For alternative recording processes (not involving material motion) this is not a concern. Examples of polymers used in this mode include polysiloxanes (11).

In the air-sandwich structure, which consists of two disks bonded face to face and separated by a spacer-defined air gap, the substrate becomes the protective layer. Very high quality optical substrates are necessary because the write and read functions take place through the disk. The air gap is advantageous for ablative media. Other related structures have been disclosed in which a thin polymer film is supported physically or aerodynamically some distance above the recording surface (12).

7.4 Recording Media

A variety of organic-polymeric-based materials have been investigated for optical recording, including dyes (pigments), dye (pigment)-polymer composites, dye-polymer solutions, and polymer-metal-layered or particulate structures. In all instances, the light absorption function is provided by the dye or metal, and the polymer serves the role of binder and film former.

The four major laser marking processes that will be discussed in this section are depicted in Figure 7.5. Processes a and b are termed ablative recording and involve material displacement to create some form of a pit. Bubble recording, process c, also involves material flow to create domed structures. The information recorded in these systems is read out optically by sensing the reflectivity differences between the marked and unperturbed surface. Process d is nondisruptive and involves some optically detectable transformation in the film (e.g., phase change or aggregation-deaggregation). Examples of organic-polymeric write-once media, which function by all four mechanisms, are found in the literature. Erasable organic-polymeric media have been described for processes a, b, and c.

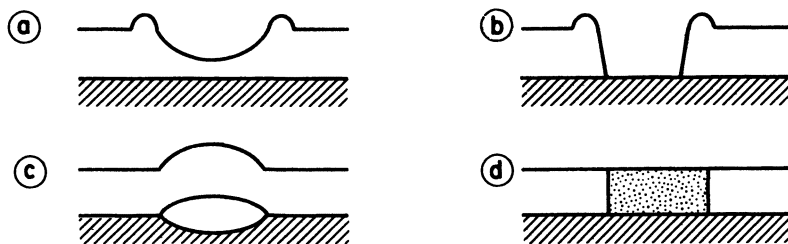


Figure 7.5. "Marks" produced in laser recording: (a) shallow pit, (b) deep pit, (c) bubble deformation, and (d) optical property change.

Determining and comparing sensitivity and performance is often difficult when reviewing organic-polymeric recording materials. No standardized testing methodology exists, and limited data are found in most patent references. However, organic-polymeric media have been reported that exhibit performance comparable to or better than tellurium-based thin films (often cited as a technological standard), which meet the technological need for sensitivity.

7.4.1 Write-Once Media

7.4.1.1 ABLATIVE RECORDING

Ablative recording has been reported in thin films of dyes (13), dye-polymer composites (14), and dye-polymer solid solutions (15). Although the mechanism of the pit-forming process is not yet fully understood, the process is a thermal one. Light absorbed in the film is instantaneously converted into heat. Because organic-polymeric materials have low thermal diffusivities ($D \sim 10^{-3} \text{cm}^2 \text{s}^{-1}$), the heat is localized in the irradiated zone for the duration of the short ($<100\text{-ns}$) exposure. Within the uncertainties of the thermal profile calculations, temperatures high enough ($>1000^\circ\text{C}$) to degrade and volatilize organic-polymeric materials are produced. This localized superheating creates pits (Figure 7.6) through an ablative and polymer flow process. The pit structure produced in dye (pigment) films is more consistent with a volatilization (sublimation) event.

Several classes of dye absorb in the near-IR region. These classes include materials with the structures shown in Chart 7.1 as well as cyanines and phthalocyanines. Recording in thin dye layers formed either by solvent casting or vacuum deposition has been reported. Kivitz et al. (16) recorded pits in a thin vanadium phthalocyanine film with $1\text{-}\mu\text{s}$, 6-mW pulses of 800-nm light. Gravesteyn and van der Veen (17) demonstrated the very high sensitivity of thin layers of a squaric acid dye and a polymethine dye to light from a Kr^+ laser (799 nm). By using 80-ns pulses having energies $>5\text{ nJ}$, well-defined micrometer-sized pits were produced. Both dye films had threshold energies in the $0.1\text{--}0.2\text{-nJ}$ range and CNR values from 55 to 65

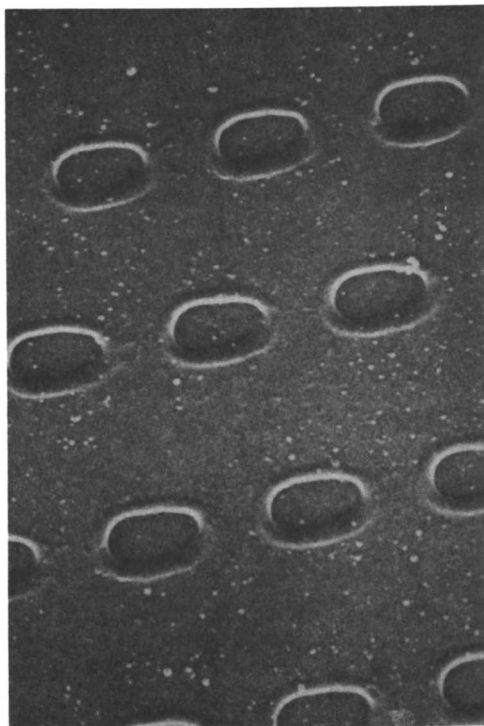


Figure 7.6. SEM photograph (40° tilt) of pits recorded in a dye-polymer/Al structure. (Reproduced with permission from reference 15. Copyright 1981 American Institute of Physics.)

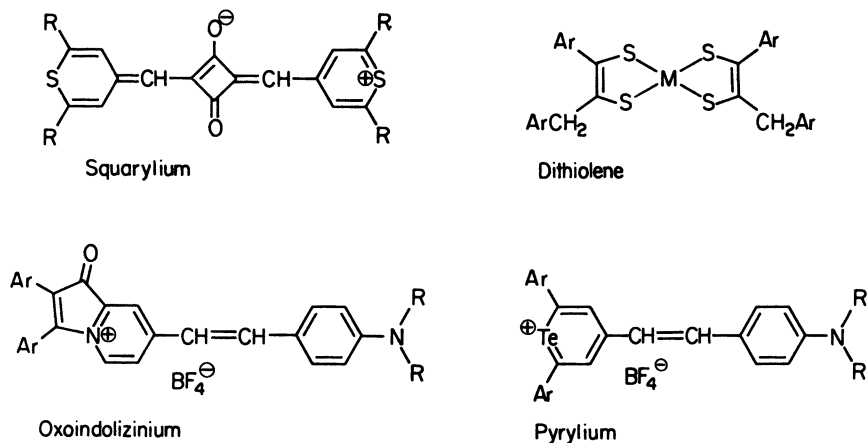


Chart 7.1. Examples of near-IR absorbing dyes for diode laser recording.

dB. Dye stability through 10^5 read-out cycles was demonstrated. One of the major difficulties encountered in dye films is the propensity of the amorphous material to undergo crystallization with subsequent deterioration of recording performance.

Examples of particulate media include dispersions of carbon black (18) and metals (19) in polymers. These films are not optically isotropic and generally exhibit low sensitivities, probably resulting from scattering effects. The key to this medium is the achievement of very uniform, small (10^2 – 10^3 -Å) particles uniformly dispersed in a polymer matrix.

Dye-polymer solid solutions appear to offer the most attractive approach for producing high-sensitivity, thin-film recording media. Examples of such composites are found in optical, electrophotographic, and semiconductor technologies. To form a true molecular dispersion, the dye and the polymer must be soluble (compatible) at the appropriate loading. For the film thicknesses and uniformity required for optical recording, spin-coating methods can be used. The coating and drying dynamics that control film thickness and morphology have been treated experimentally (20) and theoretically (21). Dye concentration will depend on the absorption and extinction coefficients at the recording wavelength, and for typical dyes, loadings of 10–50 wt % are necessary. Optimizing film thickness and recording structure to achieve an optical interference condition aids in maximizing absorption in the thin film at reduced dye levels.

Dye-polymer solutions have been studied in a number of laboratories (22, 23), and detailed morphological and recording sensitivity analyses have been published. Johnson and Law (22) investigated the structure and sensitivity (at 457 nm) of a yellow *p*-*N,N'*-dialkylaminobenzylidene malononitrile dye in a number of polymer binders. They reported that the threshold recording energy, E_{th} , is determined primarily by film absorption. Wrobel et al. (23) also studied in detail the pit formation process in a blue-sensitive coumarin dye in a cellulose nitrate polymer. The performance of this 488-nm write and 633-nm-read medium is shown in Figure 7.7. At a thickness of 1300 Å on an aluminum reflector, this medium exhibits a threshold energy of a few milliwatts (mW), and the CNR saturates at power levels >10 mW at a value of 55–60 dB. Although these studies have been carried out with blue-sensitive dyes, they represent the most detailed published information, and the design and mechanistic principles can be translated directly to the commercially important IR-absorbing dyes.

On the basis of published information, a set of design criteria for dye and polymer materials can be defined for optical recording. The primary function of the dye molecule is to absorb the incident laser energy. Several groups have shown that the sensitivity of dye-polymer media is largely determined by the optical efficiency of the thin film. Optical efficiency is a measure of the optical energy coupled into the film and is a function of the dye concentration, the dye absorption coefficient, and the layer thickness.

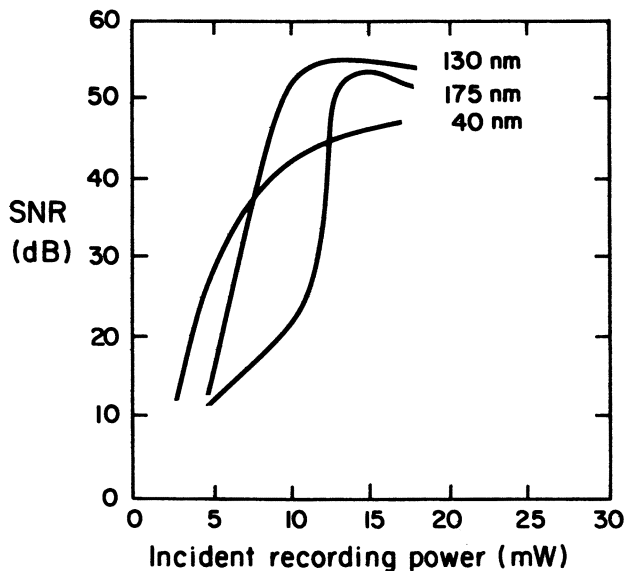


Figure 7.7. Effect of recording layer thickness on performance for a dye-polymer layer. The recording was done at 488 nm; the phase readout was done at 633 nm. The abbreviations SNR and LWL denote the signal-to-noise ratio and the laser write layer, respectively. (Reproduced with permission from reference 15. Copyright 1981 American Institute of Physics.)

In typical thin-film recording media, light absorption can be enhanced by setting up an antireflection condition in a multilayer structure. The energy absorption profile is then determined by using the complex and real indexes of refraction of the components in a multilayer interference calculation rather than from the simple Beer's law method. Dyes should have absorption coefficients as high as possible at the writing wavelength because this characteristic will maximize optical density at minimum dye loadings. Maximizing optical density is an advantage because dye-polymer solubility control can be a difficult problem. There is also a limit to increasing recording-film thickness to increase absorptivity. At film thicknesses greater than ~ 1000 Å, the ablative recording sensitivity starts to decrease as a result of the amount of material that must be displaced to form the pit. Dye concentration in the polymer is determined by the chemical structure and solubility characteristics of the dye and the binder-polymer molecules. For most dye-polymer combinations, dye loadings beyond 40 to 50 wt % result in heterogeneous films with undesirable microcrystals.

Electronically excited dye molecules can undergo a number of decay processes including radiative deactivation by fluorescence or phosphorescence and nonradiative deactivation by internal conversion and intersystem crossing. Because the marking event is so fast (< 50 ns), triplet-state processes can be ignored and only the singlet-state manifold need be considered.

Energy released in nonradiative internal-conversion events will be instantaneously transferred into vibrational, translational, and rotational motions of the dye and polymer molecules generating heat. Ideal dyes, therefore, should have high quantum yields for internal conversion ($S_n \rightarrow S_1 \rightarrow S_0 + \text{heat}$) with minimal radiative (fluorescence) energy losses, and they should have environmental and light stability consistent with archival (10 years) demands. Over the life of an optical disk, both the recorded and unexposed areas of a disk could be exposed to a considerable dose of light from tracking and reading laser functions; thus, light stability is a key requirement.

Law et al. (24) described a recording layer composed of a carbocyanine dye in a poly(vinyl acetate) matrix. A 1050-Å film containing 20 wt % dye produced micrometer-sized pits on exposure to 5-ns pulses from a dye laser (835 nm). Patent references disclose dye-polymer films obtained using dyes with general structures shown in Chart 7.1, and high performance sensitivities to diode laser recording are claimed (25–28).

Law and Johnson (22, 29) published the most detailed analysis of the role of the polymer chemical and physical properties on the sensitivity and performance of dye-polymer solutions. Their key results are collected and summarized in Table 7.3. They investigated addition- and condensation-type polymers and probed the effect of physical properties such as glass transition

Table 7.3. Effect of Polymer Binder on the Threshold Recording Energy at 475 nm for 60-nm-Thick Polyester Yellow Doped Films

<i>Polymer</i>	<i>Dye Loading (wt %)</i>	T_g (°C)	<i>Surface Tension (n·N/M)</i>	M_w ($\times 10^3$)	E_{th}
Poly(vinyl acetate)	5	35	37		21.7
	10				10.9
	20				2.5
	40				1.6
Poly(<i>n</i> -butyl methacrylate)		18			7.7
Poly(vinylbutyral)		53	25		4.8
Poly(isobutyl methacrylate)		54			6.3
Poly(<i>sec</i> -butyl methacrylate)		67			4.8
Copoly(styrene(7)-acrylonitrile(3))		101	42		2.4
Poly(methyl methacrylate)		105	39		4.6
Polycarbonate		150	35		2.6
Polysulfone		190	41		6.5
Copoly(styrene(8)-isobutyl methacrylate(2))		78		45	2.9
			40	2.7	
			32	3.9	
			23	2.6	
			15	2.6	
			6	3.6	

NOTE: The doped polyesters are 20 wt % dye unless otherwise stated.

The glass transition temperature was determined by differential scanning calorimetry.

Surface tension values are from *Polymer Handbook*; 2nd ed.; Wiley: New York, 1975.

Values of E_{th} are in arbitrary units based on a 15-nm Te monolayer reference film having $E_{th} = 3.2$ (0.1 nJ) under identical conditions.

temperature (T_g), surface tension, and molecular weight (equivalent to melt viscosity) on the recording sensitivity.

Analysis of the data in Table 7.3 showed that the dominant factor in determining the sensitivity of the medium was the absorption efficiency of the film. Variations observed in the threshold energies (E_{th} , a measure of the energy required to raise the temperature of the film to a value at which hole opening is initiated) were shown to result from differences in the 457-nm reflectivity/absorbance of the actual films resulting from polymer refractive index differences and binder-induced spectral shifts (solvatochromism) of the dye. Comparison of films of equal absorbance indicated equivalent E_{th} values. Therefore, polymer properties such as T_g , surface tension, and molecular weight have no significant impact on the sensitivity of the medium. This finding was rationalized in terms of the very rapid (<50 ns) rate of the hole-opening event and the extremely high local temperature (>1000 °C). Because the physical properties under investigation are associated with relaxation times many orders of magnitude slower, they probably have no influence on the energetics of the hole initiation process.

Although the physical parameters of the polymer binder do not influence recording sensitivity, they do have an effect on determining the final dimensions of the pit. In an experiment in which they monitored reflectivity from a pit area following hole initiation with an 8-ns pulse, Law and Johnson (29) were able to follow the postinitiation stage involving mass transport of material. A series of polystyrenes covering a molecular weight range from 4000 to 670,000 were used as the dye binder. The initial component of the postinitiation stage was essentially independent of molecular weight at molecular weights from 4000 to 20,000. Maximum reflectivity contrast (and hence, final pit size) was achieved within ~30 ns. At molecular weights greater than 20,000, however, a slower component is introduced, which manifests itself in a reduction in signal contrast. This relaxation process is dependent on molecular weight and is slower for higher molecular weights (e.g., for a molecular weight of 37,000, relaxation from initial to final hole configuration occurs in ~250 ns, whereas at molecular weights >400,000, the process takes ~2 μ s). The transition point is close to the reported value of the entanglement molecular weight for polystyrene. These results were interpreted by assuming that some initially displaced polymer material flows back into the pit, thus reducing pit size and decreasing signal contrast and overall medium performance. The molecular weight dependence is consistent with an elastic response of the viscoelastic polymer melt following displacement resulting from chain-entanglement effects. Lower molecular weight polymer binders produce the best shaped pits with optimal signal contrast and CNR.

The requirements for the dye-polymer combination are that they form a molecular solution and be coatable from solution. The composite must remain compatible and stable over the life of the optical disk. To maintain pit integrity, the composite T_g should be greater than 80 °C.

One of the concerns associated with ablative recording in dye-polymer media is the formation of small debris particles. These particles, which are created during the ablative pit forming process and are composed of dye-polymer or degradation products, can redeposit on the disk surface. They can be seen in Figure 7.6. In high-density storage, a considerable amount of debris can accumulate on the surface to become a source of noise. Gupta (30) showed that thin ($<0.5\text{-}\mu\text{m}$) ceramic or polymer overcoats can eliminate debris with minimal loss in recording sensitivity and CNR.

7.4.1.2 BUBBLE RECORDING

The mechanism of bubble recording (Figure 7.5) is also thermal. A typical recording structure is composed of a thin absorbing layer (metal, ceramic), a polymer layer, and a reflective substrate (31, 32). Optical energy absorbed in the upper layer is converted into heat, which causes localized vaporization at the interface with the polymer. The trapped vapor deforms the hot absorber layer to produce a bubble-shaped microstructure. The role of the polymer is to produce vapor, and a variety of materials are described, (e.g., poly(methyl methacrylate), poly(α -methylstyrene), and polycarbonate. If the local temperature is high enough, any polymer should function, and the use of additives such as plasticizers and vapor-producing agents should enhance performance.

One of the major problems associated with bubble media is the ability to generate well-defined, well-structured deformations. Distorted, cracked, and collapsed structures adversely affect performance, and uncertainty arises in whether adequate control over the bubble-forming process can be achieved.

7.4.1.3 PHASE-CHANGE RECORDING

This mode of recording is depicted in Figure 7.5. Because the film structure does not change, the optically induced transformation must be optically detectable so that the recorded signal can be read out. Several inorganic-type media have been described (33). Examples of organic media include photobleachable (34) and photochromic (35) dyes in polymer matrices, neither system being sensitive in the important IR region of the spectrum. Asano et al. (36) discussed a particulate medium composed of microdomains (100 \AA large) of metal (e.g., Te and Bi) dispersed in a polymer matrix. Recording is accomplished by thermal conversion of amorphous into crystalline domains. The recording layer was prepared by simultaneous vacuum evaporation of the metal and glow-discharge polymerization of a gaseous monomer such as styrene. Reflectivity changes of 20% after recording were claimed in a 900-\AA polystyrene-Te film containing 40 vol % Te. Performance deteriorates at higher recording powers where ablation starts to compete with the phase-change process.

Auerbach (37) recorded with a diode laser in a thin film of a solvent-coated polymer-metal ion salt complex (e.g., poly-2-vinylpyridine-AgNO₃). Using short-duration pulses (120 ns) of 820-nm light (10 mW), he showed that high reflectivity marks could be created that could be read with a lower power diode laser. The mechanism is believed to involve thermally induced electron transfer from the polymer to the metal ion forming localized metal areas ($\text{Ag}^+ + e \rightarrow \text{Ag}^0$). The concept is not limited to silver; salts of gold, copper, and tellurium can be used. Polymers other than vinylpyridine that can form charge-transfer complexes with metal ions should function as electron-transfer binders.

Michl and co-workers proposed (38) and demonstrated (39) a novel nondeformation recording concept based on a dye-polymer thin film. Marking is achieved by laser-induced thermal relaxation of the birefringence in a stretched, partially oriented thin film. This change in birefringence can be used to read out the information by monitoring the change in polarization of the reading beam in either a transmission or reflection mode. A thin (~5- μm) film of a vinyl chloride-vinylidene chloride copolymer doped at ~5 wt % with a polymethine dye was recorded with pulses of 250 μs or longer from a 5-mW GaAlAs laser operating at 823 nm. The marks were ~3 μm in diameter and were visible in an optical microscope with crossed polarizers as dark spots on a light background. For long exposure times (>750 μs), actual holes were burned into the film. Below 100 μs , no marking was detected. The marking function was attributed to a thermal relaxation of birefringence, and the threshold nature of the process suggests that read-out could be accomplished without damage to the material. Although this concept is interesting, the system as described is too low in sensitivity to be practical. Also, issues relating to fabrication of thinner, more uniform higher-birefringence films and long-term relaxational stability must be addressed.

7.4.2 Reversible (Erasable) Media

Examples of organic-polymer-based reversible media are few. In the inorganic category, reversible phase-change materials and magneto-optic systems appear to be the leading candidates. Both systems can be considered as examples of nondeformation recording.

7.4.2.1 PHASE-CHANGE RECORDING

Mey (40) disclosed a novel dye-polymer-based recording medium that operates by an aggregation-deaggregation mechanism. Although only limited performance data are presented, the concept is unique and could be general. The active layer consists of discrete particles (dimensions <1000 Å) of a cocrystalline complex of a dye with a polymer dispersed in a continuous phase of the same polymer. Exposing this aggregated film to a laser pulse

resulted in an instantaneous deaggregation process, which is accompanied by a significant shift in the absorption spectrum of the film. Recording at 580 nm with an energy of about $1 \text{ nJ}/\mu\text{m}^2$ in a pyrylium-polycarbonate aggregate film produced a hypsochromic shift of about 100 nm. A large number of dye-polymer combinations were disclosed with pyrylium-type dyes in polymers containing alkylidenediarylene repeat units (e.g., bis-phenol-A-polycarbonate), being the preferred materials. The recording mechanism is believed to be thermal, and a thermal erasure (reaggregation of the dye-polymer complex) was also demonstrated. Because both record and erase could be carried out without disrupting the film, significant softening of the matrix is apparently not necessary to enable the aggregation and deaggregation processes to occur. Ota (41) reported reversible recording in an organic analog of the Te/TeO₂ system, which functions by an amorphous-crystalline switching mechanism. The active medium consists of microdomains of a transition metal β -diketonate in a polymer (e.g., polystyrene, polyester, polycarbonate) matrix. In the specific examples described, the complexes were members of the general class of Cu^{II} bis(1-*p*-alkylphenylbutane-1,3-diketonates), which are sensitive in the UV region and have $T_g \sim T_{\text{cryst}}$. The condition of $T_g \sim T_{\text{cryst}}$ may facilitate the domain morphological interconversion. Recording was conducted with nanosecond pulses of 377-nm radiation from an N₂ laser, which converts the amorphous into crystalline domains. Read-out was achieved with a He-Ne laser at 633 nm in either the reflective or transmissive mode. Remelting and rapid quenching of the crystalline particles returned the system to its original amorphous structure. A claim was made that this process could be accomplished with a laser. Unfortunately, little information is available on the stability, sensitivity, and erasure capabilities of this interesting medium. The phase-change concept should be generally applicable to organic dye-polymer composites, and it is hoped that this preliminary work will stimulate further interest and activity in the area.

7.4.2.2. ABLATIVE RECORDING

Reversible recording in ablative dye-polymer media has recently been reported (42-44). The basic concept involves refilling the pits by a thermally induced flow of surrounding material to regenerate a smooth surface that can be rewritten. This erasable process appears to depend on the use of low-melt-viscosity, low-softening-temperature polymers (oligomers) as the binder matrix. Such materials will enable rapid refilling of the pits during the erase cycle. Kuder and East (45) disclosed low molecular weight polyamides based on dimer acids (e.g., the Unirez and Emerez series). The recording media of Kuroiwa et al. (46) are based on pigments dispersed in polystyrene thermoplastic oligomers ($M_n \sim 400-3000$). Marking was achieved in a copper phthalocyanine-PS (polystyrene) film (2.8 μm thick, 1:10 ratio

of dye to binder) by using a 10- μ s pulse of 10 mW from a He-Ne (633-nm) laser. The pits could be erased by heating for 8 s at 90 °C on a hot plate or by using a defocused He-Ne laser beam (10 mW, 1 mm/s scan rate). Erasure did not alter the optical properties of the film nor did it affect the recording sensitivity (for up to 10 write-erase cycles).

Gupta and Strome (43, 44) described an ablative dye-polymer recording system that functions in a reversible mode when overcoated with a thin, transparent ceramic film. The overcoat serves to restrain debris formed during the ablative recording event and to entrap material flow during pit formation. Ceramics (e.g., SiO₂, SiO, MgF₂, and glass) are the preferred overcoat materials, but polymers such as poly(vinylimidazole) and poly-*p*-xylylene can also be used. In addition to film-forming properties, the overcoat material should have low thermal conductivity to avoid heat loss during recording, low adhesion to the recording layer, and should exhibit minimal thermal flow during pit formation.

The recording process appears to be identical with that for conventional ablative recording. The overcoat prevents loss of material but still allows pit formation in the active underlayer. Microscopic analysis reveals that the overcoat layer deforms slightly during recording to form a dome over the pit. This phenomenon is shown clearly in the pit cross-section micrograph in Figure 7.8. Erasure is best carried out with a low-power laser with a beam elongated in the in-track direction to achieve a long exposure time. Defocusing the beam toward the outer edges of the pit also aids in softening the rim material and reflowing it back into the pit. The erase process regenerates a smooth recording surface that can be recorded with no loss in sensitivity. The record-erase-record sequence is shown in Figure 7.9. The optimum overcoat thickness appears to be that which absorbs enough heat generated during the recording process to undergo plastic deformation as the pit is formed. Dome formation is critical in providing volume for unrestrained radial material flow to form the rim and shape the pit. Overcoat layers that are too thin tend to form nonsymmetrical domes that have a tendency to fracture and collapse; thus, the media CNR and error level are adversely affected. Layers that are too thick are too rigid, and very high recording-power levels are necessary to generate enough heat for deformation. For typical dye-polymer media, an overcoat thickness of 50–100 nm appears to give well-shaped pits and domes having CNR values close to that found in nonovercoated layers.

Dye-polymer recording media similar to those described in reference 47 demonstrated (43, 44) CNR values >50 dB (8.8-MHz carrier, 30-KHz bandwidth, 20-m/s tangential disk velocity) that remained unchanged through 4×10^4 write-erase cycles. Writing was accomplished with an 830-nm diode laser operating in the range of 12–16 mW; erasure was accomplished with 3.5 mW of continuous power. For complete erasure, three or four disk cycles are required. Single-pass erasure will be necessary for a

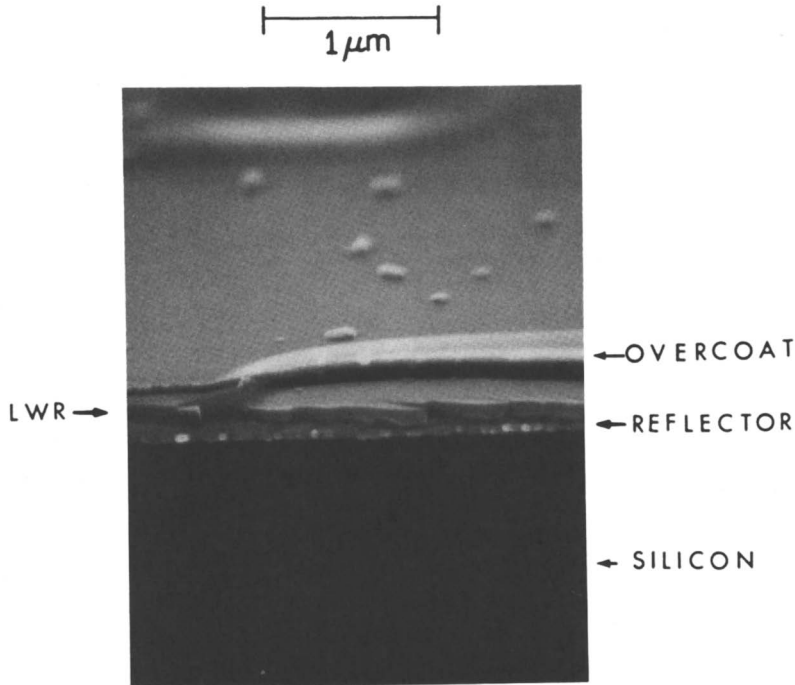


Figure 7.8. SEM photograph of the cross-section of a pit recorded in a dye-polymer film through a thin (50-nm) ceramic overcoat. (Reproduced with permission from reference 44. Copyright 1986 American Institute of Physics.)

practical system, and this may be achieved with a reshaped erase beam with an intensity profiled to favor softening and reflow of the rim areas. Data rates of 5 Mbits/s were reported with defect densities of 10^{-5} – 10^{-6} , which remained unchanged through the erase cycling.

Abbreviations and Symbols

CNR	carrier-to-noise ratio
D	(1) diffusivity (2) disk cross-section
DRAW	direct read after write
E_{th}	threshold recording energy
I	intensity
L	distance
M_n	number-average molecular weight
T_g	glass transition temperature

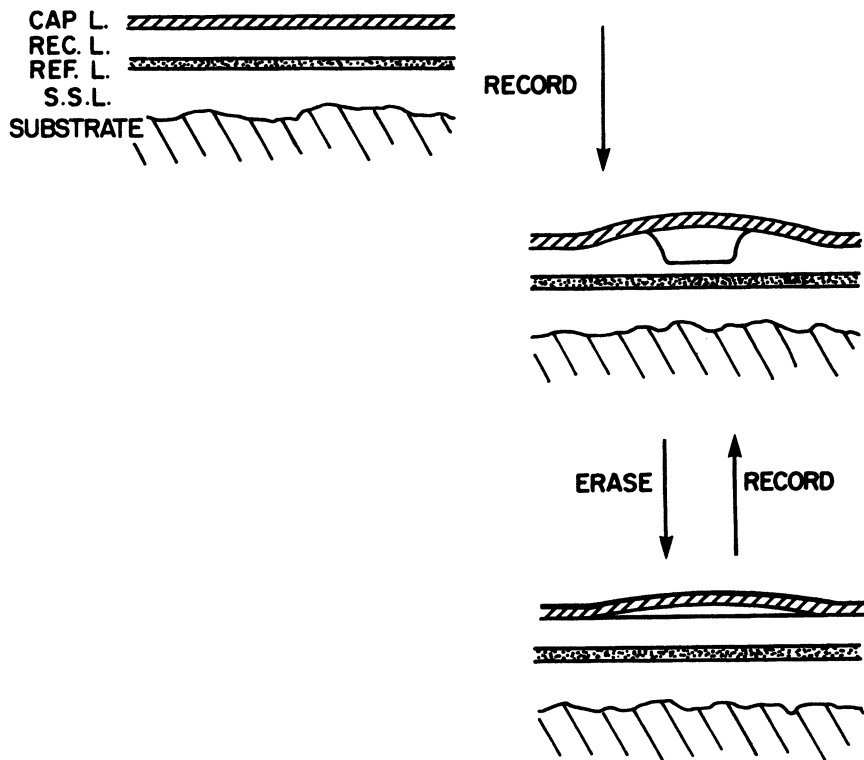


Figure 7.9. The reversible ablative recording process in a dye-polymer medium overcoated with a thin restraining layer. The capping layer (CAP L.), recording layer (REC L.), reflective layer (REF L.), and surface smoothing layer (S.S.L.) are indicated.

References

1. Pearson, J. M. *CRC Crit. Rev. Solid State Mater. Sci.* 1986, 13, 1.
2. Smith, T. W. *J. Vac. Sci. Technol.* 1981, 18, 100.
3. Kirkland, C. *Plast. Technol.* 1985, April, 73.
4. van den Broek, A. J. M.; Haverkorn van Rijsewik, H. C.; Legierse, P. E. J.; Lippits, G. J. M.; Thomas, G. E. *J. Radiat. Curing* 1984, 11, 2.
5. Ohsawa, S.; Tusge, M.; Takatsu, A.; Okunishi, T.; Tanaka, J.; Mikami, S. *Tech. Dig. Top. Meet. Opt. Data Storage* 1985, Paper ThCC4-1.
6. *Plast. Ind. News* 1986, March, 34.
7. Lefebvre, D.; Jasse, B.; Monnerie, L. *Polymer* 1982, 23, 706.
8. Hahn, B. R.; Wendorff, J. H. *Polymer* 1985, 26, 1619.
9. Kloosterboer, J. G.; Lippits, G. J. M. *J. Radiat. Curing* 1984, 11, 10.
10. Takeshima, M.; Funakoshi, N. *J. Appl. Polym. Sci.* 1986, 32, 3457.
11. Bell, A. E.; Bartolini, R. A.; Spong, F. W. *RCA Rev.* 1979, 40, 345.
12. Wheeler, J. W.; Gupta, M. C.; Kurtz, C. N. *Proc. SPIE Opt. Storage Media* 1983, 420, 39.
13. Jipson, V. B.; Jones, C. R. *J. Vac. Sci. Technol.* 1981, 18, 105.

14. Smith, T. W.; Wychick, D. J. *Phys. Chem.* **1980**, *84*, 1621.
15. Howe, D. G.; Wrobel, J. J. *J. Vac. Sci. Technol.* **1981**, *18*, 92.
16. Kivitz, P.; de Bont R.; van der Veen, J. J. *Appl. Phys.* **1981**, *A26*, 101.
17. Gravesteijn, D. J.; van der Veen, J. *Philips Tech. Rev.* **1984**, *41*, 325.
18. O'Reilly, J. M.; Mosher, R. A.; Goffe, W. L. *Photogr. Sci. Eng.* **1979**, *23*, 314.
19. Drexler, J. J. *J. Vac. Sci. Technol.* **1981**, *18*, 87.
20. Law, K. Y. *Polymer* **1982**, *23*, 1627.
21. Washo, B. D. *IBM J. Res. Dev.* **1977**, *21*, 190.
22. Johnson, G. E.; Law, K. Y. *Proc. SPIE Opt. Storage Media* **1983**, *420*, 336.
23. Wrobel, J. J.; Marchant, A. B.; Howe, D. G. *Appl. Phys. Lett.* **1982**, *40*, 928.
24. Law, K. Y.; Vincett, P. S.; Johnson, G. E. *Appl. Phys. Lett.* **1981**, *39*, 718.
25. Gravesteijn, D. J.; Steenbergen, C.; van der Veen, J.; Nijssen, W. P. M. U.S. Patent 4 508 811, 1985.
26. Crandall, R. S.; Bloom, A. U.S. Patent 4 320 489, 1982.
27. Wadsworth, D. H.; Thomas, H. T.; Fletcher, G. L.; Weidner, C. H. U.S. Patent 4 446 223, 1984.
28. Detty, M. R.; Thomas, H. T. U.S. Patent 4 584 258, 1986.
29. Law, K. Y.; Johnson, G. E. *J. Appl. Phys.* **1983**, *54*, 4799.
30. Gupta, M. C. *Appl. Opt.* **1984**, *23*, 3950.
31. Maffit, K. N.; Robbins, W. B.; Wilson, R. F. European Patent 58496, 1982.
32. Cornet, J. U.S. Patent 4 360 895, 1982.
33. Takenaga, M.; Yamada, N.; Nishiuchi, K.; Akihara, N.; Ohta, T.; Nakamura, S.; Yamashita, Y. *J. Appl. Phys.* **1983**, *54*, 5376.
34. Carlson, C. O.; Bernstein, H. L.; Stone, E. U.S. Patent 3 465 352, 1981.
35. Brettle, J., personal communication, 1984; Plessey Research Ltd., United Kingdom, Photochromic Data Sheets.
36. Asano, Y.; Yamazaki, H.; Morinaka, A. *Jpn. J. Appl. Phys.* **1982**, *22*, 480.
37. Auerbach, A. *Appl. Phys. Lett.* **1984**, *45*, 939.
38. Puebla, C.; Michl, J. *Appl. Phys. Lett.* **1983**, *42*, 570.
39. Murthy, P. S.; Klingensmith, K. A.; Michl, J. *J. Appl. Polym. Sci.* **1986**, *31*, 2331.
40. Mey, W. U.S. Patent 4 513 071, 1985.
41. Ota, K. Japanese Patent 58 199345, 1983.
42. Gupta, M. C.; Wrobel, J. J.; Strome, F. C. U.S. Patent 4 527 173, 1985.
43. Gupta, M. C.; Strome, F. C. *Tech. Dig. Top. Meet. Opt. Data Storage* **1985**, Paper WBB1-1.
44. Gupta, M. C.; Strome, F. C. *J. Appl. Phys.* **1986**, *60*, 2932.
45. Kuder, J. E.; East, A. J. European Patent 0 097 509, 1984.
46. Kuroiwa, A.; Namba, K.; Asami, S.; Aoi, T.; Takahashi, K.; Nakagawa, S. *Jpn. J. Appl. Phys.* **1983**, *22*, 340.
47. Molaire, M. F. U.S. Patent 4 499 165, 1985.

RECEIVED for review April 15, 1987. ACCEPTED September 17, 1987.

AUTHOR INDEX

- Baker, Gregory, 271
Bowden, Murrae J., 1, 75
Ito, Hiroshi, 109
Iwanagi, Takao, 109
Nonogaki, Saburo, 109
- Pearson, James M., 331
Roberts, G. G., 225
Ueno, Takumi, 109
Williams, David, 297
Willson, C. Grant, 75, 109

AFFILIATION INDEX

- Bell Communications Research, 1, 75, 271
Eastman Kodak Company, 297, 331
Hitachi, Ltd., 109
- IBM Almaden Research Center, 75, 109
University of Oxford, 225

SUBJECT INDEX

A

- Ablative imaging systems, 65
Ablative recording
 decay processes for marking event, 344–345
 dye–polymer solutions as medium, 343
 for recording media, 341
 mechanism of pit-forming process, 341
 particulate media, 343
 problem of debris in dye–polymer media, 347
 thin dye layers as medium, 341, 343
Acetylene, polymerization with epoxide- or carbonyl-functionalized polymer, 288
Acid-catalyzed thermolysis of polycarbonate, 172*f*
Acoustoelectric devices, 259–260
Acrylates as photopolymerizable resin, 68, 70
Acrylic acid-based resin, 146
Acrylic disks, advantages and disadvantages, 335
Adhesives for integrated circuits, requirements, 14
AgCl–As₂S₃, 172
Ag₂Se–Ge₂Se_{1.5} resists
 development of latent image, 174
 anisotropic wet chemical etching, 177*f*
 chemical basis, 174
Ag₂Se–Ge₂Se_{1.5} resists—*Continued*
 edge-sharpening effect, 174–175
 imaging mechanism, 175*f*
 in multilayer resist system, 176
 mechanism of edge-sharpening effect, 176*f*
 photodoping process, 174
 properties, 175–176
 sensitivity, 177*t*
Air-sandwich structure, 340
Aldehyde reactions, 168
Aliphatic diol 4,5-disulfonate structure, 125*f*
Aliphatic diol 4,5-disulfonate-based resist
 adjustment for generation of square-wave relief pattern, 127
 application, 127
 bleaching properties, 126*f*
 development rate function, 130*f*
 print quality, 127*f*
 spectra of unexposed and bleached materials, 126*f*
Aliphatic polysilane(s)
 imaging layer for bilevel oxygen RIE
 image transfer, 196
 structure, 196
 UV spectra, 196*f*
Alkoxy-substituted poly(phenylenevinylene)s, 290
N-Alkyldiazopiperidinedione, photolysis, 89*f*
All-reflecting 1:1 projection optical system, 117*f*

AUTHOR INDEX

- Baker, Gregory, 271
Bowden, Murræ J., 1, 75
Ito, Hiroshi, 109
Iwanagi, Takao, 109
Nonogaki, Saburo, 109
- Pearson, James M., 331
Roberts, G. G., 225
Ueno, Takumi, 109
Williams, David, 297
Willson, C. Grant, 75, 109

AFFILIATION INDEX

- Bell Communications Research, 1, 75, 271
Eastman Kodak Company, 297, 331
Hitachi, Ltd., 109
- IBM Almaden Research Center, 75, 109
University of Oxford, 225

SUBJECT INDEX

A

- Ablative imaging systems, 65
Ablative recording
 decay processes for marking event, 344–345
 dye–polymer solutions as medium, 343
 for recording media, 341
 mechanism of pit-forming process, 341
 particulate media, 343
 problem of debris in dye–polymer media, 347
 thin dye layers as medium, 341, 343
Acetylene, polymerization with epoxide- or carbonyl-functionalized polymer, 288
Acid-catalyzed thermolysis of polycarbonate, 172*f*
Acoustoelectric devices, 259–260
Acrylates as photopolymerizable resin, 68, 70
Acrylic acid-based resin, 146
Acrylic disks, advantages and disadvantages, 335
Adhesives for integrated circuits, requirements, 14
AgCl–As₂S₃, 172
Ag₂Se–Ge₂Se_{1.4} resists
 development of latent image, 174
 anisotropic wet chemical etching, 177*f*
 chemical basis, 174
Ag₂Se–Ge₂Se_{1.4} resists—*Continued*
 edge-sharpening effect, 174–175
 imaging mechanism, 175*f*
 in multilayer resist system, 176
 mechanism of edge-sharpening effect, 176*f*
 photodoping process, 174
 properties, 175–176
 sensitivity, 177*t*
Air-sandwich structure, 340
Aldehyde reactions, 168
Aliphatic diol 4,5-disulfonate structure, 125*f*
Aliphatic diol 4,5-disulfonate-based resist
 adjustment for generation of square-wave relief pattern, 127
 application, 127
 bleaching properties, 126*f*
 development rate function, 130*f*
 print quality, 127*f*
 spectra of unexposed and bleached materials, 126*f*
Aliphatic polysilane(s)
 imaging layer for bilevel oxygen RIE
 image transfer, 196
 structure, 196
 UV spectra, 196*f*
Alkoxy-substituted poly(phenylenevinylene)s, 290
N-Alkyldiazopiperidinedione, photolysis, 89*f*
All-reflecting 1:1 projection optical system, 117*f*

- Antireflection coating materials
 mode of action, 95
 types, 95
- Antireflective coating
 limitations, 190
 properties, 190
 as isolation layer, 188, 190
- Applications of ultrathin films, 255
- Area-selective metallization
- ArF contact etching
 experimental setup, 208*f*
 image formed, 209*f*
- ArF projection etching, experimental setup, 208*f*
- Arylazide decomposition, 140
- Aufbau principle, 28
- AZ1350 resist, reduced sensitivity in the mid-UV region, 122
- AZ13501 resist, spectra of unexposed bleached materials, 123*f*
- AZ1350J resist
 computer-simulated resist profiles, 131*f*
 top imaging resist for DUV blanket exposure-PCM, system, 180
- AZ1450 resist, photosensitivity at different laser peak powers, 210*f*
- AZ2400 resist
 dynamic bleaching absorption spectra, 124*f*
 suitability for mid-UV lithography, 124
 transmittance spectrum, 124*f*
- Azide-cyclized polyisoprene photoresists, network formation, 140-141
- Azide-phenolic resin-based resist(s)
 change in resist profiles with development time, 146
 characteristics, 146
 commercial sources, 148
 composition, 142
 rates of development, 142
 resist thickness versus exposure time, 144-145*f*
 simulation of profile, 147*f*
 simultaneous exposure to mid-UV and DUV radiation, 146
 spectral transmittance, 143*f*
 UV transparency, 146
- Azide sensitizer systems
 azide-cyclized polyisoprene, 140-141
 azide-phenolic resin, 142-148
- B**
- Band-gap energy, 29
- Band theory of solids, 28-30
 band formation obtained by mixing of electronic states, 29*f*
- Barrier coating(s)
 protection against alpha particles, 18
 use of silicones, 17
- Behavior of poled polymer films
 field-induced alignment of Disperse Red I in PMMA, 314
 molecularly doped polymer liquid crystalline system, 315-316
- Behavior of poled polymer films—
Continued
 polar alignment of γ -polybenzyl-L-glutamate, 317
- Benzophenone, for improvement of poly(olefin sulfones), 139
- Bilayer dry process with photoinitiated interfacial polymerization of Si-containing monomer, 168*f*
- Bilayer negative dry-development scheme, 167*f*
- Bilayer resist system
 patterns formed, 189*f*
 properties, 176
- Bilevel RIE-PCM scheme
 organometallic polymers, 192
 poly(dimethyl-diphenylvinylsiloxane)-hard-baked AZ1350J system, 192
 polysiloxane, 192
- Bipolaron
 definition, 274
 energy levels, 34*f*
 signature, 274
- Birefringence, 68
 changes across an injection-molded polycarbonate disk, 339*f*
 distribution of an injection-molded polycarbohydrate disk, 338*f*
- Bisarylazide-rubber resists, crosslinking reactions, 141*f*
- Bisazide-rubber resists, 76
- 2,6-Bis(4'-azidobenzal)-4-methylcyclohexanone, structure, 140*f*
- 3,3'-Bisazidophenyl sulfone, structure, 141
- Bisdiallylpolycarbonates, use as optical disk substrates, 63
- Bispyridylethylene
 imaging layer in Kodak 809 resist, 186
 structure, 186*f*
- Bis(*p*-toluenesulfonate)-2,4-hexadiyne-1,6-diol
 cubic susceptibility, 252
 tensor coefficients, 252
- Bis(trimethylsilyl)acetamide, 163
- Block copolymers, preparation, 288*f*, 289
- Bubble recording
 principle, 347
 problems, 347
 recording structure, 347
 suitable polymers, 347
- Built-on mask process, 87*f*
 absorbance of materials, 86*f*
- Built-on mask materials
 characteristics, 84-85
 imines, 85
 perhalohydrocarbons, 85
- 9-Butyl-10-anthrylpropionic acid, structure, 227*f*
- tert*-Butyl ester-onium salt resist, quality of projection printed images, 157*f*
- tert*-Butyl ester resists
 overall reaction, 156
 positive and negative images, 157*f*
 quantum efficiency, 156
 quantum yield, 156

4-*tert*-Butylphthalocyaninosilicon,
dichloride, structure, 227f

C

- C_{2v} symmetry, 310
- Cadmium dimethylarachidate
change in carboxylate stretching with
number of monolayers, 237f
reciprocal capacitance versus number of
monolayers, 237f
X-ray photoelectron signal intensity, 237f
- Centrosymmetric crystals, polarization, 55–
56
- Characterization of Langmuir–Blodgett films
Auger electron spectroscopy, 236
Brillouin scattering, 237
electron diffraction, 234
ellipsometry, 236
inelastic tunneling spectroscopy, 237
infrared spectroscopy, 236
neutron diffraction and reflection, 234
optical techniques, 234, 236
photoacoustic spectroscopy, 237
Raman spectroscopy, 236
reflection high-energy electron diffraction,
234
secondary-ion mass spectrometry, 236
X-ray diffraction, 234
X-ray photoelectron spectroscopy, 236
- Charge-transfer resonance, 305
- Charge carriers, 26
- Charged solitons, formation, 36
- Chemical amplification, 87–90, 154
tert-butyl ester, 155
tert-butyl ester polymers, 155f
carbonate groups, 155
use in resist design, 154–156
- Chemical stabilization
antioxidants, 279
choice of counterion, 279
dienophiles, 279
N-bromosuccinimide, 279
poly(methyl acetylene), 279
- Chemical stabilization of conducting
polymers, 279–281
- Chemically effective field-effect transistor,
43f
- Chemistry for generation of third dimension
in resists, 103f
- Chip protection
barrier coatings, 17
choice, 17
encapsulation, 17f
methods, 16–17
- Chlorinated polymethylstyrene resist, print
of lines and spaces, 151f
- Chloromethylated polydiphenylsiloxane,
192, 194
- Chloromethylated polystyrene
contrast, 151
DUV sensitivity, 151
- Chlorotrimethylsilane, 163
- Chromophore design and synthesis,
requirements, 327
- Circuit board, 3f
- CMS, *See* Chloromethylated polystyrene
- Coherence length, 323
- Commercial photoresists
AZ1350, 122
AZ13501, 123f
AZ2400, 123, 124f
HPR204, 124f
Kodak 809, 183
- Composites, preparation, 283
- Computer-simulated resist profiles, 131f
- Conducting polymers
chemical stabilization, 279–281
commercial applications, 37
difficulties in commercialization, 37
example with degenerate ground states,
275
from flexible polymers, 277
methods of stabilization, 278
polyacetylene, 272
possible applications, 272
required characteristics, 273
route to stability 277–278
stability, 275–276
stabilization, 278–281
stabilization by encapsulation, 278–279
types of materials sought, 272–273
- Conduction
electronic, 26
ionic, 26
mechanism, 30–37
origin, 32
- Conductivities of metallic, semiconducting,
and insulating materials, 27f
- Conjugated polymers, types according to
ground states, 274, 275, 276f
- Contact printing
improved resolution with DUV radiation,
112
in image processing, 76
resolution, 112
- Contact printing with excimer lasers, 200–
202
image quality, 201
quality and resolution, 200–201
- Contrast enhancement, 82–85
- Contrast enhancement lithography, 83f
resolution improvement, 83f, 84
- Contrast enhancement materials
principle, 82, 83f
structures of dyes, 84f
suitable dyes, 82, 84
- Conventional discharge lamp
emission of DUV photons, 113
mechanism for excitation, 113
output at various wavelengths, 112
- Coumarin 6, structure, 183f
- Cresol-formaldehyde novolac resin
in positive photoresists, 119
matrix material, 79f
structure, 121f
- Cross-linked negative resist, swollen images,
142f

- Cross-linked poly(pyrrole-*g*-styrene) copolymers, 287–288
- Crystal structure optimization
enhancement of nonlinear efficiency, 248
for second-order effects, 248
for third-order effects, 248
- Cubic susceptibilities, favorable structure, 252
- Cyclized polyisoprene-based resists
DUV sensitizers, 141
drawbacks, 141
- Cyclized rubber–bisazide formulation
advantages, 141
resolution, 144
swelling, 144
- D**
- Deep-UV applications
hardening, 198
multilayer resist systems, 178–198
- Deep-UV blanket exposure–PCM systems
capped resist image, 181*f*
diazquinone resist–PMMA two-layer scheme, 182*t*
effects of phenolic resins on interfacial layer formation, 183
line-width variations, 183
materials for planarizing layer, 183
poly(*p*-vinylphenol) as matrix resin, 183
principle, 185
problems, 180, 183
schemes, 185*t*
uncapped resist image, 181*f*
- Deep-UV contact printing, mechanical defects, 178
- Deep-UV contact/proximity printer
optical layout of illuminator, 116*f*
optical system, 116*f*
spectral output, 116*f*
- Deep-UV hardening of photoresists, 198, 199*f*
- Deep-UV imaging RIE–PCM resist systems, 191*t*
- Deep-UV light sources, 112–115
deuterium lamps, 114
excimer lasers, 114
microwave-powered Hg discharge lamps, 114
pulsed Xe lamps, 114
- Deep-UV lithography
correction of chromatic aberration, 213
definition, 109
dissolution inhibitor system, 128
effective wavelengths, 110
future directions, 213–215
historical development, 111–112
improved exposure systems for vacuum UV, 215
light sources, 112–115
need for improvement in mask making, 213
printer systems, 115–119
ring-field projection systems, 214
- Deep-UV lithography—*Continued*
step-and-scan systems, 214*f*
trend toward higher resolution and larger chips, 214
use of fluoride optical elements, 213
- Deep-UV lithography exposure equipment
developments, 112
essential requirements, 111
mirror-lens-based projection systems, 111
- Deep-UV positive resists
class based on poly(isopropenyl ketone) polymers, 137
poly(isopropenyl ketones), 138*t*
poly(olefin sulfones), 138*t*
- Deep-UV printer systems
contact/proximity printers, 115
projection printers, 115
- Deep-UV projection printers
band-pass filters, 117
flexibility, 117
illumination and projection systems, 119*f*
illumination source, 117
optical and scanning configuration, 117*f*
optical output at wafer plane, 120*f*
optics system, 118*f*
principle, 115, 117
projection optics, 118*f*
- Deep-UV resist materials
diazoketones, 87
dry-developable resists, 158–172
dual-tone resists, 152–157
improvement, 85
inorganic negative resists, 172–177
lipophilic carboxylic acid *o*-nitrobenzyl esters, 85
methyl methacrylate copolymers, 136*t*
negative resists, 140–152
o-nitrobenzylcholal system, 88*f*
PMMA, 111
positive resists, 119–140
- Deep-UV resist systems, improvement of dry etch resistance, 139
- Deep-UV resists, 85, 87
outputs at various wavelengths, 90*f*
systems based on chemical amplification, 88
- Degenerate four-wave mixing, 59
principle, 59*f*
- Design criteria for dye and polymer materials for optical recording, 343–344
absorption coefficients, 344
dye concentration, 344
film thickness, 344
light stability, 345
optical efficiency, 343
- Device fabrication, consideration in molecular electronics, 39
- Diacetylenic acids, for Langmuir–Blodgett films, 230
- Diazoketones, use in DUV resists, 87
- 5-Diazo-Meldrum's acid
photochemical decomposition, 132*f*
photolysis, 130, 132*f*
structure, 129*f*

- 5-Diazo-Meldrum's acid-based resists
absorbance spectra, 132*f*
drawbacks, 130
- Diazonaphthoquinone, dissolution inhibitor
in positive photoresists, 119
- Diazonaphthoquinone–novolac resist(s)
images photoetched with excimer laser,
209
use in DUV lithography, 128
- Diazonaphthoquinone
photochemical transformations, 121*f*
structure, 121*f*
- Diazonaphthoquinone sensitizer,
photochemical transformation, 121*f*
- Diazoquinone–novolac materials,
manipulation of exposure wavelength,
85
- Diazoquinone–novolac resin, composition,
79*f*
- Diazoquinone–novolac resists, 75–80
characteristics, 77
for mid-UV application, 125–126
nonlinear dissolution kinetics, 77
outstanding characteristics, 121
resolving ability, 77
- Diazoquinone–novolac systems
changes in dissolution rate, 80
image reversal, 80–82
mechanism for dissolution, 79–80
productivity loss, 88
resist contrast, 79
sensitivity limit, 87
- Differential solubility, 9
- Differential solubility by altered polarity of
side-chain groups, 153
- 3,4-Dimethoxybenzoic acid, improvement of
PMIPK, 137
- 4,4'-*N,N*-Dimethylaminonitrostilbene
hyperpolarizability tensor values, 305*f*
polar profile, 316*f*
- N,N'*-Diocetadecylthiacyanine, use in
fluorescence studies, 239, 240*f*
- DIP (dual in-line package), 15*f*, 19
- Direct-write laser techniques, problems,
200
- Direct-read-after-write feature, 332
- Disk fabrication
2P replication process, 336
control of birefringence, 335–336
injection molding, 336–338
technical problems, 335
- Disk intrinsic defect level, 333
- Disk mass production
injection molding, 68
photopolymerization replication, 68, 69*f*
- Dissolution inhibitor resists, 119–131
for DUV application, 128–131
for mid-UV application, 122–128
- Dissolution kinetics, linear versus nonlinear
system, 80*f*
- Dithiolene, structure, 342*f*
- Divalent ions, effect on Langmuir trough,
241
- Doped conjugated polymers
conductivity, 32*t*
structures, 32*t*
- Doped polyacetylene, energy levels of
defect structure, 34*f*
- Doping in polymers, 30
- DRAM (dynamic random access memory),
chip, 78*f*
- DRAW (direct read after write), feature, 332
- Dry-developable resists
plasma-developable resists, 158–166
properties, 158–172
self-developing resists, 166–171
thermally developable resists, 171–172
- Dry-film photoresist
application to substrate, 22
process, 23*f*
structure, 22
- Dry process for multilevel resists, 101*f*
- Dual-tone resists, poly(*p*-formylloxystyrene),
153
- Dual in-line package, 15*f*, 19
- DUV, *See* Deep UV
- Dye–polymer-based nondeformation
concept, 348
- Dye–polymer layer, effect of recording layer
thickness on performance, 344*f*
- Dye–polymer media, sensitivity, 343
- Dye–polymer solutions
absorption efficiency, 346
effect of polymer properties on sensitivity
and performance, 345
sensitivity, 346
threshold energies, 346
- Dyed resists, 94
exposure doses for imaging, 95
- Dynamic-random-access-memory chip, 78*f*

E

- Effect of polymer binder on threshold
recording energy, 345*t*
- Effect of $\chi^{(2)}$ on conversion efficiencies, 324
- Electric susceptibility functions for various
types of interacting field components,
300*t*
- Electrical conductivity, 26
- Electrical energy at high frequencies, 26
- Electromagnetic radiation, interaction with
molecules, 53, 55
- Electron beam lithography
applications, 110
electron beam system and exposure
process, 6*f*
limitations, 110
resolution, 110
 ω -tricosenoic acid, 253
- Electron behavior in an electromagnetic
field
dipolar contribution to current density,
303
perturbation to Hamiltonian, 303
- Electron spectroscopy for chemical analysis,
spectra of organometallic polymer
films, 98–99*f*
- Electron tunneling, evidence, 239

- Electronic applications of polymers
 circuit board, 2, 4
 historical development, 2
- Electronic states in crystals, 28
- Electronic states of conducting polymers, 273–278
 one-electron model for electronic states in organic polymers, 273–276
- Electronic transmission versus optical transmission, 44
- Electrooptic effect, *See* Pockels effect
- Encapsulated chip prior to transfer molding, 17f
- Encapsulation
 for ablative recording, 339
 requirements, 339
- Encapsulation techniques, 278–279
 effective barriers, 278
 epoxy matrix, 278
 poly(*p*-xylylene), 278
- Energy states for insulator, semiconductor, and metal, 30f
- Energy transfer
 effect of barrier thickness on rate, 239
 sensitizing molecule to acceptor molecule, 238, 239f, 240f
- Environmental factors affecting chips, 16
- Environmental stability of conducting polymers
 effect of chemical transformation of doping sites, 276–277
 effect of matrix stability, 277
 effect of pressure on polyacetylene films, 276
- Epoxy polymers, use in transfer moldings, 18
- Epoxy resins, 14, 16
- Erasable dye–polymer recording scheme, 67f
- Erasable media, *See* Reversible media
- Erasable optical-recording materials, 65–66
- Erasure techniques, 66, 68
- ESCA, *See* Electron spectroscopy for chemical analysis
- Ethylene
 band formation, 28
 band formation by mixing of electronic states, 29f
- Excimer laser lithography
 contact printing, 200–202
 in vacuum-UV region, 201
 photoetching of organic materials, 207f
 projection printing, 202–207
- Excimer laser photoetching organic materials
 basis of etching, 207
 etching with ArF laser, 207
 experimental setups, 208f
 image quality, 209f
 polyimide etching with XeCl laser, 207
- Excimer lasers
 applications, 114–115
 comparison with UV lasers, 114
 drawbacks, 115
- Exotic solvents for conducting polymers, 293
- Exposing radiation in imaging systems, 110
- Exposure tools, all-reflecting optics, 85
- Expressions for $\langle \cos \theta \rangle$, 314
- Expressions for estimating values of $\chi_{xxx}^{(2)}$ and $\chi_{xxx}^{(3)}$ in various environments, 313, 314f
- ## F
- Factors affecting $\chi^{(2)}$, 308–309
- Fermi level, 28
- Fiber-drawing apparatus, 45f
- Field-effect transistor, 257f
- Field-effect transistors, use of Langmuir–Blodgett films as gate insulators, 43f
- Figures of merit, 246f
- Flexible circuitry, application, 21f
- Flexible polymers
 conversion to conducting polymers, 277
 conversion to rigid conducting materials, 277f
- Focused-UV-laser techniques, 200
- Free space image at wafer plane, 128f
- Frequency mixing, principle, 301
- Full-wafer excimer laser projection exposure, 206f
- ## G
- GaAs– ω -tricosenoic acid MISS device, 256f
- GeSe bilayer system, resolution, 193f
- Ge₂Se₁₁ resist
 anisotropic wet chemical etching, 177f
 DUV sensitivity, 177t
- Graft and block copolymers, 285–289
 comb-like copolymers, 286
 formation by doping, 286f
 formation from multiple catalytic sites of soluble substrate polymer, 286
 introduction of solubilizing groups, 285–286
 synthesis of polyacetylene-containing polymers, 287f
- Guided-wave optics, 50
- ## H
- Harmonic conversion efficiency in waveguide under phase-matched conditions, 325f
- Heat-shrinkable tubing for protection of spliced fibers, 49f
- Hemicyanine–nitrostilbene, nonlinear response, 250–251
- Hemicyanine, structure, 249f
- Hexamethyldisilazane, 163
- Hg
 energy level diagram, 114f
 energy levels, 112–113
- Hg discharge lamp
 doping with Zn or Cd, 114

- Hg discharge lamp—*Continued*
 improvement of efficiency, 114
 output inefficiency, 117
- High-aspect-ratio images from aliphatic polysilane—hard-baked photoresist, 197*f*
- High-aspect-ratio images from oxygen RIE pattern transfer, 194*f*
- High-quality thin films in photoresist applications, requirements, 298
- High-resolution exposure equipment, 100
- HMDS (hexamethyldisilazane), 163
- HPR204 resist, dynamic bleaching absorption spectra, 124*f*
- Hückel molecular orbital theory, 28
- Hyperpolarizability
 associated molecular properties, 248
 contributions to value of second-order term, 56
 molecular properties affecting values, 56
 nonlinear response to radiation, 53
- Hyperpolarizability tensor factors
 acceptor electronegativity, 306
 charge density, 306
 conjugation length, 306
 donor electron-donating ability, 306
 resonance interaction, 306
- Hyperpolarizability tensor values for single molecules, 307*t*
- Hyperpolarizability tensor(s), 304–306
 components for a single molecule, 304
 ensemble of molecules, 299
 for free frequency interchange in lossless media, 310
 for molecule with intense intramolecular charge-transfer transitions, 304
 model with nonpolar ground state and polar lowest excited state, 305–306
 perturbation, 303–304, 305
 single molecule, 299, 303–304, 305
- I**
- Image-reversal process
 addition of base for decarboxylation, 81
 base catalysis, 81*f*
 flood exposure, 81
 patterned exposure, 80–81
- Image transfer by oxygen RIE, 96
- Image transformation in resists, 8*f*
- Imaging process
 early methods, 75
 materials for early methods, 76
 microlithographic trends, 38*f*
 resolution of early methods, 76
 resolution of modern methods, 77
- Imines, use in built-on mask process, 85
- In situ polymerization
 block copolymers, 283
 polybutadiene, 283
 terpolymers, 283
- Indenone, improvement of PMMA structure, 137
- Induced asymmetry in polymers, 299
- Induced polar alignment
 in anisotropic medium, 313
 order parameter, 313
- Induced polarization
 in a single molecule, 298–299, 303
 in an ensemble of molecules, 299
- Induced voltage, 245–246
 change with number of layers deposited, 246
- Injection molding
 injection—compression versus straight injection, 337
 need for high levels of cleanliness, 337
 orientation distribution in molded disks, 337
 techniques to reduce birefringence and improve stability, 337
- Inorganic negative resists
 AgCl-As₂S₃, 172
 Ag-GeSe systems, 172
 Ag₂Se-C₂Se_{1.33}, 174
 drawbacks, 176
 GeSe chalcogenide glass, 172
 properties, 172
- Inorganic resists, reciprocity failure, 211
- Integrated circuit(s)
 fabrication, 14
 packaging, 14
 size of circuit elements, 109
- Integrated optics, 50
- Intractable polymers, preparation of soluble derivatives, 283–284
- IPPhK (isopropenyl phenyl ketone), 138
- Isopropenyl phenyl ketone, 138
- K**
- Kodak 809 resist
 top imaging resist for DUV blanket exposure—PCM systems, 183
 UV transmission characteristics, 184*t*
 UV transmission characteristics in mid-UV exposure—PCM scheme, 187*f*
- KrF excimer laser projection printing
 images printed, 205*f*
 setup, 204*f*
- L**
- Langmuir–Blodgett alternate multilayers, 318*f*
- Langmuir–Blodgett film(s)
 applications, 42, 44, 243
 applied research areas, 242–243
 as biosensors, 258
 as insulators, 258
 characteristics, 41
 characterization, 234, 236–238
 control of orientation, 243–244
 definition, 236
 deposition with hydrophilic substrate, 226, 229*f*, 230

- Langmuir–Blodgett film(s)—*Continued*
 deposition with hydrophobic substrate, 230
 design of monolayer assemblies, 230–231
 early applications, 236
 effect of subphase composition, 226
 electron beam lithography, 253
 enhanced device processing, 252, 255
 example in nonlinear optics, 249–252
 for studies of energy transfer in complex monolayers, 238–239
 impetus for study, 225
 in acoustoelectric devices, 259–260
 in molecular electronics, 40–44
 in nonlinear optics and physics, 243–244, 248, 313
 in optical sensors, 258–259
 in pyroelectric devices, 244
 in semiconductor devices, 257–258
 industrial applications, 243
 investigation of intermolecular interactions, 238
 limitations, 42
 metal ion incorporation, 241
 minimal scattering, 328
 model for energy transfer between molecules, 239f
 model of cooperating molecules on substrate, 238
 modern developments, 230–233
 modification of effective barrier height at semiconductor surface, 253, 255
 molecular designs, 41–42
 monolayer isotherm, 42f
 nonlinear applications, 248–249
 passive layer in enhanced devices, 252–253
 patternwise delineation, 328
 phthalocyanines for monolayer assemblies, 231
 porphyrins for monolayer assemblies, 231
 preparation, 226–230
 properties, 230
 prospects for molecular and supermolecular electronics, 266–267
 quartz oscillator, 260
 requirements for use in optical technologies, 328
 resemblance to biological membranes, 241
 sensors and transducers, 257–260
 stability requirement of monolayer assemblies, 231
 suitable materials, 40
 superconducting quantum interference devices, 255
 surface acoustic wave oscillator, 260
 surface pressure, 40–44
 thickness control, 328
 transfer to substrate, 41
 types of deposition, 230
 unique features, 242–243
 use in field-effect transistors, 42, 43f
 use in fundamental research, 238
 use in physical studies of biological molecules, 241
- Langmuir–Blodgett film(s)—*Continued*
 with C_{∞} symmetry, 310, 311f
 Y-type deposition, 226, 229f, 230
 Y-type dipping sequence, 232f
 Y-type film with noncentrosymmetric character, 233f
- Langmuir–Blodgett technique, 40
 application to hemicyanine dye and nitrostilbene derivative, 317–319
 for assembly of films with noncentrosymmetric ordering and C_{∞} symmetry, 317–318
 for preparation of polydiacetylene crystals, 59–60
 sequence, 41f
- Langmuir troughs
 recent developments in design, 231, 233
 rotating-substrate arrangement, 233
 technique for damage-free deposition, 255
- Laser marking process, 341f
 ablative recording, 341–347, 349–351
 bubble recording, 347
 recording based on optical property change, 347–349
- Laser microchemical processing, practical applications, 200
- Laser projection system, print quality, 203f
- Lasers
 ArF, 201
 F₂, 201
 in maskless patterning technology, 198, 200
 KrF, 201, 202, 203
 spatial coherence, 198
 XeCl, 206
- LB film(s), *See* Langmuir–Blodgett film(s)
- Lens systems, improvement of resolution, 85
- Limitations imposed by phase-matching requirements on interaction length, 323–324
- Line width control, 92, 94
 use of antireflection coating, 95
 use of dyes, 94
- Line width variation caused by overcut resist profiles, 149f
- Linearly responsive resist, image reproduction, 129f
- Lipophilic carboxylic acid *o*-nitrobenzyl esters, use in DUV resists, 85–87
- Liquid crystalline polyesters, characteristics, 25
- Lithium niobate
 damage threshold, 57
 use in integrated optics, 51
- Lithographic process, overview 4–5
- Lithography, 109
 with traditional lasers, 198
- LMR, *See* Low-molecular-weight resist
- Low-cost packaging methods, 19
- Low-molecular-weight resist
 developer, 157
 dissolution differentiation, 157
 structure, 158f

M

- Macroscopic nonlinearities by intramolecular processes, 308–309
- Macroscopic polarization, expression, 248
- Magneto-optical recording, 66
- Main-chain scission resists, 131–140
- Maskless patterning technology, ceramic substrate, 200
- Meander patterns, electrical probe yield versus size and wavelength, 122*f*
- Melt-shear technique, 60
- Metal–insulator–semiconductor devices diode, 257*f*
use in field-effect transistor, 257
- Metal–insulator–double semiconductor devices, 255, 256*f*
- Metal-ion-containing multilayer, applications, 241–242
- Methacrylonitrile, improvement of PMMA structure, 137
- 2-Methyl-4-nitroaniline, nonlinear optical properties, 57
- MIBK (methyl isobutyl ketone), use in uncapped process, 180, 183
- Micro resist for shorter wavelengths, 142
cause of solubility decrease, 146, 148
effect of development time, 147*f*
mask in RIE, 150*f*
overcut profile, 146, 149*f*
quality of print by broad-band exposure, 149*f*
scanning exposure times required, 146
simulated profiles, 148*f*
simultaneous exposure to mid-UV and DUV radiation, 146
undercut profile, 146, 149*f*
- Microbending loss, 46
- Microelectronics revolution, influence on modern society, 44
- Microlithographic patterning, generation of third dimension, 100
- Microlithographic processes
influence of topographic features on layers, 90, 91*f*
resolution limits, 90
topographic features of devices, 91*f*
- Minimum device feature size,
microlithographic trends, 38*f*
- MIS, *See* Metal–insulator–semiconductor
- MISS, *See* Metal–insulator–double semiconductor
- Molecular and crystal frames of reference for a noncentrosymmetric crystal, 309*f*
- Molecular electronics
definition, 40
in integrated circuit fabrication, 39
use of polymers, 38
- Molecular interconnects, 39
- Molecular switch, requirements, 39
- Molecularly doped polymer, requirements for use in optical technologies, 327
- Molecules for Langmuir–Blodgett films
diacetylenic acids, 230
- Molecules for Langmuir–Blodgett films—
Continued
phthalocyanines, 231
porphyrins, 231
 ω -tricosenoic acid, 230
- Monolayer assemblies, reproducibility of physical parameters, 237*f*, 238
- Monolayer parameters, reproducibility, 237–238
- Monomolecular assemblies, support matrices for dye molecules, 225–226
- MRS, *See* Micro resist for shorter wavelengths
- Multilayer resist systems
components, 178
DUV blanket exposure–PCM systems, 17, 178–190
principle, 178
processes, 179*f*
RIE–PCM systems, 190–198
- Multilayer resist(s)
DUV applications, 178–198
processes, 179*f*
- Multilevel resist process(es), 90–100, 95*f*
dry process, 100, 101*f*
image transfer by oxygen RIE
trilayer process, 96, 97*f*, 98
- Multilevel resist technology
applications, 95
solution to topography problem, 95

N

- N-channel metal oxide semiconductor, manufacture, 183
- N doping, 33
- Near-IR absorbing dyes for diode laser recording, 342*f*
- Negative photoresists, 140
- Negative plasma development by selective silylation, 165*f*
dry-developed images, 165*f*
- Negative resists
azide sensitizer systems, 140–148
polystyrene-based systems, 148–152
- Negative-top resist–PCM system
advantages, 188
Ag₂Se–GeSe–PMMA, 188
MRS–PMMA, 188,
PSTTF as imaging layer, 188
- Negative-tone resists, 76*f*
- Neutral solitons, origin of free spins, 35–36
- Nitrene reactions, 140, 141*f*
- o*-Nitrobenzylcholate(s)
photochemical decomposition, 130, 133*f*
structure, 131*f*
- o*-Nitrobenzylcholate-based resists,
characteristics, 131
- o*-Nitrobenzyl ester, photochemical decomposition, 133*f*
- Nitrostilbene, structure, 249*f*
- Noncentrosymmetric molecules
design techniques, 57

- Noncentrosymmetric molecules—*Continued*
 polarization, 55
 Noncentrosymmetric structures, generation, 231
 Nonlinear applications, requirement, 249
 Nonlinear coefficients
 molecularly doped poled polymers, 312
 single crystalline materials, 312
 Nonlinear optical effects occurring through $\chi^{(2)}$, 300f
 frequency mixing, 301
 Pockels effect, 301
 second harmonic generation, 299–301
 Nonlinear optical effects occurring through $\chi^{(3)}$, 302f
 optical bistability, 301–302
 optical phase conjugation, 302–303
 third harmonic generation, 301
 Nonlinear optical properties
 effect of fluids caused by neighboring molecules, 306
 effect of molecular orientation, 306
 Nonlinear optics
 explanation of effects, 53
 fundamental concepts, 297
 interaction of electromagnetic fields with materials, 53
 origin of effects, 53
 origin of nonlinear effects, 299–303
 Novolac resists, planarizing layers for trilevel RIE-PCM system, 190
- O**
- Onium salt cationic photoinitiators, photochemistry, 156f
 Onsager expression, 308
 Optical-recording disk substrates
 bisdiallylpolycarbonates, 63
 PMMA, 63
 poly(4-methyl-1-pentene), 63
 requirements, 63
 suitable polymers, 63
 Optical audio disk
 analysis of electrical output, 62
 digital format, 62
 Optical digital recording
 device options, 65
 laser-induced ablation, 65
 suitable materials, 65
 thin-film decomposition, 65
 use of polymers, 65
 Optical disk
 protective coatings, 68
 protection schemes, 340f
 Optical disk media
 air-sandwich structure, 338
 encapsulation, 338–339
 protection schemes, 338–340
 Optical disk substrates
 contaminant removal, 334
 material requirements, 333–334
 polyacrylics, 334–335
 polycarbonates, 334
 Optical disk substrates—*Continued*
 selected physical properties, 334t
 suitable polymers, 334–335
 Optical efficiency, 343
 Optical fibers
 attenuation losses, 47
 cabling, 47
 coating procedure, 45
 connections for spliced fibers, 47, 49f
 fusion splicing, 47
 packaging for cables, 47, 48f
 packaging of spliced fibers, 47, 49f
 unsuitability for long-distance transmissions, 47
 Optical film
 coating design, 46, 47
 coating technique, 45–46
 function of coating, 46
 Optical information storage, video disk, 60
 Optical multiplexer, 51f
 Optical projection printing, advantages and disadvantages, 180
 Optical recording systems
 materials for transparent disks, 333
 techniques for disk manufacture, 333
 Optical transmissions
 advantage, 45
 capacity, 45
 driving force, 44–45
 light sources, 44
 Optical waveguide fabrication, 50–51
 ion-exchange process, 51–52
 photolocking technique, 52–53, 52f, 54f
 refraction index requirement, 52
 Optical waveguides, 51
 Optimum harmonic conversion efficiency, 323
 Optoelectronic devices, 247–252
 Organic resist materials, inadequate etching durability, 192
 Organic superlattice with unique polar axis, 244f
 Organosilicon resists for bilayer multilevel resist systems, 12–13t
 Orientational distribution function
 anisotropic medium, 313
 isotropic medium, 313
 Orientation zones in disks, 337–338
 Oxidation–reduction process, 274
 3-Oximino-2-butanone methacrylate, improvement of PMMA structure, 135, 137
 Oxindolizinium, structure, 342f
 1-Oxo-2-diazonaphthoquinone-4-arylsulfonate, structure, 125f
 1-Oxo-2-diazonaphthoquinone-5-arylsulfonate, structure, 121f
 Oxygen etch barrier, use of silicon or tin, 194
- P**
- P doping, 33
 PCM, *See* Portable conformable mask

- Perhalohydrocarbons, use in built-on mask process, 85
- PGMA [poly(glycidyl methacrylate)], 134, 135*t*
- Phase-change recording
principle, 347-348
suitable organic media, 347-348
- Phase-matched and non-phase-matched harmonic generation, 322*f*
- Phase-matched interaction of polar point groups, 309*t*
- Phase matching, for large harmonic conversion efficiencies, 326
- Phase mismatch factor versus degree of phase mismatch, 323, 324*f*
- Photo-Fries degradation, 153*f*
- Photochemical acid generators, 156*f*
properties, 156
- Photochemical hole burning, 66
- Photochemical induction of differential solubility, 119, 120
- Photolithography, 109-110
basic steps, 5*f*
conventional light source, 112
extension of resolution by short-wavelength UV radiation, 110
- Photonic applications of polymers
integrated optics, 50-53
nonlinear optics, 53-60
optical fiber coating, 45-50
optical recording media, 60-70
photonic circuits, 50
regeneration of light intensity during long-haul transmission, 50
- Photopolymerization process for replication of video disks, 69*f*
- Photoresist, bleaching at different laser peak powers, 210*f*
- Photosensitive polyimides, chemistry, 11*f*
- Phthalocyanine, modification of effective barrier height at semiconductor surface, 253, 255
- Pierls transition, 30
- PIPTBK, *See* Poly(isopropenyl *tert*-butyl ketone)
- Pit formation in dye-polymer by superheating, 342*f*
- Pit recording in dye-polymer film through ceramic overcoat, 351
- Planar waveguide, main features, 319
- Planarization
effect on resolution, 91
global, 91
local, 91
- Plasma-developable negative resists
cationic polymerization, 166
ion implantation, 163*f*
postirradiation radical grafting reactions, 166
- Plasma-developable photoresist, X-ray resist system, 158
- Plasma-developable photoresist process, 159*f*
- Plasma-developable resists
bisazide-polyisoprene, 162-163
design types, 162
- Plasma-developable resists—*Continued*
ion implantation, 162
resists based on acrylic copolymer containing silicon side groups, 162
system based on bisarylazide and aliphatic matrix resin, 15
- Plasma-developable UV-sensitive resists, use of positive-negative working resist system, 163
- Plasma development process, 160*f*
- Plasma electrons, energy, 113, 114
- PMGI, *See* Poly(dimethyl glutarimide)
- PMIPK, *See* Poly(methyl isopropenyl ketone)
- PMMA, *See* Poly(methyl methacrylate)
- Pockels effect, 56
principle, 301
- Polar alignment, 309-311
factor favoring high second-order tensor(s), 310
induced polar alignment, 313
order parameter, 313
orientational distribution function, 313
- Polar crystal, 56
- Polar order, effect on $\chi^{(2)}$
- Polarization, 53
in centrosymmetric crystals, 55-56,
in noncentrosymmetric and centrosymmetric media, 55*f*
in noncentrosymmetric molecules, 55
induction by external electric field, 57
nonlinear effect, 56
- Polarizing effect, expression, 248
- Polaron, 274
energy levels, 34*f*
- Poled polymer film applications, waveguide nonlinear optics, 319
- Poling a polymer film, 310*f*
- Poling profile for Disperse Red I in PMMA, 315*f*
- trans*-Polyacetylene
doping, 275*f*
soliton, 35
structure, 274*f*
unique characteristics, 33
- Polyacetylene(s)
as semiconductors, 29
block copolymers
anion to Ziegler-Natta transformation, 288
metathesis polymerization of cyclooctatetraene with tungsten catalysts, 289
polymerization with epoxide- or carbonyl-functionalized polymer, 288
preparation, 288
stabilization by encapsulation, 278
conductivity, 30
defect structures arising from isomerization, 35-36
energy diagram of ground-state geometric isomers, 35*f*
energy levels of geometric isomers, 35
geometric isomers, 35
latexes, 281
preparation by Feast technique, 37

- Polyacetylene(s)—*Continued*
 stabilization by encapsulation, 278
 suspensions, 281
 synthesis by Durham route, 291*f*, 292*f*
- Polyacetylene-polyethylene composites,
 preparation, 282
- Polyacrylics, 334–335
- Polyaldehyde, acid-catalyzed
 depolymerization, 169*f*
- Poly(alkylthiophene)s
 polythiophenes, 284
 preparation of soluble derivatives, 284
- Poly(3-alkylthiophene)s, conductivities, 285*f*
- Poly(arylene vinylene)s, 292
 synthesis, 292*f*
- γ -Polybenzyl-L-glutamate, enhanced polar
 alignment, 317*f*
- Poly[bis(*p*-toluenesulfonate)diacetylene],
 structure, 299*f*
- Poly(butene-1-sulfone), 138
- Poly(*tert*-butoxycarbonyloxystyrene) as
 protective agent, 100*f*, 101*f*
- Polycarbonate-onium salt resist, positive
 images by thermal development, 173*f*
- Polycarbonates, for injection molding of
 optical disks, 334
- Polydiacetylene(s)
 cubic-nonlinearity-related effects, 57, 59
 cubic susceptibility, 251*f*
 polymerization, 58*f*
 techniques of crystal preparation, 59–60
- Poly(2,3-dichloropropyl acrylate), 158
- Poly(dimethyl-diphenylvinylsiloxane)-hard-
 baked AZ1350J system, 194*f*
- Poly(dimethyl glutarimide)
 pattern obtained by DUV exposure, 188*f*
 planarizing layer for DUV blanket
 exposure-PCM systems, 186
 properties, 186
 structure, 137*f*
 thermal stability of pattern, 189*f*
 use in aqueous-base-developable bilayer
 PCM system, 186
- Poly(*p*-disilanylenephenylene), structure,
 196*f*
- Poly(*p*-formyloxystyrene) resists, positive
 and negative images, 154*f*
- Poly(glycidyl methacrylate), 134, 135*t*
- Poly(5-hexen-2-one sulfone), 138
- Polyimides, 14, 16
 as adhesives, 14, 16
 as substrates in printed wiring boards, 20
 in packaging, 19
 planarizing layers for trilevel RIE-PCM
 system, 190
 protection against alpha particles, 18
 use in resists, 11
 useful characteristics, 11
- cis*-1,4-Polyisoprene, structure, 140*f*
- Poly(isopropenyl *tert*-butyl ketone)
 cleavage, 139*f*
 Norrish type I cleavage, 139*f*
- Polymer(s)
 application-dependent properties, 311
 applications, 47
 as insulating materials, 26
- Polymer(s)—*Continued*
 as optical disk substrates, 63
 in electronic packaging, 14–20
 in optical recording media
 imaging layers, 63–68
 optical coating, 68–70
 substrates, 63
 in recording media, 340–351
 minimal scattering, 328
 passive applications, 53
 patternwise delineation, 328
 photonic applications, 44–45
 relative conductivities, 272*f*
 requirements for use in optical
 technologies, 328
 thickness control, 328
 use for optical core, 47
- Polymer applications
 active versus passive, 1
 disk packaging, 332
 disk substrates, 332
 erasable materials, 66, 67*f*
 interconnection of chips, 14
 optical digital recording, 65
 protection of chips, 14
 protective configurations, 332
 waveguides, 52
- Polymer-based recording materials in write-
 once systems, 331
- Polymer design and lithographic
 characteristics
 chemical modifications for solubility, 7,
 9
 matrix polarity and differential solubility,
 9
- Polymer physical characteristics
 effect of molecular weight on reflectivity
 contrast, 346
 effect on final pit dimensions, 346
- Polymethacrylate polymers, lithographic
 properties, 135*t*
- Polymethacrylate positive DUV resists, 135*t*
- Poly(methyl acetylene), stabilization by free-
 radical scavengers, 279
- Poly(methyl isopropenyl ketone)
 cleavage, 138
 effect of *tert*-butyl substitution, 138
 in plasma-developable resists, 159
 planarizing layer for DUV blanket
 exposure-PCM systems, 183, 186
 UV transmission characteristics in mid-UV
 exposure-PCM scheme, 187*f*
- Poly(methyl isopropenyl ketone)-azide
 resist, plasma development 161*f*
- Poly(methyl methacrylate)
 advantages, 133
 as DUV resist, 111
 as planarizing layer for resists, 95
 as positive resists, 77
 bottom planarizing layer for DUV blanket
 exposure-PCM system, 180
 direct photoengraving, 169
 dissolution kinetics, 133
 drawbacks, 134
 exposure to excimer laser, 201
 photolysis, 135*f*

- Poly(methyl methacrylate)—*Continued*
 planarizing layer for DUV blanket exposure PCM systems, 183, 186
 printing of Y-I bars, 134*f*
 radiation-induced chain scission, 135*f*
 transmission spectra, 49
 use as isotropic host medium, 57
 use as optical disk substrates, 63
- Poly(methyl methacrylate-*co*-methacrylic acid), exposure to excimer laser, 201
- Poly(methyl methacrylate) image, capped or uncapped structures, 179*f*, 180
- Poly(methyl methacrylate) resist, UV transmission characteristics, 184*f*
- Poly(4-methyl-1-pentene), use as optical disk substrates, 63
- Poly(olefin sulfones)
 poly(butene-1-sulfone), 138
 poly(5-hexen-2-one sulfone), 138
- Poly(*p*-phenylene), structure, 274*f*
- Polyphthalaldehyde-onium salt resist, 168–169
 positive image with KrF excimer laser, 171*f*
 self-developed images, 170*f*
- Polyphthalaldehyde sensitivity to radiation, 169
- Poly(pyrrole)
 effect of counterion on stability, 280
 suspensions, 282
- Poly(pyrrole) benzenesulfonate, effect of sodium hydroxide on stability, 280
- Poly(pyrrole) perchlorate, 280
- Poly(pyrrole) phthalocyanine, 280
- Polysilanes
 aliphatic repeating unit, 196*f*
 backbone scission, 195
 lithographic properties, 195
 photobleaching and blue shift of aliphatic polymers, 196
- Polysiloxanes
 for ablative recording, 340
 imaging layer in bilevel RIE-PCM scheme, 192
 structure, 192*f*
- Polystyrene-based cross-linking negative DUV resists, 150*t*
- Polystyrene-based negative resists, 148–152
 chloromethylated polystyrene, 151
 limitations, 151
 new materials, 152
- Polystyrene, 151
- Polystyrene-tetrathiofulvalene
 differential solubility by change in polarity of pendant groups, 152
 properties, 152
 structure, 152*f*
- Polystyrene-tetrathiofulvalene-PMMA system, advantages, 188
- Polystyrene-tetrathiofulvene resist, imaging mechanism, 152*f*
- Poly(sulfur nitride), source of conducting property, 29
- Polythiophenes, preparation of soluble derivatives, 284
- Polytrimethylsilylstyrene, spectra after electron spectroscopy for chemical analysis, 195*f*
- Poly(*p*-vinylphenol), 146
 matrix resin for DUV blanket exposure-PCM systems, 183
 structure, 142*f*
- Portable conformable mask process, 178
- Portable conformable mask systems
 negative-top resist, 188, 191*t*
 with DUV blanket exposure, 17, 178–190
 with RIE, 190*t*
- Positive photoresists, 9
 composition of conventional materials, 119
 diazoquinone-novolac systems, 121
 dissolution-inhibitor systems, 119–131
 reduced sensitivity in the mid-UV region, 122
 undesirable optical characteristics, 123*f*, 124*f*
- Positive resists
 linear dissolution kinetics, 77
 main-chain scission, 131–140
 PMMA, 77
- Potassium dihydrogen phosphate, damage threshold, 57
- Precision-molded plastic connector, 49*f*
- Precursor polymer preparation, 289–293
 dehydrohalogenation of poly(vinyl chloride), 289–290
 Durham route to polyacetylene, 290, 291*f*
 indirect synthesis of
 poly(phenylenevinylene), 290
 temperature-controlled retro-Diels-Alder reaction, 290
- Prepreg process, 20, 22*f*
- Printed wiring boards
 direct molding, 25
 fully additive process, 25
 impact of high-speed electronics, 26
 partially additive process, 25
 prepreg process, 20, 22
 propagation delay, 26
 speed penalty, 26
 substrate materials, 20–26
 techniques for making conductor paths, 23, 25, 24*f*
 trends, 25
- Projection printing
 effect of exposure wavelength reduction, 112
 positive resists, 77
 with excimer lasers, 202–207
 laser projection set up, 202, 204–205
 laser source coherence, 202
 print quality, 203*f*, 204
 scanning laser beam system, 202, 203*f*
 use of commercial projection printer, 205–206
 use of DUV and vacuum UV excimer lasers, 206–207
 use of modified full-field scanning projection system, 206
- Protected phenolic resin, IR spectra, 102
- Protection of optical fibers by coatings, 46*f*

- Protective coatings
 air-sandwich configuration, 68
 conformal coatings, 68
 cross-linked siloxane elastomers, 68
 polymeric encapsulated structures, 68
- Proximity printing
 effect of exposure wavelength reduction, 112
 effect of wavelength on intensity function, 112
 resolution, 112
- PSTTF, *See* Polystyrene-tetrathiofulvalene
- Pyridinium tetracyanoquinodimethane on quartz, 266
- Pyroelectric coefficient(s), 245, 246*t*
- Pyroelectric current, 245
- Pyroelectric devices, 244–247
 advantages, 245
 ferroelectric liquid crystals, 245
 Langmuir–Blodgett films, 246–247
 poly(vinyl difluoride), 245
- Pyroelectric effect, 245
- Pyroelectric response, constraints, 246–247
- Pyrrrole
 chemical polymerization, 283
 electropolymerization, 283, 287–288
 polymeric latex dispersion, 282
 polyacetylene electrodes, 280
- Pyrylium, structure, 342*f*
- Q**
- Quartz oscillator, 260, 261*f*
 Langmuir–Blodgett films, 260–261
 response characteristics, 260, 262*f*
- R**
- Radiation-induced conversion of polymer, 100
- Random access memory devices, time evolution, 38
- Random copolymers
 acetylene and methylacetylene, 284–285
 acetylene and phenylacetylene, 284–285
- RD2000N resist
 image formed with KrCl excimer laser, 212*f*
 resist thickness versus development time, 144–145*f*
- Reactive ion etching
 image transfer materials, 96
 image transfer process, 96
 in modern image processing, 76
 in multilevel resist processing, 96
 with MRS, 150*f*
 with PCM systems, 190–198
- Reactive ion etching–PCM systems
 organometallic resists, 192
 use in DUV lithography, 190, 191*t*
- Reciprocity failure in inorganic resists, 211*f*
- Recording media, properties, 331
- Reflection high-energy electron diffraction
 nitrostilbene, 235*f*
 ω -tricosenoic acid, 236*f*
- Reflective notching, 92
- Refractive index dispersion associated with optical transition, 322*f*
- Refractive index of organic polymers, suitability for parametric processes, 324
- Relationship between microscopic and macroscopic nonlinearities, 306–311
- Relationship of $\chi^{(1)}$ and $\chi^{(3)}$ to molecular quantities, 306, 308
 in centrosymmetric media, 308
 in isotropic media, 308
- Relationship of $\chi^{(2)}$ to molecular tensor components, 308–309, 310
- Resist images
 slopes of latent image, 82*f*
 wall slopes, 82
- Resist materials, 4–14
 for high-resolution lithography, 153
 important characteristics, 5
 innovations, 95–96
 research focus, 77
 resolution, 7
 tone reversal, 156–157
 unique properties required, 7
- Resist performance factors
 exposure absorption, 211–212
 optical density, 212–213
 spectral characteristics, 213
- Resists
 absorption characteristics, 211–213
 behavior in excimer laser irradiation, 207–213
 chemical modifications, 10
 definition of circuit pattern, 4
 effect of diazoquinone–novolac systems on contrast, 79
 passivation by silicon dioxide, 10
 reciprocity behavior in excimer laser exposure, 209, 210*f*, 211
- Resists allowing third dimension
 hardening process, 104
 image-reversal process, 104*f*
 image of two-level structure, 105*f*
 three-tone mask exposure, 104
- Resists, formation of three-dimensional relief structure, 4–5
- Resolution limit of imaging systems, 110
- Resolution loss in resist imaging, 91–92
- Reversible phase-change recording
 mechanism 349
 medium based on aggregation–deaggregation 348–349
 preferred materials, 349
 system based on amorphous crystalline switching mechanism, 348
- Reversible ablative recording
 basis of erasure process, 349
 ceramics as overcoat materials, 350
 copper phthalocyanine–polystyrene film for marking, 349–350
 dome formation, 350

Reversible ablative recording—*Continued*
 dye-polymer medium overcoated with a thin restraining layer, 352*f*
 erasure by difocused laser beam, 350
 erasure by heating, 350
 overcoat deformation during recording, 351*f*
 polymers as overcoat materials, 350
 principle, 349
 suitable materials, 349
 use of polystyrene thermoplastic oligomers, 349–350

Reversible media, 348–351
 ablative recording, 348–351
 phase-change recording, 348–349
 requirements, 333

RHEED, *See* Reflection high-energy electron diffraction

RIE, *See* Reactive ion etching

Ring-field projection system, 215*f*

S

SAW, *See* Surface acoustic wave

Scanning point source system, 203*f*

Second-order nonlinearities, 303–306
 perturbation of hyperpolarizability tensor, 303–304, 305

Second harmonic generation, 53
 applications, 248
 coherence length, 323
 compounds with high coefficient, 249*f*
 dependence on areal density of dye, 251–252
 ideal structure, 250
 in waveguides versus bulk, 321–325
 lithium niobate, 248
 3-methyl-4-nitroaniline, 248
 non-phase-matched and phase-matched harmonic generation, 322*f*
 optimum harmonic conversion efficiency, 323
 principle, 299–301
 refractive index dispersion associated with optical transition, 322*f*
 requirements of materials, 56
 structural requirements, 248

Selective surface metallization, approaches, 98, 100

Self-developing resists, 166–171
 chemical basis, 169
 polyaldehyde based, 168–169

Semiconductor barrier height modification, 253, 255

Semiconductor devices, 257–258

Sensors and transducers
 acoustoelectric devices, 259–260
 optical sensors, 258–259
 quartz oscillator, 260
 semiconductor devices, 257–258
 surface acoustic wave oscillator, 260

SHG, *See* Second harmonic generation

Silicon
 effect on oxygen plasma etch rate, 195

Silicon—*Continued*
 photochemical elimination for positive-tone plasma development, 162*f*
 semiconductor for integrated circuits, 42
 use in resists, 10

Silylation
 for negative resists, 163–164, 166
 for positive resists, 166

Soliton, 33
 definition, 274
 distribution of spin and charge density, 36
 signature, 274
 spin-charge configuration, 34*f*, 35

Speckle phenomenon, 114

Spectral deflection of cold mirrors, 116*f*

Spinless conductivity, 32, 33

Squarylium, structure, 342*f*

Standing wave(s), 92
 interference of transmitted light, 93*f*

Standing-wave effect, reduction, 94

Stearic acid
 compression by barrier, 226, 228*f*
 phase transformation during compression, 226
 structure, 227*f*

Step-and-scan principle, 214*f*

Supermolecular structures, in studies of biological systems, 241

Surface-layer-imaging process, 99*f*

Surface acoustic wave device
 comparison with single-crystal resonator, 263
 Langmuir-Blodgett film, 263
 lithium niobate dual line, 265*f*
 pyridinium tetracyanoquinodimethane, 263
 quartz dual delay, 266*f*

Surface acoustic wave dual delay line oscillator, 264*f*

Surface acoustic wave oscillator
 common devices, 260, 262–266
 piezoelectric Langmuir-Blodgett films, 260, 262–266
 principle, 263

Surface details in a prepatterned optical disk, 336*f*

Surface passivation of silicon-containing resist, 10*f*

Surface plasmon resonance, principle, 258, 259

Surface potential, change with number of layers, 246, 247*f*

T

Tape automated bonding, 19*f*

TE modes, 326

Temperature-dependent polarization, 245

Terpolymer resist, planarizing layer for DUV blanket exposure-PCM systems, 186

Thermally developable resists
 development by heating, 171

Thermally developable resists—*Continued*
 polycarbonates sensitized with onium salts, 171–172
 poly(olefin sulfones) sensitized with pyridine *N*-oxides, 171
 Thin-film recording media, determination of energy absorption profile, 344
 Third-order susceptibility tensor
 fundamental properties of materials, 252
 value, 250*f*
 Third harmonic generation
 applications, 248
 as function of wavelength, 251*f*
 diacetylene-based Langmuir–Blodgett films, 252
 gallium arsenide, 248
 polyacetylene, 248
 structural requirements, 248
 Three-layer DUV flood exposure–PCM systems, 190*t*
 Three-layer PCM systems, 188, 190
 Threshold energy, 346
 TM-guided modes
 factors affecting refractive index, 320
 refractive index dispersion curves, 320*f*
 TM modes, 320, 326
 conversion in a multilayer Langmuir–Blodgett waveguide, 326*f*
 electric field distributions in a symmetric waveguide, 319*f*
 Topographic features
 effect on line width variations, 94*f*
 effect on reflection from resist-substrate interface, 92
 effect on resolution, 92*f*
 effect on thickness of resist coating, 92
 Tractable materials, design approaches, 281
 Transfer molding
 epoxy polymers as molding compounds, 18
 molding formulations, 18–19
 requirements of molding compounds, 18
 Transport via structural defects, 32
 ω -Tricosenoic acid
 electron beam lithography, 253
 molecules for Langmuir–Blodgett films, 230
 properties, 230, 252
 structure, 227*f*
 Trilayer process
 early versions, 96
 resist images, 97*f*
 sequence, 95*f*
 simplification and improvement, 96–98
 Trilevel RIE–PCM system
 elimination of intermediate layer, 192
 inorganic resist systems, 192
 principle, 190
 types of planarizing layers, 190
 Trimethylstannylstyrene–*p*-chlorostyrene 1:1 copolymer, structure, 194*f*
 Tunneling devices, 255–256
 Two-layer DUV flood exposure–PCM systems, 182*t*, 185*t*

U

Ultrafast signal processing technologies, 59
 UV hardening of photoresist, 199*f*

V

Vacuum-UV excimer laser system, 202*f*
 Valence band splitting, 31*f*
 Vapor development, 166
 Very large scale integration
 microlithography, 174
 Video disk
 analog format, 60
 creation of imaging layer, 63
 double-sided design, 64*f*
 electrical output, 60, 61*f*
 information storage and conversion, 60
 relation between pit pattern and read-out signal, 62*f*
 subbing layer, 65
 topography, 61*f*
 Video disk imaging layer, need for defect-free surface, 65
 VUV (vacuum UV) excimer laser system, 202*f*

W

Waveguide design
 coupling of modes, 325–326
 phase matching, 325–326
 Waveguides
 advantages, 319
 formation, 319
 Wavelength dispersion of phase-matching thickness, 321*f*
 Wire bonding, 16
 Write-once media
 performance criteria, 332*t*
 threshold recording behavior, 333
 Write-once systems
 direct-read-after-write features, 332
 suitable materials, 331

X

$\chi^{(2)}$ values for second harmonic generation, 312*f*
 Xe–Hg lamp, spectral irradiance, 120*f*
 X-ray lithography, resolution, 110
 X-ray photoemission for study of organic materials on surfaces, 241
 X-ray resist system
 components, 158
 principle, 158–159

Z

Ziegler–Natta polymerization, 76*f*